

NASA/CR—1999-209164/VOL2



# Stirling Space Engine Program

## Volume 2—Appendixes A, B, C, and D

Manmohan Dhar  
Mechanical Technology Inc., Latham, New York

Prepared under Contract NAS3-25463

National Aeronautics and  
Space Administration

Glenn Research Center

---

August 1999

Note that at the time of printing, the NASA Lewis Research Center was undergoing a name change to the NASA John H. Glenn Research Center at Lewis Field. Both names appear in these proceedings.

Available from

NASA Center for Aerospace Information  
7121 Standard Drive  
Hanover, MD 21076  
Price Code: A18

National Technical Information Service  
5285 Port Royal Road  
Springfield, VA 22100  
Price Code: A18

## TABLE OF CONTENTS

SECTION	PAGE
<b>Volume II</b>	
<b>APPENDIX A: HEATER HEAD DEVELOPMENT</b>	
A.1 Starfish Heater Head Program.....	1
A.2 Task Narrative: 1/10 <sup>th</sup> Segment and Full-Scale Heat Pipes Heat Pipe Processing Procedure.....	11
A.3 Detailed Procedure: Sodium Filling and Processing.....	17
<b>APPENDIX B: CTPC COMPONENT DEVELOPMENT</b>	
B.1 Introduction .....	35
B.2 High-Temperature Organic Materials .....	36
Memorandum: High-Temperature Organic Material Evaluation Tests, Phase II .....	36
Memorandum: High-Temperature Adhesive Tests.....	39
B.3 Heat Exchanger Fabrication.....	45
MSR 567: Metallographic Examination of an EDM Recast Layer in IN718.....	45
MSR 652: Evaluation of Chemical Milling Procedures for Starfish Heater Head .....	53
MSR 642: Metallurgical Evaluation of Two Starfish Heater Head Machining Test Samples .....	61
MSR 586: Preliminary Evaluation of Chemical Milling as a Finishing Operation on Inconel 718 .....	67
MSR 690: Metallurgical Evaluation of CTPC Cooler Assembly Fabrication Samples .....	81
B.4 Pages intentionally omitted.....	94-110
B.5 Beryllium Issues.....	111
MSR 640: Displacer Dome to Displacer Base Braze Test Evaluation .....	111
MSR 632: Results of Beryllium Coating Adhesion Tests.....	119
MSR 589: Metallurgical Failure Analysis of Chrome-Oxide-Coated Beryllium Cylinder .....	131
Memorandum: Displacer Rod End Plug Braze Evaluation Tests.....	137
B.6 Sodium Issues .....	141
Note: Refractory Metal Coating.....	141
MSR 602: Liquid Metal Corrosion Resistant Coatings .....	145
MTI 91TR56: Heat Pipe Fatigue Test Specimen Metallurgical Examination .....	171
B.7 Wear Couple Tests .....	203
Report: Pad-on-Disc Wear Couple Tests.....	203
Report: Wear Couple Tests, New Karner Road (NKR) Rig .....	217
B.8 Pressure Boundary Penetrations .....	223
Instrumentation Ring Seal: Test Arrangement and Results.....	223
B.9 Heating System Heaters.....	225
Report: Slot Heaters for Starfish Heater Head.....	225
Report: CTPC Heat Pipe Heater Development.....	259
B.10 Cooler Flow Test.....	271
Test Arrangement and Results.....	271
<b>APPENDIX C: UDIMET TESTING</b>	
C.1 Report: Selection of the Reference Material for the Space Stirling Engine Heater Head.....	273
C.2 Memorandum: Udimet 720LI Creep Test Result Update.....	293

## **TABLE OF CONTENTS (continued)**

<b>SECTION</b>	<b>PAGE</b>
C.3 Memorandum: Final Summary of Space Stirling Endurance Engine Udimet 720LI Fatigue Testing Results.....	298
C.4 Udimet 720LI Weld Development Summary .....	305
C.5 Memorandum: Udimet 720LI Creep Test Final Results Summary .....	313
APPENDIX D: CTPC COMPONENT DEVELOPMENT PHOTOS .....	415



## APPENDIX A: HEATER HEAD DEVELOPMENT

### A.1 Starfish Heater Head Program

#### One Tenth Segment Heat Pipe

The One Tenth Segment Heat Pipe was processed according to the established procedure and sealed (pinched off and welded) between July 6 and 7, 1992. The heat pipe was tested for thermal performance between July 9 and 10, 1992. The heat pipe operated at 777°C, 4500 watts; 652°C, 4500 watts; and 527°C, 4500 watts. Each of the three tests were run for at least 15 minutes at steady state.

The One Tenth Segment Heat Pipe has demonstrated its capability to meet the full scale testing requirements. No hot spots were observed, no condenser draining problems were indicated, and no heat pipe limits were found in the testing range.

Since no heat pipe limits were found in the specified testing range, MTI (M. Dahr) requested an additional test be conducted to determine the maximum heat transport capability at 665°C.

The heat pipe was positioned and instrumented similar to the tests conducted earlier with the exception of additional type K thermocouples mounted onto the heat input face, heater head and sides. A total of 29 thermocouples were mounted onto the heat pipe as shown in Figure 1. The heat pipe/gas gap calorimeter assembly was mounted onto Thermacore's quartz lamp test station. The heat pipe was oriented in its normal operating position, top plane parallel to the ground. Trace heating electrical resistance heaters were attached to the heater head and top plate areas to assist in isothermalizing the cold startups. The entire heat pipe assembly was insulated with 3-4 inches of high temperature ceramic fiber.

The heat pipe was tested on August 25, 1992. At 665°C the heat pipe transported a maximum of 8248 watts. The test was terminated when the temperature of the water cooled aperture plate positioned between the heat pipe and quartz lamps exceeded design limits. The maximum heat pipe limit may be determined, but only with modifications to the testing apparatus.

The data for this performance test were plotted and are included as Figures 2 - 6. The test data plotted for each figure ~~is~~ discussed separately below.

ARE

■ In Figure 2 the average temperature was calculated and plotted for thermocouple locations at the heater head nose (tc#11-18), midline (tc#19-22), end (tc#23-24), back(tc#25-27), and vapor core (tc#28-29). The power delivered to the heat pipe, transported by the heat pipe, and the difference between these two values are also plotted. The data indicates that the surface temperature of the heater head condenser is in good agreement with the heat pipe vapor core temperature.

In Figures 3-6 the individual temperatures of the heat input or heater head face region were plotted along with the power input, output and difference. Also plotted are the average vapor core temperatures and the average vapor core temperature plus the conductive delta T through the heat input wall. This combined temperature was calculated and plotted so to provide a direct comparison between the heat input region and the average heat pipe temperature. The conductive delta T calculated was based on the maximum heat transport measured during test and the heat input area. The heat flux was  $21\text{W}/\text{cm}^2$  which translates into a  $62^\circ\text{C}$  temperature difference through the wall.

■ In Figure 3 face thermocouples 1 and 2 are plotted separately. These temperatures are within the  $62^\circ\text{C}$  heat pipe wall conduction band.

■ In Figure 4 face thermocouples 3 and 4 are plotted separately. These temperatures are much higher than the average heat pipe temperature and may be attributed to the thermocouples being directly illuminated by the quartz lamps and not being properly attached to the heat pipe wall, or an additional temperature difference caused by the evaporation and/or boiling heat transfer mechanism. The temperature readings were not increasing with time; therefore, the wick structure was not at a dryout limit.

■ In Figure 5 face thermocouples 5,6 and 7 are plotted separately. The temperature at thermocouples 5,6 and 7 are much higher than the average heat pipe temperature indicating a possible thermocouple attachment problem, or additional temperature difference caused by the evaporation and/or boiling heat transfer mechanism. The temperature readings were not increasing with time; therefore, the wick structure was not at a dryout limit.

■ In Figure 6 face thermocouples 8,9 and 10 are plotted separately. The temperature at thermocouples 9 and 10 indicate a potential attachment problem or additional temperature difference caused by the evaporation and/or boiling heat transfer mechanism. The temperature readings were not increasing with time; therefore, the wick structure was not at a dryout limit. Thermocouple 8 is in good agreement with the average heat pipe temperature.

The heat pipe wick structure, two layers of 100 mesh screen, is not a high performance design. Operation at  $21\text{W}/\text{cm}^2$  is considered to be excellent performance for the current design. If higher heat fluxes are desired, the wick structure and heat pipe envelope design should be reconsidered.

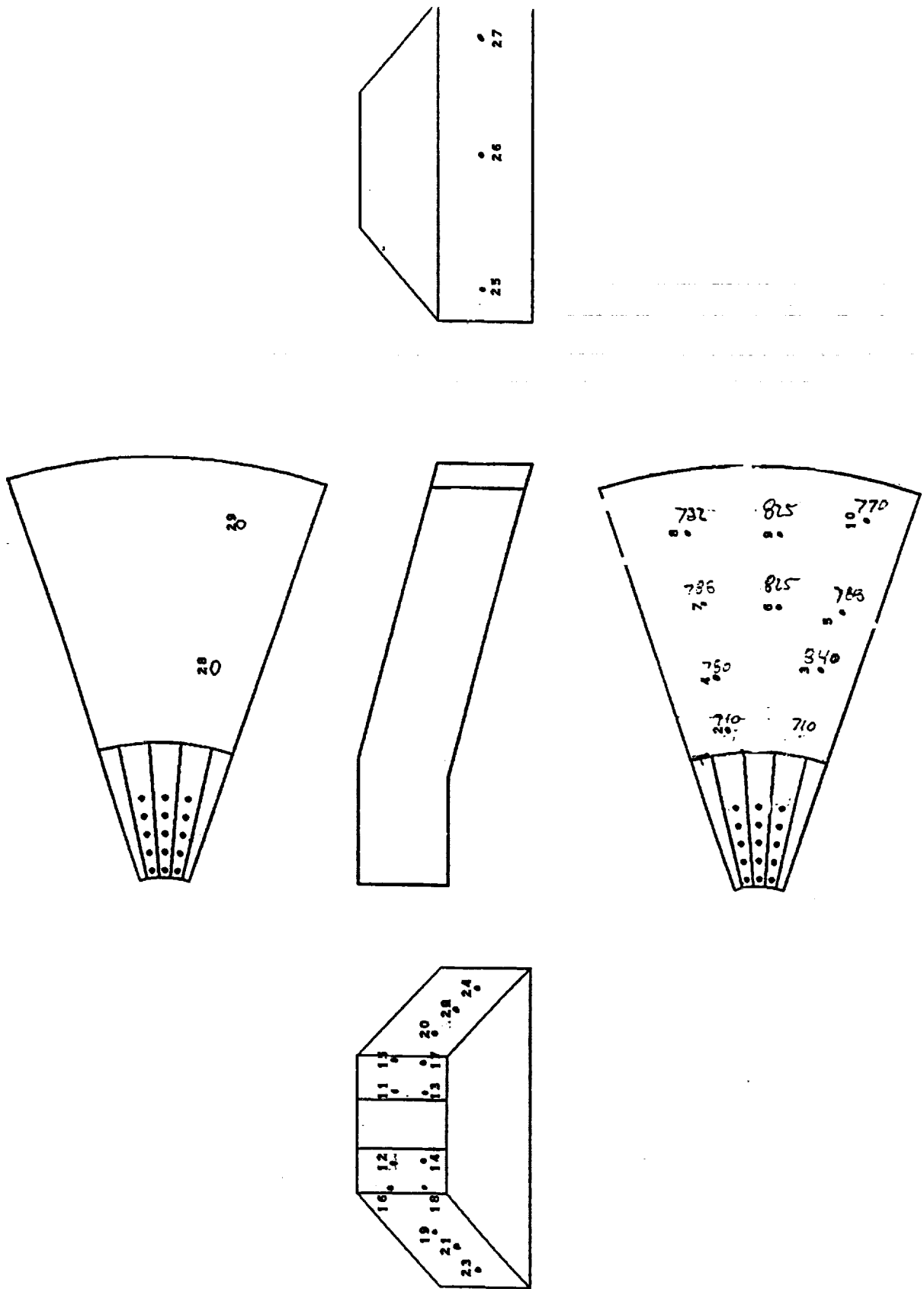


FIGURE 1 THERMOCOUPLE LOCATIONS

Mtlmaxq.dsf/mtlmaxq.grf Sept. 18, 1992 12:35:55 PM

# Heat Pipe Maximum Power Transport at 665 C 1/10 Segment Starfish Heater Head

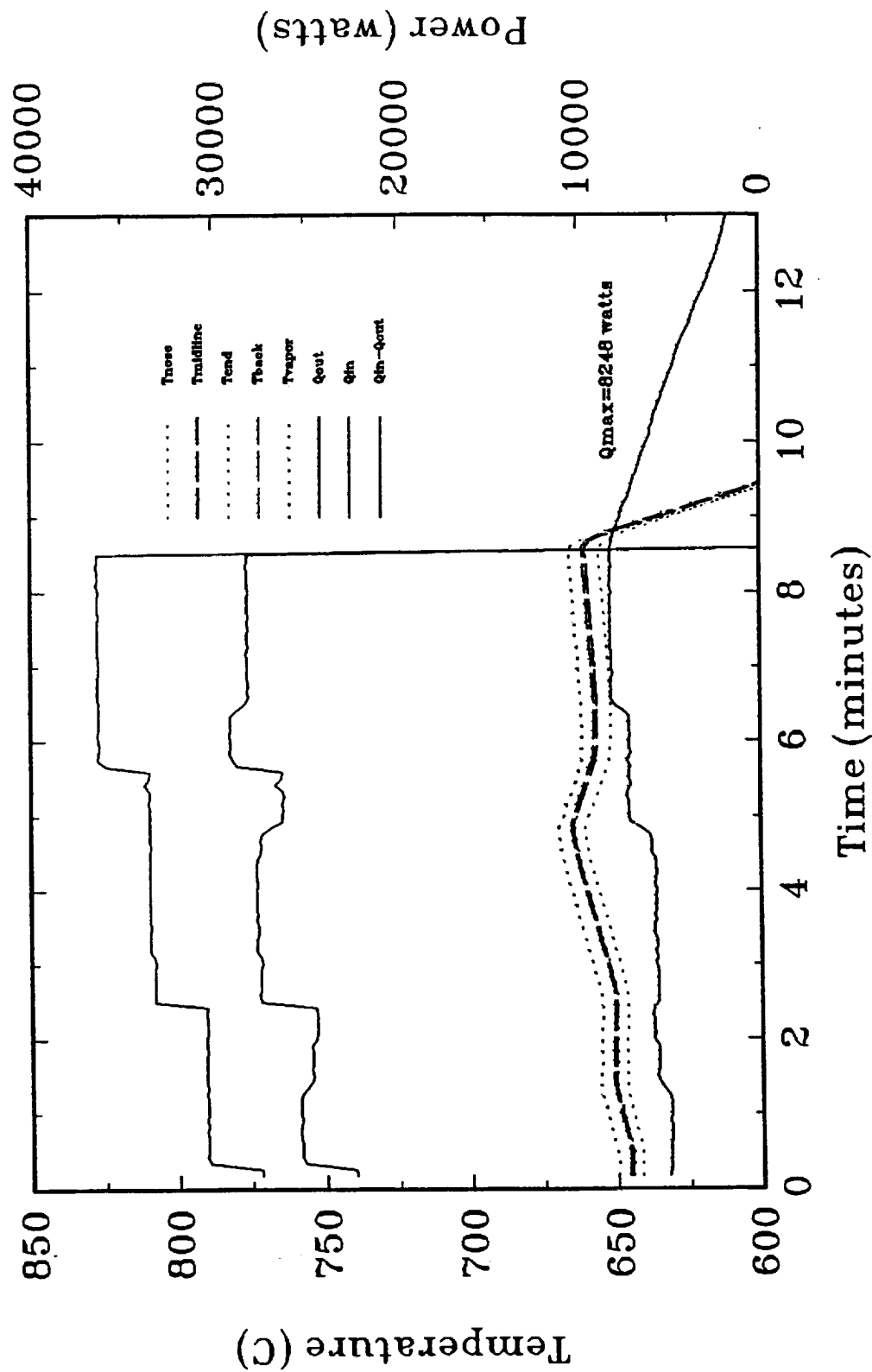


Figure 2

# Heat Pipe Maximum Power Transport at 665 C 1/10 Segment Starfish Heater Head

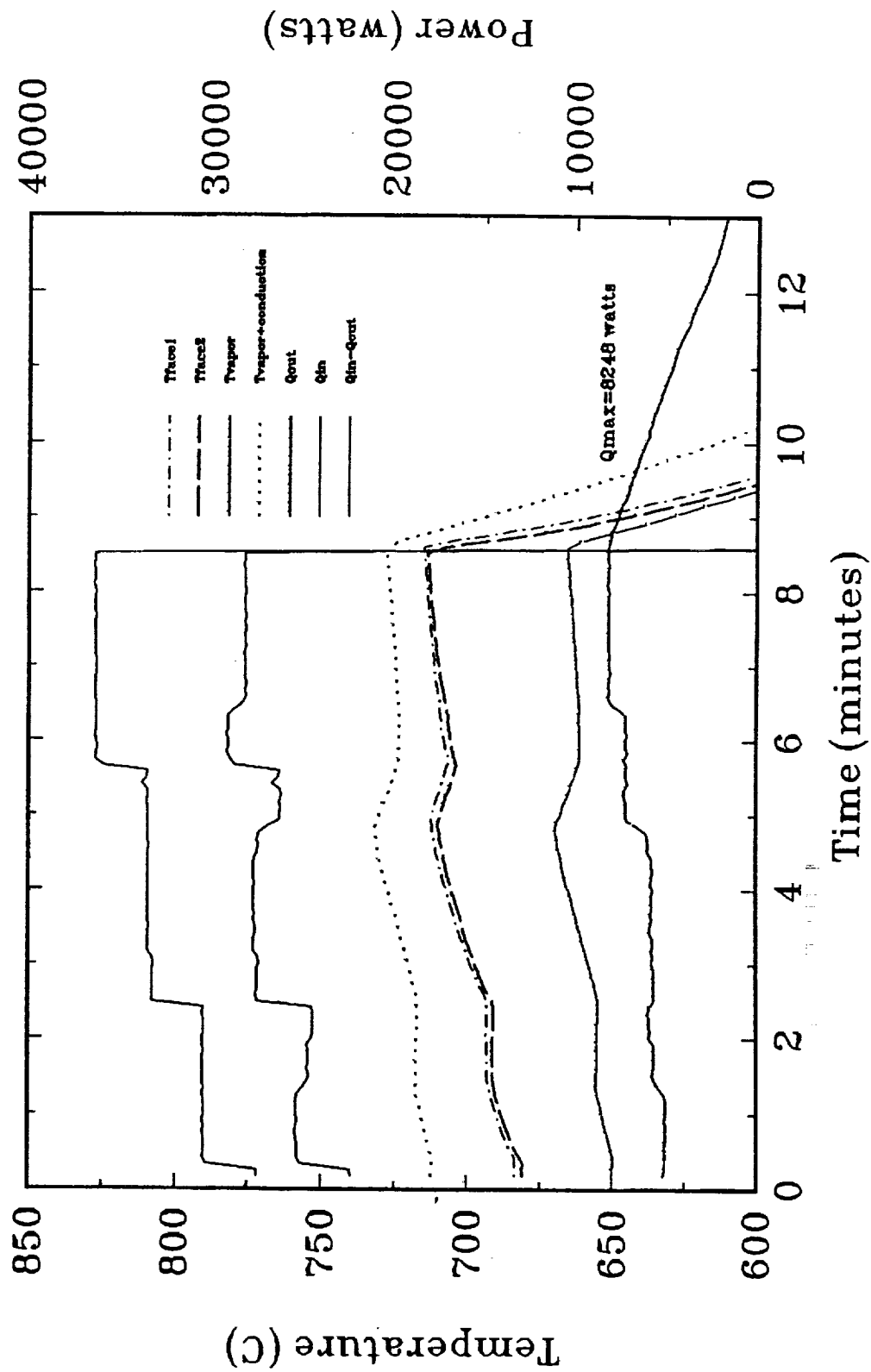


Figure 3

mtimaxq.dsf/mtimaxq2.grf Sept. 18, 1992 6:47:18 AM

# Heat Pipe Maximum Power Transport at 665 C 1/10 Segment Starfish Heater Head

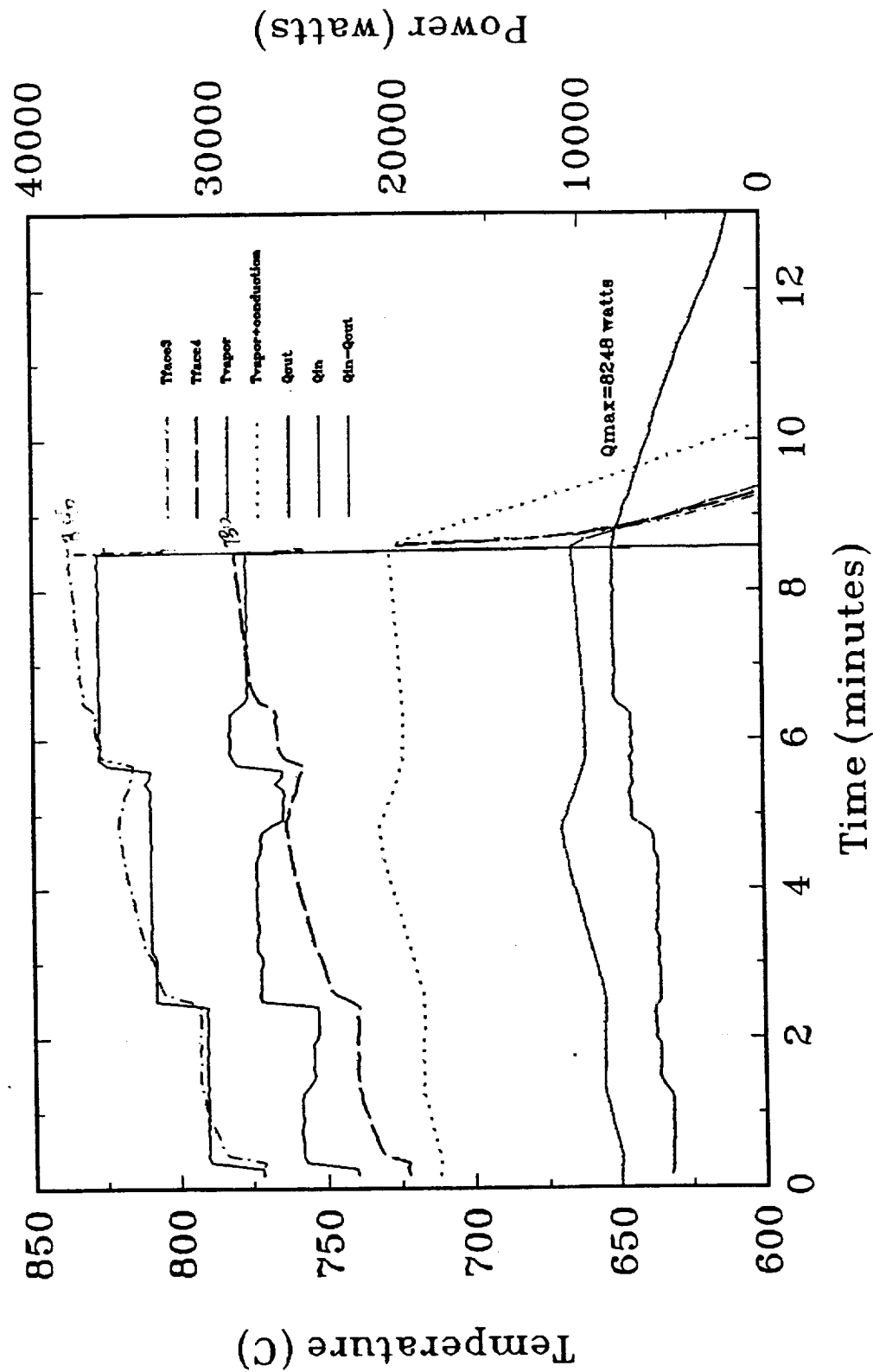


Figure 4

# Heat Pipe Maximum Power Transport at 665 C 1/10 Segment Starfish Heater Head

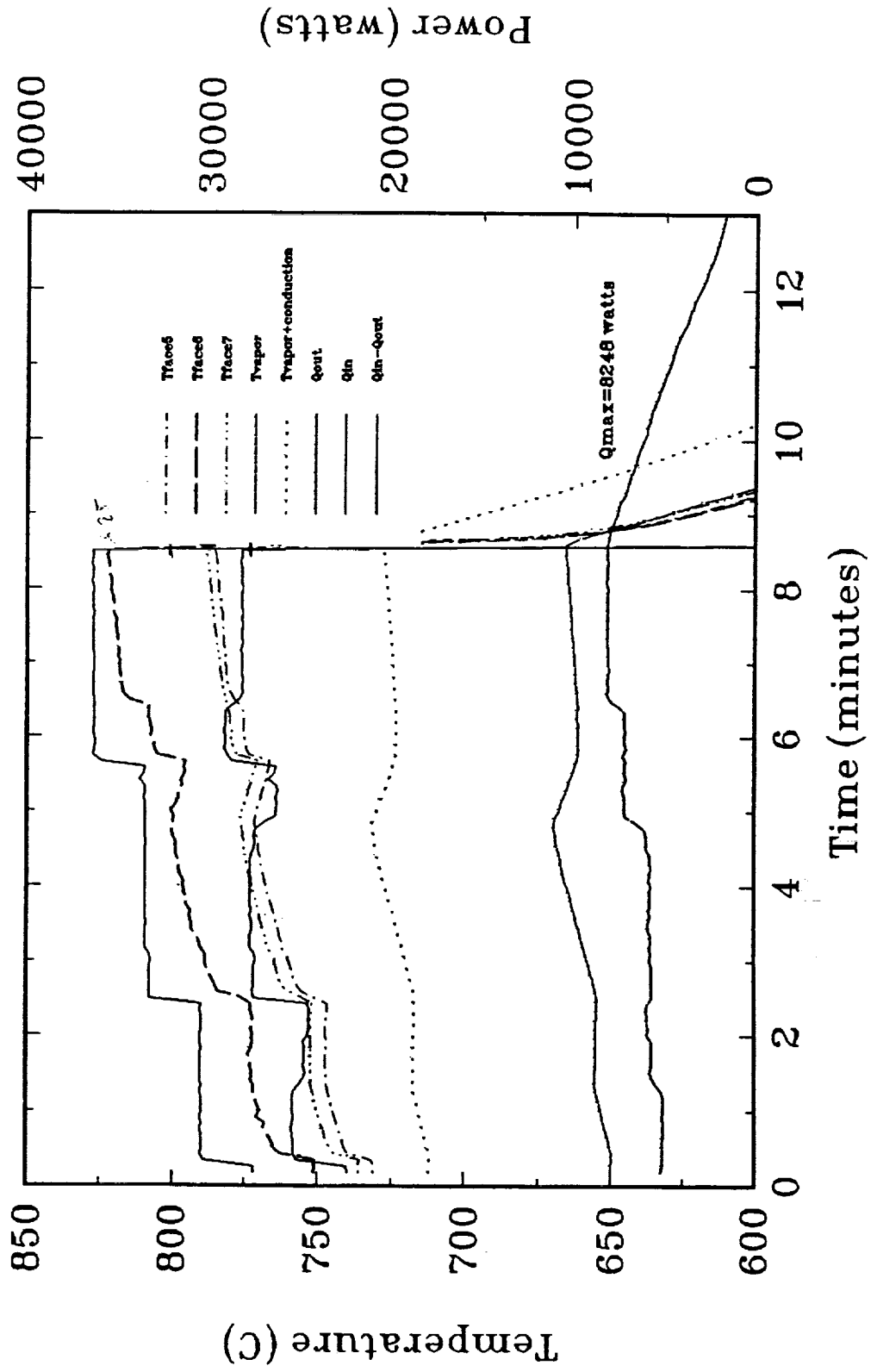


Figure 5



# Heat Pipe Maximum Power Transport at 665 C 1/10 Segment Starfish Heater Head

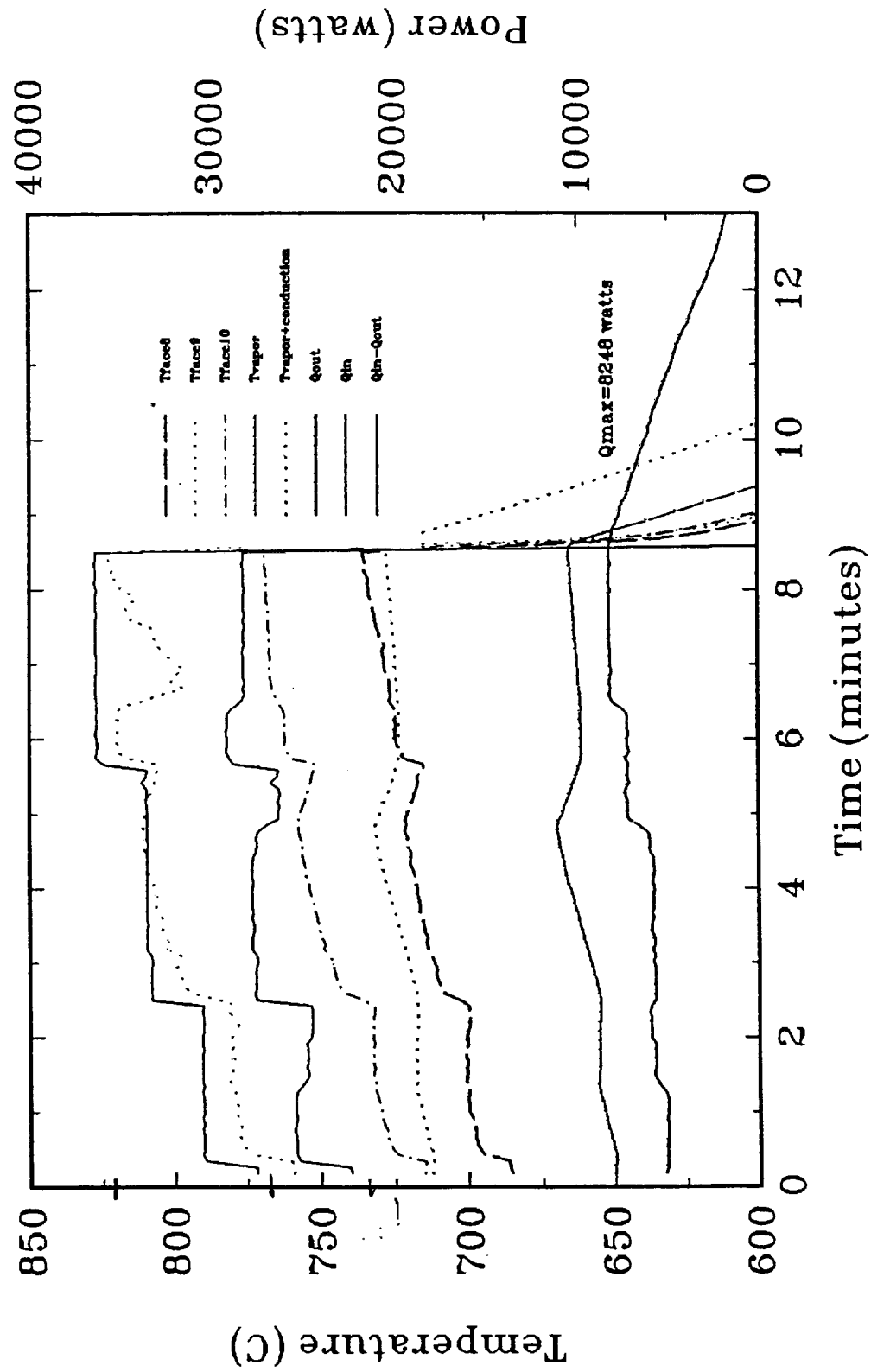


Figure 6



## **A.2 Task Narrative: 1/10<sup>th</sup> Segment and Full-Scale Heat Pipes Heat Pipe Processing Procedure**

### **Fluid Optimization and Non-Condensable Gas Removal**

This procedure documents the heat pipe processing procedure that will be used to process the 1/10<sup>th</sup> segment and full scale heat pipes for the Starfish heater head heat pipe program. The procedure is a step by step narrative of the tasks required to optimize the fluid charge (sodium) and remove non-condensable gas (NCG) from the heat pipe vapor space prior to final sealing of the heat pipe. The procedure begins at the point where the heat pipe has been welded, leak checked, and filled with sodium metal at ETEC.<sup>1</sup> There are two high temperature valves attached to the heat pipe for charging the working fluid and venting NCG.

There are two goals that must be accomplished during the heat pipe processing task. First, the NCG must be removed from the vapor space. If NCG, such as argon, nitrogen, and hydrogen, is not removed from the vapor space prior to final sealing, it will be swept to the condenser section of the heat pipe by the sodium vapor flow. The gas will reside in the condenser section increasing the resistance to heat transfer. This will result in a higher heat pipe operating temperature to transfer the required power or the heat pipe will transfer less than the required amount of power at the heat pipe operating temperature design point. NCG can result from a variety of sources. Several of the more common sources are the following: argon or nitrogen introduced during fluid charging, dissolved gases in the working fluid, chemical reaction of the working fluid with incompatible materials (envelope, wick structure, contaminants), and outgassing of the heat pipe envelope material at elevated temperatures. Proper selection of envelope and wick structure materials, careful preparation of the heat pipe prior to sodium metal charging, and careful control of the sodium charging process greatly reduce the potential for a performance limiting NCG problem. The processing procedure is a final effort to further increase the probability of success by actively removing NCG while operating the heat pipe at design point conditions.

The second goal that must be accomplished during the processing procedure is to insure that the sodium metal fluid charge is sufficient in quantity to allow for both startup and operation across the specified temperature range and not so excessive that the excess fluid results in pool boiling "chugging" that may cause excessive vibration and/or is excessive enough to fill and block off part of the condenser section. The orientation of the heat pipe and the heat pipe geometry have been selected to minimize the probability of an excess fluid charge problem. Any significant under charge or over charge will be discovered during the NCG removal operation. A significant over charge will be apparent if there is vibration caused by the excess fluid pool boiling and/or if a cold puddle of fluid collects in the condenser section. In the case of an over charge situation, the excess fluid will simply be removed into a processing dump tank. A significant under charge will be apparent if there are hot spots in the evaporator section indicating wick dryout. In the case of an under charge situation, the heat pipe would be returned to ETEC or Thermacore for additional fluid charging.

---

<sup>1</sup> See page 130 in Volume 1 for final ETEC and Thermacore roles in heat pipe processing

## TASK NARRATIVE

- 1.0 Instrument the heat pipe as shown in Figure 1. Set up the heat pipe and auxiliary equipment as shown in Figures 2 and 3. Pinch and weld the fill tube attached to valve V3 before proceeding to step 2.0.
- 2.0 Open valves V1 and V2 and vacuum pump the vapor space of the heat pipe. Continue pumping until the vacuum pressure is  $< 10^{-3}$  torr.
- 3.0 Once the vacuum pressure is less than  $10^{-3}$  torr, begin to apply heat to the three heaters; H1 - Top Plate Heater, H2 - Bottom Plate Heater, and H3 - Heater Head Heater. Heat the unit until liquid sodium begins to fill the dump pot, probably around 350 - 500 °C. At this point close valve V1 to prevent excessive sodium removal. Continue to heat the heat pipe to 675-725°C. Note: During startup adjust heater powers such that all thermocouples remain within 100 °C of each other.
- 4.0 Operate the heat pipe at 675-725°C for  $< 10$  hours. Remove any NCG through valve V1 by briefly opening the valve until the heat pipe is isothermal. Operating for 1 - 2 hours against the valve with no sign of NCG generation is a practical indication that the NCG is removed. Note: If significant fluid under or over charge is detected as described in the introduction paragraphs above, corrective action must be taken as described.
- 5.0 When NCG is eliminated at 675-725°C, increase the heat pipe operating temperature to 775-785°C, hold at temperature  $< 0.5$  hours. Return the heat pipe to 675-725°C and remove NCG. Repeat Step 5.0 a maximum of 3 times. If NCG is still present contact MTI engineering. Total Time at temperatures above 775°C should be  $< 3.0$  hours.
- 6.0 Once the heat pipe is determined to be isothermal with no sign of NCG, the fill tubes will be pinched and welded to seal the heat pipe and remove the high temperature valves.
- 7.0 The heat pipe will be cooled to room temperature and is then ready for calorimeter installation and performance testing.

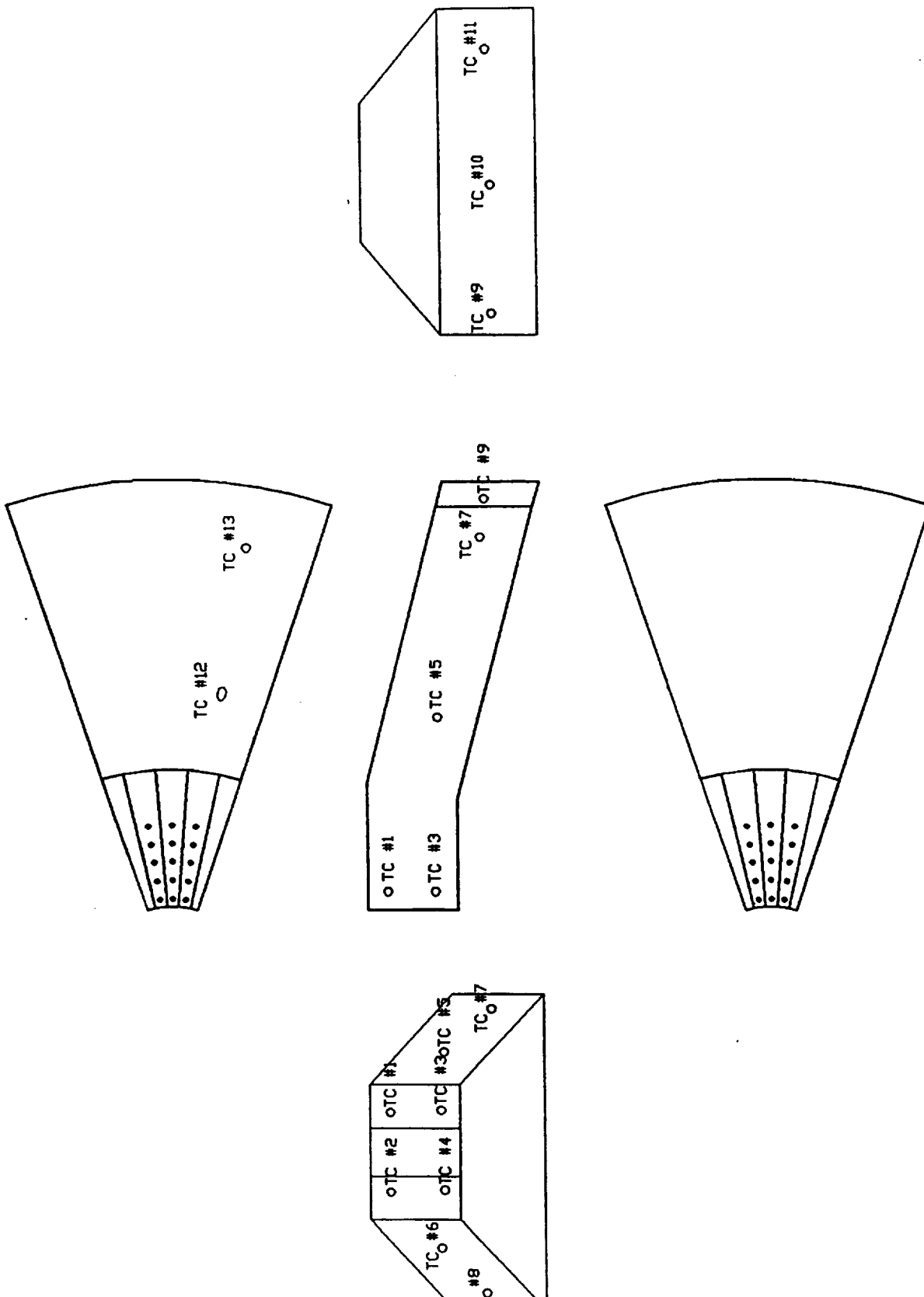
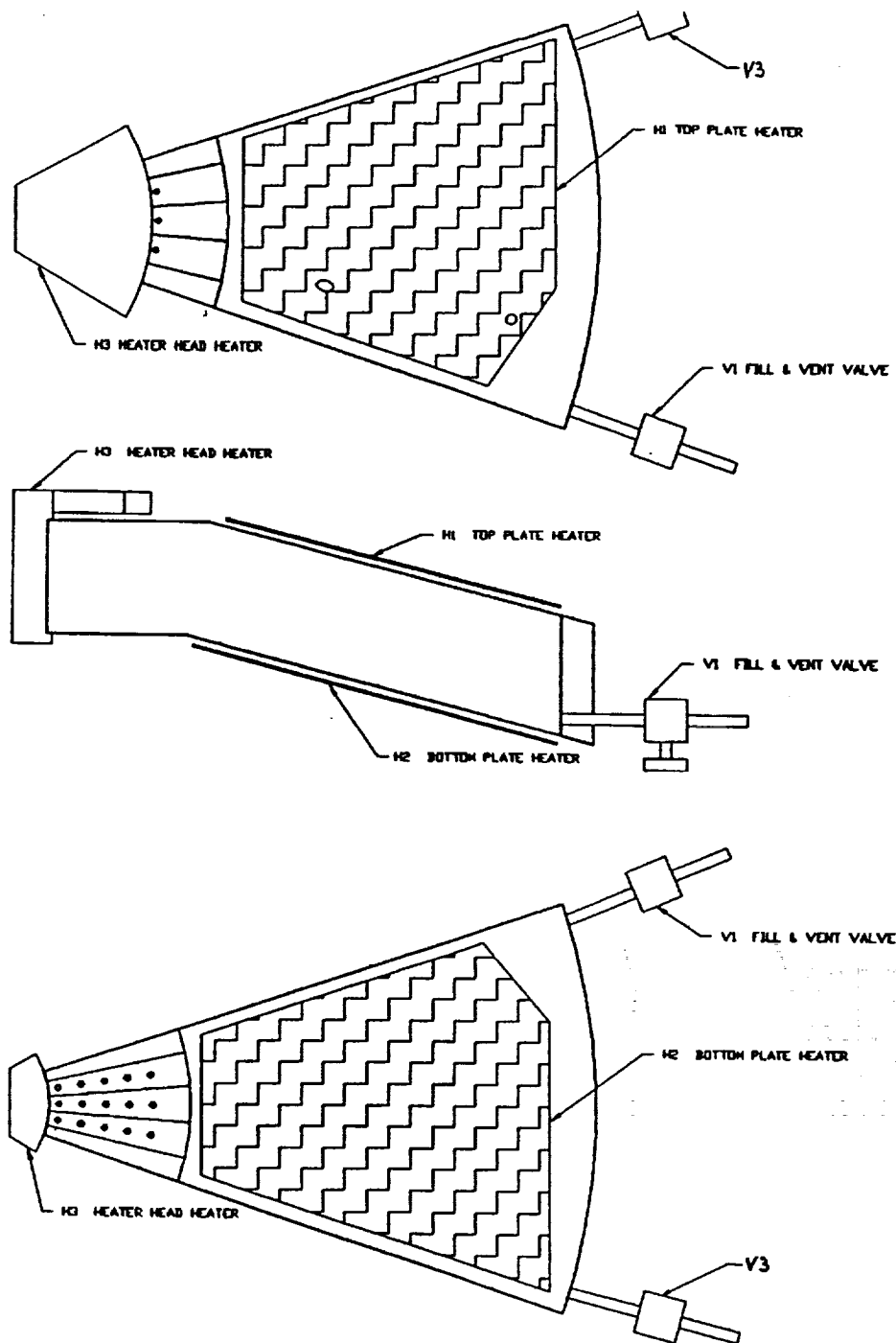


Figure A1. Thermocouple Layout



NOTE: ALL SURFACES INSULATED WITH HIGH TEMPERATURE MINERAL INSULATION EXCEPT WITHIN 15 INCHES OF FILL & VENT VALVE.

Figure A2. Processing Heater Layout

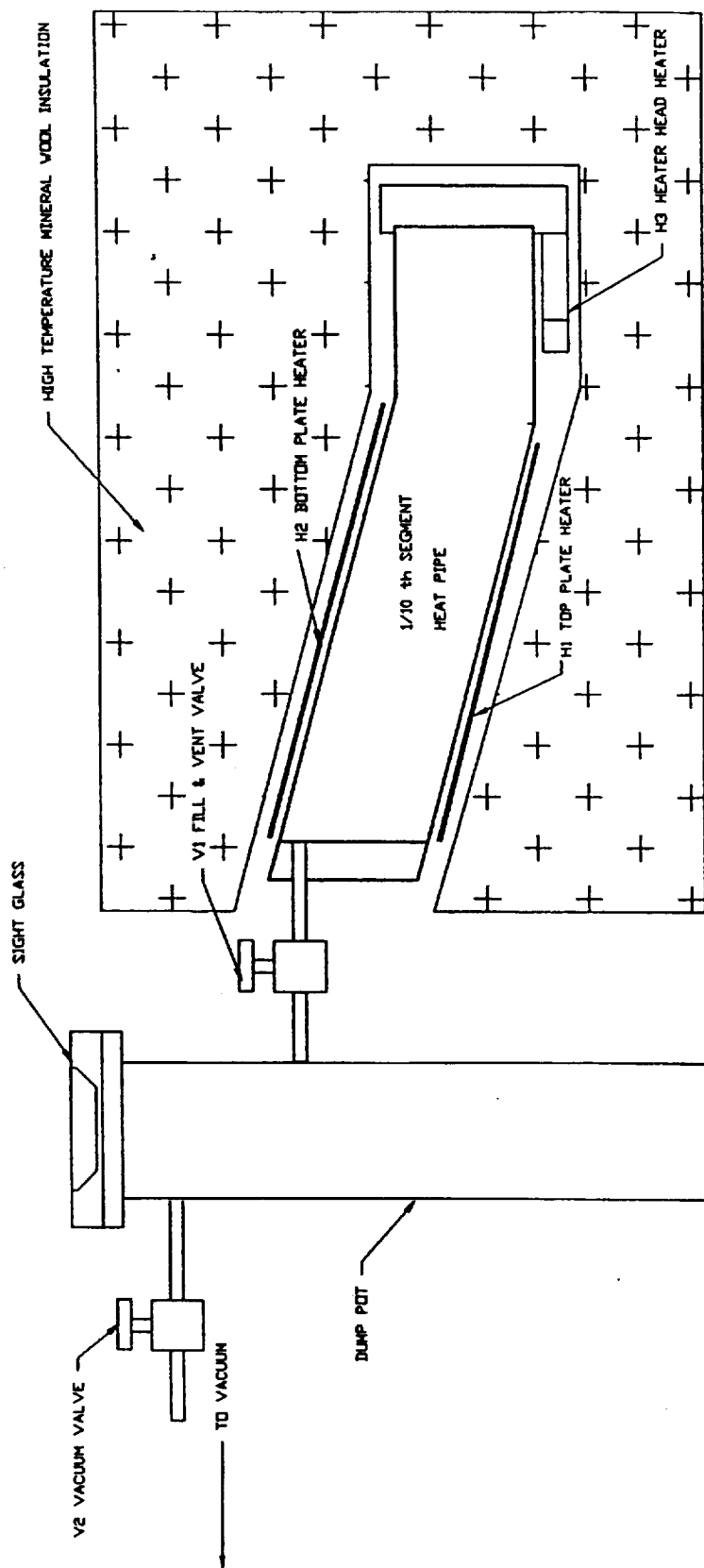


Figure A3. Heat Pipe Processing Layout





### **A.3 Detailed Procedure: Sodium Filling and Processing**

## **SODIUM FILLING AND PROCESSING PROCEDURES FOR THE SODIUM-FILLED HEAT PIPE (SFHP)**

### **BACKGROUND**

At this point in time, the wick structure has been installed in the SFHP; the SFHP has been through the vacuum reduction of oxides; the final heat pipe closure welds have been made; the heat pipe has been vacuum age hardened; the high temperature Swagelok valves have been installed; and, the SFHP has been leak checked via a helium mass spectrometer. The SFHP has been delivered to Thermacore for sodium charging and heat pipe processing.

### **RESTRICTIONS FOR HEAT PIPE PROCESSING**

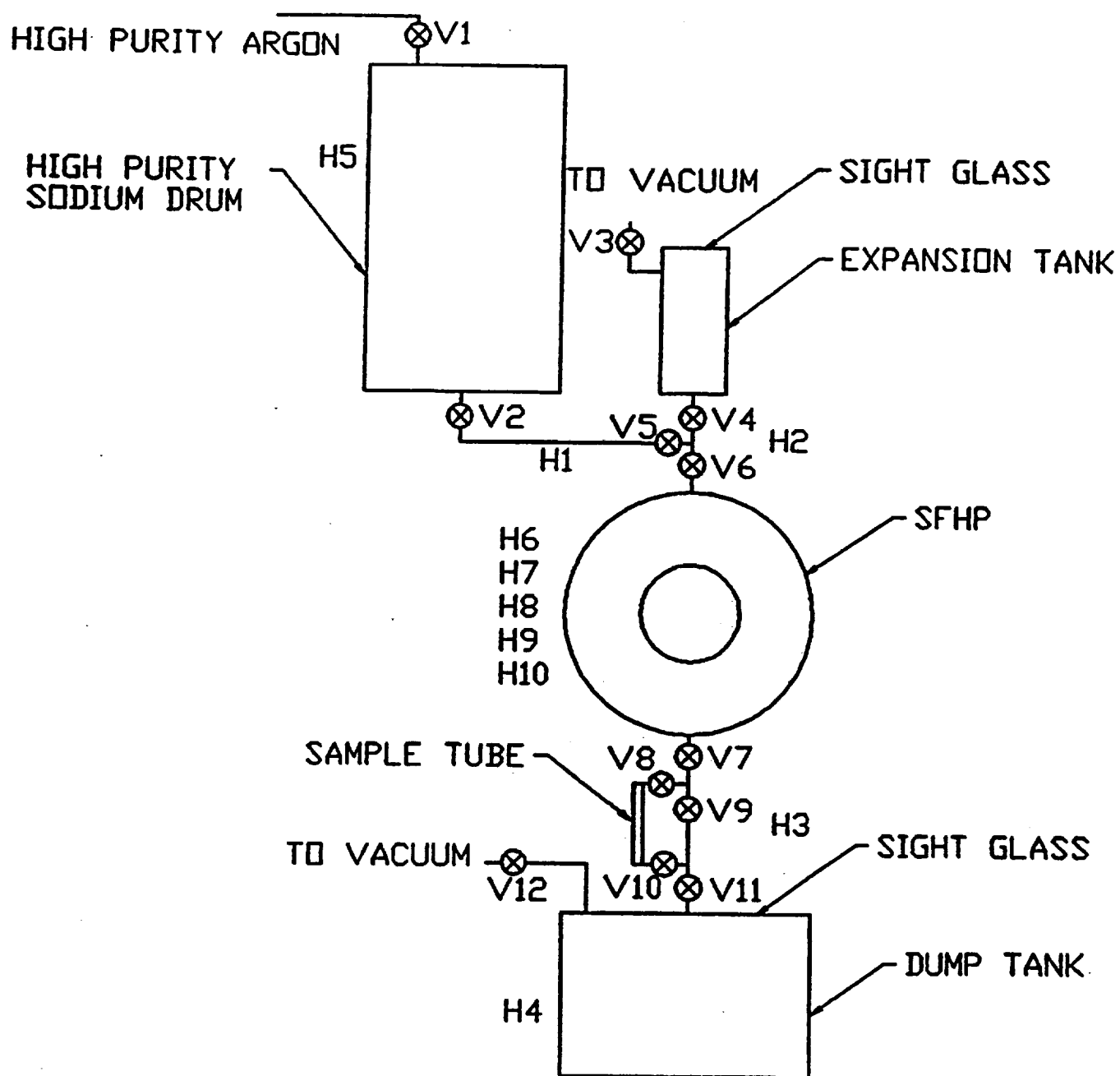
- A. Time at temperature of the heater head/heat pipe assembly shall be restricted as follows:
  - A.1 Total time at 675-725°C; less than 10 hours.
  - A.2 Total time at 725-785°C; less than 5 hours.
  - A.3 Maximum temperature at any point on the assembly shall not exceed 785°C.
- B. Maximum temperature gradient shall not exceed 100°C between any two thermocouples attached to the assembly.
- C. Thermocouples shall be attached in locations shown in Figure 1 of Appendix A as a minimum. Additional thermocouples may be attached at Thermacore's discretion provided the guidelines in Restriction D are followed. Additional thermocouple locations are shown in Figure 3 of Appendix A.
- D. Spot-welding to this material has been shown to produce microfissures below the surface. For this reason, the areas indicated in Figure 2 of Appendix A shall have no thermocouples attached, nor shall any spot-welding for any other reason be done in these areas.

### **PROCEDURE**

- 1.0 Upon receipt, inspect the heat pipe as received and inform MTI of its condition. Note any abnormalities.
- 2.0 Weigh the heat pipe including the Swagelok plugs.

- 3.0 Install the heat pipe in the fill system oriented with the fill and discharge valves at the high and low points to assure complete filling and draining. The entire system is welded and helium mass spectrometer leak checked. See Figure 1 - Sodium Charging System.
- 4.0 Install heater H6 through H10 onto the SFHP. These heaters will be strategically placed to achieve uniform heating and temperature control. **NOTE: The heaters will be attached to the upper and lower evaporator section plates with spotwelded stainless steel straps. NO SPOTWELDS WILL BE ALLOWED ON THE AREAS HIGHLIGHTED IN APPENDIX A, FIGURE 2.** Heaters in these regions will be attached to stainless steel plates and loosely clamped to the condenser section. Also, there will be an internal heater in the displacer section of the SFHP. This heater will be self contained and slid loosely into the displacer cylinder I.D. A cover plate will close off the engine side of the SFHP. The enclosed volume will be kept under a constant purge of high purity argon during any heating cycle of the SFHP to minimize internal oxidation of the heater head holes.
- 5.0 Apply vacuum to the entire filling system (fill line, expansion tank, SFHP, discharge line, sample tube, and dump tank). Once a vacuum has been established, heat the entire filling system assembly to 425°C for approximately 24 hours to degas the system. The vacuum will be drawn through a liquid nitrogen trap to prevent backstreaming of pump oil.
- 6.0 Charge the SFHP with the first of four fluid charges. The fill procedure is described in detail in Sections 6.1 through 6.8.
  - 6.1 Melt the sodium in the high purity sodium drum and achieve stable temperature at 120°C. At this time valve V2 is closed and V1 is open to a low pressure supply of ultra high purity argon. All other valves are open and vacuum is still applied to the system.
  - 6.2 Close valves V4, V5, V6, V7, V8, V9, V10, and V11. Vacuum is still being applied to the expansion tank and the dump tank.
  - 6.3 Energize heaters H1, H2, and all SFHP heaters (H6-H10). Adjust power to achieve a temperature of 120-150°C.
  - 6.4 Slowly open valve V2. Sodium should now fill the volume between V2 and V5.
  - 6.5 Slowly open valve V5. Sodium should now fill the volume enclosed by V2, V4, and V6.

FIGURE 1. SFHP SODIUM CHARGING SYSTEM



- 6.6 Slowly open valve V6. Sodium should be filling the entire SFHP. Once the sodium flow has stopped, indicated by zero flow of high purity argon into valve V1, open valve V4 while looking in the sight glass on the expansion tank. The sodium should begin to fill the expansion tank indicating that the SFHP is full. Close valve V5 to stop the flow of sodium.
- 6.7 With the vacuum continuing to draw on the expansion tank, increase the heater power to heaters H6-H10 until the entire SFHP is at 425°C. The expansion tank should fill because of the sodium density change with temperature. This is another indication that the SFHP is entirely full.
- 6.8 Soak at 425°C for approximately 24 hours.
- 7.0 Drain the first fluid charge to the dump tank. The detailed procedure is described below in Sections 7.1 through 7.7.
- 7.1 Energize heaters H3 and H4 and adjust power such that the temperature of the plumbing leading to the dump tank and the dump tank itself is approximately 120-150°C. Turn off the heaters H6-H10.
- 7.2 Slowly open valve V7. Sodium should fill to valves V8 and V9.
- 7.3 Slowly open valve V8. Sodium should fill the sample tube to valve 10.
- 7.4 Slowly open valve V10. Sodium should fill to valves V9 and V11.
- 7.5 Slowly open valve V11. Sodium should drain into the dump tank. Visually verify flow through the sight glasses on the expansion tank and the dump tank. Continue to draw a vacuum on the expansion tank and the dump tank. All flow should be the result of gravity only.
- 7.6 Once the flow of sodium has stopped, indicated visually through the sight glasses, close valve V7. Continue to draw a vacuum on the discharge section of the system. Also, maintain a temperature in this section of approximately 120-150°C for the rest of the procedure.
- 7.7 At this point the discharge section is under vacuum through the dump tank and the SFHP and expansion tank are under vacuum through the expansion tank. The system is now ready for the second fill charge. Energize heaters H6-H10 and adjust the power to achieve a temperature of approximately 120-150°C.

- 8.0** Charge the SFHP with the second of four fluid charges. The fill procedure is described in detail in Sections 8.1 through 8.4.
- 8.1** Close valve V4.
- 8.2** Slowly open valve V5. Sodium should be filling the entire SFHP. Once the sodium flow has stopped, indicated by zero flow of high purity argon into valve V1, open valve V4 while looking in the sight glass on the expansion tank. The sodium should begin to fill the expansion tank indicating that the SFHP is full. Close valve V5 to stop the flow of sodium.
- 8.3** With the vacuum continuing to draw on the expansion tank, increase the heater power to heaters H6-H10 until the entire SFHP is at 425°C. The expansion tank should fill because of the sodium density change with temperature. This is another indication that the SFHP is entirely full.
- 8.4** Soak at 425°C for approximately 24 hours.
- 9.0** Drain the second fluid charge to the dump tank. The detailed procedure is described below in Sections 9.1 through 9.4.
- 9.1** Turn off the heaters H6-H10.
- 9.2** Slowly open valve V7. Sodium should drain into the dump tank. Visually verify flow through the sight glasses on the expansion tank and the dump tank. Continue to draw a vacuum on the expansion tank and the dump tank. All flow should be the result of gravity only.
- 9.3** Once the flow of sodium has stopped, indicated visually through the sight glasses, close valve V7. Continue to draw a vacuum on the discharge section of the system. Also, maintain a temperature in this section of approximately 120-150°C for the rest of the procedure.
- 9.4** At this point the discharge section is under vacuum through the dump tank and the SFHP and expansion tank are under vacuum through the expansion tank. The system is now ready for the third fill charge. Energize heaters H6-H10 and adjust the power to achieve a temperature of approximately 120-150°C.
- 10.0** Charge the SFHP with the third of four fluid charges. The fill procedure is described in detail in Sections 10.1 through 10.4.
- 10.1** Close valve V4.

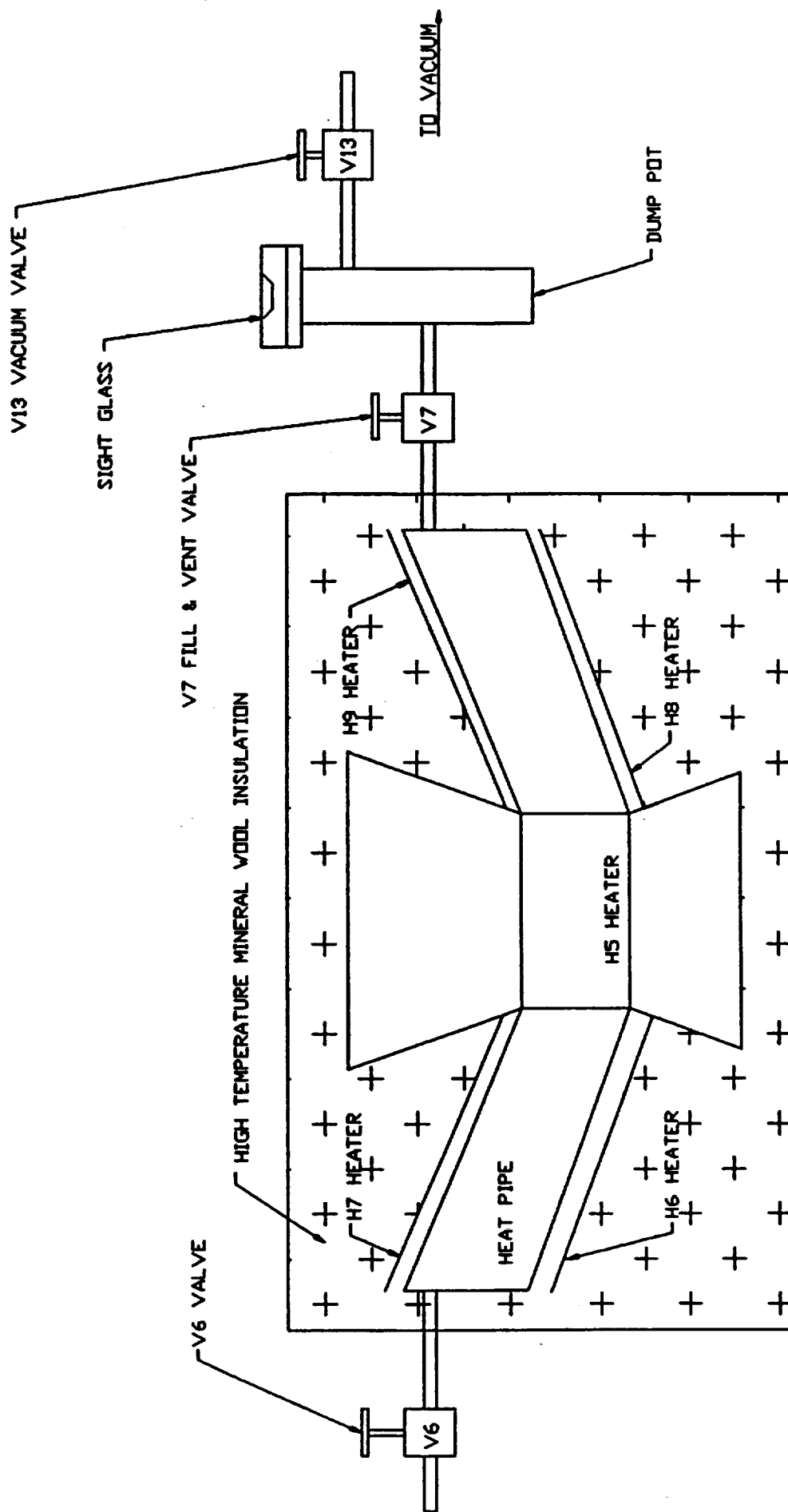
- 10.2 Slowly open valve V5. Sodium should be filling the entire SFHP. Once the sodium flow has stopped, indicated by zero flow of high purity argon into valve V1, open valve V4 while looking in the sight glass on the expansion tank. The sodium should begin to fill the expansion tank indicating that the SFHP is full. Close valve V5 to stop the flow of sodium.
- 10.3 With the vacuum continuing to draw on the expansion tank, increase the heater power to heaters H6-H10 until the entire SFHP is at 425°C. The expansion tank should fill because of the sodium density change with temperature. This is another indication that the SFHP is entirely full.
- 10.4 Soak at 425°C for approximately 24 hours.
- 11.0 Drain the third fluid charge to the dump tank. The detailed procedure is described below in Sections 11.1 through 11.4.
- 11.1 Turn off the heaters H6-H10.
- 11.2 Slowly open valve V7. Sodium should drain into the dump tank. Visually verify flow through the sight glasses on the expansion tank and the dump tank. Continue to draw a vacuum on the expansion tank and the dump tank. All flow should be the result of gravity only.
- 11.3 Once the flow of sodium has stopped, indicated visually through the sight glasses, close valve V7. Continue to draw a vacuum on the discharge section of the system. Also, maintain a temperature in this section of approximately 120-150°C for the rest of the procedure.
- 11.4 At this point the discharge section is under vacuum through the dump tank and the SFHP and expansion tank are under vacuum through the expansion tank. The system is now ready for the forth and final fill charge. Energize heaters H6-H10 and adjust the power to achieve a temperature of approximately 120-150°C.
- 12.0 Charge the SFHP with the forth and final fluid charge. The fill procedure is described in detail in Sections 12.1 through 12.4.
- 12.1 Close valve V4.
- 12.2 Slowly open valve V5. Sodium should be filling the entire SFHP. Once the sodium flow has stopped, indicated by zero flow of high purity argon into valve V1, open valve V4 while looking in the sight glass on the expansion tank. The sodium should begin to fill the expansion tank indicating that the SFHP is full. Close valve V5 to stop the flow of sodium.

- 12.3 With the vacuum continuing to draw on the expansion tank, increase the heater power to heaters H6-H10 until the entire SFHP is at 425°C. The expansion tank should fill because of the sodium density change with temperature. This is another indication that the SFHP is entirely full.
- 12.4 Soak at 425°C for approximately 24 hours.
- 13.0 Drain the third fluid charge to the dump tank. The detailed procedure is described below in Sections 13.1 through 13.6.
- 13.1 Turn off the heaters H6-H10.
- 13.2 Slowly open valve V7. Sodium should drain into the dump tank. Visually verify flow through the sight glasses on the expansion tank and the dump tank. Continue to draw a vacuum on the expansion tank and the dump tank. All flow should be the result of gravity only.
- 13.3 After approximately one-half of the fluid charge has been drained, close valves V10 and V8 trapping a sodium sample for oxygen analysis at ETEC. Ship the sample to ETEC for oxygen analysis.
- 13.4 Slowly open valve V9 and continue to drain the SFHP. Following the removal of all sodium in the vertical orientation, the heat pipe will be separated from the sodium drum. The SFHP will be rotated to the normal operating orientation to allow fluid trapped in the upper pockets and along the ribs to flow to the outer ring. The rotation will be made possible through flexible metal bellows placed between the expansion tank and the SFHP and between the dump tank and the SFHP. In the normal orientation or with a slight tilt (3-5°) towards valve V7, the remainder of the fluid charge can be discharged.
- 13.5 Once the flow of sodium has stopped, indicated visually through the sight glasses, close valve V7. At this point, all heaters in the discharge section of the system can be turned off and the discharge section can be removed by pinching and welding the tube outboard of valve V7.
- 13.6 The heat pipe should still have a partial fill charge (approximately 450 grams, conservative estimate based on ETEC 1/10th Segment filling) because the wick structure will remain saturated. The heat pipe is now ready for the additional make-up charge of approximately 450 grams (plus 50, minus 0).

- 14.0 Charge the heat pipe with the additional sodium required to achieve a fluid charge of 850 grams (plus 100, minus zero). The detailed procedure is described below in Sections 14.1 through 14.4.
- 14.1 Close valve V6.
- 14.2 Slowly open valve V5 allowing the expansion tank to fill with sodium to a predetermined fill charge level. The level will be visually verified. Close valve V5 when the correct fluid charge is achieved.
- 14.3 Slowly open valve V6 and allow the make-up fluid charge to drain into the heat pipe by gravity.
- 14.4 When the entire fluid charge is in the SFHP, close valve V6. Turn off all heaters in the entire fill system. The fill and expansion tank sections of the system can be removed by pinching and welding the tube outboard of valve V6.
- 15.0 Remove all heaters and instrumentation and weigh the heat pipe to verify the correct fluid charge has been achieved.
- 16.0 Re-install the heaters and instrumentation. Set up the SFHP as shown in Figure 2 - SFHP Processing Layout. The SFHP should be oriented upside down relative to normal operation. A cover plate should be installed across the engine side of the SFHP and an argon purge should be established to minimize internal oxidation of the heater head.
- 17.0 Weld on a processing tank. The tank is used to vent non-condensable gases through. Draw a vacuum on the processing tank through valve V13.
- 18.0 Open valve V7. The SFHP should already be under vacuum so no rise in vacuum pressure should be detected.
- 19.0 Turn on heaters H6-H10, adjusting the power to each such that all temperatures on the designated thermocouples should be within 100°C of each other.
- 20.0 Continue to increase the temperature of the SFHP until liquid sodium begins to fill the processing tank, typically around 350-500°C. At this point close valve V7 to prevent excessive sodium removal. Continue to heat the heat pipe to 675-725°C.
- 21.0 Operate the heat pipe at 675-725°C for several hours. Remove any non-condensable gas (NCG) through valve V7 by briefly opening the valve until the heat pipe is isothermal. Operating for 1-2 hours against the valve with no sign of NCG generation is a practical indication that the NCG is removed. Note: If a significant overcharge of fluid is detected by seeing vibration caused by pool boiling, the fluid can be removed at this time by leaving valve V7 open until the fluid charge is brought within range.



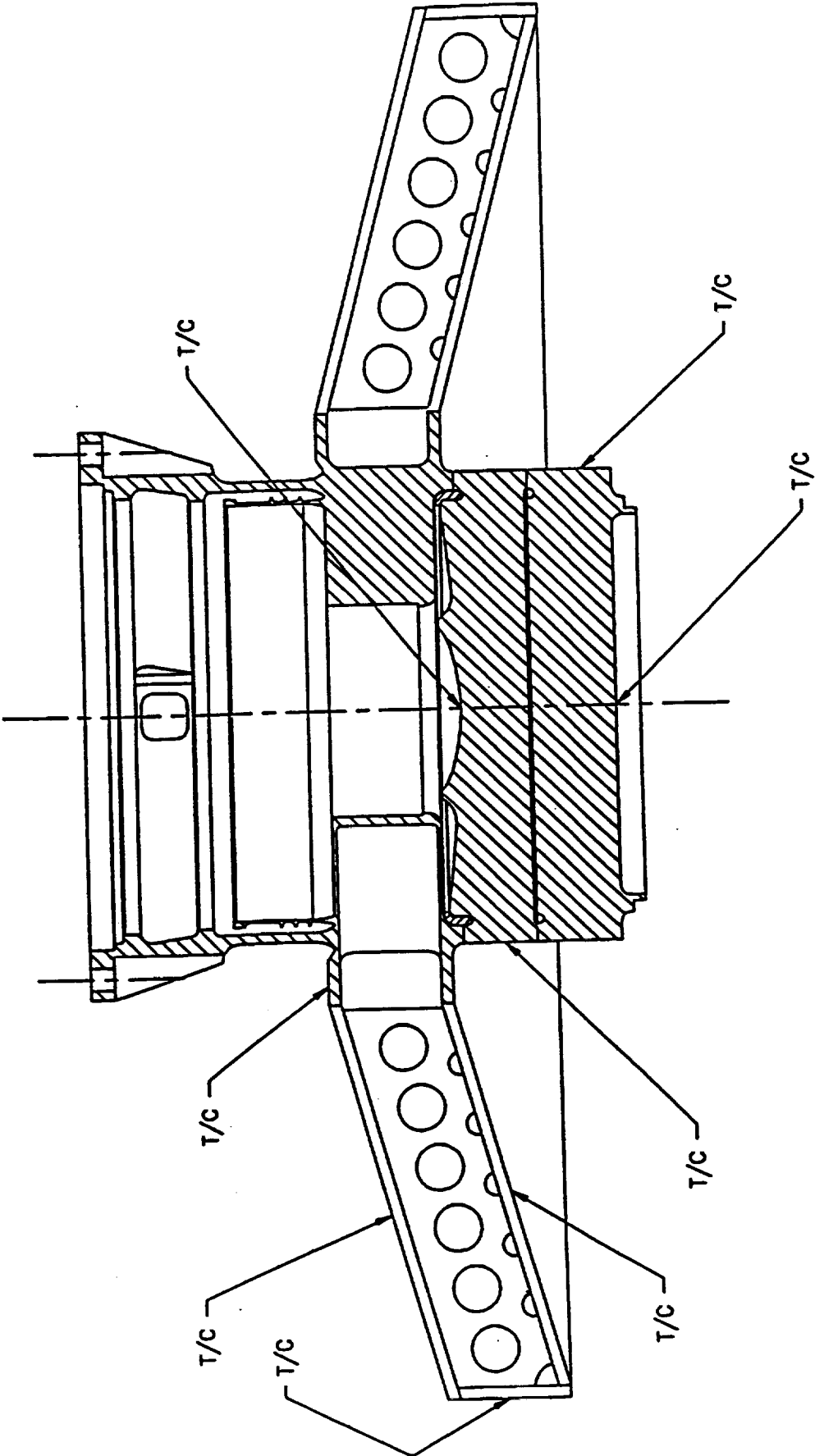
FIGURE 2. SEHP PROCESSING LAYOUT



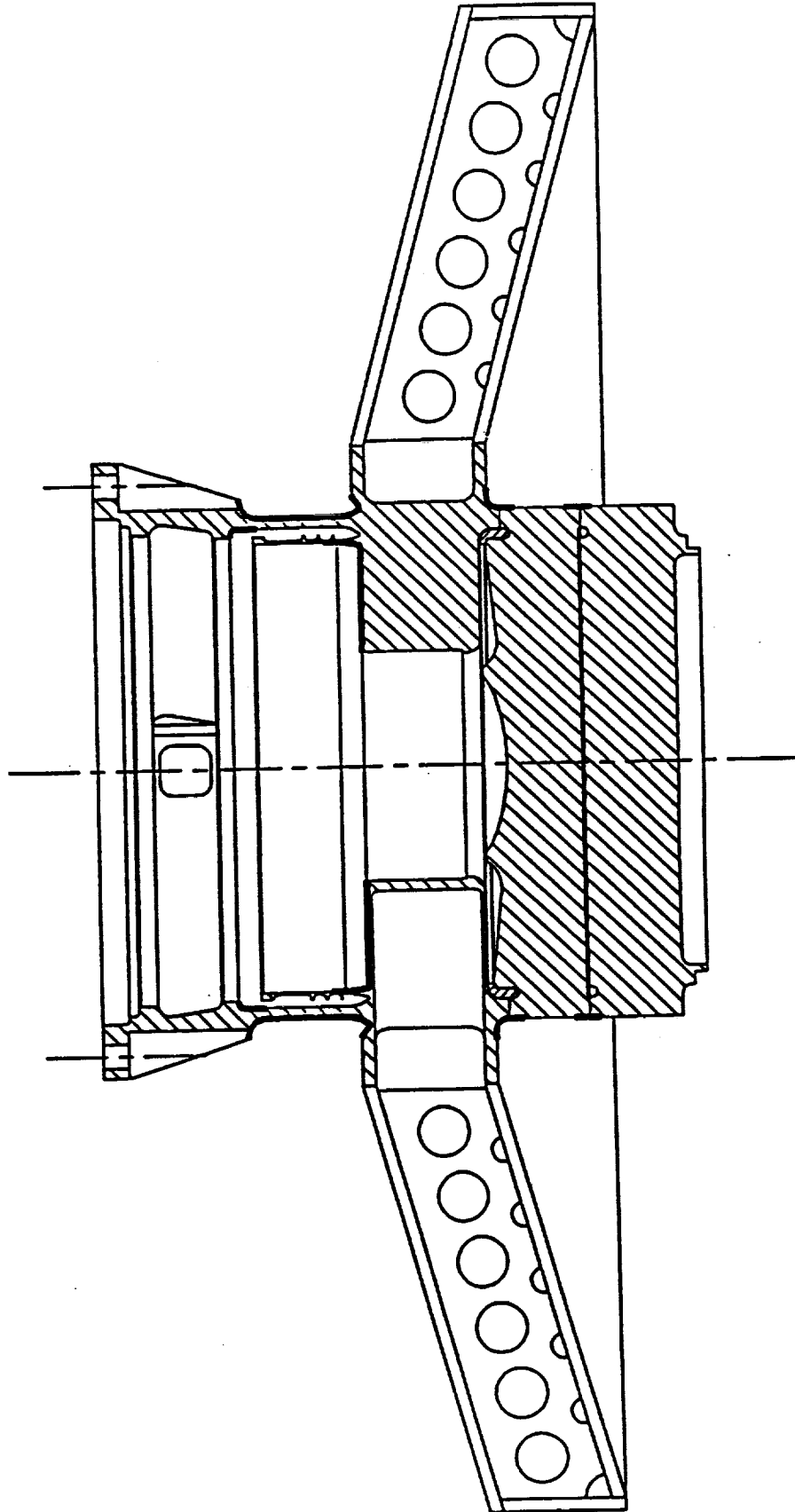
- 22.0 When NCG is eliminated at 675-725°C, increase the heat pipe operating temperature to 775-785°C, hold at temperature approximately 0.5 hours. Return the heat pipe to 675-725°C and remove any additional NCG. Repeat step 22.0 a maximum of three times. If NCG is still present contact MTI engineering. Total time at 675-725°C should be less than 10 hours. Total time at 725-785°C should be less than 5 hours. And, the maximum allowable temperature for any point on the assembly shall not exceed 785°C.
- 23.0 Once the heat pipe is determined to be isothermal with no sign of NCG, the fill tubes will be pinched and welded to seal the heat pipe and remove the high temperature valves. Valve V6 will be removed first and the heat pipe will be run up to 675°C following the weld to verify that the seal was made without introducing additional NCG. If the heat pipe is still isothermal with no sign of NCG, then valve V7 will be removed by pinching and welding the tube inboard of the valve. The heat pipe will again be operated at 675°C to verify that this seal was also made without introducing additional NCG.
- 24.0 The heat pipe will be allowed to cool to room temperature and then operated again after 12-24 hours as a final NCG check prior to packaging and delivering the SFHP to MTI.
- 25.0 Deliver the SFHP to MTI.

**Note:** Additional clarification and narration is provided in Thermacore Let11-1072.26-93 dated 2/25/93. A copy is attached as Appendix B.

APPENDIX A  
FIGURE 1: REQUIRED THERMOCOUPLE LOCATIONS

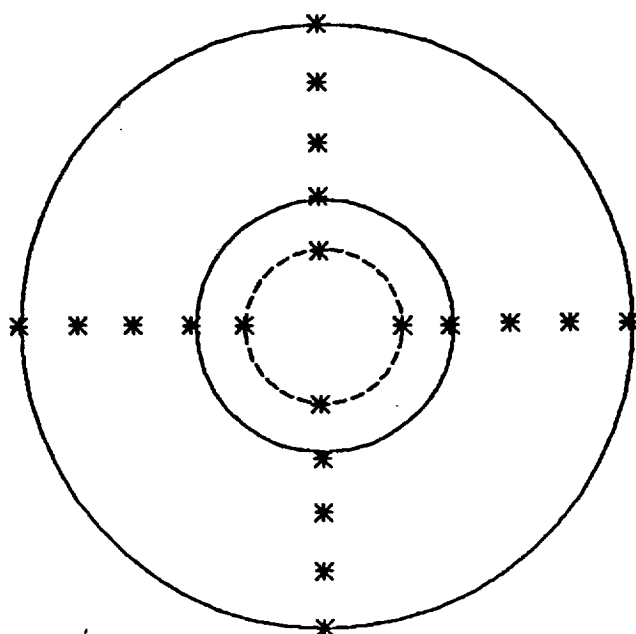


APPENDIX A  
 FIGURE 2: SENSITIVE AREAS - NO SPOT-WELDING PERMITTED



# APPENDIX A

FIGURE 3: ADDITIONAL THERMOCOUPLE LOCATION FOR PROCESSING

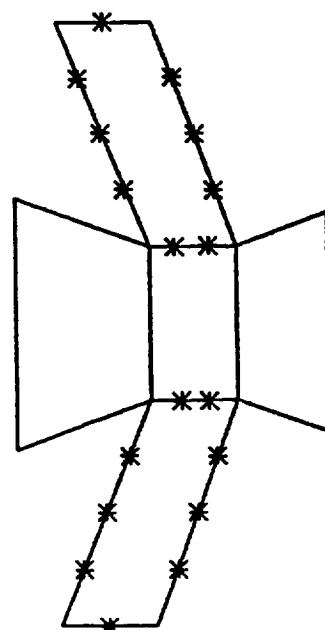


## NOTES

ASTERISKS (\*) DENOTE TYPE K  
BARE WIRE THERMOCOUPLE LOCATIONS.

THERMOCOUPLES SPOT WELDED ONTO  
HEATER HEAD SURFACE.

36 TOTAL THERMOCOUPLES PLACED---  
9 THERMOCOUPLES PER QUADRANT.



# THERMACORE

INC

780 EDEN ROAD, LANCASTER, PA 17601  
PH: 717/569-6551 FAX: 717/569-4797

In reply refer to let11-1072.26-93

February 25, 1993

Mr. Manmohan Dhar  
Mechanical Technology Inc.  
968 Albany-Shaker Road  
Latham, New York 12110

**Subject: Response to NASA Fax Dated 2/9-11/93 Regarding Sodium Fill Procedure For The SFHP**

Dear Mr. Dhar:

This letter responds to the NASA questions in their February 9-11, 1993 Fax regarding the Sodium Fill and Processing Procedure for the SFHP. Each question will be reiterated below followed by the appropriate response.

**Step 3:** *In what orientation will the pipe be mounted? If the pipe is to be mounted with the diameter between V6 and V7 vertical, to what level will the 100 mesh wicking drain in step 13.6?*

**Response:** The heat pipe will be mounted vertically between V6 and V7 during the four fill and drain steps. The final step will be to change the orientation to horizontal with the engine mating flange directed up. In this orientation the sodium trapped in the upper Starfish pockets will drain as well as any sodium held up by the support ribs. The height against gravity in this orientation is less than the static capillary height of the 100 mesh screen wick; therefore, the wick will be assumed to be fully saturated.

**Step 4:** *What heaters will be used? Size, shape, mode of attachment to the heat pipe (not Starfish)?*

**Response:** Numerous nichrome wire ceramic beaded electrical resistance heaters will be used to heat the SFHP. These heaters are typically 33 feet long and approximately .25" in diameter. The heaters will be attached to the top plate, bottom plate, and outer ring with nichrome or stainless steel straps spot welded directly to the heat pipe surface. Since no spotwelding is allowed on the heater head section, the same type heaters will be attached to stainless steel plates and placed against the heater head. Another heater, either the beaded heater type or cartridge heater type will be attached or inserted into a stainless steel round bar and placed internal to the heater head in the displacer space. Care will be taken to prevent direct contact with the pocket area of the heater head.

Step 5: *What pump and what vacuum level is advocated?*

Response: During the dry bakeout procedure, the entire system will be pumped through a turbomolecular pump backed by a conventional roughing pump. A section of tubing between the pump and the heat pipe will be placed in liquid nitrogen to prevent backsteaming of oil in case of a pump failure or power outage. The turbomolecular pump is capable of achieving a  $10^{-6}$  to  $10^{-7}$  torr vacuum; however, the vacuum in the heat pipe will most likely be less because of the conductance limit of the small tubing and valves. The 24 hour period suggested should still result in adequate degassing of surface adsorbed gases and water.

Step 6.3: *"Uniform" temperature seems a bit vague. Can an acceptable variation be defined? Moreover, can locations and number of thermocouples on the evaporator be defined whose uniformity is to be assured?*

Response: The temperature of the stock tank is not a critical parameter as long as the temperature is such that the sodium is fully melted and can flow freely through the plumbing. Operating at approximately 120°C or less is the safest temperature because 120°C is the spontaneous ignition temperature in air. Therefore, the setpoint on the stock tank will be kept at 120°C with thermostatically controlled drum heaters. The temperature of the SFHP prior to filling with sodium is also a non-critical parameter. The temperature range selected (120-150°C) seems reasonable to assure that the fill charge will remain liquid. The next step is then to increase the temperature to 425°C. Again the temperature uniformity is not critical but we believe that it can be controlled to within plus or minus 25°C; and, the heaters will be trimmed to achieve the best uniformity that is possible. If plus or minus 25°C cannot be achieved, the heaters will be redistributed until this goal can be met. Figure 1 is a sketch of the proposed thermocouple locations.

Step 6.6: *How sensitive is the pressure control on the argon supply, to indicate that a state of no flow of argon has been reached? A pressure fluctuation could give a spurious indication of liquid displacement. How good is the argon flow meter?*

Response: The sodium stock tank is not a pressure vessel; and therefore, for safety reasons the argon supply will be regulated with a oil type manometer set for less than 1 psig. The flow of argon into the sodium stock tank will be through a ball type flow meter. The accuracy of the flow meter is not critical only the indication of zero flow is important.

Step 6.7: *What is the total volume of the expansion tank, its diameter and height, and sight glass provisions be stated? How finely can the volume of sodium in the expansion tank be measured?*

Response: The total volume of the expansion tank is approximately 2500 cm<sup>3</sup>. The total volume of the SFHP is approximately 24000 cm<sup>3</sup>. A temperature increase from 120°C to 425°C will result in a liquid sodium expansion of approximately 2000 cm<sup>3</sup>. The expansion tank will be approximately 2.3 inch diameter by 36 inches in length. Each linear centimeter

corresponds to approximately 27 cm<sup>3</sup>. Liquid level pins will be placed internal to the expansion tank at 1 to 2 cm intervals to determine the fluid charge in the expansion tank. This level of accuracy will be sufficient to charge the SFHP to plus or minus 27 cm<sup>3</sup>. The sight glass is a standard off the shelf vacuum sight glass with a metal gasket seal. The sight glass is 1.5 inches in diameter. The liquid level pins can easily be seen and counted through the sight glass.

**Step 7.1:** *What is meant by "in these regions"? See comments on 6.3 above. Are we assured that the entire inner surface of the heat pipe is above 97°C?*

**Response:** "In these regions" means that the plumbing leading to the dump tank and the dump tank itself will be heated to 120-150°C such that the sodium can flow freely from the SFHP to the dump tank. As stated above for 6.3, the temperature is not critical as long as the lines and dump tank are at or near 120°C. The temperature will be determined by thermocouples placed along the plumbing lines and in or on the dump tank. During the sodium discharge step the SFHP is at 425°C as it has been for the previous 24 hours; and therefore, the temperature will surely be greater than 97°C.

**Step 11.2:** *Should volume displacements on the expansion tank and the dump tank agree, or are the markings too different in magnitude for this to be meaningful?*

**Response:** Yes, the graduations in the dump tank are much different than in the expansion tank. The dump tank is 40 times greater in volume, approximately 100,000 cm<sup>3</sup>, than the expansion tank. The graduations in the dump tank will be set at approximately 5000 cm<sup>3</sup>. The purpose is to verify that the bulk of the fluid has been discharged. The dump tank's size prohibits practical accurate measurements.

**Step 13.3:** *Is the sight glass on the dump tank used to estimate when one-half of the charge has been dumped?*

**Response:** The sight glass on the dump tank serves two purposes. The first is to visually verify good flow and grossly determine that the majority of the fluid has been discharged during the first three discharge steps. The second is to determine when one-half of the forth and final charge has been dumped. This indicates that it is time to valve off the sodium sample for oxygen analysis and to discharge the remaining fluid through the bypass plumbing. The 5000 cm<sup>3</sup> graduations will be adequate for this measurement since the SFHP volume is approximately 20,000 cm<sup>3</sup>.

**Step 13.6:** *See the comment on step 3 at the beginning. Also, will some charge be held up by the Starfish pockets? Will the ribs interfere with drainage (neglecting filleting)? Detailed calculation of the amount remaining in the wicking should be provided, for checking purposes. Recall that we have some evidence of the requirements from the one-tenth segment filling.*



**Response:** Following the removal of all sodium in the vertical orientation, the heat pipe will be separated from the sodium drum. The SFHP will be rotated to its normal operating orientation to allow fluid trapped in the upper pockets and along the ribs to flow to the outer ring. The rotation will be made possible through flexible metal bellows placed between the expansion tank and the SFHP and between the dump tank and the SFHP. In the normal operating orientation or with a slight tilt (3-5°) towards the V7 valve, the remainder of the fluid charge can be discharged. At this orientation the wick should continue to be saturated because the height against gravity is less than .3 meters. Although data from the one-tenth would be helpful to gauge the volume of the makeup fluid charge, the SFHP will be conservatively overcharged on purpose to prevent an under fill condition as was the case with the one-tenth segment. The heat pipe will be weighed after final charging to determine the total charge. During the processing steps, any resulting overcharge can be bleed off accurately into an appropriately marked dump pot.

**Step 14.3:** *Is the meniscus effect of any importance in observing the volume in the expansion tank?*

**Response:** With properly spaced liquid level pins in the tanks the fluid charge can be accurately measured. The meniscus forming on a liquid level pin is easily spotted and used as an indicator of liquid level. The diameter of the expansion tank is such that the volume of the edge meniscus is negligible. Also as stated above, there will be an intentional overcharge.

**Step 19.0:** *Rephrase suggested, "(all temperatures on the designated couples should be within 100°C of each other)".*

**Response:** The modification will be incorporated and the designated thermocouples will be called out in Figure 1 of this letter and in an additional Figure in the procedure.

**Step 20.0:** *Is this filling of the processing tank due to distillation? What exactly is the purpose of this step, since step 21.0 is supposedly available to adjust for overcharge? How do you know this step is not bringing the inventory below requirements?*

**Response:** During the time that the SFHP is being heated from room temperature to 350-500°C, a vacuum can be drawn through valve V6 to remove any non-condensable gas in the SFHP. Little if any is expected but no harm is done by drawing the vacuum. The amount of sodium leaving the SFHP as distilled vapor is negligible at these temperatures. Experience has shown that after 350-500°C, depending on the heat pipe geometry, a significant and increasing amount of vapor and liquid condensing in the plumbing between the SFHP and the processing pot will start to fill the processing pot. At this time the valve is closed. The inventory is not reduced significantly because the valve is closed at the first sign, less than 5 cm<sup>3</sup>, of sodium filling the processing tank.

**Step 21.0:** *What is the definition of isothermal? What thermocouples are being observed? What is "against the valve"? Where is the vibration being seen? Is this a sensitive method of determining overfill?*

Mr. Manmohan Dhar  
April 20, 1993  
Page 5

**Response:** Isothermal means all temperatures on the SFHP are the same. In practice, this means the thermocouple sensors are within 10-20°C and that the exposed areas where non-condensable gas should collect are visually uniform in color and optical pyrometer temperature measurements are uniform. The same criteria will be used as was used on the one-tenth segment heat pipe. Temperature uniformity as a function of time at steady state is also used to detect non-condensable gas generation. "Against the valve" means that the valve is closed. Significant overcharge can only result from a mistake during the weighing process. Significant overcharge may be several 1000's of cm<sup>3</sup>. All the note is saying is that this situation will be detectable and can be dealt with without jeopardizing the program. The chances of this type of condition are very low. In any case, if significant overcharge were present, it is typical for the entire heat pipe and mounting stand to vibrate. The most sensitive indicators are the thermocouple wires. This is not a sensitive method for determining the magnitude of the overfill condition.

**Step 23.0:** *Is there a fall back procedure for correcting for NCG seen after V6 is removed?*

**Response:** The extra valve V6 will be removed first. The order was reversed in the draft procedure. The valve V7 attached to the processing pot will be removed last. Should the sealing operation fail, the fall back position would be to cut the remaining fill tube under a high purity argon purge, weld on a new valve V7 and a new processing pot. The procedure would have to be repeated from Step 18.0. This procedure, practice welds, etc. are aimed at minimizing the risk of such an occurrence. If this condition should occur, the careful cleaning and processing will be negated; however, the heat pipe will still be useful for the several hundred hours of testing planned.

**General:** *How much charge will be in the sodium drum?*

**Response:** 400 pounds; 181.6 kg

**General:** *Can a filter be installed above the sample tube to remove any particulates which may perturb the oxygen determination at ETEC? Check with ETEC for information on this matter.*

**Response:** Thermacore has received a memo from ETEC, NASA, and MTI regarding the particulate filter. The appropriate filter will be purchased and installed in the filling system.

Thank you for reviewing the procedure and for your comments. This was a useful effort. Several key issues were identified and addressed. The responses lead to minor processing changes that will increase the probability of success. If there are any further questions, please call.

Sincerely,

  
Peter M. Dussinger  
Project Engineer/Group Leader

dlh

## **APPENDIX B: CTPC COMPONENT DEVELOPMENT**

### **B.1 Introduction**

This appendix provides detailed information to supplement the summary on component development presented in Section 10.0 of Volume I of this report.

## B.2 High-Temperature Organic Materials

### Memorandum: High-Temperature Organic Material Evaluation Tests, Phase II

TO: M. Dhar

FROM: Steve Walak *SW*

DATE: February 22, 1991

SUBJECT: High Temperature Organic Material Evaluation Tests, Phase II

#### Introduction

High temperature adhesives and organic materials are being evaluated for use in the cold end of the CTPC. The initial results of this testing were reported in the memo dated September 18, 1990. The results of testing completed after this date will be reported below.

Three materials were evaluated for thermal stability in helium at temperatures between 280°C and 330°C. The three materials included a high temperature polyimide adhesive, BR680-3, a silicon rubber adhesive, Castall S-1307 and insulation stripped from the polyimide coated wire used in the CTPC coil. A summary of the results is contained in Table 1.

The BR680-3 adhesive was also evaluated for bond strength using the test methods described in the preliminary report.

#### Results

The thermal stability of BR680-3 paste adhesive in helium at 330°C, was much better than any other organic adhesive tested at MTI. The test results indicate less than 5% weight loss after 1463 hours of exposure at 330°C, Table 1. Matri-mid 5218, previously considered to be the most stable material, lost >20% of its weight in 500 hours at 320°C.

The tensile strength of BR680-3 in steel to steel joints was poor. At room temperature the average tensile bond strength was 93 psi and after 125 hours at 325°C 4 of 5 samples fractured prior to tensile testing. The tensile strength of the single sample tested at 325°C was 50 psi.

A five layer stack up of fiberglass wrapped, flat copper wire coated with BR680-3 showed that this adhesive may be useful in coil winding. The interlaminar strength of the copper lay up appeared to be very good.

The Castall silicone was exposed to helium at 280°C and 330°C for 90 hours. After exposure at 280°C and 330°C, 4.0% and 19.3 % weight loss was recorded respectively. The material showed a slight increase in hardness but no other changes after the 280°C exposure. At 330°C the material suffered severe swelling and discoloration.

Memo to M. Dhar from S. Walak  
2/22/91

-----

The polyimide coating stripped from the CTPC wire was exposed to helium at 330°C for greater than 210 hours. The results indicate approximately 9% weight loss after 210 hours. The wire coating appeared darker after exposure but still maintained flexibility, toughness and insulating properties.

### Conclusions

The BR680-3 single component paste adhesive was found to have excellent thermal stability at temperatures up to 330°C. A five layer stack up of fiberglass wrapped, flat copper wire coated with BR680-3 demonstrated that the adhesive may be useful in coil winding applications.

Castall S-1307 silicone adhesive showed adequate thermal stability at 280°C. At 330°C severe material degradation was observed after 90 hours.

The polyimide wire coating maintained fair thermal stability at 330°C. Some weight loss and discoloration were observed after 210 hours. Exposure testing for longer times should be initiated.

cc: S. Bhate	G. Dochat
A. Brown	M. Frantsov
P. Chapman	G. Smith
M. Cronin	W. Smith

Memo to M. Dhar from S. Walak  
2/22/91

---

TABLE 1

ORGANIC OUTGASSING DATA

MATERIAL	TEMP.(°C)	TIME(HR)	ENVIRONMENT	CUMULATIVE RESIN WT. CHANGE%
BR680-3	330	125	Helium	-1.9
BR680-3	330	510	"	-2.4
BR680-3	330	963	"	-3.4
BR680-3	330	1463	"	-4.7
Castall	280	90	"	-4.0
Castall	330	90	"	-19.3
Wire Coat	330	138	"	-6.6
Wire Coat	330	210	"	-8.8

## Memorandum: High-Temperature Adhesive Tests

TO: M. Dhar  
FROM: S. Walak  
DATE: September 18, 1990  
SUBJECT: High Temperature Adhesive Evaluation Tests

### Introduction:

High temperature adhesives are being evaluated for use in the cold end of the CTPC. The uses can be divided into two primary categories: 1) Adhesive Bonding and 2) Low Stress Potting and Sealing.

The adhesive bonding applications include displacer magnet, position probe and sensor bonding. High bond strength at elevated temperature is the primary requirement in these applications.

The low stress potting and sealing applications include coil winding, coil overwraps and plunger overwraps. These applications require materials that are stable at the operating temperature and do not generate debris in the engine. Tensile strength is considered to be a secondary requirement.

### Procedures:

Material weight loss as a result of exposure time in elevated temperature helium was used as a measure of thermal stability. The materials were exposed in helium at temperatures between 275 °C and 325 °C.

The bond strength tests were performed on round steel bar stock bonded end to end. Tests were performed on 1 inch and 0.5 inch diameter samples. The ends of the bars were ground using 320 grit grinding paper prior to bonding. The bonds were tested in tension at room and elevated temperature. The elevated temperature tests were performed on samples exposed to helium at the test temperature for approximately 1 week.

The materials examined included two high temperature epoxies, Cotronics 4700 and Eccobond 104, a bismaleimide, Matrimid 5292, three polyimides, Matrimid 5218, Crest 2280 and Master Bond U845 and a ceramic adhesive, GA-100.

**Results:**

**Weight Loss**

The results of the weight loss experiments are listed in table 1. The two epoxies suffered significant weight loss at 285°C and 325°C. Samples of Cotronics 4700 lost 16% of their original weight in 50 hours of exposure at 285°C. An additional 2% was lost between 50 and 500 hours. The samples of Eccobond 104 lost 24% of their weight in 50 hours and an additional 11% between 50 and 500 hours.

The material given off by the epoxies deposited as a thick, oily resin on the inside of the sample cylinders. The epoxies appeared to be very brittle after exposure and the larger sample volumes developed cracks.

Samples of the bismaleimide, Matrimid 5292, showed an average weight loss of 5% in 50 hours of exposure at 285 °C. An additional 13% was lost between 50 and 500 hours. These results indicate that the BMI is more stable than the two epoxies but is not suited for long term use at 285 °C.

Matrimid 5218, a soluble polyimide, was tested for weight loss in helium at 275 °C and 320 °C. At 275 °C the Matrimid 5218 showed no detectable weight loss after 50 hours of exposure. After 125 hours a slight weight gain was measured. The final measurement, made after 500 hours, showed less than 1% decrease from the starting weight. These results indicate that the Matrimid 5218 is thermally stable at 275 °C.

At 320 °C Matrimid 5218 lost 9 weight percent in 50 hours and an additional 13% between 50 and 500 hours. These results indicate that M5218 is not thermally stable at 320 °C but may be considered for short term use.

The thermal stability of Master Bond U845, a thermal setting polyimide, was evaluated at 325 °C. The U845 lost 40% of its weight after 260 hours at 320 °C. These results showed no improvement over Matrimid 5218. U845 is very low viscosity and requires a carefully controlled cure cycle. These features make the U845 more difficult to work with than the Matrimid 5218.

Matrimid 5218 is currently the material of choice for the low stress potting and sealing applications. Matrimid 5218 is very stable at 275°C but begins to degrade at 320 °C. Two additional high temperature organic adhesives, American Cyanamid BR680 and Crest 2280, will be evaluated to determine if higher temperature stability can be achieved.

**Bond Strength Tests:**

A summary of the bond strength test results is shown in Table 2. The two epoxies showed excellent adhesive strength at room temperature. The tensile bond strength of Eccobond 104 was 4775 psi and Cotronics 4700 was 8600 psi as determined from single tensile tests.

Several tensile strength samples were heated in helium at 275 °C for one week and subsequently tested in air at 275°C. The tensile bond strength of Eccobond 104 and Cotronics 4700 was 615 psi and 563 psi respectively. Four additional



samples of Eccobond 104 were tested in air at 325 °C after exposure in helium at 325 °C for one week. The average bond strength of these samples was 83 psi. The maximum bond strength achieved at 325 °C was 140 psi. One sample failed during handling prior to testing. These results indicate that the two epoxies have poor adhesive strength at temperatures between 275 °C and 325 °C.

The bismaleimide, Matrimid 5292, achieved room temperature bond strengths which averaged 4238 psi with a maximum value of 7003 psi. The tensile bond strength of Matrimid 5292 at 275 °C, after exposure in helium at 275 °C, was 1798 psi. The bond strength test at 325 °C, with one week exposure in helium at 325 °C, resulted in an average tensile strength of 239 psi. Two of the six samples exposed in helium at 325 °C for one week prior to testing fractured during handling. The maximum strength obtained at 325 °C was 381 psi.

Three polyimides were subjected to similar tensile bond strength testing. Matrimid 5218 showed an average room temperature tensile strength of 2356 psi and a maximum value of 3883 psi. The tensile bond strength at 325 °C after exposure in helium at 325 °C for one week was 38 psi.

The Master Bond U845 showed poor bond strength performance at both room temperature and at 325 °C. Six test samples were assembled for room temperature testing and 4 fractured during handling prior to testing. The bond strength of the 2 remaining pieces averaged 1324 psi. Three additional samples were exposed to helium at 325 °C for one week. These three samples also fractured prior to testing.

The average room temperature tensile bond strength of Crest 2280 was 4220 psi and the maximum was 7538 psi. Three samples were exposed to helium at 325 °C for one week. One 0.5 inch diameter sample fractured during handling after high temperature exposure. The other two samples gave an average tensile bond strength of 718 psi and a maximum of 967 psi.

The ceramic adhesive, GA-100, was tested at room temperature and at 325 °C after exposure to helium at 325 °C for one week. The room temperature tensile bond strength for the GA-100 sample tested was 1942 psi. Two samples were exposed at 325 °C for one week prior to testing at 325 °C. One sample fractured during handling after the high temperature exposure and the second sample achieved a tensile strength greater than 1146 psi.

### Conclusions:

The two epoxies, Cotronics 4700 and Eccobond 104, showed poor thermal stability in helium at 275 °C and 325 °C. The bismaleimide, Matrimid 5292, degraded at a slightly slower rate but was still unstable at these temperatures. Matrimid 5218, a soluble polyimide, was stable in helium at 275 °C but was not stable at 325 °C. At present Matrimid 5218 is the material of choice for low stress potting and sealing applications.

The tensile bond strength of the epoxies degraded severely at elevated temperatures. These materials are not considered useful at 275 °C and 325 °C. The Matrimid 5292, a bismaleimide, maintained a tensile bond strength of approximately 1800 psi at 275 °C and 230 psi at 320 °C. This material may be considered for use in specific applications at these temperatures.

The highest elevated temperature tensile bond strength obtained with an organic adhesive was achieved with Crest 2280, a polyimide. After exposure for one week in helium at 325°C the Crest 2280 maintained an average strength of 718 psi at 325°C. This material appears to be suited for adhesive bonding in low to moderate stress applications.

The ceramic adhesive, GA-100, maintained excellent tensile bond strength at 325°C. The ceramic is inherently brittle and should not be used in shock or impact loading situations.

The three materials which may be considered for bonding applications at temperatures between 275°C and 325°C are Matrimid 5292, Crest 2280 and GA-100. The bond strength tests showed that improper application of these adhesives can result in bond failure at relatively low loads. Bonding conditions and procedures appear to be as important as the adhesive used.

**Table 1**  
**ORGANIC OUTGASSING DATA**

MATERIAL	TEMP.(°C)	TIME(HR)	ENVIRONMENT	CUMULATIVE RESIN WT. CHANGE%
C4700	285	50	Helium	-15.85
C4700	285	125	"	-16.95
C4700	285	500	"	-18.26
EB104	285	50	"	-24.18
EB104	285	125	"	-29.55
EB104	285	500	"	-35.04
EB104	325	50	"	-33.45
BMI(5292)	285	50	"	-5.11
BMI(5292)	285	125	"	-10.42
BMI(5292)	285	500	"	-23.31
M5218	275	50	"	-0.18
M5218	275	125	"	+2.95
M5218	275	500	"	-0.68
M5218	320	50	"	-8.90
M5218	320	125	"	-14.9
M5218	320	500	"	-22.2
M5218	310	210	"	-13.5
U845	325	260	"	-40.60

**Table 2**  
**BOND STRENGTH**

MATERIAL	PRE-TREATMENT (°C/HR)	TEST TEMP. (°C)	BOND STRENGTH (PSI - Ave./Max.)
EB104	NONE	R.T.	4775
"	275/175	275	615
"	325/175	320	*83/140
C4700	NONE	R.T.	8600
"	275/175	275	563
BMI5292	NONE	R.T.	4238/7003
"	275/175	275	1798
"	320/175	320	*229/ 381
M5218	NONE	R.T.	2356/3883
"	320/175	320	38
CREST 2280	NONE	R.T.	4220/7538
"	325/175	320	*718/967
U845	NONE	R.T.	*1324/1477
"	320/175	320	*0
GA-100	NONE	R.T.	1942
"	325/175	320	>1146*

\* Indicates that test samples failed during handling prior to testing.

## B.3 Heat Exchanger Fabrication

## MSR 567: Metallographic Examination of an EDM Recast Layer in IN718

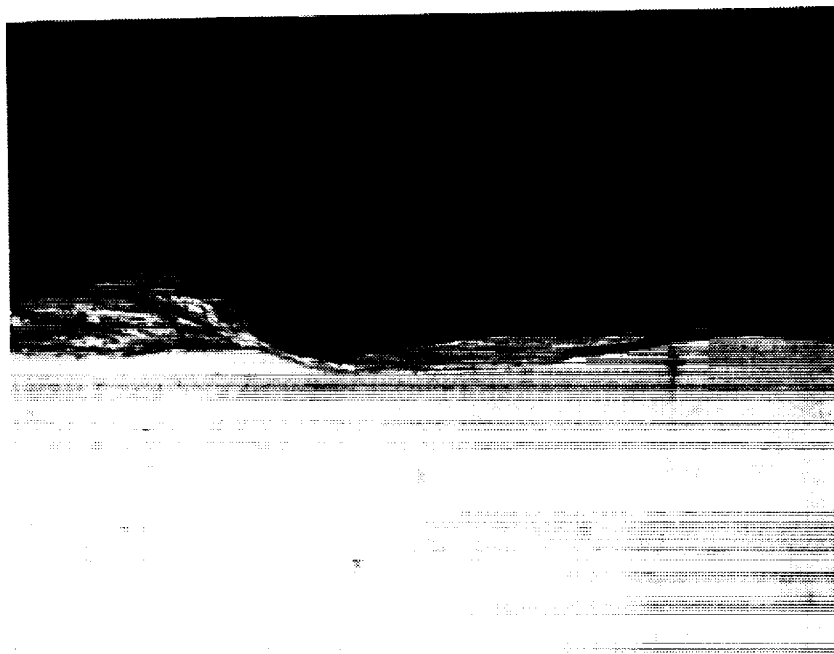
TO: Mike Walsh  
FROM: S. Walak *SW*  
DATE: April 11, 1989  
SUBJECT: Metallographic Examination of an EDM Recast Layer in IN718,

On February 14, 1989 a section of IN718 plate with several 1 mm holes was delivered to the Materials Analysis Laboratory for examination. The holes had been made by eletro-discharge machining. The machining parameters were selected to simulate the conditions to be used in cutting the gas flow holes in the proposed CTE starfish heater head. Longitudinal sections and cross-sections from several of the holes were prepared for metallographic examination. The sections were examined to determine the depth of effected metal below the machined surface.

A distinct recast layer was observed at the edge of all the holes examined. The maximum thickness of the layer was between 25 and 50 microns (1 to 2 mils). The general structure of the layer is shown in Figures 1 through 4.

Several microcracks were also observed in the recast layer, Figures 5 and 6. The maximum depth of the cracks was approximately 15 microns (0.5 mils). These cracks appeared to be contained in the recast layer and did not penetrate into the unaffected metal.

/cn



L567-3 400X  
FIGURE 2 - RECAST LAYER IN IN718 EDM HOLE.  
(LONGITUDINAL SECTION, ETCHED).

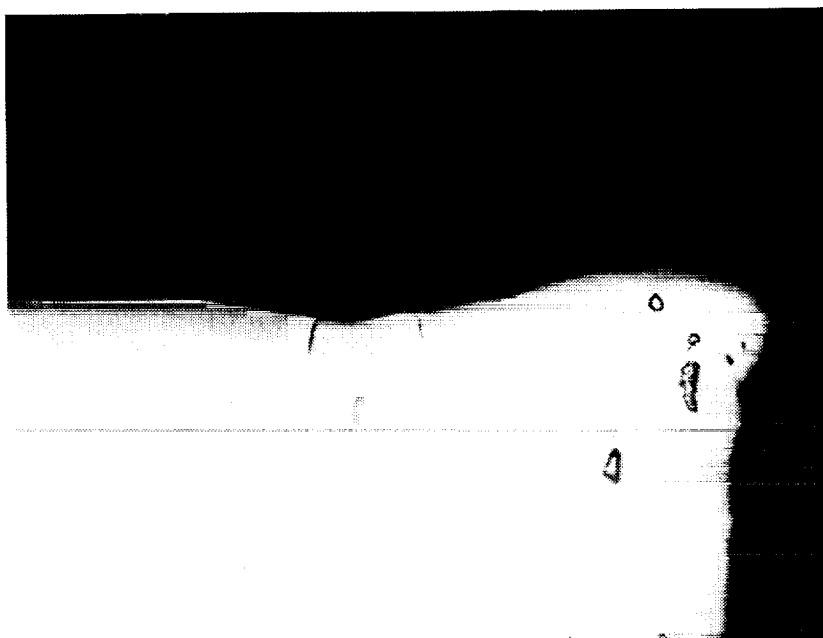


L567-4 200X  
FIGURE 3 - RECAST LAYER IN IN718 EDM HOLE.  
(CROSS-SECTION, ETCHED).

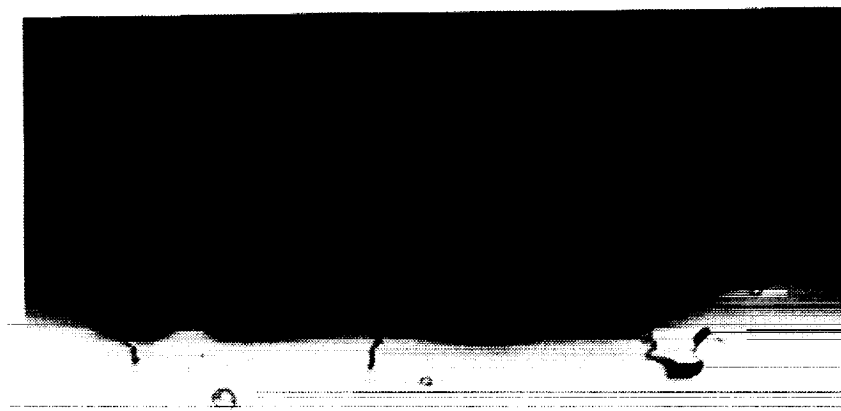


L567-8 400X  
FIGURE 4 - RECAST LAYER IN IN718 EDM HOLE.  
(LONGITUDINAL SECTION, UNETCHED).

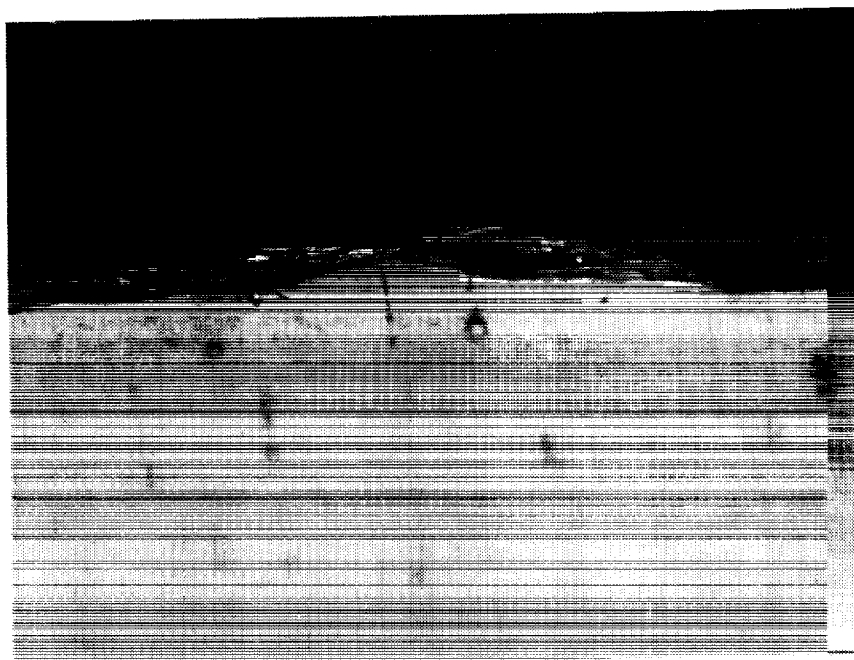




L567-6 400X  
FIGURE 5- MICROCRACKS IN AN IN718 EDM RECAST  
LAYER. (LOGITUDINAL SECTION, UNETCHED).



L567-9 400X  
FIGURE 6 - MICROCRACKS IN AN IN718 RECAST LAYER.  
(LOGITUDINAL SECTION, UNETCHED).



L567-1 400X  
FIGURE 1 - RECAST LAYER IN IN718 EDM TEST HOLE.  
(LONGITUDINAL SECTION, ETCHED)



**MSR 652: Evaluation of Chemical Milling Procedures for Starfish Heater Head**

**TO:** Gary Antonelli  
**FROM:** Steve Walak *SW*  
**DATE:** July 26, 1991  
**SUBJECT:** Evaluation of Chemical Milling Procedures for  
Starfish Heater Head Machining.

The heater head pockets on the Component Test Power Converter (CTPC) will be fabricated by a combination of conventional milling, electro-discharge machining (EDM) and chemical milling. In October 1990, several single pocket demonstration samples were fabricated at Speedring Inc., Cullman, AL using these techniques and prepared for metallographic examination at MTI.

Cracks 0.001 to 0.002 inches deep were observed on the chemically milled surfaces during this examination. These cracks appeared to be caused by grain boundary corrosion in the chemical milling solution. The initial results also implied that residual surface stress added to the cracking problem. The results of this examination were reported in MSR 642, see attached copy.

As a result, additional samples were sent to Speedring Inc. to determine if the surface cracks could be eliminated by milling beyond any residual surface stress or by using a different chemical milling solution. Pieces of the original demonstration samples were milled to determine if removing an additional 0.002 inches of metal would eliminate the surface cracks. Inconel 718 bar stock polished by standard metallographic techniques was milled 0.002 inches to evaluate different milling processes on low stress surfaces. The procedures used for chemical milling are shown below.

**Procedure 1:**

- Step 1) Chemical milling
  - 80% Nitric acid
  - 20% Hydrofluoric acid
  - Room temperature

**Procedure 2:**

- Step 1) Activation  
65% HCl  
35% H<sub>2</sub>O  
130°F, 5 to 10 minutes
- Setp 2) Chemical milling  
68% HCl  
6% Nitric Acid  
3% Phosphoric Acid  
5% Hydrofluoric Acid  
18% Ferric Chloride  
120-130°F, Mill Rate 0.001 inch in 5 minutes

**Results**

Metal removal by procedure 1, 80% nitric and 20% hydrofluoric acid at room temperature, was very slow. Several days were required to remove the requested 0.002 inches of metal. During milling additional acid was reportedly added to keep the solution active.

Metallographic examination revealed that the surface of the polished bar stock was significantly rougher after chemical milling by procedure 1. However, surface cracking was limited to a depth of <0.0003 inches, Figure 1. Cracks extending approximately 0.002 inches below the surface were observed in sections from the single pocket samples remilled by procedure 1, Figure 2.

Metal removal was much faster by procedure 2. The total time required to remove 0.002 inch was approximately 10 minutes. Metallographic sections from both samples milled by procedure 2 showed no surface cracking, Figures 3 and 4. Small surface pits, approximately 0.001 inch in depth, were observed on the polished bar stock, Figure 5.

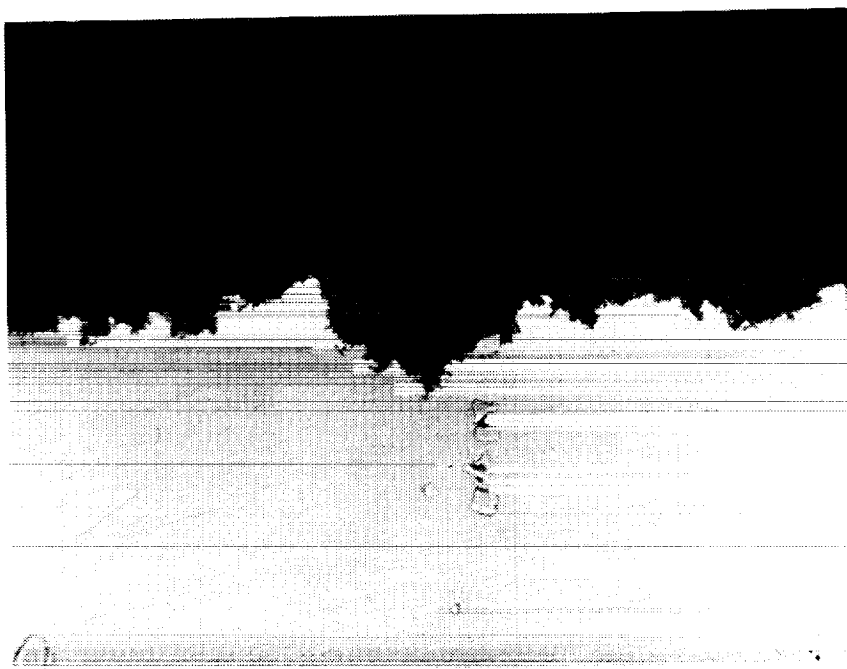
**Conclusions**

Surface cracks observed in IN718 after chemical milling appear to result from grain boundary corrosion in the Speedring chemical milling solution, procedure 1. High residual surface stress was not required for cracking to occur in this solution. No cracks were observed in samples milled by procedure 2.

The EDM recast layer on the starfish heater head can be effectively removed by chemical milling by procedure 2. Some minor surface pitting can be expected, <0.001 inch, but is not expected to be detrimental to component performance.

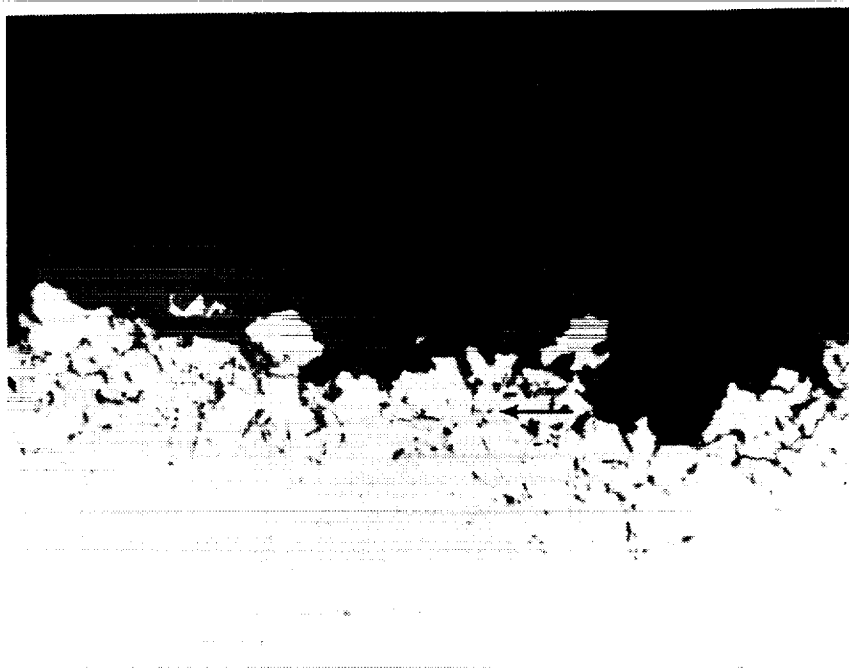
cc: P. Chapman  
M. Cronin  
M. Dhar  
G. Dochat  
G. Smith

MSR 652



L652-1 400X  
FIGURE 1 - CHEMICALLY MILLED SURFACE ON POLISHED  
IN718, Solution #1.

MSR 652



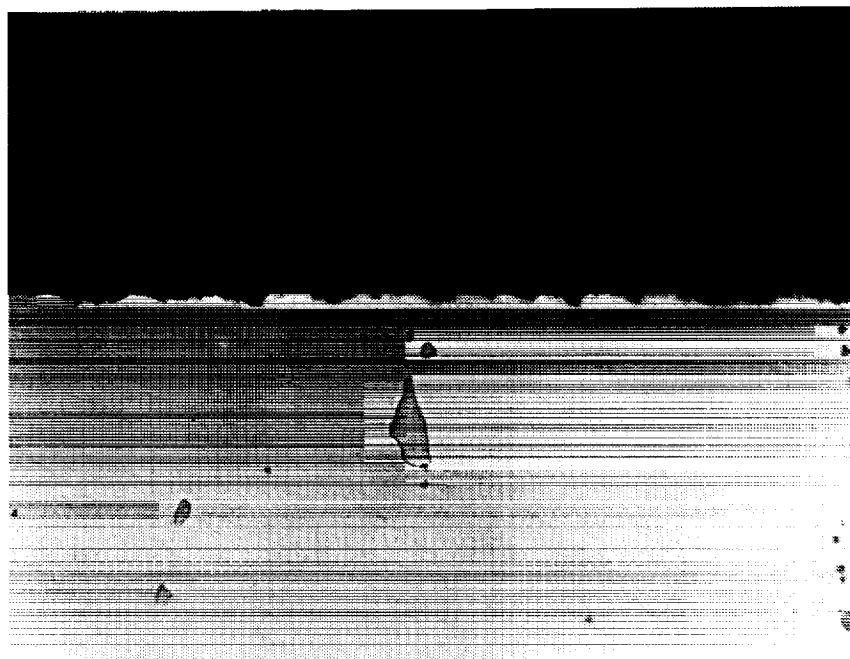
L652-6

400

FIGURE 2 - CHEMICALLY MILLED SURFACE ON A SECTION FROM  
A SINGLE POCKET DEMONSTRATION SAMPLE, SOLUTION 1  
(NOTE: SURFACE CRACKS AT ARROW)

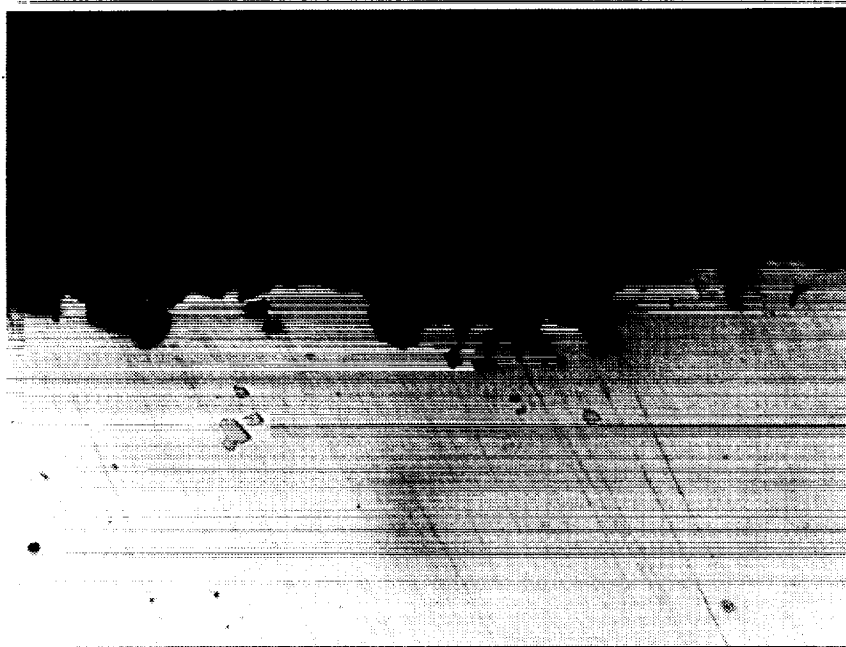


MSR 652



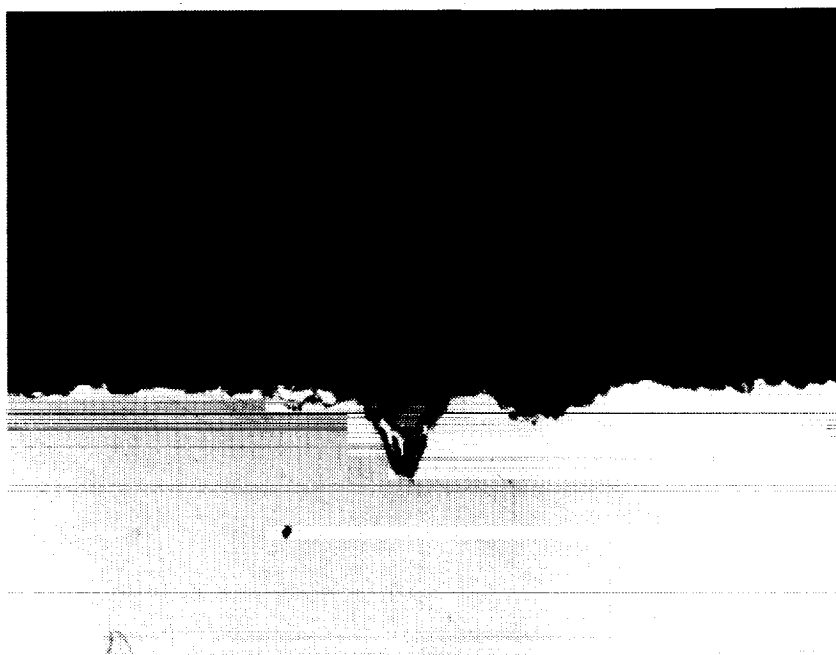
L652-4 400X  
FIGURE 3 - CHEMICALLY MILLED SURFACE ON POLISHED  
IN718, SOLUTION #2

MSR 652



L652-7 400X  
FIGURE 4 - CHEMICALLY MILLED SURFACE ON SECTION FROM  
A SINGLE POCKET DEMONSTRATION SAMPLE,  
SOLUTION #2.

MSR 652



L652-5 400X  
FIGURE 5 - LARGEST PIT OBSERVED ON THE POLISHED IN178  
AFTER CHEMICAL MILLING IN SOLUTION #2.  
(PIT DEPTH IS APPROXIMATELY 0.001 INCH)

=====

=====

=====

=====

=====

=====

=====

=====

=====

=====

=====

=====

=====

=====

=====

=====

=====

=====

=====

=====

=====

=====

=====

**MSR 642: Metallurgical Evaluation of Two Starfish Heater Head Machining Test Samples**

TO: G. Antonelli  
FROM: S. Walak *SW*  
DATE: November 16, 1990  
SUBJECT: Metallurgical Evaluation of Two Starfish  
Heater Head Machining Test Samples

**INTRODUCTION**

On October 16, 1990 two samples were delivered to the Materials and Failure Analysis Laboratory for metallurgical evaluation. The samples were fabricated to demonstrate proposed methods for machining the pockets in the CTPC Starfish heater head. The test samples, MTI Part #1042-0280, were machined from annealed Inconel 718 at Speedring Incorporated, Cullman, AL.

The samples were machined from round bar stock using a combination of lapping, conventional milling, electrodischarge machining (EDM) and chemical milling. The outside of the parts were formed by lapping parallel faces on round bar stock and machine milling the remaining surfaces. Conventional milling was used to start the internal pocket in one of the lapped faces. EDM was used to finish the pocket to near final configuration. The entire part was then exposed to a chemical milling solution to remove an estimated 0.0008 inch recast layer from the EDM surface. Chemical milling was performed at room temperature using a solution of 80% nitric acid and 20% hydrofluoric acid. The milling time was reported to be several hours.

Metallographic sections were removed from each sample and prepared for microscopic examination. The sections were taken from the root, the side wall radius and the side wall of each sample.

**RESULTS**

Fine microcracks were observed in all of the as-polished cross sections. The cracks were intergranular and extended approximately 0.001 to 0.002 inches below the surface. The cracks were most severe on the EDM and the conventionally milled surfaces, Figures 1 and 2.

Examination of the polished and etched sections revealed that most of the EDM recast layer was removed by the chemical milling solution. Thin sections of the recast layer were observed at a few locations but were not directly related to the microcracks, Figure 3.

The microcracks appear to result from an interaction between the chemical milling solution and the residual stress layer generated during preliminary machining.

Corrosion experts at INCO Alloys, Huntington, WV have indicated that hydrogen assisted cracking or stress corrosion cracking in the residual stress layer is the probable source of the microcracks. Molecular hydrogen generated as a by product of the chemical milling operation is the most likely source of the problem.

#### CONCLUSIONS

High residual stress and the corrosive agent must be present simultaneously for microcracks to form. Elimination of either the corrosive agent or the residual stress will eliminate the cracking problem.

Annealing parts prior to chemical milling will remove the residual stress layer and should eliminate the cracking problem. The annealing heat treatment is performed at 1725 to 1750 °F for 15 to 30 minutes and is followed by an inert gas cool to room temperature.

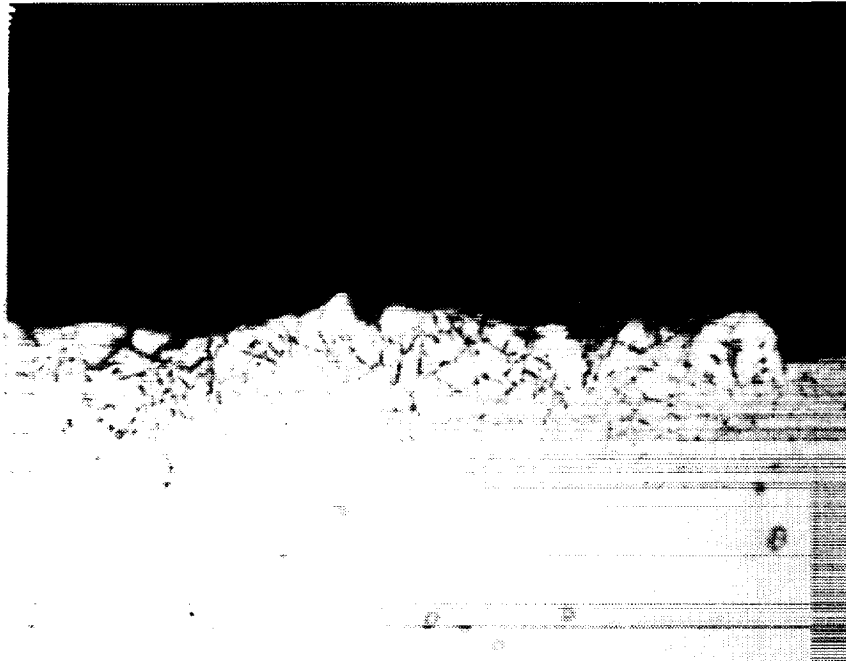
The microcracks may also be eliminated by chemically milling enough material to remove the entire residual stress layer. Chemical removal of approximately 0.003 inches of material from the machined part should eliminate the entire residual stress layer. Cracks would not be expected to propagate beyond this region.

#### RECOMMENDATIONS

Previous samples have been chemically milled without any incidence of surface cracking, see attached MSR 586. The chemical milling techniques described in MRS 586 should be used in removing the recast layer from the pockets of the starfish heater head.

Additional samples should be fabricated to assure that proper processing techniques have been established. The fabrication of additional samples should demonstrate that the annealing heat treatment and/or the removal of additional material by chemical milling will eliminate surface cracking.

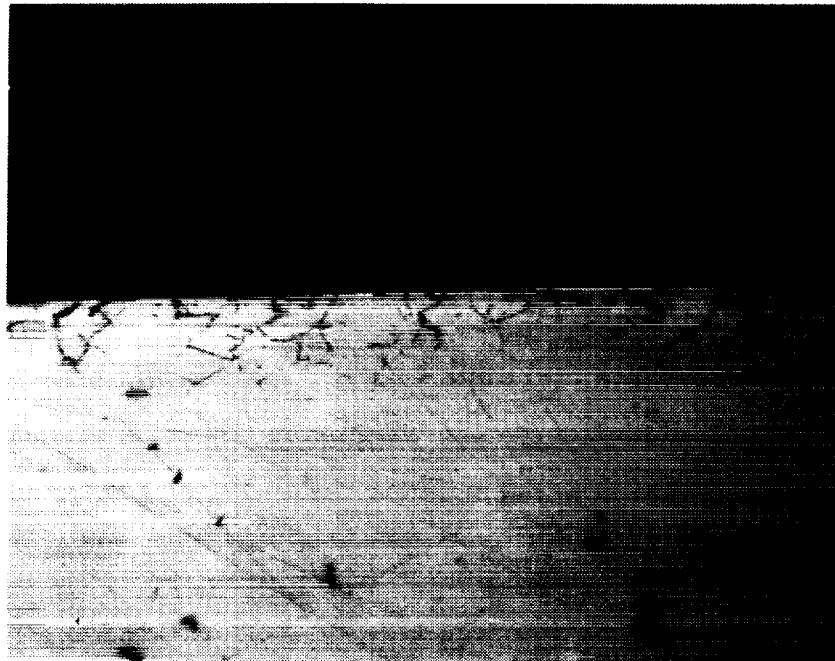
cc: P. Chapman  
M. Cronin  
M. Dhar  
G. Dochet  
D. Harris  
G. Smith



L642-2

400X

FIGURE 1 - SURFACE MICROCRACKS OBSERVED ON AN EDM  
AND CHEMICALLY MILLED SURFACE.

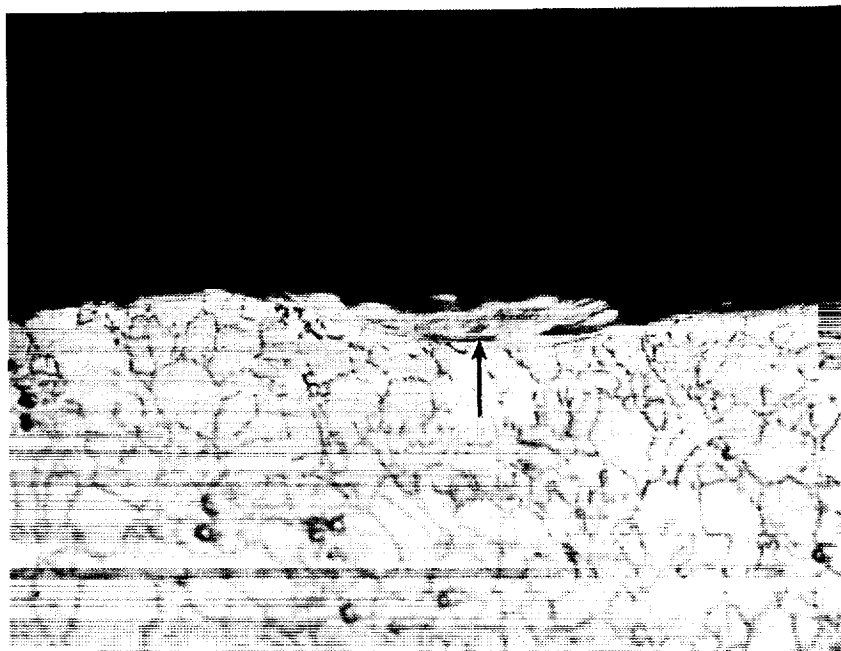


L642-5

400X

FIGURE 2 - SURFACE MICROCRACKS OBSERVED ON A  
CONVENTIONALLY MILLED AND CHEMICALLY  
MILLED SURFACE.





L642-10

400X

FIGURE 3 - REMAINS OF THE RECAST LAYER ON EDM  
POCKET SURFACE. (ARROW).



## MSR 586: Preliminary Evaluation of Chemical Milling as a Finishing Operation on Inconel 718

TO: M. Walsh  
FROM: S. Walak *SW*  
DATE: July 31, 1989  
Date:  
SUBJECT: Preliminary Evaluation of Chemical Milling as a  
Finishing Operation for Inconel 718

The chemical milling process has been discussed as a potential method for removing the EDM recast layer on the CTE Starfish Heater Head. The process is used commercially to remove EDM recast layers in IN718 and appears to be a strong candidate for use on the CTE. In this investigation, two Inconel 718 test samples were chemically milled at Tech Met Incorporated to evaluate the process as a possible finishing operation for the internal bore of the Heat Pipe Fatigue Test Specimen (HPFTS). The HPFTS is being designed to simulate material exposure conditions in the fin section of the CTE Star Fish Heater Head. Finishing the internal bore of the HPFTS by chemical milling will more closely represent the probable surface condition of the Inconel 718 in the fin section of the CTE Heater Head.

The test samples for chemical milling were 4 inch long bars with 0.5625 inch diameter holes drilled longitudinally through the bar center. One of the Inconel 718 test bars was solution annealed and the other was fully hardened according to AMS 5663.

Two steps were used in the milling process:

STEP 1) Activation Solution

65% HCl  
35% H<sub>2</sub>O  
130 Degrees F, 5 to 10 minutes

STEP 2) Chemical Milling Solution

68% HCl  
6% Nitric Acid  
3% Phosphoric Acid  
5% Hydrofluoric Acid  
18% Ferric Chloride  
120-130 Degrees F, Mill Rate 0.001 inch in 5 minutes

The inside diameter of the test samples were enlarged  $0.006 \pm 0.001$  inch by chemical milling. Inspection reports after milling confirmed that the requested

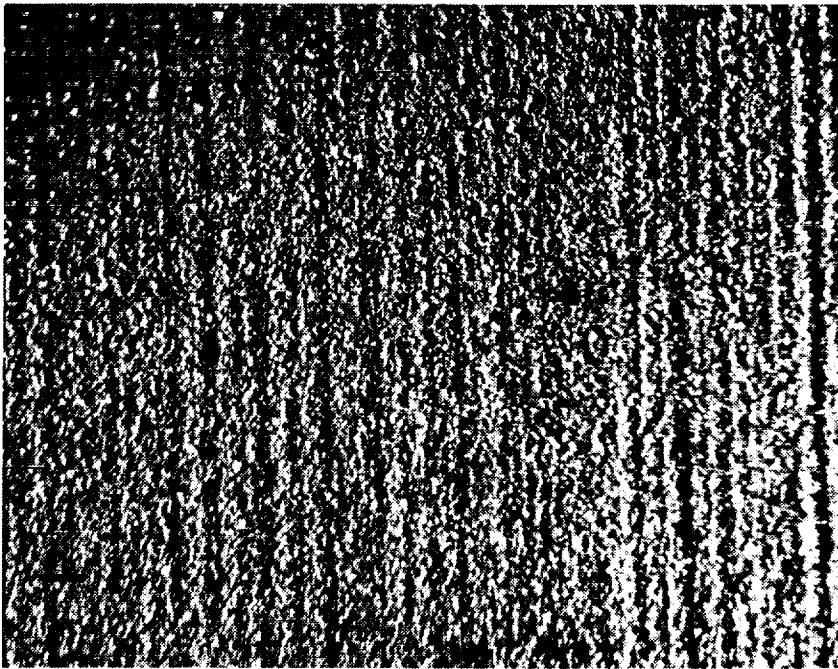
dimensional control was maintained, Appendix A. The surface roughness of the bore after milling was approximately 100 micro-inches on the annealed sample and 35 micro-inches on the aged hardened samples. The surface topography after milling appeared to duplicate the original machined surface, Figures 1 and 2.

Cross-sections through the chemically milled surfaces appeared to indicate that the roughened surface of the annealed material was a result of larger grains in this material, Figures 3 and 4. The surfaces of both samples appeared to be in good condition with no indications of surface cracks or pits.

Examination of the chemically milled surfaces in the Scanning Electron Microscope (SEM) revealed that the milling process left the non-metallic inclusions in the Inconel 718 raised above the metal surface, Figures 5 and 6. These inclusions could be deposited in the liquid metal during initial contact. The effect of small quantities of these materials in liquid sodium should be evaluated.

Chemical milling appears to be a sound method for finishing the Inconel 718 heat pipe fatigue test specimen. It has been shown that material removal can be controlled to  $\pm 0.0005$  inch and surface cracking or pitting is not a problem. Samples of electro-discharge machined Inconel 718 should be chemically milled to confirm that the process is applicable to the CTE Star Fish Heater Head.

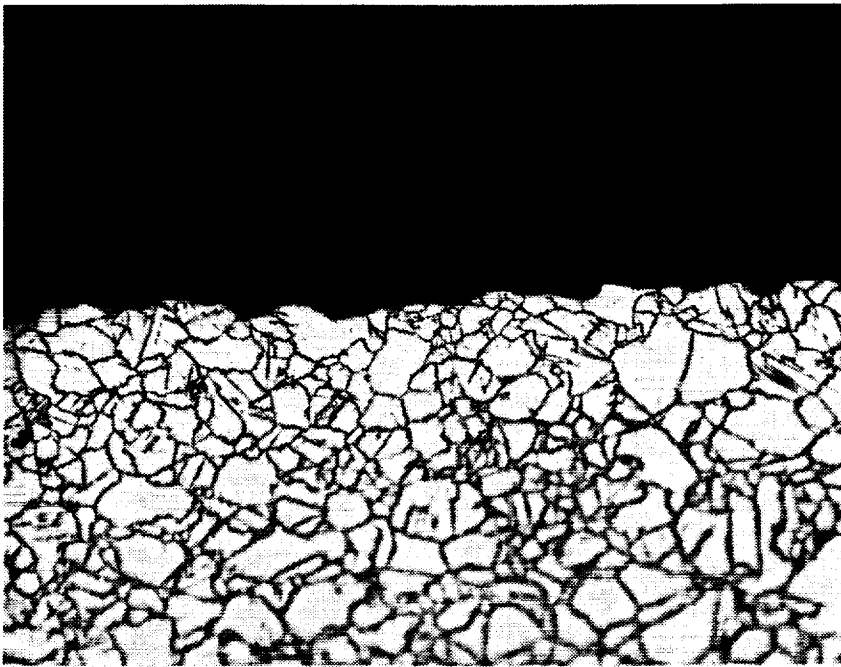
cc: G. Antonelli  
A. Brown  
M. Cronin  
M. Dhar  
G. Smith



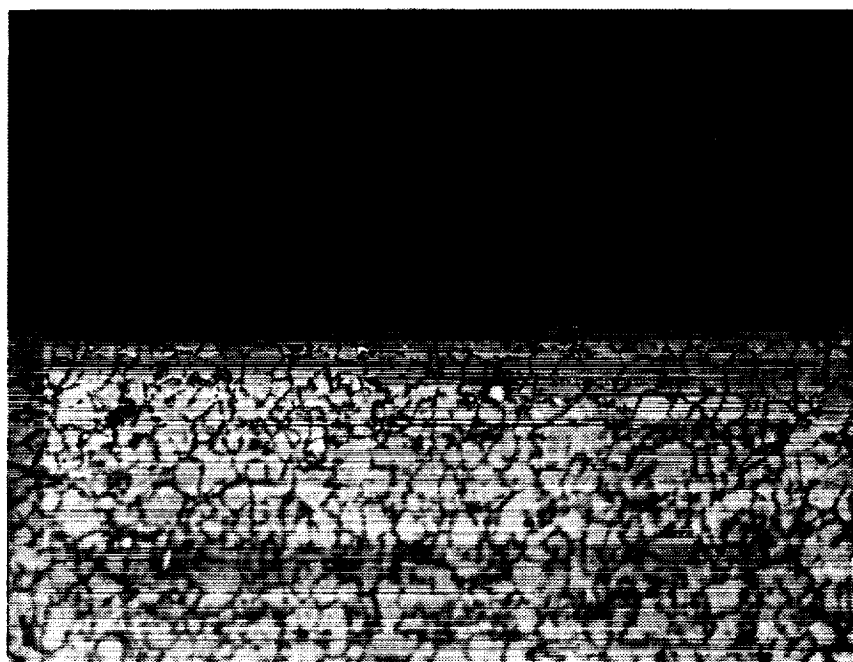
L586-1 20X  
FIGURE 1 - SURFACE TOPOGRAPHY OF THE ANNEALED  
IN718 AFTER CHEMICAL MILLING.



**L586-2** **20X**  
**FIGURE 2 - SURFACE TOPOGRAPHY OF THE AGE HARDENED**  
**IN718 AFTER CHEMICAL MILLING.**

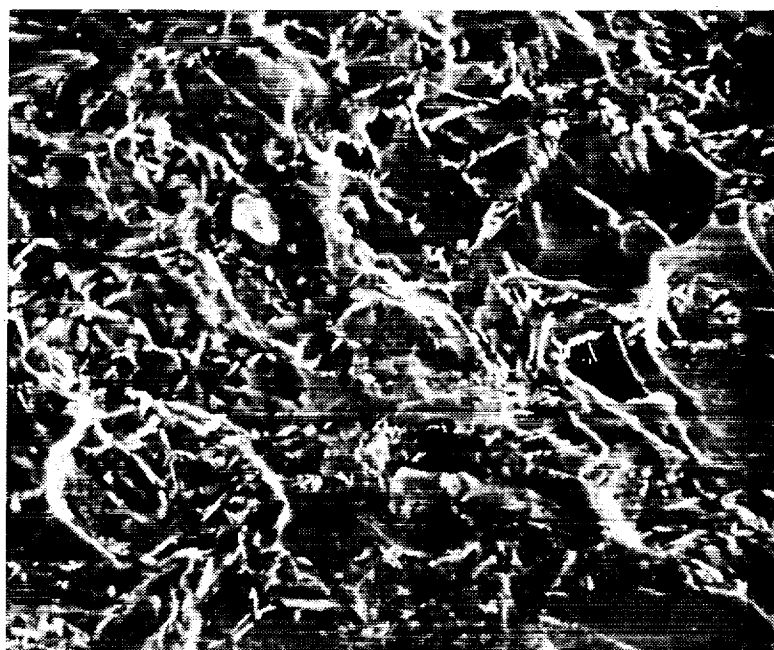


L586-31 400X  
FIGURE 3 - CROSS-SECTION SHOWING THE CHEMICALLY  
MILLED SURFACE OF THE ANNEALED IN718

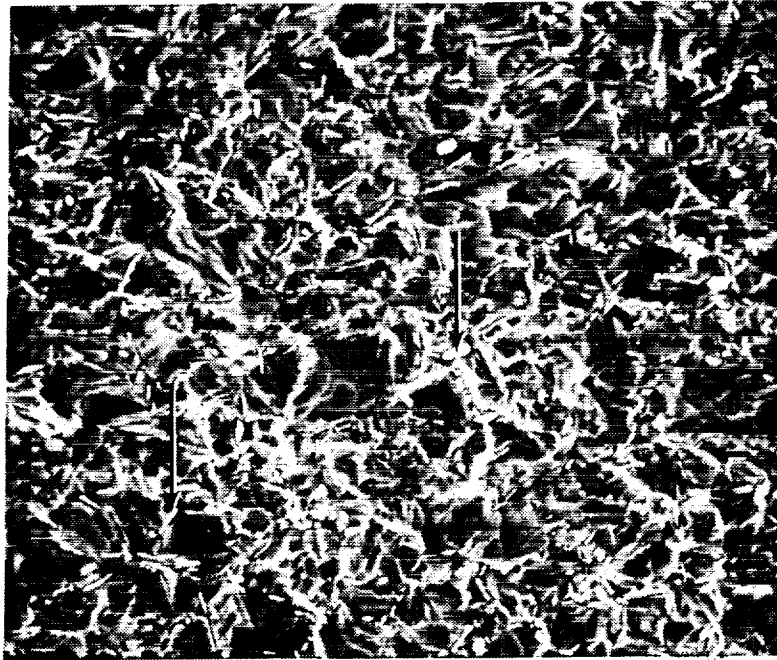


**S586-4** **400X**  
**FIGURE 4 - CROSS-SECTION SHOWING THE CHEMICALLY**  
**MILLED SURFACE OF THE AGE HARDENED IN718**





**S586-2** **1000X**  
**FIGURE 5 - CHEMICALLY MILLED SURFACE ON THE ANNEALED**  
**MATERIAL SHOWING EXPOSED INCLUSIONS (ARROWS)**



**S586-6** **1000X**  
**FIGURE 6 - CHEMICALLY MILLED SURFACE ON THE AGE**  
**HARDENED MATERIAL SHOWING EXPOSED INCLUSIONS (ARROWS)**

## APPENDIX A

DATE 5-8-99		ORDER NO.	INSPECTION RECORD		QUALITY	MATERIAL	QWR NO.	REV
SHEET NO. 1 OF 1		1050-91863			1	INCONEL 718		
NAME OF PART		SERIAL NUMBER	TIME		PLATING OR COATING			
Life Hardened Specimen		2						
DRAWING DIMENSIONS		ZONE	Pos #1	Pos #2	Pos #3	Pos #4	TEST	ACCEPT
							PHYS NO	REJECT
1	1/16" Ø		.5035	.5635	.5636	.5634		✓
2								
3	Roundness		.0001	.0001	.0001	.0001		✓
4								
5	Concentricity		.003	.0024	.001	.0038		✓
6								
7								
8								
9								
10								
11								
12								
13								
14								
15								
16								
17								
18								
19								
20								
21								
22								
23								
24								
25								

TYPE OF INSPECTION		CORRECT EACH TO	
<input type="checkbox"/> RECEIVING	<input type="checkbox"/> IN PROCESS - AT STATION	QC FILE PHOTO FILE PHOTO CONT.	DATE
		COMPANY INSPECTOR	5-8-99
		1. B. B. B.	
		SOURCE INSPECTION	
		PART OR LOT	
		ACCEPT	✓
		REJECT	

Rev. 1/86 821780

Nov 1/86 021780

DATE: 5-8-89		ORDER NO.	INSPECTION RECORD		QTY	MATERIAL	DWG NO.	REV
SHEET NO. 1 OF 1		1050-91P03			1	INCOREL 718		
NAME OF PART		SERIAL NUMBER	HEAT TREAT		PLATING OR COATING			
Annealed Specimen		1						
DRAWING DIMENSIONS		ZONE	Pos 1	Pos 2	Actual Dimension	Pos 3	Pos 4	SIZE HARD NO.
1	11010 P		.5640	.5638		.5635	.5635	✓
2			.0002	.0002		.0002	.0003	✓
3	Roundness		.010	.0074		.0048	.0034	✓
4	Concentricity							
5								
6								
7								
8								
9								
10								
11								
12								
13								
14								
15								
16								
17								
18								
19								
20								
21								
22								
23								
24								
25								

TYPE OF INSPECTION		COMES 1 EACH TO		DATE		PART OR LOT	
<input type="checkbox"/> RECEIVING	<input type="checkbox"/> IN PROCESS - AT STATION	QC FEE PROJ FEE PHOD CONT.		5-8-89		ACCEPT	
<input type="checkbox"/> QUOTE		COMPANY INSPECTOR		T. Bentley		REJECT	
		SOURCE INSPECTOR					

Rev. 1/88 021780



DATE 5-11-87		ORDER NO. 1250-91863	INSPECTION RECORD		QUANTITY 1	MATERIAL 111CONE 718	DWG NO.	REV.
NAME OF PART UNLOCATED SPECIMEN			SERIAL NUMBER	TEST TREAT	PLATING OR COATING	Chem. milled	DWG NO.	REV.
DRAWING DIMENSIONS			ZONE	Pos #1	Pos #2	ACTUAL DIMENSION	Pos #3	Pos #4
1	Hole Ø			Pos #1	Pos #2		Pos #3	Pos #4
2				.5675	.5694		.5696	.5695
3	Roundness			.0025	.0005		.0004	.0006
4	Concentricity			.010	.0076		.0050	.0032
5								
6								
7								
8								
9								
10								
11								
12								
13								
14								
15								
16								
17								
18								
19								
20								
21								
22								
23								
24								
25								

TYPE OF INSPECTION

☐ RECEIVING

☐ IN PROCESS - AT STATION

☐ OTHER

CONES LEACH TO QC FILE PRIOR TO PROD CONT.

COMPANY INSPECTOR

DATE 5-17-87

PART OR LOT

ACCEPT

REJECT

Rev. 1/86 821780





**MSR 690: Metallurgical Evaluation of CTPC Cooler Assembly Fabrication Samples**

**To:** G. Antonelli  
**From:** S. Walak *SW*  
**Date:** 25 March 1992  
**Subject:** Metallurgical Evaluation of Component Test Power Converter Cooler Assembly Fabrication Samples, MSR 690

Three test samples and several tube assemblies which demonstrated fabrication techniques proposed for use on the CTPC cooler were delivered to the Materials Analysis Laboratory for metallurgical examination between October 1991 and February 1992. The cooler tube to insert braze joint and the cooler tube to outer shell electron beam weld were the primary focus of the metallurgical evaluation.

The results of the metallurgical analysis were reported verbally to expedite improvements in the fabrication process. The present report will briefly summarize the final assembly procedure and the results of the three demonstration samples.

The cooler samples consisted of an Inconel 718 outer shell, Inconel 625 cooler tubes and Nickel 201 tube inserts, Figures 1 and 2. The sample outer shell was fabricated from a cylinder, approximately 2.5 inches long and 3.0 inch outside diameter, with 0.25 inch thick

IN718 plates electron beam welded to each end. A series of 0.375 inch diameter holes were drilled into each end plate for installation of the cooler tubes. The cooler tubes were IN625 with electroless nickel plating applied to the entire I.D. surface and a 0.025 inch length at each end of the O.D. surface. The cooler tube inserts were bonded to the cooler tubes by brazing with the electroless nickel-phosphorous plating.

The cooler test sample fabrication procedures were revised slightly after assembly of the first and second samples. The procedure used for the final sample is expected to be identical to that used on the CTPC cooler. The final test sample was fabricated as follows:

- 1) Remove electroless Ni plating from 0.25" length at each tube end (I.D. and O.D.)
- 2) Place tubes into welded cooler shell  
(Approximately 0.001" loose fit)
- 3) Place tube inserts into tubes  
(Approximately 0.001" loose fit)
- 4) Electron Beam Weld cooler tube to cooler shell
- 5) Tack weld insert to cooler tubes
- 6) Braze insert to cooler tube

## RESULTS

Individual cooler tube and insert braze assemblies were the first test hardware to be examined. Metallographic examination was performed on 5 transverse sections from one tube and a full length longitudinal section from a second tube. The braze joint between the tube and tube insert appeared to be of very good quality,

Figure 3. Some porosity and unbonded regions were observed at several locations along the braze joint, Figures 4 and 5. Measurements of the porosity and unbonded length showed that more than 82% of the braze joint examined was bonded well. The unbonded regions appeared to concentrate near one end of the tubes. No definite answer was obtained for this phenomenon but it was postulated that braze alloy may have been scraped from the inner diameter of the tube during assembly leaving the joint insufficient braze alloy at one end of the tube.

The cooler tubes in the first full tube and shell assembly were initially brazed to the shell assembly. Leak checks of the assembly after brazing revealed a significant amount of leakage at the tube to shell braze. Attempts to seal the leaks with electron beam welding resulted in more leakage and extensive cracking. The cracking was attributed to phosphorous contamination from the nickel phosphorous plating on the cooler tubes.

The difficulties encountered in brazing the cooler tubes resulted in a decision to attempt electron beam welding as the primary method of joining the tubes to the shell. Prior to electron beam welding the nickel phosphorous plating would be removed from a 0.25 inch length of the tube to eliminate phosphorous contamination cracking. These changes in fabrication procedure were incorporated into the second cooler tube and shell assembly. The first assembly was not subjected to metallographic analysis because it was no

longer representative of the revised fabrication procedure.

The second cooler assembly was examined for both braze and weld joint quality. The welds between the cooler tube and outer shell contained no cracks or incomplete fusion but relatively large pores were observed at the base of the welds, Figure 6. The minimum thickness of the weld, excluding the porosity, was approximately 0.017 to 0.020 inches. It was recommended at the time that electron beam weld parameters be adjusted to obtain additional weld penetration.

The braze joint quality was good and appeared to be similar to the first sample examined.

The third cooler assembly was fabricated using procedures finalized for use with actual engine hardware. The cooler tube inserts were dimensioned with approximately 0.001 inch clearance to facilitate assembly. Electroless nickel plating was removed from the tube ends prior to welding. Metallurgical examination of the brazed tubes indicated a joint efficiency of approximately 90% in two tubes sectioned at four locations, Figure 7. The weld between the tube and tube shell again contained relatively large pores at the base of the weld but no indications of cracking or incomplete fusion were present, Figure 8.

## CONCLUSIONS

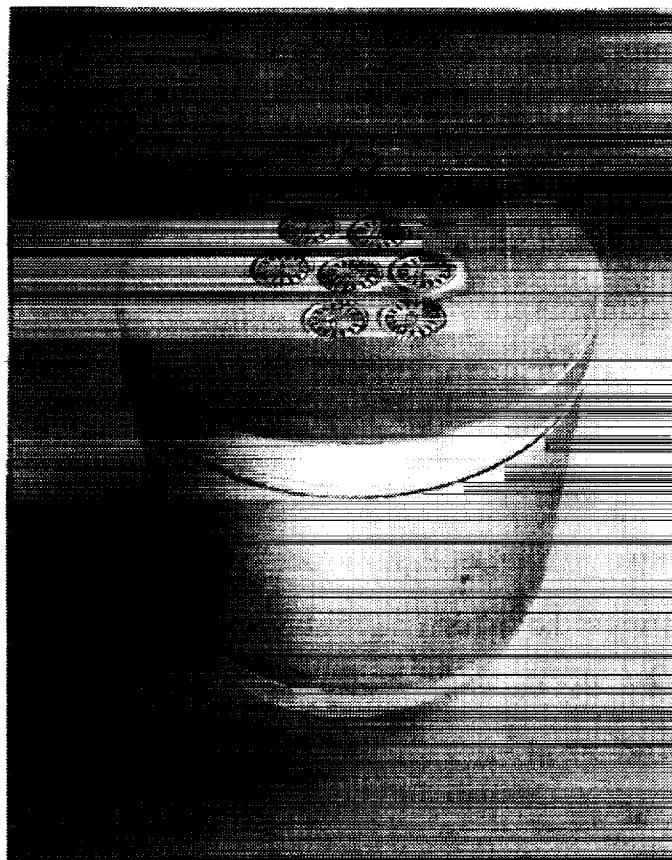
Three samples were used to demonstrate cooler assembly techniques and evaluate the quality of the tube to tube insert braze and the tube to tube shell electron beam weld. Several changes in the assembly techniques were identified and incorporated into the final fabrication approach.

The metallurgical evaluation confirmed that the tube to tube insert braze was of very good quality with approximately 90% braze efficiency in the final demonstration assembly.

The weld joint between the cooler tube and shell appeared to be of acceptable quality. Large pores at the base of the weld were observed and attempts to eliminate them should be made. The cause of the pores is not certain but may be a result of the gap between the cooler tube and shell.

/dr

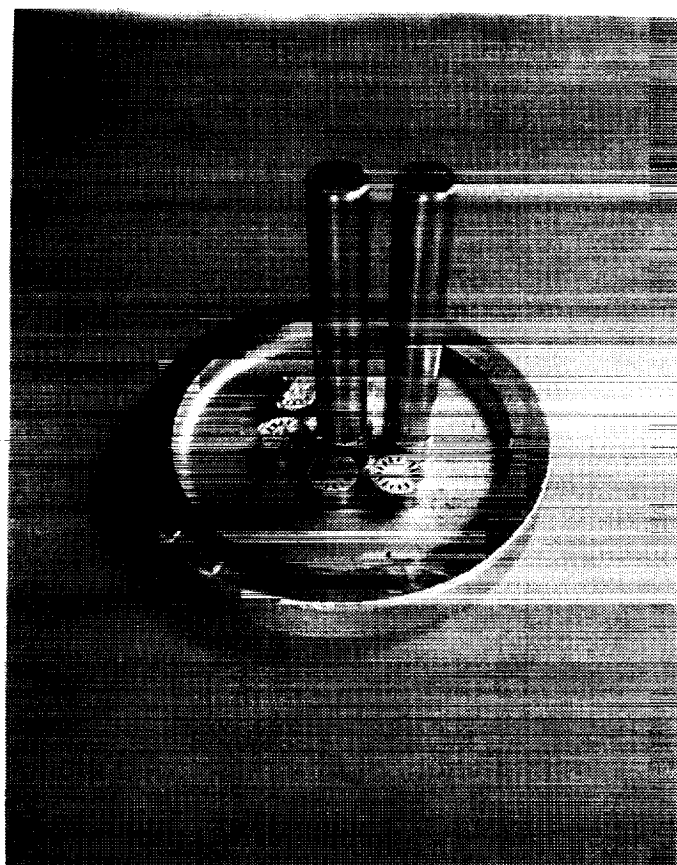
cc: P. Chapman  
M. Cronin  
M. Dhar



L713-02

0.8X

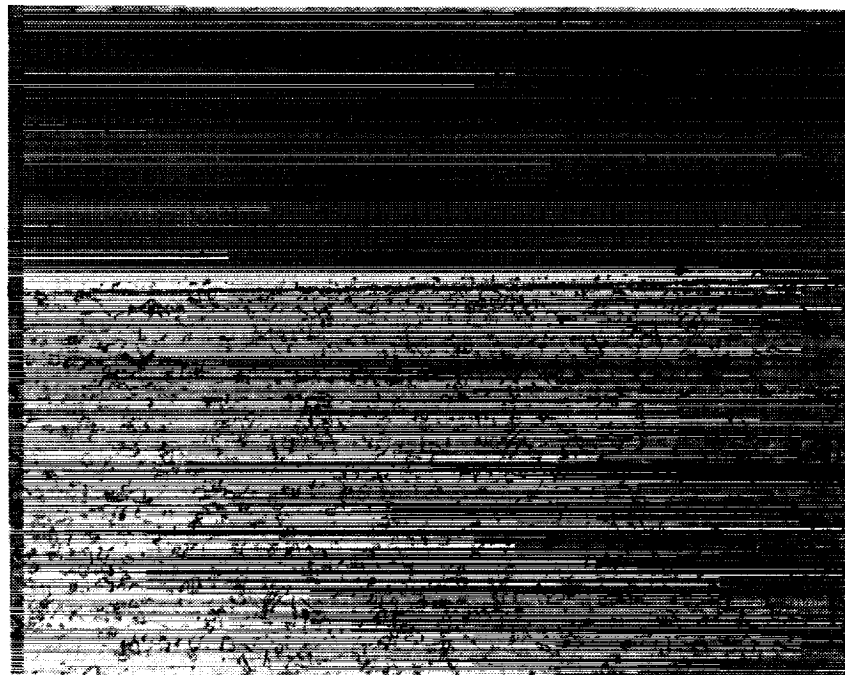
Figure 1 - Cooler Fabrication Sample



L713-04

0.8X

**Figure 2 - Cooler Fabrication Sample  
After Initial Sectioning  
for Metallographic Examination**

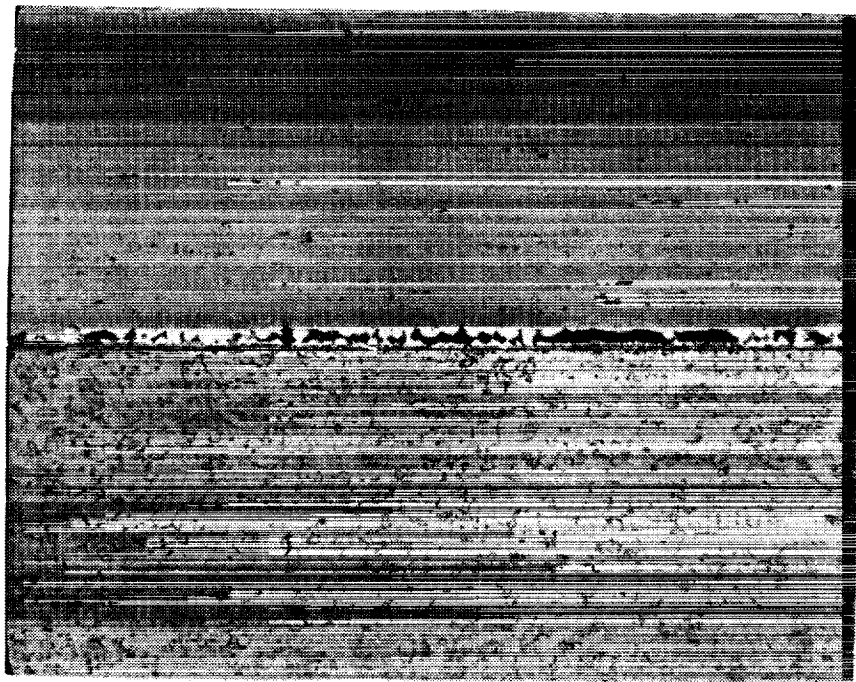


L713-04

0.8X

**Figure 3 - Photomicrograph of Cooler Tube  
(Top) to Insert (Bottom) Braze  
Joint (Longitudinal Section)**

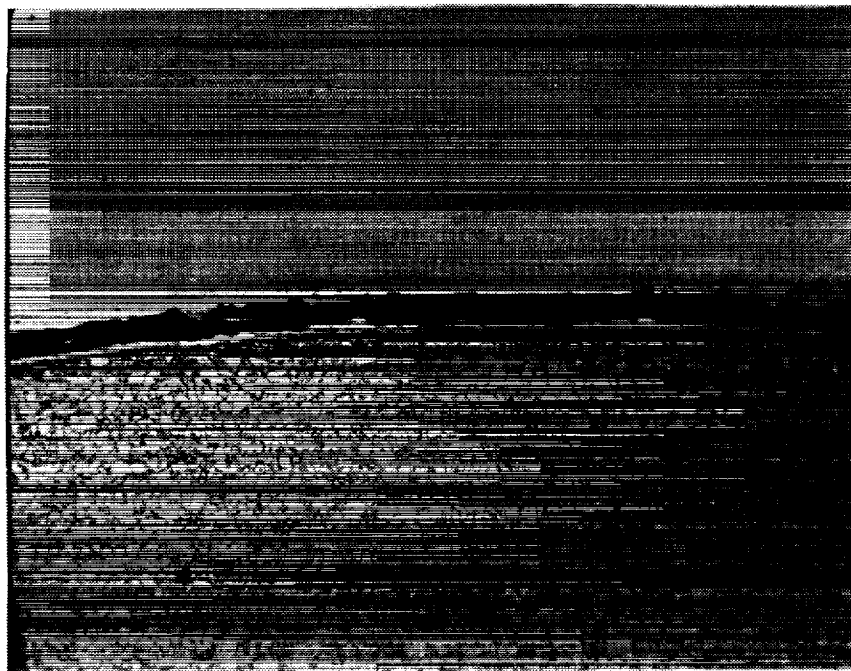




L672-08

125X

**Figure 4 - Cooler Tube (Top) to Insert  
(Bottom) Braze Joint in a  
Region of Porosity  
(Longitudinal Section)**



L672-11

125X

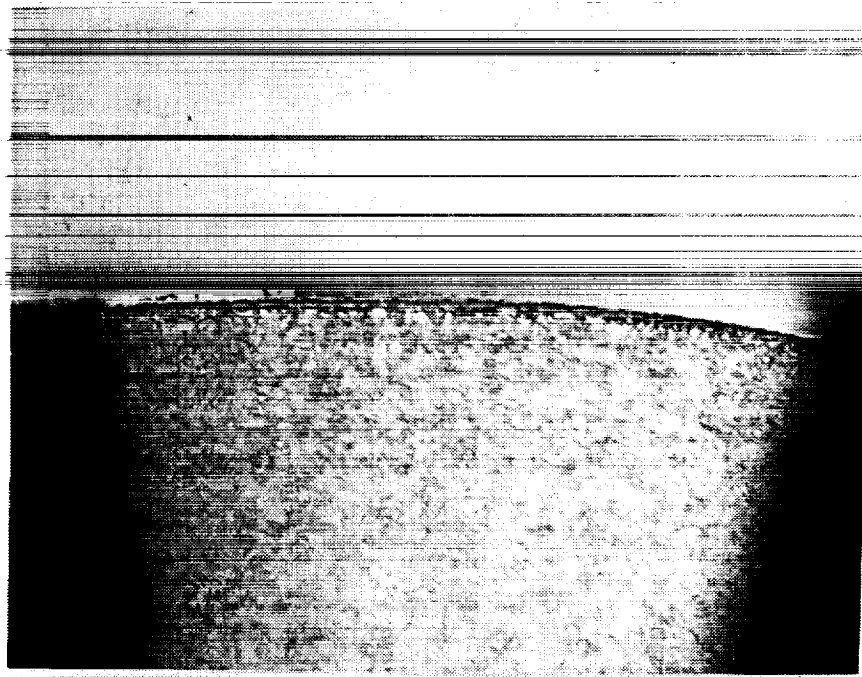
**Figure 5 - Cooler Tube to Insert Braze  
Joint in an Unbonded Region  
(Transverse Section)**



L686-02

125X

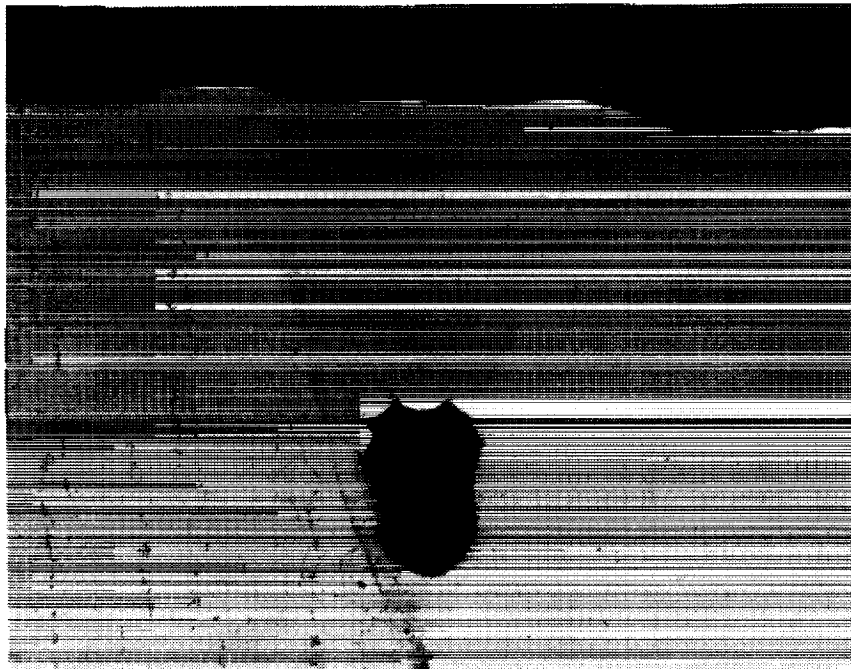
**Figure 6 - Metallographic Section Through  
a Cooler Tube to Shell Electron  
Beam Weld. Note Porosity at Arrows**



**L690-13**

**90X**

**Figure 7 - Representative Cooler Tube  
(Top) to Insert (Bottom)  
Braze Joint from the Third  
Test Sample**



L690-04

90X

**Figure 8 - Cooler Tube to Shell Electron  
Beam Weld. Note Porosity at  
Base of Weld**

[illegible]

1. 2. 3. 4. 5. 6. 7. 8. 9. 10. 11. 12. 13. 14. 15. 16. 17. 18. 19. 20. 21. 22. 23. 24. 25. 26. 27. 28. 29. 30. 31. 32. 33. 34. 35. 36. 37. 38. 39. 40. 41. 42. 43. 44. 45. 46. 47. 48. 49. 50. 51. 52. 53. 54. 55. 56. 57. 58. 59. 60. 61. 62. 63. 64. 65. 66. 67. 68. 69. 70. 71. 72. 73. 74. 75. 76. 77. 78. 79. 80. 81. 82. 83. 84. 85. 86. 87. 88. 89. 90. 91. 92. 93. 94. 95. 96. 97. 98. 99. 100. 101. 102. 103. 104. 105. 106. 107. 108. 109. 110. 111. 112. 113. 114. 115. 116. 117. 118. 119. 120. 121. 122. 123. 124. 125. 126. 127. 128. 129. 130. 131. 132. 133. 134. 135. 136. 137. 138. 139. 140. 141. 142. 143. 144. 145. 146. 147. 148. 149. 150. 151. 152. 153. 154. 155. 156. 157. 158. 159. 160. 161. 162. 163. 164. 165. 166. 167. 168. 169. 170. 171. 172. 173. 174. 175. 176. 177. 178. 179. 180. 181. 182. 183. 184. 185. 186. 187. 188. 189. 190. 191. 192. 193. 194. 195. 196. 197. 198. 199. 200. 201. 202. 203. 204. 205. 206. 207. 208. 209. 210. 211. 212. 213. 214. 215. 216. 217. 218. 219. 220. 221. 222. 223. 224. 225. 226. 227. 228. 229. 230. 231. 232. 233. 234. 235. 236. 237. 238. 239. 240. 241. 242. 243. 244. 245. 246. 247. 248. 249. 250. 251. 252. 253. 254. 255. 256. 257. 258. 259. 260. 261. 262. 263. 264. 265. 266. 267. 268. 269. 270. 271. 272. 273. 274. 275. 276. 277. 278. 279. 280. 281. 282. 283. 284. 285. 286. 287. 288. 289. 290. 291. 292. 293. 294. 295. 296. 297. 298. 299. 300. 301. 302. 303. 304. 305. 306. 307. 308. 309. 310. 311. 312. 313. 314. 315. 316. 317. 318. 319. 320. 321. 322. 323. 324. 325. 326. 327. 328. 329. 330. 331. 332. 333. 334. 335. 336. 337. 338. 339. 340. 341. 342. 343. 344. 345. 346. 347. 348. 349. 350. 351. 352. 353. 354. 355. 356. 357. 358. 359. 360. 361. 362. 363. 364. 365. 366. 367. 368. 369. 370. 371. 372. 373. 374. 375. 376. 377. 378. 379. 380. 381. 382. 383. 384. 385. 386. 387. 388. 389. 390. 391. 392. 393. 394. 395. 396. 397. 398. 399. 400. 401. 402. 403. 404. 405. 406. 407. 408. 409. 410. 411. 412. 413. 414. 415. 416. 417. 418. 419. 420. 421. 422. 423. 424. 425. 426. 427. 428. 429. 430. 431. 432. 433. 434. 435. 436. 437. 438. 439. 440. 441. 442. 443. 444. 445. 446. 447. 448. 449. 450. 451. 452. 453. 454. 455. 456. 457. 458. 459. 460. 461. 462. 463. 464. 465. 466. 467. 468. 469. 470. 471. 472. 473. 474. 475. 476. 477. 478. 479. 480. 481. 482. 483. 484. 485. 486. 487. 488. 489. 490. 491. 492. 493. 494. 495. 496. 497. 498. 499. 500. 501. 502. 503. 504. 505. 506. 507. 508. 509. 510. 511. 512. 513. 514. 515. 516. 517. 518. 519. 520. 521. 522. 523. 524. 525. 526. 527. 528. 529. 530. 531. 532. 533. 534. 535. 536. 537. 538. 539. 540. 541. 542. 543. 544. 545. 546. 547. 548. 549. 550. 551. 552. 553. 554. 555. 556. 557. 558. 559. 560. 561. 562. 563. 564. 565. 566. 567. 568. 569. 570. 571. 572. 573. 574. 575. 576. 577. 578. 579. 580. 581. 582. 583. 584. 585. 586. 587. 588. 589. 590. 591. 592. 593. 594. 595. 596. 597. 598. 599. 600. 601. 602. 603. 604. 605. 606. 607. 608. 609. 610. 611. 612. 613. 614. 615. 616. 617. 618. 619. 620. 621. 622. 623. 624. 625. 626. 627. 628. 629. 630. 631. 632. 633. 634. 635. 636. 637. 638. 639. 640. 641. 642. 643. 644. 645. 646. 647. 648. 649. 650. 651. 652. 653. 654. 655. 656. 657. 658. 659. 660. 661. 662. 663. 664. 665. 666. 667. 668. 669. 670. 671. 672. 673. 674. 675. 676. 677. 678. 679. 680. 681. 682. 683. 684. 685. 686. 687. 688. 689. 690. 691. 692. 693. 694. 695. 696. 697. 698. 699. 700. 701. 702. 703. 704. 705. 706. 707. 708. 709. 710. 711. 712. 713. 714. 715. 716. 717. 718. 719. 720. 721. 722. 723. 724. 725. 726. 727. 728. 729. 730. 731. 732. 733. 734. 735. 736. 737. 738. 739. 740. 741. 742. 743. 744. 745. 746. 747. 748. 749. 750. 751. 752. 753. 754. 755. 756. 757. 758. 759. 760. 761. 762. 763. 764. 765. 766. 767. 768. 769. 770. 771. 772. 773. 774. 775. 776. 777. 778. 779. 780. 781. 782. 783. 784. 785. 786. 787. 788. 789. 790. 791. 792. 793. 794. 795. 796. 797. 798. 799. 800. 801. 802. 803. 804. 805. 806. 807. 808. 809. 810. 811. 812. 813. 814. 815. 816. 817. 818. 819. 820. 821. 822. 823. 824. 825. 826. 827. 828. 829. 830. 831. 832. 833. 834. 835. 836. 837. 838. 839
---

Year	1990	1991	1992	1993	1994	1995	1996	1997	1998	1999	2000	2001	2002	2003	2004	2005	2006	2007	2008	2009	2010	2011	2012	2013	2014	2015	2016	2017	2018	2019	2020	2021	2022	2023	2024	2025	2026	2027	2028	2029	2030	2031	2032	2033	2034	2035	2036	2037	2038	2039	2040	2041	2042	2043	2044	2045	2046	2047	2048	2049	2050	2051	2052	2053	2054	2055	2056	2057	2058	2059	2060	2061	2062	2063	2064	2065	2066	2067	2068	2069	2070	2071	2072	2073	2074	2075	2076	2077	2078	2079	2080	2081	2082	2083	2084	2085	2086	2087	2088	2089	2090	2091	2092	2093	2094	2095	2096	2097	2098	2099	2100
1990	1991	1992	1993	1994	1995	1996	1997	1998	1999	2000	2001	2002	2003	2004	2005	2006	2007	2008	2009	2010	2011	2012	2013	2014	2015	2016	2017	2018	2019	2020	2021	2022	2023	2024	2025	2026	2027	2028	2029	2030	2031	2032	2033	2034	2035	2036	2037	2038	2039	2040	2041	2042	2043	2044	2045	2046	2047	2048	2049	2050	2051	2052	2053	2054	2055	2056	2057	2058	2059	2060	2061	2062	2063	2064	2065	2066	2067	2068	2069	2070	2071	2072	2073	2074	2075	2076	2077	2078	2079	2080	2081	2082	2083	2084	2085	2086	2087	2088	2089	2090	2091	2092	2093	2094	2095	2096	2097	2098	2099	2100	

[illegible][illegible][illegible][illegible]

## MSR 640: Displacer Dome to Displacer Base Braze Test Evaluation

TO: G. Antonelli  
FROM: S. Walak *SW*  
DATE: February 8, 1991  
SUBJECT: Displacer Dome to Displacer Base Braze Test Evaluation

Six samples representing the braze joint between the Inconel 718 displacer dome and the beryllium displacer base were received by the Metallurgy and Failure Analysis Group for evaluation. Metallographic sections were prepared from each of the samples and examined under an optical microscope. The strength of each braze joint was evaluated qualitatively by peeling the IN718 ring from the beryllium ring after sectioning. Room temperature compressive shear strength tests were performed on two assemblies brazed using the most promising temperature cycle.

Electrolytic plating was used to apply the braze alloy to all of the assemblies. A layer of silver, 0.001 inches in thickness, was deposited on the beryllium. A layer of copper, 0.0003 inches in thickness, was then deposited over the silver. When heated to the brazing temperature this combination of silver and copper was expected to melt and form an alloy similar in composition to BAg-8. A flash of electroless nickel, 0.0003 inches in thickness, was applied to the IN718 to improve surface wetting and braze flow.

Prior to brazing, all of the parts were heated at 1325 to 1375°F for 5 minutes to test the plating adhesion. The parts were then assembled and vacuum brazed at temperatures between 1435°F and 1520°F.

**RESULTS**

The first assembly was brazed at temperatures between 1455°F and 1475°F for 5 minutes. This cycle provided the best results of all the braze cycles tested. Three samples were brazed under these conditions. The braze joint thickness was 0.001 to 0.002 inches and full braze alloy penetration was observed. Some areas of the braze appeared to be copper rich, but alloy melting appeared to be nearly complete, Figure 1.

During metallographic sectioning pieces the IN718 ring pulled away from the beryllium. Several other sections were removed and no debonding was observed. The joint failures occurred at the beryllium to braze alloy interface.

Two additional assemblies were brazed at 1455 to 1475°F. These rings were brazed with a slight offset so that a room temperature compressive shear test

could be performed. The first assembly was subjected to a 20,000 pound load which generated approximately 4040 psi shear stress in the joint. The load was applied and removed ten times without failure.

This assembly was sectioned after compression testing. Several pieces were cut from the ring. During sectioning the IN718 ring was pulled from the beryllium in some areas while in others debonding was not observed. Attempts to pry the IN718 ring from the beryllium showed that significant force was required to initiate a crack in the braze joint. The failures in this assembly occurred at the electroless nickel to IN718 interface, Figure 2.

The final assembly brazed at 1455 to 1475°F was also subjected to a room temperature compressive shear test. The maximum load at failure was 30,000 pounds, approximately 6060 psi in shear. The failure occurred at the beryllium to braze alloy interface, Figure 3.

Two assemblies were brazed at 1500°F and 1520°F for 10 to 15 minutes. Attempts to section these samples resulted in complete separation of the Inconel from the beryllium. Large sections of the joint could be debonded with minimal hand force. Metallographic sections showed that the joint failure occurred in the diffusion zone between the beryllium and the braze alloy, Figure 4. These braze joints were significantly weaker than those brazed at the intermediate temperature, 1455 - 1475°F.

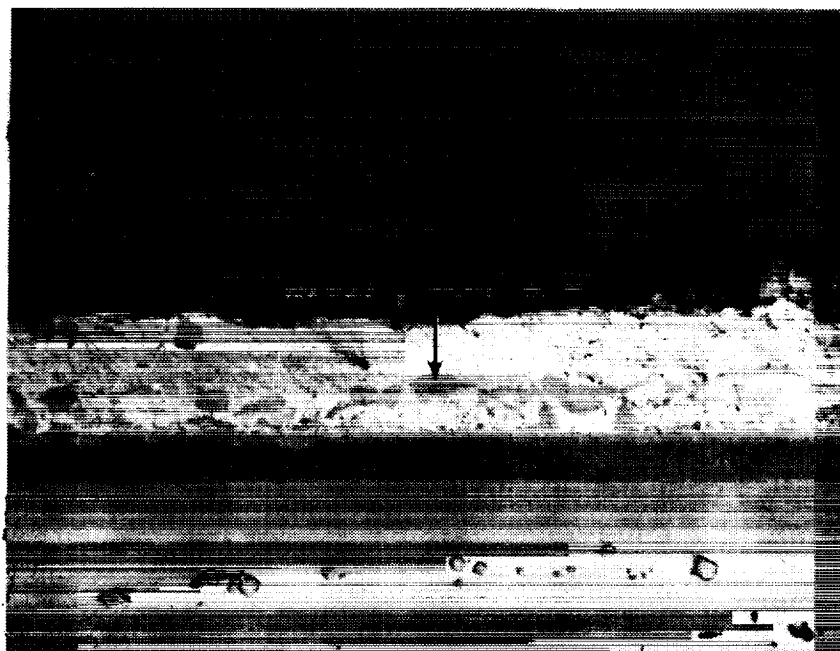
A single sample was brazed at 1435 to 1455°F for 5 minutes. This low temperature sample performed similar to the intermediate temperature braze during sectioning. Several pieces debonded during sectioning while others survived. Metallographic sections revealed that the copper plating in the braze joint had not completely melted, Figure 5. The braze joint could be separated with hand pressure and seemed to be weaker than the intermediate temperature sample. The failures occurred at the interface between the Be and the braze alloy.

## CONCLUSIONS

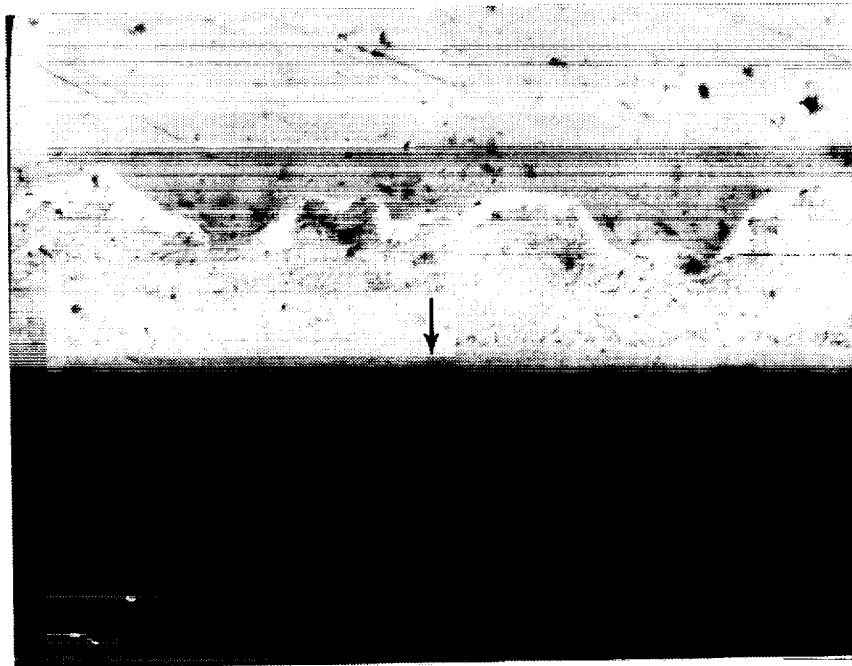
The intermediate temperature braze cycle, 1455 - 1475°F for 5 minutes, produced the strongest braze joints. Full joint penetration and nearly complete melting were observed. Braze joint failures during sectioning indicate that the tensile strength of the braze was relatively low. However, the compressive shear strength was determined to be 6060 psi at room temperature. Shear loads expected in the braze joint during actual engine operation have been estimated at less than 100 psi. It appears that the intermediate temperature braze cycle will provide adequate strength in actual operation.

Additional samples to be tested at operating temperatures under fatigue loads should be tested to confirm the mechanical performance of these joints.



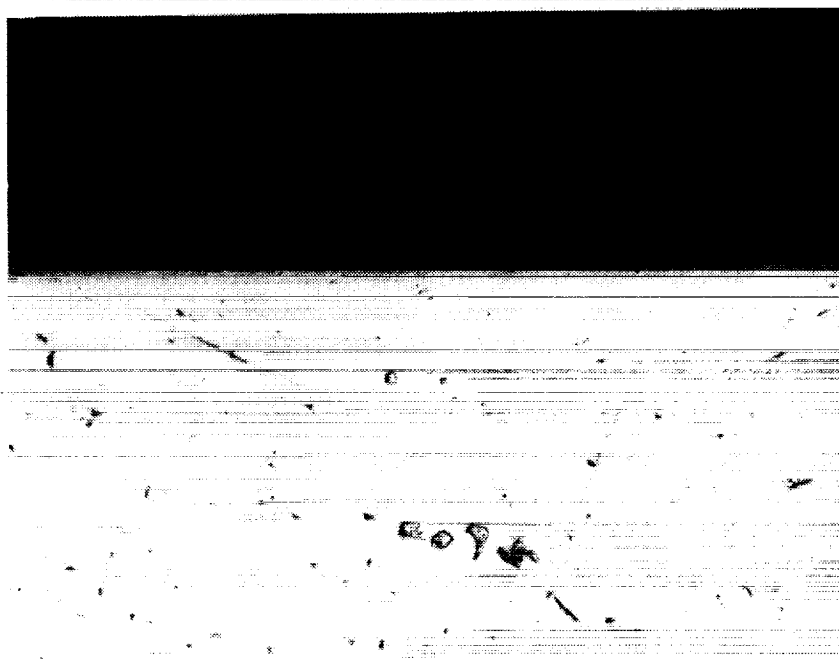


L640-1 400X  
FIGURE 1 - BERYLLIUM (TOP) TO IN718 (BOTTOM) BRAZE  
JOINT SHOWING COPPER RICH REGIONS (ARROW)



L640-9

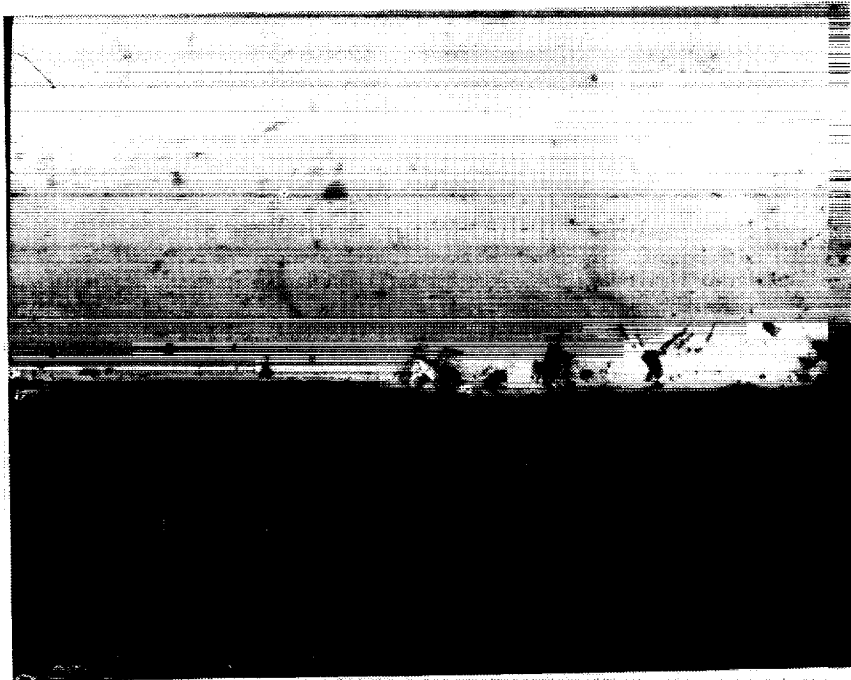
400X



L640-10

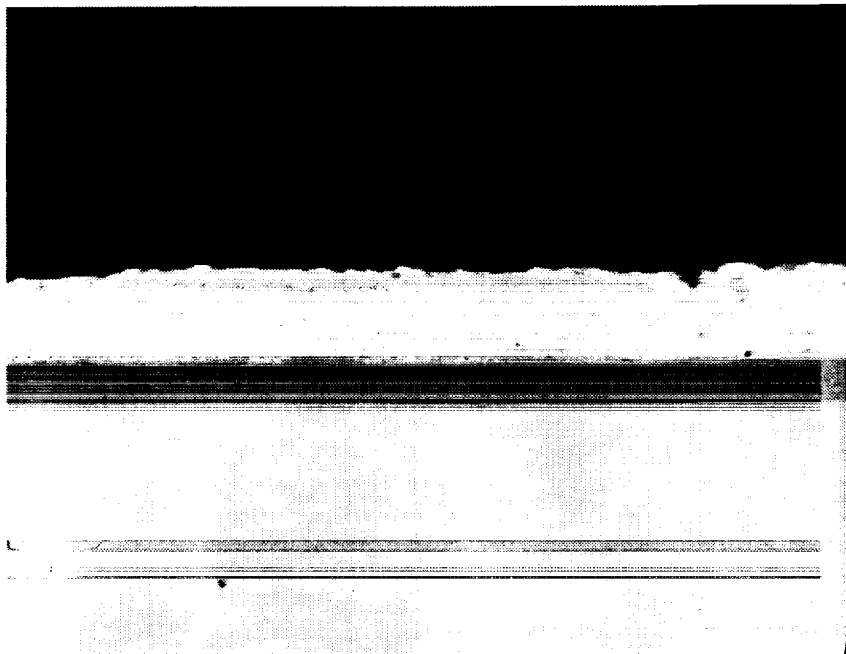
400X

FIGURE 2 - BERYLLIUM WITH BRAZE ALLOY ATTACHED (TOP) AND IN718 (BOTTOM) SHOWING FAILURE AT THE ELECTROLESS NICKEL (ARROW) TO IN718 INTERFACE.



L640-11

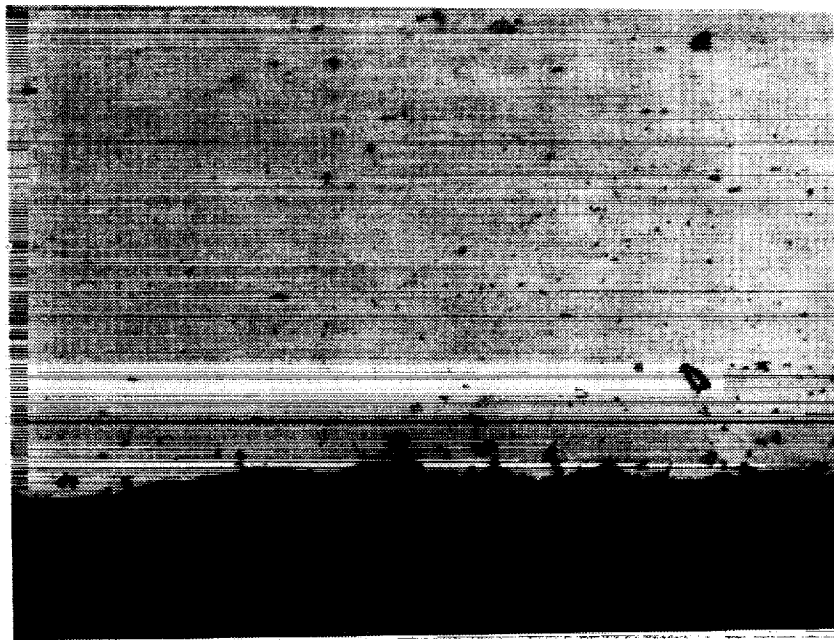
400X



L640-12

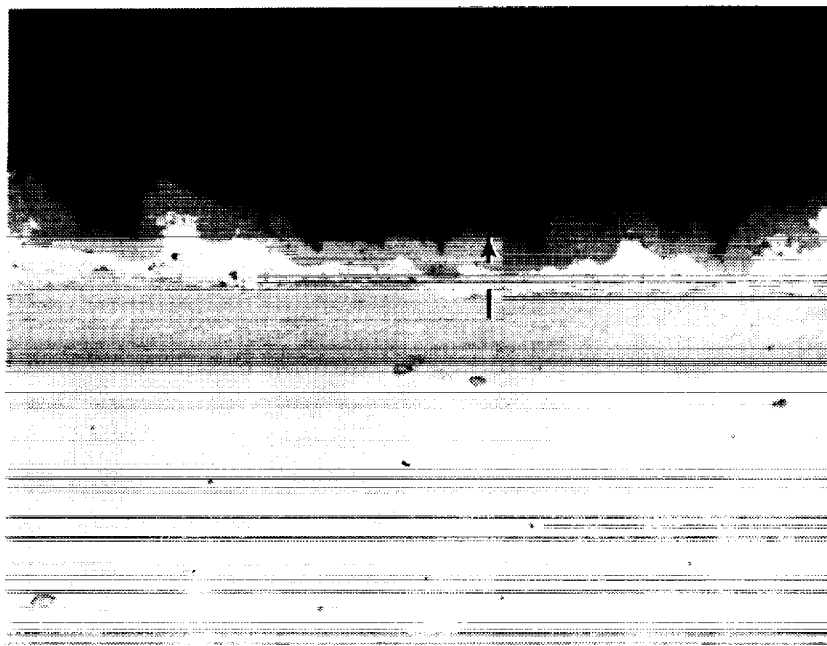
400X

FIGURE 3 - BERYLLIUM (TOP) AND IN718 (BOTTOM) BRAZE JOINT AFTER SHEAR TEST SHOWING FAILURE AT THE BERYLLIUM TO BRAZE METAL INTERFACE.



L640-5

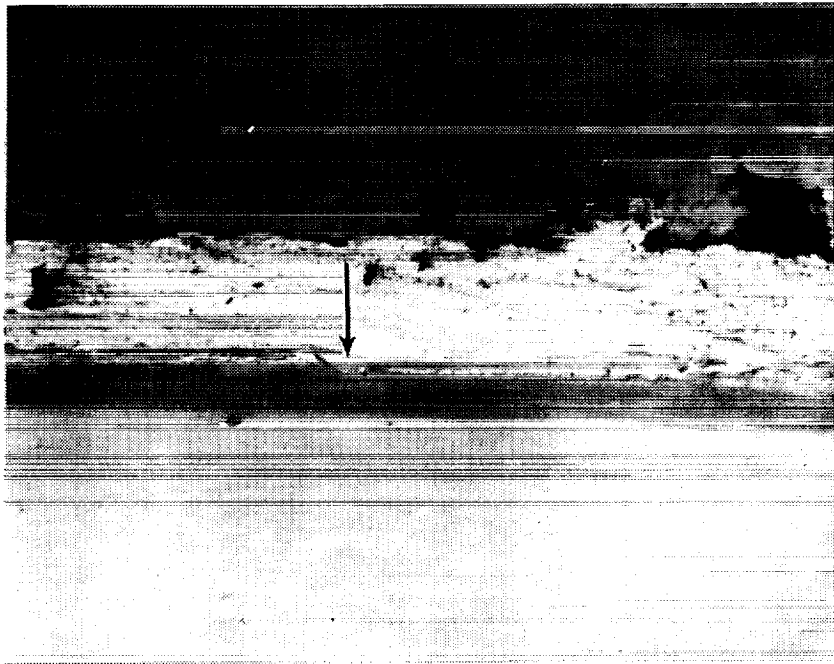
400X



L640-4

400X

FIGURE 4 - SAMPLE BRAZED AT 1500°F FOR 10-15 MINUTES  
SHOWING SEPARATION ALONG THE DIFFUSION ZONE  
(ARROW) BETWEEN THE BERYLLIUM (TOP) AND THE  
BRAZE ALLOY (BOTTOM).



L640-6 400X  
FIGURE 5 - BERYLLIUM (TOP) AND IN718 (BOTTOM) BRAZED  
AT 1435°F-1455°F SHOWING INCOMPLETE MELTING  
OF THE COPPER PLATING (ARROW).



**MSR 632: Results of Beryllium Coating Adhesion Tests**

TO: Alec Brown  
FROM: Steve Walak *SW*  
DATE: May 6, 1990  
SUBJECT: Results of the Beryllium Coating Adhesion Tests

**Introduction**

Electroless nickel plating and plasma sprayed aluminum oxide coatings are being evaluated for use on beryllium components in several areas of the Component Test Power Converter (CTPC). Concern over poor coating adhesion was raised after a chrome oxide coating applied by Kaman Sciences spalled from a beryllium test ring during final machining. Metallurgical analysis of the coating failure revealed that a metallurgical reaction between the electroless nickel under coating and the beryllium substrate was the primary cause for the failure. The results of this analysis were reported in MSR 589.

The current investigation was initiated to evaluate the strength of the bond between beryllium and the two coatings.

**Procedures**

The samples for all tests were cut from 2 inch diameter by 1 inch long coated beryllium rings. The test rings were manufactured and coated at Speed Ring Incorporated, reference P.O. 903-02782 and 903-02829. A metal stub, contoured to match the outside diameter of the test sample, was attached to the coating using Eccobond 104 epoxy adhesive. This stub was used to fixture the samples in the MTS tensile testing equipment. Samples were roughened using 180 grit abrasive paper to improve the epoxy adhesion.

Aluminum oxide and electroless nickel plated samples were tested as received and after exposure to 300 °C helium for 500 hours. Two samples of electroless nickel plated beryllium were also exposed to a simulated braze cycle. The brazing cycle simulated the conditions required for brazing the IN718 displacer dome to the beryllium base. The temperature cycle was performed in a helium atmosphere as follows:

- Slow Ramp to 1325 °F - 5 Minute Hold - Furnace Cool to Room Temp.
- Slow Ramp to 1475 °F - 5 Minute Hold - Furnace Cool to Room Temp.
- Approximate Time For Each Thermal Cycle - 6 Hours

Metallographic sections were prepared from the as received samples and from each of the exposed samples. The sections were examined to determine if a reaction between the base metal and the coating had occurred. Two tensile test samples were run for each coating and exposure condition. The maximum load was recorded

for each test. Visual examination was used to determine if the failure occurred in the epoxy bond or in the bond between the coating and substrate.

## **Results**

### **Aluminum Oxide**

The metallographic sections of the as received aluminum oxide coating and the aluminum oxide coating exposed to 300 °C helium for 500 hours showed no indications of a reaction between the coating and the substrate, Figures 1 and 2.

The average stress at failure in the coating bond strength tests was 1220 psi for both the as received samples and the samples exposed to 300°C helium for 500 hours. Visual examination revealed that failure of all the test specimens occurred in the epoxy bond, Figure 3. These results indicate that the bond strength of the aluminum oxide was greater than 1220 psi and was not affected by exposure at 300°C.

### **Electroless Nickel Plate**

The metallographic sections of the as received electroless nickel plated beryllium showed no signs of interaction between the coating and the base metal, Figure 4. The sections exposed for 500 hours at 300 °C did reveal a slight interaction layer. Careful examination of the section revealed what appeared to be a 1 to 2 micron interaction layer, Figure 5.

The average stress at failure for the as received electroless nickel plate was approximately 1220 psi and both failures occurred in the epoxy bond. This indicates that the bond strength of the as received electroless nickel coating was greater than 1220 psi.

The average stress recorded at failure in the bond tests on the electroless nickel plate after exposure in helium at 300 °C for 500 hour was approximately 630 psi. Visual examination revealed that the coating had been pulled away from the substrate in a local area around the epoxy joint, Figure 6. These tests indicate that the coating bond strength had degraded with exposure at 300 °C.

The metallographic section of the electroless nickel plate exposed to the simulated brazing thermal cycle revealed a distinct reaction layer approximately 10 microns thick. Cracks and other defects were observed along the beryllium to nickel interface, Figure 7. The stress at failure in the coating bond test was 76 psi for this sample. Visual examination revealed that the bond between the coating and the substrate had failed. A large area of coating delamination was observed, Figure 8. These tests indicate that severe degradation of bond strength results from exposing nickel plated beryllium to the brazing temperatures. A summary of all the test results is shown in Table 1.



TABLE 1

<u>MATERIAL</u>	<u>EXPOSURE</u>	<u>TENSILE TEST RESULTS*</u>	<u>MET.SECTION**</u>
(Al <sub>2</sub> O <sub>3</sub> )Be	None	Epoxy/1220	No Interaction
"	300 °C/500 Hr	Epoxy/1220	No Interaction
E-Ni/Be	None	Epoxy/1220	No Interaction
"	300 °C/500 Hr	Coating/630	Slight Layer
"	Braze Cycle (1325 °F+1475°F)	Coating/76	Distinct Layer

\* Tensile Test Results indicate the failure location and stress level at failure in psi.(Location/Stress Level(psi))

\*\* Met.Section - Results of the metallographic sections. Describes the condition of the coating Be interface.

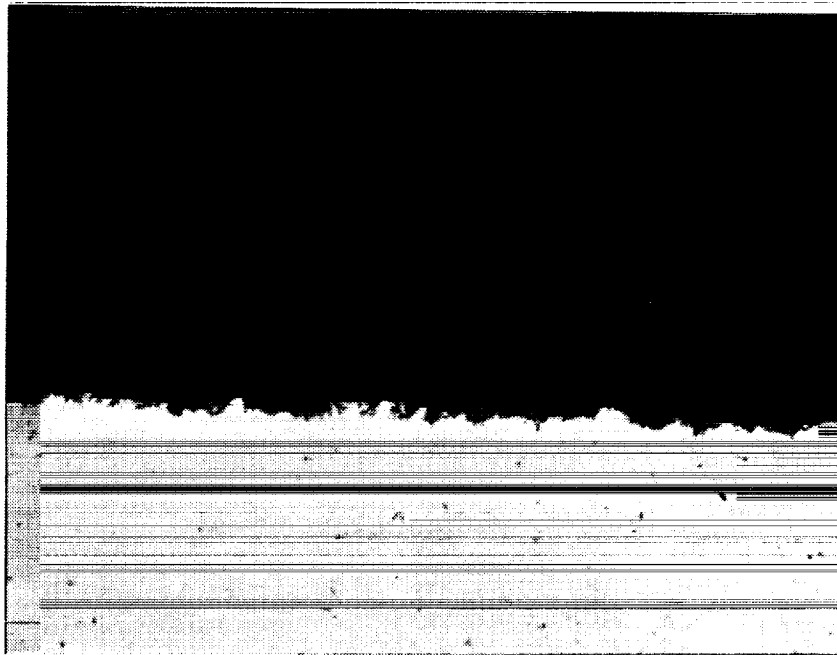
### Conclusions

The tensile bond strength of the electroless nickel plating on beryllium was greater than 1220 psi as received from the vendor. Exposure to 300 °C helium for 500 hours reduced the coating bond strength to approximately 630 psi. The adhesion of the nickel plate after 500 hours at 300°C appeared to be adequate to prevent coating failure in low stress areas. Exposure at this temperature for longer periods of time would likely reduce the bond strength further. Additional testing would be required to address this issue.

Exposure of the nickel plated beryllium to a simulated brazing thermal cycle reduced the coating bond strength to 76 psi and extensive coating delamination occurred during the tensile test. A metallurgical reaction between the nickel plate and the beryllium appears to be the cause for reduced bond strength. Electroless nickel plated beryllium should not be subjected to brazing conditions.

The tensile bond strength of the plasma sprayed aluminum oxide coating was greater than 1220 psi as received from the vendor and after exposure to 300°C helium for 500 hours.

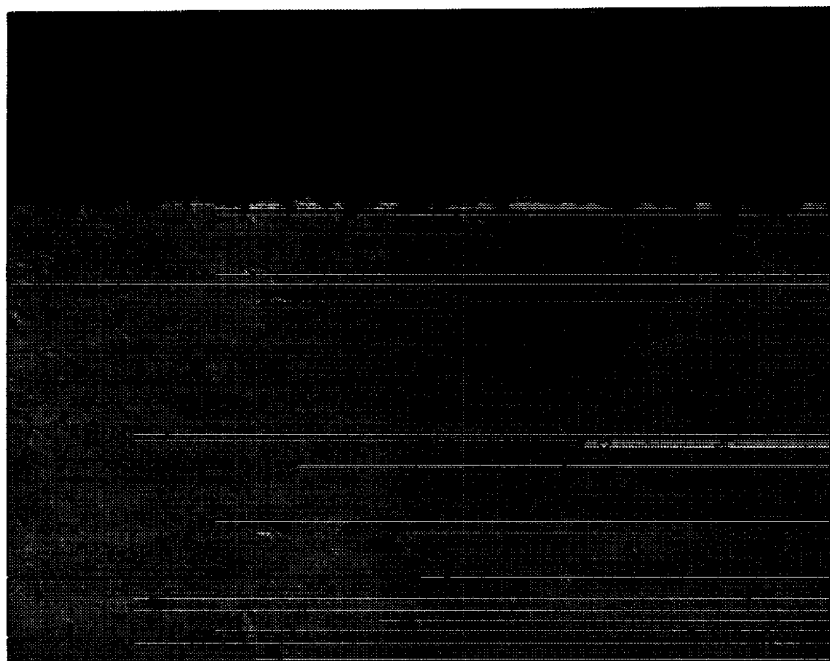
cc: G. Antonelli  
P. Chapman  
M. Cronin  
M. Dhar



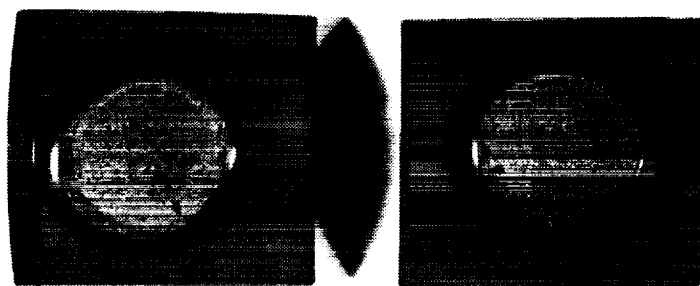
L532-14

X400

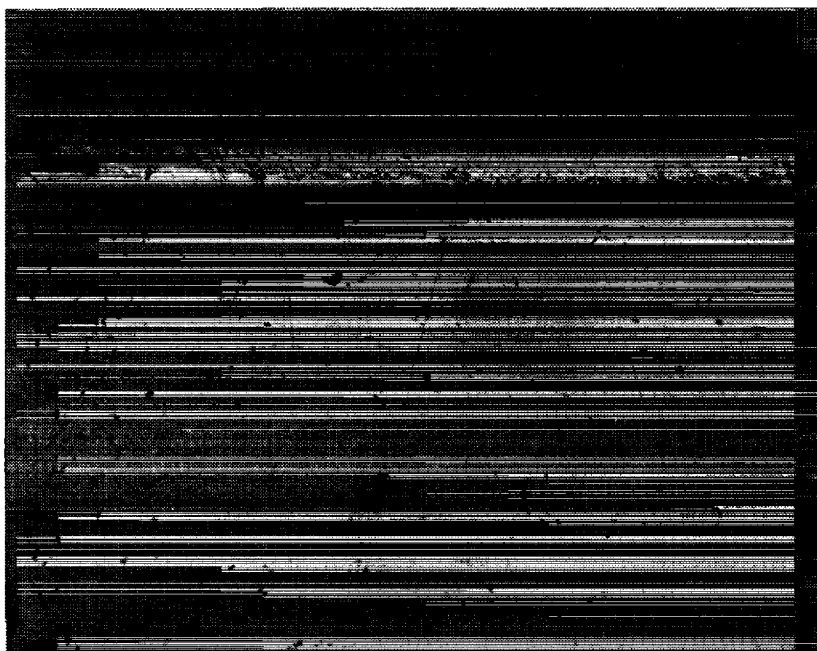
FIGURE 1 - PLASMA SPRAYED ALUMINUM OXIDE (TOP) ON  
BERYLLIUM (BOTTOM) AS RECEIVED FROM THE VENDOR



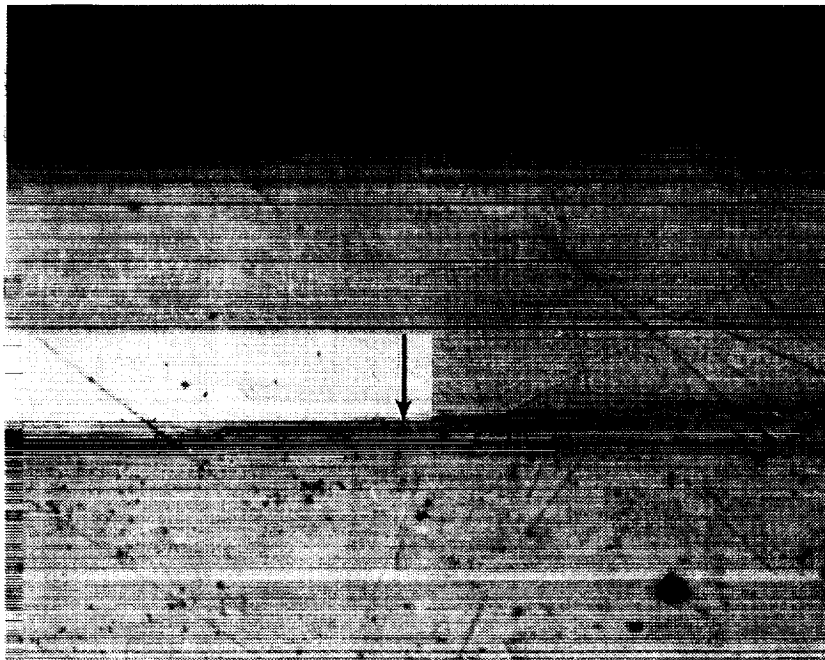
L632-20 X400  
FIGURE 2 - PLASMA SPRAYED ALUMINUM OXIDE (TOP) ON  
BERYLLIUM (BOTTOM) AFTER 500 HOUR EXPOSURE  
AT 300°C



L632-26 X1.6  
FIGURE 3 - ALUMINUM OXIDE COATING BOND STRENGTH SAMPLE  
AFTER TEST SHOWING EPOXY BOND FAILURE



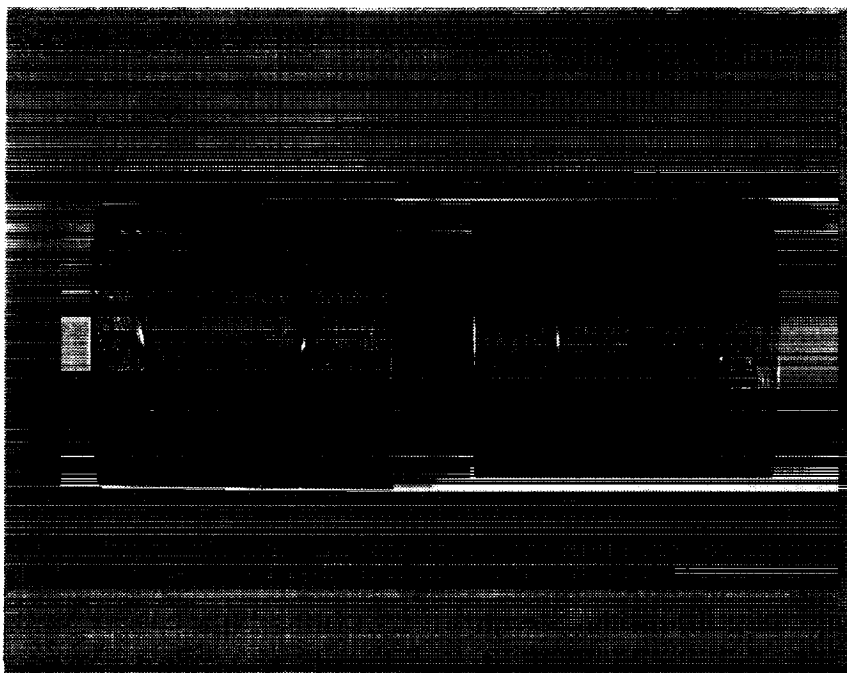
L632-10 X400  
FIGURE 4 - ELECTROLESS NICKEL PLATE (TOP) ON BERYLLIUM  
(BOTTOM) AS-RECEIVED FROM THE VENDOR



L632-2

X400

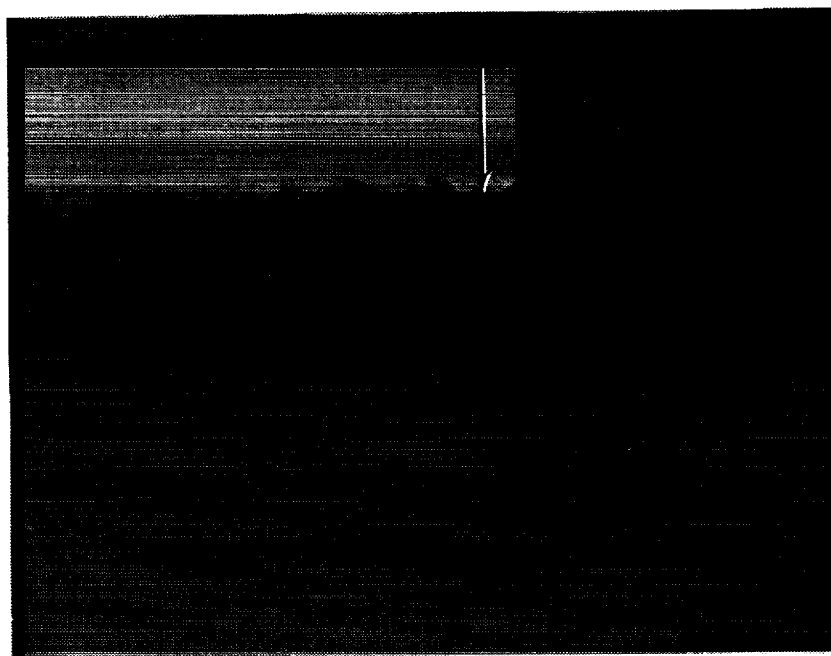
FIGURE 5 - SLIGHT INTERACTION LAYER (ARROW) AT THE ELECTROLESS NICKEL (TOP) TO BERYLLIUM (BOTTOM) INTERFACE AFTER EXPOSURE TO 300°C FOR 500 HRS.



L632-25

X1.6

FIGURE 6 - ELECTROLESS NICKEL PLATED BOND STRENGTH  
SAMPLE AFTER TESTING. THE SAMPLE EXPOSED  
TO 300°C HELIUM (LEFT) FAILED AT THE COATING  
TO SUBSTRATE INTERFACE.



L632-8

X400

FIGURE 7 - REACTION LAYER (ARROW) BETWEEN ELECTROLESS  
NICKEL (TOP) AND BERYLLIUM (BOTTOM) AFTER  
EXPOSURE TO A SIMULATED BRAZE CYCLE.





L632-24 X1.0  
FIGURE 8 - COATING DELAMINATION ON ELECTROLESS NICKEL  
BOND STRENGTH TEST SAMPLE AFTER EXPOSURE  
TO A SIMULATED BRAZE CYCLE.



**MSR 589: Metallurgical Failure Analysis of Chrome-Oxide-Coated Beryllium Cylinder**

TO: G. Antonelli cc: M. Cronin  
FROM: S. Walak *SW* M. Dhar  
DATE: July 12, 1989 A. Brown  
SUBJECT: Metallurgical Failure Analysis M. Walsh  
of a Chrome Oxide Coated Beryllium Cylinder, MSR 589.

On June 5, 1989 a chrome oxide coated beryllium cylinder was delivered to the Materials and Failure Analysis Group for examination. The chrome oxide coating had spalled from the surface of the beryllium (Be) during grinding. The coating was applied to the outside diameter of the cylinder by a slurry application and high temperature bake process at Kaman Science, Colorado Springs, CO. The Kaman coating process included six individual two hour bake cycles at 1000°F. Electroless Ni plate was applied to the cylinder prior to chrome oxide coating.

**RESULTS**

Metallographic examination of coating flakes and coating attached to the beryllium cylinder showed that debonding occurred between the Ni plate and the Be, Figure 1. The coating fracture appeared to propagate along an intermetallic layer formed between the electroless Ni and the Be, Figure 2. Chemical analysis using the electron microprobe analyzer indicated that the layer contained primarily Ni and Be. The dark speckles in the layer contained high concentrations of oxygen and appeared to be oxide particles, figure 3.

A metallographic section was prepared from a Beryllium test sample coated with electroless Ni and plasma sprayed chrome oxide. This coating had been ground successfully. The intermetallic layer observed in the sample coated by Kaman was not observed in the plasma sprayed coating, Figure 4.

**CONCLUSIONS**

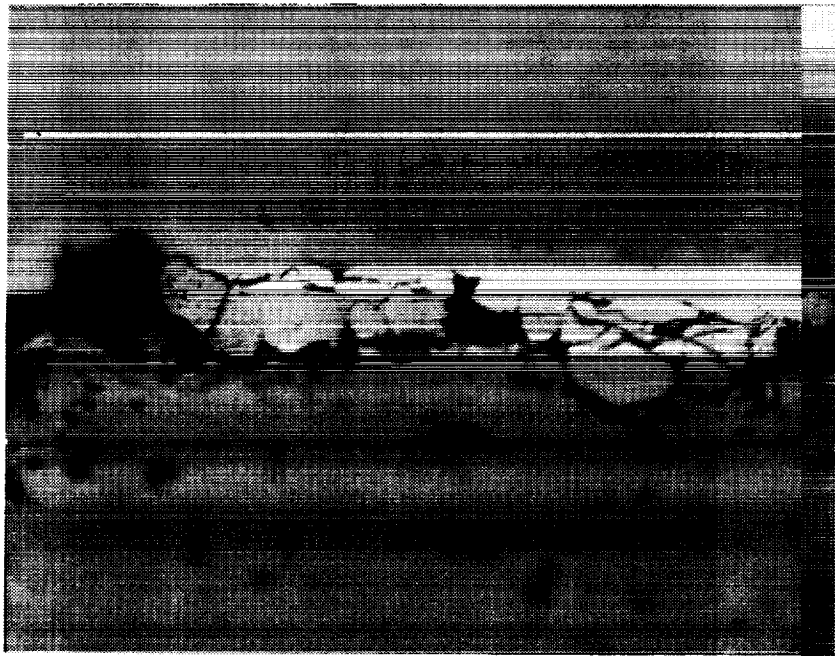
The electroless Ni/Kaman chrome oxide coating failed at the bond between the Ni plate and the Be cylinder. The failure initiated in a brittle layer formed at the electroless Ni to Be interface during elevated temperature exposure in the Kaman coating process. The Ni/Be intermetallic layer was not observed in the plasma sprayed sample confirming that elevated temperature exposure is required formation.

**RECOMENDATIONS**

Beryllium test specimens coated with electroless nickel should be subjected to heat treatment cycles similar to those encountered in the Kaman process, examined metallographically and subjected to adhesion tests. This type of test would confirm that high temperature exposure is the cause of poor coating adhesion of the Kaman coating.



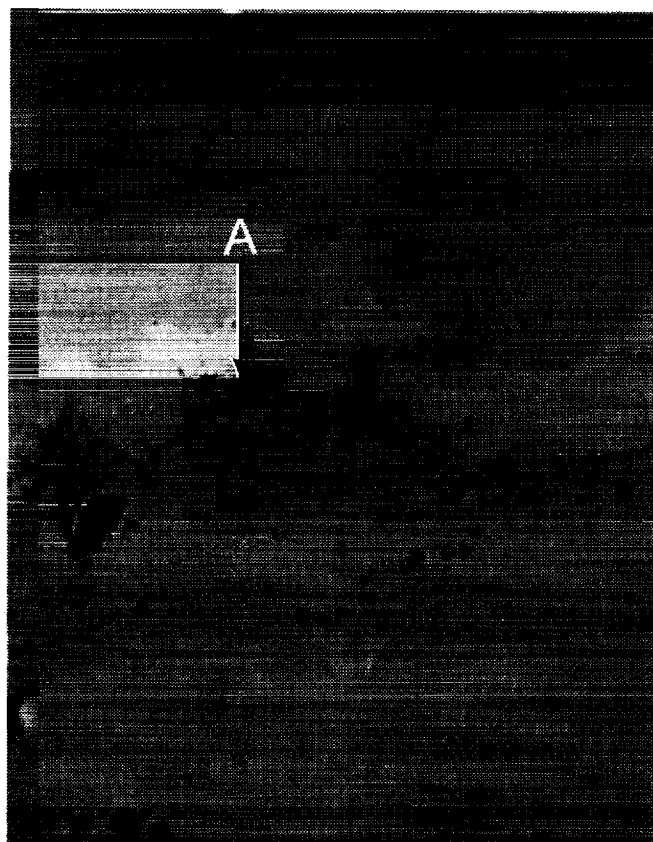
L589-6 400X  
FIGURE 1 - METALLOGRAPHIC SECTION SHOWING CRACKS  
IN THE BOUNDARY LAYER (ARROW) BETWEEN THE ELECTROLESS  
NICKEL PLATE (TOP) AND THE BERYLLIUM (BOTTOM)



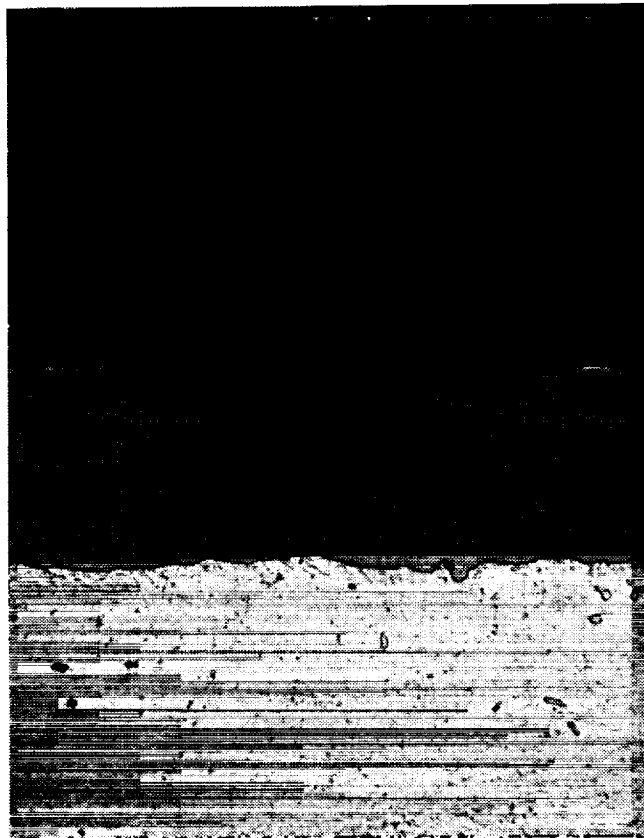
L589-7

1000X

FIGURE 2 - METALLOGRAPHIC SECTION SHOWING FRACTURE  
PATH ALONG THE BOUNDARY LAYER BETWEEN THE NICKEL  
PLATE (TOP) AND THE BERYLIUM (BOTTOM)



L589-2 1000X  
FIGURE 3 - PHOTOMICROGRAPH SHOWING OXIDE PARTICLES  
(A) AND THE TWO PHASE BOUNDARY LAYER BETWEEN THE  
NICKEL PLATE (TOP) AND BERYLIUM (BOTTOM)



L589-17 400X  
FIGURE 4 - PHOTOMICROGRAPH SHOWING PLASMA SPRAYED  
CHROME OXIDE (TOP) AND ELECTROLESS NICKEL (MIDDLE)  
ON BERYLIUM (BOTTOM)





## Memorandum: Displacer Rod End Plug Braze Evaluation Tests

TO: M. Dhar  
FROM: S. Walak *SW*  
DATE: March 1, 1991  
SUBJECT: Displacer Rod End Plug Braze Evaluation Tests

Displacer rod end plug braze samples, MTI part 1042C13-0246 Rev A, were tested by the Materials and Failure Analysis Group at MTI. The 3 test samples were machined and brazed at Speedring Incorporated, Cullman Al. The braze was made using an aluminum alloy according to Speedring procedure SR-3602.

The braze joint between the displacer rod and the rod end plug will be subjected to a 70 Hertz cyclic load in the CTPC. The shear stress in the joint is estimated to be approximately  $\pm 187$  psi. The braze joint is expected to operate in the range of 275°C to 320°C.

The three braze samples were tested in compression fatigue at temperatures between 150°C and 320°C. The fatigue loads applied generated an alternating shear stress of  $\pm 300$  psi in the braze joint. This shear stress is approximately 1.5 times the alternating shear stress expected in the actual engine components. The test conditions of 370  $\pm 300$  psi were very conservative due to the 370 psi mean stress. In the engine components the mean stress will be zero.

### Results

The first fatigue test was run continuously at 320°C. The cyclic load frequency was varied between 50 and 80 Hertz. The applied shear stress in the braze joint was 370  $\pm 300$  psi. After approximately 1.5 to 2.0 million cycles a slight drift in the test load was noted. Fine tuning of the load and frequency controls were unsuccessful in eliminating the load drift. At 2,447,000 cycles the test was shut down and the specimen examined. The braze joint had failed allowing the outer ring to move. After the braze failed, the load was supported by direct contact with the end plug.

In testing the second sample, limits were set to end the test when approximately 0.03 inches of slip occurred along the braze joint. This test was run with a shear stress of 370  $\pm 300$  psi, a frequency of 70 Hertz and temperatures between 150 and 320°C. A summary of the test cycle is shown in table 1. The test specimen survived more than 29 million cycles, 115 hours, of testing at temperatures between 150°C and 300°C. After an additional 1,434,000 cycles, 5.7 hours, at 320°C the braze joint failed.

Slip along the braze joint was limited to 0.03 inches in the third test also. The test was run at 275°C. The shear stress in the joint was 370  $\pm 300$  psi and

Memo to M. Dhar from S. Walak  
March 1, 1991

---

the frequency was 70 Hertz. This test was run for 57,279,600 cycles, 227 hours, without failure. Inspection of the sample after testing indicated that the braze joint had not failed.

### Conclusions

Test samples representing the displacer rod to end plug joint were successfully brazed using Speedring procedure SR-3602. The cyclic shear strength of the aluminum braze was shown to be inadequate at 320°C. In two separate tests joint failures occurred after approximately 1.4 to 2.5 million load cycles. The total test time was approximately 5 to 9.5 hours.

The strength of the aluminum braze was found to be adequate at 275°C. More than 57 million load cycles were applied to a sample at 275°C without joint failure. The conservative load conditions in this test, 370 +/-300 psi, give additional confidence in the results.

Higher strength braze alloys, i.e., silver alloys, should be used for applications requiring 320°C operation, figure 1.

cc: G. Antonelli  
A. Brown  
P. Chapman  
G. Dochat  
G. Smith

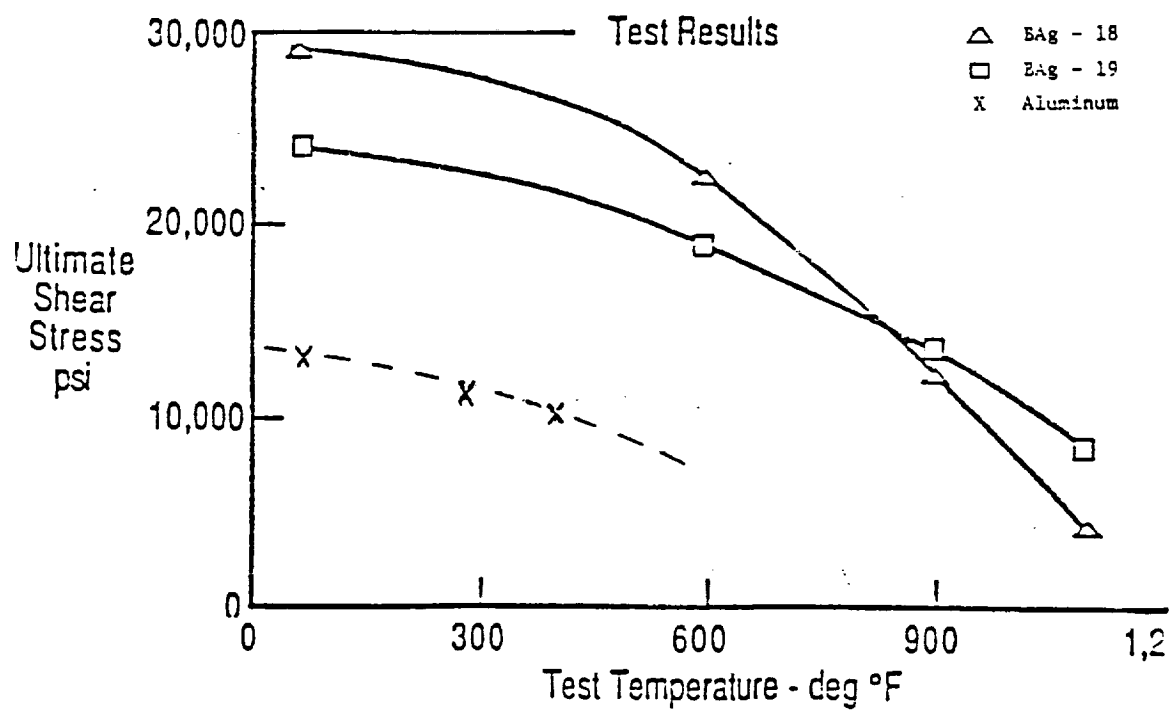


FIGURE 1

Ultimate Shear Stress versus Temperature Plot For  
Beryllium to Beryllium Joints Brazed with Two Silver  
Alloys and an Aluminum Alloy.  
(Electrofusison and Brushwellman Product Data)

Memo to M. Dhar from S. Walak  
March 1, 1991

---

TABLE 1  
TEST #2 LOAD AND TEMPERATURE SUMMARY

<u>CYCLES</u>	<u>TEMPERATURE(°C)</u>	<u>COMMENTS</u>
1,948,400	150	No failure
5,709,500	250	No failure
12,240,100	300	No failure
1,440,600	320	Test failure

## B.6 Sodium Issues

### Note: Refractory Metal Coating

Wedge shaped test samples representative of the finned section of the CTE Star Fish Heater Head were delivered to Synterials Inc., Herndon VA to be coated with Mo and Nb metal by chemical vapor deposition. A protective coating may be necessary if Inconel 718 is shown to have poor sodium corrosion fatigue resistance in tests at MTI.

Synterials Inc. has made several attempts to deposit molybdenum (Mo) and niobium (Nb) on the inside of the wedge shaped samples. Two test runs have been made with Mo and a single run has been made with Nb. All test samples were coated with a 2 to 5 micron thick layer of electroless nickel prior to chemical vapor deposition.

In the first Mo test run reactive gas was supplied uniformly to the reaction chamber. No special effort was made to direct the gas inside the wedge of the test sample. Molybdenum was deposited on the outside of the test sample but not inside the wedge as required.

A reactive gas delivery nozzle was constructed and used on the second Mo test run. This nozzle directed reactive gas into the test sample wedge. In this coating cycle molybdenum was deposited to a depth of approximately one (1) inch into the the opening of the sample. The molybdenum thickness was approximately 2 to 5 microns as determined by metallographic sectioning. The coating trial was run at 800 C for 2 hours.

A single niobium coating trial was run. The reactive gas was delivered directly to the inside of the wedge as in the second molybdenum run. Niobium was deposited on the entire internal surface but the coating thickness was approximately 2 to 5 microns. The test sample was held at 800 C for 2 hours during the coating cycle.

Final coating runs will be attempted with both Mo and Nb. Gas flow rates will be lowered and coating times will be increased in an attempt to coat at the base of the wedge and increase the coating thickness.

#### ALUMINIDE COATING

In aluminizing treatments elevated temperature exposure in an aluminum rich environment causes interdiffusion between nickel and aluminum at the surface of the base material. The treatment generates a layer of NiAl or Ni<sub>2</sub>Al<sub>3</sub> approximately 0.002 to 0.005 inches in thickness. Pack and slurry aluminizing treatments can be used to coat the heater head.

The slurry process would be likely to produce a more uniform coating on a complex geometry such as the CTE Star Fish Heater Head. The coating is applied by dipping the component in a slurry and heating to elevated temperature causing aluminum diffusion into the surface. The coating cycle includes a heat treatment at 925 to 1050 C for between 3 and 4 hours. The effect of this exposure on the base material properties would need to be considered in the overall heat treatment cycle.

Slurry dipped aluminide coatings can be applied to the heater head by Chromally Inc. of Orangeburg, NY.

Two wedge shaped Inconel 718 test samples are currently being manufactured at MTI for trial coating runs at Chromally.

#### CHEMICAL MILLING

Samples of age hardened and annealed Inconel 718 were chemically milled to remove 0.003  $\pm$  0.0005 inch of material from the surface of an internal bore. The test samples were manufactured to represent a section of the HPFTS.

The chemical milling was performed by Tech Met Inc., Glassport Pa. Two chemical solutions are used in the milling process:

STEP 1) Activation Solution

65% HCl

35% H<sub>2</sub>O

130 Degrees F, 5 to 10 minutes

STEP 2) Chemical Milling Solution

68% HCl

6% Nitric Acid

3% Phosphoric Acid

5% Hydrofluoric Acid

18% Ferric Chloride

120-130 Degrees F, Mill Rate 0.001 inch in 5 minutes

The test samples have been examined at MTI and a detailed report of the surface condition is being written. Additional samples may need to be tested to confirm that EDM layers can be removed from the CTE Heater Head Fins.





**MSR 602: Liquid Metal Corrosion Resistant Coatings**

TO: M. Dhar  
FROM: S. Walak *SW*  
DATE: September 22, 1989  
SUBJECT: Liquid Metal Corrosion Resistant Coatings

Several coatings were investigated as possible corrosion protection for Inconel 718 exposed to high temperature liquid metal in the CTE star fish heater head. The three coatings investigated were, niobium (Nb) and molybdenum (Mo) deposited by chemical vapor deposition (CVD) and an aluminum diffusion coating applied by a pack cementation process.

Coating thickness requirements were determined from estimates of the expected corrosion rate of the coating in liquid sodium at 1050°K and the diffusion rates between the coatings and the base metal. The life of the heater head was assumed to be 60,000 hours. Based on these calculations between 0.002 and 0.005 inch thick coatings were required for 60,000 hour performance without surface degradation.

Test samples representing individual pockets of the CTE star fish heater head heat exchanger were manufactured and delivered to vendors for coating of the internal pocket, Figure 1. Synterials Incorporated, Herndon VA and Chromalloy Incorporated, Orangeburg NY were selected to apply the CVD and the aluminide coatings respectively. Both companies reviewed sketches of the Star Fish Heater Head and indicated they could apply the coatings to the full sized component if the initial testing was successful. Synterials was the only CVD company which could accommodate the full size CTE heater head in their CVD chamber and deposit refractory metal coatings.

**RESULTS****CVD Refractory Metal Coating**

Significant time delays and technical problems were encountered during CVD coating at Synterials. The internal pocket of a test sample was coated with Nb but satisfactory results could not be obtained with Mo. The CVD coating cycle and processing details are described in a letter report from Synterials in Appendix A.

Dr. R.Engdahl, Synterials Incorporated, indicated that the main problem encountered with the CVD process was delivery of reaction gas to the base of the internal pocket. Several runs were attempted using different delivery systems and only marginal success was obtained.

The test sample coated with Nb was sectioned and carefully examined at MTI. The internal surfaces of the pocket appeared to be coated uniformly and no indications of flaking or chipping of the coating were identified, Figure 2.

Metallographic sections of the coated surface revealed that the Nb was deposited over a thin layer of thin nickel. The nickel plate was non-uniform but averaged about 75 micro-inches in thickness. The Nb layer was between 75 and 120 micro-inches in thickness and extremely uniform from the root to the open end of the pocket, Figures 3 and 4. The irregular layer of nickel below the Nb appeared to be the main cause of coating non-uniformity, Figure 5. Electron microprobe x-ray analysis was used to confirm that Nb had been deposited, Figure 6.

A section cut from the side wall of the test sample was subjected to thermal cycling to evaluate coating adhesion. The sample was cycled between room temperature and 1050°K five times. Small areas of flaking were observed after testing, Figure 7.

### Aluminide Coating

The pack aluminide coating is applied by heating the part in a powder pack containing aluminum and aluminum containing compounds. The aluminum in the pack reacts with the metal surface and forms a coating of aluminide intermetallics with the base metal.

The MTI test samples were heat treated for 20 hours at 1800°F during the aluminide coating deposition. The extended exposure at 1800°F is not expected to affect the performance of the IN718 base metal.

The inside pocket of the test sample appeared to be coated uniformly with the exception of a slight difference in reflectivity between the root and the open end of the test sample, Figure 8. Closer examination revealed that the difference resulted from a variation in surface finish between the two areas. The surface roughness near the root and the open end of the aluminide coated test sample was 33 micro-inches and 44 micro-inches center line average respectively. The surface finish of the IN718 prior to coating was 12 micro-inches center line average.

Metallographic sections through the coating revealed that the coating thickness ranged from approximately 0.0013 to 0.002 inches. The thicker regions of coating were found near the root of the test sample and the thinner regions were found near the open end of the test sample, Figures 9 and 10. The overall uniformity of the coating appeared to be quite good. Inclusion of particles from the pack was observed at some locations near the root of the pocket.

A section cut from the side wall of the test sample was subject to thermal cycling. The coating adhesion appeared to be good after five cycles between room temperature and 1050°K, Figure 11. Small chips of coating were removed from the cut edge of the sample but mechanical damage is the suspected cause for this damage.

Additional samples are being prepared for thermal cycling tests. The results of the additional tests will be used to confirm the current results.

## **CONCLUSIONS**

Deposition of refractory metal coatings on the Star Fish Heater Head Fins by CVD appears to be a difficult procedure. The depth to width ratio of the individual pockets requires special gas delivery fixturing. The difficulties encountered in coating a single pocket sample has shown that extensive development work would be required before the Star Fish heater head could be coated successfully.

The pack diffusion aluminide coating process appears to be capable of providing a uniform protective coating to the Star Fish heater head fins. The coating is uniform and of good quality from the root to the open end of the fin. Detailed discussions with the coating vendor would be required to assure successful coating of the entire heater head. The preliminary test results seem to indicate that the aluminide coating would be a reasonable coating for liquid metal corrosion protection.

/cn

cc: G. Antonelli  
A. Brown  
M. Cronin  
G. Dochat  
P. Chapman  
M. Walsh  
D. Jones  
G. Smith

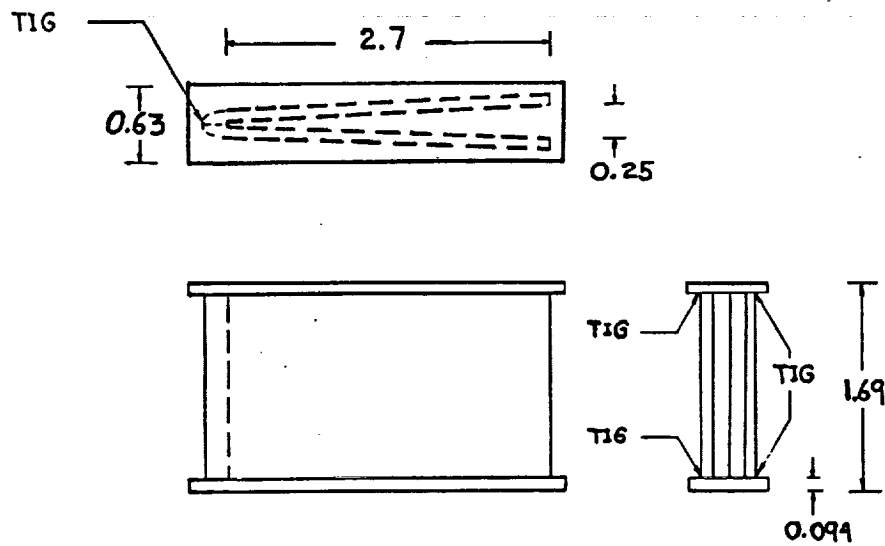
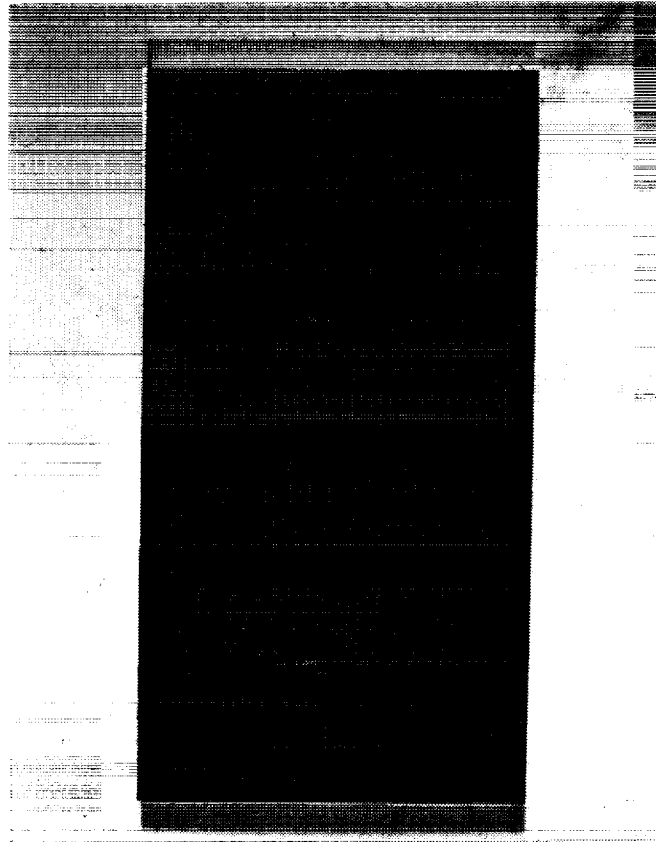
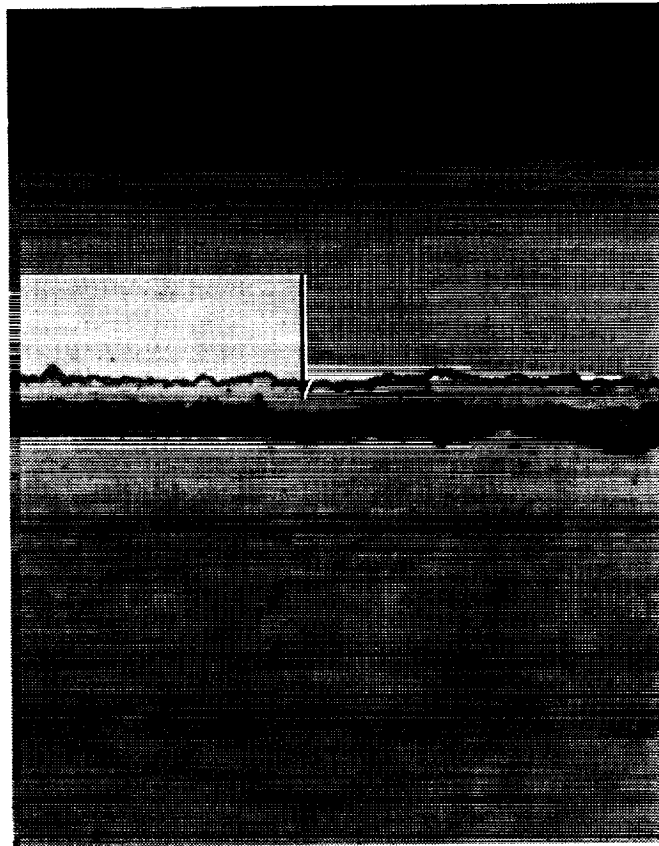


FIGURE 1 - SKETCH OF COATING TEST SAMPLES



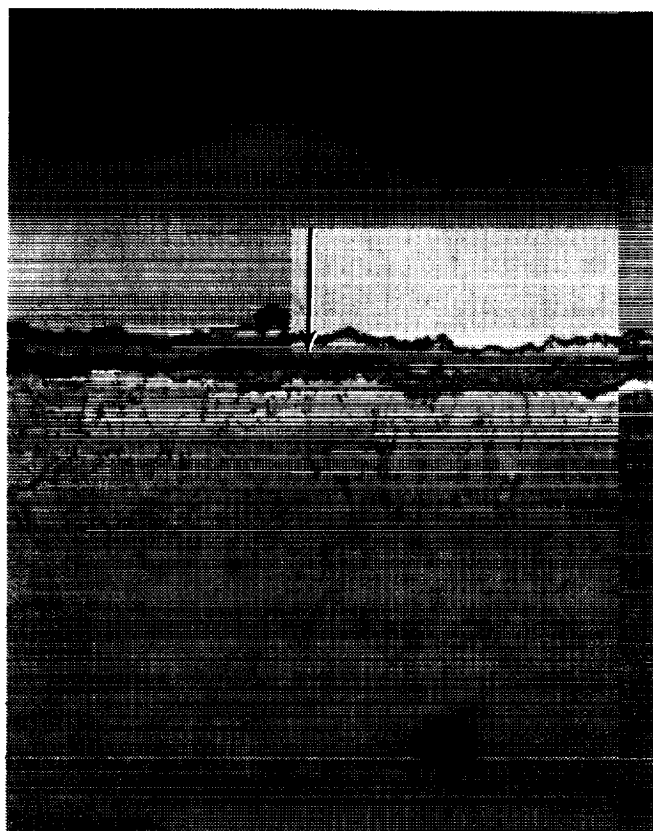
L602-21 1.8X  
FIGURE 2 - NIOBIUM COATED TEST SAMPLE SIDE WALL, INTERNAL  
SURFACE, AFTER SECTIONING



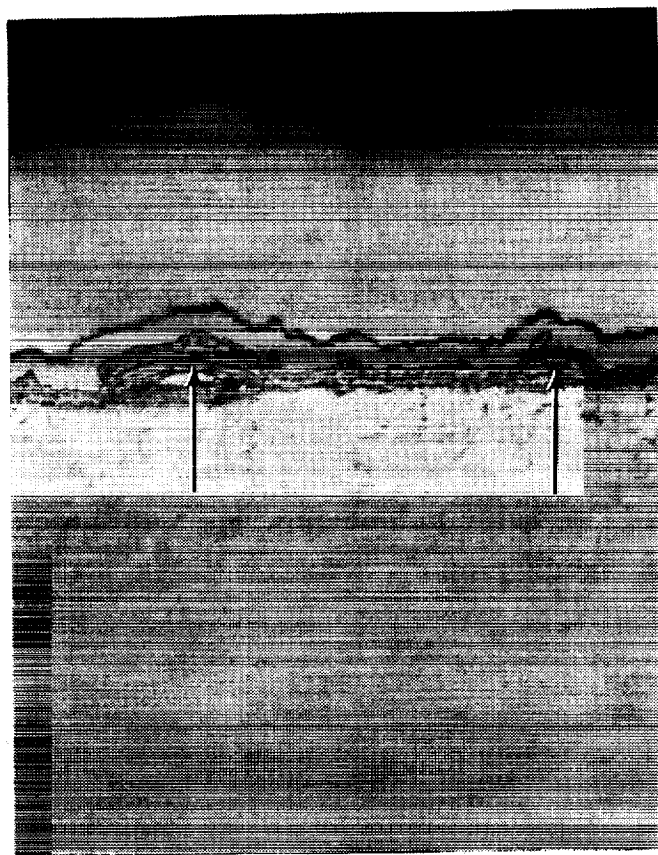
L602-20

1000X

FIGURE 3 - CROSS-SECTION OF THE Nb LAYER (ARROW) NEAR  
THE OPEN END OF THE SAMPLE



L602-11 1000X  
FIGURE 4 - CROSS SECTION OF THE Nb LAYER (ARROW) NEAR  
THE ROOT OF THE TEST SAMPLE



L602-19

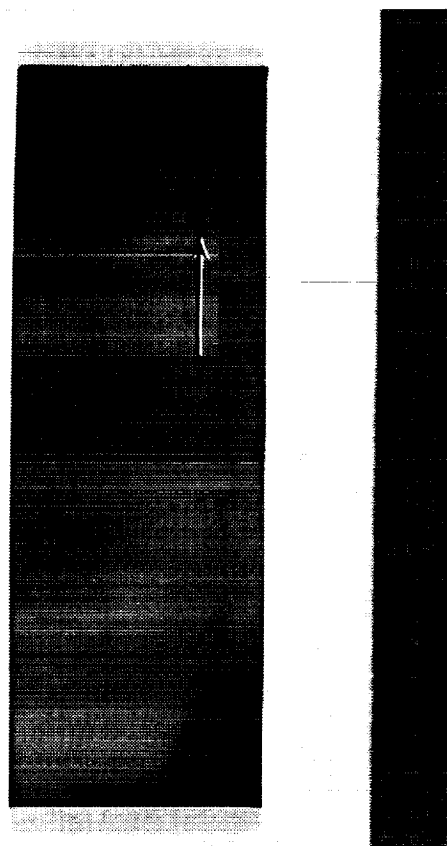
1000X

FIGURE 5 - CROSS-SECTION OF THE Nb COATING SHOWING DEFECTS  
IN THE NICKEL PLATE (ARROW)





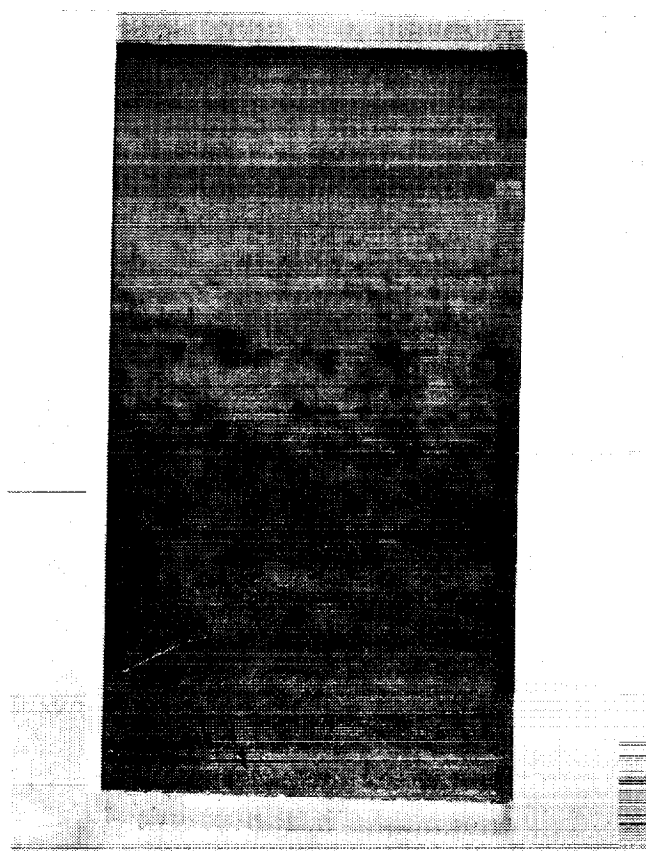
L602-5 2000X  
FIGURE 6 - ELECTRON MICROPROBE X-RAY DOT MAP SHOWING THE  
WIDTH OF THE Nb LAYER (WHITE DOTS INDICATE THE PRESENCE  
OF NIOBIUM)



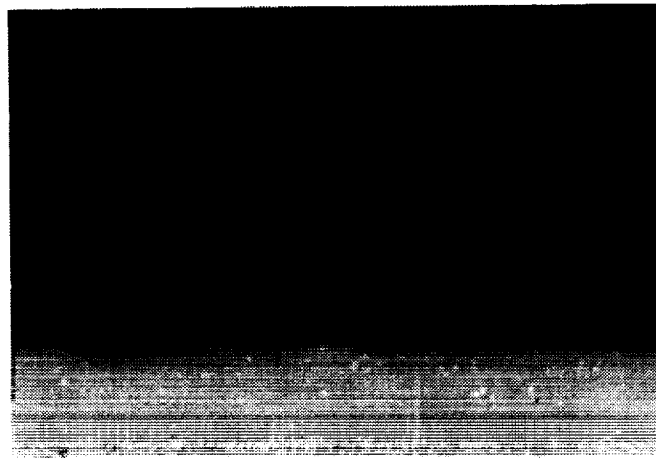
L602-23

1.8X

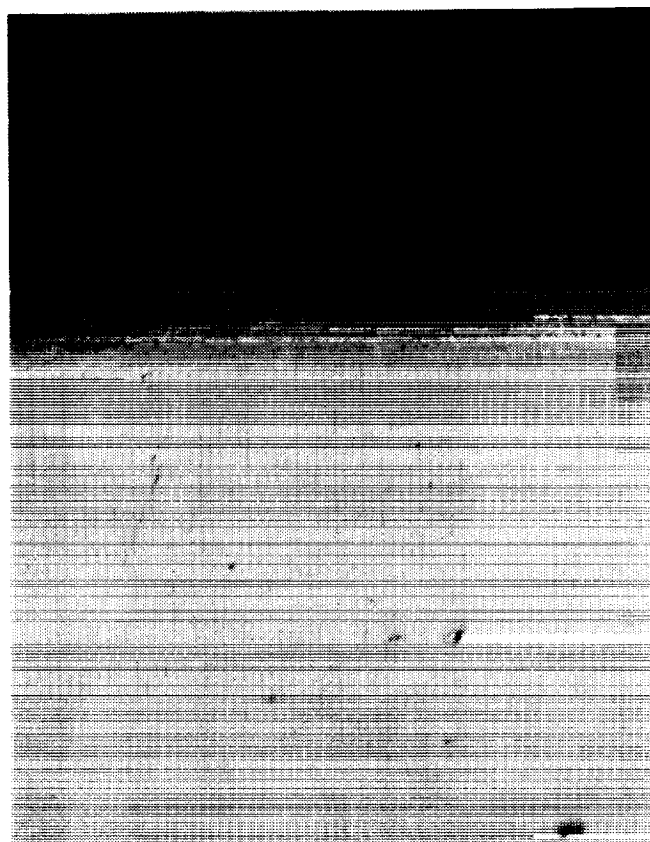
FIGURE 7 - Nb COATING TEST SAMPLE. INTERNAL SIDE WALL  
SURFACE AFTER THERMAL CYCLING (NOTE COATING FLAKES AT  
ARROW)



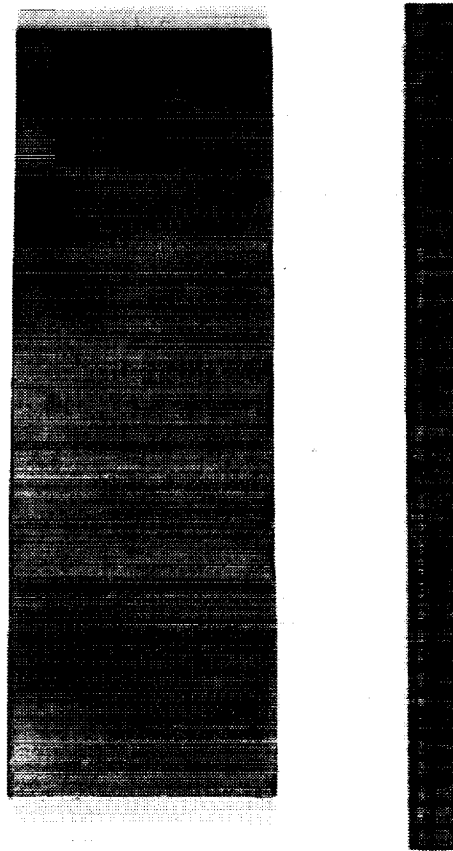
L602-22 1.8X  
FIGURE 8 - NICKEL ALUMINIDE COATED TEST SAMPLE INTERNAL  
SIDE WALL SURFACE



L602-9 400X  
FIGURE 9 - NICKEL ALUMINIDE COATING NEAR THE ROOT OF  
THE TEST SAMPLE (0.002 INCH THICKNESS)



L602-10 400X  
FIGURE 10 - NICKEL ALUMINIDE COATING NEAR THE OPEN END  
OF THE TEST SAMPLE (0.00125 INCH THICKNESS)



L602-24

1.8X

FIGURE 11 - NICKEL ALUMINIDE COATED TEST SAMPLE SIDE  
WALL INTERNAL SURFACE AFTER THERMAL CYCLING

## **APPENDIX A**

# Synterials

---

October 3, 1989

Ms. Susan T. Piechnik  
Mechanical Technology Incorporated  
968-969 Albany-Shaker Road  
Latham, New York 12110

Subject: Report on the Synterials effort to coat the internal surface of a cavity formed by Inco 718 with Mo. and as an alternate, Nb.  
P.O. 90304271.

Figure 1. illustrates the shape of the cavity to be coated. This cavity was selected as representative of a shape that was under consideration for an engine application which would require the coating to be tolerant of liquid sodium at 1400 F. The effort was to demonstrate that Synterials could deposit a coating acceptable for this application.

The Synterials initial set-up for these trials consisted of a lance and a support structure for the test part configured for use in a vacuum CVD facility. The lance consisted of two concentric tubes which directed the flow of the chlorinated Mo. or Nb. and the hydrogen reducing agent into the cavity to be coated. The hydrogen flowed down the inside tube, and the chlorinated metal flowed in the annulus between the inside and outside tube. The cavity was located directly in front of the concentric tubes so that the effluent gases would be directed into the cavity where the chlorinated metal would be reduced by the hydrogen to produce the desired coating. The Inco 718 cavity was pretreated by a coating of electroless nickel prior to the CVD coating.

The set-up was changed during the testing period to incorporate a funnel type arrangement which directed the deposition gases into the cavity approximately 1 1/4 inches or about one-half way. The funnel crosssection was rectangular with dimensions approximately 1/8 by 1 1/4 inches at the discharge end. A third major change was to introduce a prereaction chamber, prior to the funnel, to provide more time and better mixing between the time the hydrogen and the chlorinated metal were introduced and they arrived at the cavity surface for deposition.

The deposition temperature was selected to be 880 C for all tests. The initial deposition pressure was set at one Torr. Other pressures tested ranged up to 30 Torr. The metal chlorination rate was typically 1/4 gram per minute.



# Synterials

---

Ms. Susan Piechnik, Oct 3, 1989, page 2, P.O. 90304271 Report.

Figure 2. is a view showing the lance, the prechamber, the funnel arrangement leading to the test specimen and the test specimen all mounted in the support frame. This entire frame assembly is installed in the CVD chamber for the coating of the test specimen. Figure 3. is a view of the funnel arrangement installed in the test specimen. In this view, the prechamber and the lance have been removed. Figure 4. is a view of the lance looking at the concentric tube arrangement for control of the deposition gasses. The large cylindrical shaped part on the outside of the concentric tubes is to provide for a slip connection to the premix chamber. In operation, the material mounted on the rack and the rack rotate about the central axis. The lance is not connected to the rack and is stationary during the deposition operation.

During the initial tests, it was found that the majority of the metal deposition took place downstream from the specimen. Figure 5. is a diagram of the specimen showing the location of the section lines used to expose the coating distribution and thickness. For the Mo., the polished specimens indicated that at the open end, and for approximately 3/4 of an inch into the cavity, the Inco 718 was covered by the Mo. coating. Also, the coating penetrated into the weld region satisfactorily. However, the coating was only about two microns thick. It was also noted that the nickel coating was very thin to nonexistent at the closed end of the cavity. For the Nb. the results were better in that Nb. was observed in the bottom of the cavity but no nickel was observed. The thickness at the open end and at 0.4 inches from the closed end of the cavity was approximately 2 microns. The nickel also showed some blistering.

Based on these tests, a test sample was coated with Nb. By repeating the coating effort three times, with inspections between each coating trial, we believe that the coating thickness was built up to approximately 2 mils. This specimen was delivered on 7/19/89.

To achieve additional Mo. coating in the bottom of the specimen cavity, a funnel configuration was designed and fabricated. This hardware is shown in Figure 3. with the specimen sample in place. Tests with this design indicated that more Mo. was being deposited at the open end, but that the coating thicknesses in the bottom of the cavity was still insufficient. The next effort was to increase the deposition pressure from approximately 10 Torr to 30 Torr. This resulted in a rough Mo. deposit that we considered unsuitable for the sodium environment. Next, we enlarged the entrance chamber leading to the funnel. Although this helped some, it still was not good enough for the application.

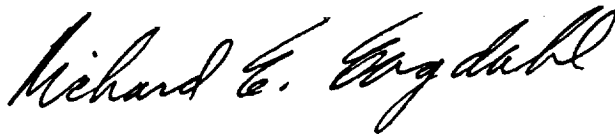
# Synterials

Ms. Susan Piechnik, Oct 3, 1989, page 3, P.O. 90304271

Our next effort was to have been to enlarge the prechamber by a factor of about four. However, at this time Mr. Walak said that we should stop the work. The sample specimen with the last Mo. coating is enclosed with the Mo. and the Nb. sectioned specimens from the previous efforts.

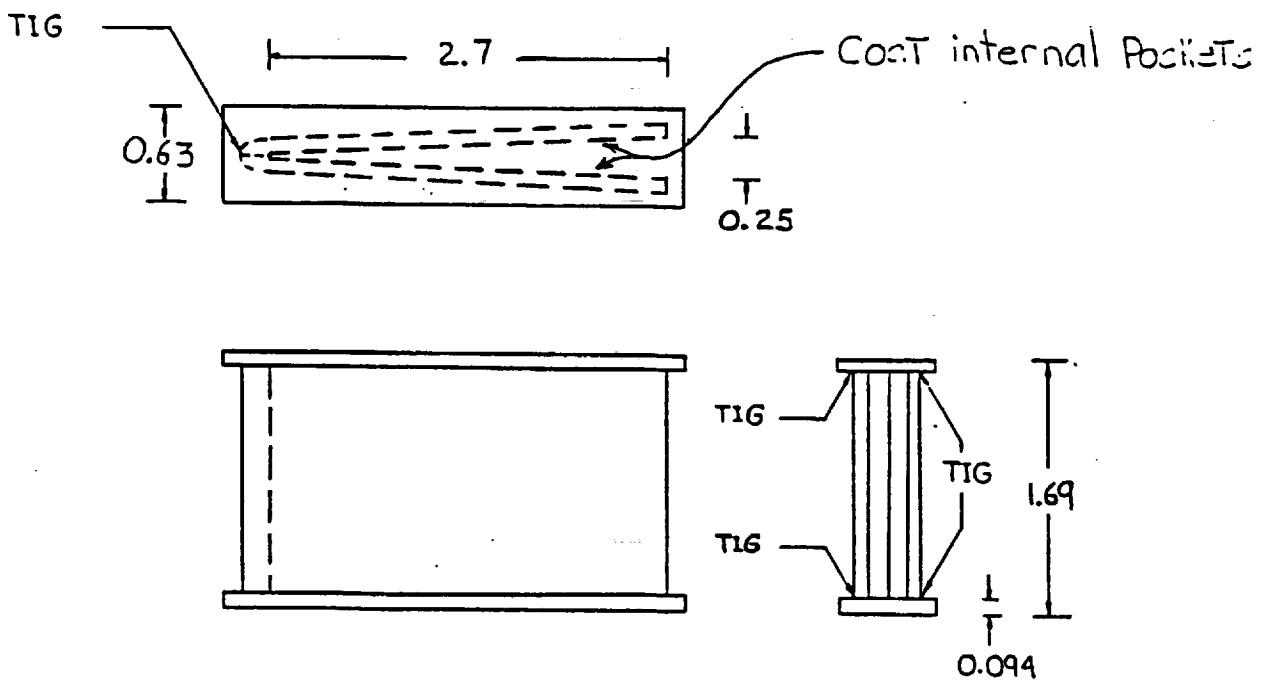
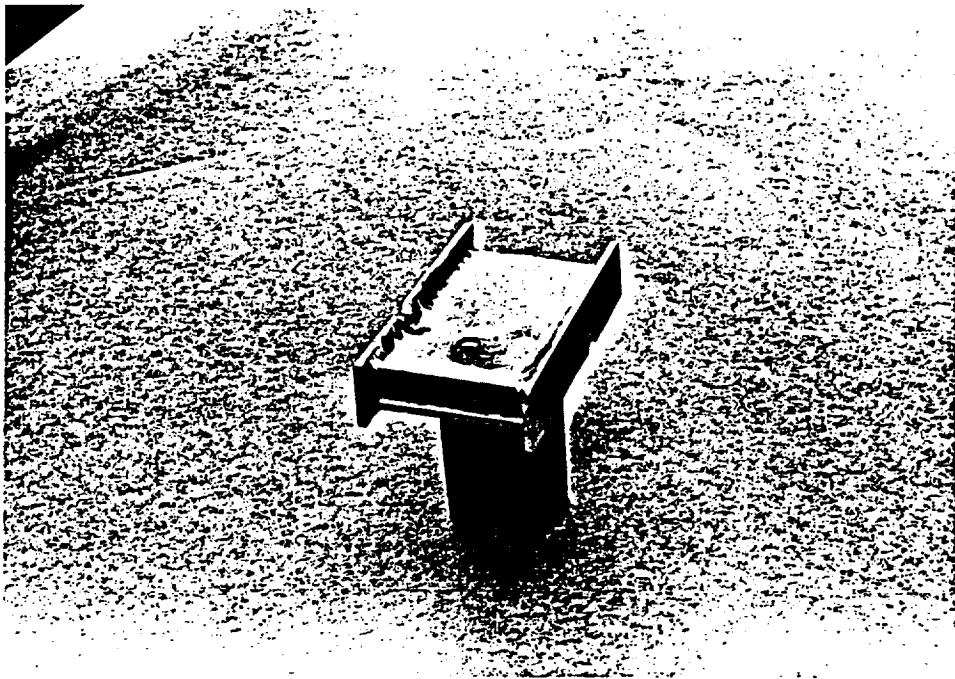
We trust that this report contains all the information that you need for your program. Should there be additional data required, we would be pleased to respond to your requirements.

Sincerely,

A handwritten signature in cursive script, reading "Richard E. Engdahl". The signature is written in dark ink and is positioned above the typed name and title.

Richard E. Engdahl  
President

RE/bl



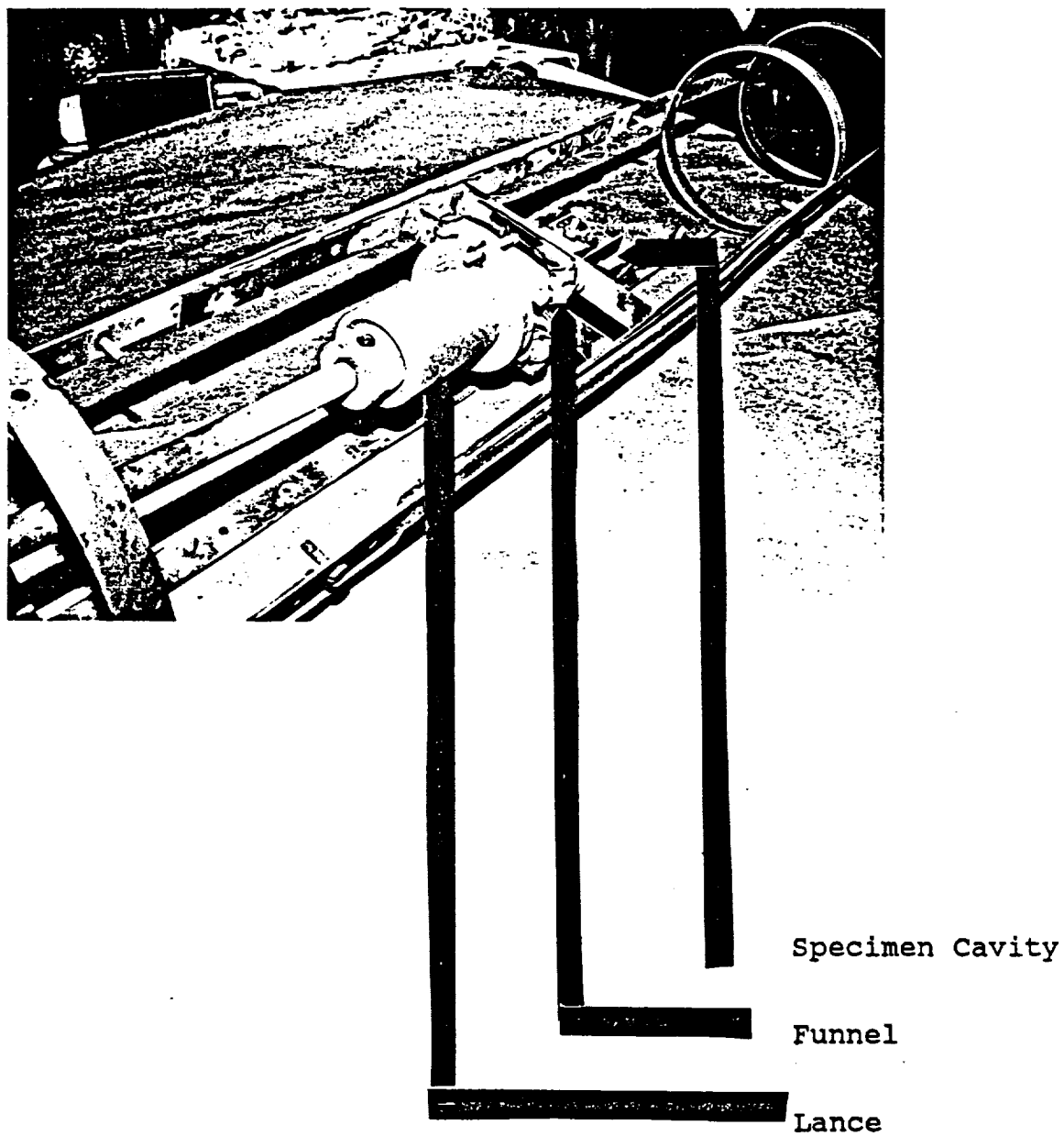


Figure 2. View of the CVD coating fixture.

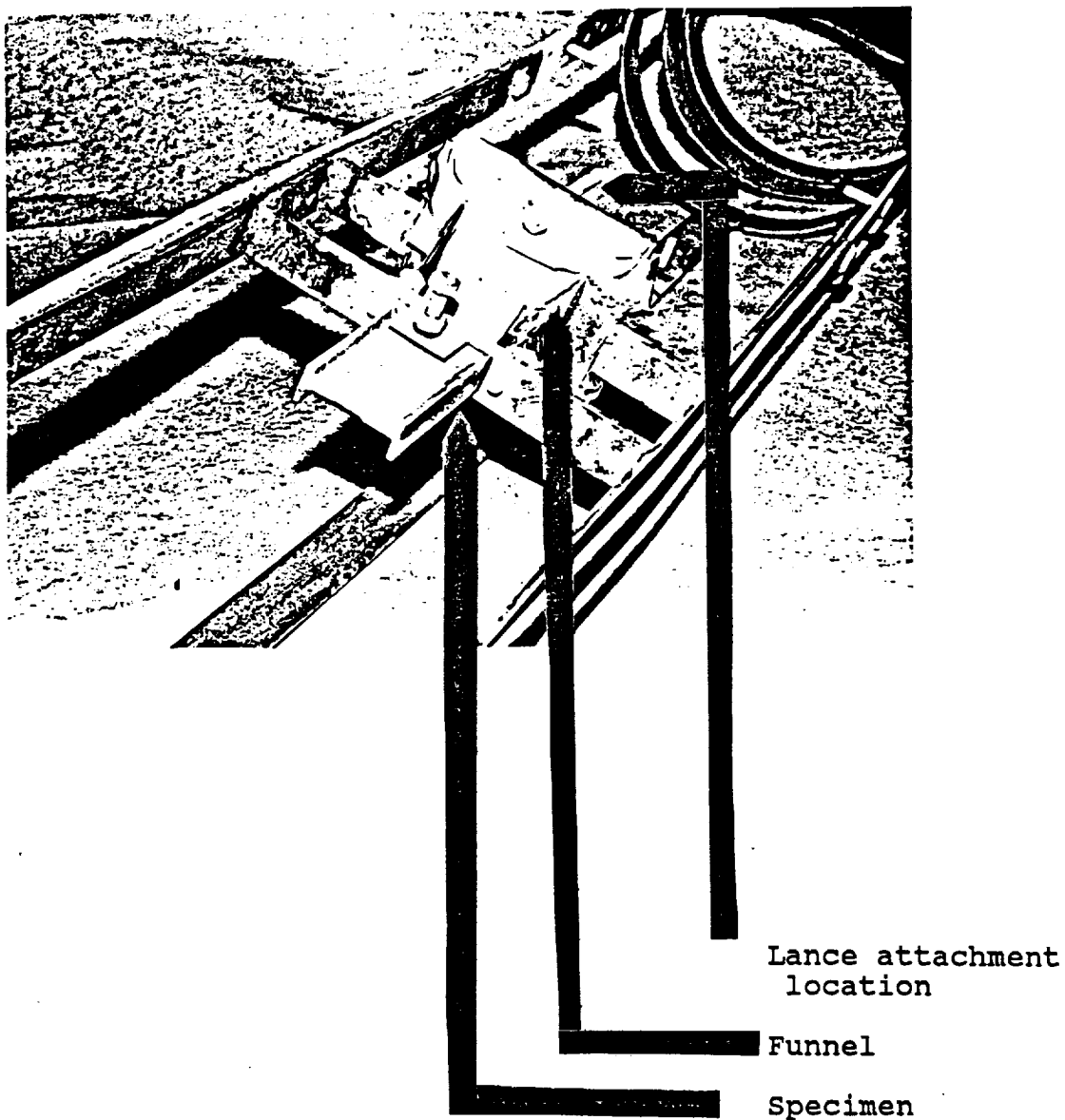
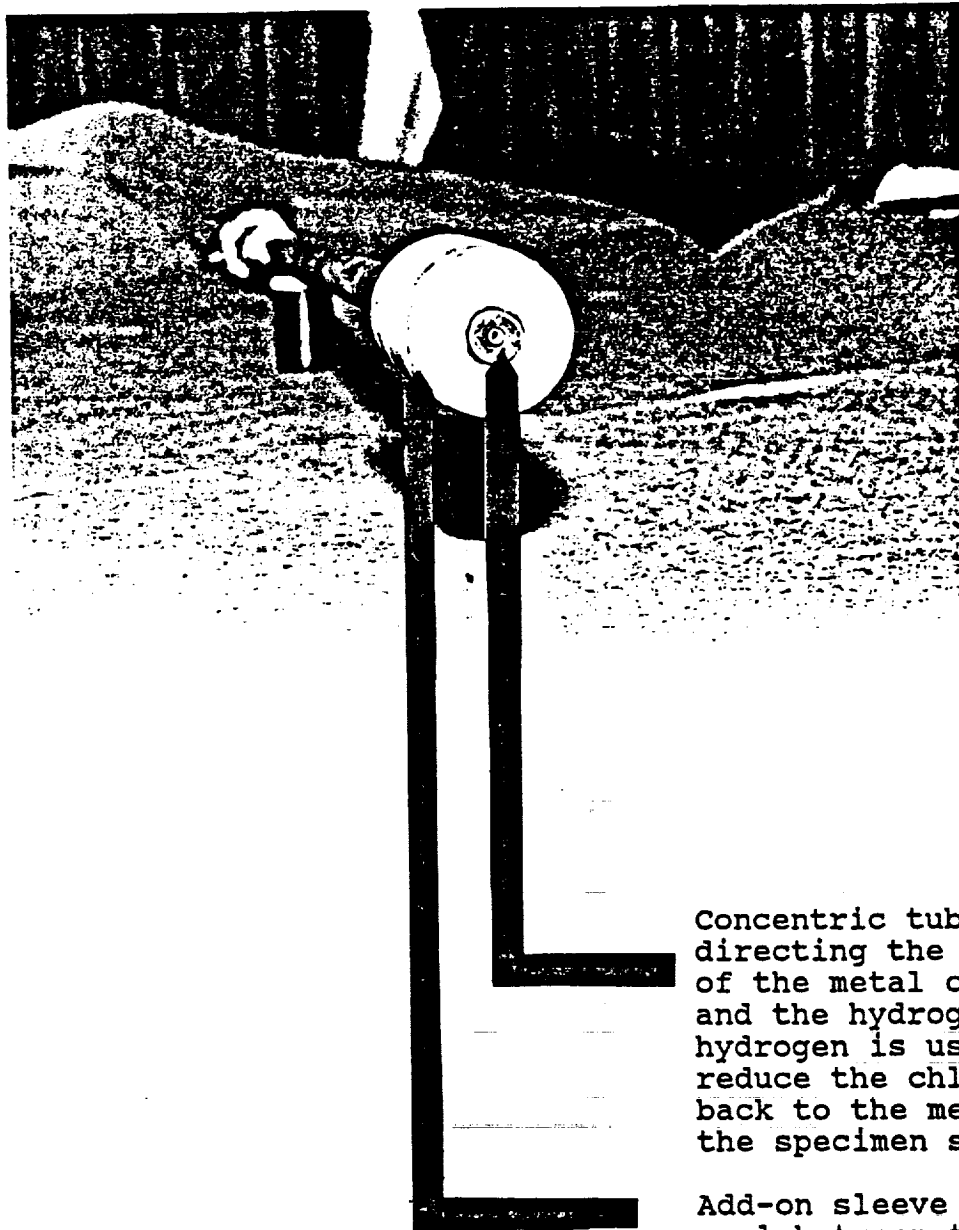


Figure 3 View of the support structure for the funnel and the specimen.



Concentric tubes for directing the discharge of the metal chloride and the hydrogen. The hydrogen is used to reduce the chloride back to the metal at the specimen surface.

Add-on sleeve used to seal between the lance and the funnel.

Figure 4 View of the lance use to chlorinate the metal and to introduce the metal chloride with the hydrogen.

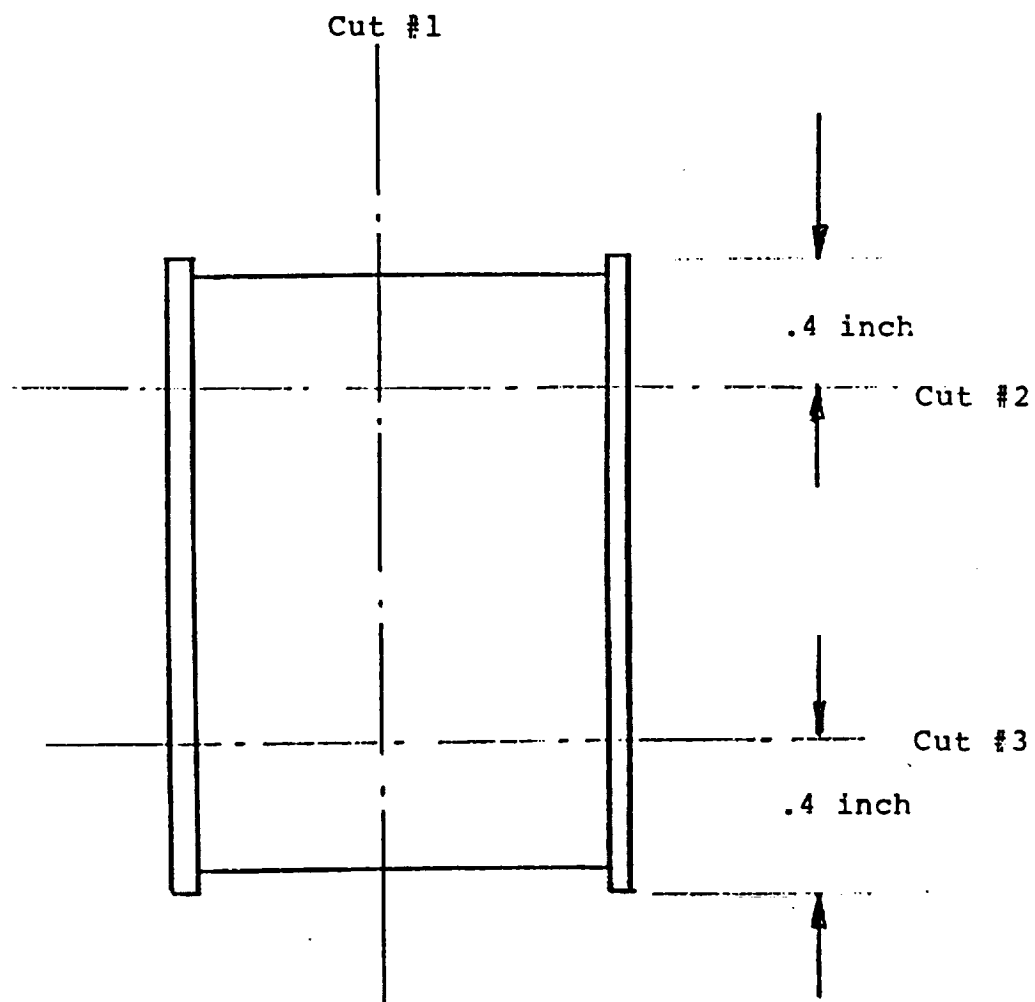


Figure 5. Sectioning plan for the cavity specimen

Figure 6A

SEM view of the  
Mo. coating at the  
#1 cut location.  
(see figure 5)

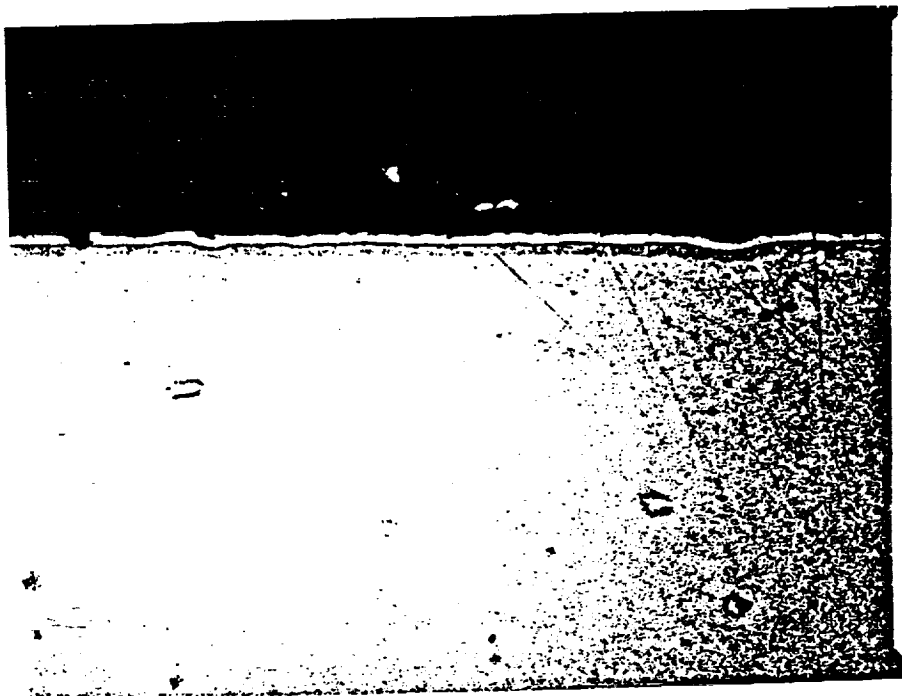
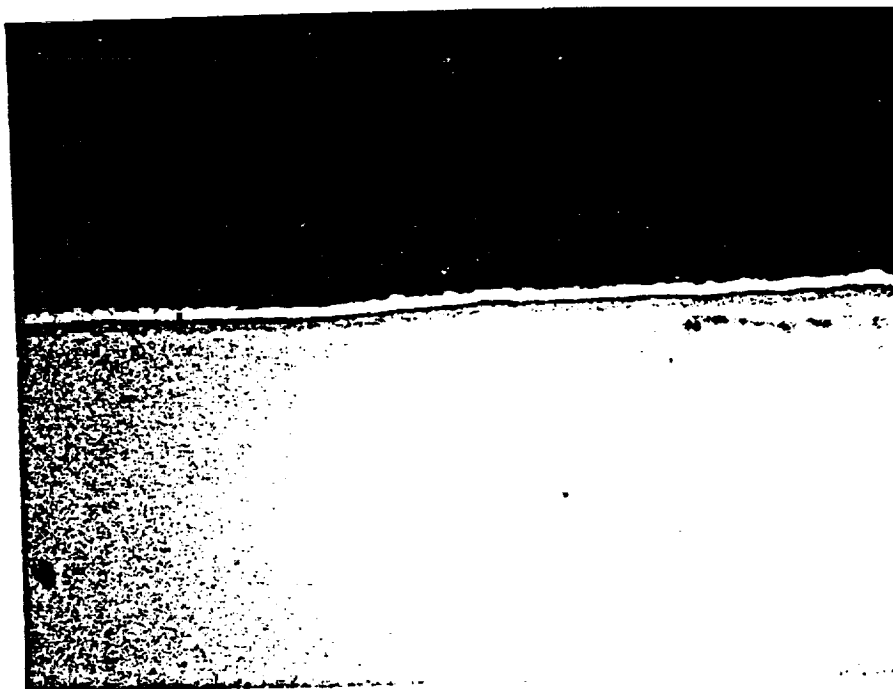


Figure 6B

SEM view of the Mo.  
coating at the  
cut #2 location.  
(see Figure 5)





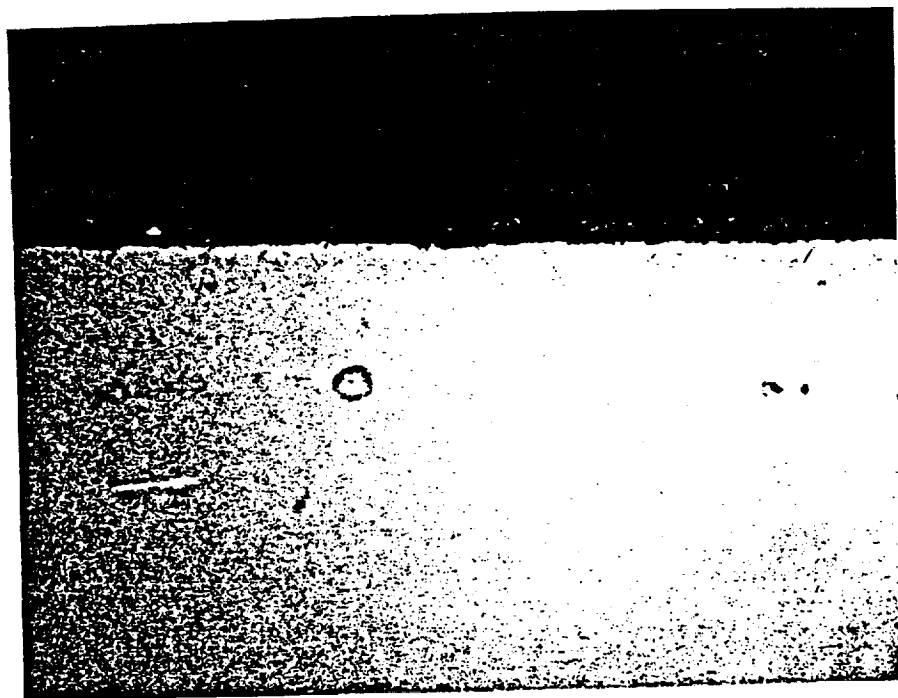


Figure 7. SEM view of the Mo. coating at the cut #3 position. The view indicates that neither the electroless nickel or the Mo. coated the Inco 718 at the cut #3 position.

Figure 8A

SEM view of  
the Nb. coating  
at the #2  
location.  
(see figure 5)

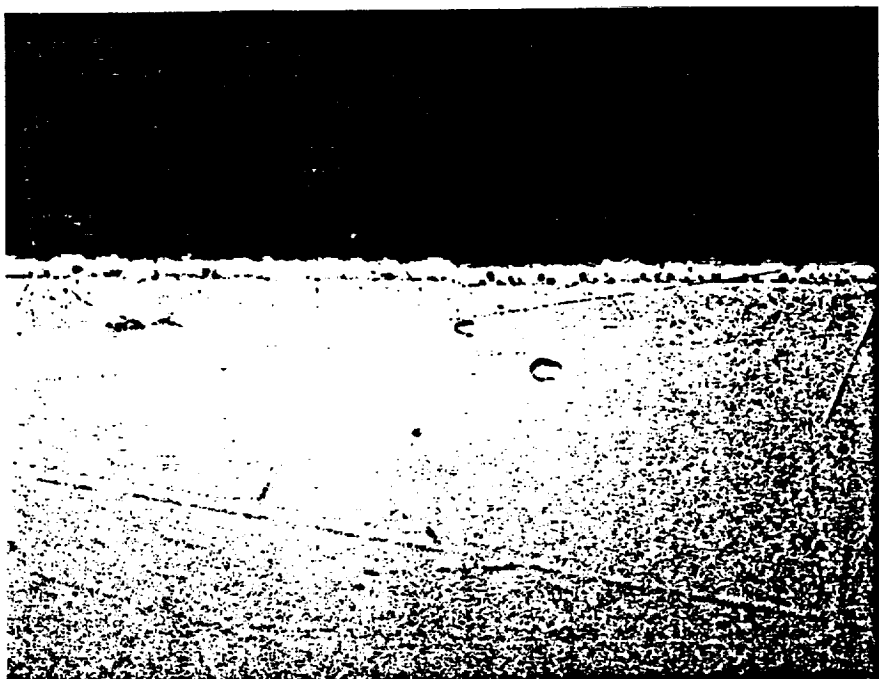
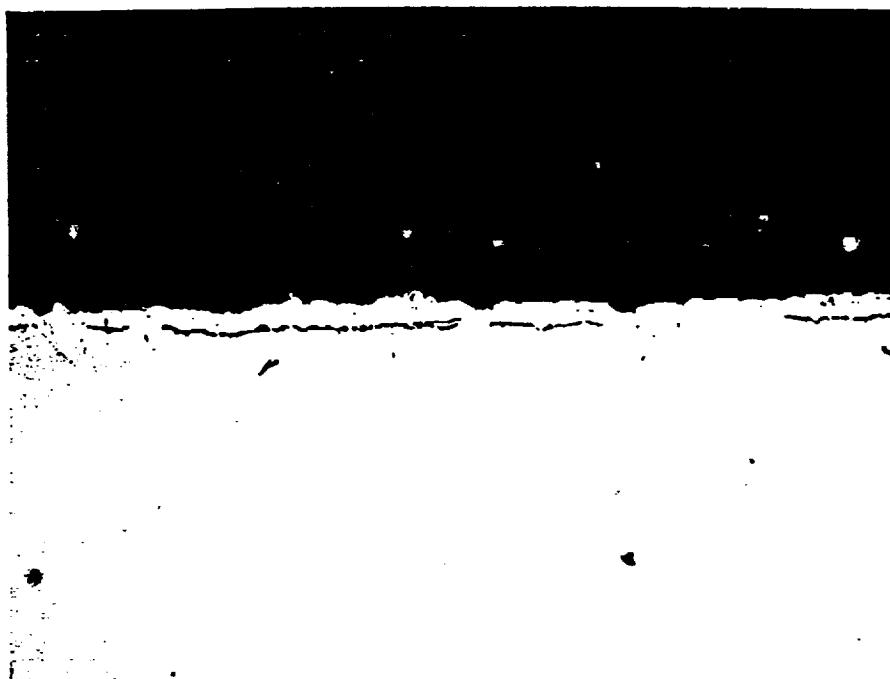


Figure 8B

SEM view of the  
Nb. coating at the  
cut #3 location.  
(see figure 5)



# Heat Pipe Fatigue Test Specimen Metallurgical Evaluation

Steven E. Walak and Michael J. Cronin  
*Mechanical Technology Incorporated*  
*Latham, New York*

Toni Grobstein  
*NASA-Lewis Research Center*  
*Cleveland, Ohio*

January 1992

Prepared for  
Lewis Research Center  
Under Contract NAS3-25463



## SUMMARY

A sodium-charged Inconel 718 heat pipe with an Ni-200 screen wick was operated for 1090 hr at temperatures between 950 K (1250°F) and 1050 K (1430°F) while being subjected to a mean tensile stress of (21 ksi) and a cyclic tensile stress of  $\pm 34$  MPa (5 ksi). The heat pipe survived the thermal-mechanical testing sequence and was then sectioned for metallographic and electron microprobe examination. The examination revealed only minor changes in the surface topography and chemistry of the sodium-exposed Inconel 718. Stress-accelerated corrosion, stress corrosion cracking, extensive grain boundary attack and liquid metal embrittlement were not observed.

A surface layer depleted in Cr, Nb, Ti, and Al was formed on the Inconel 718 in all sodium-exposed regions of the heat pipe. Fe and Mo concentrations were also reduced slightly in the condenser. In contrast to previous studies [4], the Ni concentration at the surface of the heat pipe increased as a result of sodium exposure. Chemical interaction between the Ni-200 wick and the Inconel 718 wall appeared to be the reason for the increased Ni concentration in the surface layer.

The depth of the surface layer ranged from 5 to 25  $\mu\text{m}$  (200 to 1000  $\mu\text{in.}$ ) and was directly related to the location of the surface in the heat pipe. The depth of the layer was slightly greater in the condenser section than in the evaporator section of the heat pipe. The variation in reaction layer depths, combined with deposits containing Ni, Nb, Fe, and Cr in the evaporator, indicates that material was transferred from the condenser to the evaporator by the sodium liquid and vapor flow.

## 1.0 INTRODUCTION

The component test power converter (CTPC) is a limited-life (<10,000 hr), laboratory test engine being developed to demonstrate the feasibility of free-piston, Stirling-cycle engine technology for space power conversion applications. The CTPC is designed to operate on thermal energy provided via a sodium metal heat pipe system operating at temperatures to 1050 K (1430°F) with a condenser heat flux of 25 W/cm<sup>2</sup>. The unique heat pipe system design minimizes the number of welded or brazed joints operating at elevated temperatures by integrating the CTPC's heater head directly with the heat pipe. In this configuration, regions of the integrated heater head/heat pipe are exposed to condensing sodium vapor, a mean stress of 145 MPa (21 ksi), and a cyclical stress of ±21 MPa (3 ksi). The heater head and heat pipe will be fabricated from Inconel 718.

The vapor and liquid dynamics in an operating heat pipe system result in liquid metal exposure conditions that are very different from those observed in pumped or flowing-loop systems. Thermal energy input at the heat pipe's evaporator generates pure sodium vapor in the working fluid. The vapor flows to the heat pipe's condenser, where thermal energy is extracted, causing the vapor to condense on the heat pipe wall. The condensed liquid is then pulled back to the evaporator by the capillary action of a wick structure within the heat pipe.

Laboratory testing is planned for the CTPC and heat pipe system to confirm the basic design concept and identify areas for further development. However, prior to full-scale engine testing, additional information is required to confirm the mechanical properties and corrosion resistance of nickel-based superalloys in liquid sodium heat pipe systems. The limited data that are available on nickel-based alloys in liquid sodium were primarily generated in flowing-loop systems for nuclear reactor applications and are not directly applicable to the heat pipe environment.

Therefore, to obtain more specific data, a heat pipe fatigue test specimen (HPFTS) was constructed and tested. The HPFTS was subjected to creep and fatigue loads during elevated-temperature operation to evaluate the corrosion resistance and mechanical performance of a sodium-filled Inconel 718 heat pipe. The test was designed to simulate the stress, temperature, and sodium exposure conditions in the most highly stressed region of the CTPC heat pipe system during the planned laboratory testing.

This report describes the test procedures used and presents the findings of the metallurgical analysis conducted on the HPFTS after test completion.

## 2.0 PROCEDURES

### 2.1 Test Specimen Components

The HPFTS, shown in Figure 1, consisted of a heat pipe envelope, wick, end caps, and attachment fixturing. Inconel 718 was used for the heat pipe envelope and end caps. The wick was fabricated from 200 mesh Ni-200 screen, with a wire diameter of 0.05 mm (0.002 in.). Commercially pure sodium was used as the working fluid. The compositions of the Inconel 718, the Ni-200 screen material, and the sodium are identified in Table 1.

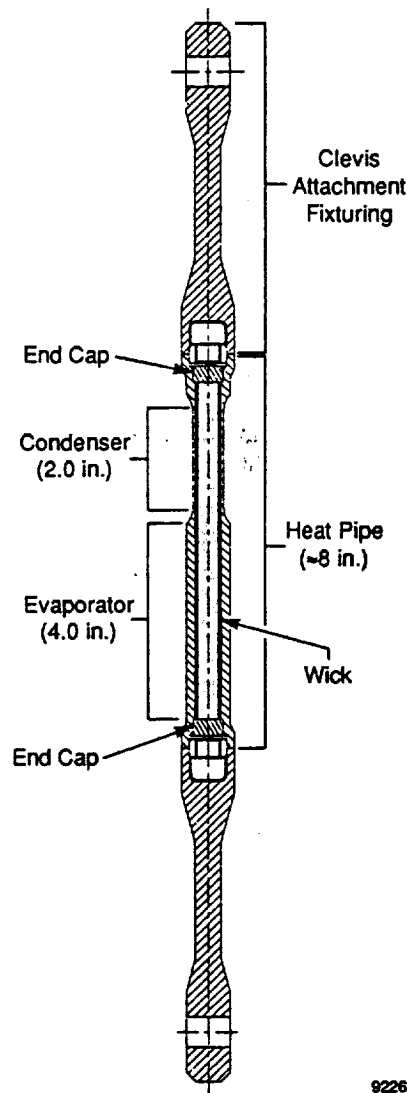


Figure 1. Heat Pipe Fatigue Test Specimen

Table 1. Material Compositions

Element	Inconel 718 (Weight %)	NI-200 (Weight %)	High-Purity Sodium* (ppm)
Ag	-	-	<3
Al	0.56	-	13
B	-	-	<13
Ba	-	-	<25
Be	-	-	<3
C	0.04	0.03	-
Ca	-	-	13
Cd	-	-	<25
Co	-	-	<13
Cr	18.45	-	<13
Cu	-	-	10
Fe	19.03	0.07	20
K	-	-	625
Li	-	-	<3
Mg	-	-	8
Mn	0.07	0.14	3
Mo	3.07	-	<25
Na	-	-	Balance
Nb	5.18	-	-
Ni	52.10	99.65	<13
Pb	-	-	<13
Rb	-	-	<25
Si	0.12	0.04	13
Sn	-	-	<13
Ti	0.98	0.01	<25
V	-	-	<13
Y	-	-	<25
Zn	-	-	<125
Zr	-	-	<25

\*Oxygen concentration of the sodium was not available.

91TR56

The heat pipe envelope was fabricated from 32 mm (1-1/4 in.) diameter Inconel 718 bar stock, AMS 5662, and was approximately 203 mm (8.0 in.) in length with an internal diameter of 12.7 mm (0.5 in.). The pipe condenser was 51 mm (2 in.) long, with a wall thickness of 1.6 mm (0.062 in.). The evaporator was 102 mm (4 in.) long, with wall thickness of 4.8 mm (0.19 in.). The difference in wall thickness ensured that the most severe stress conditions were obtained in the condenser to best simulate the conditions that would be experienced during CTPC laboratory testing. The highest stress in the CTPC heat pipe system under development occurs at the outer edge of the heater head fins, as shown in Figure 2.

The CTPC heat pipe condenser will be fabricated using a combination of conventional milling, electro-discharge machining (EDM), and chemical milling. Chemical milling will be used to remove the recast layer generated by the EDM process. To simulate the surface condition expected in the highest-stress region, the internal bore of the HPFTS was finished by chemical milling. The surface finish after chemical milling was measured at 1.5  $\mu\text{m}$  (60  $\mu\text{in.}$ ). A typical chemically milled surface is shown in Figure 3.

## 2.2 Test Specimen Assembly

The HPFTS components (heat pipe envelope, wick screen, end caps) were degreased in trichloroethane, a water-based detergent cleaning solution, and rinsed in deionized water. To assemble the wick, two layers of the Ni-200 screen were wrapped on a preoxidized stainless steel mandrel, inserted into the heat pipe envelope, and sintered at 1273 K (1832°F) for 30 min. The pipe was cooled to room temperature, the mandrel removed, and the screen spot welded to the heat pipe wall.

A 51 mm (2.0 in.) long, 99.5%-pure vanadium wire was inserted into the heat pipe for use in determining the oxygen content of the sodium working fluid after testing. The procedure to be used was a variation of the V-wire equilibration technique described in ASTM test method C997-83, sections 65 to 74. However, review of the testing requirements after HPFTS fabrication and assembly revealed that this technique was not viable for determining oxygen in the HPFTS due to the method's low detection limits (<15 ppm) [1, 2]\*. The V-wire was left in the heat pipe but was not used for analysis.

The heat pipe envelope was sealed with Inconel 718 end caps, which were tungsten inert gas (TIG) welded to the ends of the pipe. A 6.4 mm (0.25 in.) outside diameter Inconel 718 tube, with a 1.6-mm (0.063 in.) wall, was placed in one of the end caps to allow for sodium filling.

The heat pipe was charged with 10 grams of sodium metal using a push pot assembly and sealed with a high-temperature sodium service valve in an argon gas purged dry box. The pipe was heated at 928 K (1211°F) for 1-3/4 hr and 1123 K (1562°F) for 5 min in a vacuum of approximately  $2.7 \times 10^{-3}$  Pa to remove noncondensable gas and optimize the sodium fluid charge. The fill tube was then sealed by electric resistance welding in the vacuum chamber and operated in vacuum at 1123 K (1562°F) for approximately 10 min to ensure complete sealing of the fill tube.

Attachment fixturing was electron beam welded to the ends of the heat pipe. The entire HPFTS was vacuum heat treated according to the following schedule:

- 1227 K (1750°F) 1 hr argon gas cool
- 991 K (1325°F) 8 hr cool to 894 K (1150°F) at 55 K/hr (100°F/hr)
- 894 K (1150°F) 8 hr furnace cool to room temperature.

---

\*Numbers in brackets indicate references listed in Section 6.0.



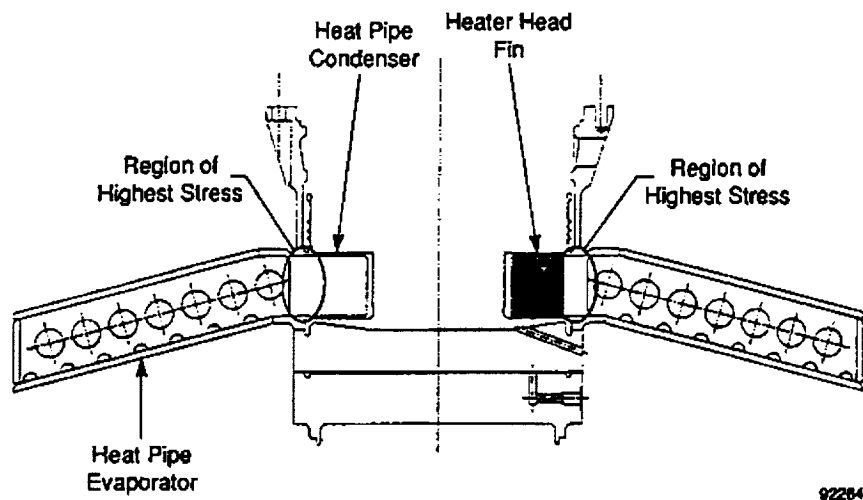


Figure 2. Component Test Power Converter (CTPC) Heater Head and Heat Pipe System Cross Section

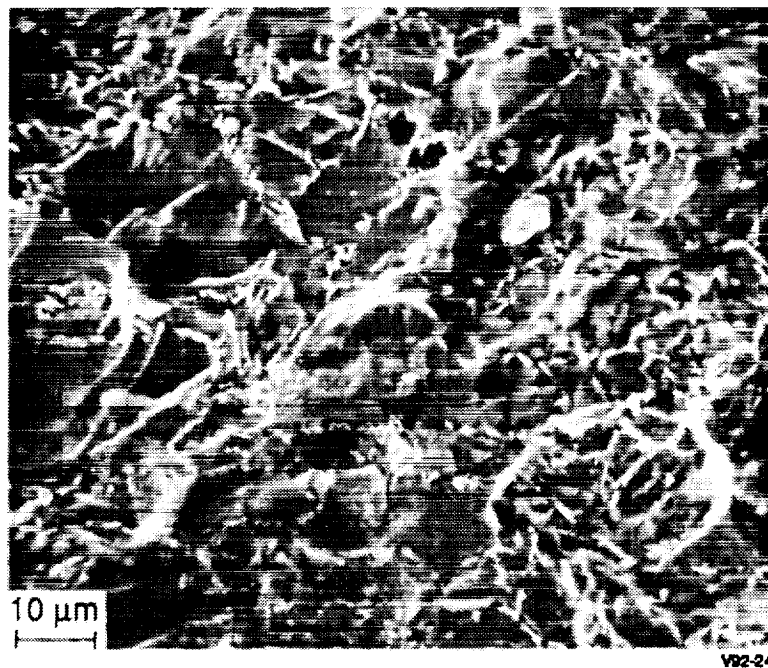


Figure 3. Scanning Electron Micrograph of an Inconel 718 Surface After Chemical Milling

## 2.3 Test Setup and Conditions

Under actual operating conditions, the highest-stress region of the CTPC heat pipe (Figure 2) will be exposed to condensing sodium vapor, elevated temperature, and combined static and cyclic mechanical loads. The sodium exposure, temperature, and stress conditions for the HPFTS were designed to simulate this region.

The HPFTS was enclosed in a stainless steel chamber (see Figure 4). The chamber was continuously purged with argon during testing to minimize external oxidation and the hazard of a sodium fire if heat pipe failure occurred. The HPFTS was tested in a vertical orientation, with the condenser above the evaporator, which allowed gravity to assist fluid transfer to the evaporator. The evaporator was heated by radiation from two 360-W, 60.3 mm (2.38 in.) inner diameter, half shell electric resistance heaters. The condenser cooled passively by conduction to the ends of the HPFTS and by radiation to the stainless steel enclosure. The estimated heat flux at the condenser was  $<5 \text{ W/cm}^2$ .

The HPFTS was subjected to 36 test sequences under thermal and mechanical load for a total test time of 1090 hr. Maximum temperatures in the condenser were 1000 K (1340°F) or 1050 K (1430°F), depending on the test sequence being conducted. Total hours at specific condenser temperatures were: 775 hr at 950 K (1250°F), 275 hr at 1000 K (1340°F), and 40 hr at 1050 K (1430°F). These operating times and temperatures were shown to produce approximately 2% creep in independent creep tests. Creep strain was not recorded during heat pipe testing. Temperature was monitored with type K thermocouples at ten locations along the length of the heat pipe. A plot (Figure 5) of the

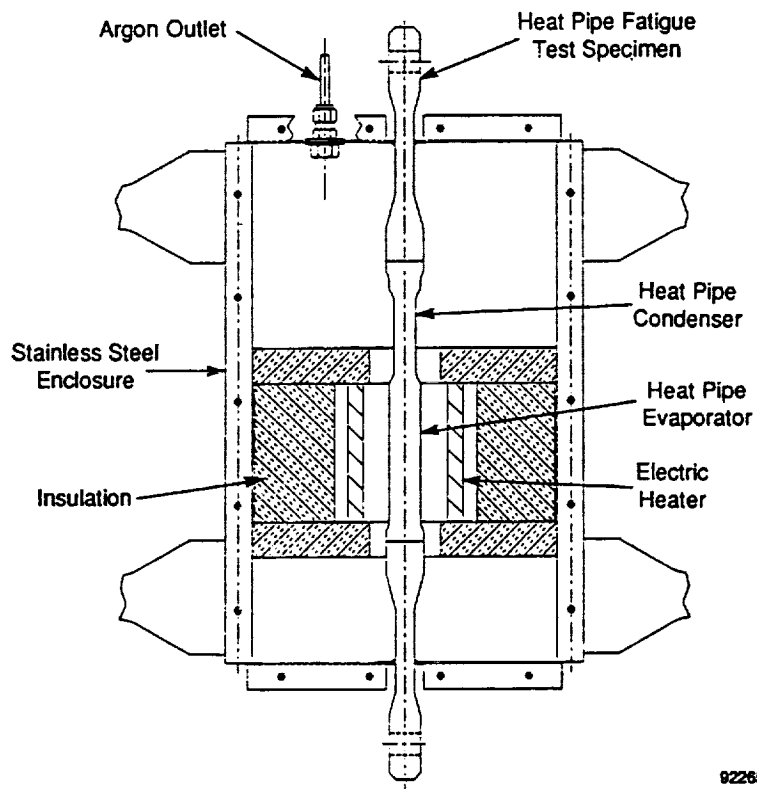


Figure 4. Heat Pipe Fatigue Test Setup

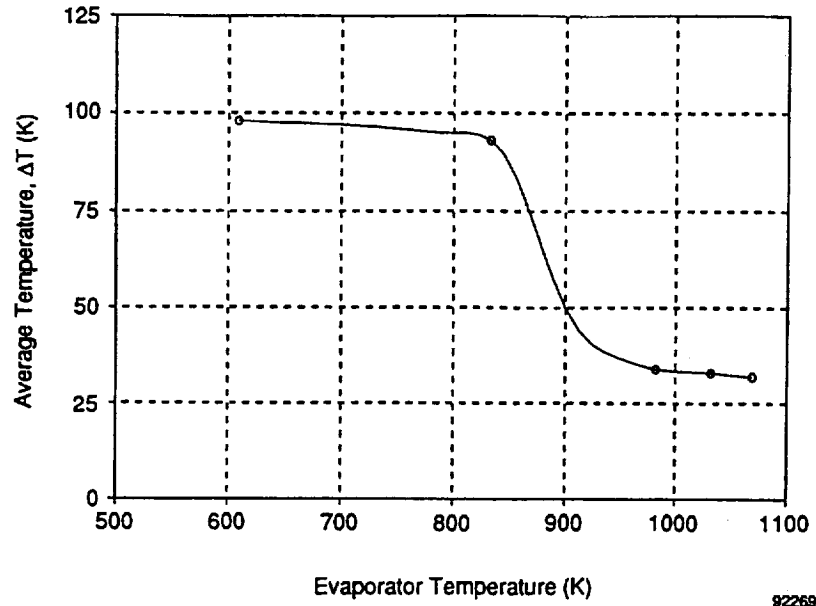


Figure 5. Difference in Average Outside Wall Temperature Between Evaporator and Condenser as a Function of Average Evaporator Temperature

difference in average outside wall temperature between the evaporator and condenser,  $\Delta T$ , as a function of the average outside wall temperature of the evaporator shows a significant drop in  $\Delta T$  at evaporator temperatures above approximately 900 K (1160°F). The internal temperature drop along the length of the heat pipe was estimated to be approximately 70 K (125°F) at temperatures below 900 K (1160°F), and <5 K (10°F) at temperatures above 925 K (1205°F).

The mechanical load remained the same for all sequences: 145 MPa (21 ksi) mean stress and  $\pm 35$  MPa (5 ksi) cyclic stress. During a test sequence, the load cycle was controlled using load response feedback. A typical test sequence, shown in Figure 6, consisted of the following steps:

1. A 145 MPa (21 ksi) mean stress was applied to the heat pipe condenser at room temperature to simulate initial CTPC pressurization with He at 150 bar.
2. Heat was applied to the evaporator until the condenser temperature reached 950 K (1250°F), simulating heat pipe system start-up.
3. A cyclic stress of  $\pm 35$  MPa (5 ksi) at 70 Hz was applied in addition to the mean stress to simulate the pressure wave in the operating CTPC with an added 14 MPa (2 ksi) safety factor.
4. Depending on the sequence being conducted, the condenser temperature was increased to either 1000 K (1340°F) or 1050 K (1430°F) after 10 to 20 hr of operation at 950 K (1250°F).
5. The HPFTS continued to operate to the end of the test sequence under load at the higher temperature to simulate CTPC operation at higher temperatures.
6. At the end of the test sequence, the cyclic stress was removed and the heater turned off to allow the heat pipe to cool.
7. When the external heat pipe wall at the evaporator reached a temperature of 421 K (300°F), the mean stress was removed to simulate CTPC shutdown.
8. Testing was resumed immediately with the next test sequence.

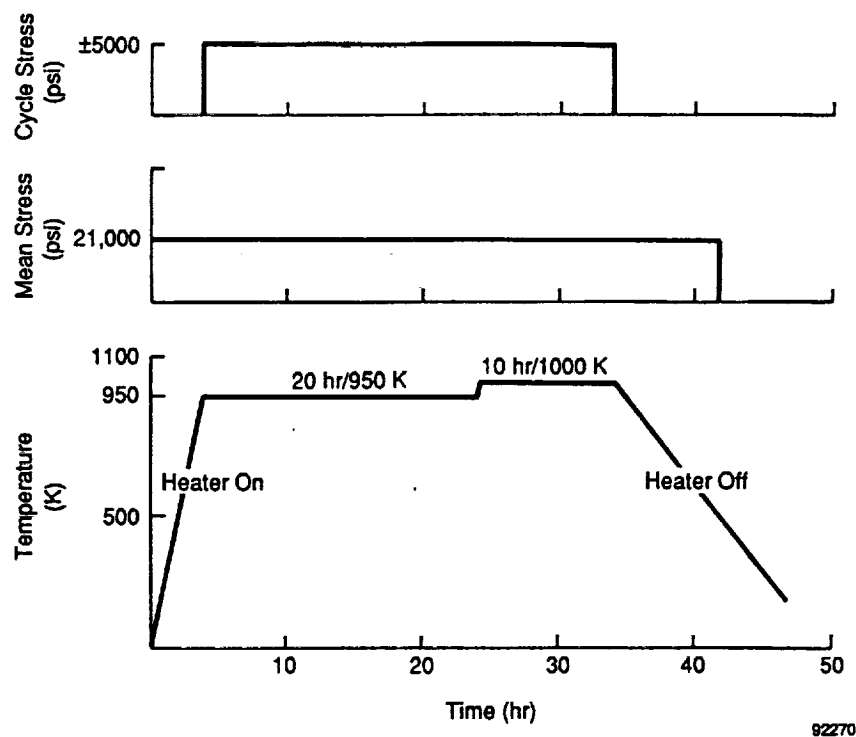


Figure 6. Typical Test Sequence

## 2.4 Test Specimen Preparation for Analysis

After completion of the 1090-hr fatigue test, the HPFTS was prepared for metallurgical analysis. The attachment fixtures were cut from the ends of the heat pipe. The heat pipe was cut across its diameter in the condenser using a slow-speed diamond saw with a mineral oil lubricant under an argon gas purge.

Sodium was removed from the heat pipe sections by immersion in alcohol. The two heat pipe pieces were submerged in a 50/50 mixture of butyl and propyl alcohols, and the sodium was allowed to react with this mixture for several hours. The pipe was then transferred to a mixture of methyl and ethyl alcohols to continue the reaction process. The total time the pieces were submerged in the alcohols was approximately 24 hr. Final sodium removal was performed in methyl alcohol with intermittent vibration in an ultrasonic cleaner for approximately 12 hr.

Longitudinal cuts were made along two lines approximately  $180^\circ$  apart using an abrasive cut-off wheel and water lubrication. The abrasive wheel cuts were made only through the depth of the heat pipe wall to avoid damaging the wick. The wick was then carefully sectioned along the same two cut lines using surgical scissors and a scalpel. The resulting four pieces were then submerged in ethyl alcohol and vibrated in an ultrasonic cleaner.

## 2.5 Specimen Analysis

Metallographic sections of the wick and heat pipe wall were prepared from the evaporator and condenser. A JEOL T-300 scanning electron microscope equipped with a Tracor Northern TN-200 energy dispersive x-ray analysis system was used to examine the wick and wall surfaces. Electron microprobe analysis using a JEOL 733 Superprobe equipped with a complete wavelength dispersive x-ray spectral (WDS) analysis system was used for quantitative chemical analysis of the metallographic sections.

### 3.0 RESULTS

The wick and heat pipe appeared to be in very good condition after sectioning and cleaning, showing no visible signs of corrosion attack. The only visually noticeable effect of sodium exposure was a metallic-looking deposit on the wick over a 25.4 mm (1.0-in.) length at the base of the evaporator (see Figure 7\*). The metallographic analysis, however, did produce evidence of localized corrosion.

#### 3.1 Wick

Scanning electron microscope examination of the metallic-looking deposit at higher magnification revealed that the wick was fully coated by the deposited material, as shown in Figure 8. The diameter of the wire in the specimen increased from 0.050 mm (0.002 in.) to approximately 0.076 mm (0.003 in.).

Many of the wires with the heaviest deposits were observed to have a central core surrounded by an outer shell, as can be seen in Figure 9. The compositions of the outer shell and central core were examined using WDS analysis on polished metallographic sections. The outer shell contained approximately 80% Ni and 20% V with the concentration of V gradually decreasing toward the central core. The central core was nearly pure Ni with <1% V. A slight increase in Cr and O was also observed at the outer edge of the wire deposit. Table 2 lists the concentration of elements in the deposited material from three locations on the wire cross section.

The wick wires were not significantly changed in regions away from the base of the evaporator. No measurable change in wire diameter was observed in the upper regions of the evaporator or in the condenser. Grain boundary etching was the only noticeable effect of sodium exposure in these regions (see Figure 10). No change in wire chemistry was detected with WDS analysis.

A second type of deposit was observed in a small area approximately 44.5 mm (1.75 in.) above the base of the evaporator. The location of the deposit is suspected of corresponding with the region of contact between the V-wire and the heat pipe wall but this could not be confirmed. In this region, a cluster of crystals containing Ni and V with small additions of Nb, Cr, Al, Ca, Si, C, and O was formed on the wick as shown in Figure 11. WDS analysis on the as-deposited material was used to estimate the concentration of these elements in the deposit. The analysis results are given in Table 3. The Ca, Si, C, and O appeared to be concentrated in nodules attached to the crystal surface as shown in Figure 12.

#### 3.2 Heat Pipe Wall

Scanning electron microscopy was used to examine the heat pipe wall for evidence of surface corrosion. Fine surface pits, <1.5  $\mu\text{m}$  (60  $\mu\text{in.}$ ) in diameter, were observed at the evaporator base to a height of approximately 25.4 mm (1.0 in.) (see Figure 13). The pitted region corresponded with the region of the wick that was coated with the vanadium-containing deposits. Exposure to excess sodium liquid accumulated at the base of the evaporator appears to be the reason for the surface changes observed in this region. The maximum depth of the fine surface pits was <10  $\mu\text{m}$  (400  $\mu\text{in.}$ ) as revealed by metallographic sections (Figure 14). The intensity of pitting gradually decreased at distances greater than 25.4 mm (1.0 in.) from the evaporator base and no fine surface pits were observed above approximately 51 mm (2 in.) (Figure 15).

The condenser wall was faceted as a result of surface etching, with the most significant etching occurring in the lower 32 mm (1.25 in.) of the condenser (Figure 16). The faceted surface was not observed above approximately 38 mm (1.5 in.) into the condenser (Figure 17). Limited vapor flow

---

\*Due to the large number of figures and tables in this section, they are included at the end of the text in their order of reference.

resulting from a build-up of noncondensable gas or excess sodium metal are probable explanations for the lack of etching at the condenser end.

A surface layer, appearing white in etched metallographic sections, was observed on all heat pipe surfaces exposed to sodium during testing (Figure 18). The layer is thought to result from a change in base metal surface chemistry due to interaction with the high-temperature sodium metal. The thickness of the layer was approximately 15 to 25  $\mu\text{m}$  (600 to 1000  $\mu\text{in.}$ ) in the evaporator and 5 to 10  $\mu\text{m}$  (200 to 400  $\mu\text{in.}$ ) in the condenser.

WDS analysis results, presented in Table 4, indicated that the concentrations of Cr, Nb, Al, and Ti were reduced and the concentration of Ni was increased in the layer relative to the nominal alloy composition. The concentrations of Fe and Mo were reduced slightly in some locations. An average layer composition, calculated from data taken at several locations in the evaporator and condenser, indicated that the changes in Cr, Fe, Ni, and Mo concentration were more pronounced in the condenser. All composition data used in the average calculation were taken at 2 to 3  $\mu\text{m}$  (80 to 120  $\mu\text{in.}$ ) below the sodium-exposed surface.

Knoop microhardness measurements were taken in the surface layer and the unaffected heat pipe material. The surface layer hardness was approximately 203 KHN and the unaffected Inconel 718 was 435 KHN, indicating a significant reduction in surface hardness.

In addition to the surface changes discussed above, the concentration of grain boundary carbides was reduced at the sodium-exposed surface (Figure 19). The grain boundary carbides were affected to a depth of 25 to 30  $\mu\text{m}$  (1000 to 1200  $\mu\text{in.}$ ). Depletion of carbides was observed in both the evaporator and condenser. Metallographic sections revealed that some carbides exposed to the sodium were being dissolved and leached from the surface (Figure 20).

A small region of more extensive corrosion was observed approximately 44.5 mm (1.75 in.) above the base of the evaporator. The depth of attack in this region was approximately 35  $\mu\text{m}$  (1400  $\mu\text{in.}$ ), as shown in Figure 21. The reason for accelerated corrosion at this location is not certain but is suspected of corresponding with the contact area between the V-wire and the heat pipe wall. Accumulation of liquid sodium with a high concentration of oxygen contamination is thought to be the reason for the local corrosion mechanism. Table 5 provides the results of the WDS analysis of the corrosion product and white regions in the base metal adjacent to the corrosion product.

The corrosion product remained in the surface pits after sectioning and cleaning with alcohol and water. WDS analysis showed that the chemical composition of the corrosion product was similar to sodium-chromium-oxygen compounds observed in 300 series stainless steels exposed to high-oxygen sodium [3]. Fe, Ni, Nb, Al, and Ti were also observed in the corrosion product formed in Inconel 718.

As indicated in Table 5, the white regions in the base metal adjacent to the corrosion product were depleted in Cr, Nb, Al, and Ti and enriched in Ni. The concentration of Fe and Mo, 18.8% and 3.9% respectively, showed little change from the nominal alloy concentration of 19.0% Fe and 3.1% Mo.

Crevices at the ends of the pipe were examined for signs of accelerated corrosion. The locations of these crevices is shown in Figure 22. Minor grain boundary attack, <10- $\mu\text{m}$  (400  $\mu\text{in.}$ ) deep, was observed in metallographic sections from the evaporator crevices (see Figure 23). A larger, local pit was observed in a metallographic section from the condenser, Figure 24. Several metallographic sections taken from adjacent regions contained no indications of pitting. The cause of the pit in the condenser crevice could not be identified conclusively. Accelerated corrosion from contamination accumulated in the crevice or a simple defect in the end cap weld are two possible explanations.

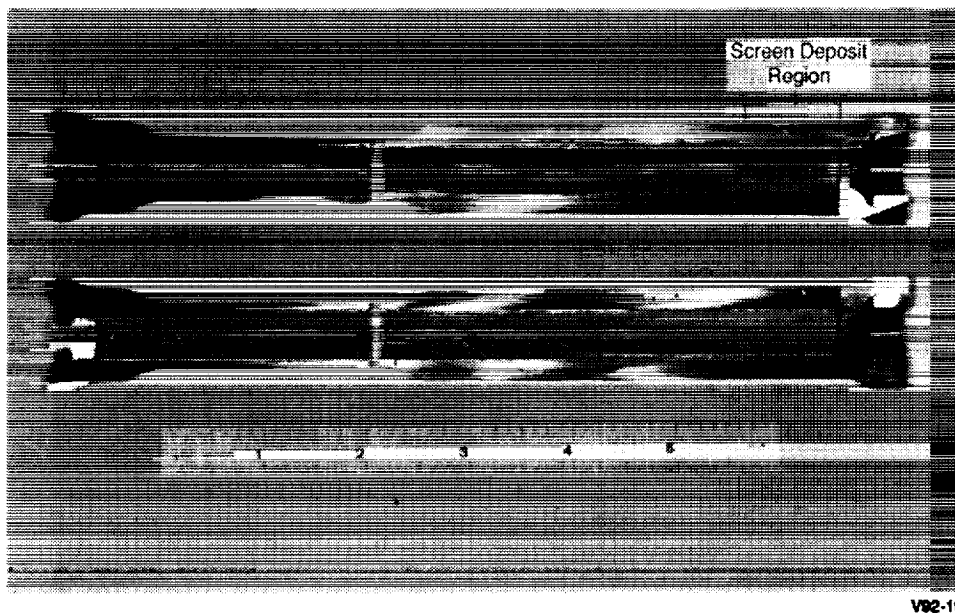


Figure 7. Heat Pipe Fatigue Test Specimen After Sectioning and Alcohol Cleaning

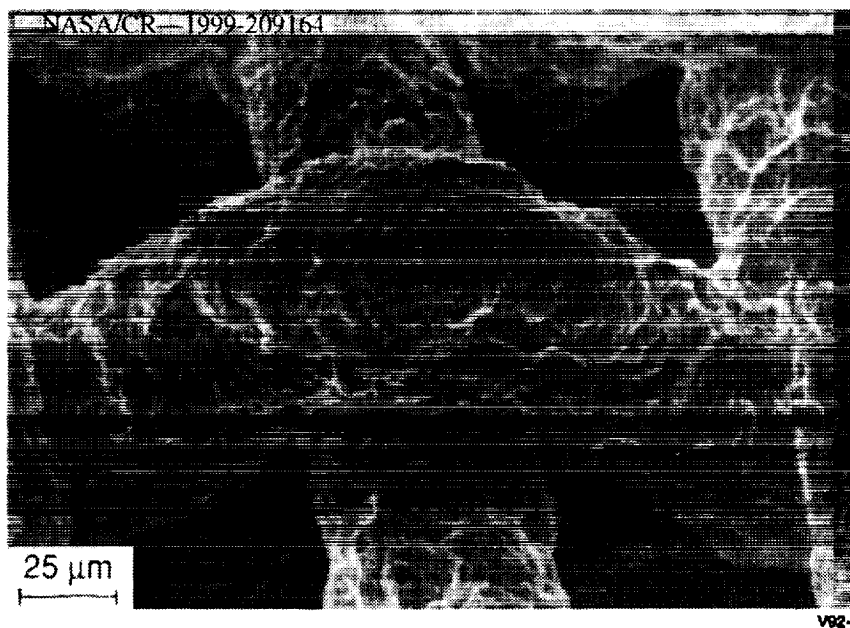


Figure 8. Scanning Electron Micrograph of Wick at Evaporator Base

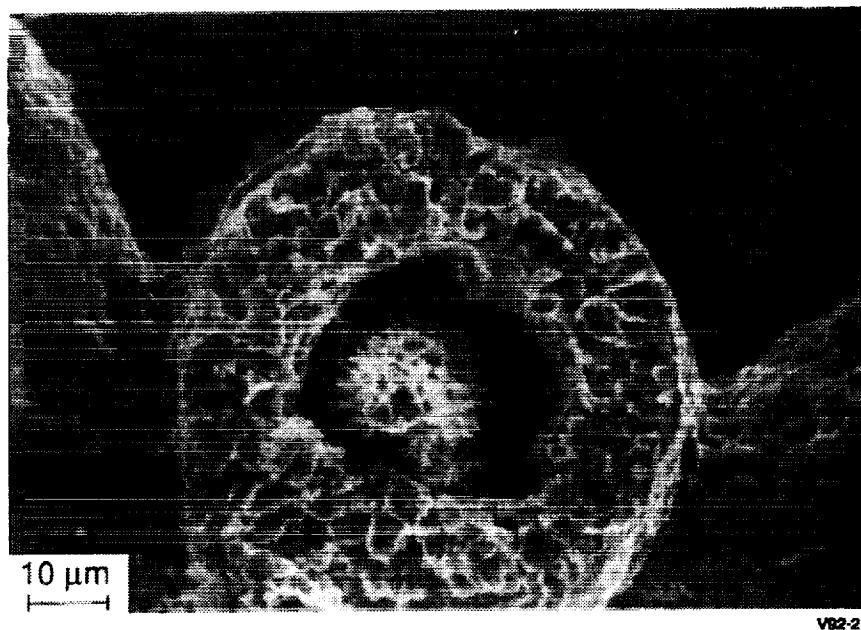


Figure 9. Scanning Electron Micrograph of Fractured Wire in Deposit Region Showing Cored Structure

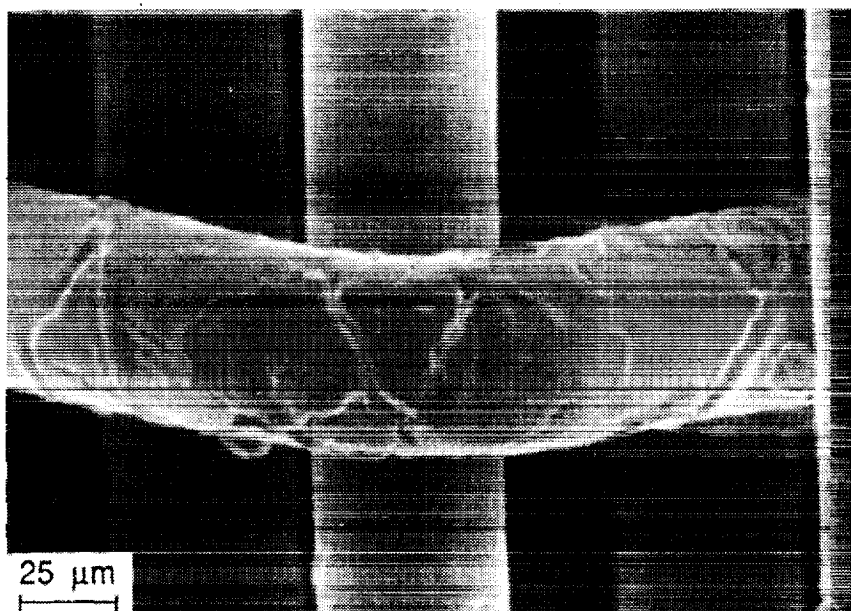
Table 2. Nominal and Post-Test Compositions of Wick from Lower Evaporator

Element	Nominal Ni-200 (Weight %)	Post-Test from Three Wire Locations		
		Outer Edge (Weight %)	Mid-Radius (Weight %)	Central Core (Weight %)
Al	—	•	•	•
C	0.03	•	•	•
Cr	—	0.62	0.12	0.14
Fe	0.07	0.12	0.28	0.23
Mn	0.14	0.19	0.35	0.44
Mo	—	•	•	•
Nb	—	•	•	•
Ni	99.65	76.80	92.50	97.70
O	—	1.60	0.98	0.78
Si	0.04	—	—	—
Ti	0.01	0.14	0.17	0.16
V	—	20.55	5.61	0.54

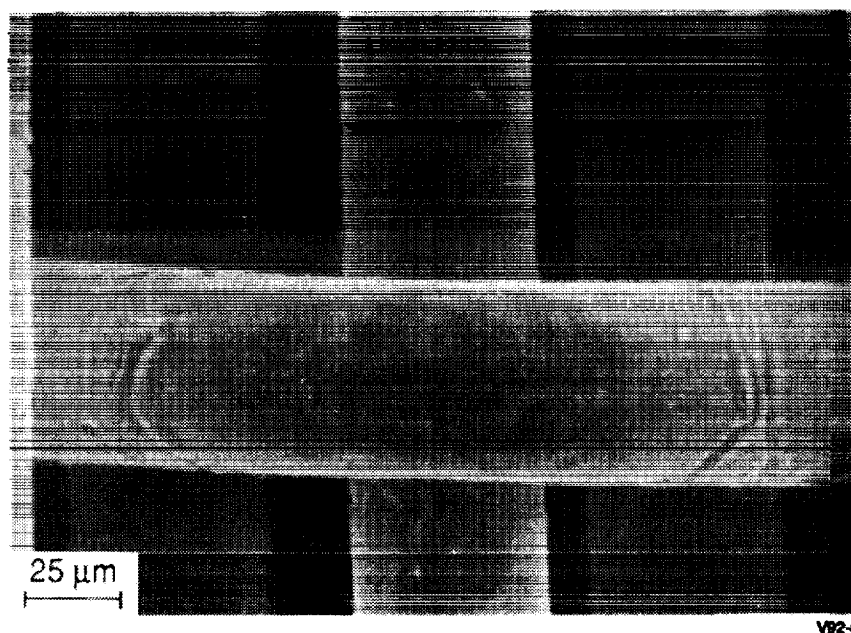
91TR58

\*Concentration below detectable limit.





**a) Condenser**



**b) Upper Evaporator**

**Figure 10. Scanning Electron Micrograph of Wick**

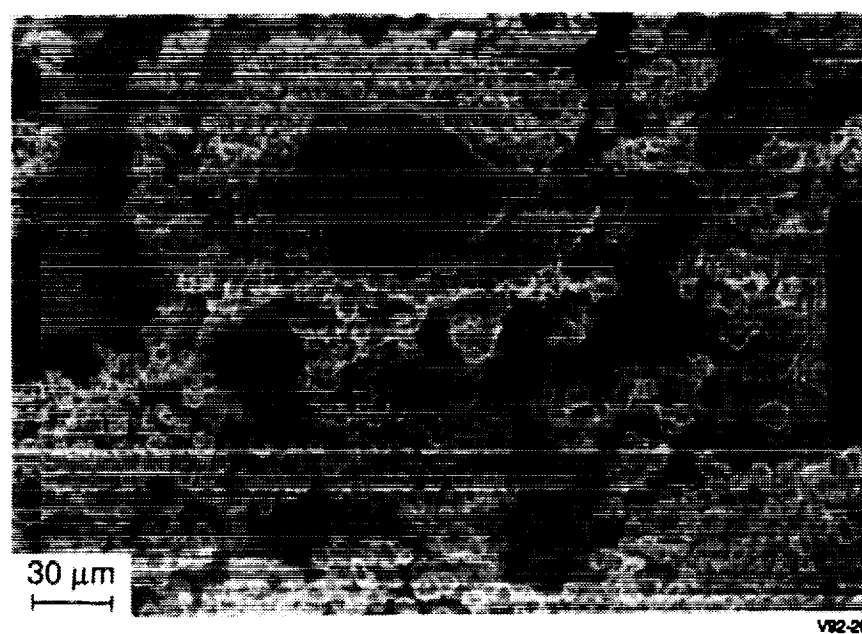
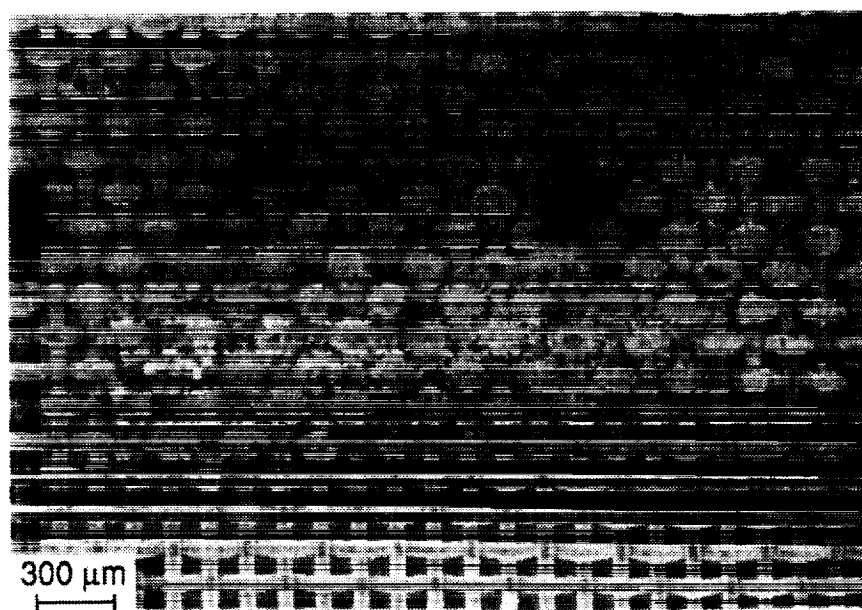


Figure 11. Scanning Electron Micrograph of Screen Deposits in Evaporator

Table 3. Composition of Crystalline Deposit from Lower Evaporator

Element	Deposit Concentration (Weight %)
Al	0.30
C	0.30
Ca	0.51
Cr	0.47
Fe	0.04
Mn	*
Mo	*
Nb	0.87
Ni	72.26
O	3.90
Si	0.07
Ti	*
V	21.27

\*Concentration below detectable limit.

91TR56

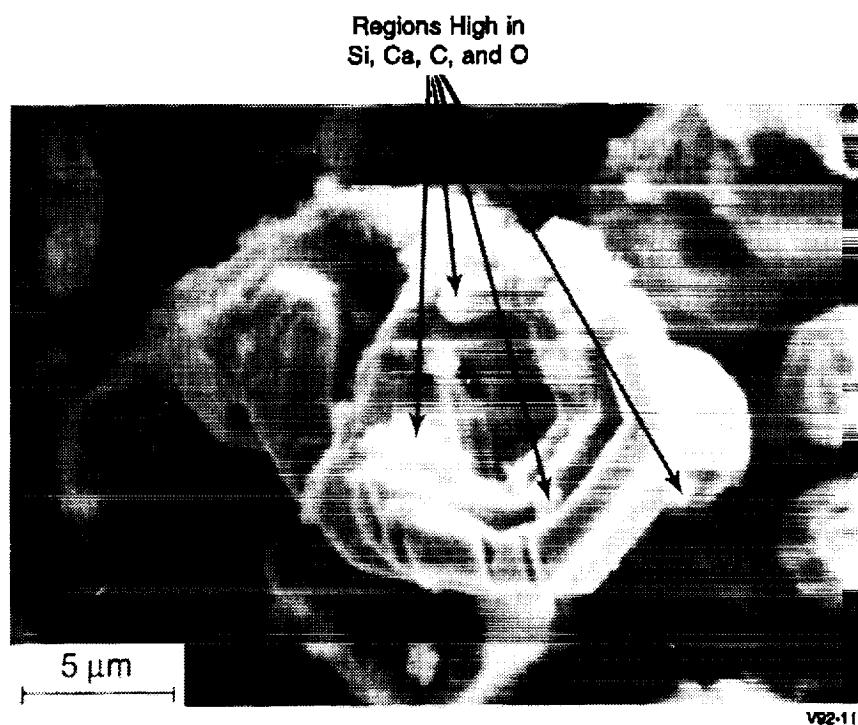
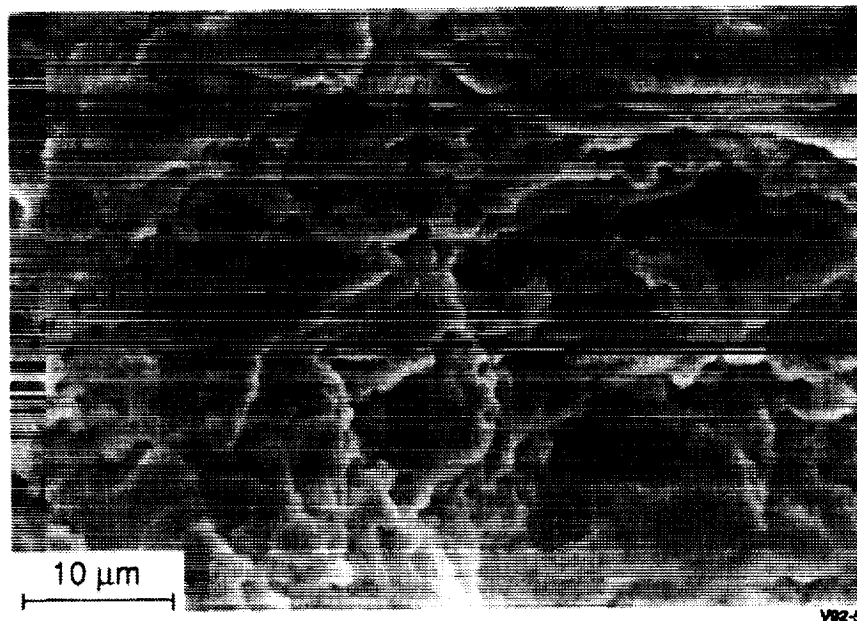
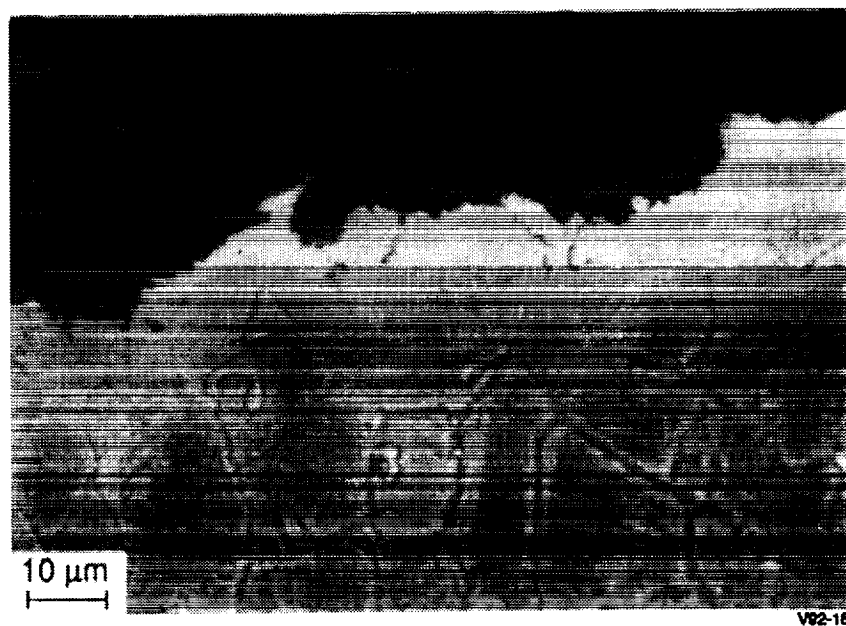


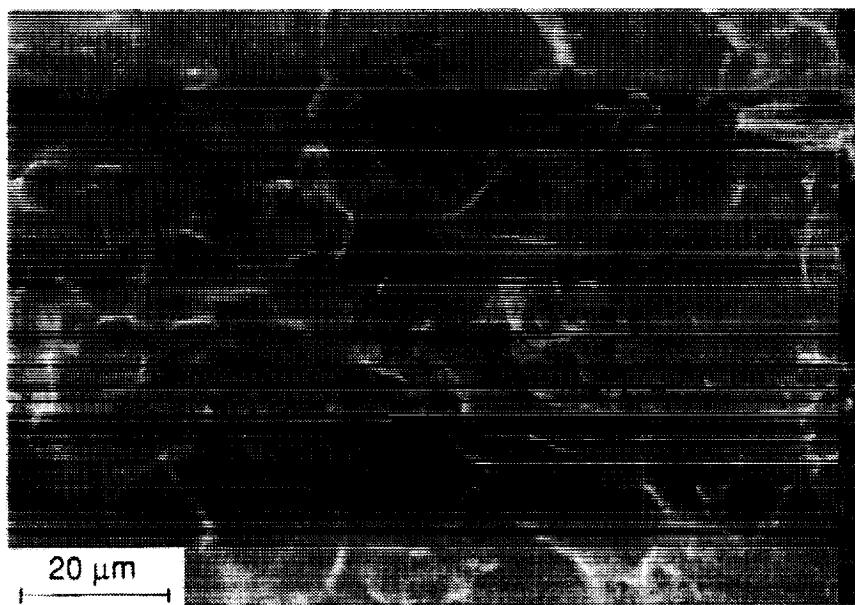
Figure 12. Secondary Electron Image of Screen Deposit in Evaporator



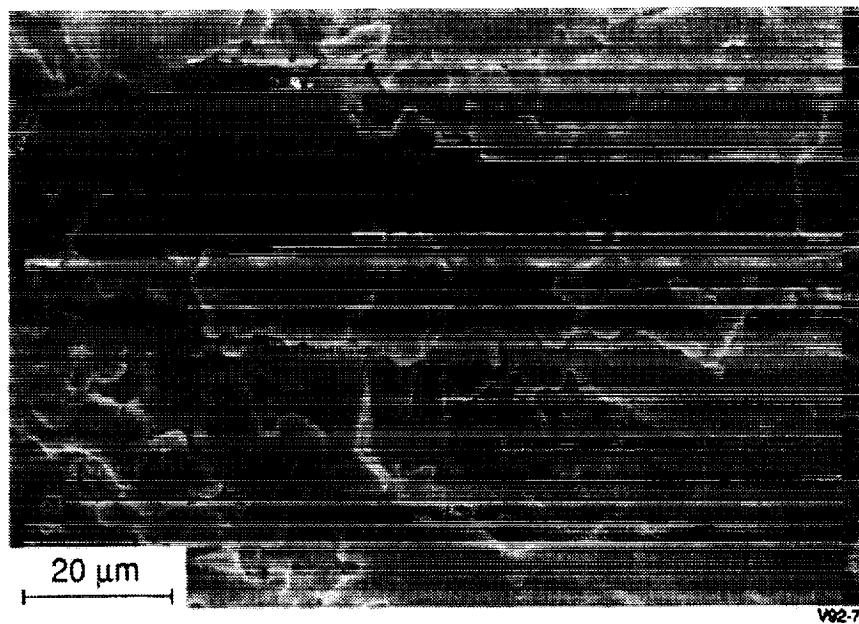
**Figure 13. Scanning Electron Micrograph of Inconel 718 Heat Pipe Wall at Evaporator Base**



**Figure 14. Optical Micrograph of Fine Surface Pitting on Heat Pipe Wall at Evaporator Base**

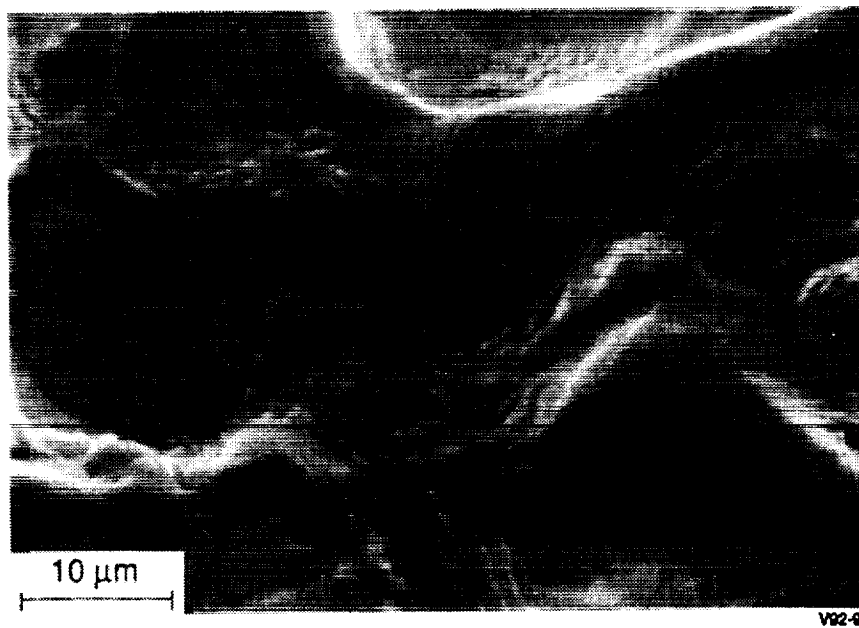


**a) 2.0 in. Above Base**

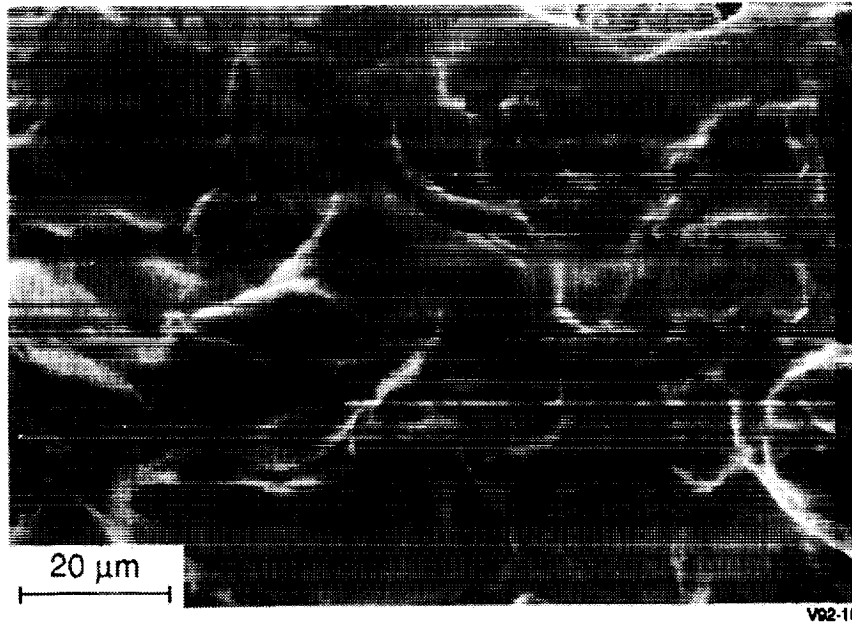


**b) 1.25 in. Above Base**

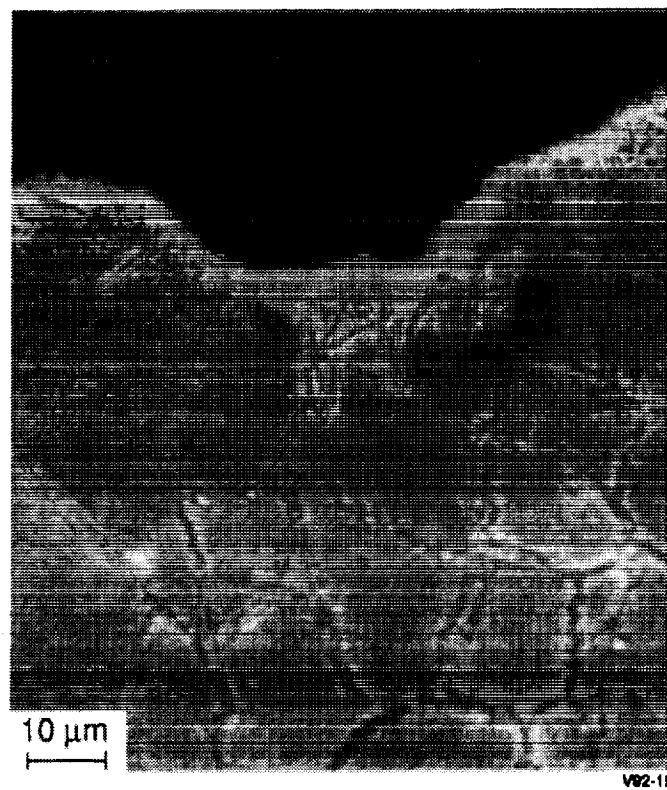
**Figure 15. Scanning Electron Micrographs of Heat Pipe Wall  
at Two Locations Above Evaporator Base**



**Figure 16. Scanning Electron Micrographs of Faceted Surface in Condenser**



**Figure 17. Scanning Electron Micrograph of Heat Pipe Wall Surface in Upper Half of Condenser**



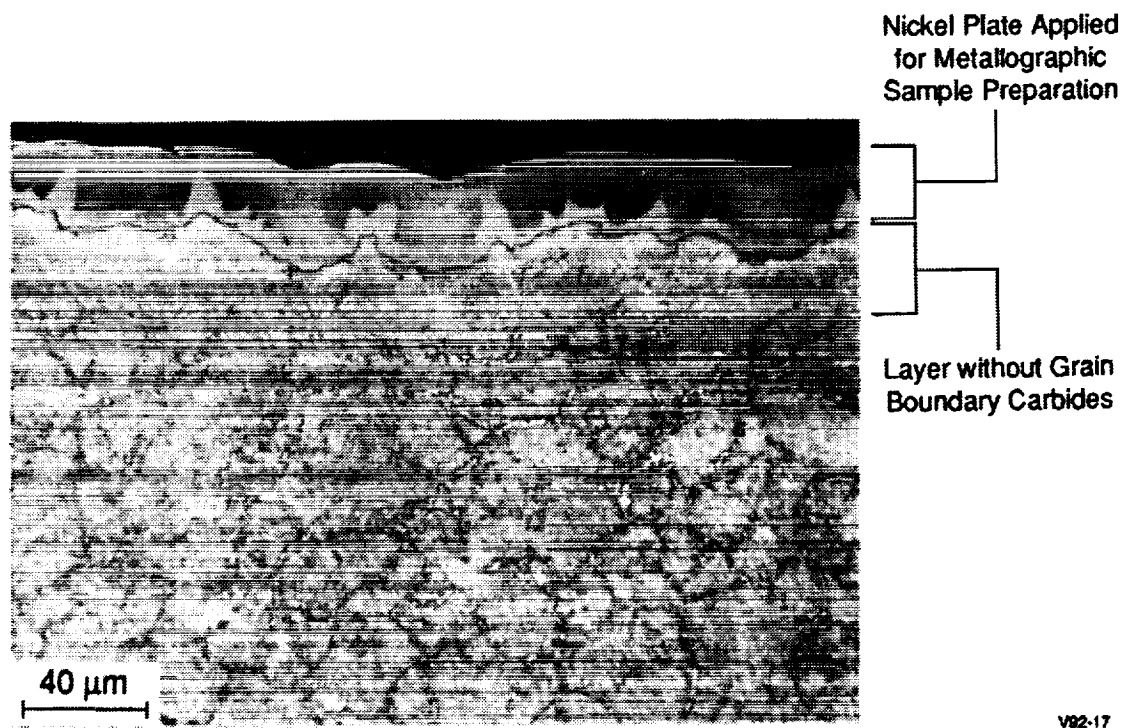
**Figure 18. Optical Micrograph of Inconel 718 Surface Layer (White) in Condenser**

Table 4. Comparison of Heat Pipe Wall Surface Layer and Nominal Alloy Compositions

Element	Nominal Inconel 718 (Weight %)	Evaporator Surface* (Weight %)	Condenser Surface* (Weight %)
Al	0.56	0.05	0.25
C	0.04	0.00	0.00
Cr	18.45	15.49	11.61
Fe	19.03	18.48	13.76
Mn	0.07	0.05	0.04
Mo	3.07	3.03	2.38
Nb	5.18	1.68	2.23
Ni	52.10	60.10	69.19
O	—	0.08	0.01
Si	0.12	0.00	0.01
Ti	0.98	0.22	0.44
V	—	0.82	0.11

\*Average values calculated from WDS analysis, 2 to 3  $\mu\text{m}$  below sodium-exposed surface.

91TR56



V92-17

Figure 19. Optical Micrograph of Inconel 718 Surface Layer in Evaporator



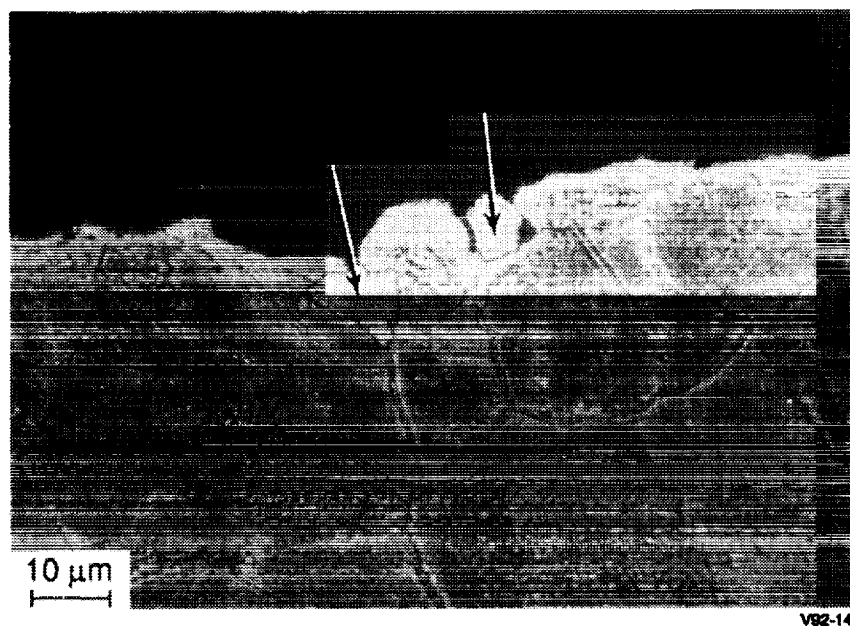


Figure 20. Optical Micrograph of Inconel 718 Carbides Partially Dissolved at Sodium-Exposed Surface (Arrows)

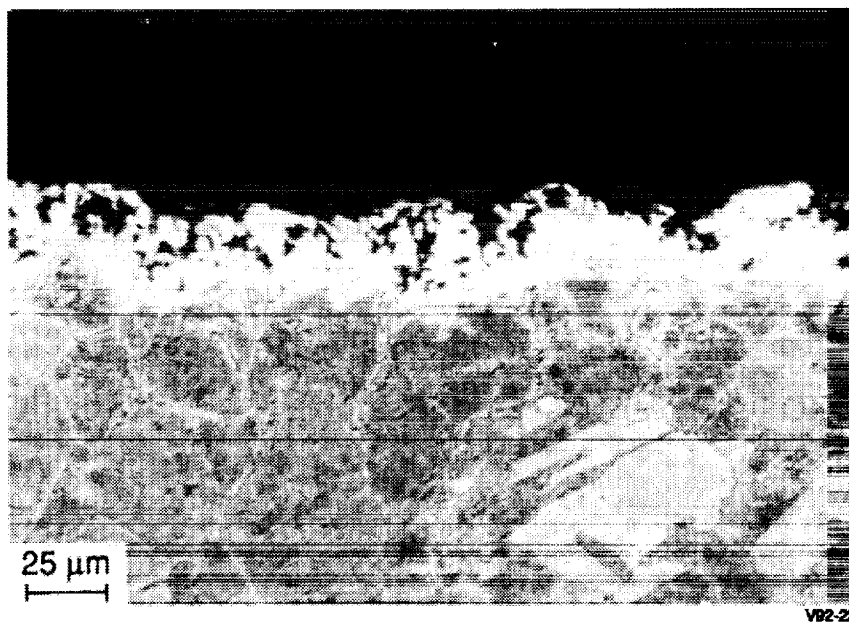
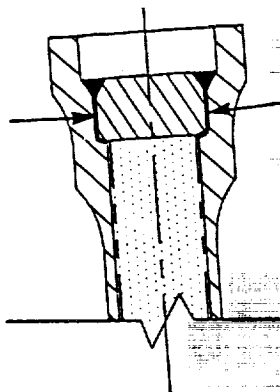


Figure 21. Optical Micrograph of Oxygen-Accelerated Corrosion

Table 5. Comparison of Corrosion Product and White Region with Nominal Alloy Composition

Element	Nominal Inconel 718 (Weight %)	Corrosion Product (Weight %)	White Region (Weight %)
Al	0.56	0.39	0.05
C	0.04	0.00	0.00
Cr	18.45	49.50	7.91
Fe	19.03	1.03	18.80
Mn	0.07	0.00	0.06
Mo	3.07	0.77	3.94
Na	—	1.64	0.00
Nb	5.18	3.09	0.39
Ni	52.10	3.22	68.73
O	—	39.69	0.00
Si	0.12	0.00	0.00
Ti	0.98	0.60	0.08
V	—	0.06	0.04

91TR56



92266

Figure 22. Heat Pipe End Cap Crevices (Arrows)

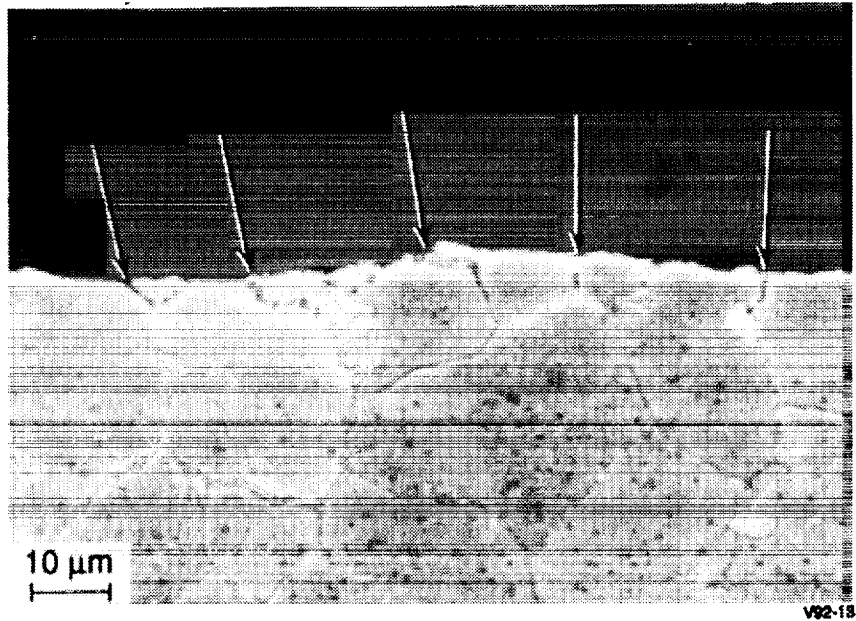


Figure 23. Optical Micrograph of Exposed Inconel 718 in Evaporator End Cap Crevice with Limited Grain Boundary Attack (Arrows)

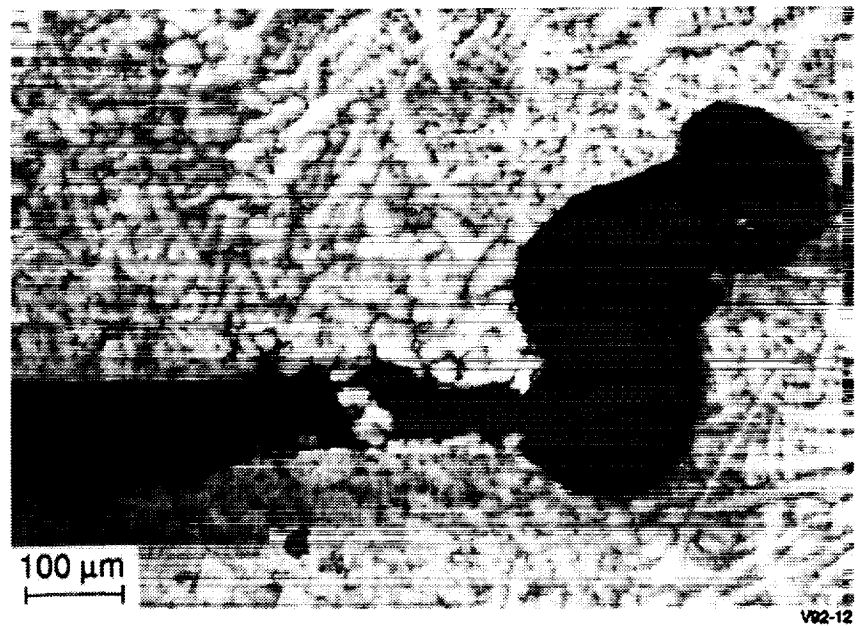


Figure 24. Optical Micrograph of a Pit in Condenser End Cap Crevice

## 4.0 DISCUSSION OF RESULTS

### 4.1 Heat Pipe Exposure Conditions

Surface topography changes observed in the Ni-200 wick and the Inconel 718 heat pipe wall indicated that three primary sodium exposure/interaction regions were present along the length of the operating HPFTS. These regions, shown in Figure 25, appear to result from exposure to:

- Condensing sodium vapor and pure sodium liquid (condenser)
- Evaporating sodium and sodium liquid containing moderate levels of contamination and solute (upper evaporator)
- Excess liquid sodium containing a high concentration of contaminants and solute (evaporator base).

### 4.2 Surface Chemistry

Surface chemistry changes have been observed in 300 series stainless steels and Ni-based alloys exposed to flowing sodium in the hot zone of nonisothermal pumped loops [4, 5]. Surface layers depleted in Cr and Ni and enriched in Fe were formed in the stainless steels. The surface of Inconel 718 exposed to sodium under similar conditions was found to be depleted in Cr, Ni, Nb, and Al and enriched in Fe and Mo.

A surface layer depleted in Cr, Nb, Ti and Al was formed on the Inconel 718 in all regions of the HPFTS. Fe and Mo concentrations were also reduced slightly in the condenser. In contrast to previous observations [4], the Ni concentration at the surface of the Inconel 718 heat pipe increased as a result of sodium exposure. This increase appears to occur because of the large surface area of the Ni-200 wick in proximity to the Inconel 718 and the limited solubility of Ni in sodium, approximately 3.9 ppm at 1050 K (1430°F) [6].

Ni and Ni-based alloys exposed to high-temperature sodium are thought to corrode by dissolution of Ni from the metal surface [7, 8]. The rate of dissolution is directly related to the difference between the concentration of Ni in the sodium and the maximum solubility of Ni in sodium at the test temperature. The rate of Ni loss from the surface can be described by the equation:

$$J = k(C - c)$$

where:

J = rate of Ni dissolution

k = solution rate constant

C = solubility of Ni in sodium at the temperature of interest

c = actual concentration of Ni in the sodium.

The surface area of the Ni-200 wick was estimated to be more than five times the surface area of the Inconel 718 heat pipe wall. Based on the area of surface exposed, the wick has the potential of providing five times more Ni than the wall in a given period of time. In addition, the concentration of Ni is 52% in Inconel 718 and 99.6% in the Ni-200 wick, which again favors dissolution of Ni from the wick. The sodium is thought to be saturated with Ni, supplied primarily by the wick, thus limiting dissolution of Ni from the heat pipe wall.

Limited dissolution of Ni combined with leaching of Cr, Nb, Ti, and Al from the Inconel 718 resulted in a relative increase of Ni at the sodium-exposed surface.

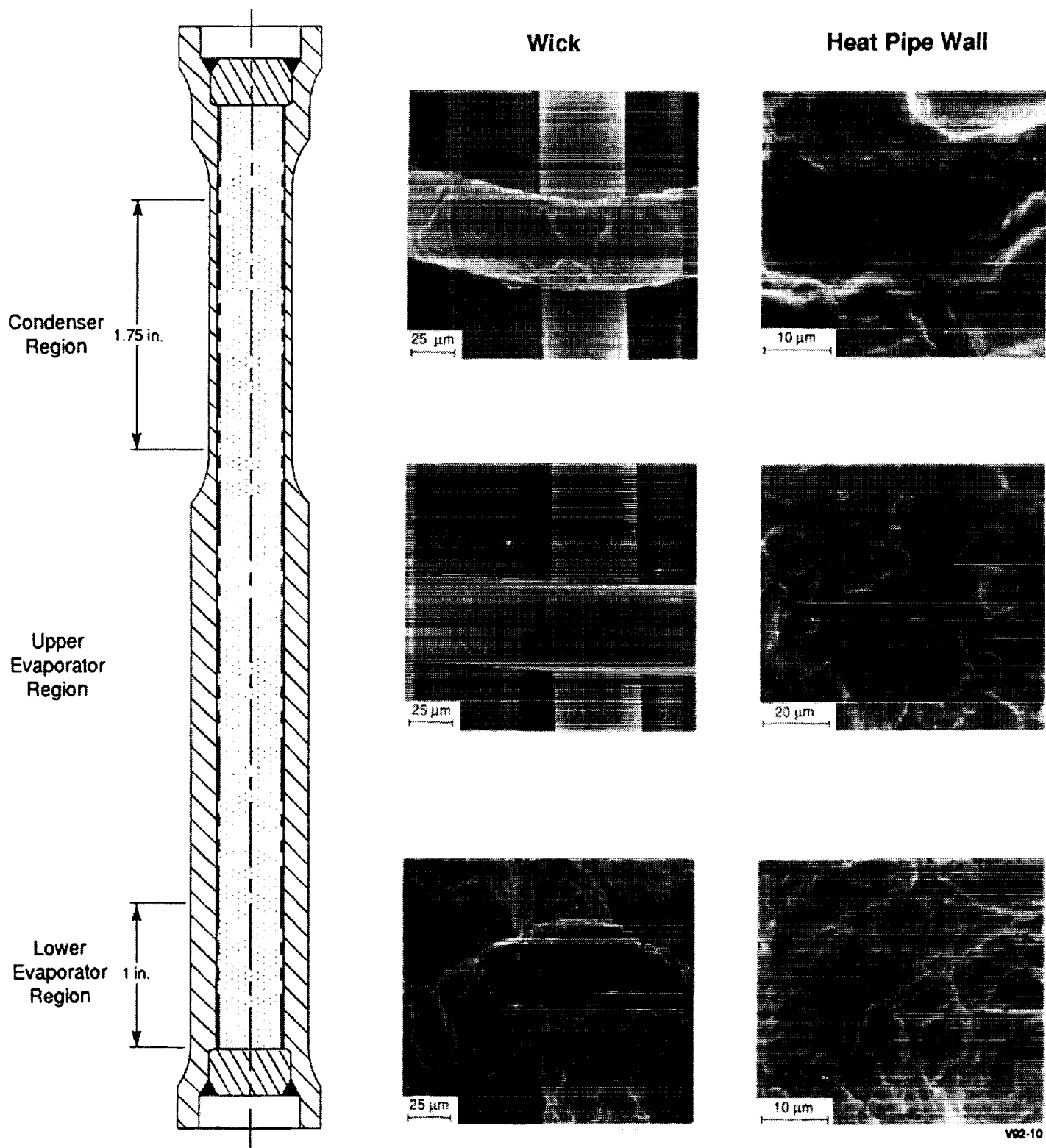


Figure 25. Three Primary Interaction Regions Along Heat Pipe Length

Low microhardness values observed in the white etching surface layer correlate well with reduced concentrations of Nb, Al, and Ti. The high strength of age-hardened Inconel 718 is generated by precipitation of Nb-rich  $\text{Ni}_3(\text{Nb, Ti, Al})$ , also known as  $\gamma''$  [9]. Low concentrations of Nb, Al, and Ti, as observed in the surface layer, will reduce the amount of  $\gamma''$  and result in low strength and hardness.

Interaction between the wick and wall materials was found to have a strong influence on surface chemistry changes and dissolution rates in the sodium heat pipe environment. The current CTPC heat pipe design specifies 316L stainless steel, containing approximately 10% Ni, for the wick material. The limited concentration of Ni available in the 316L stainless steel will allow the sodium to remove larger concentrations of Ni from the CTPC heat pipe wall before the Ni solubility limit is reached. As a result, a surface layer depleted in Ni is expected in the Inconel 718 exposed in the CTPC heat pipe.

#### 4.3 Mass Transfer

In an operating heat pipe, pure sodium vapor formed in the evaporator flows to the condenser where heat is extracted. Heat removal causes the vapor to condense as a pure liquid. Based on the dissolution rate equation described in Section 4.2, elements that are soluble in liquid sodium will be removed from the heat pipe condenser wall due to the small concentration of solute in the pure sodium liquid. The liquid returns to the evaporator, transferring the solute accumulated from the heat pipe wall to the liquid sodium collected in the evaporator. Here, the solute concentration increases as pure sodium vapor is again formed. Thus, a net transfer of material from the condenser to the evaporator is expected.

Low heat flux rates and the complex interaction of the Inconel 718/Ni/V system made it difficult to confirm this operating mechanism but several factors supporting this theory were observed in the HPFTS. These observations were as follows:

- Deposits containing Ni, Nb, Fe, and Cr formed in the evaporator, confirming the transport of soluble elements to that area. Vanadium from the pure V-wire, included in the heat pipe for oxygen analysis after testing, was also a major constituent in the evaporator deposits. The vanadium appears to be transferred directly through excess sodium liquid without transport through the vapor phase or migration along the length of the heat pipe.
- Changes in surface chemistry were observed in both the condenser and evaporator but greater changes occurred in the condenser. This observation indicates that the dissolution potential is stronger in the condenser, which supports the theory of condenser-to-evaporator mass transfer.
- The thickness of the white etching surface layer observed in the sodium-exposed Inconel 718 was approximately 15 to 25  $\mu\text{m}$  (600 to 1000  $\mu\text{in.}$ ) in the evaporator and 5 to 10  $\mu\text{m}$  (200 to 400  $\mu\text{in.}$ ) in the condenser. Removal of material through mass transfer is thought to be the cause for the thinner layer in the condenser. This observation also supports the theory of mass transfer in the heat pipe system.

#### 4.4 Local Accelerated Corrosion

A region of accelerated corrosion attack in the heat pipe evaporator appeared to result from a local increase in oxygen concentration in the sodium. It has been shown that sodium chromite,  $\text{Na}_2\text{CrO}_3$ , and sodium ferrite,  $\text{Na}_2\text{O-Fe}_2\text{O}_3$ , can form in 300 series stainless steels exposed to sodium containing >20 ppm oxygen [3, 10]. The concentrations of Cr and O in the corrosion product in the HPFTS were similar to those of sodium chromite observed previously [3]. The Inconel 718 corrosion product also contained Fe, Nb, Ni, Ti, and Al. Crystallographic analysis was not performed to fully characterize the corrosion products.

The relative increase in Ni and Mo concentration in the white etching zone surrounding the corrosion product indicates that these elements are relatively insensitive to the concentration of oxygen in the sodium. The slight reduction in Fe concentration and the large reduction of Cr, Nb, Al, and Ti concentration in the zone surrounding the corrosion product indicate that these materials are more sensitive to the presence of oxygen.

## 5.0 CONCLUSIONS AND RECOMMENDATIONS

The conclusions reached from the metallurgical evaluation of the HPFTS are as follows:

- Three primary sodium interaction regions were observed in the HPFTS and are expected to be present in the CTPC heat pipe. These regions will correspond with the lowest point in the evaporator, the upper evaporator, and the condenser. The interaction and corrosion mechanisms operating in the CTPC heat pipe are expected to be the same as those observed in the HPFTS, even with increased heat flux.
- Stress-accelerated corrosion, stress corrosion cracking, extensive grain boundary attack, and liquid metal embrittlement were not observed in any region of the HPFTS and are not expected in the CTPC heat pipe.
- Transfer of Ni, Cr, Nb, Fe, and C from the condenser to the evaporator was observed in the HPFTS and is expected to occur in the CTPC heat pipe. The rate of dissolution and deposit formation, i.e., mass transfer, will be increased relative to the rate in the HPFTS due to the increased sodium flux rate.
- Interaction between the heat pipe wick and wall materials has a major influence on the surface chemistry changes occurring in liquid sodium heat pipes. Changing the wick material, i.e., from Ni-200 to 316 stainless steel, will affect the rate of Ni dissolution and mass transfer from the heat pipe wall.
- Regions of oxygen-accelerated corrosion were present in the HPFTS and are expected to occur in the CTPC heat pipe evaporator. Failure of the CTPC heat pipe resulting from this type of corrosion is not expected due to the limited depth of attack ( $<35\text{ }\mu\text{m}$  (1400  $\mu\text{in.}$ )), the thick wall structure in the CTPC evaporator (6.3 mm (0.25 in.)), and careful control of initial sodium purity.
- The cause of the large pit, 300 to 400  $\mu\text{m}$  (0.012 to 0.016 in.) in depth, observed in the crevice at the end of the heat pipe condenser was not identified conclusively. Therefore, reasonable efforts should be made to minimize crevices in the CTPC heat pipe.

A better understanding of the processes that occur in a heat pipe system will enable the design of future engines to be enhanced and may provide the opportunity to extend the life of long-life engines. Therefore, additional development studies on alkali-metal/nickel-based superalloy heat pipes are recommended to define the effects of:

- Wick material on heat pipe wall corrosion, surface chemistry, and mass transfer
- Alkali metal flux rate on mass transfer
- Alkali metal heat pipe exposure on the long-term creep rate and fatigue resistance of nickel superalloys.



## 6.0 REFERENCES

1. Hooper, A. J., and E. A. Trevillion. "Oxygen Analysis of Sodium by Equilibration with Vanadium: An Assessment." *Journal of Nuclear Materials* 48 (1973):216-222.
2. Smith, D. L. "An Equilibration Method for Measuring Low-Oxygen Activities in Liquid Sodium." *Nuclear Technology* 11 (1971):115-119.
3. Hiltz, R. H. "The Corrosion of Stainless Steel in Oxygen-Contaminated Sodium at 1200°F and 1400°F." *Corrosion by Liquid Metals*. Edited by J. E. Draley and J. R. Weeks. Plenum Press, 1970.
4. Whitlow, G. A., et al. "Sodium Corrosion Behavior of Alloys for Fast Reactor Applications." In *Proceedings of the TMS-AIME Symposium on Chemical Aspects of Corrosion and Mass Transfer in Liquid Sodium*, Detroit, October 19-20, 1971.
5. Berkey, E., and G. A. Whitlow. "Microstructural and Compositional Changes in Sodium-Exposed Stainless Steel by Scanning Electron Microscopy." In *Proceedings of the TMS-AIME Symposium on Chemical Aspects of Corrosion and Mass Transfer in Liquid Sodium*, Detroit, October 19-20, 1971.
6. Weeks, J. R., and H. S. Isaacs. "Corrosion and Deposition of Steels and Nickel-Based Alloys in Liquid Sodium." In *Volume 3 of Advances in Corrosion Science and Technology*. Plenum Press, 1973.
7. Tyzack, C. "The Behaviour of Materials in Liquid Sodium." In *Proceedings of the Symposium on Advances in Materials*. Institution of Chemical Engineers, Northwestern Branch, Manchester, England, 1964.
8. Tortorelli, P. F. "Fundamentals of High-Temperature Corrosion in Liquid Metals." In *Volume 13 of Metals Handbook*, 9th ed. American Society for Metals, 1987.
9. Eiselstein, H. L. "Metallurgy of a Columbium-Hardened Nickel-Chromium-Iron Alloy." *Advances in the Technology of Stainless Steels and Related Alloys*. ASTM Special Technical Publication No. 369, 1965.
10. Baker, M. G. and D. J. Wood. "The Chemical Composition of Corrosion Products in Liquid Sodium." In *Proceedings of the TMS-AIME Symposium on Chemical Aspects of Corrosion and Mass Transfer in Liquid Sodium*, Detroit, October 19-20, 1971.



### Report: Pad-on-Disc Wear Couple Tests

#### INTRODUCTION

This report summarizes the results of wear couple testing conducted using a 'pad on disc' test rig to evaluate surface coatings for the CTE engine seal surfaces. The rig is located at the Latham facility. Follow on tests performed on an 'oscillating shaft' test rig at the NKR facility are reported separately.

The Component Test Engine (CTE) being designed and built under the space power project will advance the technology as represented by the Space Power Research Engine (SPRE).

A major new requirement for CTE is that the engine cooler will operate at temperatures up to 525K, consequently the power piston and cold side of the displacer will operate at temperatures in the 525K to 575K range.

As with SPRE the displacer and power piston will operate with extremely small clearances in the seals and bearings. (.0005 to .0007 inches )

Occasional rubbing contact in the seal regions has been difficult to avoid completely on previous engines in which the cooler operated at about 300K. This has been especially true for the displacer which typically has tight clearance seals on three different concentric surfaces. At the higher temperature of 525K it is more difficult to control thermal distortions than in the lower temperature engines.

Past experience at MTI led to the selection of chrome oxide coatings on both surfaces of tight clearance seals and bearings for SPRE. Galling problems have been avoided but rubbing contact in the displacer seals has been difficult to avoid completely and has required extremely precise alignment during assembly. If rubbing contact occurs with two hard surfaces it has usually required engine disassembly, cleaning and realignment of the mating parts.

Based on this experience it was decided to investigate wear couples other than chrome oxide against chrome oxide for CTE. The desire is for a wear couple in which occasional light rubbing will not affect engine operation. The thinking is that if one surface is hard and the adjacent surface is relatively soft that the soft surface would wear slightly to accommodate small interferences which might occur due to thermal distortions.

#### SOFT COATINGS

In the 525 to 575K temperature range there are relatively few options for a soft surface. The TFE based materials such as Rulon F and J were exposed to temperature in a helium atmosphere and it was determined that they were not capable of operating at 575K. They lost significant weight and became less flexible.

Carbon graphite was identified as the most promising candidate. Two types from Pure Carbon Co were selected for evaluation. P-3310 is a low (.5%) porosity graphite and P5N is a high (10%) porosity graphite. The porosity of P5N could increase seal leakage so P-3310 was the preferred selection.

Another material considered as possible but less promising was PS212 (70% Chromium Carbide-15%silver-15%barium/calcium fluoride) developed for high temperature bearing applications at NASA Lewis. This is not strictly speaking a soft material but has good low friction characteristics at elevated temperature.

Since carbon graphite cannot be applied in very thin sections, being made from a sleeve which is shrunk or press fitted into cylinder bores or over piston surfaces it is not a desirable candidate for the appendix gap seal between the displacer and the cooler. This gap is slightly larger than the seals, being a nominal .002 inches, but has proved to be more difficult to align precisely on SPRE and rubbing has occurred in this seal during transient operating conditions.

Several flame spray applied abradable coatings using METCO materials were identified as possible alternates to carbon graphite particularly for the appendix gap.

#### HARD COATINGS

The hard coatings identified as options were :

Hardened Electroless Nickel

Plasma sprayed chrome-oxide

Plasma sprayed aluminum oxide

Titanium nitride

SPEEDRING CO was the primary supplier of the precision beryllium parts on SPRE and it was anticipated that this company would fabricate some or all of the precision beryllium parts on CTE.

SPEEDRING routinely applies aluminum oxide to beryllium surfaces so for this reason it was selected as the favored hardcoat. Hard nickel and chrome-oxide parts were purchased but titanium nitride was not pursued.

#### TEST EQUIPMENT

The test equipment used for tests reported herein was the Pad on Disc test machine located at MTI's Latham facility. A schematic is shown in Figure 1 and a photograph in Figure 2.

In this machine a 2.0 inch diameter disc .5 inch thick is mounted on a horizontal shaft which can be rotated at a preselected speed.

The o.d. of the disc is one test surface. A pad with a raised test surface .375 inch wide by .5 inch long is supported by an arm and contacts the top of the rotating disc at top dead center. The dead weight of the arm applies a load of 1.0 lb. to the pad.

The contact force between the pad and the disc can be adjusted by adding dead weight to the arm or supporting some of the arm weight with a spring.

The end of the arm can be connected to a load cell which measures the tension induced in the arm by frictional drag on the pad at the contact surface. A strip chart recorder is used for this.

Two banks of resistance heaters can be positioned around the test pieces to control the temperature measured by a thermocouple located on the arm near the pad.

For test conditions not requiring the spring to counteract some of the dead weight of the arm, a loosely fitting cover can be installed and an inert gas environment established around the test pieces by a continuous gas purge from a high pressure bottle.

#### TEST PROCEDURE

In all cases the outer surface of the disc was the hard surface and the pad was the soft surface.

Before starting a test the surface finish of the disc was measured. At intervals during a test the pad was removed and the geometry of the wear path recorded. For the initial tests using hard nickel to debug the rig and develop the test procedure a height gage was used along with weight measurements. These did not prove sufficiently accurate. For most of the tests an optical comparator was used to measure the wear path geometry. This was a groove with a 1.0 inch radius since this is the radius of the disc.

The contact pressure during a test was calculated by dividing the arm load by the contact area, the contact area being the width of the wear path groove times the width of the pad (.375 inch).

Some initial testing was done at various disc rotating speeds. Friction characteristics were not sensitive to this so 2500 rpm was selected as the reference test speed. This corresponds approximately to the maximum velocity during the sinusoidal motion of the engine displacer and power piston.

If debris of sufficient quantity was generated it was collected on a filter paper or for some of the abradable materials it collected on the pad and was manually removed.

TABLE 1 summarizes the results of the tests conducted.

TABLE 1

DISC Finish (Date)	Pad	Temp Gas	Time incr mins	Load lbs	Wear width ins	Wear depth mils	Pres psi	Wear mils/ hour	Frict Coef.
Nickel 3310	Graphite	20C	60	1.0	.07	.4	.		.16
		Air	60	2.0	.08	.4	67		.17
			60	3.5	.08	.4	116		.13
Nickel 3310	Graphite	300C	60	1.0	.05	.1			.06
		He	60	2.0	.065	.1	82		.05
			60	3.5	.10	.09	113		.05
Al-ox 3310	Graphite	20C	60	1.0	.135	1.4			.19
		Air	60	2.0	.145	1.6	38		.19
			60	3.5	.155	2.1	62		.14
Al-ox 3310	Graphite	300C	60	1.0	.085	.3			.19
		He	60	2.0	.09	.4	61		.20
Al-ox	Graphite	20C	60	1.0	.120	1.5			.22
		He							
----- Wear measurements above this line are not accurate -----									
Al-ox (10/11)	Graphite 3310	20C	20	1.0	.090	1.0			
		He	20		.105	1.3	27	.9	
			20		----	----			
			20	2.0	.105	1.4			
(10/11)			20		.120	1.8	47	1.2	
			20		.125	2.1	44	0.9	
(10/12)			20	3.5	.095	1.2			
			20		.115	1.7	88	1.5	
			20		.125	1.9	77	.6	
Al-ox 11-14 (10/16)	Graphite 3310	20C	20	1.0	.085	.90			
		He	20		.100	1.0	29	.3	
			20		.110	1.3	25	.9	
(10/20)			10	0.5	.050	.3			
			10		.060	.4			
			10		.070	.4+	19	.5	
			10		.070	.4+			
			20		.080	.7			

Table 1 continued.

DISC Finish (Date)	Pad	Temp Gas	Time incr mins	Load lbs	Wear width mils	Wear depth mils	Pres psi	Wear mils/ hour	Frict Coef.
(10/23)			10	0.25	.050	.3			
			10		.055	.4	12	.2	
			20		.055	.45			
			20		.060	.5			
Cr-ox low (10/27)	Graphite 3310	20C Air	10	0.25	.030	.1-			
			10		.035	.1+	17	.2-	
			20		.040	.15			
			20		.040	.2			
(10/31)			10	0.5	.042	.15			
			10		.050	.2	26	low	
			20		.050	.2			
			10	1.0	.050	.25			
			10		.050	.25			
			20		.055	.35	51	<.1	
			20		.055	.35			
Al-ox 10 (11/2)	Metco 311	20C Air	10	0.25	.095	1.9			
			10		.115	2.6			
				20		.135	3.6	5	2.6
			20		.140	4.3			
			10	0.5	.140	4.5	9		
			10		.140	4.5			
			20		.140	4.5			very low
			20		.140	4.5			
			10	1.0	.150	5.4			
			10		.150	5.4			
			20		.150	5.4	18	very low	.47
			20		.150	5.4			
Al-ox (11/8)	Metco 601	20C Air	10	.25	.285	11.8			
			20		.345	13.6	2		10.8
Al-ox 100 (11/9)	Graphite 3310	20C Air	10	.25	.140	2.6			
			20		.145	2.8	5	1.2	.25
Al-ox 10 (11/9)	Metco 601	20C Air	10	.25	.095	1.7	7	3.0	.20
			20		.105	2.3			

TABLE 1 continued

DISC Finish (DATE)	Pad	Temp Gas	Time incr mins	Load lbs	Wear width mils	Wear depth mils	Pres psi	Wear mils/ hour	Frict Coef.
Cr-ox 4 (11/14)	Metco 311	20C Air	10	.25	.055	1.5	-		
			10		.070	2.0	10.5	3.0	
			20		.090	2.5	8.3	3.0	
			20		.090	2.5	7.4	0.0	
			20		.090	2.5	7.4	0.0	
Cr-ox 4 (11/16)	Metco 311	20C He	20	1.0	.105	4.2	25		
			20		.105	4.2	25	0.0	
			20		.105	4.2	25	0.0	
Cr-ox (11/27	Metco 611	20C Air	10	.25	.045	1.7	-		
			10		.050	1.9	14.0	1.2	
			20		.075	2.5	10.8	1.8	
			20		.085	2.8	8.3	.6	
			20		.085	2.8	7.8	0.0	
Cr-ox (11/28)	Metco 611	20C He	60	1.0	.125	4.5			
Cr-ox (11/29)	Metco 611	300C He	60	1.0	.080	3.1	squeal		
Cr-ox (11/30)	Metco 308	20C Air	10	.25	.045	.8	-	-	
			10		.08	1.4	10.6	3.6	
			20		.095	2.1	7.7	1.8	
			20		.100	2.4	6.8	0.9	
			20		.100	2.4	6.6	0.0	
Cr-ox (12/1)	Metco 308	20C Air	30	1.0	.135	3.1	-	Squeal	
			60		.145	3.5	19.0	.8Squeal	
Cr-ox (12/1)	Metco 308	300C He	60	1.0	.065	1.1	-	-	
Cr-ox (12/4)	Metco 308	20C Air	10	.25	.030	.5	-	-	
			10		.040	1.0	19	3.0	
			20		.045	1.0	15.7	low	
			20		.045	1.1	14.8	low	
			20		.050	1.1	14.0	low	
Cr-ox (12/5)	Metco 611	20C Air	10	.25	.030	.4	-	-	
			10		.035	.4	20.8	low	
			20		.040	.5	17.8	low	
			20		.045	.6	15.7	low	



## DISCUSSION OF RESULTS

The wear rate measurements summarized in TABLE 1 are shown graphically in Figure 3 in which the wear rate in mils per hour is plotted against contact pressure.

The emphasis was placed in testing Graphite P-3310 against aluminum oxide since this is the tentative reference selected for the CTE engine.

In the engine, interferences of the order one or two tenths of a mil are the magnitude to be relieved by wear since if more wear than this is required the additional seal clearance will induce excessive leakage losses. It is difficult to define precise requirements on the wear characteristics of the wear couples in the engine. Figure 1 shows that for relatively smooth aluminum oxide (surface finish less than 20 microins) the wear rate is in the range 1 to 2 tenths per hour at contact pressures below 10 psi.

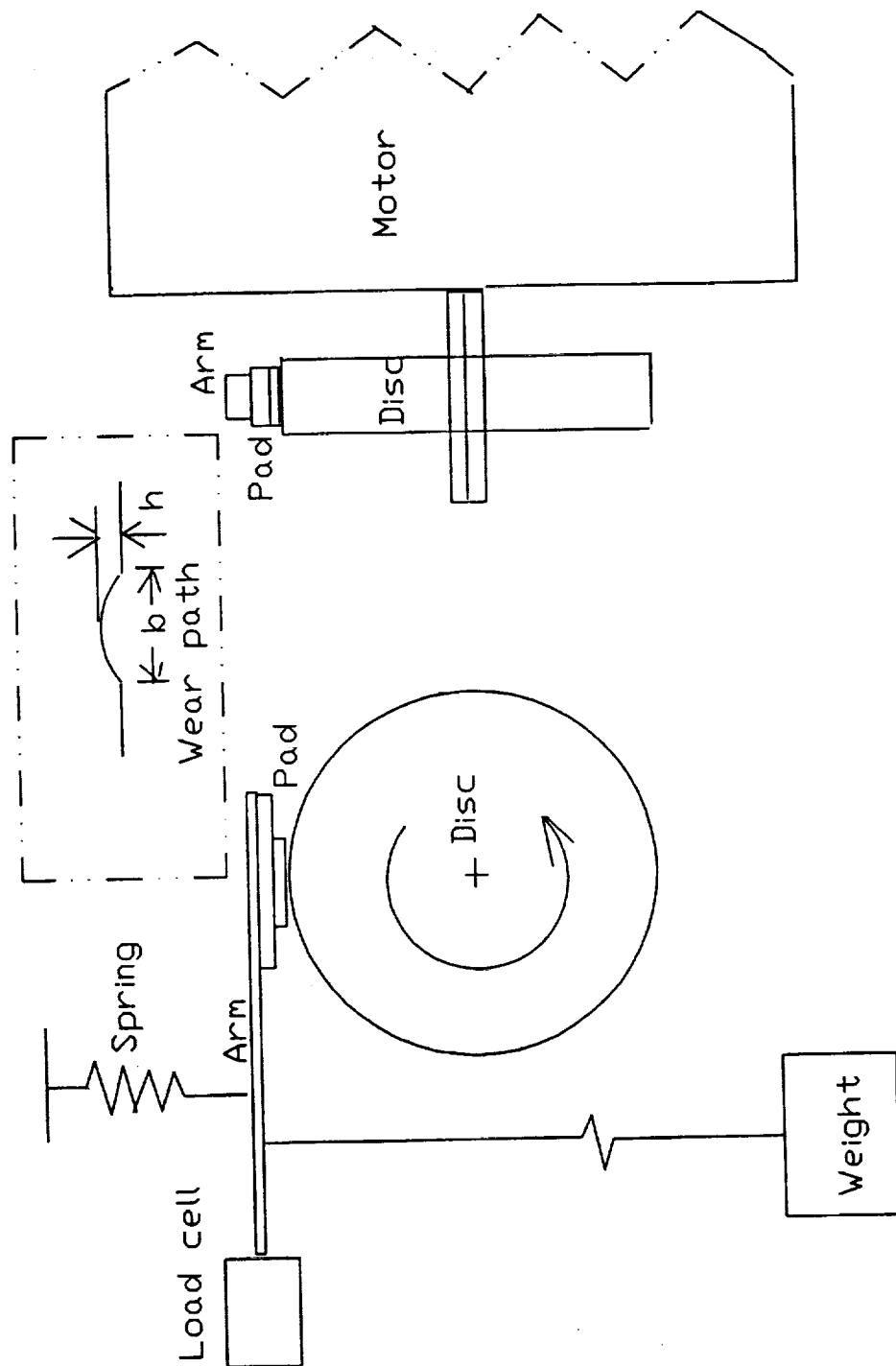
For a surface finish of 50 microins the wear rate was significantly higher for example 1.2 mils per hour at 5 psi contact pressure.

The normal finish attained on a ground plasma sprayed hard coat like aluminum oxide or chrome oxide is relatively smooth. The conclusion reached from the above tests is that intentional roughening of the surface may be desirable. If it is not practical to control on all surfaces during initial fabrication the use of local roughening at contact locations after engine test and disassembly may prove helpful.

The coefficient of friction is consistently less than 0.2 for temperatures from room temperature to 300C in both air and helium. Compared to typical values attainable with wear couples this is considered acceptable.

The debris generated by graphite P-3310 (see appendix) is a very fine dust which should not be a problem for CTE. (For RSSE this may need further review).

The abradable coatings are not promising based on the screening tests conducted. For METCO 601 the wear rate was very high and unacceptably large particles were generated in the debris. For METCO 311 the initial wear was moderate but after a few tenths were removed from the surface the wear rate was essentially zero. This suggests that after finish grinding which is required on all surfaces the wear rate would be very low. METCO 308 and 611 exhibited similar behavior to METCO 311.



PAD ON DISC TEST RIG SCHEMATIC

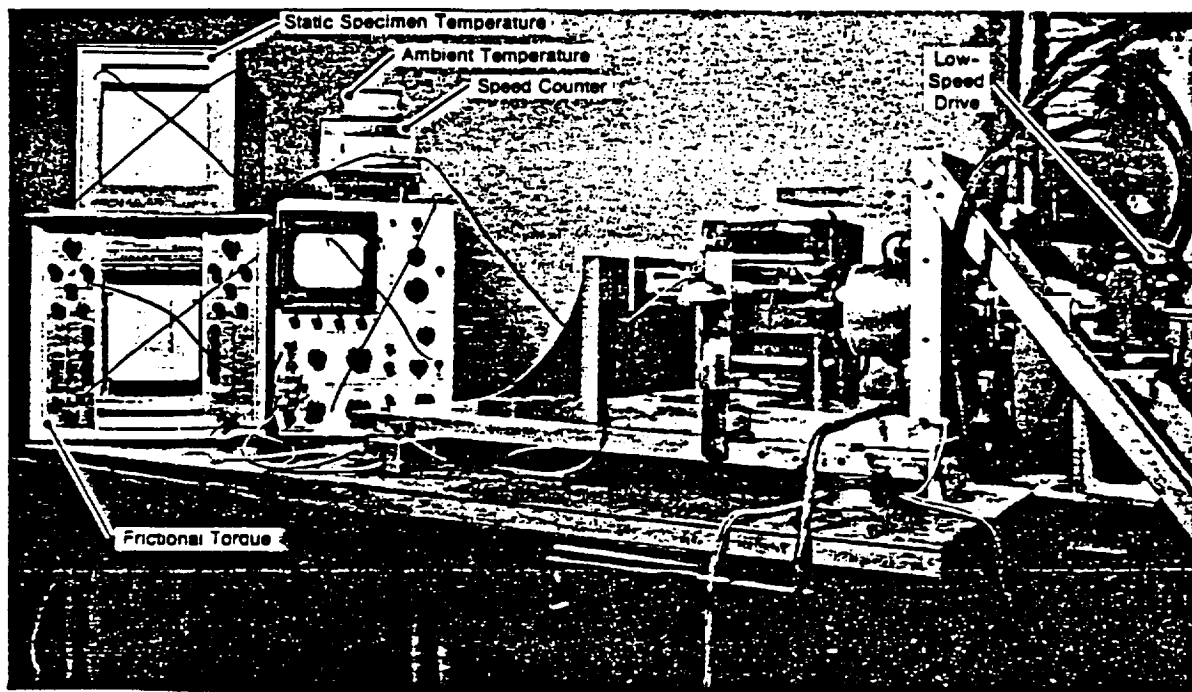


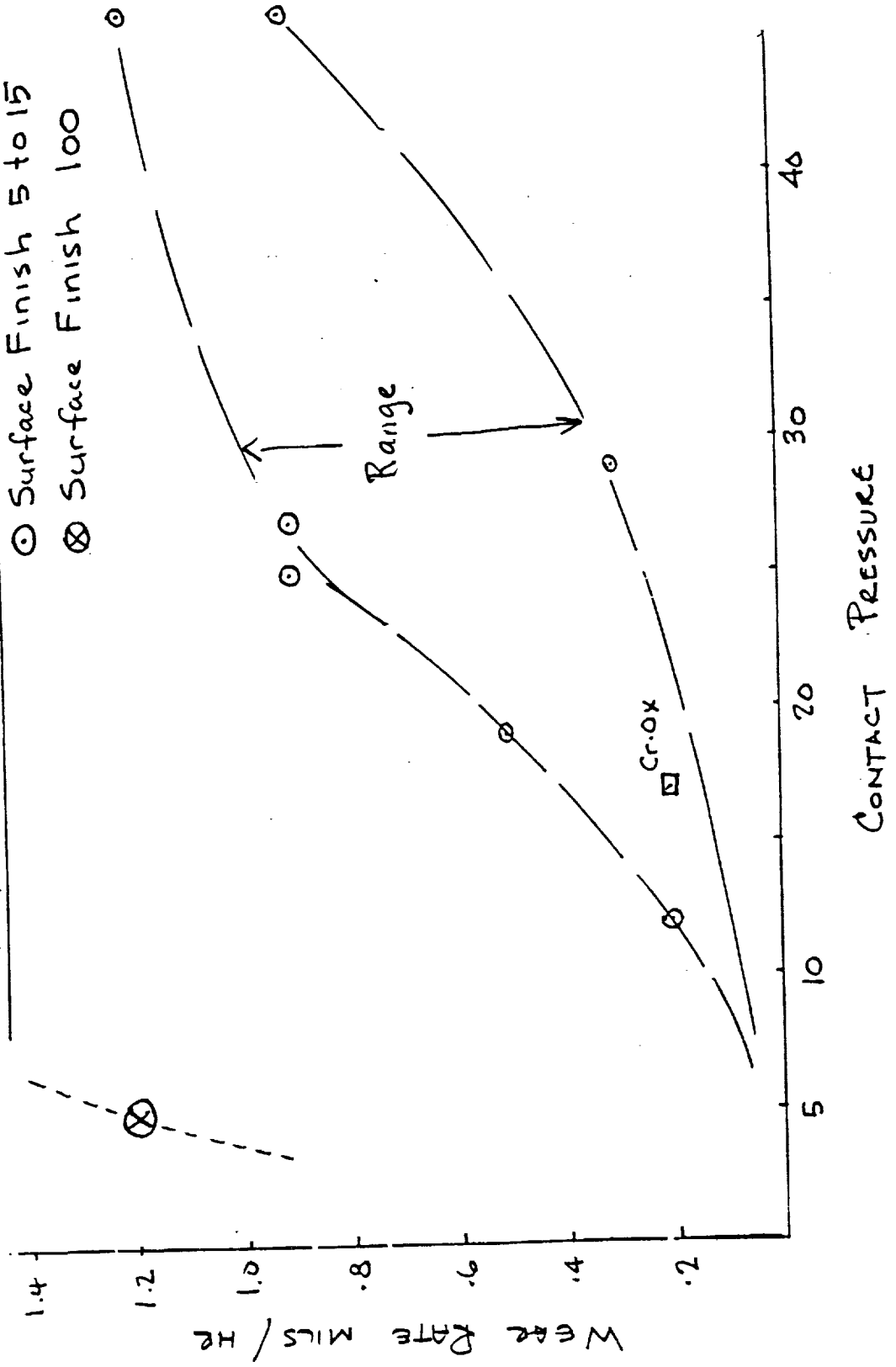
Figure 3

# WEAR TEST RESULTS

GRAPHITE P-3310 AGAINST ALUM. OXIDE

○ Surface Finish 5 to 15

⊗ Surface Finish 100



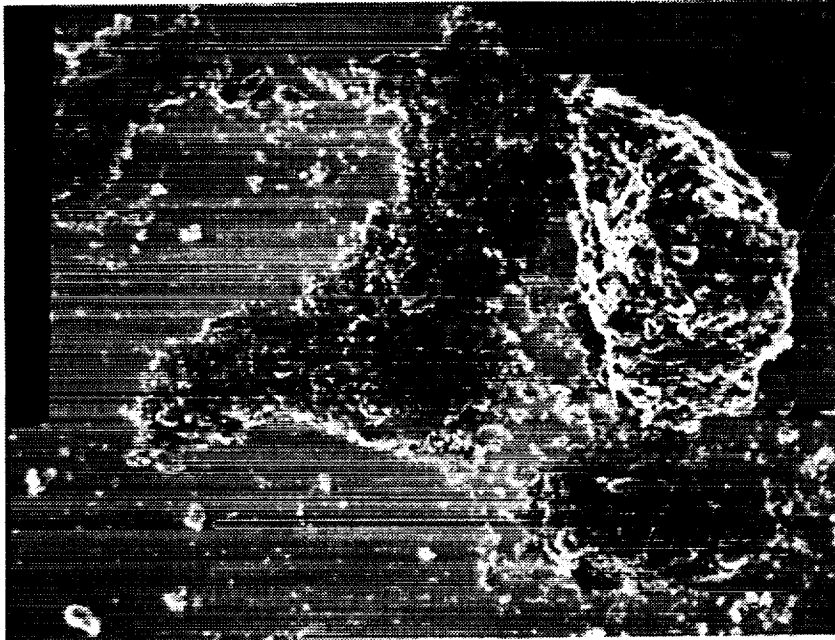
**Appendix to Pad-on-Disc Wear Couple Tests Report: MSR 595**

TO: Mike Cronin  
FROM: Lauris Petersen *L.P.*  
DATE: August 18, 1989  
SUBJECT: MSR 595 - Carbon Block/Ni-Plated Disc Wear Debris

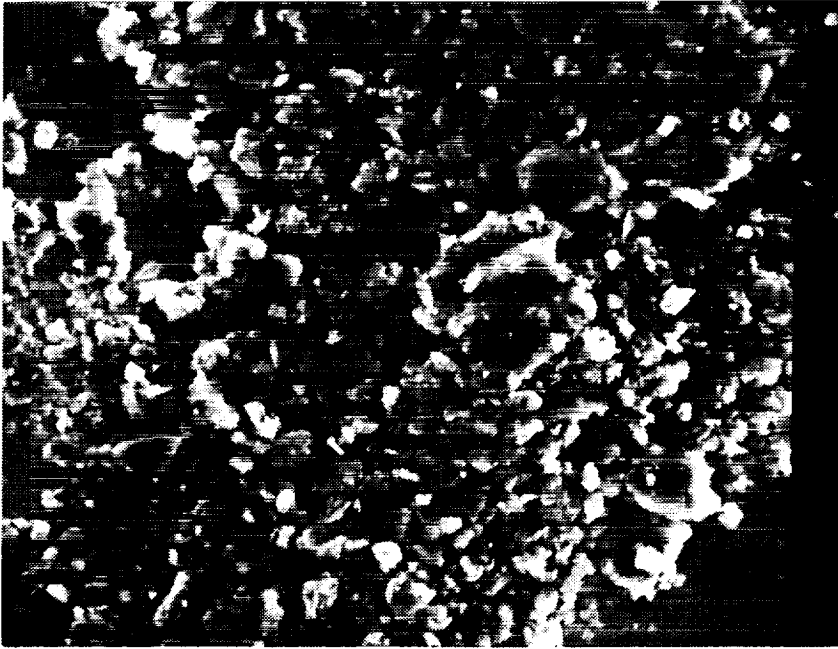
A small sample of wear debris, generated during a carbon block on nickel plated disc wear test, was delivered to the Materials Analysis Laboratory by Bob Green on August 9. This debris resulted from a 1 hour test where the block on disc contact force was 3 lbs.

The debris was examined using a scanning electron microscope (SEM). Figure 1, a SEM photograph, shows the conglomerate nature of the relatively large debris particles. The size range is 100 to 150 microns. They are rather loosely connected and easily crumble apart.

The fine particle make-up of the large conglomerate particles is evident in Figure 2. Figure 3 shows the fine particles individually. They range in size from 1 to about 15 microns.



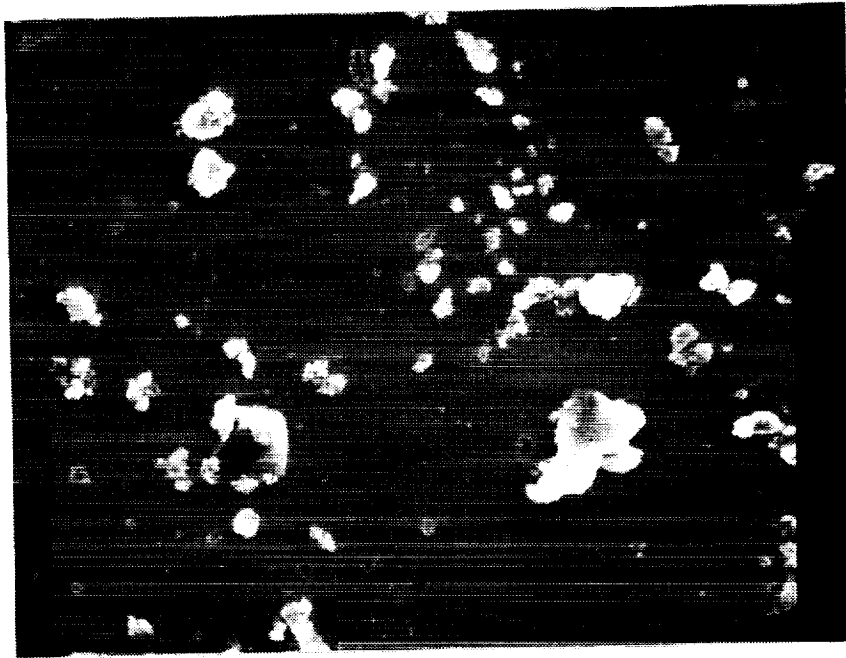
S595-14 X300  
FIGURE 1 - WEAR DEBRIS GENERATED DURING CARBON BLOCK  
Ni PLATED DISC TEST. NOTE LARGE CONGLOMERATE  
PARTICLES. (SEM PHOTOGRAPH).



S595-15

X1000

FIGURE 2 - HIGHER MAGNIFICATION OF LARGE CONGLOMERATE  
PARTICLE SHOWN AT CENTER OF FIGURE 1. NOTE MAKEUP OF  
VERY FINE PARTICLES. (SEM PHOTOGRAPH).



S595-13 X1000  
FIGURE 3 - VERY FINE INDIVIDUAL WEAR PARTICLES.  
(SEM PHOTOGRAPH).



## Introduction.

Graphite (Pure P-3310) and Aluminum Oxide ( flame sprayed by Speedring or Plasma Technologies) have been selected as the reference coatings to be applied to the adjacent surfaces of the close clearance bearings and seals on the CTE displacer and power piston assemblies.

The objectives of the wear couple testing on the NKR test rig are:

(1) assess the capability of the reference coatings to wear-in under light rubbing conditions without requiring engine shutdown to relieve local interferences.

(2) Determine the frictional resistance to be overcome during dry start conditions on internal bearings

The NKR rig allows for testing under reciprocating motion which more closely simulates the operating conditions in CTE than the unidirectional rotation of the Pad-on-Disc rig at Latham which was used for screening and high temperature tests.

Data obtained on the Pad on Disc rig suggest that the reference coating combination selected is the best of the options available for a 300C operating temperature. A variable that significantly affected wear rate was the surface finish of the aluminum oxide.

The small bearing area inherent in the pad on disc tests resulted in most of the test data being obtained above 10 psi. It is possible on the NKR rig to test at contact pressures down to about 2 psi.

The aluminum oxide in the pad on disc tests was applied by Plasma Technologies. Since Speedring and Plasma Tech. were both potential suppliers for CTE original plans called for testing samples from each supplier. Due to time limitations only Speedring samples were tested.

The design operating frequency of the CTE engine is 70 Hertz.

The nominal stroke of both the power piston and the displacer is 28 mm (1.1 in). During a typical start up the stroke is typically held at about half stroke until the temperature has stabilized then increased from half to full stroke.

At any time during this procedure it is possible that a light rub would occur. It is desirable that when this occurs (it is usually indicated by a drop in stroke or a stick slip indication of stroke) that by continuing to operate the rubbing location will wear-in in a reasonable period of time and that eventually full stroke at full frequency is attained.

The maximum velocity is 1210 fpm and the average velocity is 770 fpm.

The force tending to oppose the motion during rubbing is the product of contact pressure, contact area and coefficient of friction.

The contact pressure and area during the light rubbing conditions which are likely to be encountered during CTE testing are not predictable with any degree of accuracy. This makes it difficult to define quantitative requirements on the wear rate required.

The tests will be conducted using arbitrary loading to compare the results of reciprocating wear against rotational wear and provide a qualitative basis to assess surface finish effects.

Wear rate is traditionally plotted as a function of the product of contact pressure and surface average speed ("pv" in psi-fpm). Generally wear couples are desired which have a low wear rate at high "pv". For the CTE application the opposite is desired i.e. relatively high wear rate at low "pv".

A low coefficient of friction is desired since this translates into smaller forces during both rubbing and dry start conditions.

#### TEST SET UP

#### TEST RESULTS

The test rig has a maximum stroke capability of 22 mm ( 0.87 in ).

The rig was set up to operate at 60 hertz. A variac was used to adjust the input voltage to the linear drive motor which in turn sets the stroke of the piston. At 50 bar mean operating pressure the system is tuned for resonant operation at about 60 hertz.

The position and dimensions of the three test samples results in three different contact pressures on the three samples. These are in the ratio of 4:2:1. For the first test using smooth aluminum oxide 4 pounds was applied to the center washer. The force on the other two washers is 2 pound. The contact area is .5 sq.in for the center and lower washer and 1 sq.in for the upper washer. This results in contact pressures of 8 psi, 4 psi and 2 psi respectively on the center, lower and upper washers.

The wear rate after one hour and again after an additional 8 hours was determined from weight measurements. Optical comparator measurements were also made but it was difficult to determine wear rate from these and weight change was determined to be the most

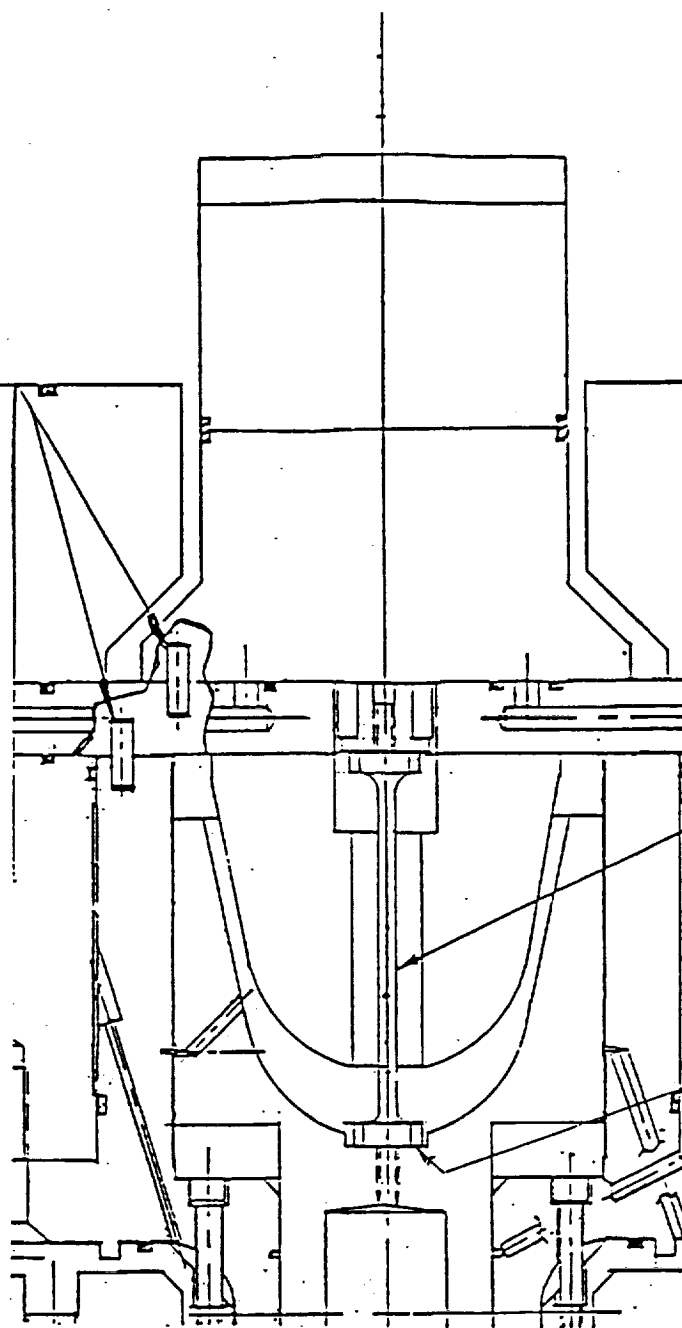
reliable indicator.

This test condition was repeated with an initially rough aluminum oxide sample with a surface finish approximately 100 microinch and a new set of graphite test samples. Following the test and measurements at a 4lb load on the center donut the test was continued with 10 lb on the center donut.

The results are plotted in Figure xx and suggest the wear rate is lower than that indicated on the pad and disc tests.

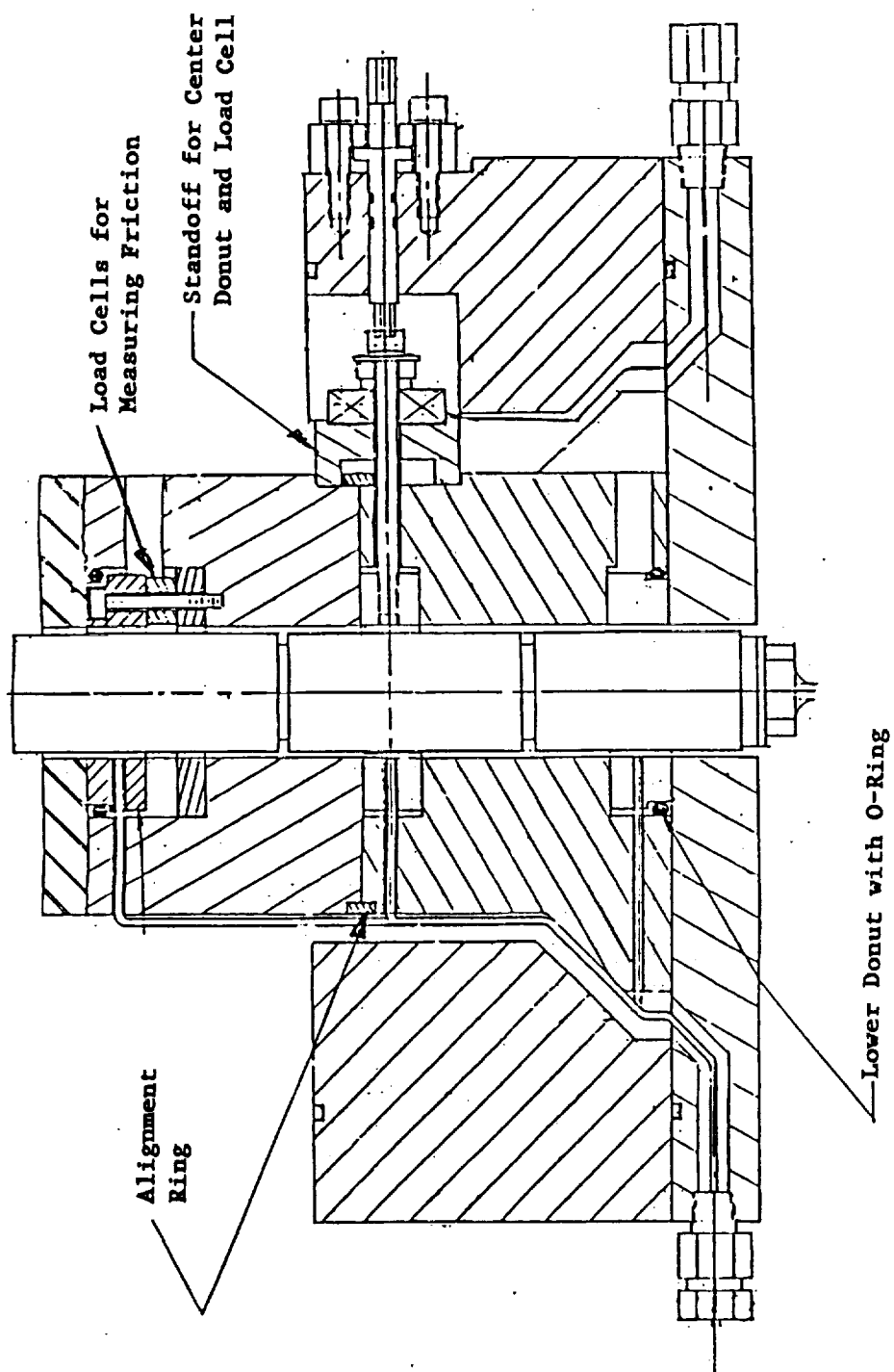
Time did not permit measurements of coefficient of friction to be made.

Alignment  
Dowels



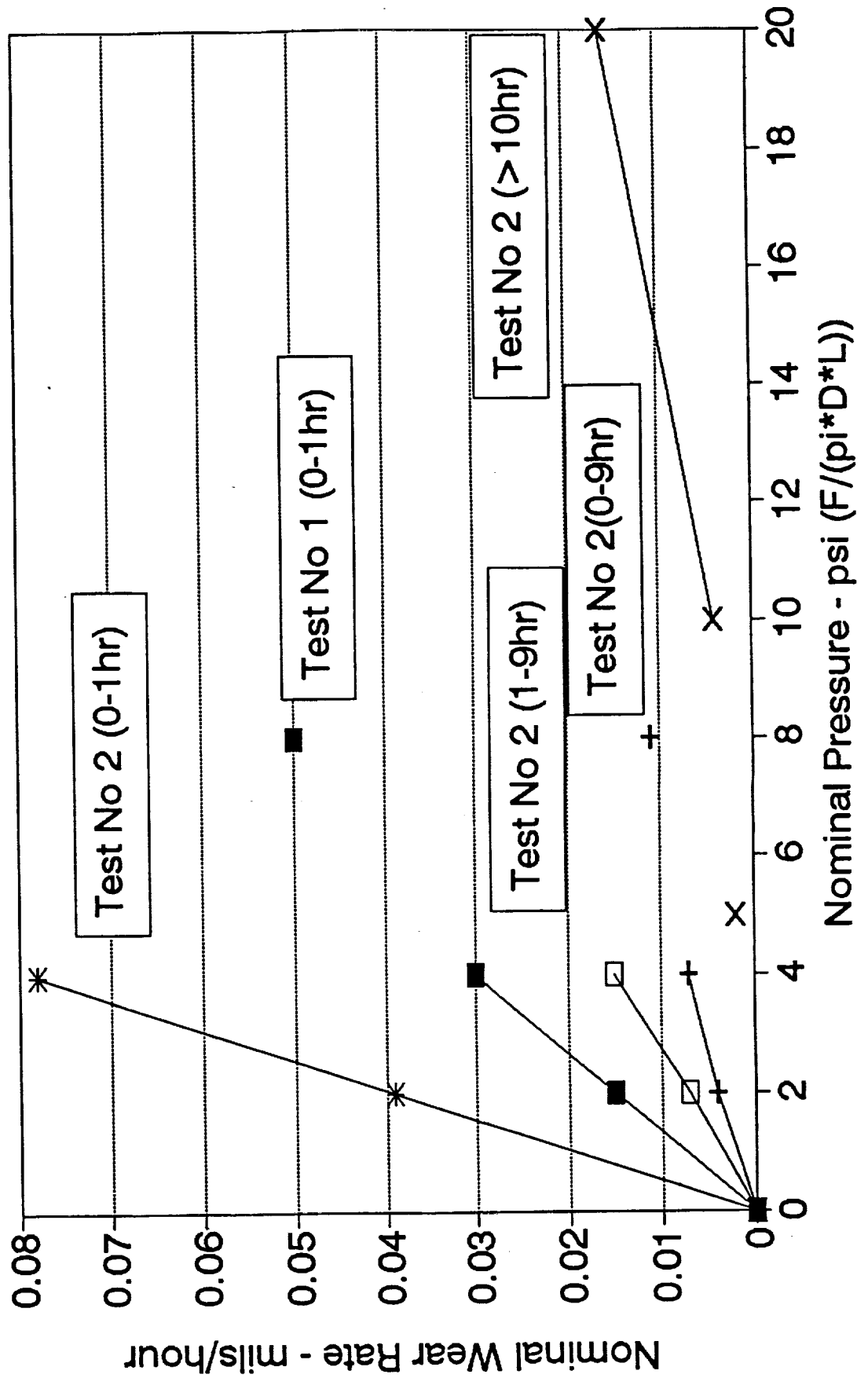
Stinger

Piston  
Mounting  
Face



# CTE WEAR TESTS NKR RIG

## P3310 Graphite vs Speedring Al.Ox.



## B.8 Pressure Boundary Penetrations

### Instrumentation Ring Seal: Test Arrangement and Results

The 'displacer post and flange' is a two piece assembly described in Section 3.3 of this report.

The outer section of the flange is the instrumentation ring. This is made of Inconel because it is subject to large compressive loads due to the bolt preload required to counteract the engine pressure loading.

The inner section of the flange is beryllium.

Various instrumentation leads must cross this joint and pass through the instrumentation ring to cross the pressure boundary of the engine.

Seals are required to preclude leakage from the compression space to the forward gas spring.

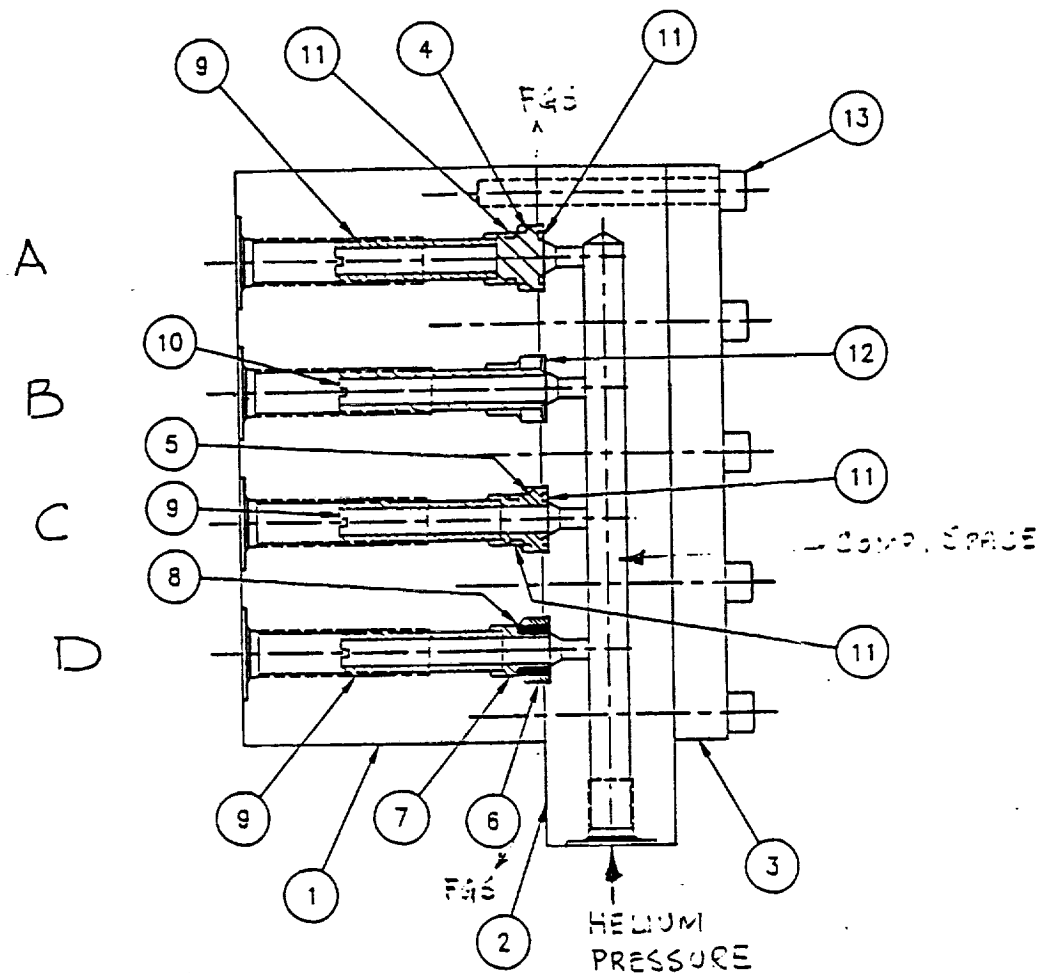
Figure 1 shows a test block which simulates the instrumentation ring (Part No 1) and the beryllium flange (Part No 2). Four feedthrough locations are designated A,B,C and D.

The arrangement at 'B' uses a silver plated belleville washer and long threads on the seal positioner to seal the joint. It was the preferred arrangement since it is possible to replace this seal without disassembling the instrumentation ring from the flange.

The arrangement at 'C' uses Kalrez O-rings to seal the joint and the arrangement at 'D' uses a preformed Grafoil gasket. These were backup approaches to 'B'.

The arrangement at 'A' is an O ring seal for possible use where for spare penetration locations with no feedthrough.

Arrangement 'B' was installed at the four penetrations and was tested by connecting a helium bottle of known volume and monitoring pressure level with time. After adding grafoil sealant to the threads the arrangement sealed with negligible leakage when tested at both room temperature and also at 250°C.



13	10	1042C10-0288P13	SOCKET HEAD CAP SCREW 1/4-20 UNC-2A X 2.25" LONG	A286
12	AR	1042B10-0302	SEAL-BELLEVILLE WASHER TYPE	AG COATED 17-7PH
11	AR	1042C10-0288P11	KALREZ O-RING #AS-568A-904	KALREZ COMPOUND 4079
10	AR	1042B03-0211	SEAL POSITIONER	INCONEL
9	AR	1042B03-0210	SEAL POSITIONER	INCONEL
8	AR	LATER	GRAFOIL SEAL	GRAFOIL
7	AR	1042B03-0213	SEAL CARRIER	INCONEL
6	AR	1042B03-0214	INSERT	INCONEL
5	AR	1042B03-0212	O-RING CARRIER	INCONEL
4	AR	1042B10-0287	BLANKING PLUG	INCONEL
3	1	1042C10-0269	CLAMPING PLATE	INCONEL
2	1	1042C10-0271	SEAL SEAT BLOCK	BERYLLIUM
1	1	1042C10-0270	SEAL HOUSING	INCONEL
ITEM NO.	QTY REQD	PART NO.	DESCRIPTION	MATERIAL

Figure 1



## B.9 Heating System Heaters

### Report: Slot Heaters for Starfish Heater Head

#### Introduction

Electrically heated silicon carbide radiant heaters sized to fit into the slots of the Starfish heater head were identified as a practical means of supplying heat to the CTPC.

The Starfish heater head was expected to be available several months ahead of the heat pipe. The slot heaters provided the option of testing the CTPC without the heat pipe and permit engine testing to continue in the event heat pipe delivery was delayed.

As the program proceeded it was decided to build a second heater head. It was planned to use slot radiant heaters for the first head and weld the heat pipe to the second head.

The 'I-squared-R Company' manufactures several types of silicon carbide heater. One standard item is an igniter. The hot zone of this is 1.5 x .7 x .14 inch. It was recognized that with some dimensional changes to the heating element that two heaters side by side in the Starfish slot could supply heat fairly evenly into the helium passages located in the wall between the slots.

Because the width of the slot at the inner end was initially 0.200 inch a heater .14 inch thick if perfectly centered had .030 inch clearance. The heater thickness was reduced to 0.120 to give a little more clearance. Subsequently the fin thickness was increased to provide more margin against breakthrough during the hole drilling process. The end result being that the nominal edge clearance between the heater and the fin is 0.030 inch.

To determine if arcing across a small gap would be a problem, a test was conducted with a standard igniter. This was mounted adjacent to an Inconel plate in a fixture such that the gap between the plate and the igniter could be adjusted. Power up to 120 Volts was supplied using a Variac for control. Tests were conducted in which the gap was progressively reduced from .060 inch down to 0.010 inch with no arcing.

At the solid outer section of the fins the pocket walls are parallel. By installing the heater elements in a parallel sided holder it is possible to locate them precisely in the slot and maintain a gap between the element and the wall. Figure 1 shows the initial design selected.

It was decided to perform a both a thermal analysis and also perform component tests to determine the power limits of the approach and the temperature distribution in the fins and the heater.

Heat transfer analysis codes at MTI did not handle radiation efficiently. Arrangements were made for an analysis to be conducted at NASA Lewis ( Pat Dunn ). For schedule reasons the procurement of heater assemblies and component test hardware proceeded in parallel with the analysis.

## THERMAL ANALYSES

The thermal analysis conducted at NASA Lewis is reported in the attached Appendix.

The analyses were conducted at a power input to the helium of 1400 Watts per slot. Two heaters are used in each slot. This results in 70 KWatts into the engine which provides margin above the 50 to 60 kWatts predicted to be required for 12.5 kWatts output at 20 to 25% efficiency.

The temperature of the fin adjacent to the helium passages is controlled primarily by the helium temperature. Temperature differences between the metal and the helium are relatively small. The film drop at design point conditions being about 20°K.

The reference hot side temperature 'Thot' is defined as the average temperature of the gas passage walls. The design point value for Thot is 1050°K.

The solid outer section of the fin (referred to as the tip in the Appendix) carries a high axial stress produced by the 150 bar helium pressure in the engine acting on the closure head. The creep strength of Inconel 718 in this section sets time limits on CTPC testing at the design point temperature. At 1050°K this limit is about 50 hours. It is thus essential that the fin tip not operate significantly higher than the section containing the helium passages.

In the thermal analyses various boundary conditions on both the temperature of the outer edge of the holder and the thermal resistance between the holder and the fin were analysed. The analysis showed that for any realistic condition at the holder to fin interface it was necessary to maintain the end of the holder close to room temperature to control the fin tip temperature.

The analysis also indicated that even with the end of the holder maintained near room temperature that the temperature at the location where the power lead is connected to the heater element inside the holder was 1120°K (1550°F). This is above the 1000°F level recommended by the manufacturer.

The temperature predicted in the hot zone of the heater is 1950°K (3050°F) which is close to the 3100°F level at which the heater supplier indicated chemical breakdown (glass formation) of the silicon carbide occurs.

The thermal analysis suggested that the heaters could supply 70 kWatts to the engine on the hot zone temperature prediction however cooling of the holder and connector appears necessary to control fin tip and power connector temperatures.

Air jets inside the holders and also between the holders were selected as a reference approach.

Based on the analytical conclusions it was decided to modify the heater element holder. It was lengthened as shown in Figure 2. Nickel was selected for the holder material because it has a higher thermal conductivity than Inconel and would draw heat from the fin tip and help keep it cooler.

Two sets of tests were initiated.

The objective of the first set (single pocket tests) was to determine heater power limits based on degradation or failure of the hot zone.

The objective of the second set of tests was to determine what cooling requirements were needed to control fin and connector temperatures.

### SINGLE POCKET TESTS

An Inconel block was available in which a prototypical pocket had been machined to evaluate the slot machining process.

A test set up was designed which utilized shop air to cool the outer faces of the block by jet impingement. A series of grooves were machined in the faces of the block so that thermocouples could be located near the inside face. Figure 3 shows the block and Figure 4 shows the test arrangement. Copper wires were forced into the outer part of the grooves to form passages for the thermocouples at the bottom of the grooves.

Air jets were also used to cool the holder.

The objective of the first set of tests was to determine the power levels at which the hot zone would break down. Figures 5 and 6 show the total heater power versus voltage for 12 heaters from the data supplied by 'I-sq-R'. The resistance of the heaters is also shown.

Figure 7 summarizes the results from the tests. The first test was conducted at a total power level of 800 Watts per heater. One heater (No 4) failed after about 2 hours and caused the other heater (No 3) to fail also.

In the next test heaters No 5 and No 6 were used. The test was started at 600 Watts per heater and a 950 °K wall temperature. The power was progressively increased as shown in the figure with heater number 6 eventually failing at the 750 Watt level after 47 hours.

In the next test No 7 and No 8 were tested at 750 Watts per heater. Glass formation was observed on No 7 after 8 hours and it eventually failed after 45 hours. No 9 was installed with No 8 and testing continued at 700 Watts per heater. No 9 failed at 30 hours.

It is observed from the results that high resistance heaters are more prone to failure than low resistance heaters and for low

resistance heaters a power level of 750 Watts per heater should give a useful life for engine testing. At this power level assuming about 100 Watts per heater is removed by cooling the holder about 650 watts per heater will be available for input to the helium. This will result in about 65 kWatts into the engine since there are 100 heaters ( 2 x 50 pockets ).

A maximum resistance of 30 Ohms at 125 Volts was specified in the purchase order for engine heaters. Most of the heaters subsequently received had a resistance less than 27 Ohms.

It was also observed from the tests that heaters did not fail without any warning. In every case a significant increase in resistance occurred before failure. Glass formation was clearly visible hours before failure. During engine tests heater resistance can be determined since the current and voltage at every heater is measured.

The installation approach will permit periodic visual inspections to be conducted.

#### FIN AND HOLDER TEMPERATURE TESTS

To assess the temperature of the fin tip and the connector inside the holder a set up was made as shown in Figure 8. Four heaters are mounted as shown. The material between the holders represents a typical fin tip. The hot zone of the four heaters was open to the air with the heat being removed primarily by radiation to the room. A flow of cooling air from a vertical tube mounted above the assembly was used to supplement the cooling of the hot zone of the heaters.

Shop air could be fed to 1/8 inch diameter stainless steel tubes mounted in the assembly to jet cool the end of the fin and/or the inside of the holder at the connector. Brass inserts in the end of the jet tubes with a drilled hole in them were used to set the jet diameter.

Air flow was measured by pressure drop across an orifice in the air supply line.

Thermocouples were installed in the sections of the fixture which represent the fin tips. These could be moved inside holes drilled in the front and back edge of the fin tips.

Initial tests were conducted with heaters in the short Inconel holders. These were followed by tests with heaters in long nickel holders.

With the long nickel holders it was determined that air cooling between the holders to help cool the fins was not needed.

It was not known if the connector had a temperature limit . An early failure suggested that it should be well cooled. After further tests were conducted it was determined that the connector could operate at 750°C (1025°K). Over 50 hours of operation on four heaters were finally conducted with no cooling at all. The front of the fin was operating at a temperature of 760°C and the back side of the fin at 745°C.

Based on these tests it is expected that no cooling will be required on the engine. In the event engine operation does not replicate the above simulation the parts needed to add jet cooling have been ordered. Figure 9 shows the arrangement that can be incorporated in engine set up if necessary.

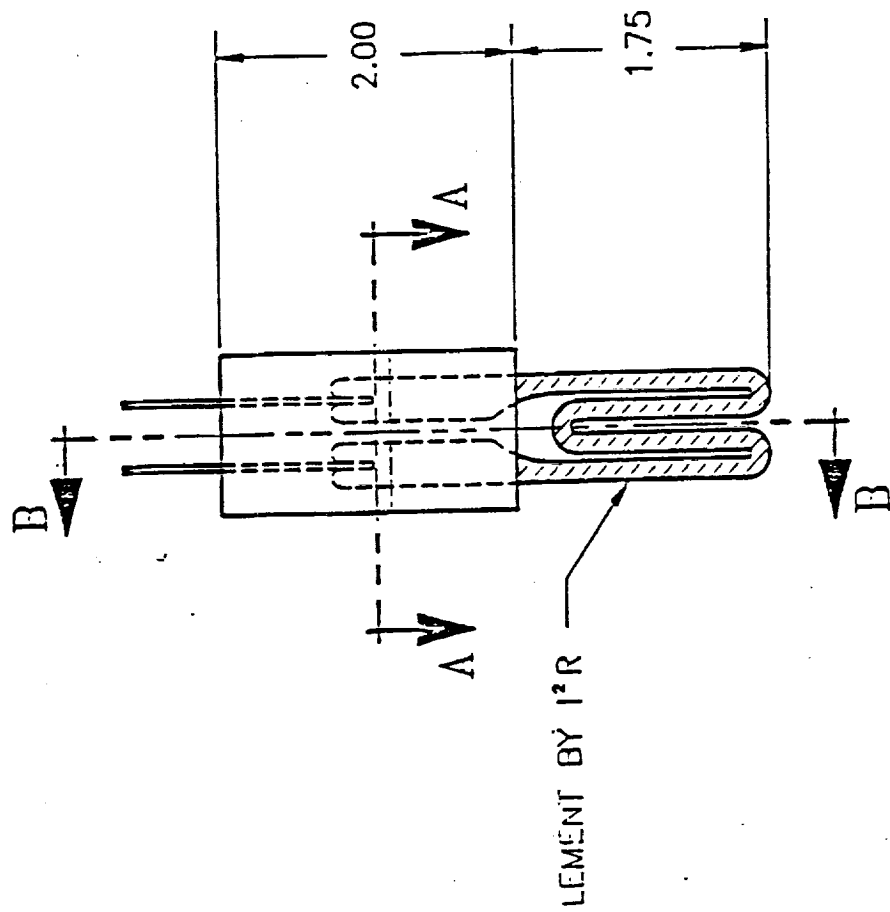
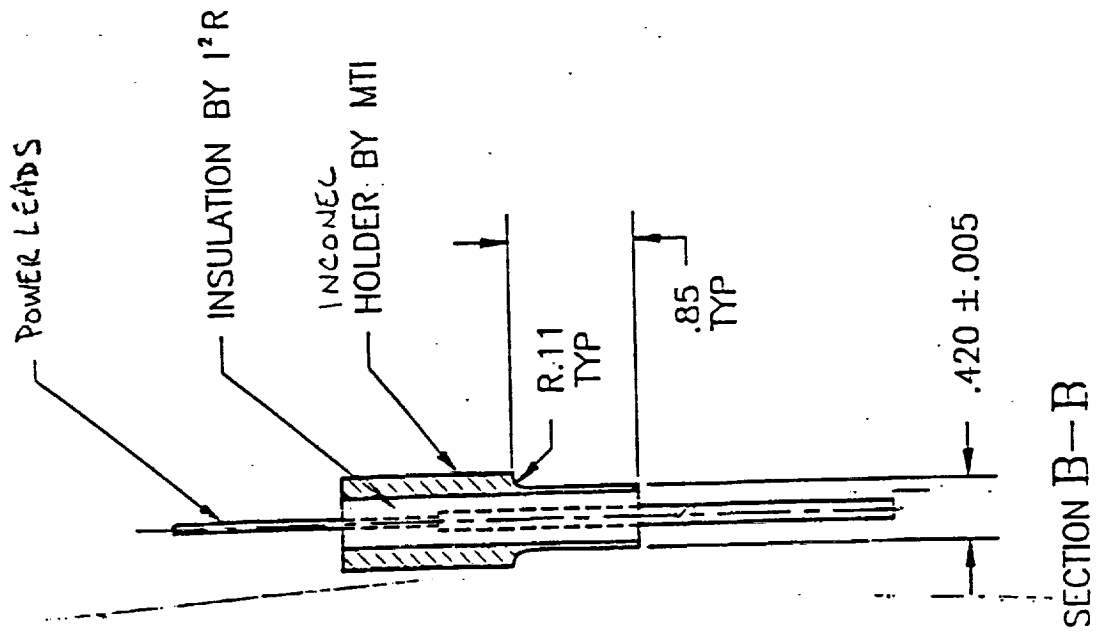
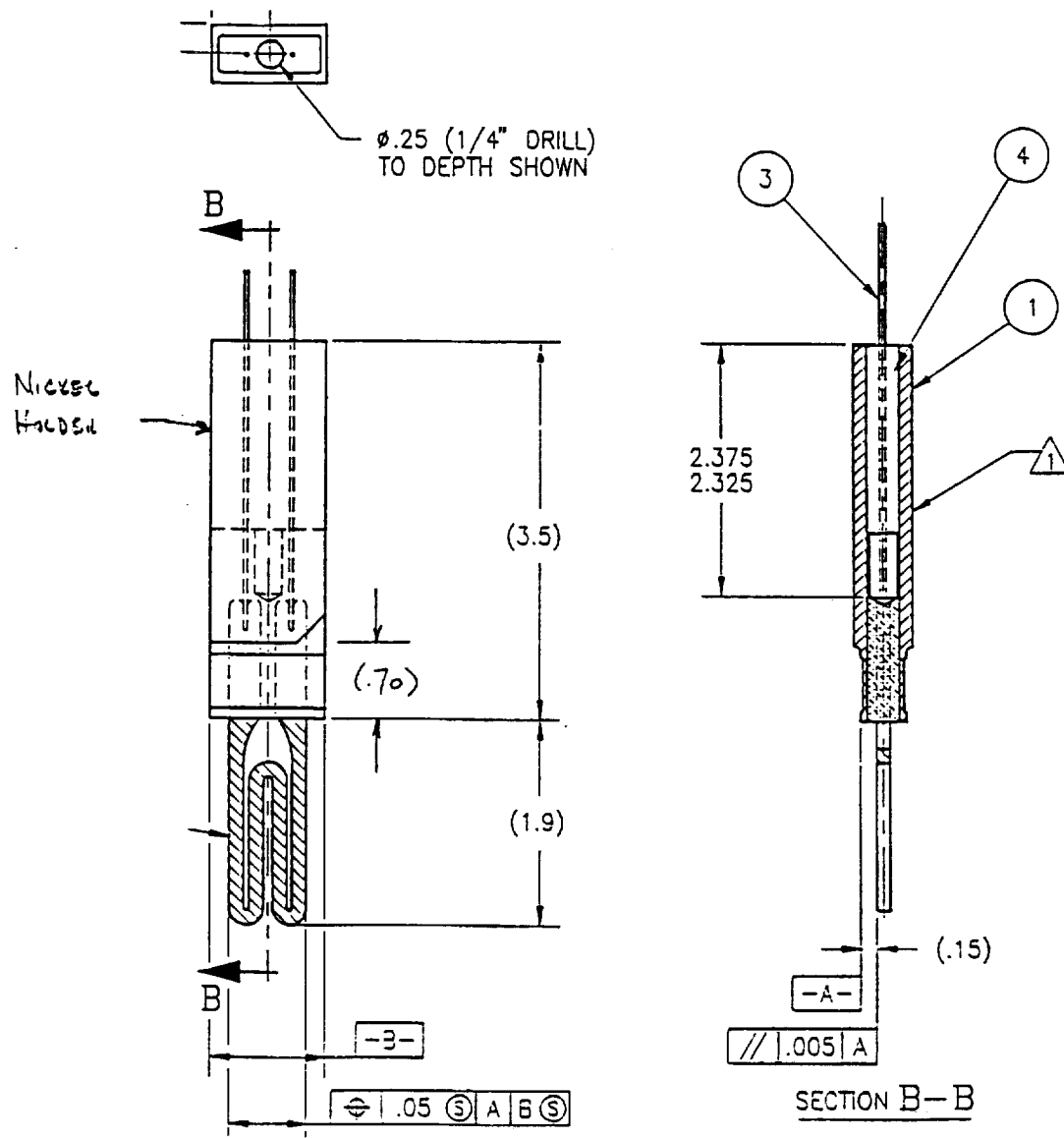
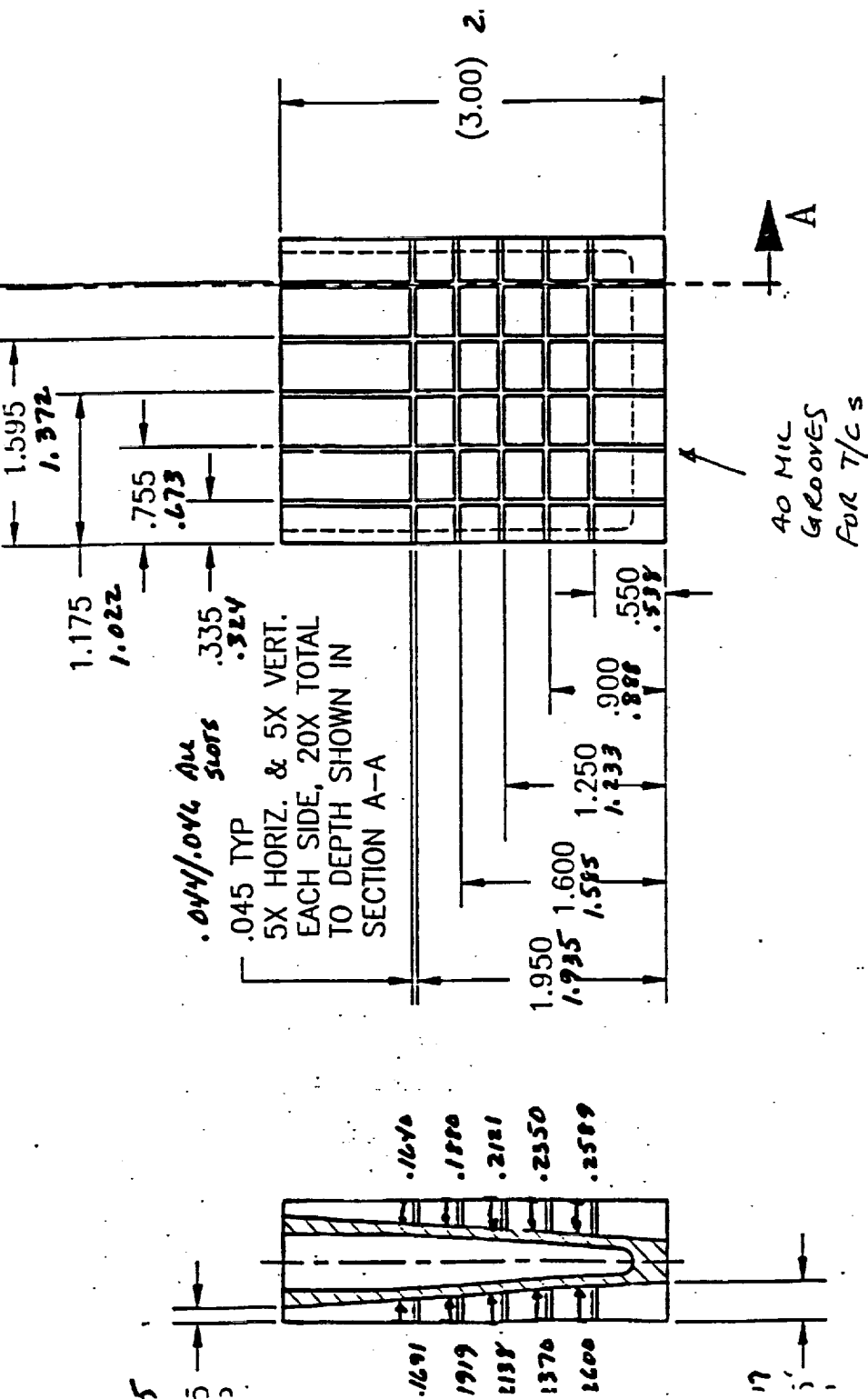


Figure 1.



POCKET RADIATOR HEATER (FINAL DESIGN)  
Figure 2

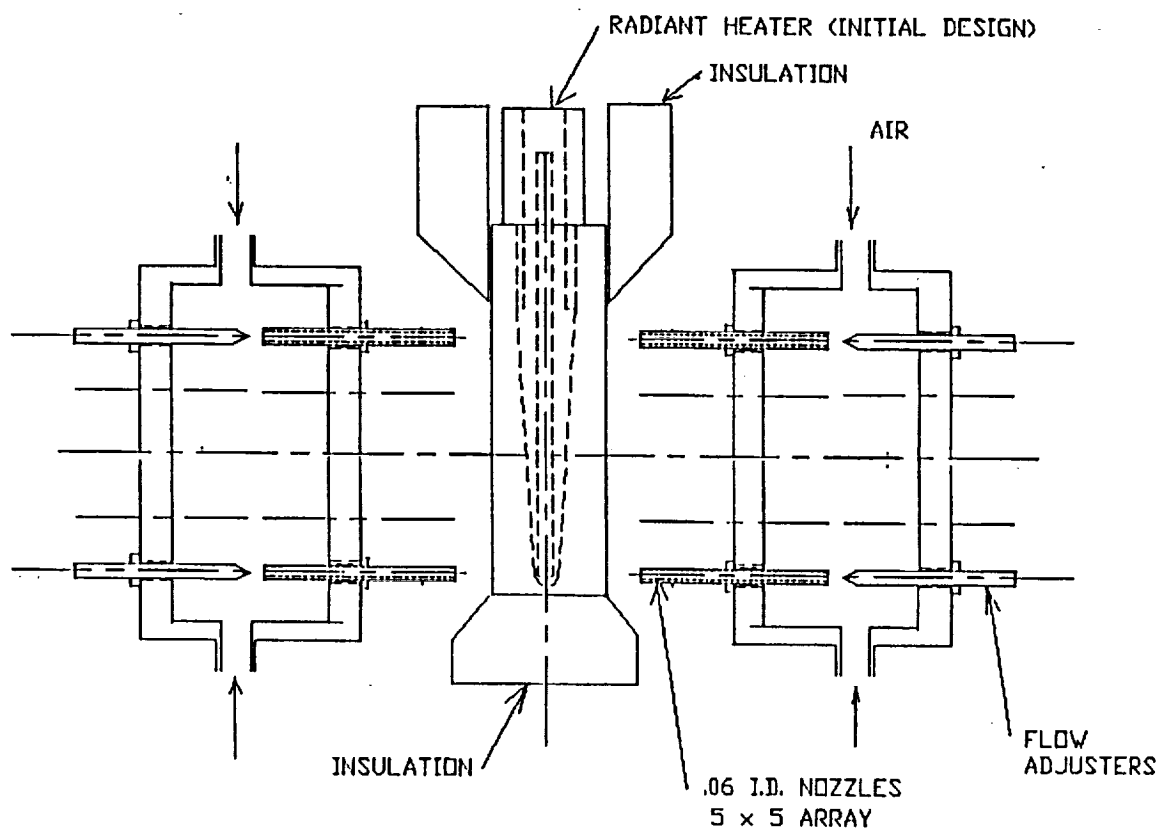


SECTION A-A STARFISH POCKET SAMPLE

Figure 3

INCHES APPROXIMATE





STARFISH RADIANT HEATER SINGLE POCKET TEST ARRANGEMENT

# HEATER POWER - VOLTAGE

## Initial design test heaters

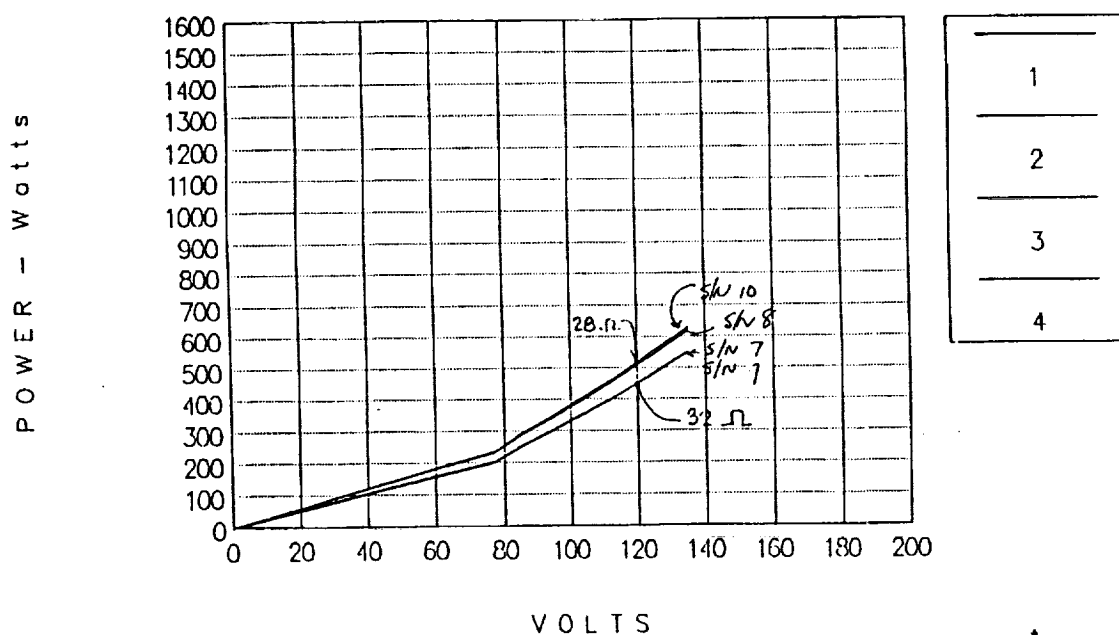
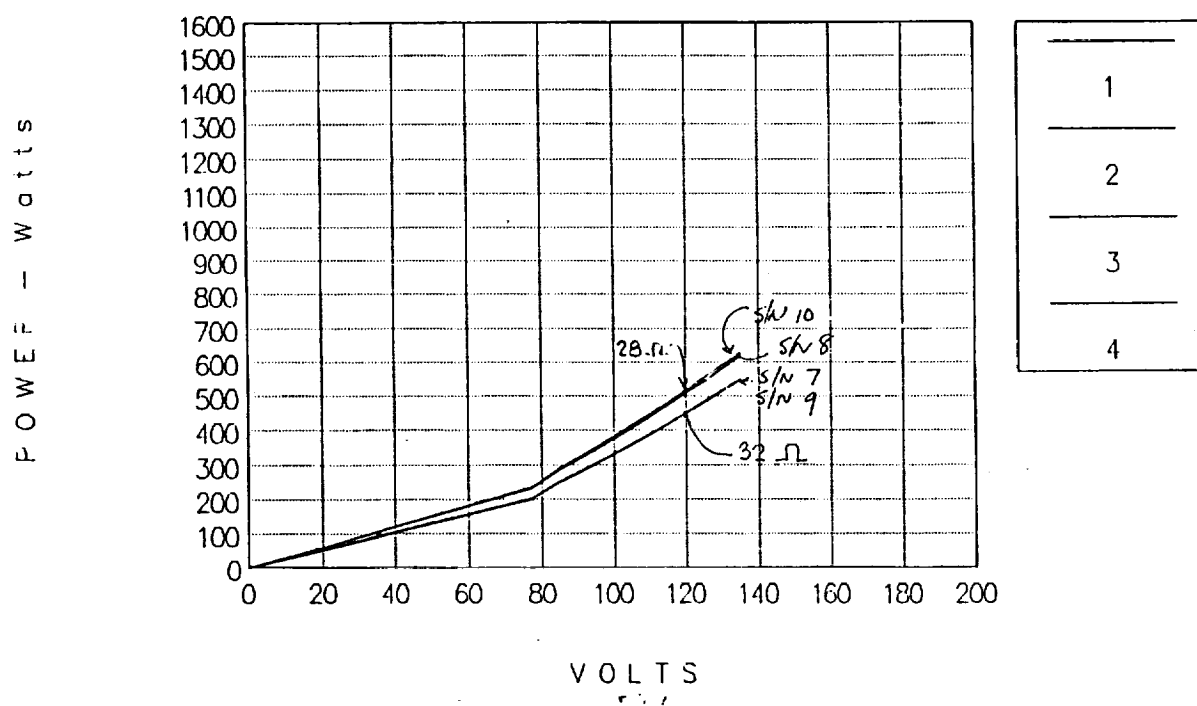


Fig 5

# HEATER POWER – VOLTAGE

## Initial design test heaters



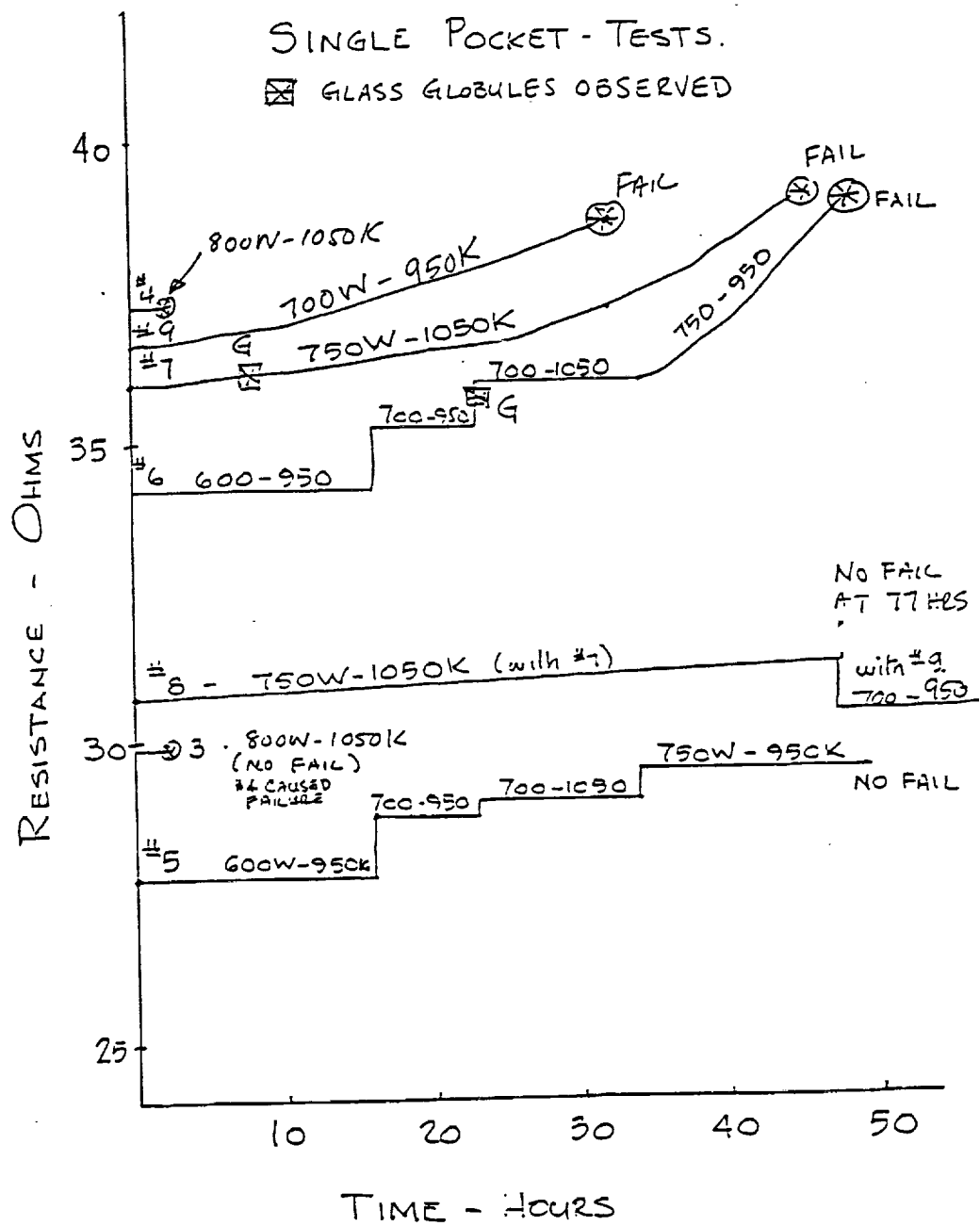
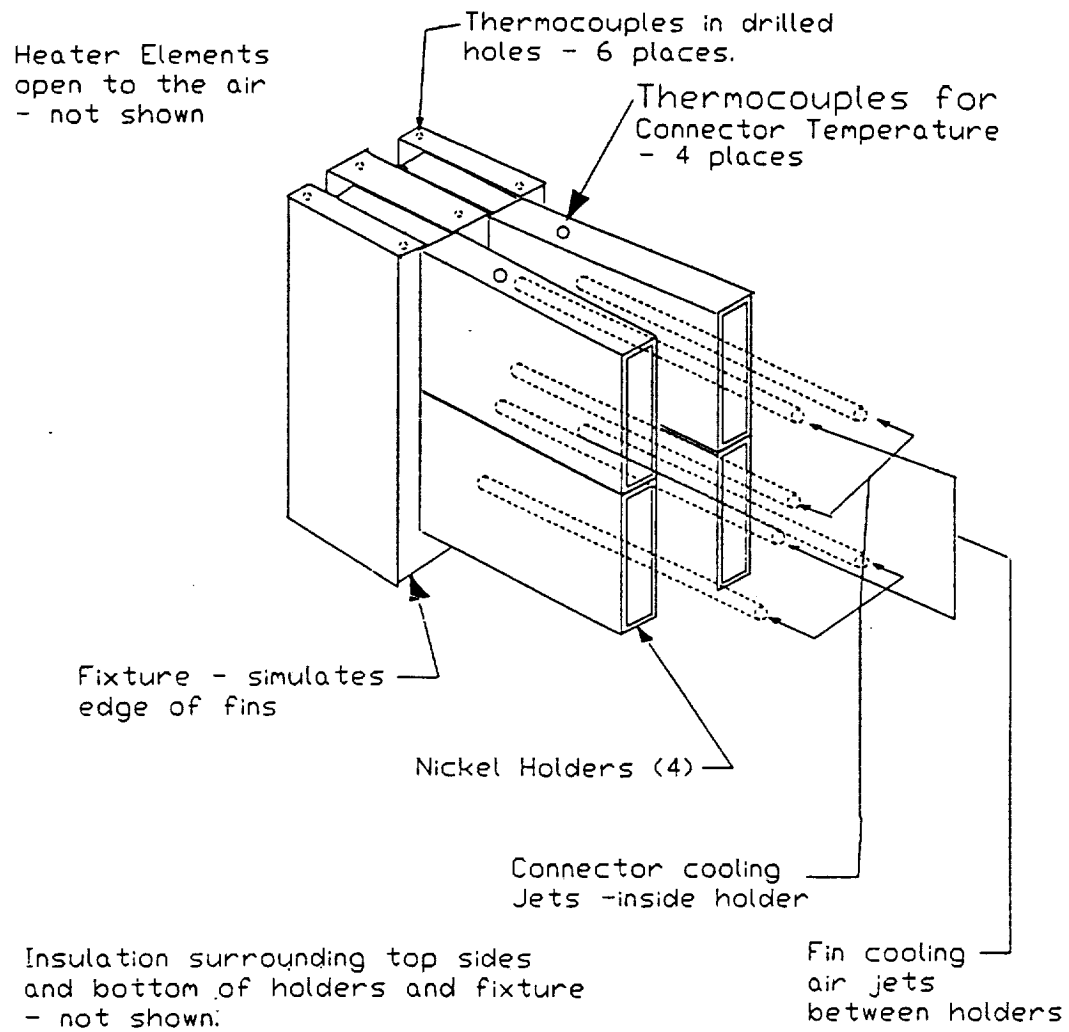


Figure 7



# SLOT RADIANT HEATERS HOLDER AND FIN COOLING SETUP

Figure 6

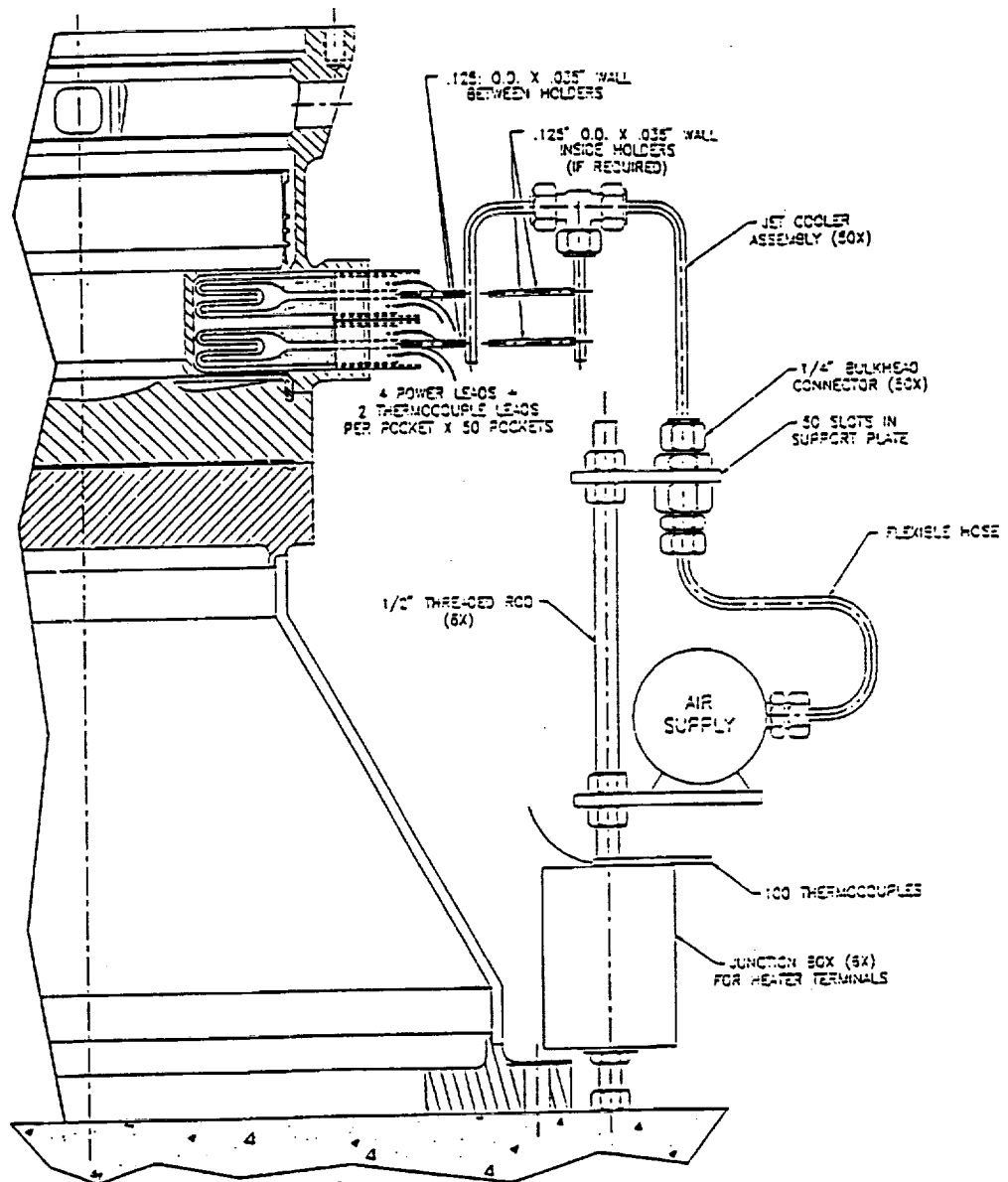


Figure 3

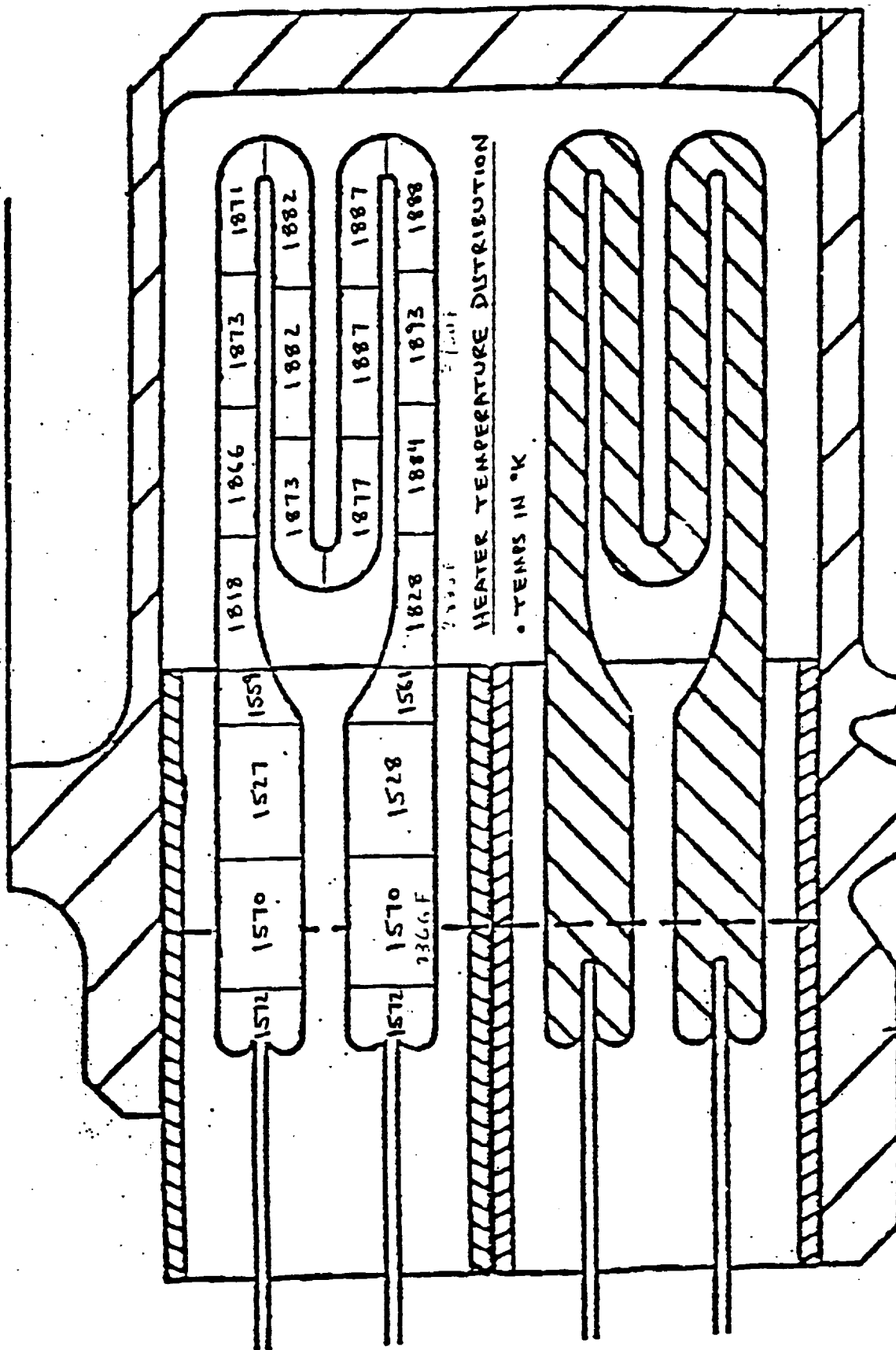
## APPENDIX TO SLOT HEATER COMPONENT DEVELOPMENT REPORT

### THERMAL ANALYSIS BY NASA.

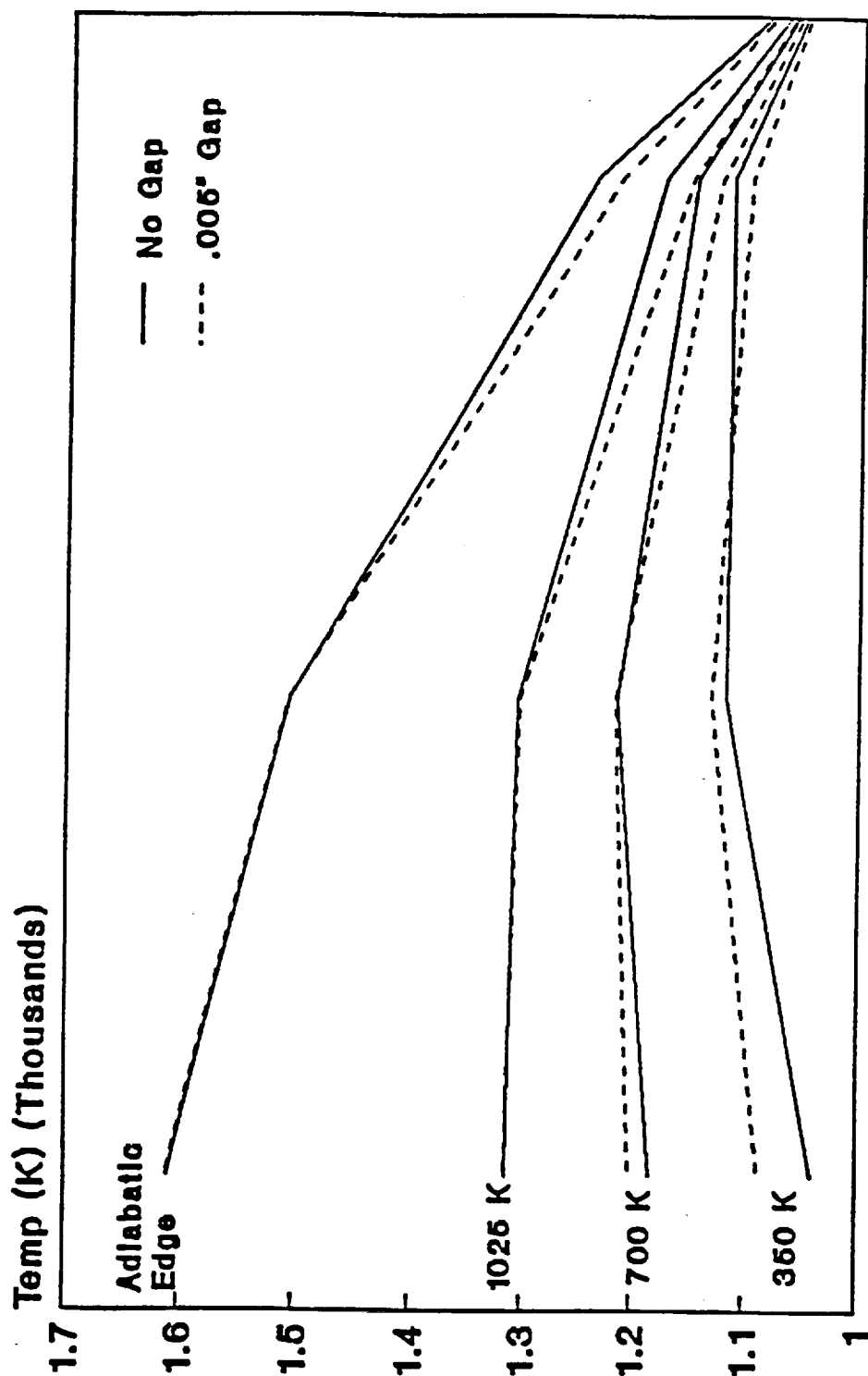
The following analysis was conducted on the initial short Inconel heater holders by P.Dunn on NASA Lewis RC.

Based on this the holder length was increases and the material changed to Nickel to increase thermal conductivity.

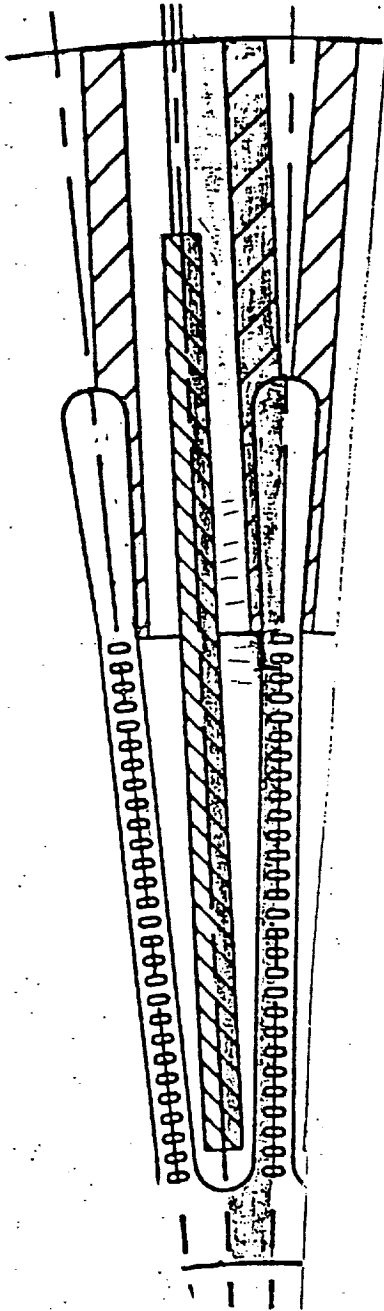
The final arrangement was not reanalyzed, the conclusions on power limits and cooling requirements were based on the tests reported in the main body of the report.

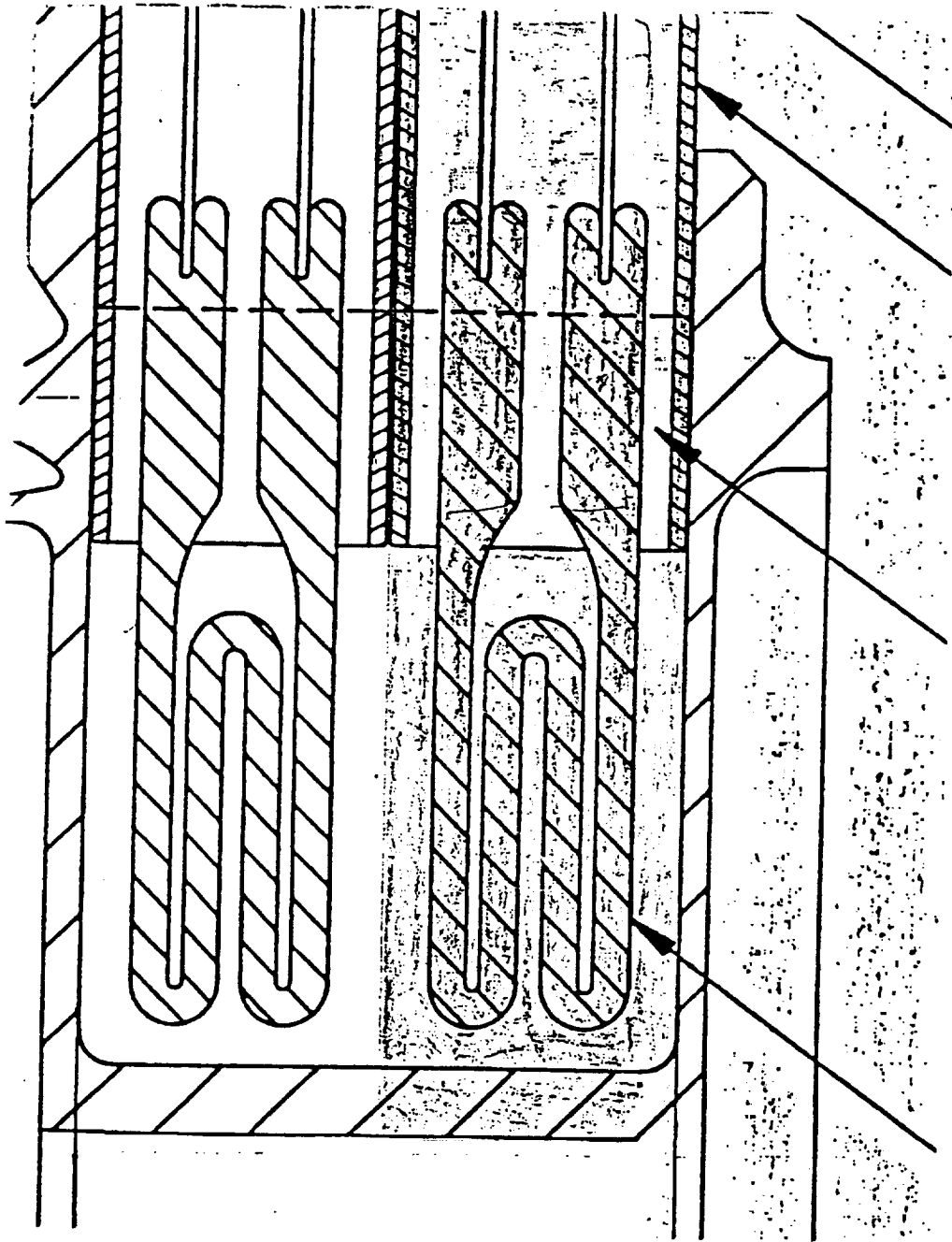


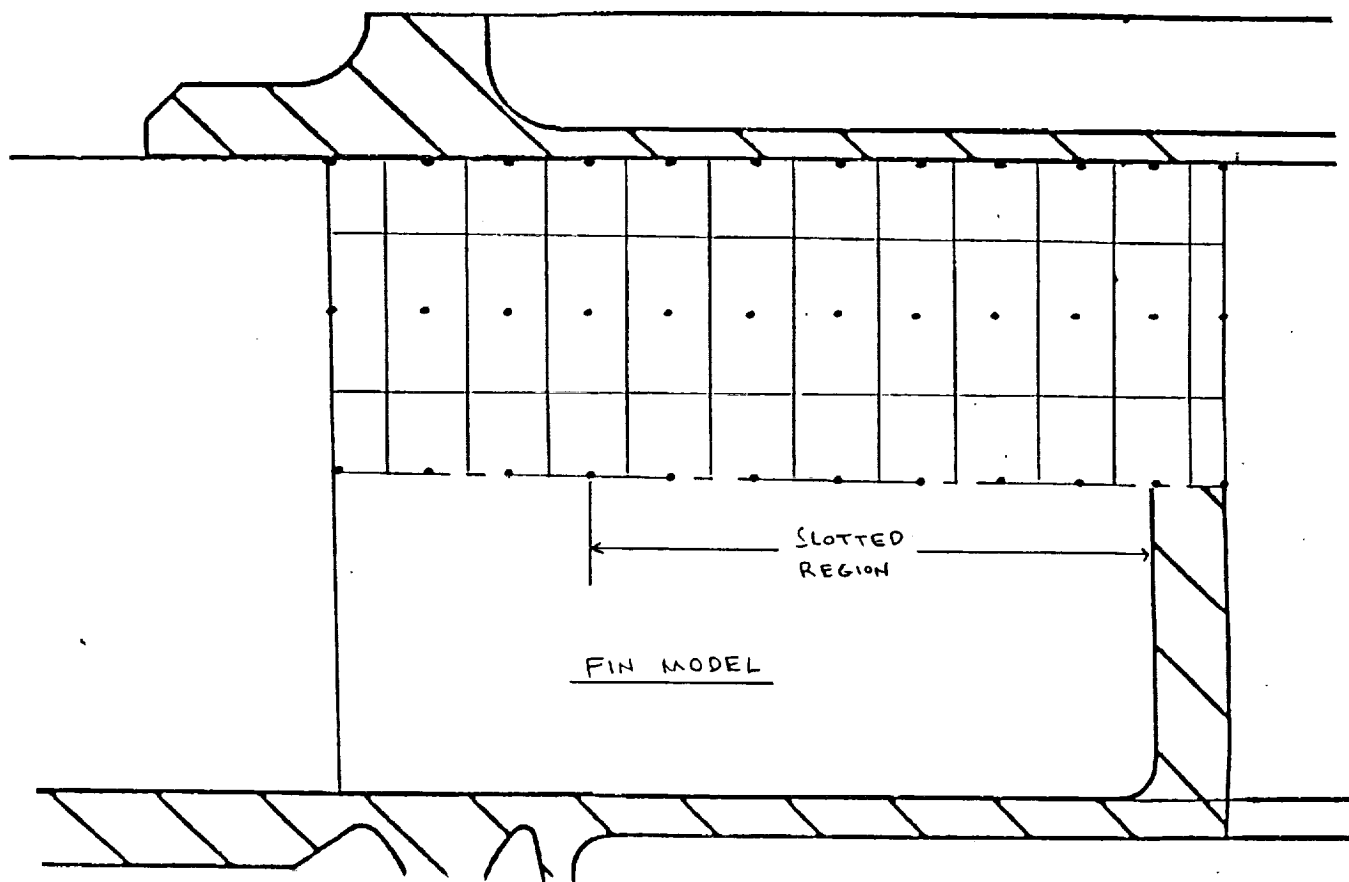


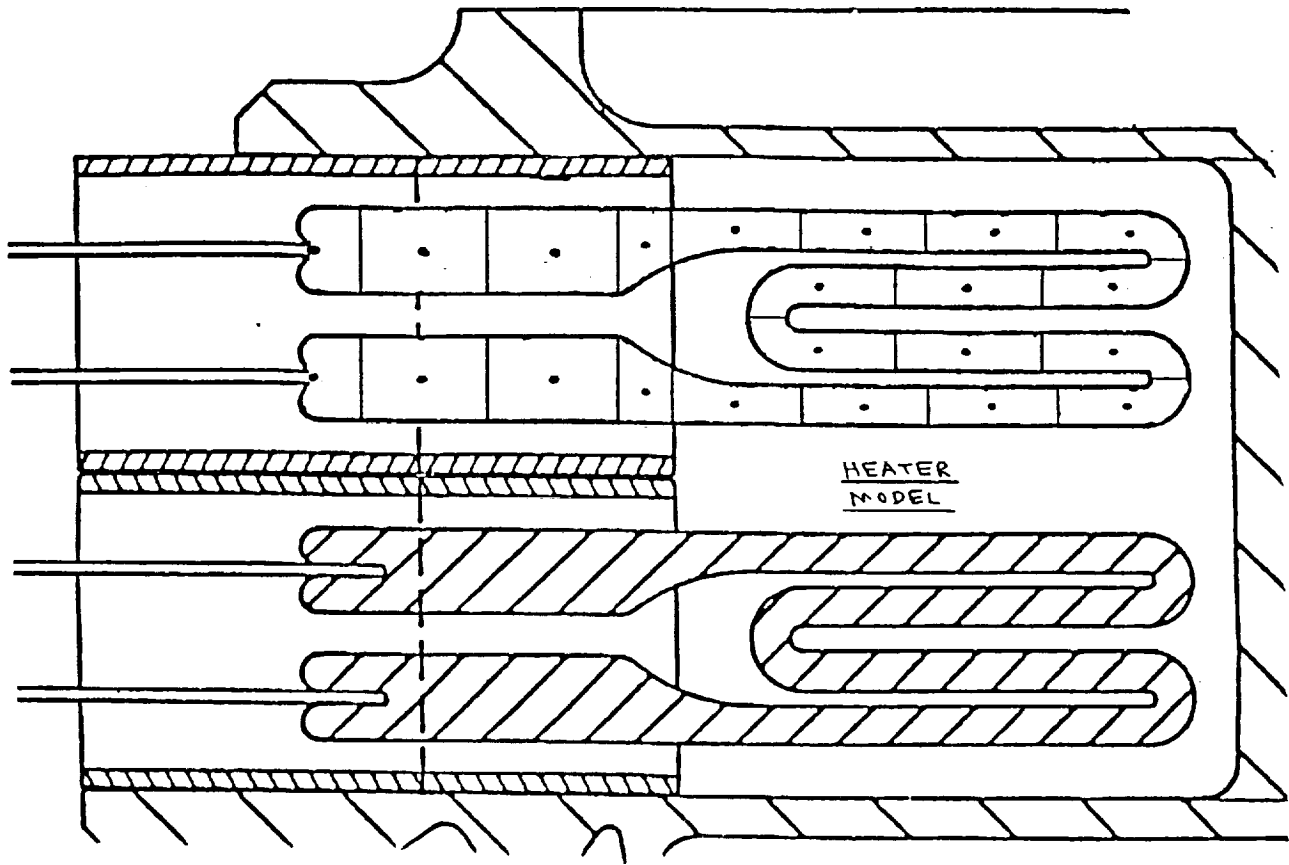


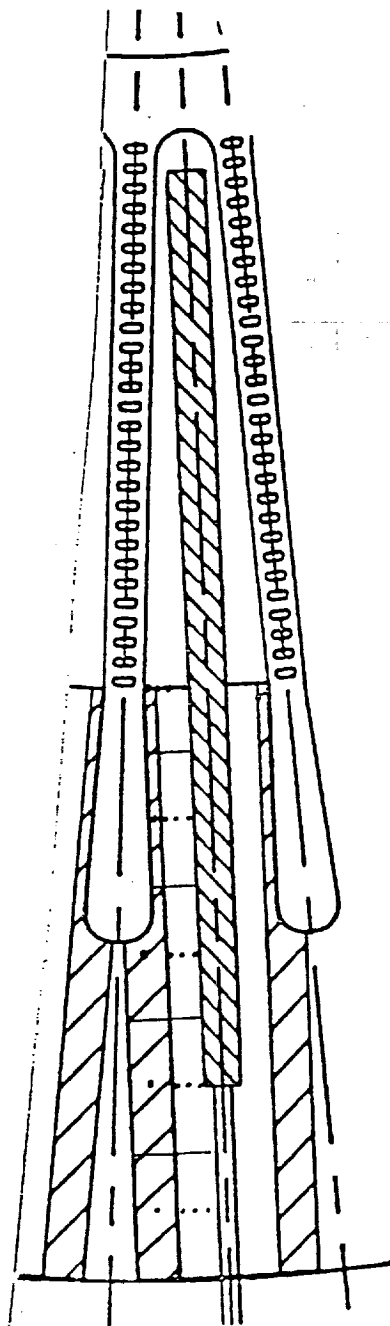
## Distance Along Tip Fin Tip Temperatures











INSULATION / INCONEL HOLDER MODEL

## MODEL NODAL BREAKDOWN

FIN 36 Nodes

HEATER 22 Nodes

INSULATION 75 Nodes

INCONEL HOLDER 26 Nodes

SLOT GAS TEMP 1 Node

ENCLOSURE AIR TEMP 1 Node

161 TOTAL NODES

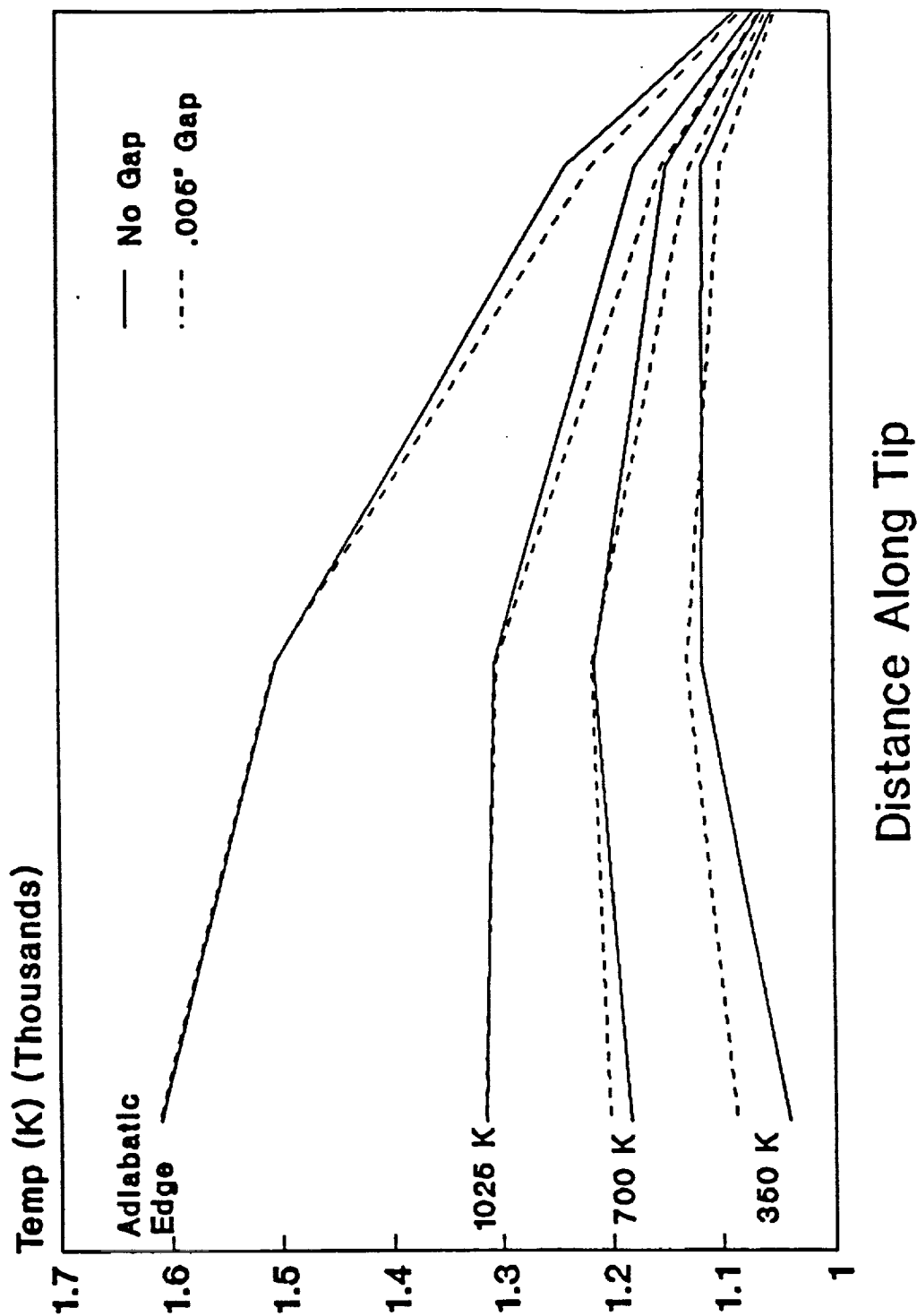
RADIATION CONDUCTORS 694

CONDUCTION CONDUCTORS 356

CONVECTION CONDUCTORS 60

1110 TOTAL CONDUCTORS

# Fin Tip Temperatures

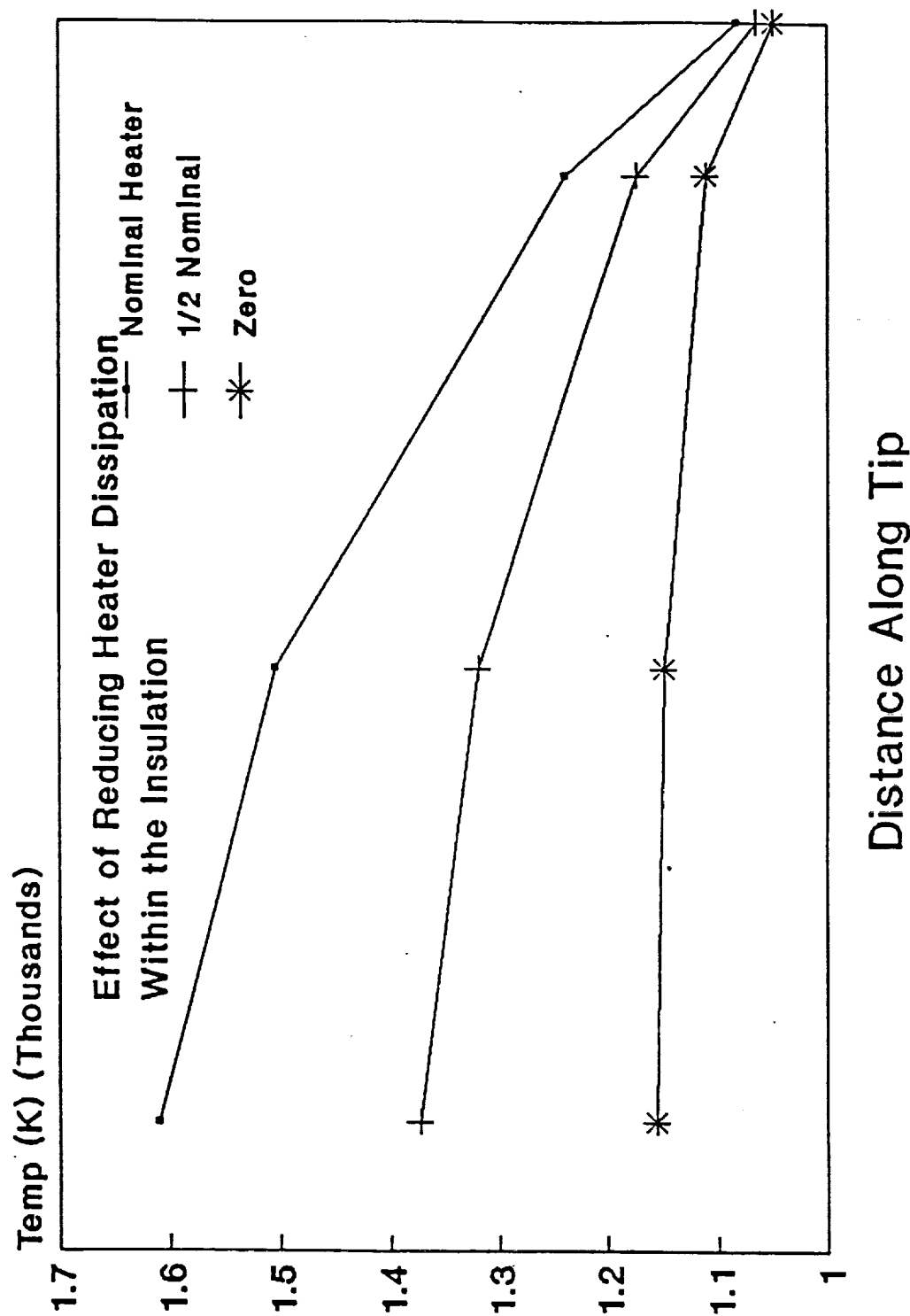


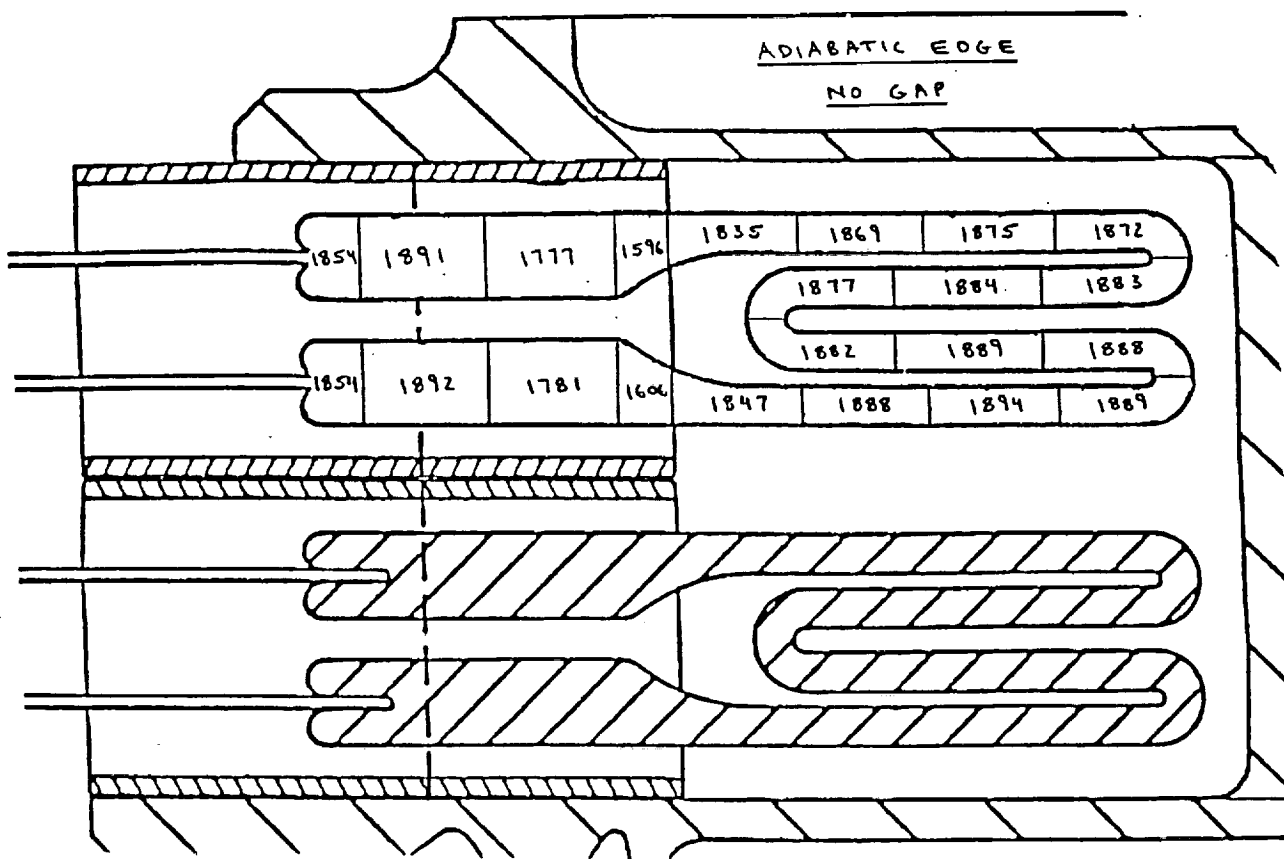


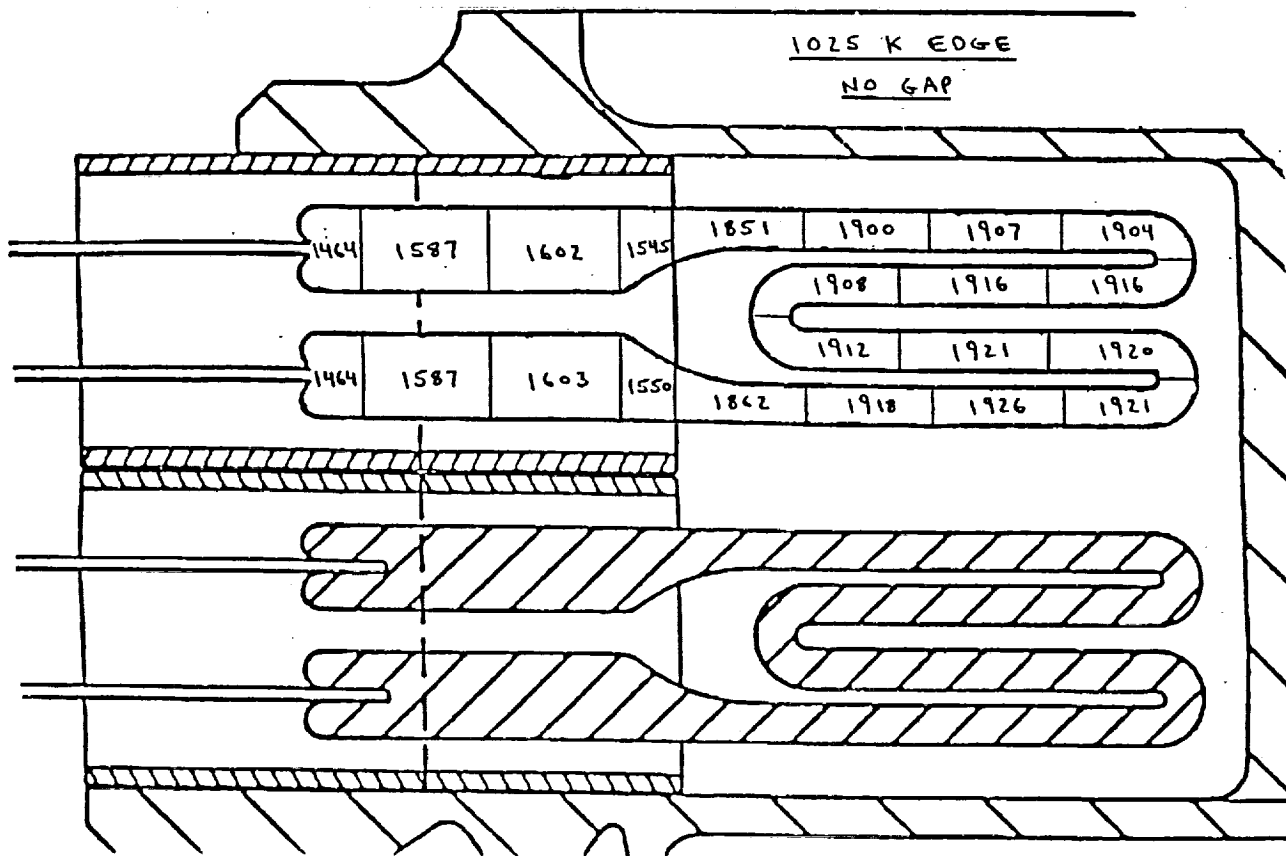
HEATER POWER REQUIREMENTS FOR A COOLED  
OUTER SURFACE

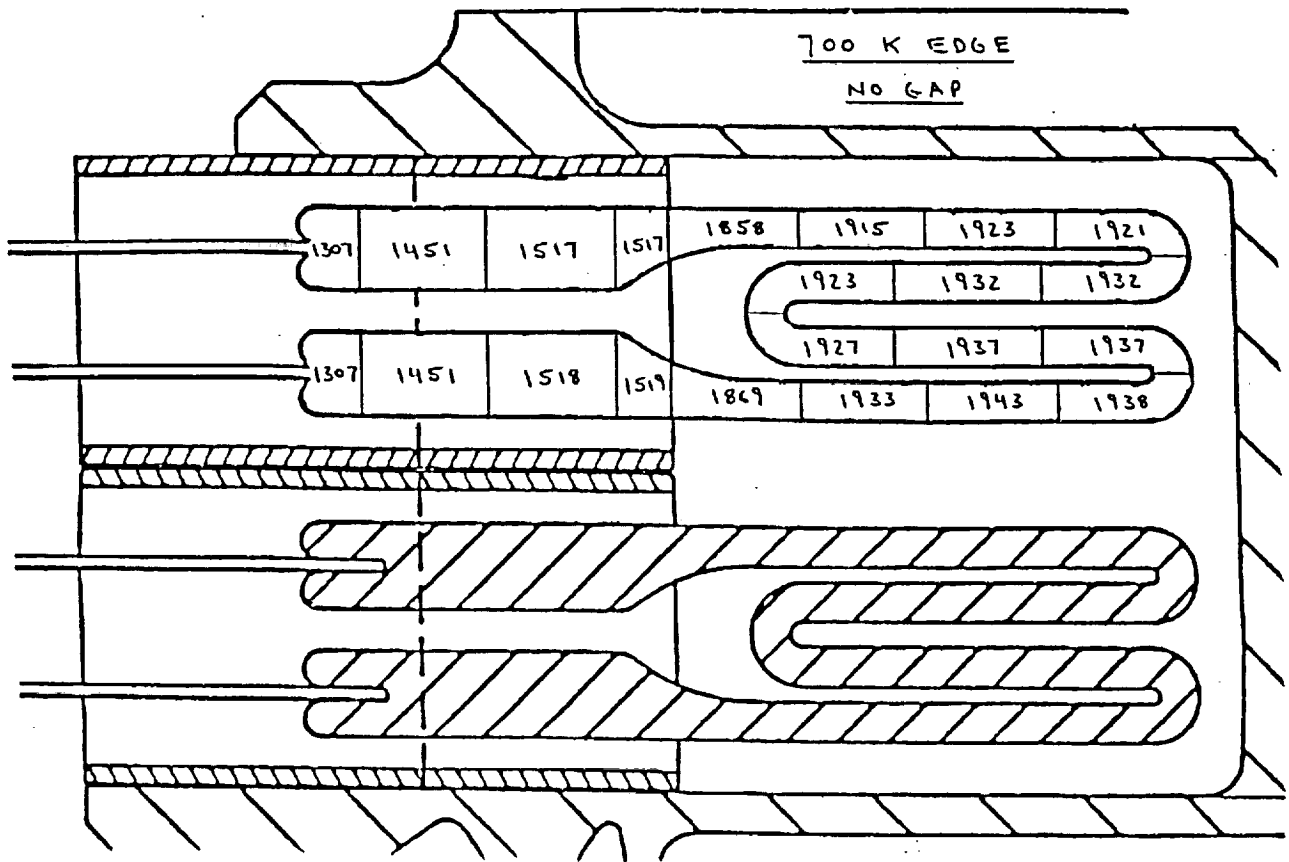
OUTER EDGE TEMP (°K)	POWER REQUIREMENT
ADIABATIC	NOMINAL (1400 W PER SLOT)
1025	1.08 NOMINAL
700	1.12 NOMINAL
350	1.15 NOMINAL

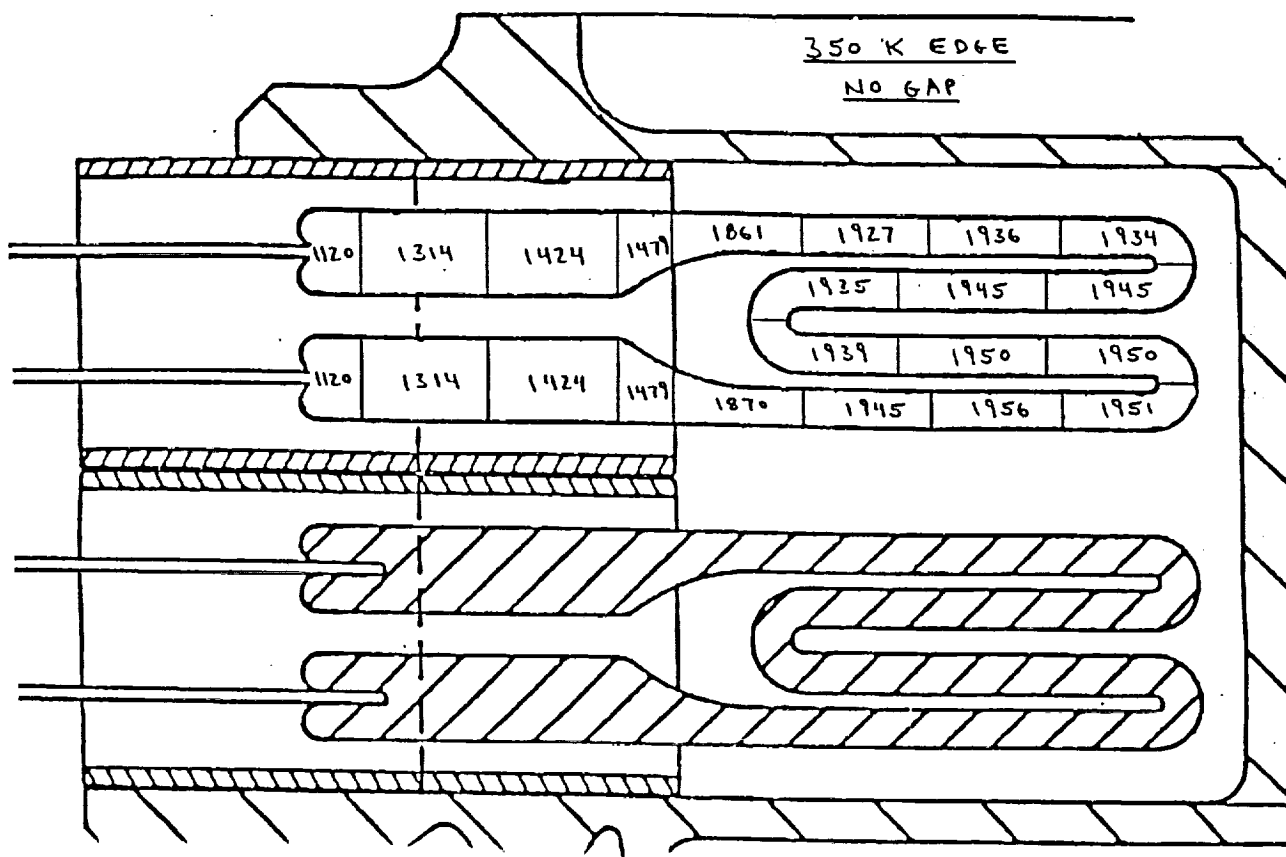
# Fin Tip Temperatures

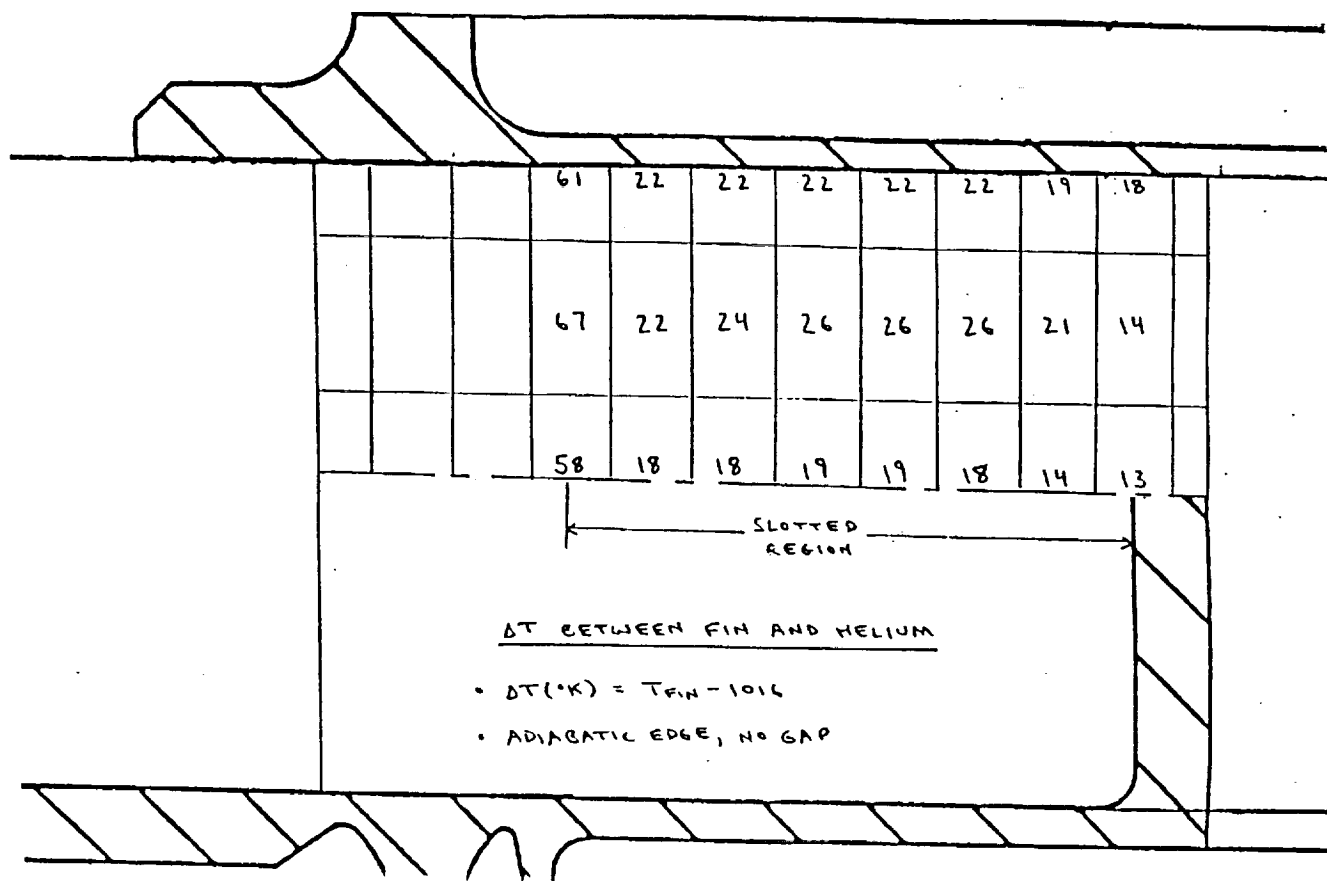


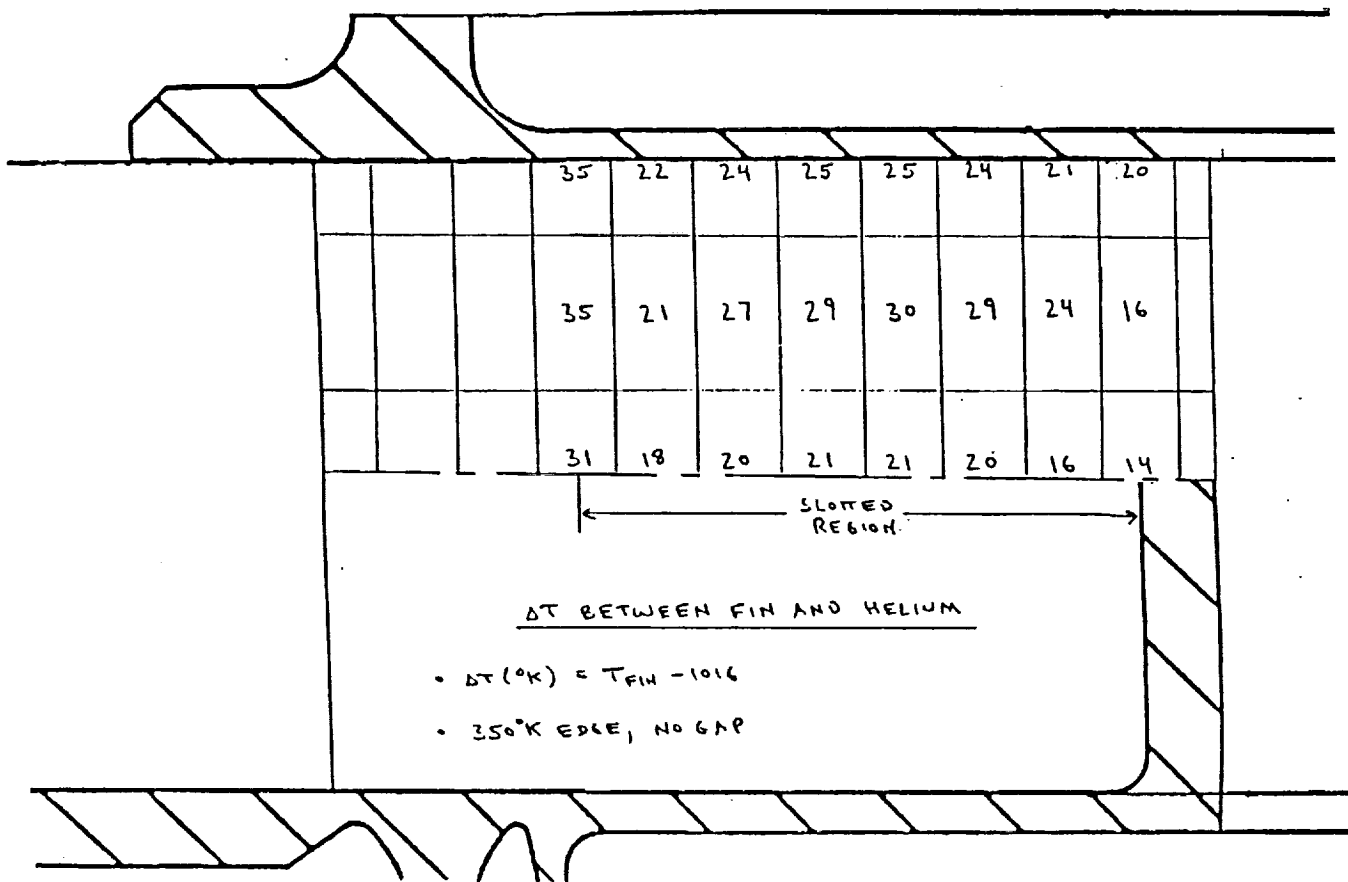








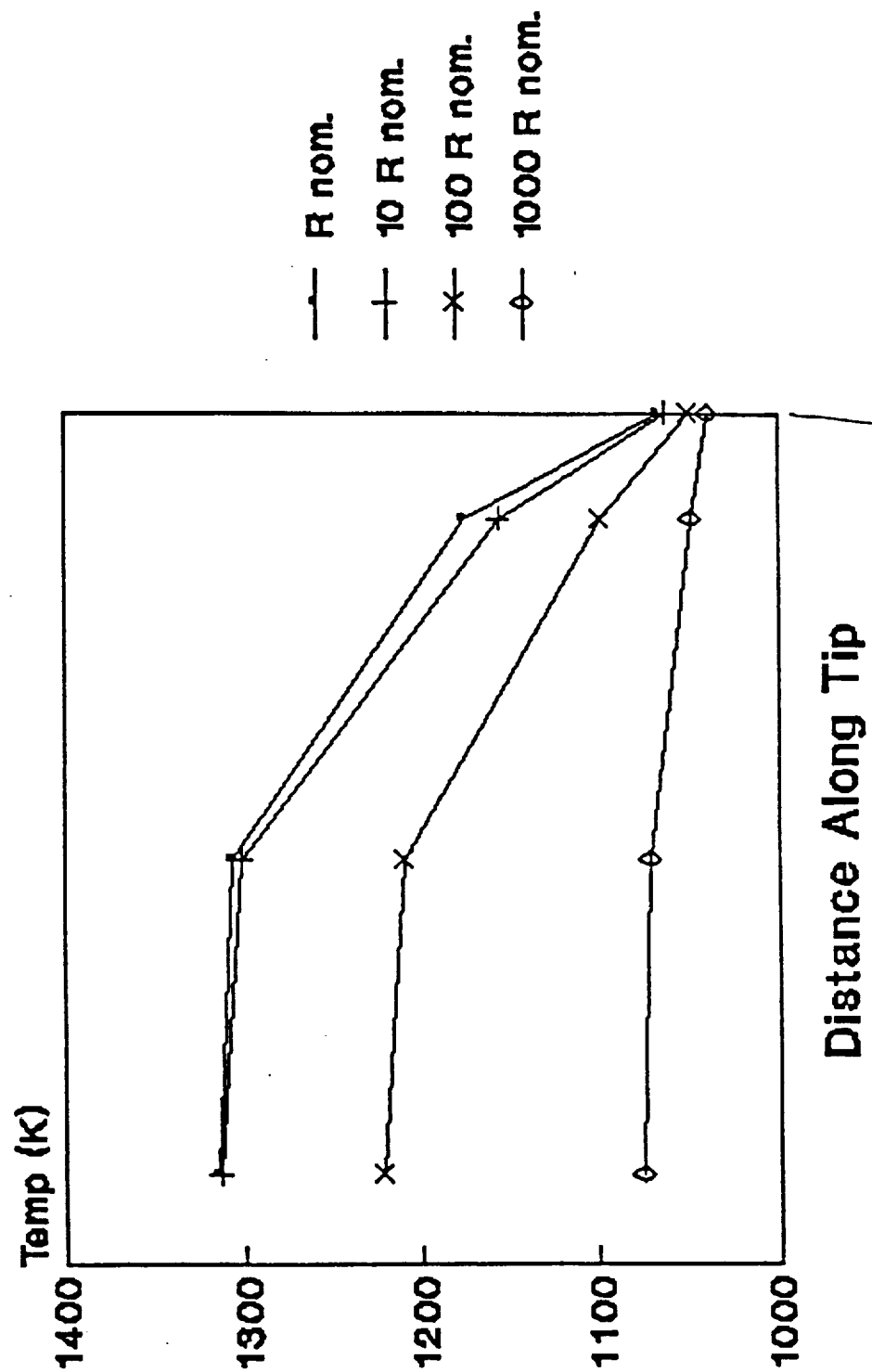






# Fin Tip Temperatures

## Edge Temp = 1025 K





## Report: CTPC Heat Pipe Heater Development

It is planned to supply heat to the CTPC heat pipe by locating a set of silicon carbide radiant heaters in an insulated cavity below the bottom plate of the heat pipe.

The cavity has an inner diameter of approximately 15 inches and an outer diameter of approximately 30 inches. The I-squared-R company makes round silicon carbide heaters referred to as 'starbars'. A copy of the data sheets on these heaters is appended.

The diameter of the heater, the length of the the hot zone, and the length of the cold leg can be specified to meet a specific application.

In the initial arrangement selected for CTPC sixty heaters .5 inch diameter with a hot zone length of 6 inches and an overall length of 13 inches were mounted radially in the cavity. The top surface of the cavity is formed by the heatpipe base plate and the remaining surfaces are high temperature insulation. The center to center spacing of the heaters is .83 inches at the inside end of the cavity and approximately 1.5 inches at the outer end of the cavity.

To demonstrate the power capability of such an arrangement a test set up was built and is shown in Figure 1. This set up simulates a 48 degree segment of the cavity and incorporates eight heaters spaced as in the full sized design.

A 1/4 inch thick Inconel 718 plate was placed over the cavity to represent the heat pipe base plate. This plate was cooled by a set of air jets impinging on the top surface of the plate. The air flow through each jet tube could be adjusted by turning a threaded rod with a tapered end into the entrance of the jet tube.

Each heater is held by a clamp around the collar to a block mounted on a support plate. High temperature silicone sheet is used as a cushion between the metal clamp and the ceramic collar.

Power to the heaters could be adjusted by three Variacs on the three legs of 208 Volts 3 phase line power.

Three heaters were connected in parallel on each of two variacs and two heaters were connected in parrallel to the third Variac.

The current to the heaters was measured by the voltage across a precision resistor at the output of each Variac. The power was determined by the product of voltage and current.

Prior to the tests fourteen heaters were individually tested in open air to determine their resistance. Heaters with similar resistances were selected to be in the same leg of the electrical

circuit to minimize power variations from heater to heater.

Temperature measurement of the top surface of the plate was determined with a thermal wand connected to the T/C input on a multimeter.

During the first tests it was found that the plate temperature could be set close to 1050°K by adjusting the jet inserts and supply pressure until the color of the plate started to glow red and was uniform at each jet.

The power to the heaters was set to give about 1300 Watts per heater. This is equivalent to a 78 kwatt power setting on 60 heaters. After about an hour one pair of heaters failed. After cooldown it was determined that the power connection had overheated.

This power lead is flat braided aluminum clamped to the end of the silicon carbide heater element. Local melting was observed.

A visit was made to the heater supplier to solicit advice on the installation and operation of heaters. The outcome was a recommendation to use 3/4 inch diameter heaters which are inherently more rugged and reliable. It was also recommended that a center to center heater spacing of at least 2" be maintained.

Heaters were ordered with 5 inch and 6 inch hot zone lengths. The overall length was 13 and 14 inches respectively. By alternating these in a 40 heater array a center to center heater spacing greater than 2" could be maintained.

Three 14 inch and two 13 inch heaters were mounted in the cavity.

The three long heaters were connected in parallel to the largest Variac and the one short heater was connected to the smaller Variacs.

After initial tests in which the temperature of the connector was monitored by touching the connector with a thermocouple during a brief power shut off it was decided to add shop air cooling to the connector end of the heater.

A 1/2 inch diameter stainless steel tube was located beneath the heaters inboard of the collars. Two 32 mil holes were drilled in the tube directly below each heater such that air from the holes would impinge on the heater.

During check out testing 10 psi shop air at the cooling manifold maintained the connectors below 400°C. The melting point of aluminum is in the 500 to 600°C range.

A steady state test was run with the power to the 5 heaters equivalent to 60 kWatts into 40 heat pipe heaters. The plate temperature was between 700 and 750°C. This test was continued

without incident for 50 hours.

The power to the heaters was increased to be equivalent to 82 kWatts into the heat pipe heaters and the test continued for an additional 50 hours without incident.

Power was raised to 93 kWatts equivalent and the test continued four heaters were still operating after 65 hours. An edge heater failed during the last few hours of this test.

Following shut down the failed heater had degraded near its tip in the hot zone. Two other heaters were showing slight glass formation.

The conclusions reached are that at a power level up to about 80 kWatts into the heat pipe heaters no degradation is observed and a relatively long life would be expected.

Above 90 kWatts some heaters will have a useful life less than 50 hours.

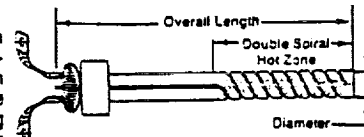
The required power input into the CTPC heat pipe is expected to be less than 60 kWatts. Allowing for thermal losses the required power input to the heaters is expected to be less than 70 kWatts.

From the above tests forty 3/4 inch diameter starbars have ample capability to meet CTPC testing needs.

Figures 2 and 3 show the final arrangement planned for engine testing.

## TYPE SER STARBAR SUPER SPIRAL BAYONET HEATING ELEMENT

**DESCRIPTION:** Made of special high density, reaction bonded silicon carbide, this element is a cylinder with both electrical connections on one end. The hot zone is formed by cutting a double spiral slot, which reduces the cross sectional area over which the current flows, resulting in higher resistance than the cold end. The cold end is formed by cutting two longitudinal slots along the length of the cylinder. The element is supplied with a ceramic collar cemented to the extremities of the cold end. The cold end of the element is flame sprayed with aluminum for a distance of about 2 inches. Flat, braided aluminum straps are held in compression with stainless steel clamps to this metallized area. The hose clamp is electrically insulated from the flat braid with high temperature fiber insulation. The aluminum braid is 10 inches long and holes are provided for easy connection to the power supply.



**OPERATING TEMPERATURES:** SER STARBARS can be operated at furnace temperatures up to 3000°F (1650°C) in air. In reducing atmospheres the maximum use temperature is 2500°F (1370°C). See Watt Loading Graph (Figure 1).

**ELECTRICAL CHARACTERISTIC:** The SER STARBAR has a negative resistance temperature characteristic from room temperature to approximately 1200°F (650°C). At this temperature it turns positive and remains so throughout its normal operating temperature range. See Typical Resistance/Temperature Characteristics Graph. The elements are calibrated at a surface temperature of 1960°F (1070°C).

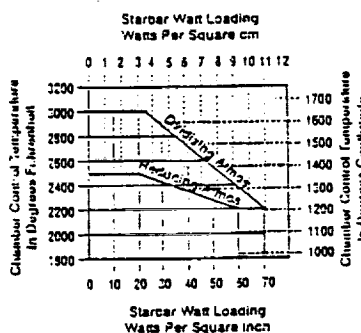
**SUPERIOR PERFORMANCE:** At 2.7 gms/cc this high density-low porosity element is able to survive severe environments. The high density prevents the internal lattice structure from being oxidized. This element, therefore, has an extremely slow aging characteristic.

### APPLICATIONS:

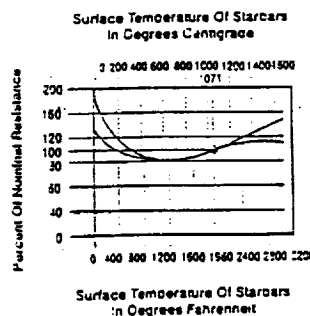
- 1) Where both electrical connections are required on one end.
- 2) Maximum temperature 3000°F (1650°C).
- 3) Cycling to 2800°F (1540°C) from ambient.
- 4) Atmospheres of Carbon, Oxygen, Water Vapor.
- 5) Where other, lower density elements perform poorly.

**MOUNTING:** SER (Bayonet) STARBARS can be mounted vertically or horizontally. When mounted horizontally, the hot end does not need to be supported. When mounting the element horizontally, however, make sure that the slot in the terminal end is not in contact with the insulation in the wall of the furnace or kiln. This is most easily accomplished by placing the slot in a horizontal position. The terminal holes should also be 10% larger than the diameter of the element.

Maximum Watt Loading  
(Figure 1)



Typical  
Resistance Temperature  
Characteristics



SQUARED ELEMENT CO., INC.

## SER STARBAR ELEMENTS IN FURNACE DESIGN:

SER STARBARS may be oriented in any position. However when the STARBAR is mounted horizontally, the slot in the cold end should also be positioned horizontally. Care should be taken to avoid inserting the STARBAR's hot zone into the insulating wall.

For proper operation, SER STARBARS should be placed no closer than two element diameters to each other, or two element diameters from a product, or furnace insulation. These spacing distances are to be measured from the element's center line.

For uniform heating of the product or load, the minimum distance between the element and stationary load is obtained by dividing the distance between the elements by 1.41. To provide uniform heating on a product moving perpendicular to the axis of the element, the minimum distance between the elements is divided by 1.73.

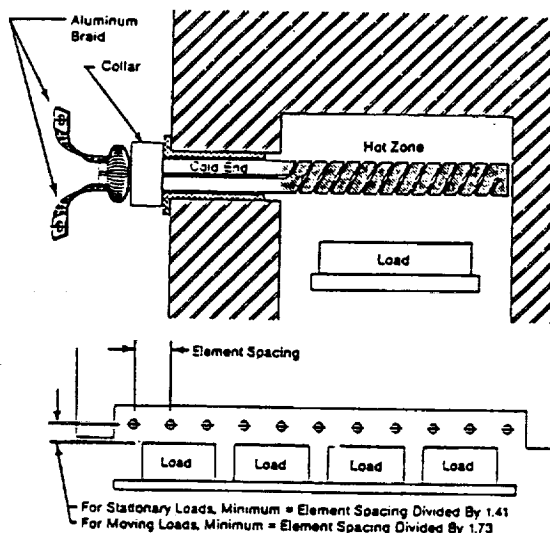


Table A  
SER STARBAR ELEMENT STANDARD SIZES AND ELECTRICAL CHARACTERISTICS:

Starbar Diameter	Maximum Heating Length	Maximum Overall Length	Nom. Ohms Per Inch Hot Section	Nom. Ohms Per Inch Cold Section	Radiating Area Sq. Inch Per Inch	Nom. Ohms Per cm Hot Section	Nom. Ohms Per cm Cold Section	Radiating Area Sq. cm Per cm
1/2 in. 1.3 cm	10 in. 25 cm	21 in. 53 cm	0.99	0.20	1.57	0.39	0.079	3.99
3/4 in. 1.6	10 25	22 56	0.79	0.14	1.96	0.31	0.055	4.98
1 in. 1.9	16 40	25 63	0.60	0.10	2.36	0.24	0.039	5.99
1 1/4 2.5	20 51	36 91	0.50	0.06	3.14	0.20	0.024	7.97
1 3/4 3.2	20 51	39 99	0.34	0.04	3.93	0.13	0.016	9.98
1 7/8 3.8	24 61	40 101	0.28	0.03	4.71	0.11	0.012	11.9
2 in. 4.4	24 61	40 101	0.24	0.02	5.50	0.09	0.008	14.0
2 1/4 5.4	24 61	48 122	0.16	0.02	6.60	0.06	0.008	16.9
2 3/4 7.0	40 102	61 155	0.10	0.01	8.64	0.04	0.004	21.9

**POWER SUPPLY CONSIDERATIONS:** Refer to the Maximum Watt Loading Graph (Figure 1) on the front page of this brochure to determine the maximum recommended watt loading for SER STARBAR elements in specific atmosphere/temperature situations.

Next, compute the total wattage output for a single element of desired length and diameter, by multiplying the maximum recommended watt loading value by the total hot zone radiating surface calculated from values shown in Table A (above).

Finally compute individual element voltage and amperage requirements

by again referring to Table A for nominal element resistance values, and use the equation  $E = \sqrt{WR}$  (where E = nominal full load voltage; W = wattage element output rating in watts; R = nominal element resistance in ohms). Knowing the voltage, current (I) is then computed by using the equation  $I = W \div E$ .

Multiple tap transformers, silicon controlled rectifiers, and saturable reactors are frequently used to control the power to the elements. When the kilowatt input to the furnace or kiln is known, and the specific STARBAR and element arrangement is known,

full power voltage can be computed using the formula  $E = \sqrt{WR}$  (where E = nominal full load voltage; W = wattage element arrangement R = network resistance of element arrangement).

SER STARBARS increase in resistance very slowly, but it is still necessary to be able to compensate for reduced output as the elements increase in resistance. A factor of 1.4 times the nominal full load voltage will accomplish this. For idling and slow heat up, 0.7 times the nominal full load voltage works well.

**CALIBRATION:** SER STARBARS are subject to a manufacturer's tolerance of  $\pm 20\%$  of nominal resistance. All elements are calibrated at least twice at 1960°F (1070°C) prior to shipping, to ensure that they are within specifications and uniform in temperature. The calibrated amperage of each element is marked on the carton, as well as on the ceramic collar cemented to the cold end. When installing, arrange elements with amperage values as close to each other as available.

**MATCHING:** Longer element life, as well as more uniform heating results, will be obtained when SER STARBARS, with similar resistance values, are installed in closely matched groups. Due to increased resistance with age, avoid installing new SER STARBARS with older, used elements. If it is necessary to replace one used element, it is advisable to replace all elements in that group. The used elements can be employed later as individual, used element replacements, or otherwise matched into used element replacement groups.

**EASE OF REPLACEMENT:** SER STARBARS can be replaced while the furnace is at operating temperature. The power to the elements being changed should be shut off. The aluminum braids can then be disconnected from the buss bar, and the old elements removed. New SER STARBARS can then be inserted into the hot furnace and reconnected to power.

**AVAILABILITY:** SER STARBARS can be shipped from stock, or within two to three weeks of receipt of order.

**OPERATION—CONTINUOUS OR INTERMITTENT:** SER STARBARS can be operated either continuously, or intermittently. At furnace control temperatures over 2800°F (1540°C), or when a glass material has coated the elements, we recommend keeping SER STARBARS above 1300°F (700°C). Note that longer life will always result from operating SER STARBARS continuously.

Table B  
PHYSICAL DIMENSIONS OF SER & TSR STARBAR ELEMENTS  
FOR TUBE FURNACE APPLICATIONS:

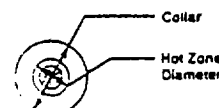
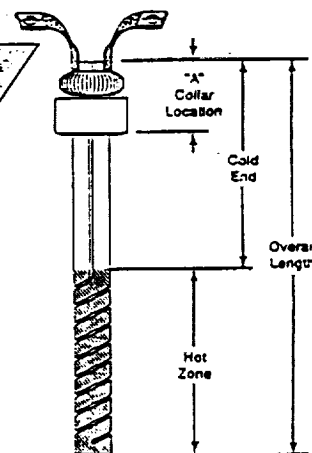
Starbar Diameter	Collar Diameter	Collar Location	Terminal Strip Amp Rating	Maximum Load Tube O.D.	Starbar I.D.
------------------	-----------------	-----------------	---------------------------	------------------------	--------------

**SER:**

1/2 in. 1.3 cm	1 1/2 in. 3.8 cm	2 in. 5 cm	50	1/2 in. 3 mm	3/16 in. 5 mm
3/4 1.6	1 1/2 3.8	2 5	50	1/2 6	3/16 8
3/4 1.9	1 1/2 3.8	2 5	50	3/16 8	3/8 9.5
1 2.5	2 1/4 5.7	2 5	50	1/2 12	9/16 14
1 1/4 3.2	2 1/4 5.7	2 5	100	9/16 14	1 1/16 17
1 1/2 3.8	2 1/4 5.7	3 7.6	100	1 1/16 21	1 1/8 24
1 3/4 4.4	3 7.6	3 7.6	100	1 1/8 24	1 1/2 27
2 5.4	3 7.6	3 7.6	100	1 3/8 30	1 5/8 33
2 3/4 7.0	3 9.5	4 10	400	1 13/16 46	1 15/16 49

**TSR:**

1 1/4 in. 4.5 cm			100	1.14 in. 29 mm	1.46 in. 37 mm
2 5.0			100	1.34 34	1.65 42
2 1/2 5.5			100	1.53 39	1.85 47
2 3/4 5.2			100	1.81 46	2.13 54
3 7.5			100	2.32 59	2.54 57

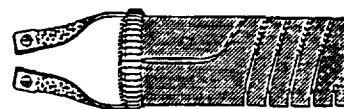




## TYPE TSR STARBAR — SUPER SPIRAL TUBULAR BAYONET HEATING ELEMENT

### DESCRIPTION:

Available in five different diameters, TSR STARBARS feature a large interior used as a heating chamber. With both electrical connections on one end, the TSR STARBAR is similar to the SER STARBAR. But the TSR STARBAR has thinner walled construction, and an internal diameter open from end to end. There is no collar. The flat, braided aluminum straps are held in place with a stainless steel clamp covered with high temperature insulation. A TSE STARBAR version is also available (see drawing). Please contact I Squared R for electrical specifications.



TSR



TSE

### OPERATING TEMPERATURES:

Same as SER (see front page).

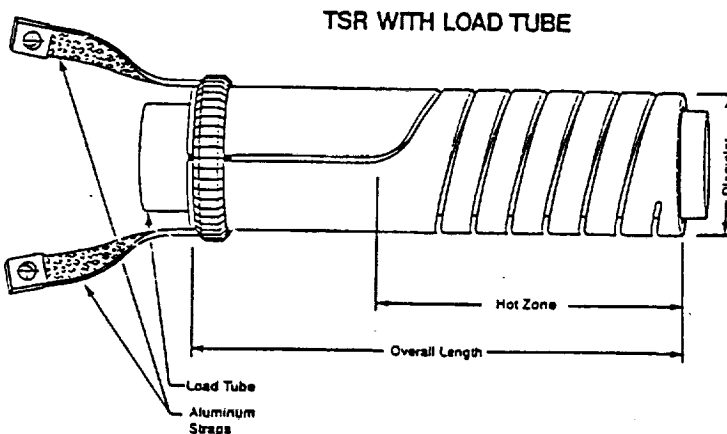
### ELECTRICAL CHARACTERISTIC:

Same as SER (see front page).

### SUPERIOR PERFORMANCE:

Same as SER (see front page).

**APPLICATION:** The TSR STARBAR makes a superior tubular furnace element capable of operating at temperatures of up to 1650°C (3000°F). The TSR STARBAR can be damaged, however, if the product being furnaceed is allowed to touch the silicon carbide walls when hot and electrically energized. To prevent this, a ceramic load tube is typically inserted into the element. A list of recommended maximum tube sizes is shown in Table B (preceding page).



**MOUNTING:** TSR STARBARS can be mounted in any orientation. When used horizontally, the slot in the cold end should be positioned horizontally, to reduce the possibility of accidental shorting from the introduction of foreign materials. Typically, TSR STARBARS will be positioned vertically, with the hot zone up, for crucible applications.

Table C

TSR STARBAR ELEMENT STANDARD SIZES AND ELECTRICAL CHARACTERISTICS:

Starbar Diameter	Maximum Heating Length	Hot Zone Diameter	Hot Zone Length	Hot Zone Area	Hot Zone Per Inch	Cold Zone Diameter	Cold Zone Length	Cold Zone Area	Cold Zone Per Inch	Overall Length	Overall Area	Overall Per Inch
1 1/4 in.	4.5 cm	12 in.	30 cm	0.68	0.14	5.5	0.27	0.055	14.0			
2	5.0	12	30	0.69	0.13	6.2	0.27	0.051	15.7			
2 1/4	5.5	12	30	0.67	0.15	6.6	0.26	0.059	16.7			
2 1/2	6.2	12	30	0.70	0.09	7.8	0.27	0.035	19.8			
3	7.5	12	30	0.70	0.10	9.4	0.27	0.039	23.9			

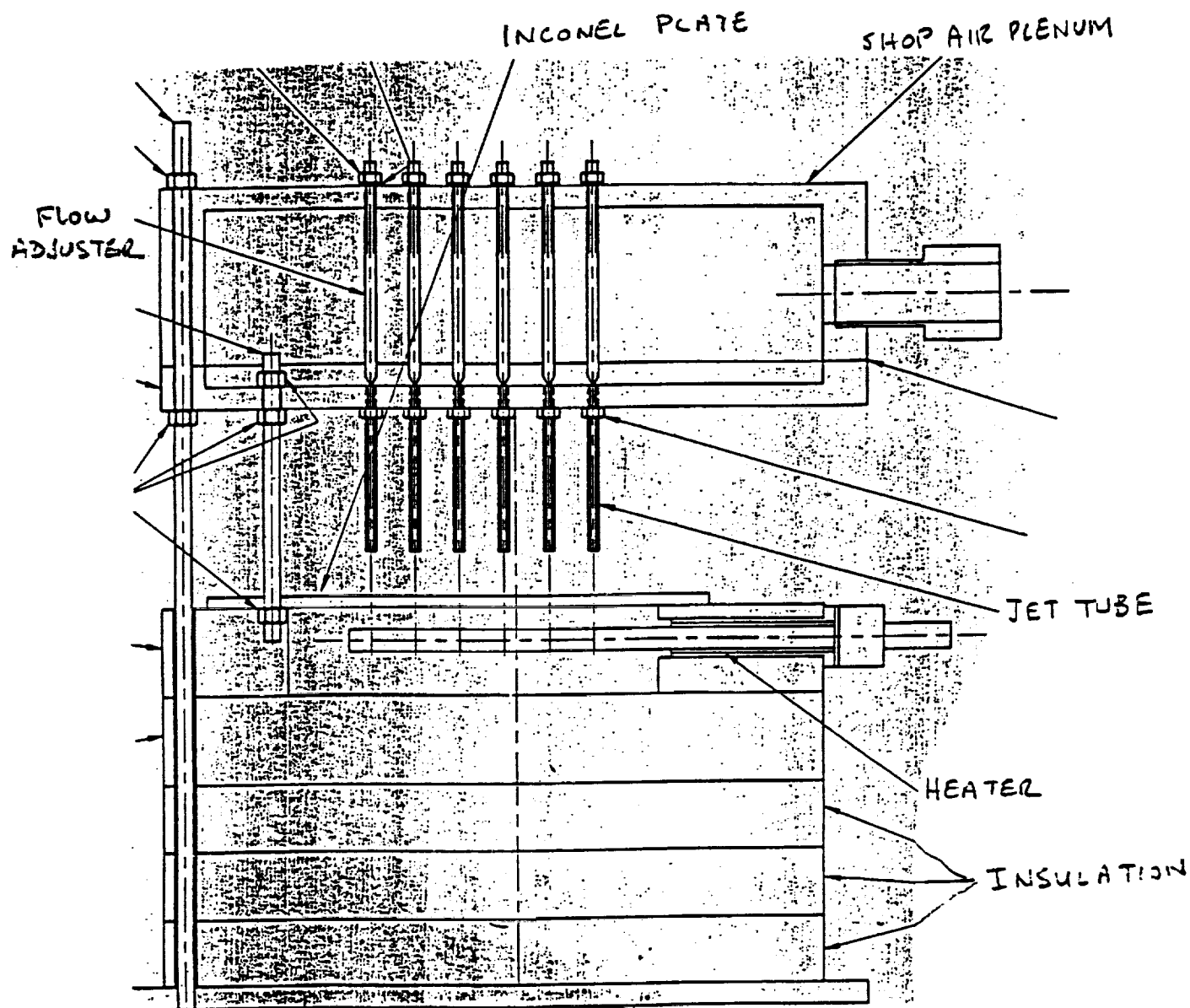
## I SQUARED R ELEMENT CO., INC.

12500 CLARENCE CENTER ROAD, AKRON, NEW YORK 14001  
Call Jack Davis For Additional Information.

(716) 542-5511

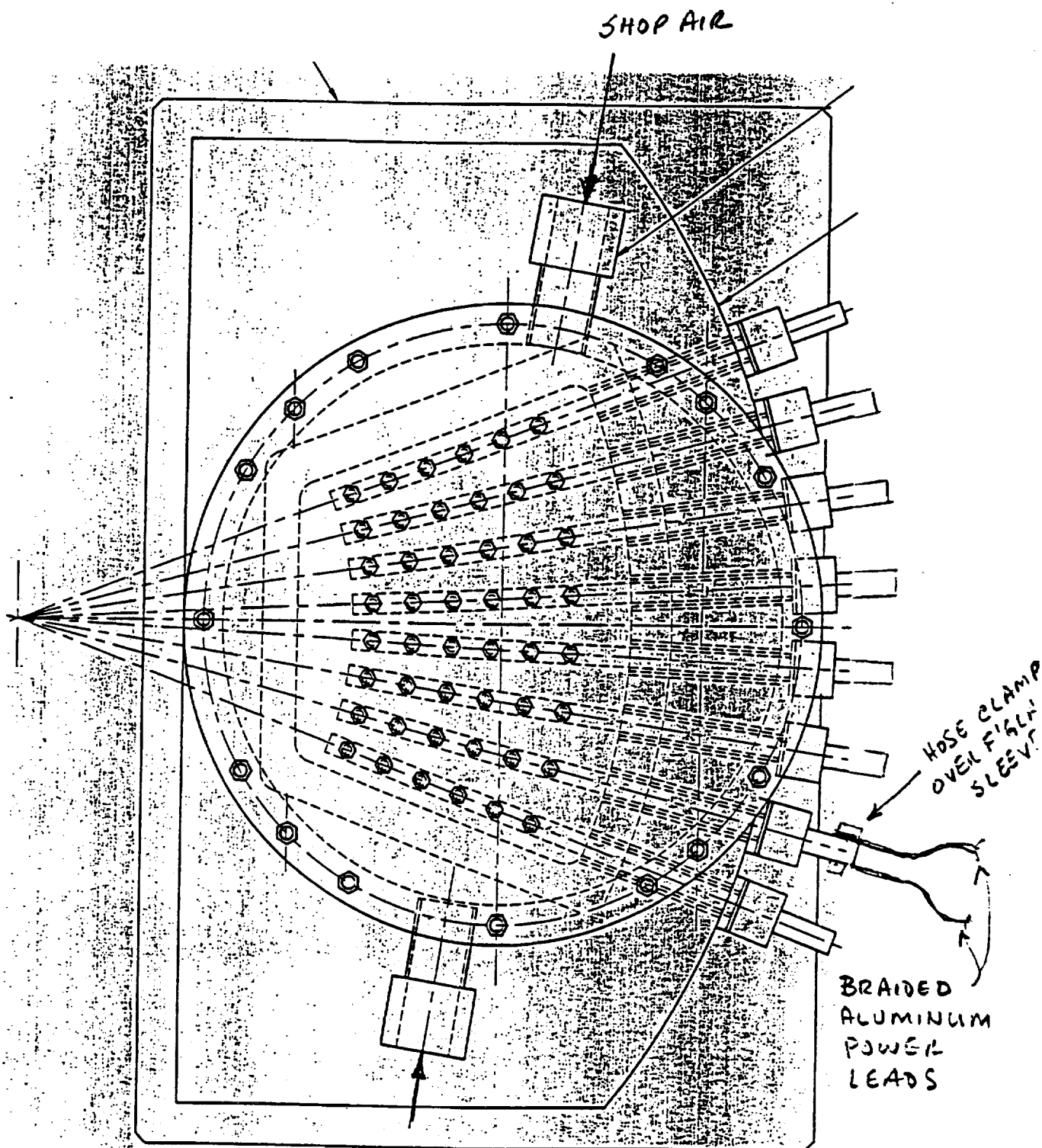
FAX: (716) 542-2100

PG. 4



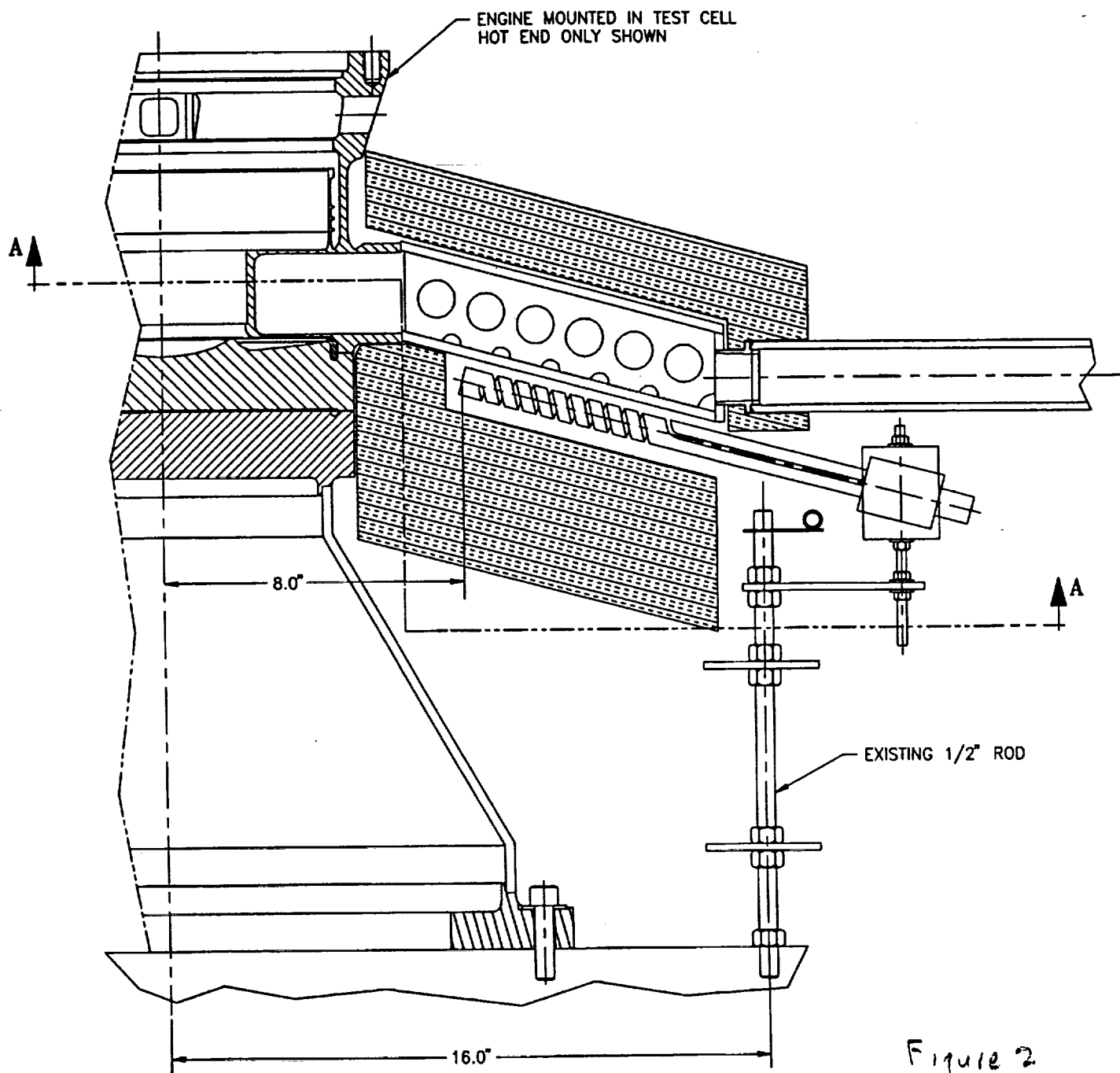
CROSS SECTION HEAT PIPE HEATER RIG.

Figure 1a



TOP VIEW HEAT PIPE HEATER RIG.

Figure 1b.



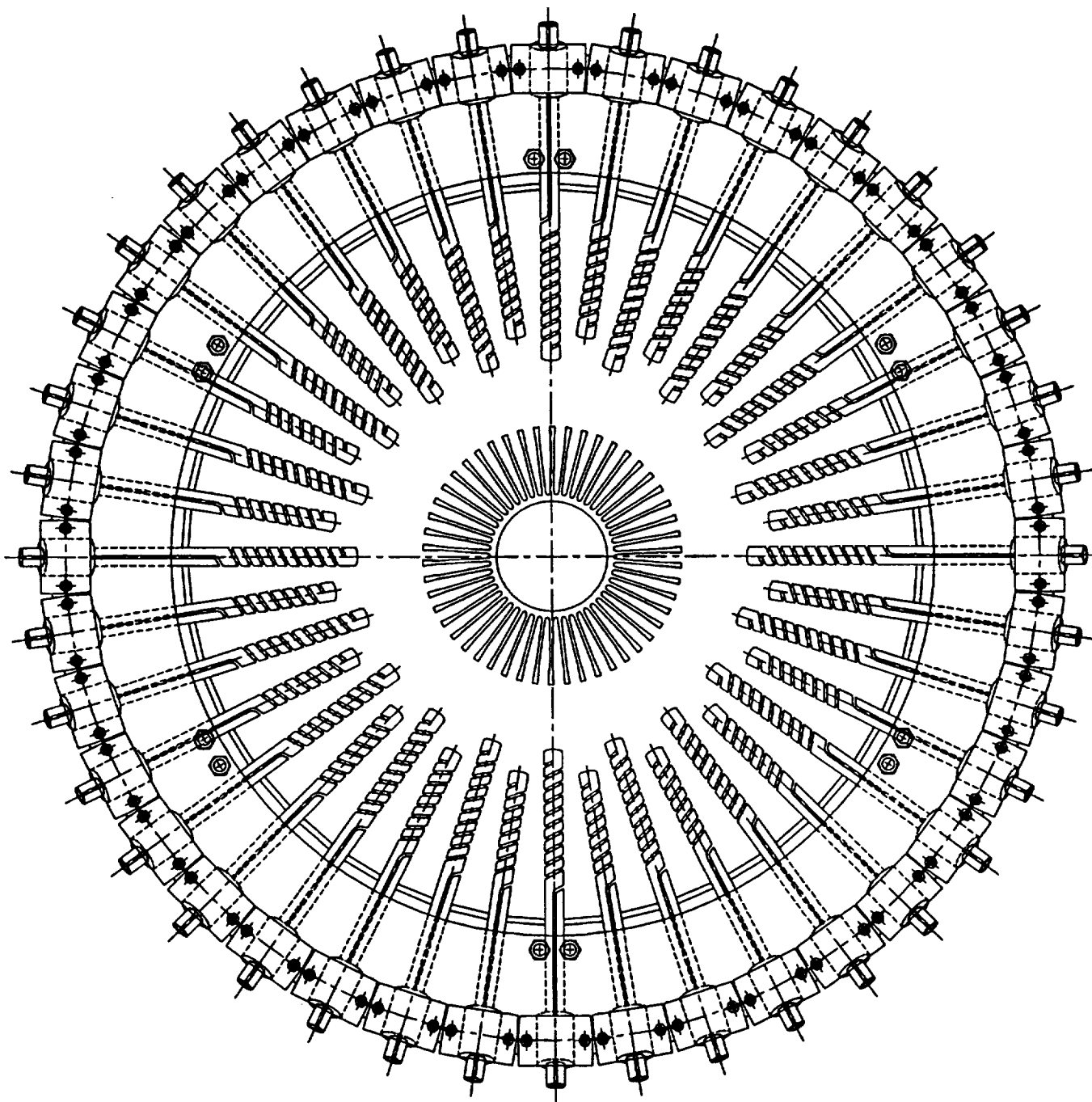


Figure 3

SECTION A-A



## B.10 Cooler Flow Test

### Test Arrangement and Results

TO: M. Dhar

DATE: 10/15/91

FROM: D. Jones

SUBJECT: Test Results From CTPC Cooler Flow Simulator Rig

#### BACKGROUND

The CTPC displacer drive (displacer cylinder, displacer, post & flange, and gas spring cylinder) is a precision assembly with very tight clearances between moving and stationary parts. The CTPC tube-in-shell engine cooler uses a dual inlet/outlet arrangement to minimize circumferential temperature variations which might affect seal clearances in the displacer drive. Due to the heater head regenerator wall length requirements, the coolant ports in the cooler were forced off-center, towards the engine cold-side. This raised concerns about coolant flow maldistribution in the cooler, and the effects on engine mechanical and thermodynamic performance.

To address these concerns 1/4 segment full-scale models of the CTPC cooler were constructed from both plastic and steel, and tests performed to evaluate coolant flow distribution. The plastic rig was tested using water, with dye injected into the flow stream to indicate flow patterns. The steel rig used electric heating elements in place of cooler tubes, instrumented with thermocouples, and was tested using the alternator cooling loop with oil coolant. The effect of a coolant flow distributor (snout) installed at the coolant inlet port was evaluated on both rigs.

#### SUMMARY OF TEST RESULTS

##### Plastic Rig

The plastic model tested with flowing water showed the dye to rapidly disperse downstream of the various injection points (at the inlet port, along the inner and outer cooler walls, and adjacent to the cooler tube sheets), indicative of good coolant flow distribution. The addition of the "snout" flow distributor resistance at the coolant inlet port did not change the dye dispersion patterns.

### Steel Rig

The steel model was tested with Paratherm-NF oil at low ( $<70^{\circ}\text{C}$ ) temperature. The only firm conclusion reached was that the snout had no effect on flow distribution. Tube surface temperatures, recorded from thermocouples staked into grooves in the heater tubes, showed non-uniform patterns which are difficult to attribute to flow maldistributions. More likely they result from variations in bonding of the thermocouples to the tubes. The addition of the snout did not change the temperature patterns. The temperature variations around the tubes showed the leading faces of the tubes to have the lowest temperatures (highest heat transfer), as expected. Again, the snout had little effect on results.

It is concluded from these tests that there will be good flow distribution in the CTPC cooler without the addition of a flow restriction at the cooler inlet and/or outlet ports.



## **APPENDIX C: UDIMET TESTING**

### **C.1 Report: Selection of the Reference Material for the Space Stirling Engine Heater Head**

In the free-piston Stirling-cycle machine, the heater head is a critical as well as difficult component to design in the system (see Figure 1). It is critical because of the multi-purpose function required of it. The heater head must function as the heat exchanger for the heat input to the power module. It also must allow for the residual heat to be rejected from the power module. Thirdly, it acts as a main pressure barrier for the working fluid in the power module. The heater head is a difficult component to design because of the severe operating conditions it must work under. For these reasons the selection of the appropriate material for the heater head is very important.

#### **OPERATING CONDITIONS**

The heater head must contain the high pressure helium in the power module. For the SSE, the internal pressure is 150 Bar (2175 psi). In addition, there is also a 12%, or 18 Bar (260 psi), pressure wave imposed on top of the mean pressure. The "hot end" of the head operates at 1050°K (1430°F) and is exposed to sodium vapor on the exterior surfaces. The "cold end" operates at 525°K (485°F) and is exposed to NaK. These temperature conditions result in a large thermal gradient along the wall of the head, causing high bending stresses at both ends. Typical stress levels in the heater head are given in Figure 2. The power module is to be designed for 60,000 hours of operation, with up to 200 start-up/shut-down cycles over its life. Thus, there are a number of possible failure modes that must be considered when designing the heater head.

#### **STRUCTURAL DESIGN CONSIDERATIONS**

##### **Short-Term Rupture**

Because the heater head is part of the main pressure vessel of the engine, the material it is made from must possess high tensile strengths over the full temperature range. From a short-term failure viewpoint, the primary stresses

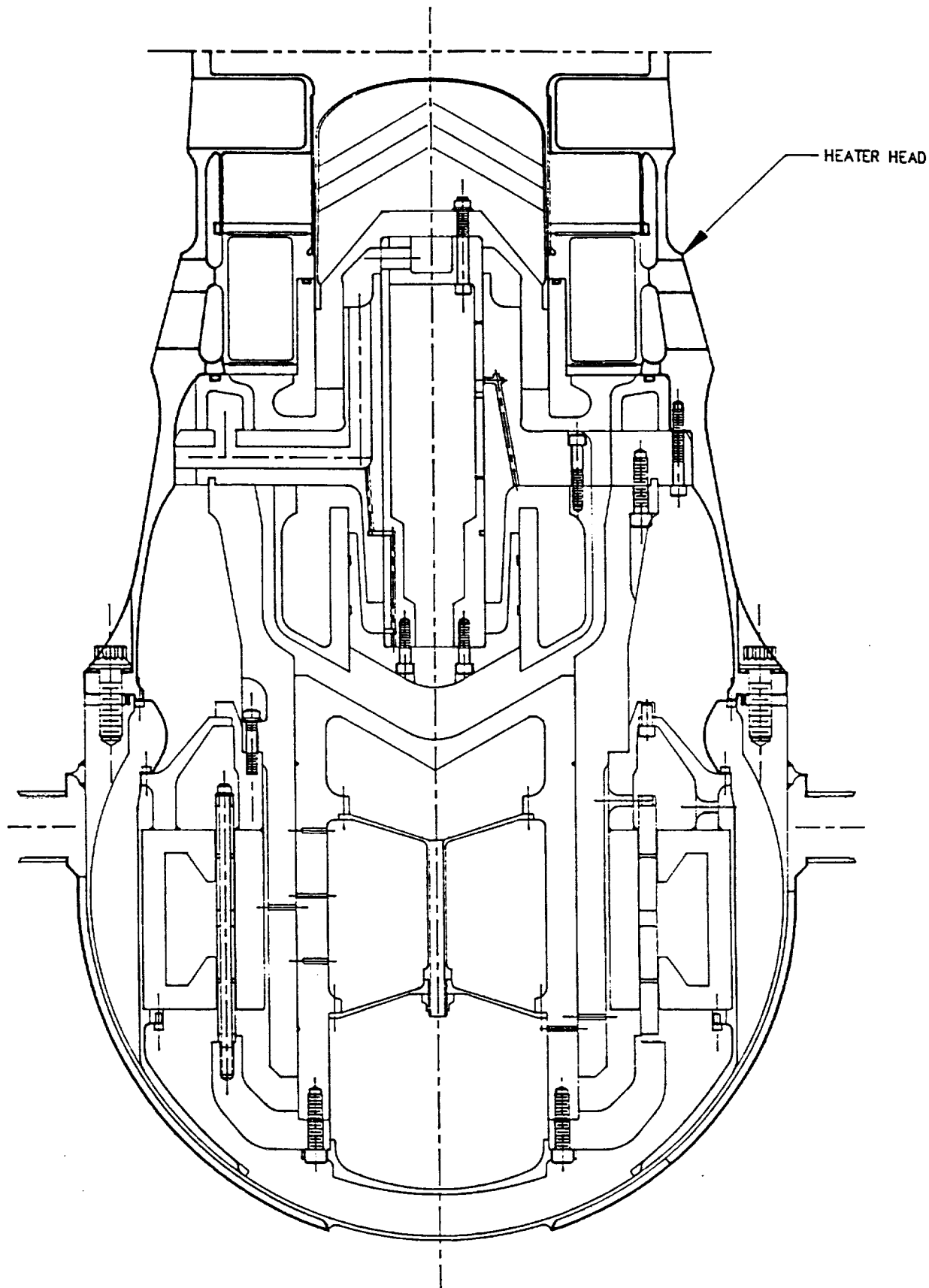


FIGURE 1: SSE FREE-PISTON ENGINE

### LOADING CONDITIONS

1. PRESSURE + TEMPERATURE
2. TEMPERATURE ONLY
3. PRESSURE ONLY

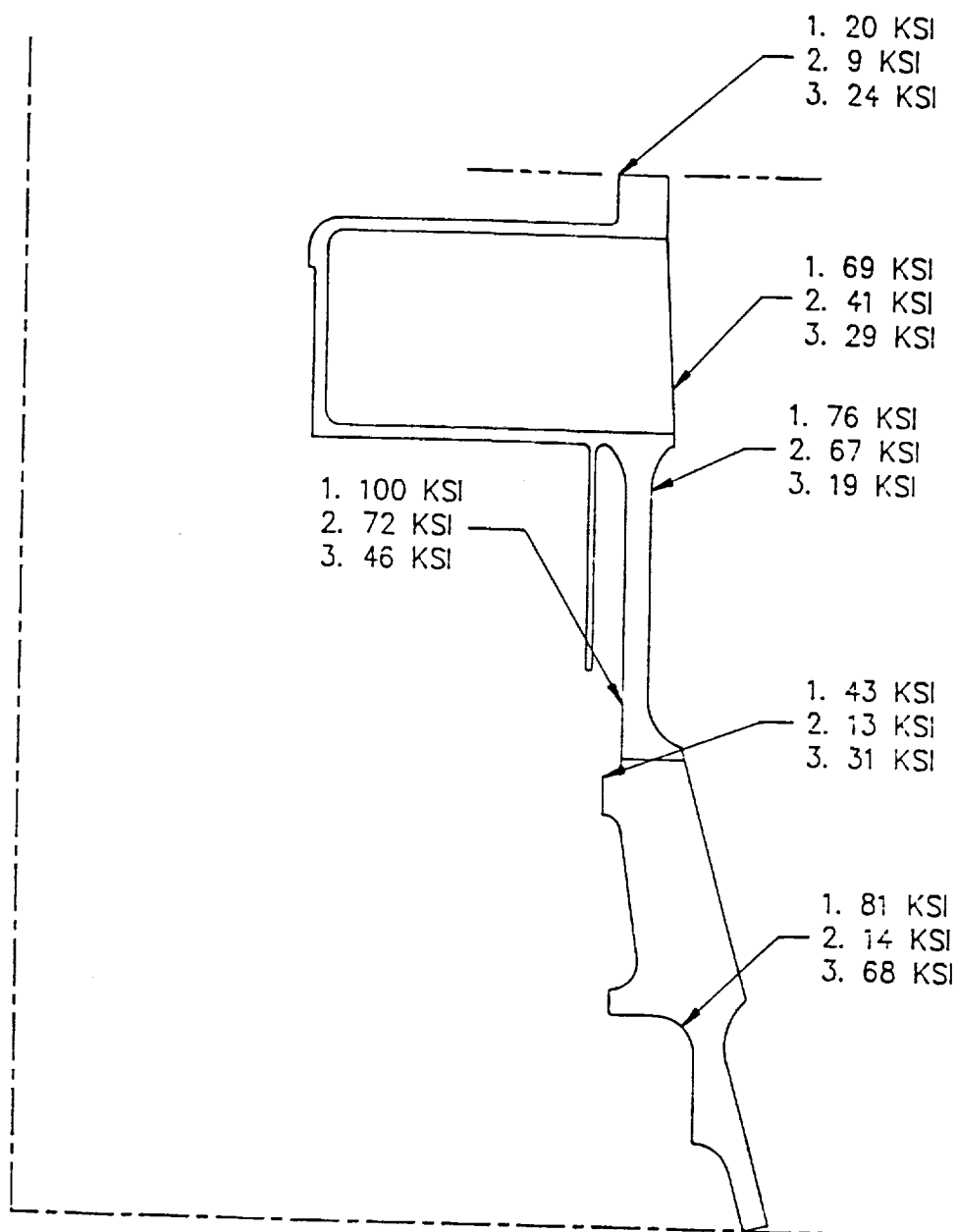


FIGURE 2: SSE HEATER HEAD, TYPICAL STRESS LEVELS (von Mises)

due to pressure are limited to  $1/2$  the ultimate strength or  $2/3$  the yield strength of the material, whichever is lower. The material with the highest tensile strengths will yield the lightest weight design, thus having an impact on the total specific mass of the power module. Table 1 lists the typical tensile strengths for candidate heater head materials at room temperature and  $1033^{\circ}\text{K}$  ( $1400^{\circ}\text{F}$ ). All of these alloys are nickel-base alloys, with the exception of HS-31, which is a cobalt-base alloy.

### Long-Term Rupture: Creep

Since the engine is expected to run for thousands of hours at high temperature and pressure levels, the heater head must be designed against creep failure. The primary stresses due to pressure are limited to the  $1\%$  creep strength or  $2/3$  the creep-rupture strength (whichever is lower) of the material under these conditions. Therefore the higher the creep strength of the material, the lighter the heater head can be, again influencing the specific mass of the power module. Table 2 lists the creep-rupture strengths for superalloys at  $1050^{\circ}\text{K}$  for an expected life of 60,000 hours.

### Fatigue

During its life, the engine may be stopped and restarted a number of times. Because the heater head has fairly high stress levels due to combined thermal and pressure loads, low-cycle fatigue must be taken into account. For most nickel-base alloys, low-cycle fatigue is only a problem if the yield stress is exceeded. Therefore, a material with a high yield strength and good ductility is desirable for this criterion.

As well as having a high mean stress due to the thermal and pressure loads, the heater head also experiences an alternating stress due to the cyclic pressure of the system. Thus the head must also be designed to resist high-cycle fatigue. Since the alternating stress is very small compared to the mean stress, the

Table 1

	Ultimate Strength, MPa (ksi)		Yield Strength, MPa (ksi)	
	R.T. ----	1033°K -----	R.T. ----	1033°K -----
Wrought Alloys				
INCONEL 718	1365 (198)	855 (124)	1124 (163)	800 (116)
UDIMET 720-CR	1117 (162)	1027 (149)	862 (125)	793 (115)
UDIMET 720-HS	1579 (229)	1069 (155)	1227 (178)	965 (140)
RENE 41	1420 (206)	1103 (160)	1062 (154)	938 (136)
Cast Alloys				
HS-31	745 (108)	483 (70)	524 (76)	241 (35)
INCONEL 713LC	896 (130)	952 (138)	752 (109)	758 (110)
MAR-M 247	965 (140)	1034 (150)	827 (120)	827 (120)

**Table 2**

Creep Rupture Strength,MPa (ksi) (60,000 hrs., 1050°K)

**Wrought Alloys**

INCONEL 718	< 69 (10)
-------------	-----------

UDIMET 720-CR	248 (36)
---------------	----------

UDIMET 720-HS	< 69 (10)
---------------	-----------

RENE 41	138 (20)
---------	----------

**Cast Alloys**

HS-31	117 (17)
-------	----------

INCONEL 713LC	228 (33)
---------------	----------

MAR-M 247	317 (46)
-----------	----------

operating point on the Goodman diagram begins to approach the ultimate tensile strength of the material. Thus a material with a high ultimate strength combined with good fatigue resistance is desirable.

### Ductility

Although not covered by any of the design criteria used for the heater head, ductility is a desirable characteristic in a material. Certain localized areas of the heater head are subject to very high secondary stresses due to temperature gradients or stress concentrations. These stresses can exceed the yield strength of the material. A ductile material will allow some local plastic deformation to occur without resulting in a failure. A common property used to compare the relative ductility between materials is the tensile elongation, obtained from a uniaxial tensile test. Table 3 lists the tensile elongation for the candidate superalloys at room temperature and at 1033°K.

Another test commonly used to quantify the ductility of a material is the Charpy V-Notch test. This test determines the relative brittleness and impact strength of a material when subjected to high strain rates. Some typical values are listed in Table 4. The importance of this material property is significant only if there is a failure of the heater head. Because the heater head has an enormous amount of energy stored in it, a catastrophic failure could result in high velocity flying debris if the head is made from a brittle material. Thus this property is often considered from a safety standpoint. Since it is difficult to determine what is an acceptable impact strength, the information in Table 4 is provided strictly for a basis of comparison. If the heater head is designed properly, a failure would never occur.

### CAST VERSUS WROUGHT ALLOY

The form that the material is available in must also be considered. Some of the wrought alloys are also available in cast form, however, some other alloys are only available in cast form.

**Table 3**

	Tensile Elongation, %	
	R.T. ----	1033°K -----
<b>Wrought Alloys</b>		
INCONEL 718	21	30
UDIMET 720-CR	6	22
UDIMET 720-HS	18	16
RENE 41	14	11
<b>Cast Alloys</b>		
HS-31	9	10
INCONEL 713LC	15	11
MAR-M 247	7	5



**Table 4**

Impact Strength, N-m (ft-lbs)

	R.T. -----	1170°K -----
Wrought Alloys		
INCONEL 718	28.2 (20.8)	-
UDIMET 720-CR	-	12 (9) {19 (14) after 10,000 hrs.}
UDIMET 720-HS	-	16 (12)
RENE 41	19 (14)	-
Cast Alloys		
HS-31	8 (6)	12 (9)
INCONEL 713LC	11 (8)	13.3 (9.8) {920°K}
MAR-M 247	-	-

## Characteristics of Cast Materials

The general advantage of casting a component is the ability to cast it to near-finished dimensions with minimal machining required, thus reducing the cost per part. Currently the "starfish" configuration is the primary choice for the heater head design (see Figure 3). An advantage of using a cast alloy would exist if the fins could be cast into the heater head. However, there is doubt whether this could be done successfully because of the thin walls and tight tolerances required by the design. The main advantage of the cast alloys is that they demonstrate higher creep-rupture strengths than the wrought alloys (Table 2). This characteristic is usually obtained by directionally solidifying the alloy. For example, the creep-rupture strength of directionally-solidified MAR-M 247 is 46 ksi. For equiaxed MAR-M 247, the creep-rupture strength drops to 39 ksi. Because the heater head requires good creep strength in at least two axes, the cast alloy must be equiaxed.

From a pressure vessel standpoint, castings have some detrimental characteristics associated with them. Typically cast alloys are lower in ductility and toughness. There is also a high risk of porosity or local voids in the casting. This may make it very difficult to seal high pressure helium for extended periods of time. Cracking due to shrinkage can also be a problem, especially if the casting has drastic section changes. Cast alloys also tend to be weaker in fatigue and are usually more sensitive to notches. From a fabrication standpoint, the cast alloys are generally more difficult to weld than the wrought alloys.

## Characteristics of Wrought Materials

Wrought alloys have several advantages over cast alloys for the heater head design. Typically, the wrought alloys have better ductility and toughness. Higher tensile strengths are generally achievable. Manufactured parts are usually superior with respect to soundness and microstructural homogeneity. Better fatigue strength and lower notch sensitivity are common. Joining wrought alloys together, either by welding or brazing, is typically easier than with the cast alloys. Welding of the precipitation-hardenable nickel-base alloys,

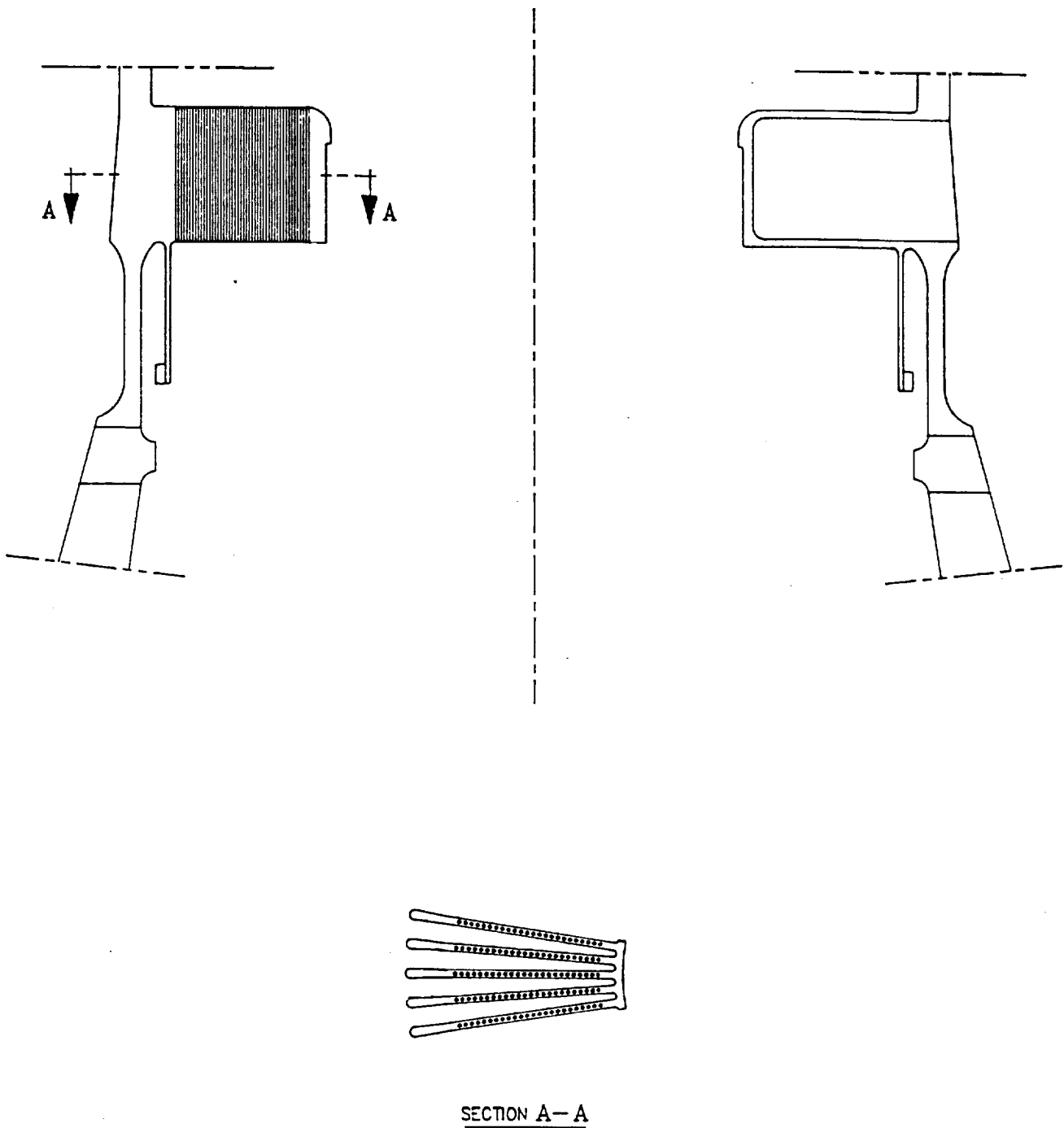


FIGURE 3: STARFISH HEATER HEAD CONFIGURATION

however, is generally difficult, primarily due to microcracking during welding and strain-age cracking during post-weld heat treatment. Though with proper care in pre-weld heating and proper joint design, many of the nickel-base wrought alloys have been successfully welded.

### SELECTION OF MATERIAL

Based on the information obtained, UDIMET 720 seems to be the material best suited for the SSE heater head. The combination of good tensile strength over a wide temperature range and high creep-rupture strength allows a low specific mass design. One advantage to UDIMET 720 is its stability over long periods of time at elevated temperatures. Figure 4 shows the impact energy versus exposure time for some nickel-base alloys (1). UDIMET 720 maintains its strength after 10,000 hours, even increasing slightly, while the others deteriorate after only 5000 hours. Another advantage to UDIMET 720 is that two different heat treatments produce different properties. The heat treatment for creep resistance (CR) produces good stress-rupture strength while maintaining good tensile and impact properties. The heat treatment for high strength (HS) produces exceptional tensile strengths and ductilities. For the starfish heater head, the intention is to perform a dual heat-treat on the part. The hot end of the head will receive the CR heat treatment to get the creep-rupture properties. The cold end will receive the HS heat treatment to obtain the high tensile strength needed at this end where the stresses are highest.

Unfortunately, UDIMET 720 is one of the precipitation-hardenable nickel-base alloys that is difficult to weld. The material is prone to microcracking during welding and strain-age cracking during post-weld heat treatment. Some welding success has been achieved using a lengthy pre-weld heat treatment and a closely controlled welding cycle and post-weld heat treatment. This was using UDIMET 720 for both the base metal and filler metal with the gas tungsten arc welding technique. Additional welding success has been achieved using UDIMET 520 as the filler metal (11). Furthermore, a procedure for weld repairing UDIMET 720 gas turbine blades using INCONEL 625 weld rod has been developed by the Kelsey-Hayes Company and has been approved by Westinghouse (2).

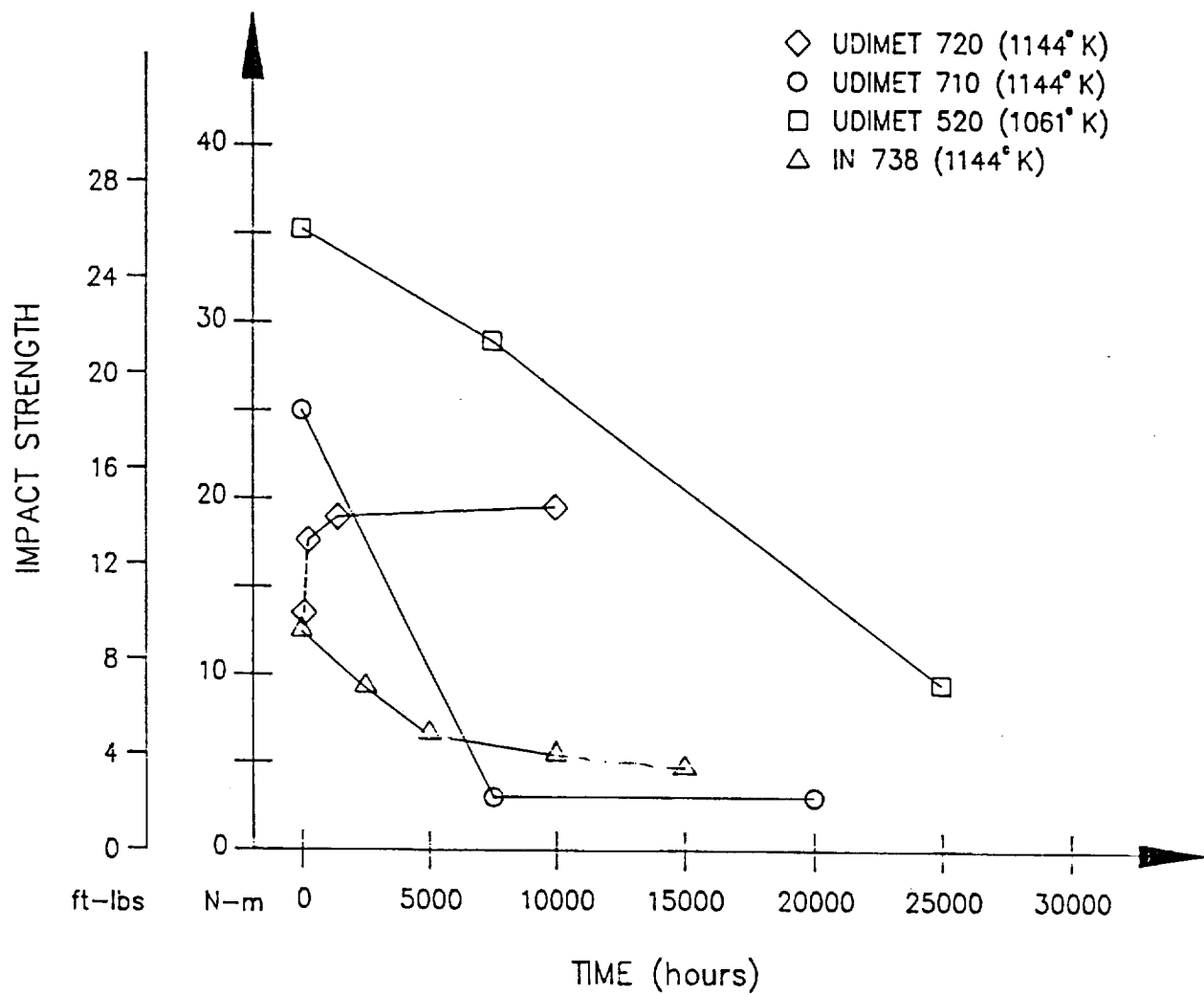


FIGURE 4: 1174° K Impact strength vs. time for several alloys exposed to elevated temperatures (in parentheses).

## DESIGN AND MANUFACTURING DATA BASE REQUIREMENTS

In order to design the starfish heater head using UDIMET 720, some mechanical properties need to be determined and some joining techniques need to be identified. Currently there is not enough data available to achieve the design goals. The following information is required to complete the detailed design of the heater head.

### Structural Information

Most of the mechanical data needed for UDIMET 720 is fatigue data. Because the Stirling engine heater head possesses a unique loading condition, not much fatigue data is available that is useful for the design. The high thermal stresses imposed on the head are strain dependent. If local yielding or creep deformation occurs, the thermal stresses are relieved, thus reducing the damaging effect they have on fatigue life. Therefore, the fatigue tests that need to be conducted should utilize strain-controlled loading. Most of the available fatigue data, especially at elevated temperatures, has been generated using load-control testing modes. Using this data would produce a very conservative, therefore heavy, design.

The following test conditions for high-cycle fatigue need to be performed for both the CR and HS heat treatments at temperatures ranging from 300°K to 1050°K:

- Strain-controlled bending fatigue with high mean strains
- Strain-controlled axial fatigue with high mean strains
- Fully-reversed bending fatigue
- Fully-reversed axial fatigue

Because the total number of stress cycles in a Stirling engine operating at 70 Hz frequency and designed for 60,000 hours operational life is very large ( $>10^{10}$  cycles), it is not practical to conduct fatigue tests to that number of cycles. Typical high-cycle fatigue tests are stopped after  $10^7$  or  $10^8$  cycle. Since nickel-base alloys do not possess true endurance limits enough data must

be collected so that the fatigue strengths can be extrapolated out to the required number of cycles.

In addition, the effect of combining the high-cycle fatigue due to the pressure wave with the low-cycle fatigue due to start/stop cycling needs investigation. If a crack initiates due to low-cycle fatigue, it would have a tendency to propagate when exposed to high-cycle fatigue. Therefore, the following combined fatigue tests need to be performed for both the CR and HS heat treatments at temperatures ranging from 300°K to 1050°K:

- Strain-controlled bending fatigue with high mean strains, intermittently returning to zero strain
- Strain-controlled axial fatigue with high mean strains, intermittently returning to zero strain

If the dual heat treatment is carried out on the heater head, the characteristics of the intermediate material need to be determined. For this material, the following tests need to be conducted at temperatures ranging from 300°K to 900°K:

- General tensile data (yield, ultimate, elongation)
- High-cycle bending fatigue with various mean stresses (load control)
- High-cycle axial fatigue with various mean stresses (load control)
- Combined high and low cycle bending fatigue, intermittent zero to max. strain
- Combined high and low cycle axial fatigue, intermittent zero to max. strain

#### Environmental Effects

Since the heater head will be exposed to high temperature sodium vapor, some testing needs to be done to see if long-term exposure will degrade the mechanical properties of UDIMET 720. The properties that need evaluation after sodium exposure are tensile strength, creep-rupture strength, and fatigue strength. Testing is required in order to determine if there is an effect on these proper-

ties. If a significant decrease in one of these strengths is noticed, then the option of protective coatings must be investigated.

### **Manufacturing Techniques**

The ability to join UDIMET 720 to itself or other alloys is critical in the fabrication of the heater head. Because of the hermeticity requirement, some final seal welds will also be necessary. It will most likely be impossible to do any pre-weld or post-weld heat treatments on these weld joints. These joints will need a readily weldable or "buttering" metal, such as INCONEL 625, which does not require the heat treatments to obtain good quality welds. Figure 5 shows probable joint locations on the starfish heater head. The following joining techniques should be investigated for the joining of UDIMET 720 to itself or to INCONEL 718 or 625:

- **Electron-Beam Welding:** This type of welding is preferred. Because the welding is done in a vacuum, the chance of producing an oxide in the joint is reduced. The oxide layer tends to increase the difficulty in welding these alloys. Also, the amount of energy input into the parts is substantially lower than other fusion-type processes, thus reducing the amount of residual stress in the joint.
- **Diffusion Bonding:** This term will be used to collectively refer to diffusion welding and diffusion brazing since the process that will be used is currently undefined. UDIMET 700, which is comparable to UDIMET 720 in weldability, has been successfully diffusion welded with joint efficiencies of 75 to 100 percent in tensile and stress-rupture strengths (5).
- **Friction Welding:** This process has been used in successfully joining alloys that are generally considered unweldable. Friction welding has also been used to join dissimilar metals that cannot be joined by other welding techniques. Again, excellent joints have been produced using this technique with UDIMET 700, with tensile and stress-rupture properties equivalent to those of the parent metal (5). Because of the nature



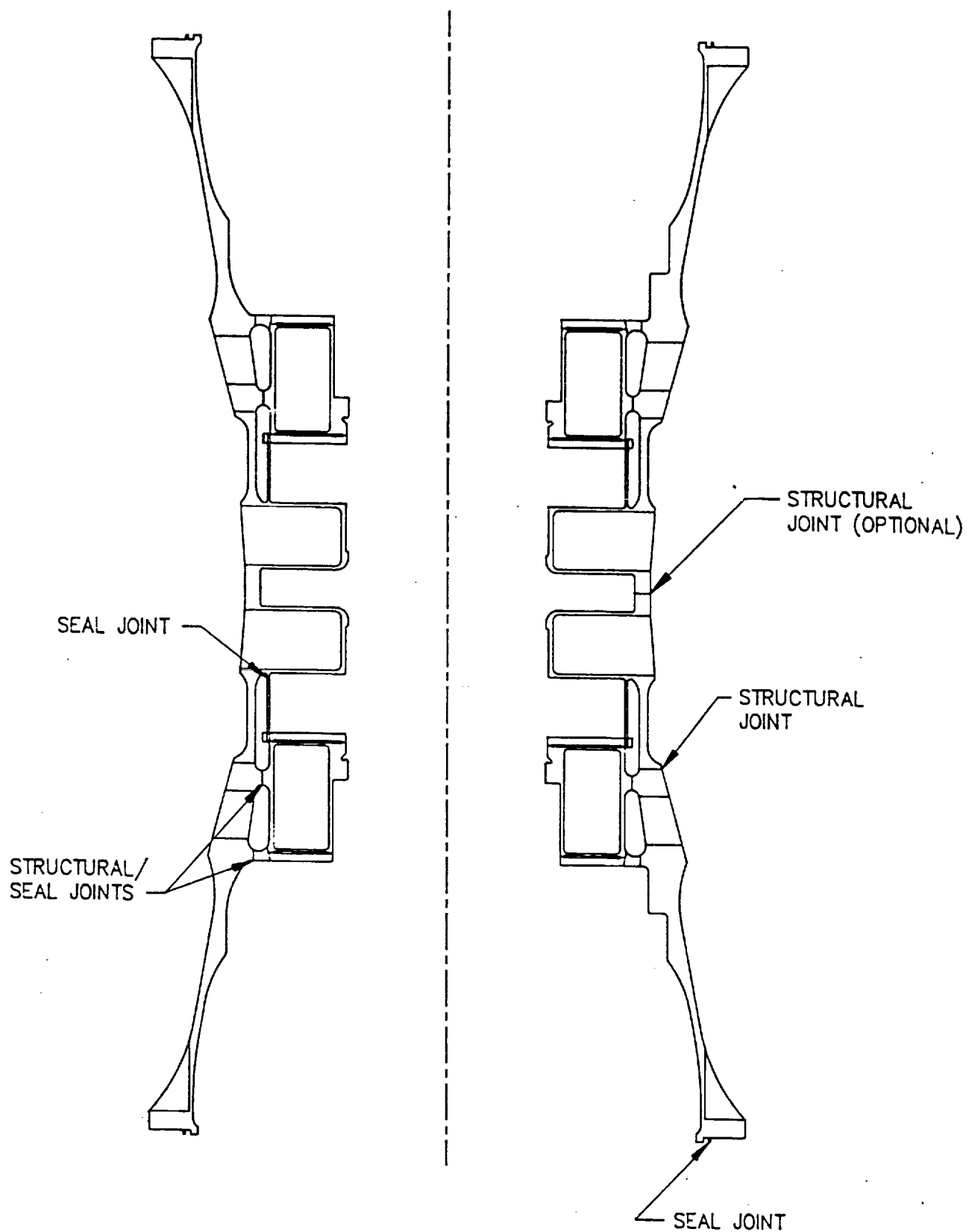


FIGURE 5: POSSIBLE JOINT LOCATIONS IN SSE HEATER HEAD

of the process, the practicality is usually limited to small diameters and may not be feasible for the joints required in the starfish heater head.

When successful joining techniques are identified, these joints should then be structurally evaluated for tensile, creep, and fatigue strenths.

### SUMMARY

UDIMET 720, with dual heat treatment, is recommended as the material for the first generation SSE starfish heater head. If the dual heat treatment cannot be successfully obtained, then UDIMET 720 with CR heat treatment can be used. This material combines the beneficial properties associated with a wrought alloy with the creep-rupture strength typical of the cast nickel-base alloys. Because the material is intended for gas turbine blades, the type of design data available is not entirely applicable to Stirling engine heater head design. This is true with most of the materials that are suitable for this component. Therefore, a fair amount of testing is required. Once the required data is obtained, the 60,000 hours life starfish heater head can then be designed as light and compact as possible.

## REFERENCES

1. Cooper, A. H., Maurer, G. E., Crombie, E. A., and Tien, J. K., "Alloy Design, Microstructure and Properties of a Boron Modified Superalloy", paper submitted to Metallurgical Transactions.
2. Hoffman, G., "Comparison of U-720 vs. INCO 738 for Gas Turbine Blade Application", Utica Division, Kelsey-Hayes Company, December 1983.
3. The International Nickel Company, Inc., "High Temperature, High Strength Nickel Base Alloys", July 1977.
4. Kattus, J. R., "Inconel Alloy 718", Aerospace Structural Metals Handbook, Code 4103, June 1986.
5. Klopp, W. D., "Udimet 700", Aerospace Structural Metals Handbook, Code 4207, June 1985.
6. Klopp, W. D., "X-40 / X-45", Aerospace Structural Metals Handbook, Code 4305, December 1985.
7. Manson, S. S., "713 LC", Aerospace Structural Metals Handbook, Code 4108, December 1976.
8. Manson, S. S., "MAR-M-247", Aerospace Structural Metals Handbook, Code 4218, December 1984.
9. Manson, S. S., "Rene 41", Aerospace Structural Metals Handbook, Code 4205, December 1972.

10. Prager, M. and Shira, C.S., "Welding of Precipitation Hardening Nickel-Base Alloys", Welding Research Council Bulletin No. 128, New York, February 1968.
11. Sczerzenie, F. E., Mancusso, S. O., Keefe, P. W., Maurer, G. E., and Boesch, W. J., "UDIMET Alloy 720", [Unrestricted, Class I Report], TR-88-002, Special Metals Corporation, New Hartford, NY, May 1988.

## C.2 Memorandum: Udimet 720LI Creep Test Result Update

To: M.Dhar

From: S.Walak *SW*

Date: September, 22 1992

Subject: Udimet 720LI Creep Test Result Update.

Udimet 720LI creep testing has been initiated to aide materials selection and to generate design data for a long life 1050K Stirling engine heater head. A summary of the tests which are in progress or have been completed is shown in Table 1.

Several conclusions drawn from the results of these tests are listed below:

1) The creep rate of cast-wrought Udimet 720LI given the full CR heat treatment appears to be lower than that expected from Larson-Miller extrapolations of "Standard Composition" Udimet 720 data from Special Metals Corporation (SMC) U720 data sheets.

MTI tests being run at 1050K and 248 MPa (36 KSI) with 0.25 inch diameter round bar test specimens cut from 4.25 inch diameter bar stock show a significant improvement in time to 0.1% creep, figure 1.

2) Five variations of Udimet 720LI were creep tested as 0.03 inch thick flat specimens and ranked on the basis of creep rate at 1050K and 248 MPa (36 KSI). The materials are listed below in descending order of creep resistance (The first listed indicates the best creep resistance):

- Cast-Wrought / CR Heat Treatment
- Powder Metal / 2300°F HIP (ASTM 4) / CR Heat Treatment
- Powder Metal / 2025°F HIP (ASTM 7-8) / CR Heat Treatment  
(-270 and -140 Mesh Starting Particle Size Showed Similar Creep Rates)
- Cast-Wrought / HS Heat Treatment
- Powder Metal / 2025°F HIP / HS Heat Treatment

3) The creep resistance of HIP consolidated U720LI powder materials were evaluated for potential use in the thin sections of the heater head fins at the helium passages. A strong desire to maintain a minimum grain size of ASTM 4, resulting in 5 grains across the thinnest sections of the heater head fins, was the driving force for this evaluation. The maximum grain size of consolidated powder U720LI was found to be equal to or finer than ASTM 4 in all conditions evaluated.

The steady state creep rate of Udimet 720LI PM(2025°F HIP)-CR was plotted as a function of the creep test stress level at 1050K,

figure 2. A straight line drawn through data points at 10, 24, 36 and 48 KSI was used to obtain the steady state creep rate at the 5 KSI, 1050K design level. The creep rate at 5 KSI and 1050K was estimated to be  $9.0 \times 10^{-5}$  %/hr which results in a time to 1% creep of approximately 11,111 hours under steady state conditions.

The results of a metallographic examination on first round creep samples after testing seemed to indicate that the CR anneal temperature had been lower than the required temperature of 2138°F. A second set of PM(2025°F HIP)-CR tests were run at 36 KSI and 1050K with material annealed at the correct temperature.

The average steady state creep rate from these tests was plotted on the creep rate versus stress plot described above, figure 2. A straight line parallel to the first round test data was drawn through the 36 KSI data point and extended to the 5 KSI design level. In this way the steady state creep rate at 5 KSI was estimated to be  $2.2 \times 10^{-5}$  %/hr. This creep rate results in 45,454 hours to 1% creep assuming a constant creep rate.

A third set of thin plate creep tests were initiated in an attempt to improve the expected time to 1% creep at 5 KSI and 1050K to the 60,000 hour design limit. These tests were run at 1050K and 248 MPa (36 KSI) using U720LI powder that was consolidated at 2300°F and heat treated to the CR condition. The average ASTM grain size of this material was ASTM 4.

The average steady state creep rate for these tests was extrapolated to the 5 KSI level as described above. The estimated steady state creep rate was  $1.3 \times 10^{-5}$  %/hr which results in a time to 1% creep at 1050K and 5 KSI of 76,923 hours. These results imply that Udimet 720LI powder HIP consolidated at 2300 °F will have sufficient life at 1050K and 5 KSI.

## CONCLUSIONS

1) Udimet 720LI appears to have creep resistance equal to or better than that report for standard composition U720 in Special Metals data sheets.

2) Udimet 720LI metal powder HIP consolidated at 2300°F appears to meet the grain size and creep requirements of the heat transfer area of the star fish heater head fins.

C.C.

A.Brown

P.Chapman

M.Cronin

M.Dhar

G.Dochat

TABLE1 - SUMMARY OF U720LI CREEP TESTS - 9/21/92

MATERIAL	STRESS	TEMP.	SPECIMEN	No. TESTS
(U720LI)	(KSI/MPA)	(K)		
ROUND A TESTS*				
*CW-CR	48/331	1050	THIN	1
*CW-CR	36/248	1050	THIN	1
*CW-CR	24/165	1050	THIN	1
*CW-CR	10/69	1050	THIN	1
*FGPM <sup>1</sup> -CR	48/331	1050	THIN	1
*FGPM <sup>1</sup> -CR	36/248	1050	THIN	1
*FGPM <sup>1</sup> -CR	24/165	1050	THIN	1
*FGPM <sup>1</sup> -CR	10/69	1050	THIN	1
CW-HS	48/331	1050	THIN	1
CW-HS	36/248	1050	THIN	1
CW-HS	24/165	1050	THIN	1
CW-HS	10/69	1050	THIN	1
FGPM <sup>1</sup> -HS	48/331	1050	THIN	1
FGPM <sup>1</sup> -HS	36/248	1050	THIN	1
FGPM <sup>1</sup> -HS	24/165	1050	THIN	1
FGPM <sup>1</sup> -HS	10/69	1050	THIN	1
ROUND B TESTS				
FGPM <sup>1</sup> -CR	36/248	1050	THIN	2
FGPM <sup>1</sup> -CR	36/248	1050	STANDARD	2
CW-CR	36/248	1050	THIN	2
CW-CR	36/248	1050	STANDARD	2
ROUND C TESTS				
FGPM <sup>2</sup> -CR	36/248	1050	THIN	2
ROUND D TESTS				
LGPM-CR	36/248	1050	THIN	2

\* = CR SOLUTION ANNEAL TEMP. MAY BE LOW IN ROUND A TESTS

CW = CAST WROUGHT

FGPM<sup>1</sup> = POWDER PROCESSED (-270 MESH)

FGPM<sup>2</sup> = POWDER PROCESSED (-140 MESH)

LGPM = ASTM 4 GRAIN SIZE POWDER HIP TEMP. = 2300°F

CR = CR HEAT TREATMENT

HS = HS HEAT TREATMENT

# UDIMET 720LI CREEP

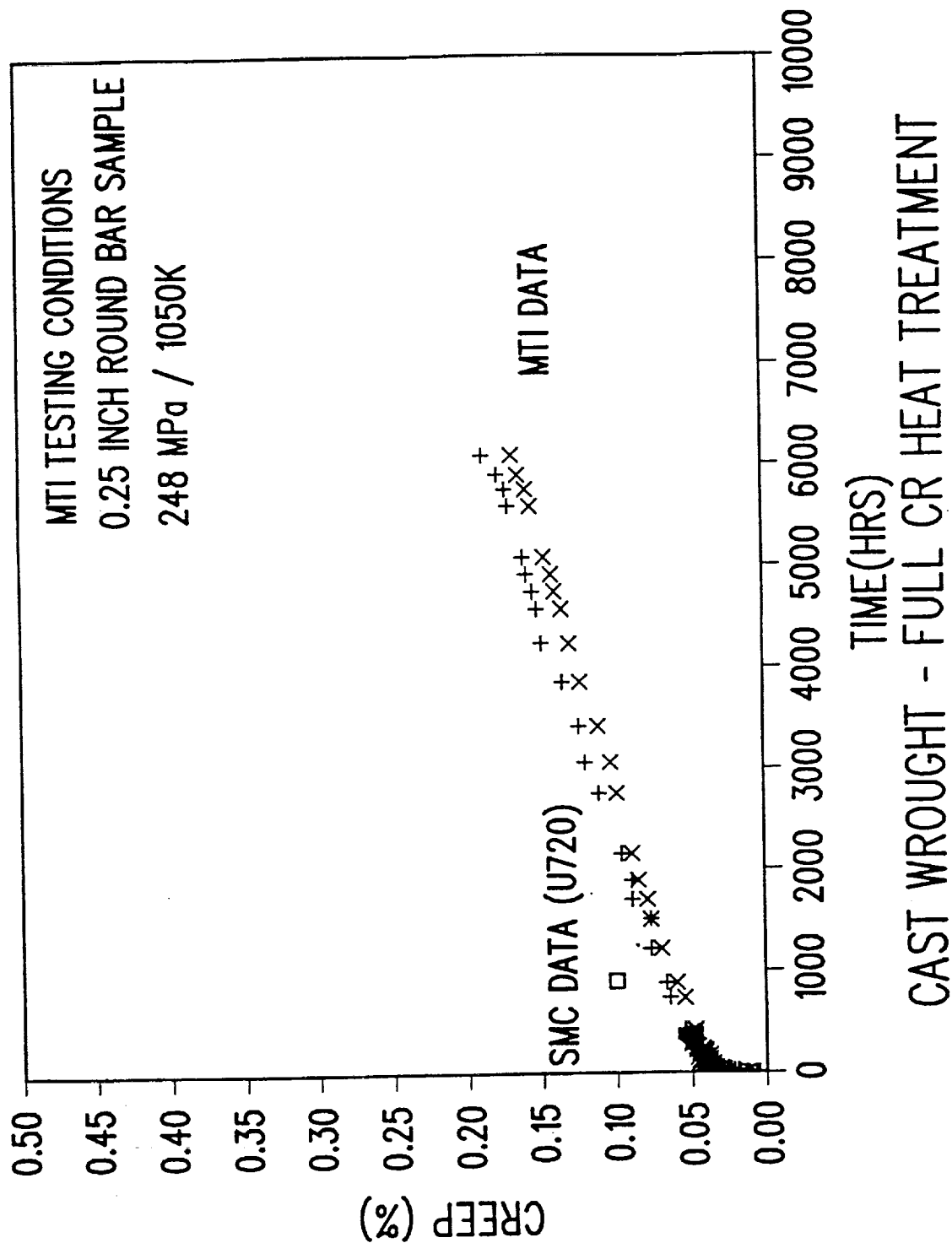


Figure 1



# CREEP RATE VERSUS STRESS

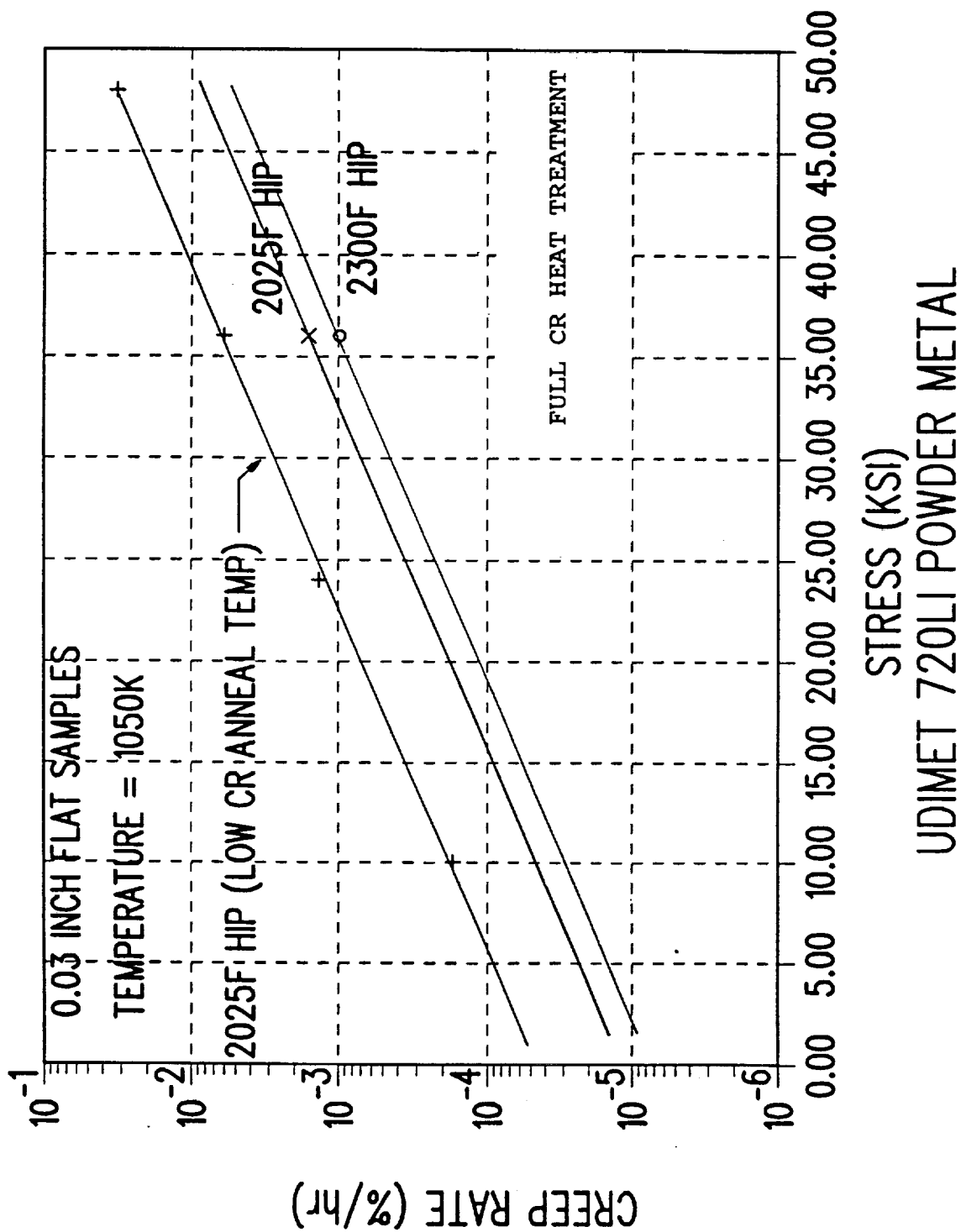


Figure 2

**C.3 Memorandum: Final Summary of Space Stirling Endurance Engine  
Udimet 720LI Fatigue Testing Results**

**To:** M.Dhar

**From:** S.Walak *SW*

**Subject:** Final Summary Of Space Stirling Endurance Engine Udimet  
720LI Fatigue Testing Results.

**INTRODUCTION**

Fatigue testing was initiated to confirm the performance of Udimet 720LI under the temperature and stress conditions anticipated in laboratory testing of the long life Component Test Power Converter. The fatigue tests were run using standard 0.25 inch gauge diameter test bars. The stress and temperature simulated the most severe fatigue conditions in both the hot and cold sections of the engine.

The testing sequence and a brief description of the results will be shown below. Detailed results are contained in the Metcut Research Associates Inc. test reports on file.

**PROCEDURES**

All Udimet 720LI used in the MTI fatigue testing program was heat treated to the CR annealed and aged condition prior to specimen machining and testing, table 1.

**TABLE 1 - UDIMET 720LI CR HEAT TREATMENT**

TEMPERATURE(°C/°F)	TIME(HRS)	COOLING
1170/2138	4	AIR COOL
1080/1976	4	AIR COOL
845/1553	24	AIR COOL
760/1400	16	AIR COOL

Fatigue tests were performed with conventional cast and wrought Udimet 720LI and with Udimet 720LI powder HIP consolidated at 2300°F. The cast-wrought material was taken from a 6.5 inch diameter bar, P.O. #00302774, and the powder metal was taken from a 2 inch diameter HIP billet, P.O.#20302369. Full CR heat treatment of the cast-wrought and powder processed material resulted in a grain size of ASTM M10 and 4 respectively.

The maximum calculated engine stresses were used to establish

appropriate fatigue test conditions. The calculated stresses were as follows:

#### Cold End Conditions

Effective Mean (1)	114.8 KSI ( $\epsilon = 0.41\%$ )	Alt. 7.6 KSI ( $\epsilon = 0.027\%$ )
Effective Mean (2)	120.4 KSI ( $\epsilon = 0.42\%$ )	Alt. 6.7 KSI ( $\epsilon = 0.024\%$ )
Principal Mean	136.5 KSI ( $\epsilon = 0.48\%$ )	Alt. 6.9 KSI ( $\epsilon = 0.024\%$ )

#### Hot End Conditions

Effective Mean	72.1 KSI ( $\epsilon = 0.32\%$ )	Alt. 7.5 KSI ( $\epsilon = 0.033\%$ )
Principal Mean	71.7 KSI ( $\epsilon = 0.32\%$ )	Alt. 8.1 KSI ( $\epsilon = 0.036\%$ )

### RESULTS

The testing sequence and a brief description of the test results will be shown below. Detailed test results are contained in the Metcut Research Associates Inc. test reports on file.

#### SCHEDULE A (REV. 2, 9/28/92)

**General:** Combination LCF/HCF tests of cast and wrought Udimet 720LI were performed at room temperature. The test material was supplied as round bar and machined to final test configuration by the testing vendor. Two tests were conducted under these conditions.

**Purpose:** This loading sequence was selected as a conservative test to confirm operation of U720LI CWCW under cold end stress and temperature conditions.

#### TESTING SEQUENCE:

- 1) Low cycle fatigue in strain control.
  - a) Run 400 cycles from 0.00% to \*0.550% strain at approximately 1 Hz.

Record and Report (As a minimum):

- A) Minimum and maximum stress at 50 cycle intervals.
- B) Total strain range during the stress cycle recorded in (A).
- C) A plot of load versus strain for each cycle recorded in (A).

(\* Caution: Application of strains greater than 0.550% +.005% are not acceptable during any cycle.)

- 2) Liquid penetrant inspect the test specimen to identify any indications of surface cracks.

- 3) Run strain controlled fatigue at the maximum allowable frequency ( $\geq 10$  Hz) between 0.450% minimum strain and 0.550% maximum strain. (Mean strain = 0.500%). Run 100,000 cycles.

- a) Record minimum and maximum load during test to determine if

the material is work hardening or softening. This data should be forwarded to MTI for review and definition of the control method to be used in step 4. MTI will respond to the testing vendor within 1 business day of the receipt of the data. The test specimen should not be removed from the test fixture prior to start of step 4.

4) Option A or Option B will be selected after review of the step 3 test data.

**Option A)**

- a) Define the minimum and maximum load,  $l_{min}$  and  $l_{max}$ , corresponding to 0.450% strain and 0.550% strain in step 3.
- b) Run 10,000,000 cycles in load control at 70 Hz between  $l_{min}$  and  $l_{max}$ .

**Option B)**

- a) Define the minimum and maximum piston displacement,  $PD_{min}$  and  $PD_{max}$  corresponding to 0.450% strain and 0.550% strain in step 3.
- b) Run 10,000,000 cycles in stroke control at 70 Hz between  $PD_{min}$  and  $PD_{max}$ .

**Option A) was selected for actual testing.**

**Record and Report (As a minimum):**

- A) Maximum and minimum stress every 500,000 cycles.
- B) Maximum and minimum piston displacement for the cycles above.

**Sequence A Results:**

Test sample 1 survived the full testing sequence.

Test sample 2 survived Step 1 LCF testing and failed at 2,324,932 cycles into Step 4 HCF testing

**SCHEDULE 1 (REV. A, 10/19/92)**

**General:** Combination LCF/HCF tests of Udimet 720LI powder metal HIP consolidated at 2300°F was performed at room temperature. The test material was supplied as round bar and machined to the final test configuration by the testing vendor. A total of two tests were performed under these conditions.

**Purpose:** This schedule was performed to compare Udimet 720LI powder HIP consolidated at 2300°F with the cast-wrought Udimet 720LI tested under schedule A, "conservative cold end", conditions.

**TESTING SEQUENCE:**

- 1) Low cycle fatigue in strain control.
  - a) Run 400 cycles from 0.00% to \*0.550% strain at approximately 1 Hz.

**Record and Report (As a minimum):**

- A) Minimum and maximum stress at 50 cycle intervals.
- B) Total strain range during the stress cycle recorded in (A).
- C) A plot of load versus strain for each cycle recorded in (A).

(\* Caution: Application of strains greater than 0.550% +.005% are not acceptable during any cycle.)

2) **Liquid penetrant inspect** the test specimen to identify any indications of surface cracks.

3) **Run strain controlled fatigue** at the maximum allowable frequency ( $\geq 10$  Hz) between 0.450% minimum strain and 0.550% maximum strain. (Mean strain = 0.500%). Run 100,000 cycles.

a) Record minimum and maximum load during test to determine if the material is work hardening or softening. This data should be forwarded to MTI for review and definition of the control method to be used in step 4. MTI will respond to the testing vendor within 1 business day of the receipt of the data. The test specimen should not be removed from the test fixture prior to start of step 4.

4) Option A or Option B will be selected after review of the step 3 test data. (Option A was selected in actual testing sequence.)

**Option A)**

- a) Define the minimum and maximum load,  $l_{min}$  and  $l_{max}$ , corresponding to 0.450% strain and 0.550% strain in step 3.
- b) Run 10,000,000 cycles in load control at 70 Hz between  $l_{min}$  and  $l_{max}$ .

**Option B)**

- a) Define the minimum and maximum piston displacement,  $PD_{min}$  and  $PD_{max}$  corresponding to 0.450% strain and 0.550% strain in step 3.
- b) Run 10,000,000 cycles in stroke control at 70 Hz between  $PD_{min}$  and  $PD_{max}$ .

Record and Report (As a minimum):

A) Maximum and minimum stress every 500,000 cycles.

B) Maximum and minimum piston displacement for the cycles above.

**Schedule 1 Results:**

Specimen 1 survived the full test sequence.

Specimen 2 survived the full test sequence.

**SCHEDULE 2, REV.C**

**General:** Fatigue test Udimet 720LI, cast wrought material with the full CR heat treatment, at 1430°F. One sample was tested according to this schedule.

**Purpose:** This schedule was run to confirm operation of cast-wrought Udimet 720LI under hot end stress and temperature conditions.

**TESTING SEQUENCE:**

1) **Strain controlled fatigue:**

a) Run 100,000 cycles between strain limits of  $\epsilon_{min} = 0.312\%$  and  $\epsilon_{max} = 0.392\%$  ( $\epsilon_{mean} = 0.352\%$ ,  $\epsilon_{alt} = \pm 0.04\%$ ) at the maximum allowable frequency  $\geq 10$  Hz.

i) Record and report minimum and maximum stress, strain and piston displacement at 10,000 cycle intervals.

ii) Maintain a continuous record of load, strain and

piston displacement.

- 2) FAX results to MTI engineering prior to running Step 3.
- 3) **Piston Displacement controlled fatigue:**
  - a) Run 10,000,000 cycles at 70 Hz to the piston displacement minimum and maximum corresponding to  $\epsilon_{\min} = 0.312\%$  and  $\epsilon_{\max} = 0.392\%$  as run in step 1.
    - i) Record and report a continuous record of load, strain and piston displacement.
- 4) FAX results to MTI for evaluation prior to the start of additional testing.
- 5) **Strain controlled fatigue:**
  - a) Run 400 cycles between strain limits of  $\epsilon_{\min} = 0.00\%$  and  $\epsilon_{\max} = 0.352\%$  at 0.1 Hz.
- 6) Repeat steps 1 through 3 as described above.

**Schedule 2 Results:** One specimen was subjected to the entire Schedule 2 test sequence without failure.

#### SCHEDULE 3, REV.A

**General:** Three fatigue tests using Udimet 720LI, cast wrought material with the full CR heat treatment, at 1430°F were run according to this test schedule.

**Purpose:** This test schedule was run to confirm operation of cast-wrought Udimet 720LI under hot end stress and temperature conditions.

#### TESTING SEQUENCE:

- 1) **Strain controlled fatigue:**
  - a) Run 5 cycles between strain limits of  $\epsilon_{\min} = 0.00\%$  and  $\epsilon_{\max} = 0.40\%$  at 0.1 Hz.
    - i) Record and report minimum and maximum stress, strain and piston displacement of each cycle.
    - ii) Maintain a continuous record of load, strain and piston displacement.
- 2) **Piston Displacement controlled fatigue:**
  - a) Run 1,000,000 cycles at 70 Hz to the piston displacement minimum and maximum corresponding to  $\epsilon_{\min} = 0.30\%$  and  $\epsilon_{\max} = 0.40\%$ . (These piston displacement values should be defined during step 1)
    - i) Record and report a continuous record of load, strain and piston displacement.
- 3) Repeat steps 1 and 2 ten times to accumulate a total of 50 strain controlled cycles and 10,000,000 piston displacement controlled cycles.
- 4) **Strain controlled fatigue:**
  - a) Run 350 cycles at 0.1 Hz to strain limits of  $\epsilon_{\min} = 0.00\%$  and  $\epsilon_{\max} = 0.40\%$ .

- i) Record and report minimum and maximum stress, strain and piston displacement at a minimum of 50 cycle intervals.
- ii) Maintain a continuous record of load, strain and piston displacement.

**Schedule 3 Results:** Three test samples were exposed to schedule 3 and all survived without failure.

#### **SCHEDULE 4, REV.A**

**General:** Three fatigue tests were run at 485°F according to test schedule 4, rev. A, using cast-wrought Udimet 720LI with the full CR heat treatment.

**Purpose:** This test sequence was similar to schedule A with less conservative load conditions. The tests were run to confirm successful operation under cold end stress and temperature conditions.

#### **TESTING SEQUENCE:**

##### **1) Strain controlled fatigue:**

- a) Run 5 cycles between strain limits of  $\epsilon_{\min} = 0.00\%$  and  $\epsilon_{\max} = 0.54\%$  at 0.1 Hz.
  - i) Record and report minimum and maximum stress, strain and piston displacement of each cycle.
  - ii) Maintain a continuous record of load, strain and piston displacement.

##### **2) Piston Displacement controlled fatigue:**

- a) Run 1,000,000 cycles at 70 Hz to the piston displacement minimum and maximum corresponding to  $\epsilon_{\min} = 0.46\%$  and  $\epsilon_{\max} = 0.54\%$ . (These piston displacement values should be defined during step 1)
  - i) Record and report a continuous record of load, strain and piston displacement.

**3) Repeat steps 1 and 2 ten times to accumulate a total of 50 strain controlled cycles and 10,000,000 piston displacement controlled cycles.**

##### **4) Strain controlled fatigue:**

- a) Run 350 cycles at 0.1 Hz to strain limits of  $\epsilon_{\min} = 0.00\%$  and  $\epsilon_{\max} = 0.54\%$ .
  - i) Record and report minimum and maximum stress, strain and piston displacement at a minimum of 50 cycle intervals.
  - ii) Maintain a continuous record of load, strain and piston displacement.

**Schedule 4 Results:** Three samples were tested as described in Schedule 4. All samples completed the test sequence without failure.

## CONCLUSIONS

The results of the Schedule 4 fatigue tests indicate that cast-wrought Udimet 720LI in the CR condition can survive cold end operating conditions. However, failure of one of two samples in the more conservative Schedule A, Rev. 2, fatigue tests revealed that the material was relatively close to the fatigue failure limit.

Udimet 720LI powder HIP consolidated at 2300°F in the CR condition appears to have better fatigue resistance than cast-wrought material under stress conditions which approximate cold end engine operation.

The results of Schedule 3 fatigue tests indicate that cast-wrought Udimet 720LI in the CR heat treat condition is acceptable for hot end engine fabrication.

C.C.

G. Antonelli

A. Brown

P. Chapman

M. Cronin

Gary Smith



#### C.4 Udimet 720LI Weld Development Summary

**To:** M. Dhar  
**From:** M. Cronin  
**Date:** 6/21/93

**Subject: UDIMET 720LI WELD DEVELOPMENT SUMMARY**

### INTRODUCTION

The two objectives for this task were:

- a) develop a weld repair procedure for the heater head, and
- b) develop a less costly, easier to use joining procedure to be used in place of conventional more costly and time consuming brazing type joining processes.

The materials evaluated in this study included:

- a) cast and wrought Udimet 720LI bar stock (U720LI-CW),
- b) HIP consolidated Udimet 720LI powder metal (U720LI-PM)
- c) wrought Inconel 718 (IN718), and
- d) wrought Inconel 617.

Note: The U720LI-PM used in this task was produced from -140 mesh powder that was HIP consolidated at 2025°F.

Initial electron beam welding trials were done on 0.25" and 0.5" flat plates cut from the ends of bars. The plates were in a fine grained solution annealed condition and were unrestrained during welding. These were used to establish voltage, current, speed and focus parameters. Voltages varied from 60KV to 150KV, current varied from 15 to 45 milliamps, and focus was varied from "under" to "over" focus. As a result of these initial trials, the following parameters were selected as the starting point: 60KV, 25 ma, 30 in/min, and sharp focus. It is interesting to note that in all of the initial trials with unrestrained plates, no cracks were found in the as welded condition.

Table 1 summarizes all the significant welding development tests. The following summarizes the results.

The first weld trials were conducted with axial butt welds. After welding parameters were established and validated, subscale radial butt welds were made to represent actual weld joints for the heater head. Finally, half scale radial butt welds simulating closure plate welds were made.



## RESULTS

### Axial butt welds.

Cracking was normally associated with the stop/start areas of the welds. Also, in these first welds, the nail heads were not machined off, except on W77-2, W7, PM-2 . Cracking was found in these highly restrained, self-mated joints. Cracking was not found in the dissimilar joints of U720LI/Inconel 718 even with the nail head in place.

### Radial butt welds

The radial butt welds simulated the closure plate welds on the heater heads. All the radial butt welds, except WR3/4, were similar metal welds. WR3/4 used fully heat treated (large grain) U720LI and Inconel 718.

Weld defects were found in all weld specimens. Either cracking or subsurface "porosity" was found. The subsurface porosity is thought to be related to hot cracking and subsequent heat treating.

The most successful weld was the thin-walled powder metal to cast-wrought U720LI. There was the typical spherical microporosity which is believed as result of argon coming out of solution during welding.

The first welds, made with U720LI CW and Inconel 718 backer rings, the Inconel 718 was found to have mixed completely through the weld, having greater concentrations iron at the bottom than at the top.

## Good Welding Practice for Nickel Based Superalloys

The following is a list of recommendations collected during the course of this project. They are listed here for future reference.

Material to be welded should be in a fine grained, solution-annealed condition. Large grained material often results in microcracking.

Use compressive shrink fits or other means of providing compressive forces on weld joints to reduce the possibility of hot cracking.

Machine the top of each weld prior to heat treatment to remove stress raisers. Welds must have a raised boss to machine off nail head and an additional boss at the weld tip if not in a backer ring.

Backer rings should be used whenever possible. They reduce/eliminate weld puddle drop during welding. They also can be a benign area for weld tip porosity in addition to controlling splatter. Backer rings are best used as separate rings. Any cracking between the parts and the backer rings tends to be perpendicular to the weld and does not run into the parts.



Heat treatment should be done very carefully. The ramp up through the  $\gamma$  precipitation range should be done as quickly as possible to prevent cracking. MTI did this by heat treating in a double chamber vacuum heat treating system. Parts are loaded into a pre-chamber and the pre-chamber is evacuated. The parts are then charged into the hot vacuum chamber of a two chamber system.

### **Other observations**

During CR anneal of the CW product form, the grains were completely recrystallized. No residual weld microstructure was evident. Grains grew across the entire weld width.

Without a backup ring, the weld puddle exhibited severe drop-out in the weld. It was not possible to obtain a full penetration weld without weld drop-out pointing the need to always use a backer ring.

Separate backer rings are recommended to avoid the possibility of any cracking at the backer ring from turning into the basemetal structure.

It was discovered that during the subsolvus solution treatment, rings cut from a 4" round bar of U720 distorted by about 0.020 inch on the diameter.

Microhardness readings were taken across several welds at each stage of the heat treatment. No significant differences were found across the welds. The parent metal and the weld metal had essentially similar hardnesses, regardless of heat treatment. The values varied from 400 to 500 Knoop (100gms, 20 seconds).

Internal weld porosity was found by MTI and NASA during microstructural review. The porosity was not evidenced by standard NDE methods such as ultrasonics or X-ray. The porosity was found to be somewhat continuous through HIPping trials at NASA. NASA suggested that the porosity may in fact be cracking which occurs sometime during the last three step in the "CR" heat treatment.

Using a dissimilar metal backer ring can be used to dope the weld metal to reduce the tendency of cracking.

EB welding fully age hardened U720LI will result in cracking.

### **CONCLUSIONS**

The most successful weld was the thin-walled powder metal U720LI to cast-wrought U720LI. It is thought that the thin wall reduces welding stresses and reduces the probability of cracking.



Self-mated welds in U720LI are susceptible to both hot cracking and strain age cracking. It may be possible to obtain acceptable welds, but further development is necessary to optimize process parameters before adequate reliability is obtained.



TABLE 1 - UDIMET 720LI WELD SPECIFICATIONS

Weld Number	<sup>1</sup> MATERIAL 1 (Preweld HT Code)	<sup>1</sup> MATERIAL 2 (Preweld HT Code)	Diameter / Thickness (Inches) / Direction <sup>4</sup>	<sup>3</sup> Weld Parameters Kilovolts / milliamps	<sup>2</sup> Backer Ring/ Material	Results
W4	U720LI-CW (EHT)	U720LI-CW (EHT)	3.0 / 0.25 ABW	60 / 25	none	Nail head not machined. Cracking at stop/start. Cracking after CR Anneal.
W6	U720LI-CW (EHT)	U720LI-CW (EHT)	3.00 / 0.50 ABW	60 / 60	none	Indications at three locations, including stop/start as welded - no obvious cracking. Nail head not machined. Heated treated per HS1 - severe cracking at start /stop location.
W77-1	U720LI-CW (EHT)	Inconel 718 (Solution Anneal)	3.0 / 0.25 ABW	60 / 25	none	Nail head not machined. Some cracking at stop/start. Post-weld heat treat 1750°Sol. with 1325 age. No cracks after heat treat.
W77-2	U720LI-CW (EHT)	Inconel 718 (Solution Anneal)	3.0 / 0.25 ABW	60 / 25	none	Cracking at stop/start. Nail head and drop-out machined off. No cracks after heat treat.
W7	U720LI-CW (CRA)	U720LI-CW (CRA)	3.0 / 0.5 ABW	60 / 60	none	No indications after welding. Nailhead and drop-out machined off. Cracking in HAZ after post- weld CRA.
PM-2	U720LI-PM (EHT)	U720LI-PM (EHT)	1.1875 / 0.25 ABW	60 / 40	none	Cracking at stop/start. Machined nailhead and dropout prior to heat treat. Drilled hole at deep indication, Cracking at hole after post weld CRA.



TABLE 1 - UDIMET 720LI WELD SPECIFICATIONS

RBW-1	U720LI-CW (EHT)	U720LI-CW (EHT)	4.0 / 0.5 RBW	60/50 Weld 1 60/60 Weld 2	S Inconel 718	Cracks at start/stop as welded. Machined nailhead, no cracks. No visible cracks after HT. Found weld metal "porosity" in cross section. Fe from Inconel 718 backer throughout weld.
RBW-2	U720LI-CW (EHT)	U720LI-CW (EHT)	4.0 / 0.5 RBW	60/50	S U720LI	Cracking at stop/start. Nailhead machined. Single 0.020 inch porosity found with X-Ray after welding. Cracking not visible after CRA and full age cycle. Subsurface porosity in weld found during metallurgical exam.
WR6A/B	U720LI-PM (EHT)	U720LI-PM (EHT)	1.75 / 0.40 RBW	60 / 60	I U720LI	No cracks after weld. Nailhead machined off. Single crack, perpendicular to weld line, found after vacuum CR solution treat. Spherical micro-porosity, 0.0009 inch, found in metallurgical exam.
WR7A/B	U720LI-PM (EHT)	U720LI-CW (EHT)	1.75 / 0.065 RBW	60 / 10	I U720LI	No cracks after weld. Nailhead machined off. No cracking after heat treat. Spherical micro- porosity, 0.0009 inch, found in metallurgical exam.
W3	U720LI-CW (CRA)	U720LI-CW (CRA)	3.9 / 0.45 ABW	60 / 55	S U720LI	Cracking found as welded, entire length of weld in the HAZ.
WR3/4	U720LI-CW (CRF)	IN718 (PA)	3.9 / 0.45 RBW	60 / 55	S Inconel 718	Cracks after weld. Cracking found on U720LI side after nailhead machined off.
HSS1	U720LI-CW (EHT)	U720LI-CW (EHT)	6.5 / 0.6 RBW		S U720LI	Not machined before heat treat. Cracking found after CRA

TABLE 1 - UDIMET 720LI WELD SPECIFICATIONS

HSS2	U720LI-CW (EHT)	U720LI-CW (EHT)	6.5/0.6 RBW		S U720LI	Nail head machined prior to heat treat. Cracking found after CRA.
W6-1	Inconel 617 (CRA)	Inconel 617 (CRA)	2.0/0.25 ABW	60/21	none	Post-weld CRA Single microcrack found at base of nailhead in one of two cross sections.
WS6/7-1	Inconel 617 (MA)	Udimet 720LI (EHT)	3.0/0.25 ABW	60/21	S Inconel 617	Post-weld CRF. No cracking or porosity found in cross sections.
WS6/7-1	Inconel 617 (MA)	Udimet 720LI (EHT)	3.0/0.25 ABW	60/21	S Inconel 617	Post-weld CRF. No cracking or porosity found in cross sections.

1 PREWELD HEAT TREATMENT CONDITIONS

(EHT) = EURO PREWELD HEAT TREAT: 1100\_C / 4 HOURS / OIL QUENCH

(CRA) = U720LI CR ANNEAL: 1170\_C / 4 HOURS / AIR COOL

(CRF) = U720LI CR ANNEAL AND AGE:

1170\_C / 4 HOURS / AIR COOL

1080\_C / 4 HOURS / AIR COOL

845\_C / 24 HOURS / AIR COOL

760\_C / 16 HOURS / AIR COOL

(PA) = IN718 ANNEAL AND PARTIAL AGE:

954\_C / 1 HOUR / AIR COOL

718\_C / 4 HOUR / AIR COOL

2 I = INTEGRAL indicates backer ring is machined into one side of the weld.

S = SEPERATE indicates backer ring is a separate component.

N = None



Mechanical Technology, Inc.

# TABLE 1 - UDIMET 720LI WELD SPECIFICATIONS

3 For all welds, the speed was 30 Inches /min and the focus was sharp, unless otherwise specified.

4 Direction, ABW = axial butt weld, RBW = radial butt weld.



## C.5 Memorandum: Udimet 720LI Creep Test Final Results Summary

To: M.Dhar

From: S.Walak *SW*

Date: March, 30 1993

Subject: Udimet 720LI Creep Test Final Results Summary.

### INTRODUCTION

Udimet 720LI creep tests were performed to generate the data necessary to assure successful operation of a long life heater head for MTI's Stirling cycle power converter designed for space applications. The design goals for the Udimet 720LI heater head were 60,000 hours of operation at 1050K with stress levels of approximately 24 KSI.

### PROCEDURES

The materials evaluated in the creep tests included cast-wrought Udimet 720LI, Udimet 720LI consolidated from -270 mesh powder metal by Hot Isostatic Press (HIP) processing at 2025°F, Udimet 720LI HIP consolidated from -140 mesh powder metal at 2025°F and Udimet 720LI HIP consolidated from -140 mesh powder at 2300°F.

The two heat treatments evaluated in the Udimet 720LI creep testing program were the standard Special Metals "HS 1" and "CR" heat treatments, Table 1.

TABLE 1 - UDIMET 720LI THERMAL TREATMENTS

#### CR HEAT TREATMENT

TEMPERATURE(°C/°F)	TIME(HRS)	COOLING
1170/2138	4	AIR COOL
1080/1976	4	AIR COOL
845/1553	24	AIR COOL
760/1400	16	AIR COOL

#### HS1 HEAT TREATMENT

TEMPERATURE(°C/°F)	TIME(HRS)	COOLING
1105/2021	2	OIL QUENCH
760/1400	8	AIR COOL

Testing was performed on 0.25 inch diameter round and 0.03 inch thick flat specimens. All tests were performed according to ASTM E-139 requirements using constant axial loading. The 0.03 inch thick flat specimens were used to access the effect of large grains in thin wall structures.

## RESULTS

A summary of all testing completed in this program is shown in Table 2. Tables and graphs of all test data have been assembled in Appendix A.

Results from the MTI Udimet 720LI creep tests which may have a direct impact on long life heater head design and material selection are listed below:

1) The creep rate of cast-wrought Udimet 720LI with the full CR heat treatment appears to be lower than that projected from Larson-Miller calculations using "Standard Composition" Udimet 720 data from Special Metals Corporation (SMC) U720 data sheets.

MTI tests run at 1050K and 248 MPa (36 KSI) with 0.25 inch diameter round bar test specimens cut from 4.25 inch diameter bar stock show a significant improvement in creep resistance for the U720LI material, figure 1.

2) Five variations of Udimet 720LI were creep tested as 0.03 inch thick flat specimens and ranked on the basis of creep rate at 1050K and 248 MPa (36 KSI). The materials are listed below in descending order of creep resistance (The first listed indicates the best creep resistance):

- Cast-Wrought / CR Heat Treatment
- Powder Metal / 2300°F HIP (ASTM 4) / CR Heat Treatment
- Powder Metal / 2025°F HIP (ASTM 7-8) / CR Heat Treatment  
(-270 and -140 Mesh Starting Particle Size Showed Similar Creep Rates)
- Cast-Wrought / HS Heat Treatment
- Powder Metal / 2025°F HIP / HS Heat Treatment

3) The creep resistance of HIP consolidated U720LI powder materials were evaluated for potential use in the thin sections of the heater head fins at the helium passages. A strong desire to maintain a minimum grain size of ASTM 4, resulting in 5 grains across the thinnest sections of the heater head fins, was the driving force for this evaluation. The maximum grain size of consolidated powder U720LI was found to be equal to or finer than ASTM 4 in all conditions evaluated.

The steady state creep rate of Udimet 720LI PM(2025°F HIP)-CR was plotted as a function of the creep test stress level at 1050K, figure 2. A straight line drawn through data points at 10, 24, 36 and 48 KSI was used to obtain the steady state creep rate at the 5

KSI, 1050K design level. The creep rate at 5 KSI and 1050K was estimated to be  $9.0 \times 10^{-5}$  %/hr which results in a time to 1% creep of approximately 11,111 hours under steady state conditions.

The results of a metallographic examination on first round creep samples after testing indicated that the CR anneal temperature was lower than the required temperature of 2138°F. A second set of PM(2025°F HIP)-CR tests were run at 36 KSI and 1050K with material annealed at the correct temperature.

The average steady state creep rate from these tests was plotted on the creep rate versus stress plot described above, figure 2. A straight line parallel to the first round test data was drawn through the 36 KSI data point and extended to the 5 KSI design level. In this way the steady state creep rate at 5 KSI was estimated to be  $2.2 \times 10^{-5}$  %/hr. This creep rate results in 45,454 hours to 1% creep assuming a constant creep rate.

A third set of thin plate creep tests were initiated in an attempt to improve the expected time to 1% creep at 5 KSI and 1050K to the 60,000 hour design limit. These tests were run at 1050K and 248 MPa (36 KSI) using U720LI powder that was consolidated at 2300°F and heat treated to the CR condition. The average ASTM grain size of this material was ASTM 4.

The average steady state creep rate for these tests was extrapolated to the 5 KSI level as described above. The estimated steady state creep rate was  $1.3 \times 10^{-5}$  %/hr which results in a time to 1% creep at 1050K and 5 KSI of 76,923 hours. These results imply that Udimet 720LI powder HIP consolidated at 2300 °F will have sufficient life at 1050K and 5 KSI.

## CONCLUSIONS

- 1) Udimet 720LI with the full CR heat treatment appears to have creep resistance equal to or better than that reported for standard composition U720, with the same heat treatment, in Special Metals data sheets.
- 2) Udimet 720LI metal powder HIP consolidated at 2300°F appears to meet the grain size and creep requirements of the heat transfer area of the star fish heater head fins.

C.C.

A. Brown

P. Chapman

M. Cronin

M. Dhar

G. Dochat

MAT'L SOURCE/  
HEAT NUMBER  
(SEE ATT.)

TABLE 2 - SUMMARY OF U720LI CREEP TESTS - 2/30/93

	MATERIAL	STRESS	TEMP.	SPECIMEN	No. TESTS
	(U720LI)	(KSI/MPA)	(K)		
	ROUND A TESTS*				
A	*CW-CR	48/331	1050	THIN	1
A	*CW-CR	36/248	1050	THIN	1
A	*CW-CR	24/165	1050	THIN	1
A	*CW-CR	10/69	1050	THIN	1
C	*FGPM <sup>1</sup> -CR	48/331	1050	THIN	1
C	*FGPM <sup>1</sup> -CR	36/248	1050	THIN	1
C	*FGPM <sup>1</sup> -CR	24/165	1050	THIN	1
C	*FGPM <sup>1</sup> -CR	10/69	1050	THIN	1
A	CW-HS	48/331	1050	THIN	1
A	CW-HS	36/248	1050	THIN	1
A	CW-HS	24/165	1050	THIN	1
A	CW-HS	10/69	1050	THIN	1
C	FGPM <sup>1</sup> -HS	48/331	1050	THIN	1
C	FGPM <sup>1</sup> -HS	36/248	1050	THIN	1
C	FGPM <sup>1</sup> -HS	24/165	1050	THIN	1
C	FGPM <sup>1</sup> -HS	10/69	1050	THIN	1
	ROUND B TESTS				
C	FGPM <sup>1</sup> -CR	36/248	1050	THIN	2
C	FGPM <sup>1</sup> -CR	36/248	1050	STANDARD	2
A	CW-CR	36/248	1050	THIN	2
A	CW-CR	36/248	1050	STANDARD	2
	ROUND C TESTS				
D	FGPM <sup>2</sup> -CR	36/248	1050	THIN	2

STANDARD = 0.25 INCH DIAMETER ROUND SPECIMEN

THIN = 0.03 INCH THICK FLAT SPECIMEN

\* = CR SOLUTION ANNEAL TEMP. MAY BE LOW IN ROUND A TESTS

CW = CAST - WROUGHT

FGPM<sup>1</sup> = POWDER PROCESSED (-270 MESH) Fine Grain

FGPM<sup>2</sup> = POWDER PROCESSED (-140 MESH) Fine Grain

LGPM = ASTM 4 GRAIN SIZE POWDER HIP TEMP. = 1200°F - Large Grain

CR = CR HEAT TREATMENT

HS = HS HEAT TREATMENT

MAT'L SOURCE/  
HEAT NUMBER  
(SEE ATT.)

TABLE 2 - SUMMARY OF U720LI CREEP TESTS - 2/30/93

	MATERIAL	STRESS	TEMP.	SPECIMEN	No. TESTS
	(U720LI)	(KSI/MPA)	(K)		
	ROUND D TESTS				
E	LGPM-CR	36/248	1050	THIN	2
	ROUND E TESTS				
B	CW-CR	36/248	1095	STANDARD	2
E	LGPM-CR	10/69	1110	THIN	2
	ROUND F TESTS				
E	LGPM-CR	36/248	1095	STANDARD	2

STANDARD = 0.25 INCH DIAMETER ROUND SPECIMEN

THIN = 0.03 INCH THICK FLAT SPECIMEN

\* = CR SOLUTION ANNEAL TEMP. MAY BE LOW IN ROUND A TESTS

CW = CAST - WROUGHT

FGPM<sup>1</sup> = POWDER PROCESSED (-270 MESH) Fine Grain

FGPM<sup>2</sup> = POWDER PROCESSED (-140 MESH) Fine Grain

LGPM = ASTM 4 GRAIN SIZE POWDER HIP TEMP. = 2300°F - Large Grain

CR = CR HEAT TREATMENT

HS = HS HEAT TREATMENT

MECHANICAL TECHNOLOGY  
PO BOX 805  
LA TIAM NY 12110

CERTIFICATE OF TEST

SPECIAL METALS CORPORATION  
MIDDLE SETTLEMENT ROAD,  
NEW HARTFORD, NEW YORK 13413

HEAT NO		SIZE				ALLOY		SMC ORDER NO		CUSTOMER ORDER NO		WEIGHT		DATE MOIDAY/YR	
89251		4" DIA.				UDIMET 720		HTI 7		00302774-2		1044		01/10/91	
C	MN	SI	CR	III	CO	FE	INO	W	TI	AL	B	ZR	S	P	
0.010	0.01	0.01	15.90	BAL.	14.66	0.07	3.03	1.24	5.08	2.70	0.0154	0.029	0.0011	0.00.	
CU															
0.03															

MATERIAL HOT ROLLED AND CONDITIONED FORGING BILLET. CHEMISTRY ON A INGOT. MATERIAL MELTED 11/22/90.  
MATERIAL ULTRASONICALLY INSPECTED TO SMC PROCEDURE PC-210 AND FOUND ACCEPTABLE.

HEAT TREATMENT	TYPE SAMPLE	TEMP °F	STRESS/ULT PSI	0.2% YIELD PSI	LIFE HRS	GAGE LGTH	ELONG %	RA %
<i>HSL - Designation</i> 2020F 2 HRS. OQ 1400F 8 HRS. AC 1200F 24 HRS. AC	COMB SR/N	ROOM 1000 1300	241,000 232,000 90,000	180,200 166,900	284.1	4D 4D 4D	21.8 20.6 14.7	21.8 22.0
GRAIN SIZE: 11-12, 1% ALA 9 STRESS RELIEVED								
HARDNESS: RC 47								

CHEMISTRY & PROPERTIES FOR INFORMATION ONLY.  
This is to certify that the above values are true and s  
to the best of my knowledge and belief

ATTACHMENT A

*[Signature]*  
AUTHORIZED SIGNATURE

MECHANICAL TECHNOLOGY INC  
PO BOX 805  
LATHAM NY 12110

# CERTIFICATE OF TEST

SPECIAL METALS CORPORATION

MIDDLE SETTLEMENT ROAD,  
NEW HARTFORD, NEW YORK 13413



HEAT NO		SIZE		ALLOY				SMC ORDER NO		CUSTOMER ORDER NO		WEIGHT		DATE MO/DAY/YR	
914120		6 1/2" DIA.		UDIMET 720				NTI 5		00302774-1				07/19/91	
C		MN	SI	CR	NI	CO	FE	MO	W	TI	AL	B	ZR	S	P
0.011		0.01	0.01	16.13	DAL	14.65	0.12	3.02	1.19	5.04	2.61	0.0131	0.029	0.0003	0.00
CU		PB-PPH	BI-PPH												
0.01		*5	*0.5												

\* DENOTES LESS THAN NUMBER. CHEMISTRY WT % UNLESS DESIGNATED PPM.  
MATERIAL FORGED AND PEELED. MATERIAL MELTED 11/09/90. INGOT DIAMETER- 20". CHEMISTRY AND PROPERTIES FOR INFORMATION  
MATERIAL ULTRASONICALLY INSPECTED PER SMC PC-231 (IMMERSION METHOD) AND FOUND ACCEPTABLE.

HEAT TREATMENT	TYPE SAMPLE	TEMP °F	STRESS/ULT PSI	0.2% YIELD PSI	LIFE HRS	GAGE LGTH	ELONG %	RA %
2020F 2 HRS. OQ 1400F 8 HRS. AC 1200F 24 HRS. AC	CONB SR/N	ROOM 1000 1300	243,400 233,100 90,000	179,900 168,700	290.5	4D 4D 4D	21.2 18.9 28.4	23.5 18.5
GRAIN SIZE: HARDNESS: RC 47;								

UDIMET 720;

This is to certify that the above values are true and accurate to the best of my knowledge and belief

ATTACHMENT B

*Authorized Signature*  
7-19-91  
AUTHORIZED SIGNATURE

# SPECIAL METALS CORPORATION

PRINCETON PLANT  
Rural Rte. 6, Box 140  
Princeton, Kentucky 42445  
(502) 365-9551

U720

-270 Mesh

BN91021

H.I.P. Consolidation S/N's:  
SMKO 4194, 4195, 4196

Certification No. 91039A

  
H. S. Cooper  


ATTACHMENT C



SPECIAL METALS CORPORATION  
PRINCETON DIVISION  
CERTIFICATION

ALLOY: U720

BLEND/LOT NUMBER: BN91021

MESH: -270

MELT STOCK SOURCE: SPECIAL METALS CORPORATION, NEW HARTFORD, NY

MASTER HEAT/INGOT NUMBER: 718783, 718781

POWDER SOURCE: SPECIAL METALS CORPORATION-PRINCETON DIVISION, PRINCETON, KY

MELTING AND ATOMIZATION PRACTICE: MASP 2014 AND MASP 3056

POWDER HEAT NUMBERS: B91410, B91411, B91412, B91413, B91414, B91415, B91418,  
BN91014

CONSOLIDATION S/N(s): SMK04194, SMK04195, SMK04196

CHEMICAL ANALYSIS: BN91021					SPECIFICATION NO.: INFO. ONLY (SEE NOTE)				
	O2	C	S	W	Mo	Co	Cr	Bi	Cu
ACTUAL	103	.006	<.001	1.22	3.00	N/A	.030	N/A	N/A
	N2	Co	Fe	Mn	Cr	V	Ti	P	NI
ACTUAL	2	14.47	.05	<.01	16.21	N/A	4.36	.007	BALANCE
	Si	Al	B	H2	NOTE: BN91021 MEETS CHEMISTRY LIMITS ON CR:16.0-17.2, C:0.006-0.012, AND B:0.01-0.02.				
ACTUAL	<.10	2.50	.014	7 ppm					

SCREEN ANALYSIS: BN91021

SPECIFICATION NO.: INFO. ONLY

MESH	PERCENT
+230	0.0
-230+270	0.2
-270+325	1.9
-325+400	17.8
-400+500	34.0
-500	46.1
TOTAL :	99.9

PHYSICAL PROPERTIES:

QUANTITATIVE T.I.P. 2165 F / 4 HOURS

	Pra TIP	Post TIP	% Diff.
SMK04194	8.1148	8.1120	0.035
SMK04195	8.1157	8.1106	0.112
SMK04196	8.1152	8.1078	0.091

100X & 1000X PHOTOMICROGRAPHS ARE INCLUDED.

BY: 

PRINCETON DIVISION

SPECIAL METALS CORPORATION  
PRINCETON, KENTUCKY 42445

SOLD TO: Mechanical Technology Inc.  
P.O. Box 805  
Latham, N.Y. 12110

SHIP TO: Mechanical Technology Inc.  
968 Albany Shaker Rd.  
Latham, N.Y. 12110

ALLOY: H.I.P.. U720

CUSTOMER ORDER NO.: P.O. 10302192 N.C. ORDER NO.: 1452

DRAWING/PART NO.: U720 HIP'd LOG ( MILL ORDER NO. MTI 008 )

SPECIFICATION NO: MILL ORDER MTI-008

DIAMETER: 1.8" APPROX.

LENGTH: 12"

MELT STOCK SOURCE: Special Metals Corporation, New Hartford, N.Y.

POWDER SOURCE: Special Metals Corporation, Princeton, Ky.

MELTING AND ATOMIZATION PRACTICE: MASP 2014 AND MASP 3056  
(Vacuum Induction Melted & Inert Gas Atomized)

HEAT NO.: 7-18783, 7-18781

MASTER POWDER BLEND: BN91021

POWDER HEAT NO.(s): B91410, B91411, B91412, B91413, B91414, B91415,  
B91418, BN91014

SERIAL NO.: SMK04194, SMK04195, SMK04196

CONSOLIDATED PRACTICE: Hot Isostatic Pressing

CONSOLIDATION DATE: 03/05/91

CONSOLIDATED SOURCE: Autoclave Toll Services, Princeton, KY

REMARKS: Logs are in decanned condition. UST inspection not performed per  
MTI Mill Order MTI-008.

By 

PRINCETON PLANT



# AUTOCCLAVE TOLL SERVICES LTD.

RURAL RTE 8, BOX 141  
PRINCETON, KENTUCKY 42445  
TELEPHONE (502) 366-0100

## CERTIFICATION

Date 03/05/91

CUSTOMER SPECIAL METALS CORP. CUSTOMER ORDER NO. P117845  
PART NO. \_\_\_\_\_ ALLOY U720  
QUANTITY 4 pcs. DESCRIPTION See Remarks  
LOT NO. \_\_\_\_\_ DRAWING NO. \_\_\_\_\_ SERIAL NO. See Remarks  
CUSTOMER SPECIFICATION ATS-006/2025 ± 25°F/14750 ± 250 psi/3 hrs.

CERTIFIED HIP NO. L1-22-02933 IN UNIT NO. 2 WAS CONDUCTED IN THE FOLLOWING  
MANNER: TEMPERATURE 2025 ± 25 °F, PRESSURE 14750 ± 250 PSI, HOLD 3 HRS  
GAS ANALYSIS: H<sub>2</sub> \_\_\_\_\_ O<sub>2</sub> \_\_\_\_\_ N<sub>2</sub> \_\_\_\_\_ CH<sub>4</sub> \_\_\_\_\_ DEWPOINT \_\_\_\_\_

## REMARKS:

Cans 2 7/8" OD x 15" Lg

SMK0's 4193, 4194, 4195, 4196

Sworn to and Subscribed to Before Me

on this 6th Day of March, 19 91

NOTARY PUBLIC

[Signature]  
My Commission Expires  
January 4, 1995

[Signature]  
Documenting By

WHITE: CUSTOMER COPY

CANARY: File Copy

PINK: Shipping Copy

# SPECIAL METALS CORPORATION

PRINCETON PLANT  
Rural Rte. 5, Box 140  
Princeton, Kentucky 42445  
(502) 365-9551

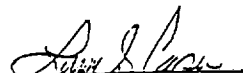
U720 LI

-140 Mesh

BN91029

H.I.P.'D S/N SMK04227

Certification No. 910072A

  
L. S. Cooper



ATTACHMENT D

SPECIAL METALS CORPORATION  
CERTIFICATION

ALLOY: U720 L.I.      H.I.P.'D: SMK04227      DIAMETER: 1.8"  
 CONSOLIDATION SOURCE AND DATE: AUTOCLAVE TOLL SERVICES, PRINCETON, KY  
 CONSOLIDATION PRACTICE: H.I.P. 2025 +25 F/ 14750 +/- 250 psi/ 4 hrs.  
 MELT STOCK SOURCE: SPECIAL METALS CORPORATION, NEW HARTFORD, NY.  
 MASTER HEAT/INGOT NUMBER: 718784, 718311  
 POWDER SOURCE: SPECIAL METALS CORPORATION-PRINCETON DIVISION, PRINCETON, KY.  
 MELTING AND ATOMIZATION PRACTICE: MASP 1028 B.  
 POWDER HEAT NUMBERS: B91417, B91418, B91415, B91421

CHEMICAL ANALYSIS: B91029							U720 L.I. CHEM.		
ANALYTE:	O2	C	S	W	Mo	Zr	Si	Al	B
ACTUAL: (Wgt. %)	.0103	.0082	.0034	1.29	2.99	.032	<.01	2.49	.015
ANALYTE:	N2	H2	Co	Fe	Mn	Cr	Ti	P	NI
ACTUAL: (Wgt. %)	.0001	N/A	14.76	.03	<.01	15.58	4.96	<.01	BALANCE

SCREEN ANALYSIS:  
Master Powder Blend: B91029

PHYSICAL PROPERTIES  
Other Data and Comments:

MESH SIZE: -140

SMK0422.7 GRAIN SIZE = 9.0 ASTM OR FINER

MESH	PERCENT
+140	.0
-140+170	.6
-170+200	2.5
-200+230	9.2
-230+270	9.5
-270+325	10.6
-325+400	17.0
-400+500	23.1
-500	27.4
TOTAL:	99.9

BY: 

L.S. COOPER  
QUALITY ASSURANCE MANAGER  
PRINCETON DIVISION



# AUTOCLAVE TOLL SERVICES LTD.

RURAL RTE 6, BOX 141  
PRINCETON, KENTUCKY 42445  
TELEPHONE (502) 366-0100

## CERTIFICATION

Date 06/06/91

CUSTOMER SPECIAL METALS CORP. CUSTOMER ORDER NO. P118046

PART NO. SMK04227 ALLOY U720

QUANTITY 1 pc. DESCRIPTION Can 3" Dia. x 15" Lg

LOT NO. \_\_\_\_\_ DRAWING NO. \_\_\_\_\_ SERIAL NO. \_\_\_\_\_

CUSTOMER SPECIFICATION ATS-006 2025  $\pm$  25°F/14750  $\pm$  250 psi/4 hrs.

CERTIFIED HIP NO. P1-32-02710 IN UNIT NO. 3 WAS CONDUCTED IN THE FOLLOWING

MANNER: TEMPERATURE 2025  $\pm$  25 °F, PRESSURE 14750  $\pm$  250 PSI, HOLD 4 HRS

GAS ANALYSIS: H<sub>2</sub> \_\_\_\_\_ O<sub>2</sub> \_\_\_\_\_ N<sub>2</sub> \_\_\_\_\_ CH<sub>4</sub> \_\_\_\_\_ DEWPOINT \_\_\_\_\_

REMARKS:

Sworn to and Subscribed to Before Me

on this 7 Day of June, 19 91

NOTARY PUBLIC

*[Signature]*

*[Signature]*  
Documented By



# AUTOCCLAVE TOLL SERVICES LTD.

RURAL RTE 4, BOX 141  
PRINCETON, KENTUCKY 42445  
TELEPHONE (502) 365-0100

## CERTIFICATION

Date 05/12/92

CUSTOMER SPECIAL METALS CORP. CUSTOMER ORDER NO. P118465  
PART NO. \_\_\_\_\_ ALLOY U720  
QUANTITY 6 pcs. DESCRIPTION Cars  
LOT NO. \_\_\_\_\_ DRAWING NO. \_\_\_\_\_ SERIAL NO. See Remarks  
CUSTOMER SPECIFICATION 2300  $\pm$  25°F/14750  $\pm$  250 psi/3 hours

CERTIFIED HIP NO. L2-22-03436 IN UNIT NO. 2 WAS CONDUCTED IN THE FOLLOWING  
MANNER: TEMPERATURE 2300  $\pm$  25 °F, PRESSURE 14750  $\pm$  250 PSI, HOLD 3 hrs.

GAS ANALYSIS: H<sub>2</sub> \_\_\_\_\_ O<sub>2</sub> \_\_\_\_\_ N<sub>2</sub> \_\_\_\_\_ CH<sub>4</sub> \_\_\_\_\_ DEWPOINT \_\_\_\_\_

### REMARKS:

S/N's: 4360, 4361, 4362, 4363, 4364, 4365, 4366, 4367

Sworn to and Subscribed to Before Me

on this 13th day of May, 19 92

NOTARY PUBLIC Thomas Ray Jones

Documented By JDH

# UDIMET 720LI CREEP VERSUS TIME

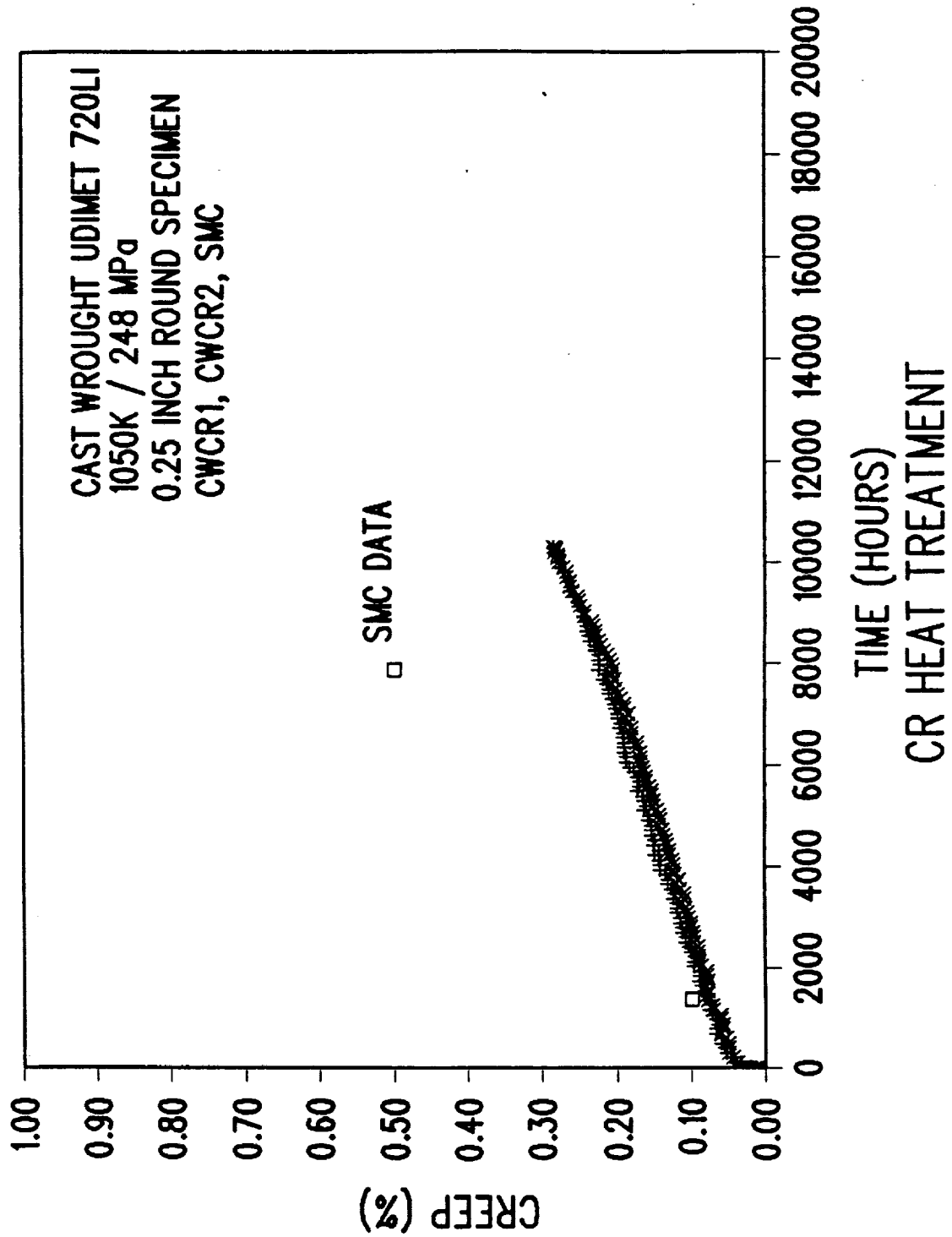


Figure 1



PO #20302369

## SPECIAL METALS CORPORATION

PRINCETON PLANT  
Rural Rte. 6, Box 140  
Princeton, Kentucky 42445  
(502) 365-9551

U720 L.I.

-140 Mesh

8N91029

H.I.P.'D S/N SMK04342, 4343, 4352

Certification No. 920368

*L. S. Cooper*  
L. S. Cooper



ATTACHMENT E

SPECIAL METALS CORPORATION  
PRINCETON DIVISION  
CERTIFICATION

ALLOY: U720 LI

H.I.P.'D BILLET FROM  
MASTER POWDER BLEND: BN91029

MESH: -140

MELT STOCK SOURCE: SPECIAL METALS CORPORATION, NEW HARTFORD, NY

INGOT NUMBER: 718783, 718781

POWDER SOURCE: SPECIAL METALS CORPORATION-PRINCETON DIVISION, PRINCETON, KY

MELTING AND ATOMIZATION PRACTICE: MASP 2012 B AND MASP 3056.

POWDER HEAT NUMBERS: B91417, B91418, B91415, BN91021

\*\*\*CHEMICAL ANALYSIS\*\*\*

	O2	C	S	W	Mo	Cb	Zr	Ta	Cu
ACTUAL	ppm 130	.009	.0002	1.25	3.00	<.01	.03	<.01	<.01
	N2	Co	Fe	Mn	Cr	V	Ti	P	NI
ACTUAL	ppm 18	14.62	.04	<.01	16.41	<.01	4.93	<.01	BALANCE
	Si	Al	B	Hf					
ACTUAL	.01	2.32	.015	<.02					

\*\*\* SCREEN ANALYSIS \*\*\* (BN91029)

PHYSICAL PROPERTIES  
Other Data & Comments

MESH	PERCENT	I.D. SMKO	PRETIP G/CC	POSTTIP G/CC	CHANGE %
+120	.0	4342	8.1141	8.1084	.070
		4343	8.1137	8.1069	.084
-120+140	.0	4352	8.1134	8.1111	.028
		4367	8.1109	8.1044	.080
-140+170	0.6 )				
-170+200	2.5 )				
-200+230	9.2 )				
-230+270	9.5 )				
-270+325	10.6 )				
-325+400	17.0 )				
-400+500	23.1 )				
-500	27.4 )				
TOTAL :	99.9				

METALLOGRAPHIC EVALUATION ACCEPTABLE

By:

*W. L. S. Cooper*

PRINCETON DIVISION

# CREEP RATE VERSUS STRESS

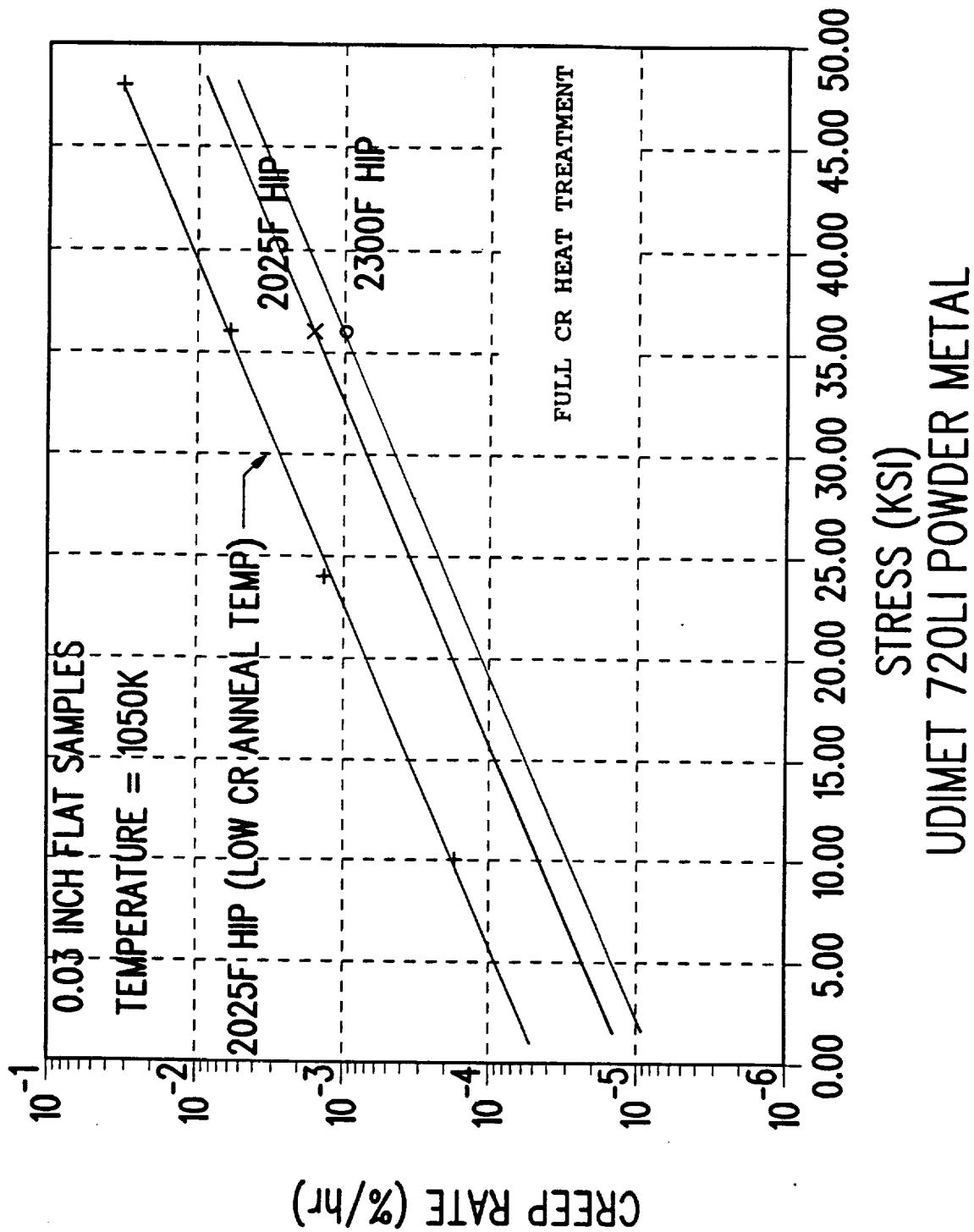
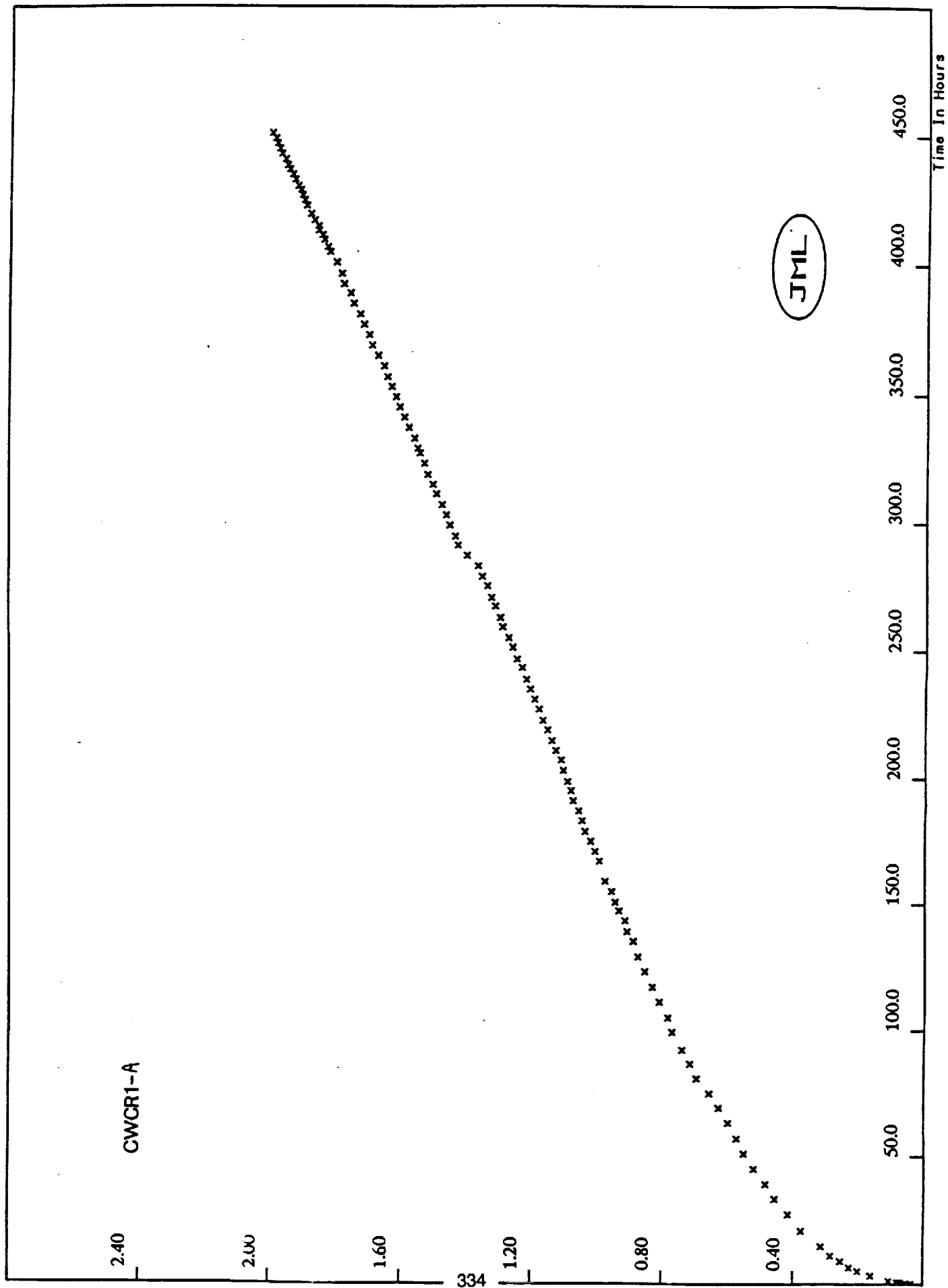


Figure 2

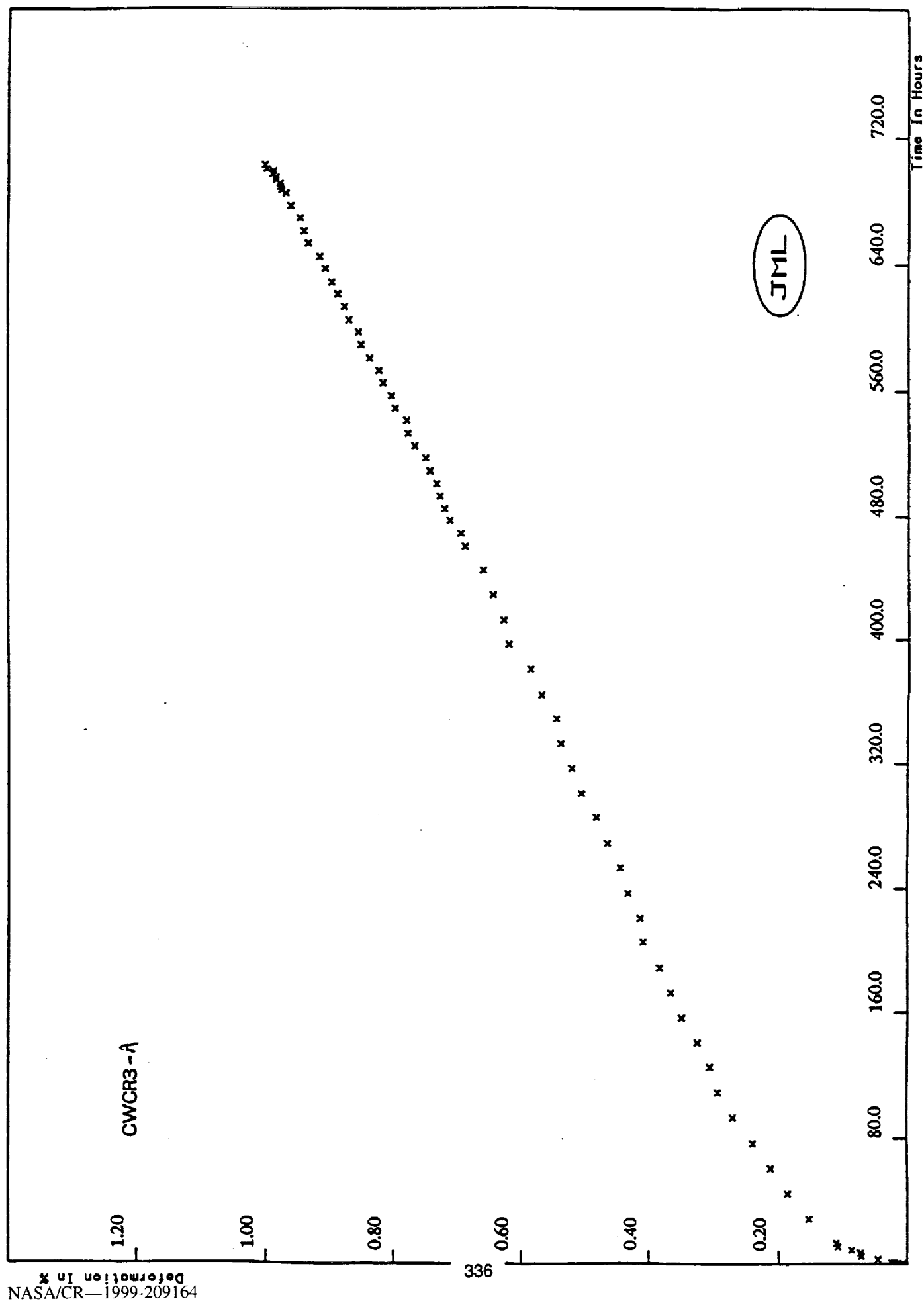
## APPENDIX A

# SUMMARY OF U720LI CREEP TESTS - 3/29/93

SAMPLE	STRESS	TEMP.	SPECIMEN	TOTAL %EL.	RUPTURE
I.D.	(KSI/MPA)	(K)		(%)	(YES\NO)
ROUND A TESTS*					
CWCR1A*	48/331	1050	THIN	2.00	NO
CWCR3A*	36/248	1050	THIN	1.00	NO
CWCR2A*	24/165	1050	THIN	0.27	NO
CWCR4A*	10/69	1050	THIN	0.31	NO
PMCR2A*	48/331	1050	THIN	1.10	YES
PMCR3A*	36/248	1050	THIN	1.80	YES
PMCR1A*	24/165	1050	THIN	1.00	NO
PMCR4A*	10/69	1050	THIN	0.36	NO
CWHS1A	48/331	1050	THIN	25.2	YES
CWHS3A	36/248	1050	THIN	44.2	YES
CWHS2A	24/165	1050	THIN	1.49	NO
CWHS4A	10/69	1050	THIN	1.02	NO
PMHS2A	48/331	1050	THIN	0.56	NO
PMHS3A	36/248	1050	THIN	2.19	NO
PMHS1A	24/165	1050	THIN	1.55	NO
PMHS4A	10/69	1050	THIN	1.00	NO
* = CR SOLUTION ANNEAL TEMP. MAY BE LOW IN FIRST ROUND TESTS					

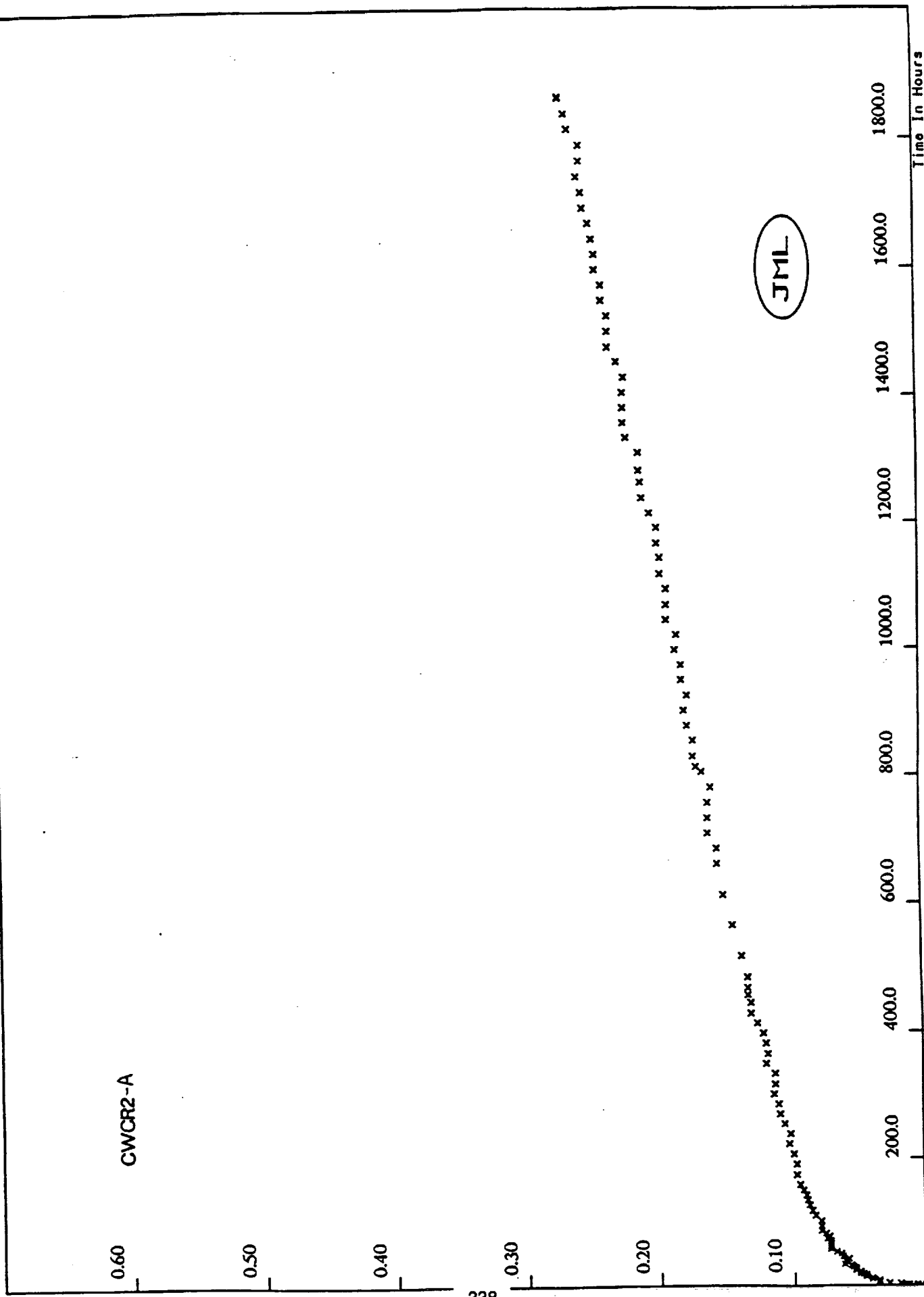


1430 F - 48.0 KSI CREEP DATA FOR CWCRI-A					
Time In Hours	Deformation %	Time In Hours	Deformation %	Time In Hours	Deformation %
0.10	0.037	178.90	1.038	336.90	1.581
0.30	0.054	183.00	1.046	340.80	1.595
0.50	0.071	186.80	1.057	344.90	1.609
0.70	0.079	190.90	1.075	348.90	1.622
1.30	0.105	194.90	1.081	352.80	1.635
3.30	0.161	198.50	1.092	356.70	1.648
5.20	0.201	203.00	1.106	360.80	1.659
6.50	0.228	207.10	1.112	364.90	1.677
9.00	0.255	210.80	1.127	368.90	1.697
11.20	0.286	214.70	1.141	372.90	1.705
14.80	0.315	218.90	1.154	376.90	1.721
20.90	0.375	222.50	1.168	380.80	1.734
27.10	0.416	226.90	1.180	385.00	1.754
33.10	0.458	230.60	1.193	389.00	1.762
39.00	0.486	234.70	1.206	392.50	1.783
45.00	0.521	238.50	1.219	396.50	1.790
51.00	0.552	243.20	1.232	400.80	1.806
57.00	0.575	246.50	1.248	404.80	1.826
63.10	0.600	251.00	1.261	406.60	1.832
69.20	0.628	254.70	1.274	409.50	1.843
75.00	0.656	258.80	1.292	411.30	1.850
81.00	0.694	262.50	1.299	413.10	1.860
86.90	0.714	267.00	1.313	414.80	1.862
92.40	0.738	270.40	1.326	417.20	1.874
99.10	0.768	275.00	1.338	419.60	1.884
104.90	0.782	278.60	1.353	422.90	1.898
111.00	0.808	282.80	1.366	425.00	1.905
116.80	0.830	287.00	1.399	427.00	1.911
123.00	0.854	291.00	1.427	429.10	1.915
128.90	0.875	294.50	1.435	430.70	1.924
135.00	0.889	298.90	1.452	433.10	1.933
138.80	0.908	302.90	1.462	435.20	1.942
143.10	0.915	306.80	1.475	437.10	1.951
147.00	0.934	311.10	1.493	438.70	1.957
150.50	0.945	314.90	1.504	441.00	1.964
154.80	0.956	318.60	1.520	443.20	1.976
159.00	0.976	323.00	1.530	445.10	1.983
167.10	0.994	327.00	1.546	447.20	1.990
171.00	1.007	328.80	1.552	449.10	1.994
175.00	1.020	332.60	1.563	451.10	2.005

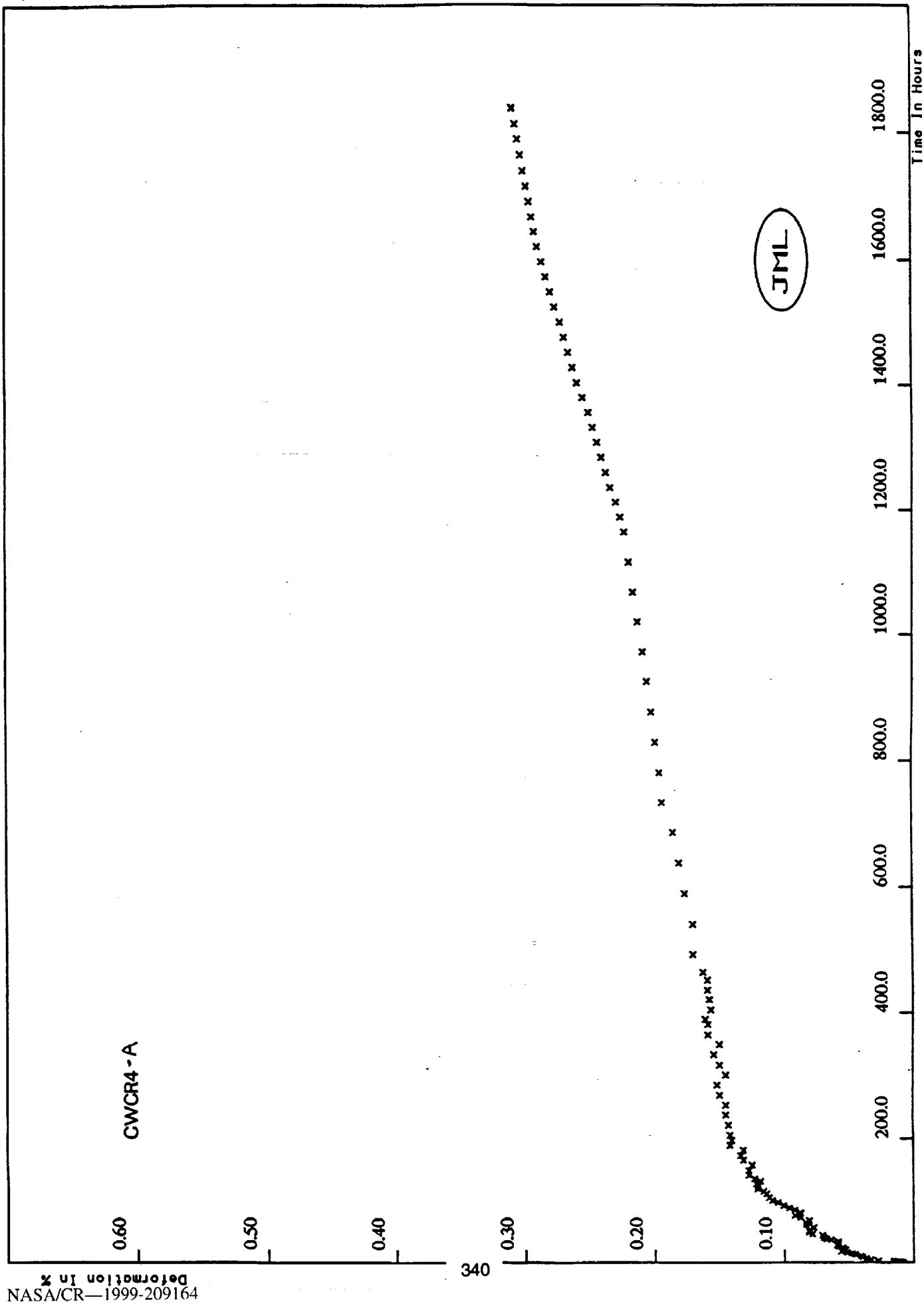




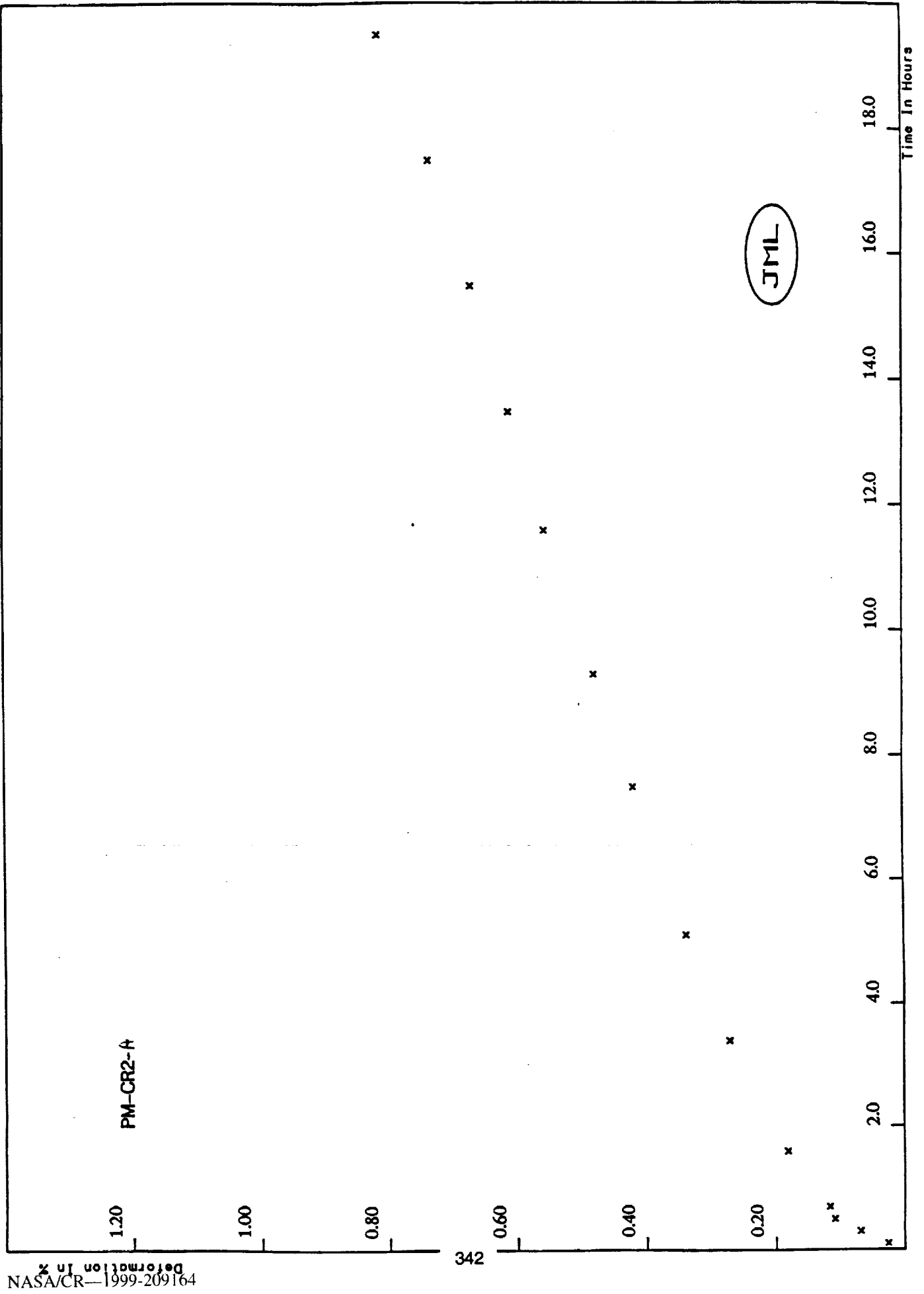
1430 F - 36.0 KSI CREEP DATA FOR CWCR3 -A			
Time In Hours	Deformation %	Time In Hours	Deformation %
0.10	-0.005	460.40	0.688
0.30	0.006	468.80	0.695
0.50	0.014	477.00	0.712
0.70	0.019	484.40	0.720
0.90	0.024	492.90	0.728
2.80	0.045	500.60	0.733
4.90	0.071	508.40	0.744
6.90	0.072	516.80	0.751
8.90	0.087	524.40	0.768
10.90	0.108	532.40	0.779
13.00	0.110	540.80	0.781
28.60	0.154	548.50	0.798
44.60	0.186	556.60	0.805
60.70	0.212	564.70	0.818
76.50	0.240	572.60	0.824
93.00	0.270	580.50	0.839
109.00	0.294	589.00	0.852
125.20	0.306	597.00	0.857
140.40	0.325	604.50	0.872
156.60	0.348	613.00	0.878
172.50	0.366	620.90	0.889
188.40	0.383	628.20	0.899
205.00	0.409	636.90	0.909
220.50	0.413	644.60	0.917
236.60	0.433	653.00	0.935
252.70	0.446	660.90	0.941
268.20	0.465	669.10	0.948
285.00	0.482	676.70	0.962
300.80	0.506	684.90	0.969
316.90	0.521	686.90	0.976
332.80	0.539	688.20	0.978
348.90	0.545	690.80	0.979
364.30	0.569	693.20	0.984
380.40	0.586	694.80	0.984
396.50	0.621	697.10	0.990
412.30	0.629	698.90	0.989
428.90	0.645	700.30	1.000
444.80	0.660	702.80	1.002



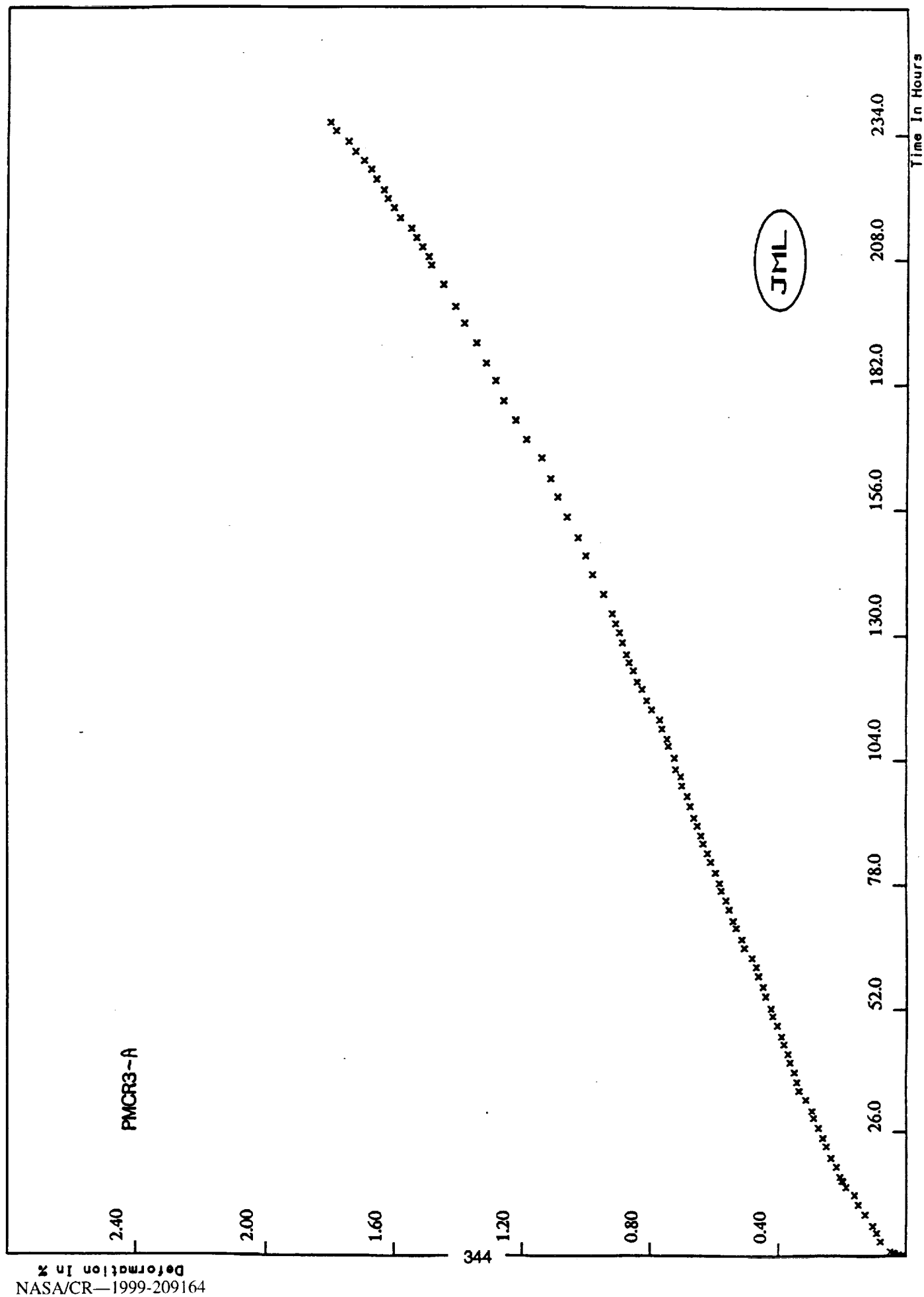
1430 F - 24.0 KSI CREEP DATA FOR CWCR2-A					
Time In Hours	Deformation %	Time In Hours	Deformation %	Time In Hours	Deformation %
0.10	0.000	142.20	0.090	951.70	0.181
0.30	0.007	150.20	0.092	975.60	0.181
0.50	0.013	158.60	0.095	999.60	0.185
0.70	0.015	174.20	0.097	1023.10	0.184
2.40	0.020	190.50	0.097	1047.50	0.192
4.20	0.029	206.60	0.099	1071.60	0.192
6.00	0.036	222.70	0.102	1095.70	0.192
8.30	0.036	238.50	0.101	1119.40	0.196
10.40	0.042	254.50	0.106	1144.30	0.196
12.20	0.042	270.10	0.109	1167.60	0.198
14.40	0.046	286.00	0.110	1191.70	0.198
16.30	0.046	302.10	0.113	1215.50	0.204
18.30	0.048	318.10	0.112	1239.50	0.209
19.70	0.051	334.50	0.112	1263.70	0.210
22.50	0.051	350.60	0.119	1282.30	0.211
24.30	0.054	366.10	0.118	1311.50	0.211
26.30	0.054	382.60	0.119	1335.50	0.220
28.20	0.054	398.50	0.121	1359.60	0.222
30.10	0.056	414.60	0.125	1383.50	0.222
32.30	0.057	430.10	0.130	1407.50	0.222
34.50	0.063	446.40	0.130	1431.10	0.221
38.50	0.062	458.60	0.132	1455.80	0.227
42.30	0.059	470.10	0.132	1478.40	0.233
46.70	0.064	486.00	0.132	1503.50	0.233
50.40	0.065	518.60	0.137	1527.50	0.233
54.00	0.068	566.30	0.143	1551.60	0.238
58.40	0.073	614.60	0.150	1575.50	0.238
62.60	0.073	663.60	0.154	1599.60	0.242
66.30	0.073	687.60	0.154	1623.30	0.242
70.30	0.073	711.60	0.161	1647.50	0.244
74.40	0.075	735.60	0.161	1671.70	0.247
78.00	0.074	759.60	0.161	1695.10	0.251
82.40	0.076	783.30	0.159	1719.10	0.252
86.50	0.079	807.50	0.165	1743.40	0.255
93.90	0.079	815.30	0.170	1767.00	0.253
102.20	0.079	831.30	0.172	1791.30	0.253
110.70	0.084	855.70	0.172	1815.90	0.262
118.10	0.086	879.10	0.176	1839.60	0.264
126.30	0.088	903.20	0.178	1863.60	0.269
134.40	0.089	927.50	0.176	1864.50	0.269



1430 F - 10.0 KSI CREEP DATA FPR CWCR4 -A					
Time In Hours	Deformation %	Time In Hours	Deformation %	Time In Hours	Deformation %
0.10	0.009	97.10	0.105	686.10	0.184
0.30	0.011	100.80	0.109	734.10	0.193
0.50	0.014	105.40	0.112	782.00	0.195
0.70	0.015	110.90	0.114	830.10	0.198
0.90	0.016	115.00	0.116	877.70	0.201
2.70	0.028	118.90	0.120	926.30	0.205
4.50	0.034	123.00	0.120	974.10	0.208
6.80	0.037	127.00	0.121	1022.00	0.212
8.80	0.040	131.00	0.118	1070.10	0.216
10.80	0.042	135.00	0.123	1118.20	0.219
13.00	0.046	141.20	0.127	1166.10	0.222
14.70	0.048	148.70	0.127	1190.00	0.225
16.80	0.053	157.10	0.125	1213.90	0.229
18.50	0.057	165.00	0.131	1238.10	0.233
21.00	0.054	172.50	0.134	1261.90	0.236
22.90	0.056	181.10	0.131	1286.10	0.240
24.80	0.056	188.90	0.141	1310.10	0.243
26.80	0.059	197.30	0.140	1334.10	0.246
28.60	0.060	205.00	0.141	1358.00	0.250
30.80	0.059	220.90	0.142	1381.70	0.254
32.60	0.059	237.40	0.144	1405.60	0.258
34.80	0.059	252.60	0.144	1430.20	0.262
37.10	0.065	268.60	0.149	1454.10	0.265
38.70	0.068	284.70	0.151	1478.00	0.268
40.70	0.070	300.50	0.144	1502.00	0.271
44.80	0.071	316.60	0.149	1526.10	0.276
46.70	0.079	333.10	0.153	1550.00	0.279
48.90	0.081	349.00	0.149	1574.10	0.282
50.80	0.081	364.60	0.158	1597.90	0.286
52.30	0.081	381.20	0.158	1622.20	0.289
56.90	0.078	388.90	0.160	1646.20	0.291
61.00	0.083	404.70	0.155	1669.60	0.293
65.00	0.083	421.00	0.157	1693.60	0.296
68.30	0.081	436.50	0.158	1717.60	0.298
73.00	0.088	452.60	0.158	1741.60	0.300
76.60	0.092	464.90	0.161	1765.80	0.302
80.50	0.088	493.00	0.169	1790.60	0.304
85.00	0.092	540.80	0.169	1814.10	0.306
88.80	0.096	589.10	0.175	1838.10	0.309
92.50	0.101	638.00	0.180	1838.90	0.309

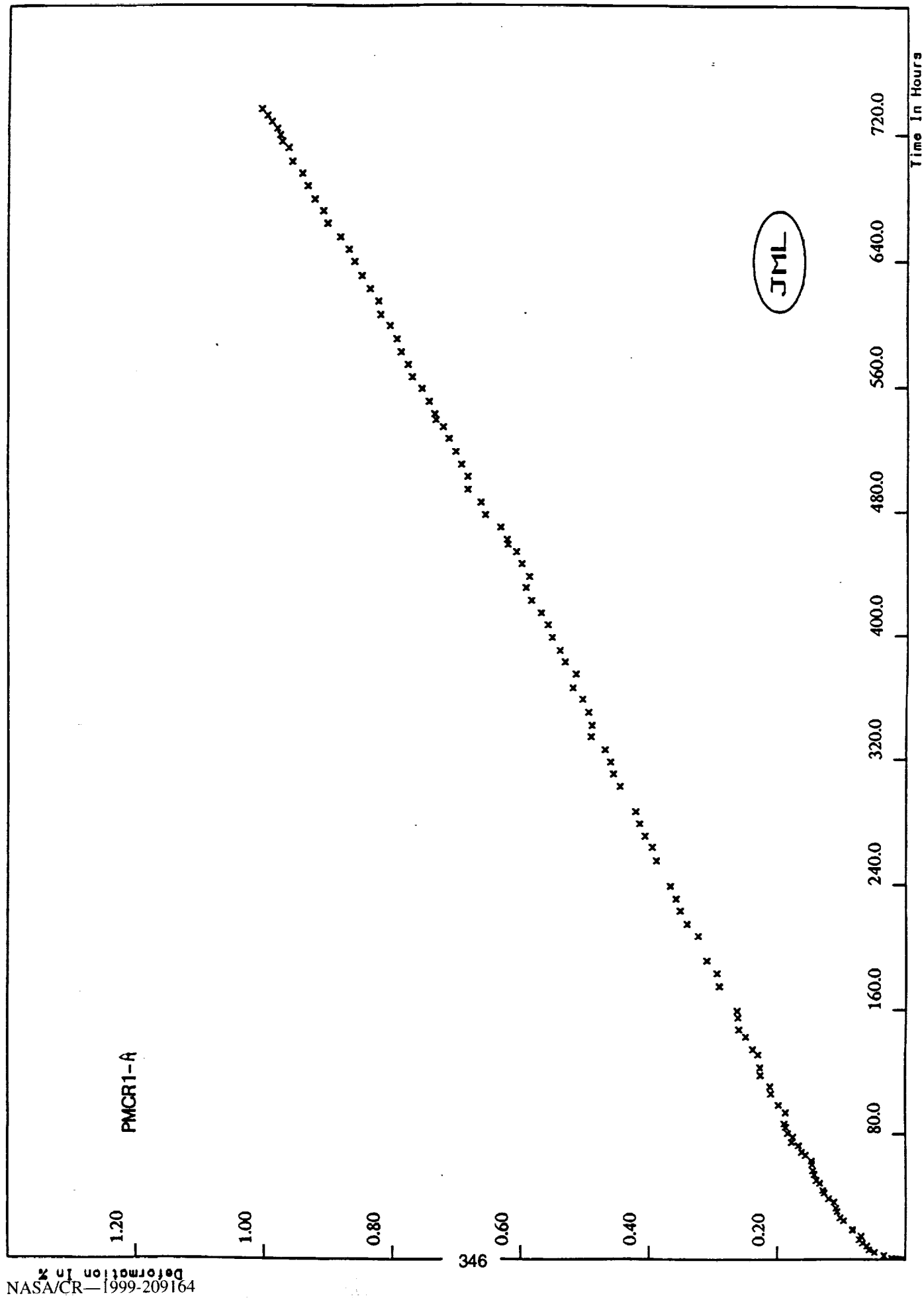


1430 F - 48.0 KSI CREEP DATA FOR PM-CR2	
Time In Hours	Deformation %
0.10	0.027
0.30	0.069
0.50	0.108
0.70	0.117
1.60	0.181
3.40	0.271
5.10	0.337
7.50	0.418
9.30	0.479
11.60	0.556
13.50	0.611
15.50	0.669
17.50	0.734
19.50	0.815

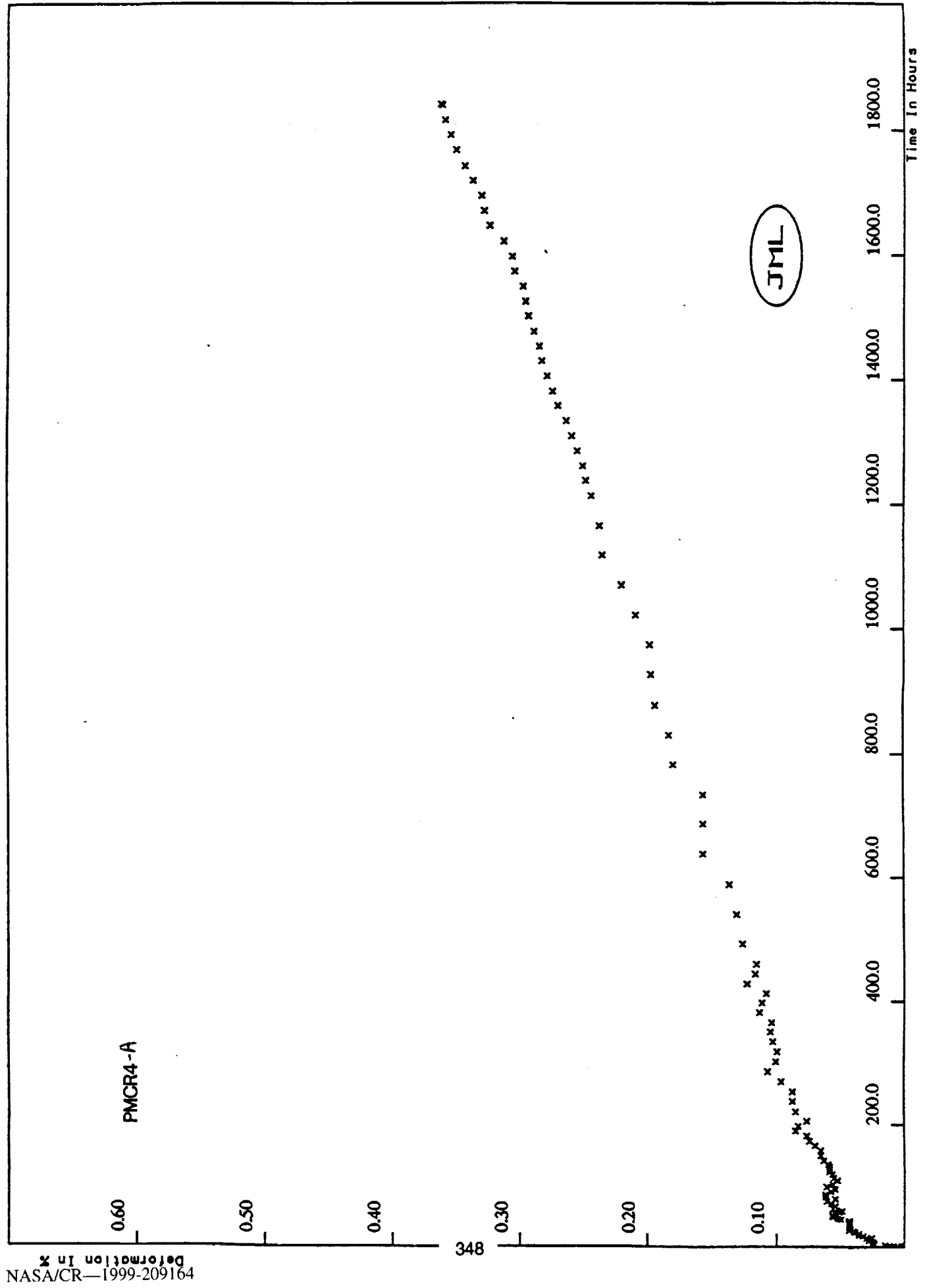




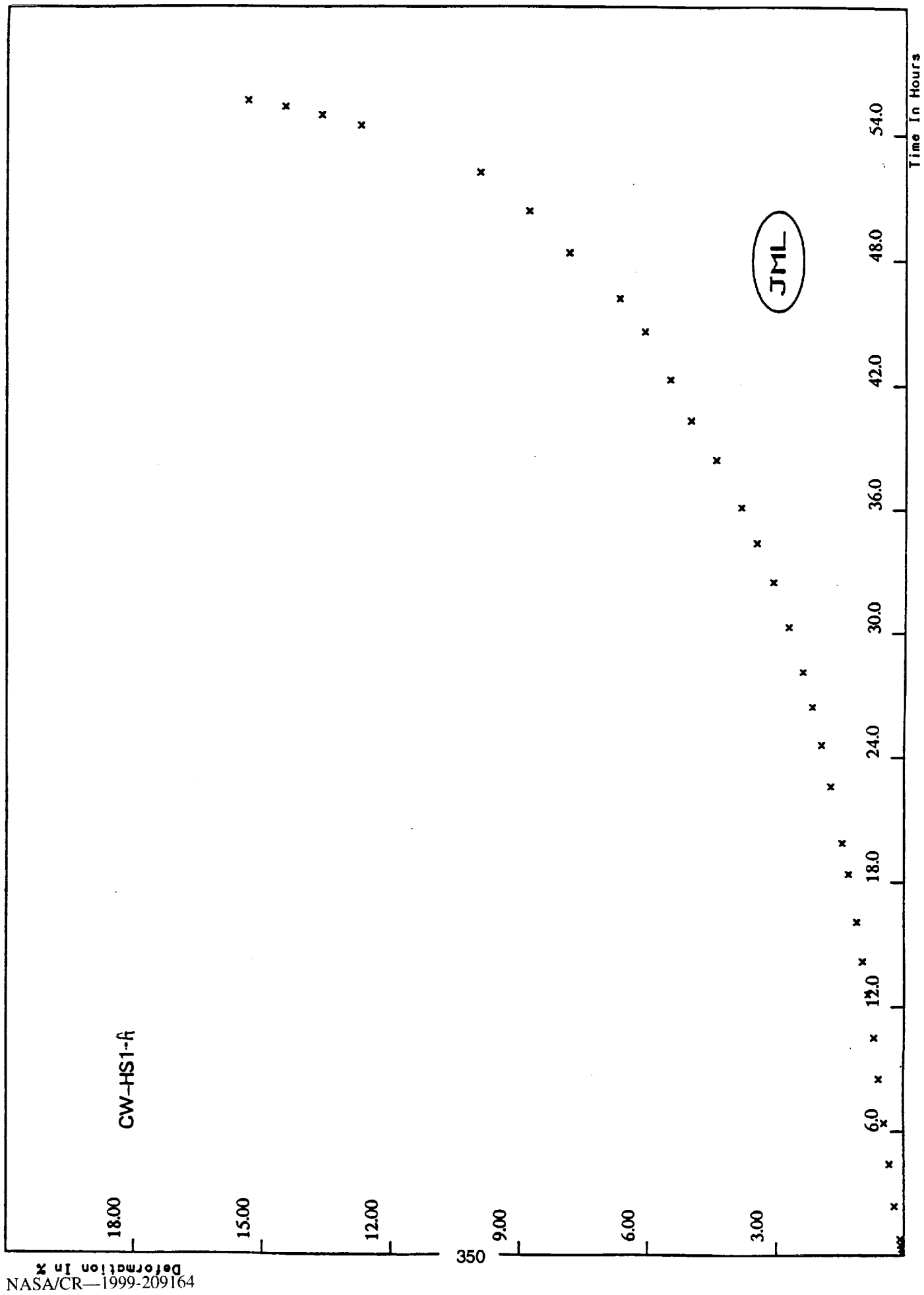
1430 F - 36.0 KSI CREEP DATA FOR PMCR3-A					
Time In Hours	Deformation %	Time In Hours	Deformation %	Time In Hours	Deformation %
0.10	0.011	60.70	0.471	132.50	0.910
0.30	0.023	62.60	0.484	134.60	0.920
0.50	0.035	64.70	0.508	138.60	0.946
0.70	0.040	66.50	0.516	142.60	0.981
1.00	0.050	68.90	0.534	146.60	1.003
3.00	0.082	70.40	0.542	150.30	1.026
4.80	0.093	72.80	0.555	154.50	1.061
6.30	0.106	74.70	0.564	158.70	1.091
8.70	0.130	76.80	0.579	162.50	1.113
10.80	0.151	78.30	0.583	166.80	1.141
12.80	0.163	80.60	0.596	170.60	1.188
14.50	0.190	82.90	0.610	174.60	1.222
15.70	0.199	84.70	0.620	178.60	1.259
15.80	0.203	86.70	0.633	182.80	1.283
16.60	0.207	88.40	0.640	186.40	1.314
18.60	0.219	90.50	0.650	190.60	1.344
20.50	0.236	92.10	0.661	194.60	1.381
22.90	0.251	94.60	0.674	198.10	1.409
24.60	0.261	96.60	0.683	202.70	1.448
26.80	0.274	98.80	0.700	206.80	1.487
28.90	0.290	100.70	0.704	208.50	1.495
30.40	0.295	102.20	0.720	210.50	1.515
32.80	0.313	104.50	0.724	212.40	1.534
34.80	0.335	107.00	0.743	214.30	1.549
36.60	0.341	108.50	0.747	216.50	1.586
38.70	0.350	110.70	0.763	218.60	1.605
40.70	0.363	112.50	0.769	220.50	1.625
42.60	0.369	114.60	0.795	222.30	1.638
44.60	0.382	116.50	0.810	224.50	1.662
46.30	0.391	118.80	0.825	226.60	1.677
48.60	0.404	120.40	0.842	228.50	1.701
50.60	0.419	122.70	0.854	230.30	1.726
52.20	0.424	124.50	0.866	232.40	1.748
54.70	0.442	126.10	0.875	234.50	1.787
56.70	0.449	128.60	0.888	236.20	1.804
58.80	0.463	130.70	0.898		



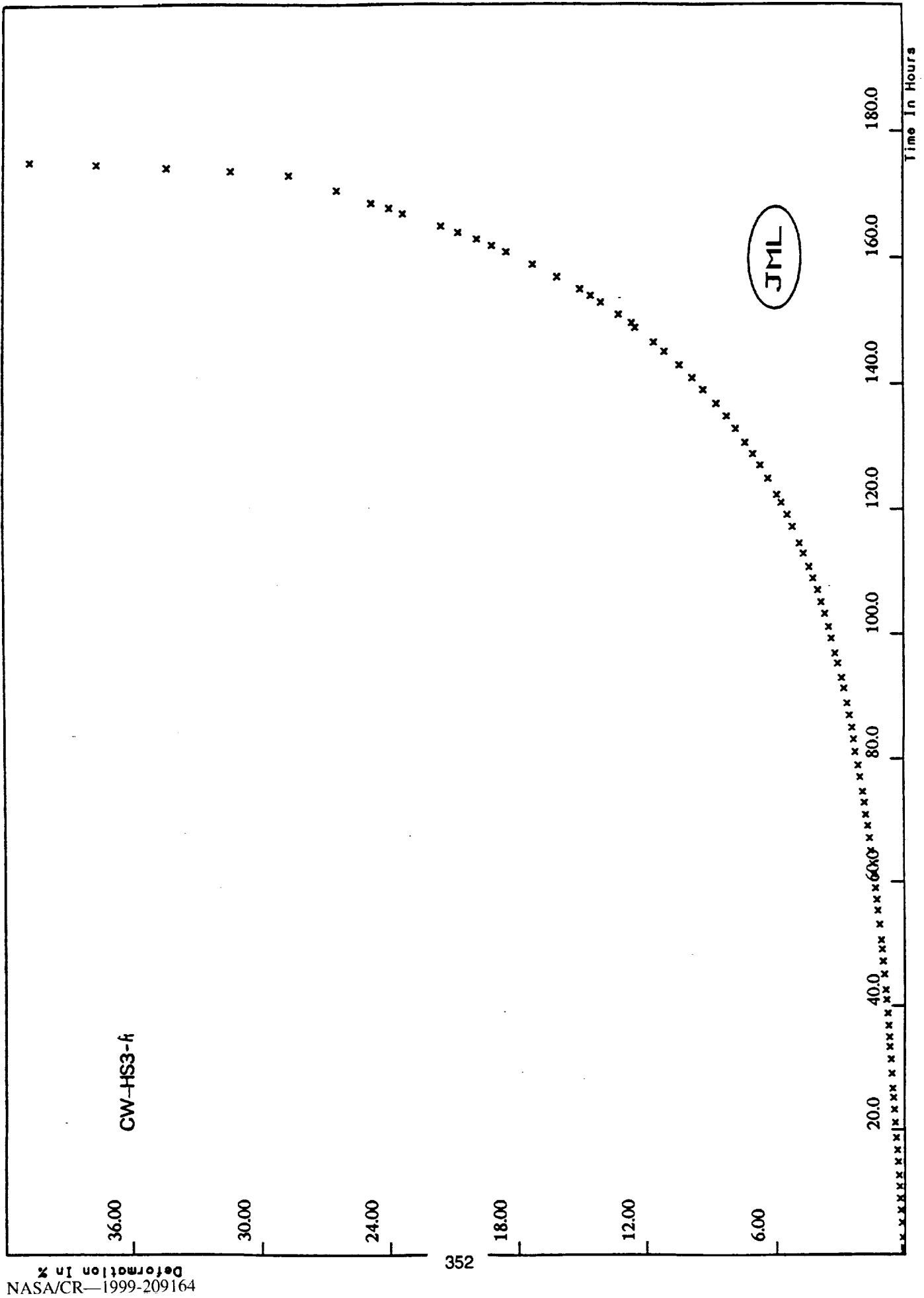
1430 F - 24.0 KSI CREEP DATA FOR PMCR1- $\beta$					
Time In Hours	Deformation %	Time In Hours	Deformation %	Time In Hours	Deformation %
0.10	0.004	122.90	0.227	458.80	0.623
0.30	0.011	131.20	0.230	462.10	0.624
0.50	0.015	134.40	0.239	470.00	0.634
0.70	0.022	142.30	0.250	478.10	0.658
2.60	0.035	146.80	0.261	486.10	0.664
4.40	0.049	154.60	0.262	494.30	0.685
6.10	0.058	158.80	0.263	502.60	0.685
8.40	0.061	174.30	0.291	510.30	0.695
10.50	0.068	182.70	0.294	518.70	0.704
12.40	0.072	190.60	0.309	526.80	0.715
14.60	0.070	206.70	0.322	534.30	0.724
18.40	0.083	214.40	0.340	538.80	0.735
19.00	0.083	222.90	0.351	542.70	0.737
24.40	0.098	230.60	0.357	550.70	0.746
26.40	0.103	238.70	0.366	558.80	0.757
30.30	0.107	254.60	0.388	566.40	0.772
32.40	0.110	263.20	0.395	574.30	0.779
36.50	0.113	270.30	0.406	582.40	0.789
38.60	0.121	278.30	0.414	590.70	0.796
42.40	0.127	286.10	0.421	598.80	0.807
44.10	0.129	302.30	0.445	605.90	0.821
48.50	0.134	310.40	0.456	614.30	0.825
50.50	0.139	318.20	0.461	622.10	0.838
54.10	0.143	326.20	0.469	630.30	0.851
56.50	0.145	334.60	0.491	639.40	0.862
60.60	0.146	342.10	0.490	647.10	0.871
62.70	0.147	350.70	0.496	655.30	0.884
66.40	0.156	358.80	0.504	663.70	0.904
68.30	0.162	366.20	0.520	671.70	0.910
72.40	0.167	374.80	0.515	679.20	0.923
74.60	0.178	382.70	0.533	687.70	0.934
78.10	0.175	390.10	0.541	695.70	0.943
80.50	0.183	398.70	0.553	703.20	0.958
84.60	0.186	407.00	0.559	711.80	0.965
86.60	0.189	414.70	0.570	715.80	0.975
94.10	0.186	422.70	0.586	719.80	0.978
98.80	0.197	430.80	0.594	723.60	0.982
106.40	0.209	438.20	0.589	727.90	0.991
110.90	0.211	446.50	0.601	731.70	0.998
118.20	0.226	454.20	0.610	735.70	1.007



1430 F - 10.0 KSI CREEP DATA FOR PMCR4-A					
Time In Hours	Deformation %	Time In Hours	Deformation %	Time In Hours	Deformation %
0.10	0.000	86.80	0.062	638.20	0.157
0.30	0.002	91.00	0.058	686.30	0.157
0.50	0.001	95.40	0.054	734.20	0.157
0.70	0.009	99.00	0.061	782.40	0.179
0.90	0.012	103.40	0.057	830.30	0.183
2.80	0.015	109.00	0.052	877.80	0.193
4.50	0.024	113.00	0.055	926.40	0.197
6.90	0.025	119.10	0.057	974.20	0.198
9.00	0.028	123.10	0.059	1022.10	0.209
10.80	0.028	127.00	0.059	1070.20	0.220
13.10	0.030	131.00	0.059	1118.40	0.235
14.80	0.026	135.10	0.060	1166.20	0.237
16.90	0.033	141.40	0.063	1214.10	0.243
18.60	0.036	148.90	0.065	1238.30	0.248
21.10	0.036	157.20	0.065	1262.00	0.250
23.00	0.039	165.10	0.070	1286.10	0.254
24.90	0.040	172.60	0.074	1310.10	0.259
26.90	0.043	181.20	0.076	1334.10	0.263
28.60	0.042	189.00	0.085	1358.10	0.270
30.90	0.043	197.50	0.083	1381.60	0.274
33.00	0.043	205.10	0.076	1405.80	0.278
34.90	0.043	220.80	0.085	1430.40	0.283
37.20	0.043	237.50	0.087	1454.10	0.285
38.90	0.043	252.70	0.087	1478.10	0.289
40.90	0.043	268.70	0.096	1502.40	0.293
42.80	0.043	284.70	0.107	1526.20	0.296
44.90	0.050	300.60	0.100	1550.10	0.298
46.80	0.052	316.60	0.099	1574.20	0.304
49.00	0.057	333.20	0.102	1598.10	0.307
50.90	0.057	349.10	0.104	1622.20	0.313
52.40	0.057	364.70	0.103	1646.30	0.324
54.90	0.054	381.30	0.113	1669.70	0.328
56.90	0.051	397.30	0.111	1693.70	0.330
58.90	0.049	412.70	0.108	1717.70	0.337
62.90	0.057	428.70	0.123	1741.60	0.343
66.90	0.054	444.60	0.116	1766.50	0.350
71.00	0.058	460.60	0.115	1790.80	0.354
75.10	0.061	493.20	0.126	1814.20	0.359
78.90	0.054	540.90	0.130	1838.20	0.361
82.60	0.062	589.20	0.136	1839.10	0.362

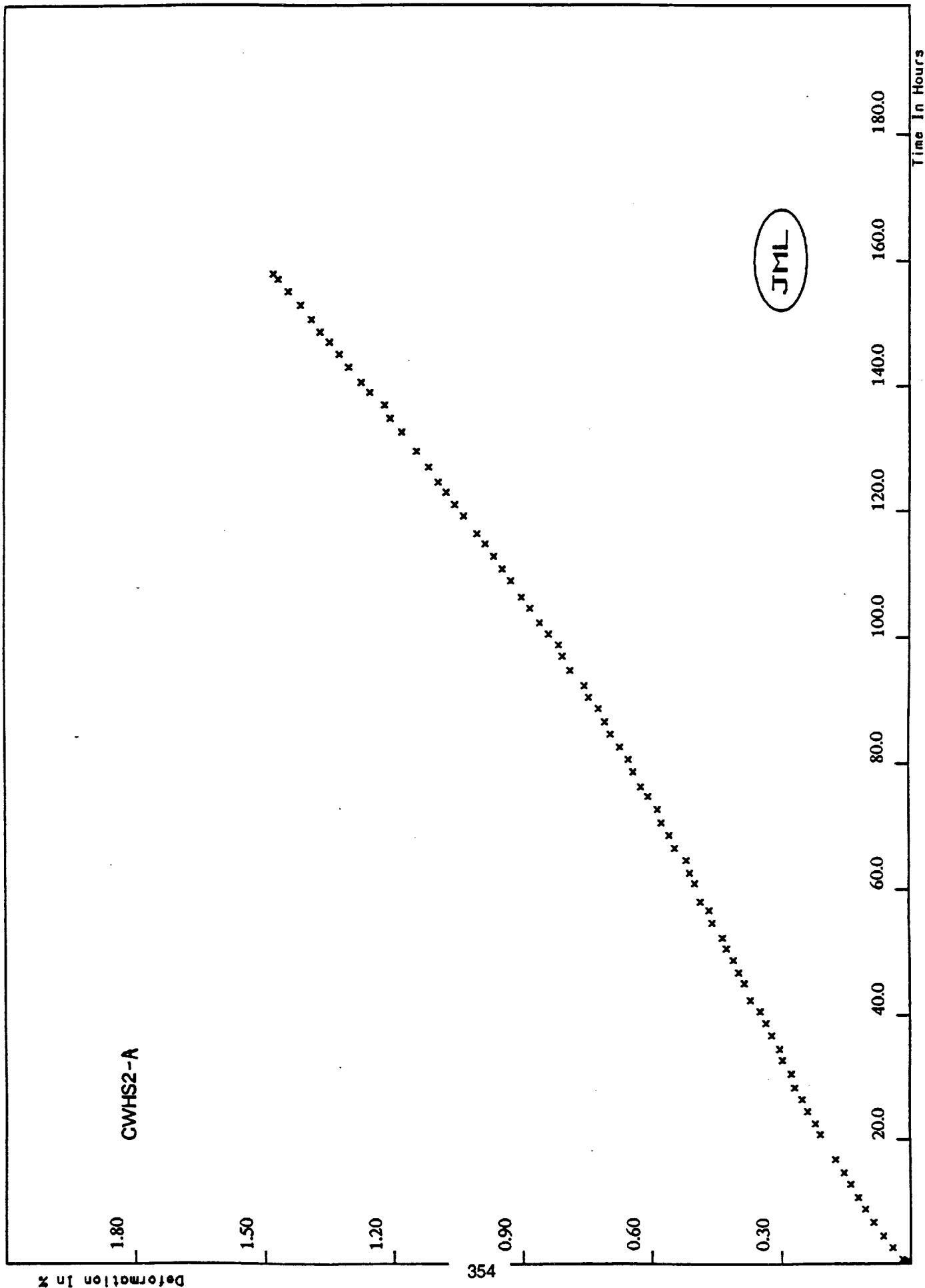


1430 F - 48.0 KSI CREEP DATA FOR CW-HS1	
Time In Hours	Deformation %
0.10	0.042
0.30	0.068
0.50	0.086
0.78	0.101
2.40	0.234
4.40	0.355
6.40	0.469
8.50	0.594
10.50	0.708
12.60	0.847
14.20	0.973
16.10	1.098
18.40	1.305
19.90	1.450
22.60	1.719
24.60	1.937
26.40	2.169
28.10	2.399
30.30	2.738
32.50	3.103
34.40	3.490
36.10	3.857
38.40	4.443
40.30	5.015
42.30	5.513
44.60	6.107
46.20	6.714
48.40	7.887
50.40	8.831
52.20	9.974
54.40	12.771
54.90	13.677
55.30	14.525
55.60	15.405





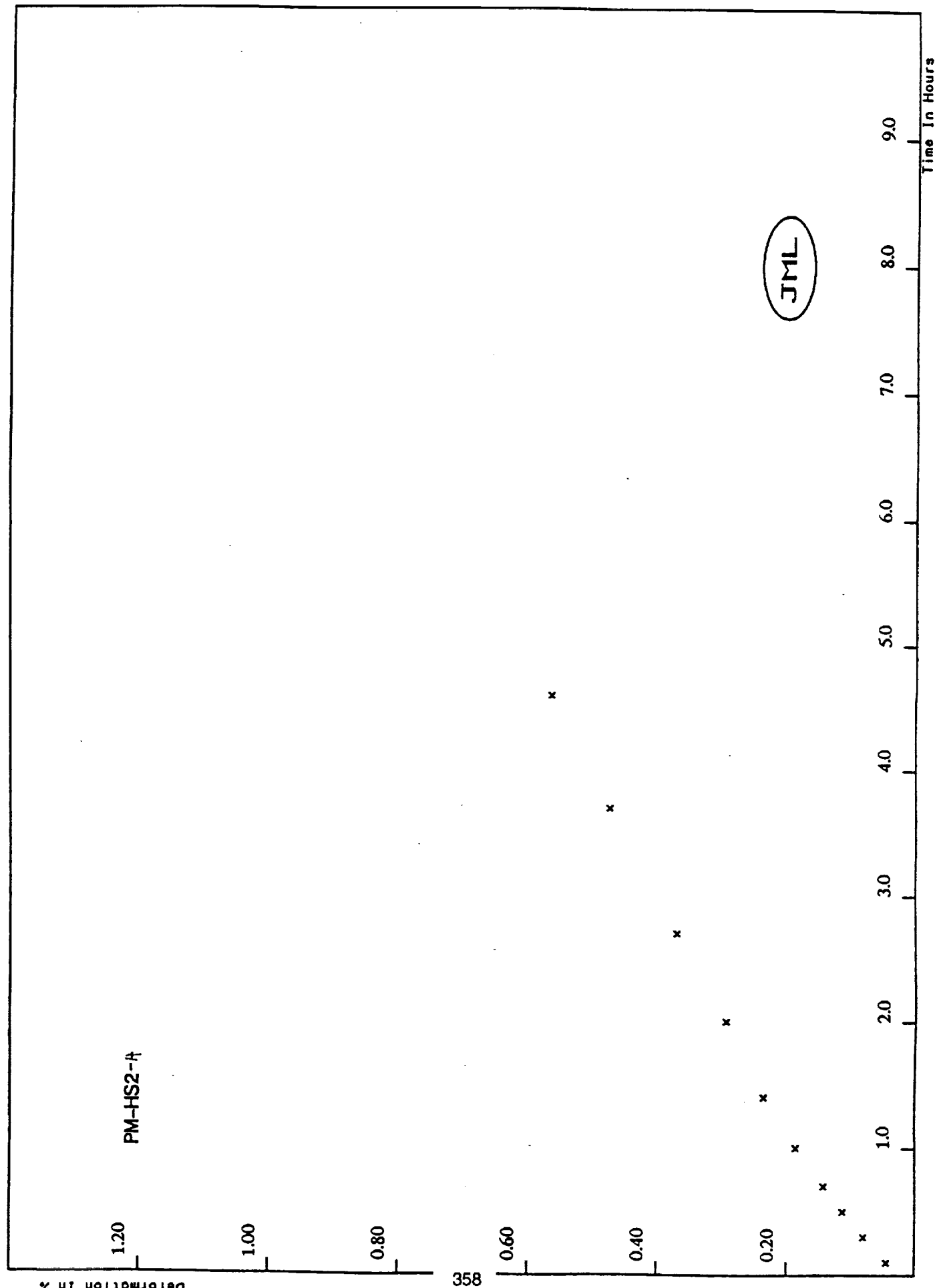
1430 F - 36.0 KSI CREEP DATA FOR CW-HS3- <sup>2</sup>					
Time In Hours	Deformation %	Time In Hours	Deformation %	Time In Hours	Deformation %
0.10	0.009	61.10	1.435	128.90	7.025
0.30	0.022	62.90	1.498	130.70	7.382
0.50	0.031	65.00	1.573	132.90	7.828
0.70	0.051	67.10	1.651	134.90	8.250
1.10	0.059	69.10	1.721	136.90	8.722
2.70	0.098	70.90	1.809	139.10	9.326
5.10	0.145	72.90	1.882	141.00	9.822
7.10	0.190	74.70	1.961	143.00	10.419
9.00	0.234	77.10	2.080	145.10	11.114
10.90	0.258	79.00	2.163	146.60	11.602
12.70	0.291	81.10	2.290	148.90	12.472
14.90	0.328	83.10	2.384	149.63	12.636
16.80	0.368	85.00	2.457	151.00	13.266
18.70	0.405	87.00	2.576	152.90	14.103
21.10	0.447	88.90	2.680	154.00	14.582
23.20	0.483	91.30	2.821	155.00	15.064
25.10	0.522	93.00	2.931	156.90	16.130
26.60	0.550	95.30	3.099	158.90	17.257
29.00	0.594	96.90	3.228	160.90	18.506
31.30	0.639	99.30	3.398	161.90	19.181
33.30	0.705	101.20	3.528	162.90	19.861
34.90	0.725	103.30	3.706	163.90	20.712
36.80	0.767	105.20	3.876	164.90	21.518
38.80	0.807	107.10	4.052	166.90	23.338
41.00	0.857	109.00	4.266	167.80	23.978
42.60	0.903	110.80	4.431	168.60	24.824
45.10	0.961	112.90	4.696	170.60	26.450
47.20	1.016	114.50	4.874	173.00	28.678
49.10	1.069	117.20	5.198	173.70	31.421
50.60	1.108	119.10	5.436	174.20	34.376
53.10	1.190	121.10	5.732	174.60	37.594
55.40	1.256	122.40	5.917	175.00	40.745
57.10	1.300	125.00	6.327	175.30	43.918
59.00	1.364	127.10	6.679		



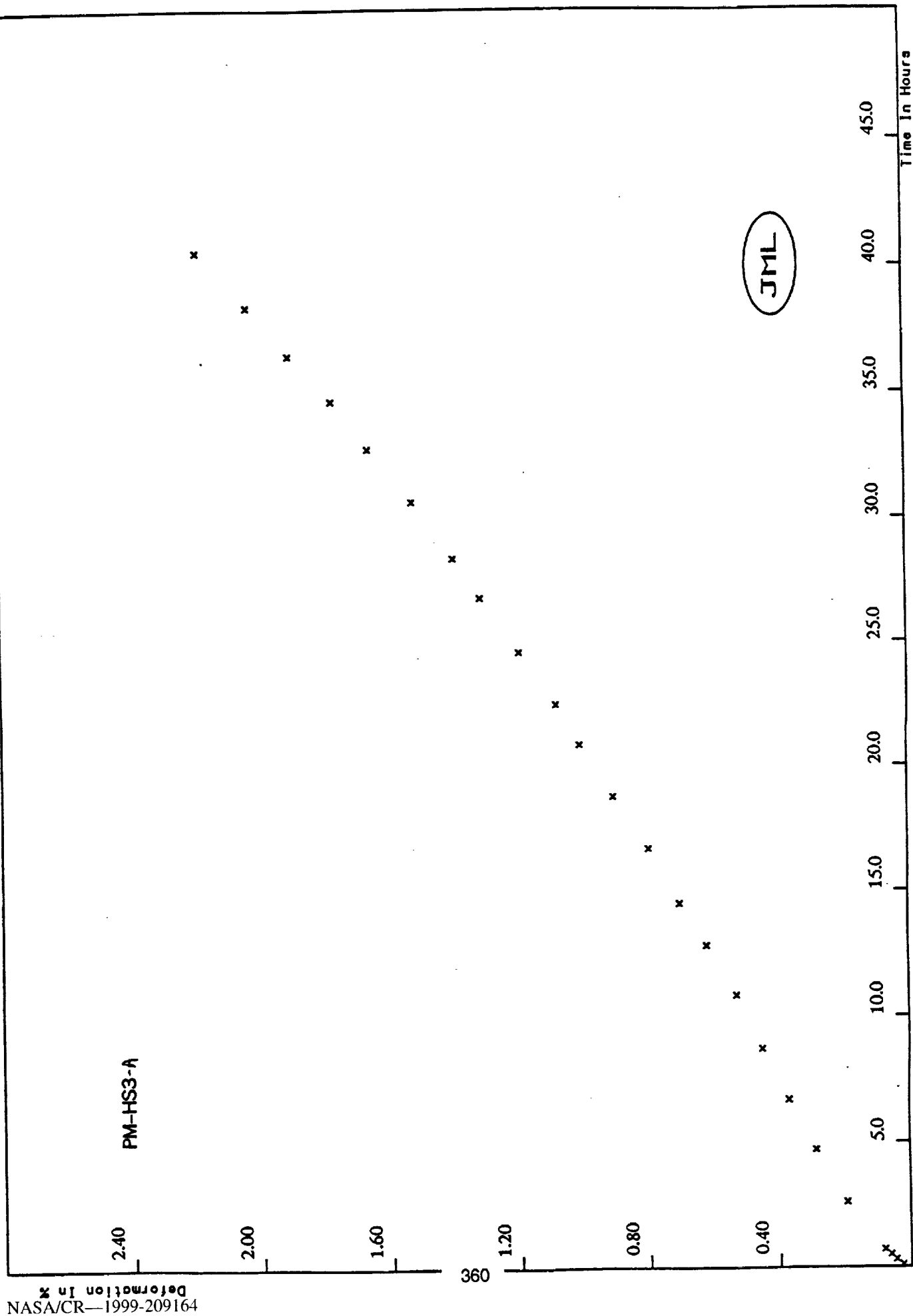
1430 F - 24.0 KSI CREEP DATA FOR CWS2-A					
Time In Hours	Deformation %	Time In Hours	Deformation %	Time In Hours	Deformation %
0.10	0.002	50.60	0.425	104.60	0.882
0.30	0.009	52.30	0.434	106.30	0.902
0.50	0.015	54.70	0.457	108.90	0.927
0.70	0.020	56.70	0.464	110.80	0.947
2.50	0.042	58.08	0.483	112.80	0.967
4.40	0.064	60.90	0.497	114.80	0.987
6.60	0.087	62.60	0.509	116.40	1.007
8.70	0.106	64.60	0.518	119.20	1.037
10.60	0.122	66.50	0.544	121.00	1.057
12.70	0.139	68.60	0.557	123.00	1.077
14.60	0.154	70.60	0.575	124.60	1.095
16.70	0.174	72.70	0.584	127.00	1.117
20.80	0.209	74.80	0.606	129.50	1.145
22.60	0.220	76.30	0.623	132.60	1.181
24.60	0.238	78.70	0.641	134.80	1.207
26.50	0.251	80.70	0.652	136.90	1.220
28.40	0.268	82.70	0.672	138.90	1.256
30.60	0.276	84.80	0.694	140.50	1.275
32.80	0.297	86.70	0.707	142.90	1.304
34.60	0.303	88.80	0.722	145.00	1.326
36.80	0.322	90.50	0.744	146.90	1.348
38.70	0.335	92.30	0.756	148.50	1.370
40.60	0.348	94.70	0.789	150.50	1.390
42.30	0.370	97.00	0.806	152.80	1.416
45.00	0.384	98.80	0.815	154.90	1.445
46.70	0.396	100.50	0.838	156.90	1.469
48.70	0.409	102.30	0.859	157.80	1.480



1430 F - 10.0 KSI CREEP DATA FOR CWHS4-A					
Time In Hours	Deformation %	Time In Hours	Deformation %	Time In Hours	Deformation %
0.10	0.015	224.50	0.337	424.10	0.693
0.30	0.012	232.80	0.350	429.10	0.704
0.50	0.014	240.40	0.358	432.30	0.708
0.70	0.015	248.30	0.377	436.90	0.715
2.60	0.031	256.90	0.387	440.40	0.728
4.50	0.033	264.30	0.400	444.90	0.738
6.80	0.039	272.40	0.415	448.60	0.745
8.40	0.045	280.20	0.424	452.80	0.760
10.60	0.046	288.70	0.440	456.70	0.765
12.70	0.050	296.30	0.452	460.80	0.773
18.70	0.063	300.60	0.460	464.20	0.780
24.50	0.068	305.00	0.465	468.70	0.793
30.60	0.076	308.70	0.476	473.00	0.803
36.50	0.090	312.80	0.480	476.80	0.815
42.70	0.096	316.80	0.491	480.70	0.821
48.10	0.102	320.10	0.498	484.80	0.823
54.60	0.104	324.70	0.502	488.30	0.831
60.00	0.118	328.90	0.506	492.70	0.844
66.30	0.117	332.80	0.515	497.20	0.851
72.20	0.128	336.60	0.526	500.80	0.858
78.60	0.139	340.70	0.534	504.60	0.867
84.90	0.149	344.80	0.541	508.70	0.873
90.50	0.154	348.80	0.548	512.70	0.886
96.30	0.156	352.90	0.552	516.60	0.893
102.70	0.165	356.70	0.565	520.40	0.899
109.20	0.175	360.90	0.571	524.90	0.906
113.00	0.178	364.60	0.571	528.40	0.912
120.90	0.188	368.70	0.586	532.70	0.919
128.30	0.199	377.00	0.592	536.10	0.926
137.00	0.209	380.90	0.606	540.80	0.932
145.00	0.226	384.50	0.613	545.10	0.938
152.30	0.225	388.90	0.621	548.60	0.949
161.00	0.238	392.70	0.631	552.80	0.956
168.70	0.261	396.90	0.634	556.80	0.958
176.90	0.262	400.60	0.647	560.30	0.969
184.80	0.276	404.50	0.652	565.10	0.978
192.50	0.285	408.30	0.654	568.40	0.984
200.10	0.293	412.70	0.667	572.70	0.997
208.60	0.313	416.20	0.675	576.20	1.008
216.90	0.328	420.70	0.686	580.90	1.021

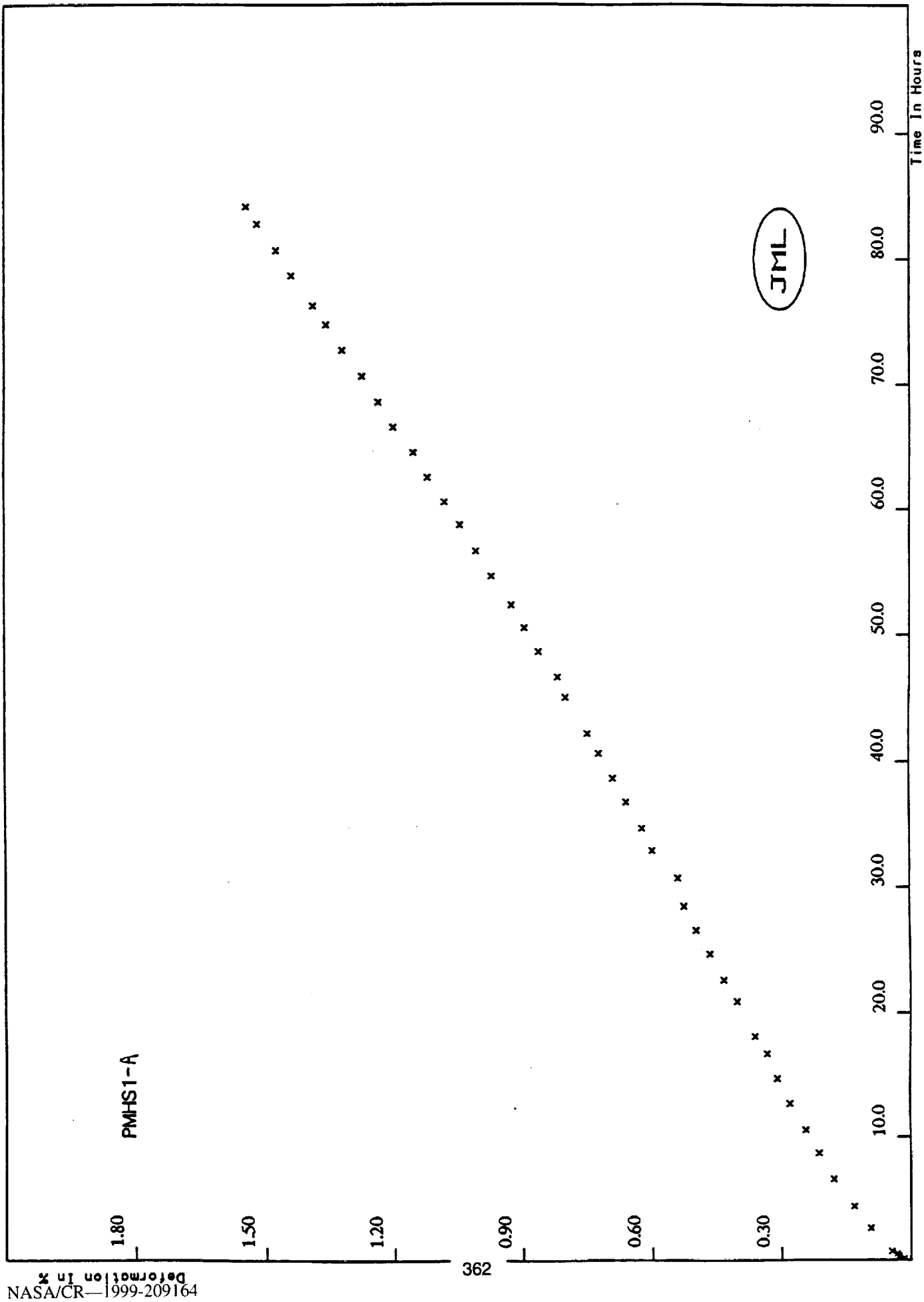


1430 F - 48.0 KSI CREEP DATA FOR PM-HS2	
Time In Hours	Deformation %
0.10	0.045
0.30	0.081
0.50	0.112
0.70	0.142
1.00	0.184
1.40	0.235
2.00	0.293
2.70	0.369
3.70	0.473
4.60	0.564

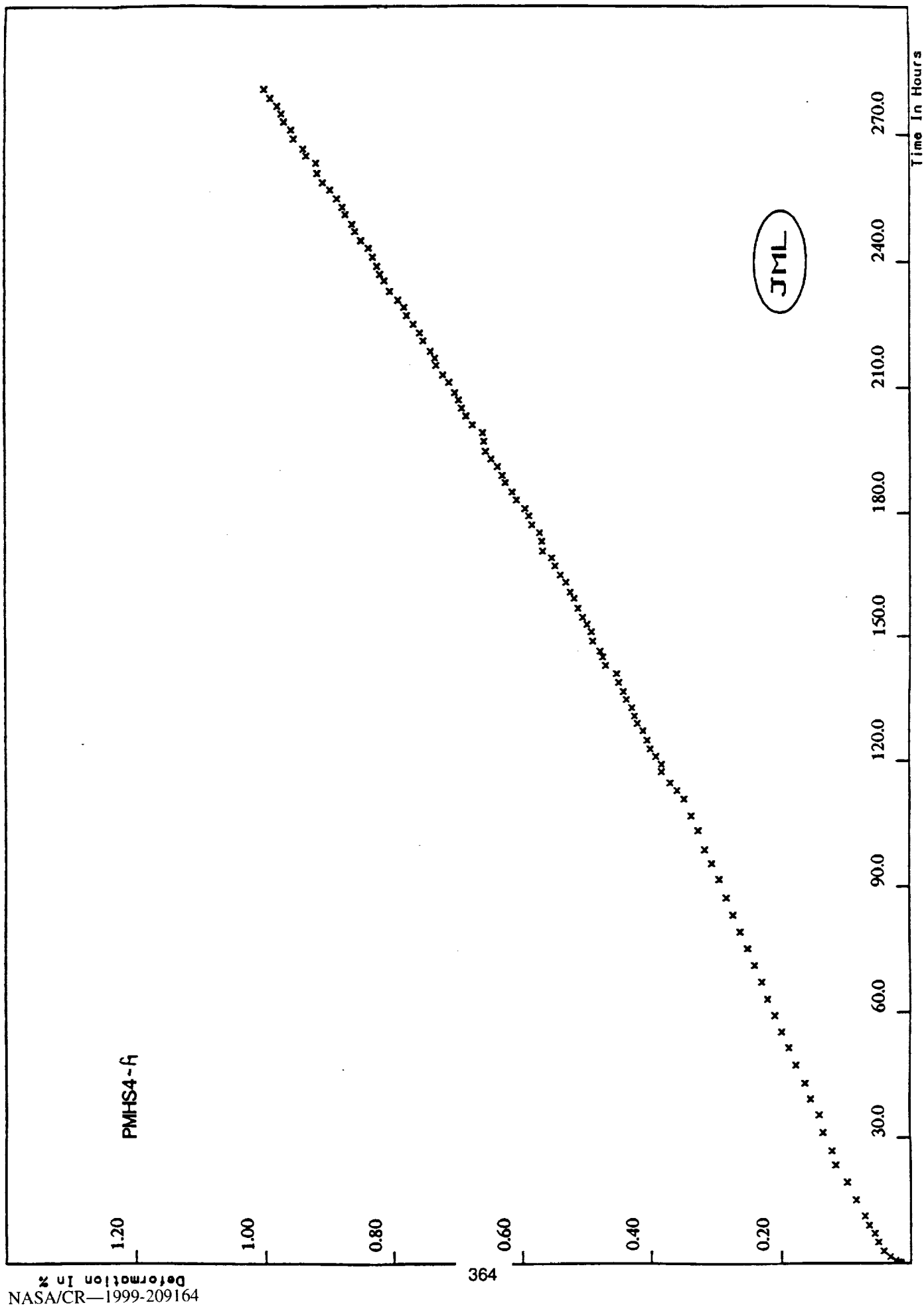




1430 F - 36.0 KSI CREEP DATA FOR PM-HS3	
Time In Hours	Deformation %
0.10	0.025
0.30	0.047
0.50	0.062
0.70	0.081
2.60	0.195
4.70	0.287
6.70	0.367
8.70	0.451
10.80	0.529
12.80	0.619
14.50	0.700
16.70	0.796
18.80	0.906
20.90	1.009
22.50	1.083
24.60	1.196
26.80	1.315
28.40	1.398
30.70	1.524
32.80	1.660
34.70	1.772
36.50	1.903
38.40	2.032
40.60	2.187



1430 F - 24.0 KSI CREEP DATA FOR PMHS1			
Time In Hours	Deformation %	Time In Hours	Deformation %
0.10	0.015	40.70	0.722
0.30	0.029	42.30	0.748
0.50	0.033	45.10	0.799
0.70	0.046	46.70	0.817
2.60	0.095	48.70	0.861
4.40	0.134	50.60	0.894
6.60	0.179	52.40	0.925
8.70	0.212	54.70	0.972
10.60	0.242	56.70	1.008
12.70	0.278	58.80	1.045
14.70	0.307	60.60	1.081
16.70	0.331	62.60	1.121
18.10	0.360	64.60	1.155
20.90	0.402	66.60	1.201
22.60	0.432	68.60	1.236
24.70	0.464	70.70	1.274
26.60	0.494	72.80	1.320
28.50	0.522	74.80	1.358
30.70	0.536	76.30	1.387
32.90	0.597	78.70	1.438
34.70	0.621	80.70	1.474
36.80	0.658	82.80	1.519
38.70	0.689	84.20	1.545



1430 F - 10.0 KSI CREEP DATA FOR PMHS4-A					
Time In Hours	Deformation %	Time In Hours	Deformation %	Time In Hours	Deformation %
0.10	0.015	123.00	0.400	203.30	0.687
0.30	0.020	125.10	0.405	205.20	0.693
0.50	0.024	127.40	0.411	207.20	0.698
0.70	0.024	129.20	0.420	208.90	0.704
1.60	0.033	130.98	0.424	211.40	0.713
3.00	0.043	133.00	0.429	213.20	0.722
5.20	0.050	135.00	0.437	215.50	0.733
7.30	0.057	136.90	0.442	217.20	0.735
9.20	0.066	139.10	0.449	218.80	0.741
11.40	0.072	141.20	0.453	221.30	0.752
15.20	0.085	143.20	0.470	223.20	0.758
19.30	0.098	145.20	0.475	225.30	0.768
23.40	0.116	146.60	0.479	227.40	0.779
26.80	0.121	149.00	0.490	229.40	0.783
31.20	0.135	151.30	0.492	231.10	0.792
35.40	0.140	153.10	0.499	233.20	0.805
39.20	0.153	154.80	0.505	235.70	0.814
43.00	0.162	157.00	0.513	237.20	0.820
47.40	0.176	159.40	0.518	239.10	0.825
51.60	0.187	160.90	0.525	241.30	0.831
55.40	0.198	163.30	0.531	243.40	0.838
59.30	0.209	165.10	0.540	245.20	0.850
63.20	0.220	167.30	0.548	247.40	0.860
67.30	0.230	169.20	0.553	249.10	0.864
71.30	0.241	170.80	0.568	251.40	0.875
75.30	0.252	173.20	0.569	253.20	0.879
79.30	0.262	175.30	0.572	255.20	0.888
83.30	0.273	177.20	0.584	257.30	0.899
87.40	0.283	179.40	0.588	259.00	0.910
91.80	0.294	181.20	0.595	261.20	0.919
95.60	0.305	183.30	0.608	263.60	0.921
98.90	0.316	185.20	0.615	265.30	0.936
103.40	0.326	187.50	0.626	266.90	0.941
106.90	0.337	189.20	0.630	269.30	0.956
110.90	0.348	191.30	0.638	271.40	0.960
113.00	0.359	193.10	0.647	273.30	0.971
114.80	0.370	194.90	0.656	275.20	0.976
117.50	0.383	197.30	0.658	277.00	0.982
119.30	0.383	199.30	0.661	278.80	0.993
121.20	0.392	201.20	0.677	280.90	1.002

SAMPLE	STRESS	TEMP.	SPECIMEN	TOTAL %EL.	RUPTURE
I.D.	(KSI/MPA)	(K)		(%)	(YES\NO)
ROUND B TESTS					
CWCR1BT	36/248	1050	THIN	0.74	YES
PMCR3BT	36/248	1050	THIN	0.54	NO
PMCR4BT	36/248	1050	THIN	0.55	NO
CWCR5BT	36/248	1050	THIN	0.73	YES
PMCR1BS	36/248	1050	STANDARD	0.51	NO
PMCR2BS	36/248	1050	STANDARD	0.51	NO
CWCR1BS	36/248	1050	STANDARD	0.284	NO
CWCR2BS	36/248	1050	STANDARD	0.284	NO



# Round B Thin Final Report

## LABORATORY REPORT

TO: Mechanical Technology Inc.  
Attn: Greg Migriditch  
P.O. Box 805  
Latham NY 12110

NUMBER: 1864-55281-1  
DATE: July 24, 1992  
AUTHORIZATION: 20302148  
Page 1 of 1

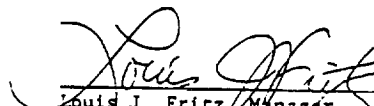
PROJECT: Creep Rupture Testing of (5) Udimer 720 Sheet Specimens Manufactured to Metcut D/N 741003-1 Mod. From Material Supplied and Identified by Mechanical Technology Inc.

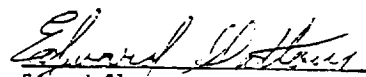
Testing is to ASTM E139.  
Nominal Gage Section: 0.030" t x 0.375" w x 1.5" long  
Temperature: 1430°F  
Stress: 36,000 psi

MRAI Number	Specimen Ident.	Time (hrs) to % Creep of					Final Creep	Duration (Hours)	Elong. (%)
		0.1	0.2	0.3	0.4	0.5			
C-61435	CW-CR-1-BT 462	2214	3914	-	-	-	.374	4416.5	.74
C-61436	CW-CR-2-BT -	-	-	-	-	-	-	497.9(a)	-
C-61437	PM-CR-3-BT 27	96	164	226	281	.542	.542	305.1(b)	-
C-61438	PM-CR-4-BT 44	126	192	253	308	.548	.548	330.1(b)	-
C-61531	CW-CR-5-BT 1904	3061	3779	4098	-	.460	.460	4116.7	.73

Notes: (a) Void test.  
(b) Test discontinued at time shown.

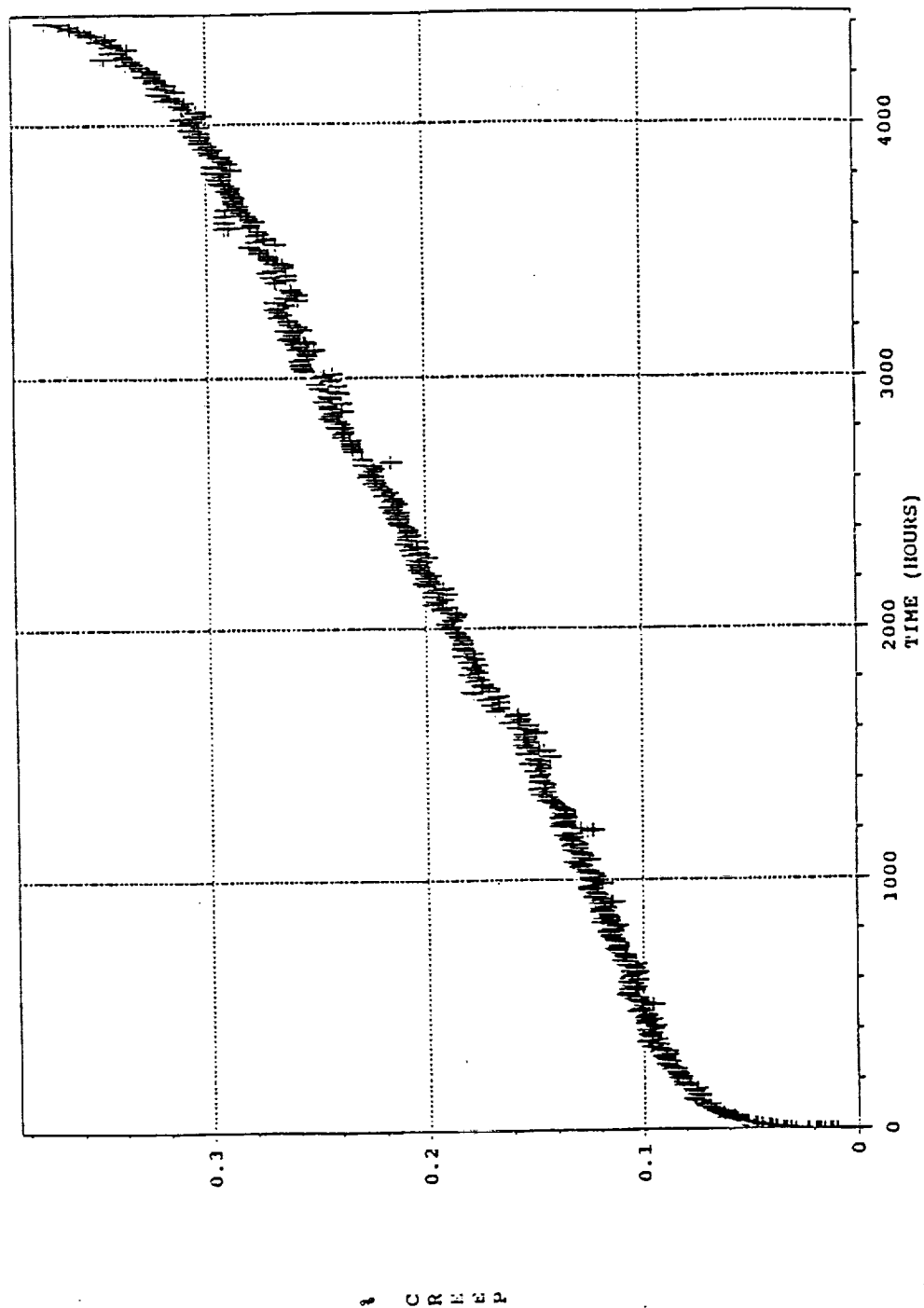
\* Full data tables are not available  
as of 1/20/93

  
Louis J. Fritz, Manager  
Creep, Stress Rupture & Tensile Testing  
EJ

  
Edward Slattery  
Supervisor

Metcut Research Associates Inc. • 5080 Rosslyn Drive • Cincinnati, Ohio 45209-1700  
Tel: (513) 271-5100 • Telex: 5131271-0511

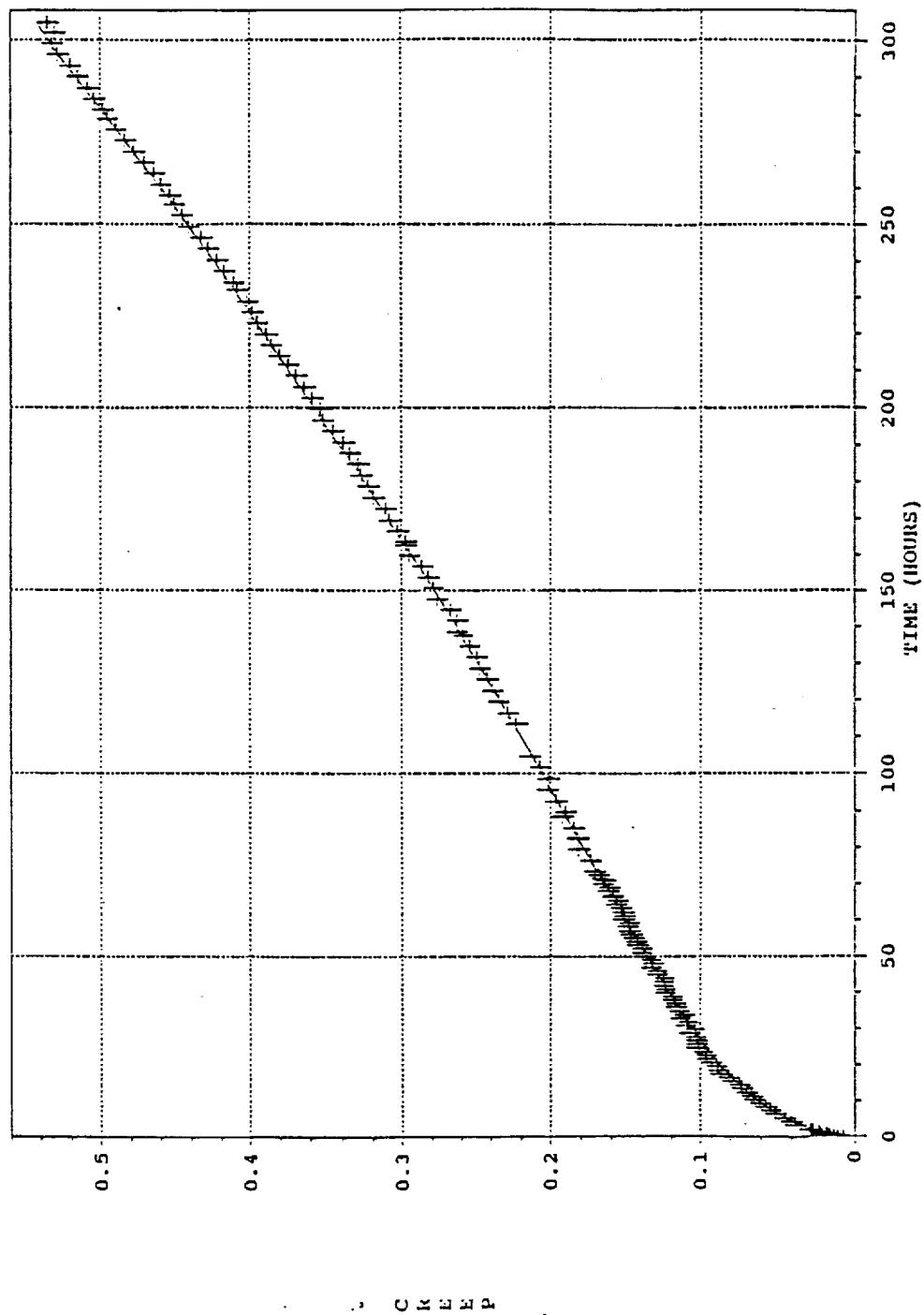
1864-55201 C61435 SPECIMEN NO CW-CR-1-DT 1430 F 36000 PSI  
 .11-462 HRS .21-2214 HRS



METCUT RESEARCH ASSOCIATES INC.  
 3580 Rosslyn Drive, Cincinnati, Ohio 45209 / (513) 271-5100

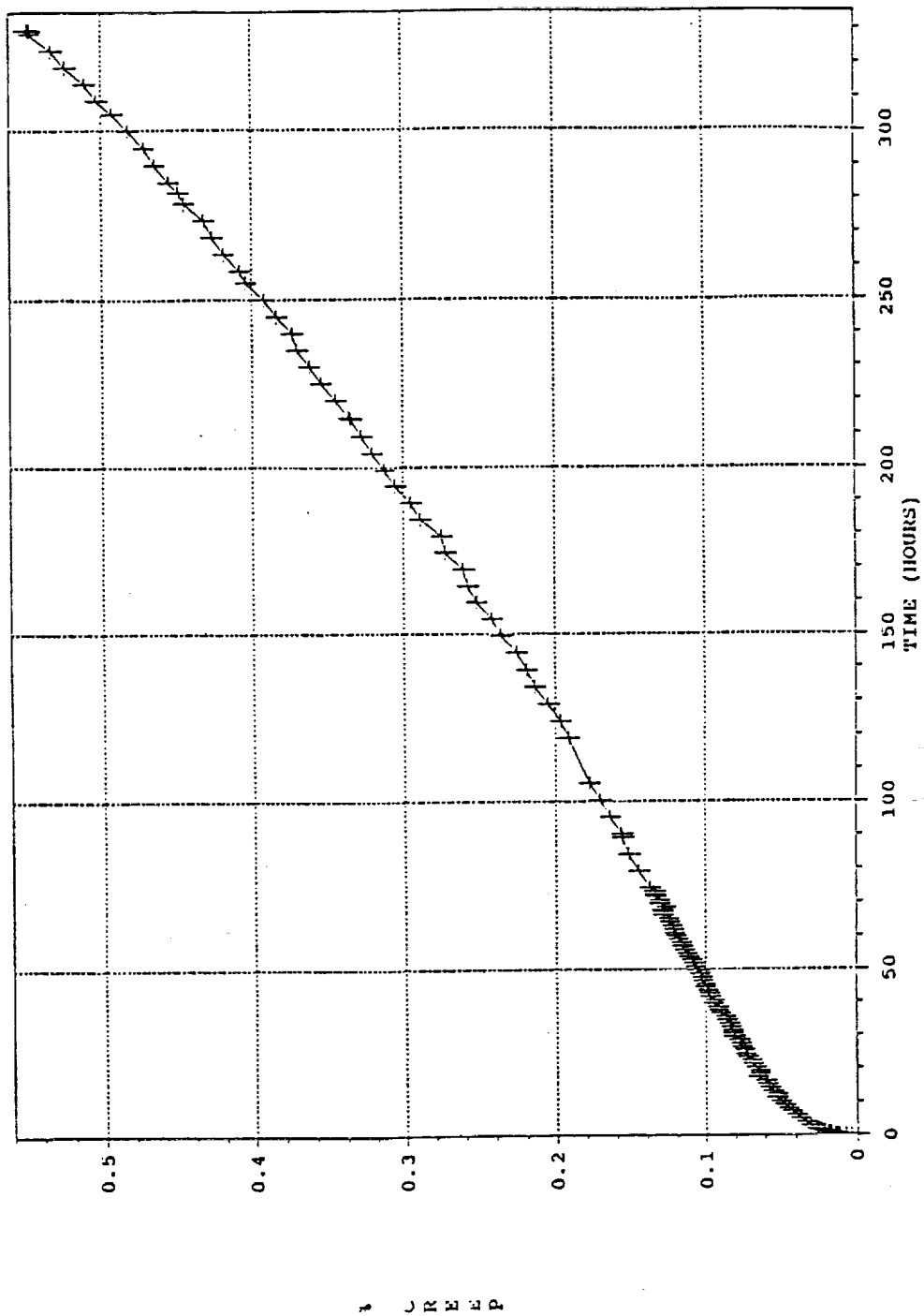


1864-55281 C61437 SPECIMEN NO PW-CR-3-BT 1430 F 36000 PSI  
 .13-27 HRS .23-96 HRS .53-281 HRS



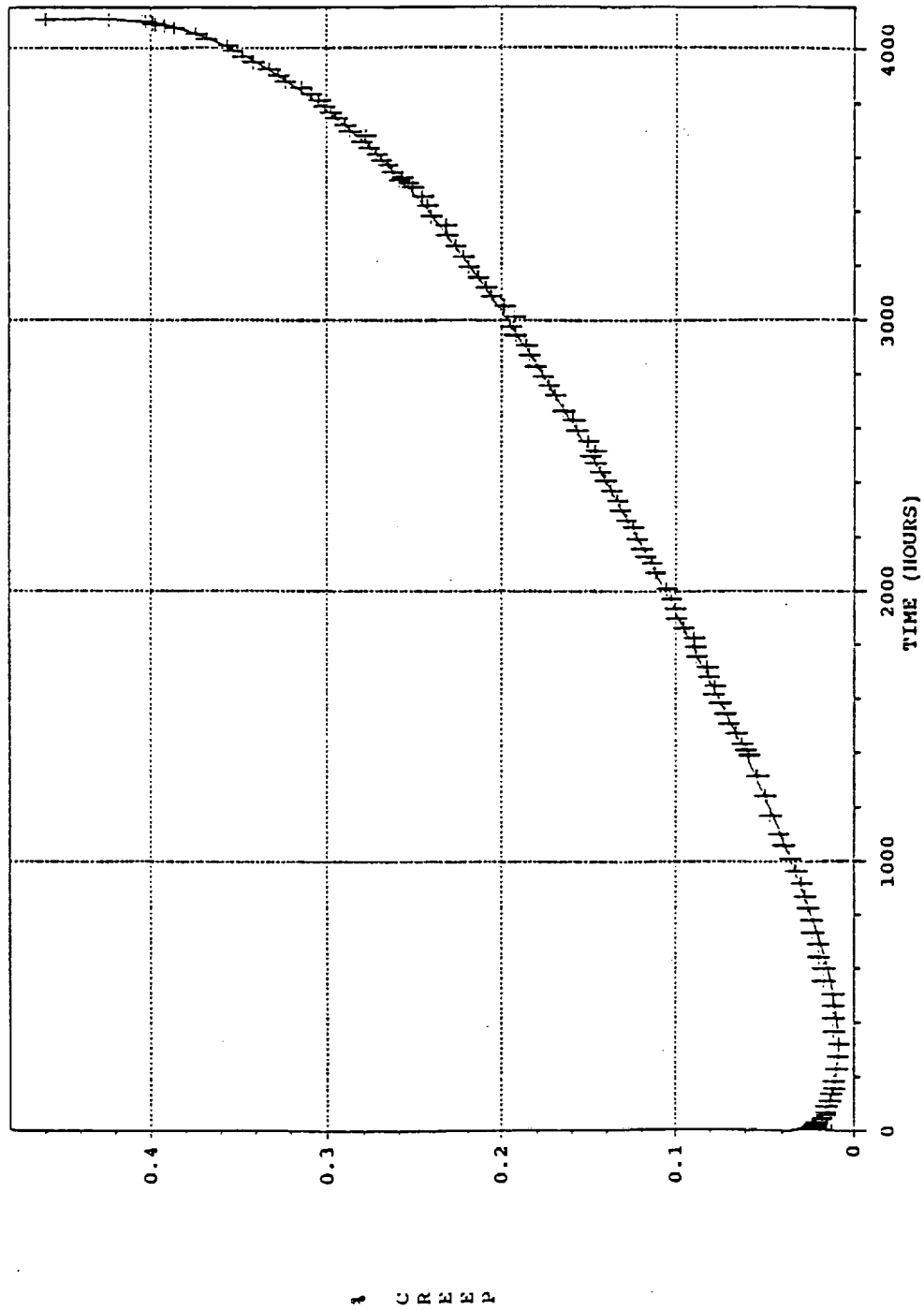
METCUT RESEARCH ASSOCIATES INC.  
 3980 Rosslyn Drive, Cincinnati, Ohio 45209 / (513) 271-5100

1864-55201 C61430 SPECIMEN NO PW-CR-4-QT 1430 F 36000 PSI  
 .11-44 HRS .21-126 HRS .51-308 HRS

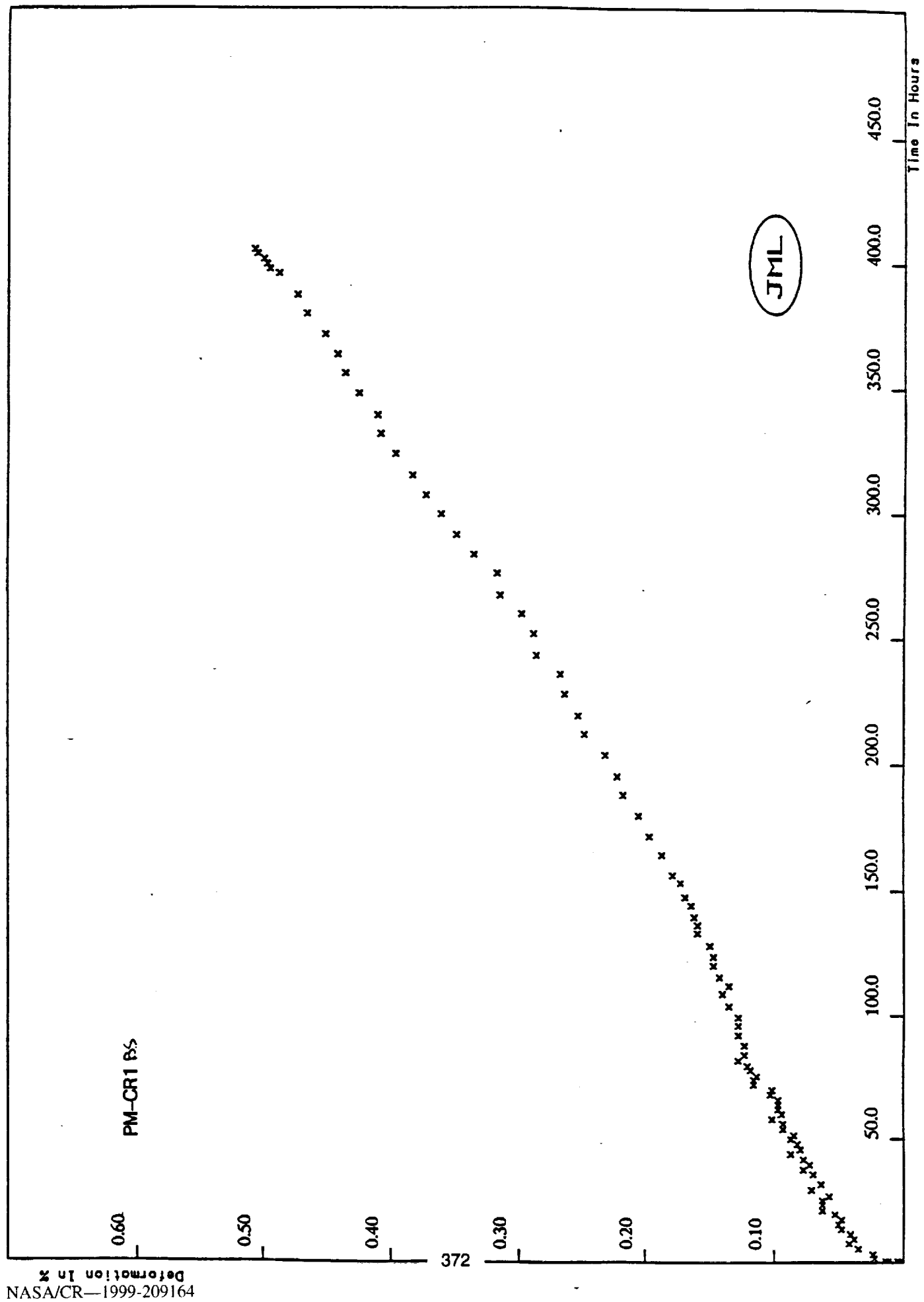


MEJOR RESEARCH ASSOCIATES INC.  
 3980 Rosslyn Drive, Cincinnati, Ohio 45209 / (513) 271-5100

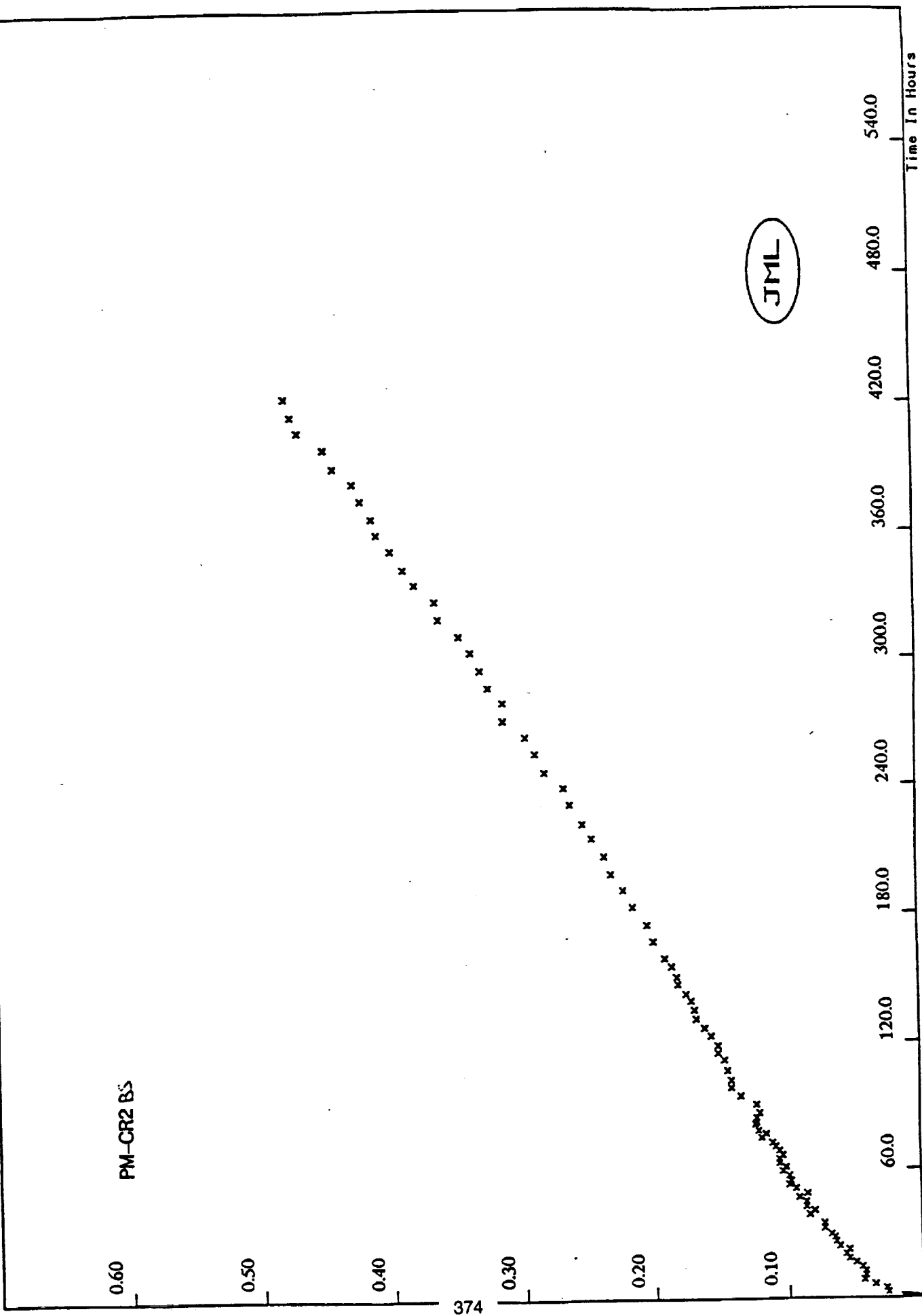
1864-55281 C61531 SPECIMEN NO CW-CK-5-DT 1430 F 36000 PSI  
 .11-1904 HRS .21-3061 HRS



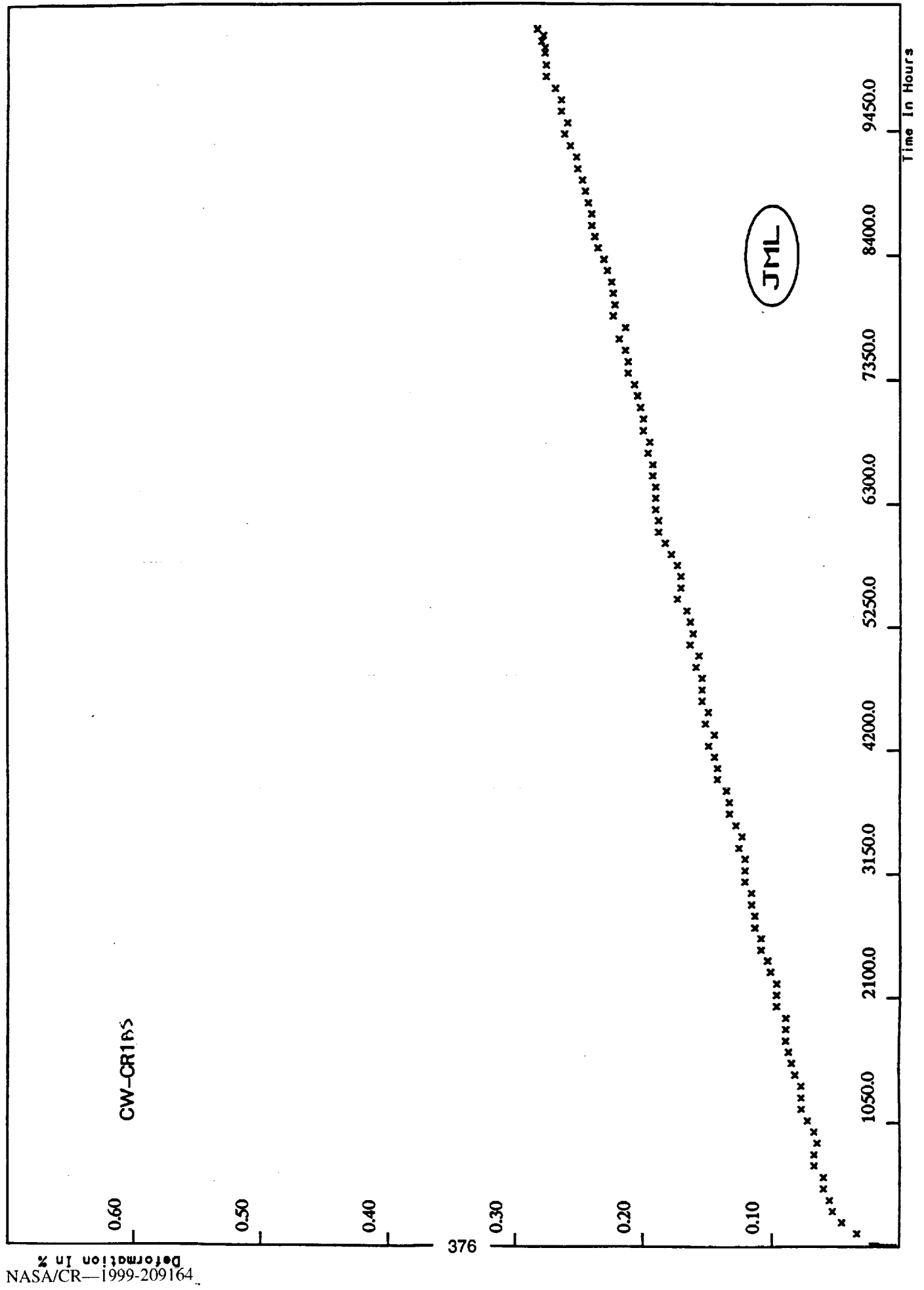
WILCOX RESEARCH ASSOCIATES INC.  
 3980 Rosslyn Drive, Cincinnati, Ohio 45209 / (513) 271-5100



1430 F - 36.0 KSI CREEP DATA FOR PM-CR185					
Time In Hours	Deformation %	Time In Hours	Deformation %	Time In Hours	Deformation %
0.10	0.002	61.80	0.096	187.80	0.217
0.30	0.012	63.60	0.096	195.20	0.221
0.50	0.005	65.60	0.096	203.70	0.231
0.70	0.014	67.80	0.102	212.00	0.248
1.60	0.023	69.60	0.101	219.30	0.253
3.30	0.024	71.80	0.115	227.90	0.263
5.60	0.035	73.70	0.115	235.70	0.267
7.80	0.042	75.20	0.113	243.20	0.286
9.60	0.038	77.60	0.118	251.90	0.289
11.70	0.041	79.40	0.120	259.90	0.298
13.70	0.048	81.50	0.128	267.20	0.315
15.70	0.051	83.80	0.123	275.90	0.318
17.70	0.048	87.70	0.123	283.30	0.336
19.80	0.053	91.80	0.128	291.30	0.349
21.40	0.063	95.80	0.128	299.70	0.361
23.60	0.063	99.10	0.128	307.30	0.373
25.50	0.063	103.70	0.135	315.20	0.384
27.10	0.058	108.70	0.140	323.80	0.397
29.60	0.071	111.90	0.135	331.90	0.409
32.00	0.064	115.30	0.142	339.10	0.411
35.90	0.070	119.80	0.147	347.80	0.426
37.70	0.077	123.30	0.147	355.80	0.437
39.60	0.072	127.60	0.149	363.30	0.443
41.70	0.077	132.70	0.159	371.50	0.452
43.80	0.087	135.90	0.159	379.70	0.467
45.60	0.079	139.20	0.161	387.10	0.474
47.90	0.082	143.80	0.164	395.80	0.488
49.80	0.087	147.20	0.168	397.60	0.496
51.30	0.084	152.80	0.172	399.60	0.498
53.80	0.093	155.90	0.178	401.60	0.500
56.00	0.093	163.80	0.186	403.80	0.505
57.80	0.101	171.30	0.196	405.50	0.507
59.80	0.094	179.70	0.205		

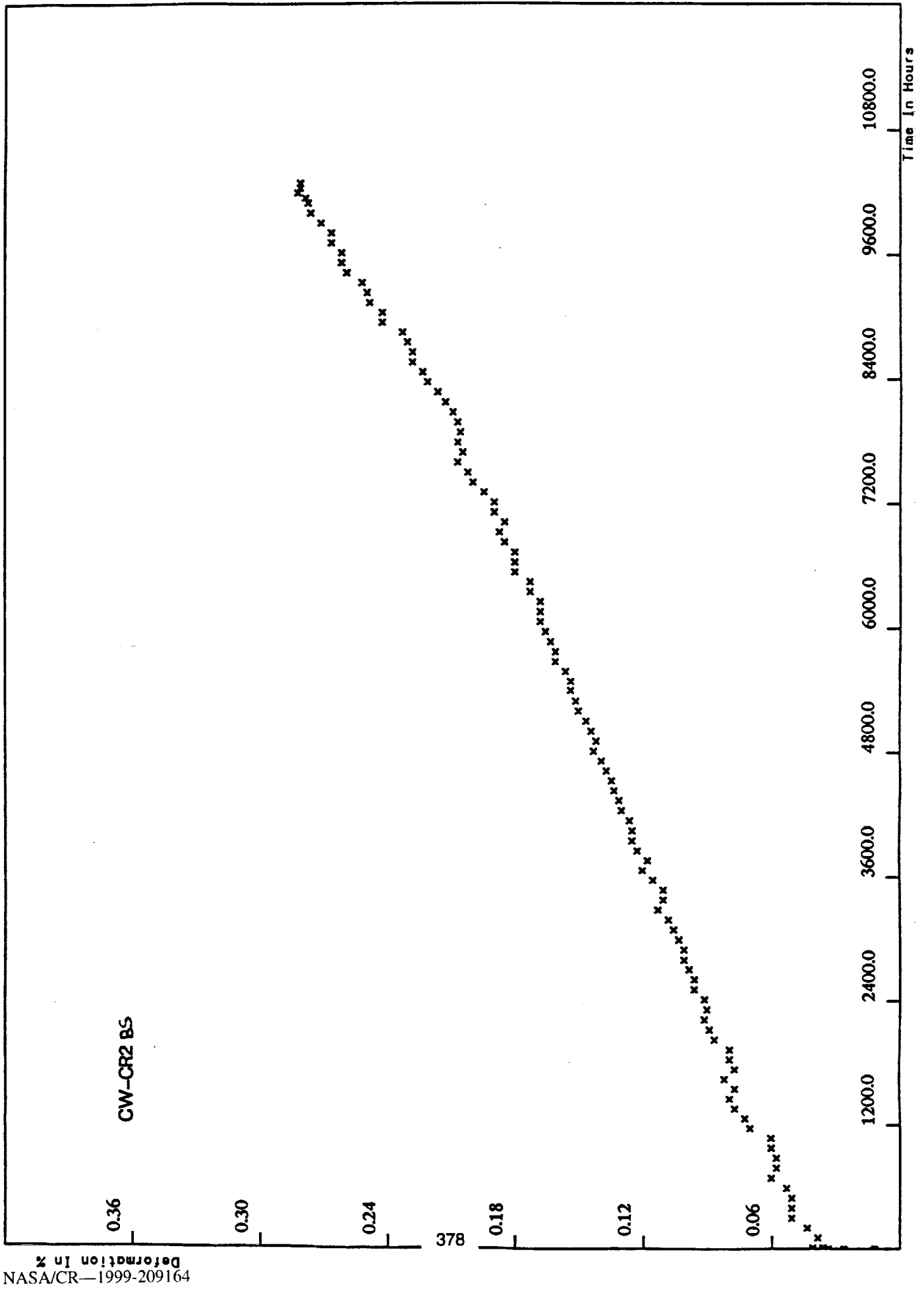


1430 F - 36.0 KIS CREEP DATA FOR PM-CR2 85					
Time In Hours	Deformation %	Time In Hours	Deformation %	Time In Hours	Deformation %
0.10	0.002	61.30	0.101	174.80	0.203
0.30	0.007	63.20	0.106	183.20	0.214
0.50	0.010	65.20	0.106	191.20	0.221
0.70	0.012	67.10	0.103	198.70	0.231
0.90	0.014	69.10	0.106	207.20	0.236
3.00	0.026	71.20	0.108	215.50	0.245
5.00	0.028	73.00	0.111	222.10	0.252
6.80	0.036	75.30	0.119	231.30	0.262
9.00	0.044	77.20	0.115	239.20	0.267
11.30	0.043	78.70	0.121	246.60	0.281
13.10	0.043	81.70	0.124	255.30	0.288
15.20	0.046	82.80	0.123	263.30	0.296
17.10	0.050	85.00	0.123	270.70	0.313
19.10	0.055	87.20	0.120	279.30	0.313
21.10	0.058	91.20	0.123	286.60	0.323
23.20	0.055	95.30	0.135	294.80	0.329
24.80	0.063	99.20	0.142	303.10	0.337
27.00	0.065	102.60	0.142	310.80	0.345
29.00	0.066	107.20	0.144	318.70	0.361
30.50	0.069	112.20	0.147	327.20	0.363
33.10	0.073	115.30	0.151	335.30	0.379
35.40	0.073	118.80	0.151	342.60	0.387
39.30	0.084	123.20	0.156	351.30	0.397
41.20	0.081	126.70	0.161	359.20	0.407
43.00	0.087	131.00	0.167	366.70	0.411
45.20	0.087	135.20	0.168	375.10	0.419
47.30	0.091	139.30	0.171	383.10	0.425
49.10	0.085	142.60	0.174	390.50	0.440
51.30	0.094	147.20	0.180	399.20	0.447
53.30	0.099	150.60	0.181	407.30	0.466
54.80	0.097	155.50	0.185	414.60	0.471
57.30	0.099	159.30	0.190	423.20	0.476
59.50	0.103	167.30	0.198		



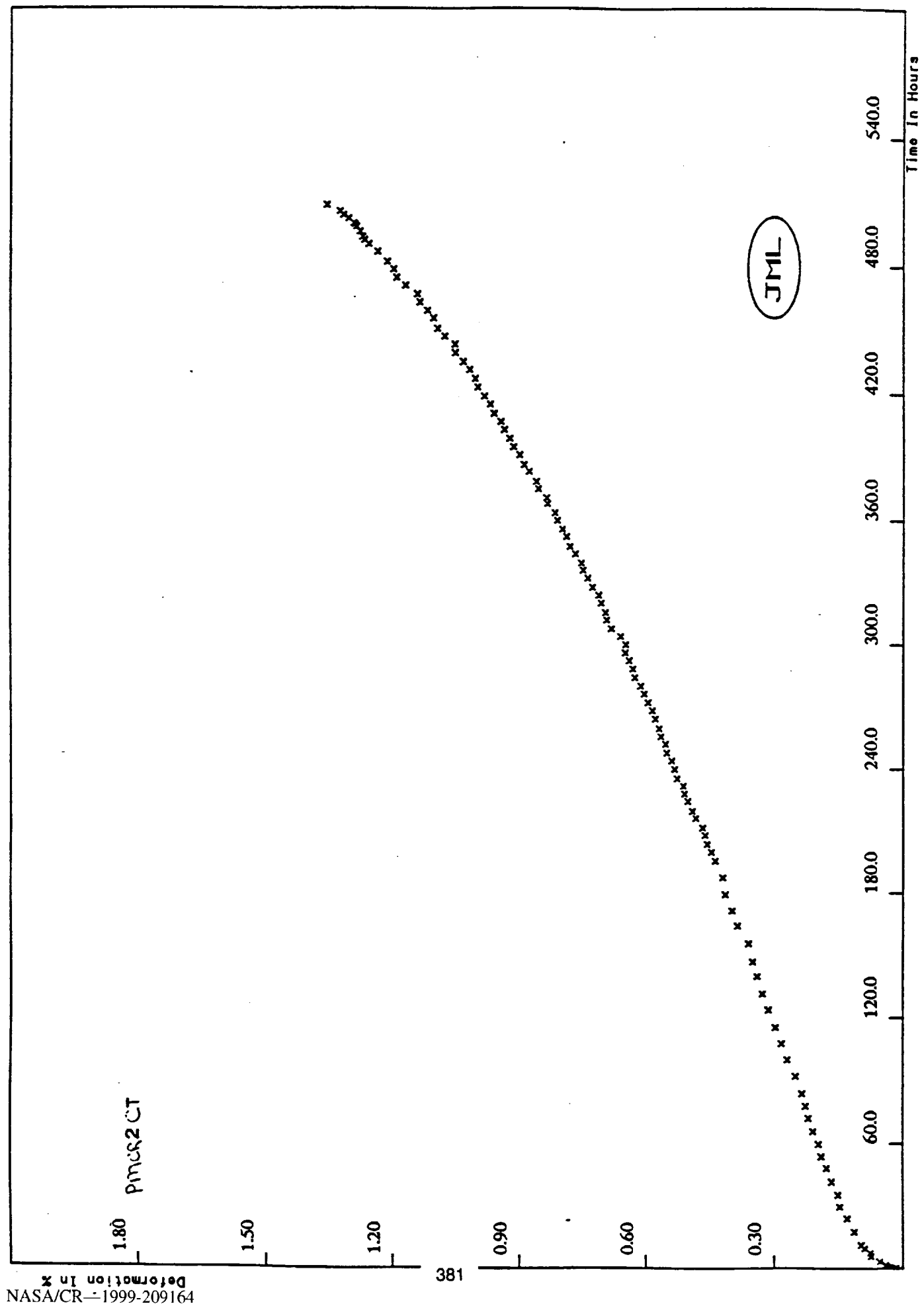


1430 F - 36.0 KSI CREEP DATA FOR CW-CR165					
Time In Hours	Deformation %	Time In Hours	Deformation %	Time In Hours	Deformation %
0.10	0.005	2987.20	0.115	6827.30	0.195
0.30	0.005	3083.80	0.120	6924.00	0.200
0.50	0.007	3179.70	0.120	7020.40	0.200
0.70	0.012	3275.90	0.120	7117.00	0.202
2.60	0.014	3371.40	0.125	7212.70	0.204
4.30	0.018	3467.30	0.123	7309.00	0.207
6.60	0.022	3563.70	0.127	7404.80	0.212
8.80	0.019	3659.40	0.132	7500.60	0.212
10.60	0.022	3755.70	0.132	7596.90	0.214
12.70	0.019	3851.80	0.135	7692.40	0.219
109.80	0.034	3948.00	0.142	7787.30	0.214
204.80	0.046	4043.80	0.142	7884.80	0.224
300.70	0.053	4139.60	0.144	7980.80	0.222
396.80	0.055	4235.90	0.149	8076.90	0.224
492.80	0.060	4331.60	0.144	8172.00	0.225
588.90	0.060	4427.80	0.152	8269.00	0.228
684.50	0.067	4524.00	0.149	8364.40	0.231
781.00	0.067	4619.50	0.154	8461.70	0.236
876.60	0.065	4715.50	0.154	8557.00	0.238
972.50	0.067	4811.30	0.154	8652.30	0.240
1068.80	0.072	4908.20	0.159	8748.80	0.240
1164.90	0.077	5003.60	0.156	8844.50	0.243
1260.90	0.077	5100.10	0.164	8940.80	0.245
1356.70	0.077	5195.80	0.161	9036.40	0.248
1452.10	0.082	5291.90	0.164	9132.90	0.251
1548.60	0.084	5387.80	0.166	9228.90	0.253
1644.30	0.087	5483.60	0.173	9324.90	0.257
1740.70	0.089	5580.00	0.171	9420.90	0.262
1836.70	0.089	5675.60	0.171	9516.50	0.260
1932.80	0.089	5771.90	0.173	9612.90	0.265
2028.90	0.096	5867.60	0.178	9708.60	0.265
2124.40	0.096	5963.90	0.183	9804.70	0.269
2219.90	0.096	6060.00	0.188	9900.80	0.277
2315.30	0.101	6155.40	0.188	9996.80	0.277
2412.00	0.103	6252.00	0.190	10092.80	0.278
2507.80	0.108	6347.00	0.190	10140.80	0.278
2603.80	0.108	6444.00	0.190	10188.50	0.280
2695.90	0.113	6540.00	0.192	10236.80	0.279
2795.30	0.113	6636.00	0.192	10284.90	0.284
2891.80	0.115	6732.10	0.196	10290.80	0.284

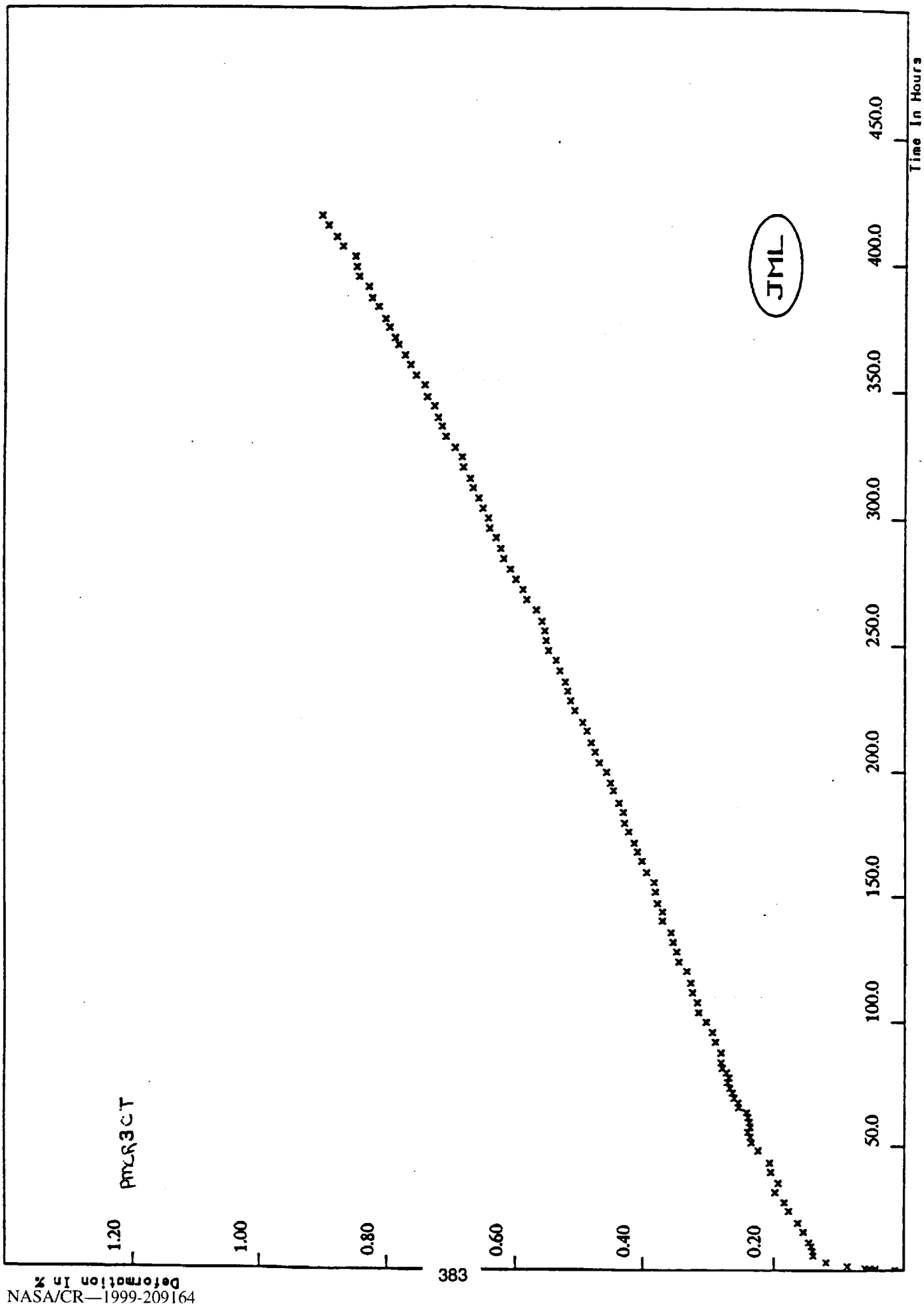


1430 F - 36.0 KSI CREEP DATA FOR CW-CR2 85					
Time In Hours	Deformation %	Time In Hours	Deformation %	Time In Hours	Deformation %
0.10	0.012	2986.30	0.103	6826.40	0.185
0.30	0.034	3082.90	0.106	6923.10	0.188
0.50	0.026	3178.80	0.108	7019.40	0.185
0.70	0.034	3274.90	0.113	7116.10	0.190
1.70	0.036	3370.50	0.111	7211.80	0.190
3.40	0.041	3466.40	0.111	7308.00	0.195
5.60	0.041	3562.80	0.115	7403.90	0.200
7.90	0.041	3658.40	0.120	7499.60	0.202
9.70	0.041	3754.80	0.118	7596.00	0.207
11.80	0.036	3850.90	0.123	7691.40	0.205
108.90	0.038	3947.00	0.125	7788.30	0.207
203.90	0.043	4042.90	0.125	7883.80	0.206
299.70	0.051	4138.60	0.126	7979.80	0.207
395.90	0.051	4235.00	0.130	8075.90	0.209
491.90	0.051	4330.60	0.131	8171.00	0.213
588.00	0.053	4426.90	0.134	8268.00	0.217
683.60	0.060	4523.10	0.135	8363.40	0.221
780.00	0.058	4618.60	0.137	8460.10	0.224
875.70	0.058	4714.60	0.140	8556.00	0.229
971.60	0.060	4810.40	0.143	8651.30	0.229
1067.90	0.060	4907.30	0.142	8747.80	0.231
1164.00	0.070	5002.60	0.144	8843.60	0.233
1260.00	0.072	5099.10	0.147	8939.90	0.243
1355.80	0.077	5194.90	0.150	9035.40	0.243
1451.40	0.079	5291.00	0.152	9131.90	0.249
1547.70	0.077	5396.90	0.154	9227.90	0.250
1643.30	0.082	5482.70	0.154	9324.00	0.253
1739.80	0.077	5579.10	0.156	9419.90	0.260
1835.80	0.079	5674.70	0.161	9515.50	0.262
1931.90	0.079	5770.90	0.161	9611.90	0.262
2028.00	0.087	5866.70	0.164	9707.60	0.267
2123.50	0.089	5963.00	0.166	9803.70	0.267
2218.90	0.091	6059.00	0.168	9899.80	0.272
2314.40	0.090	6154.50	0.168	9995.90	0.277
2411.00	0.091	6251.00	0.168	10091.90	0.278
2506.90	0.096	6346.70	0.173	10139.80	0.279
2602.90	0.096	6443.00	0.173	10187.50	0.283
2698.80	0.099	6539.10	0.180	10235.90	0.282
2794.00	0.101	6635.10	0.180	10284.00	0.282
2890.80	0.101	6731.10	0.180	10289.80	0.284

SAMPLE	STRESS	TEMP.	SPECIMEN	TOTAL %EL.	RUPTURE
I.D.	(KSI/MPA)	(K)		(%)	(YES\NO)
		ROUND C TESTS			
+ PMCR2C	36/248	1050	THIN	1.5	YES
+ PMCR3C	36/248	1050	THIN	1.0	YES



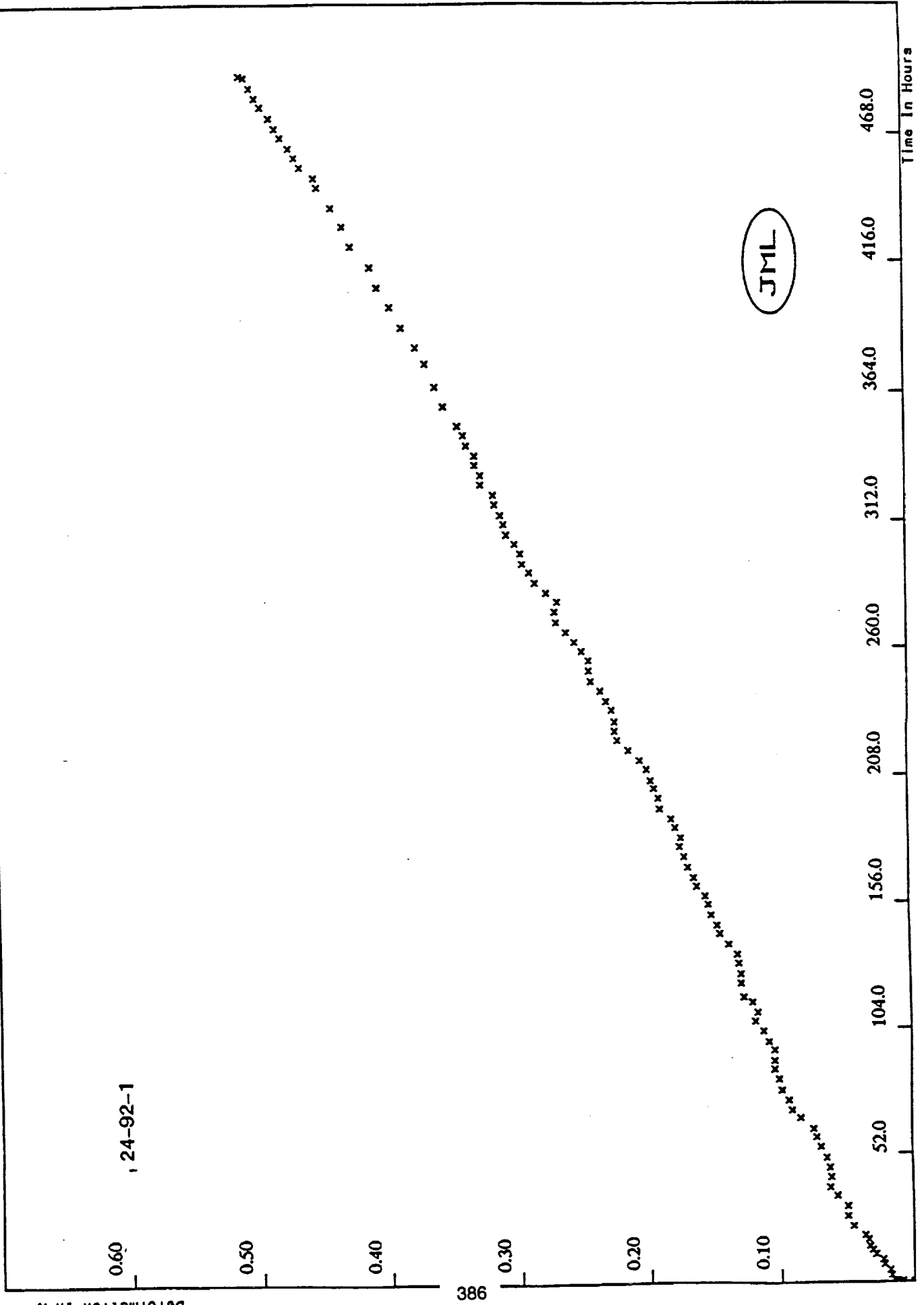
1430 F - 36.0 KSI CREEP DATA FOR PMQRZ-CT					
Time In Hours	Deformation %	Time In Hours	Deformation %	Time In Hours	Deformation %
0.10	0.016	216.00	0.482	374.70	0.856
0.60	0.030	219.30	0.490	378.10	0.861
0.80	0.036	224.10	0.501	382.90	0.878
1.00	0.040	227.80	0.510	386.20	0.890
1.80	0.040	231.60	0.512	390.80	0.901
3.30	0.054	235.20	0.527	394.70	0.915
6.00	0.074	239.80	0.533	398.60	0.924
7.70	0.076	243.80	0.540	402.70	0.937
9.80	0.089	247.70	0.552	406.70	0.945
11.40	0.098	251.80	0.555	410.40	0.961
17.70	0.113	255.50	0.566	414.80	0.970
24.10	0.129	259.20	0.570	418.70	0.984
29.80	0.146	263.70	0.579	422.70	1.000
35.40	0.150	267.70	0.587	426.70	1.006
41.60	0.165	271.70	0.596	431.00	1.019
48.10	0.177	275.70	0.605	434.60	1.034
53.70	0.189	279.60	0.614	438.80	1.053
59.60	0.195	283.80	0.627	442.80	1.054
65.60	0.208	288.00	0.632	446.60	1.078
71.70	0.219	292.10	0.641	450.20	1.095
77.60	0.227	295.80	0.650	455.10	1.105
83.60	0.234	299.80	0.649	458.80	1.119
91.90	0.249	303.70	0.661	462.70	1.137
99.90	0.268	307.60	0.683	466.70	1.143
107.70	0.282	311.70	0.694	470.70	1.171
115.60	0.296	315.30	0.697	474.60	1.193
123.90	0.312	319.90	0.707	478.70	1.199
131.70	0.326	323.80	0.713	482.20	1.214
140.10	0.338	327.60	0.729	486.90	1.237
147.20	0.348	331.90	0.739	490.70	1.258
155.80	0.358	335.90	0.750	492.60	1.268
164.20	0.384	339.20	0.755	494.00	1.273
171.30	0.396	343.70	0.768	496.50	1.279
179.30	0.412	347.30	0.781	498.90	1.287
187.30	0.418	351.90	0.789	500.00	1.291
195.40	0.436	355.70	0.799	500.50	1.294
199.70	0.444	359.80	0.811	502.80	1.306
203.40	0.455	363.30	0.817	504.50	1.318
207.70	0.460	367.80	0.835	506.10	1.326
211.30	0.466	370.50	0.837	508.90	1.357



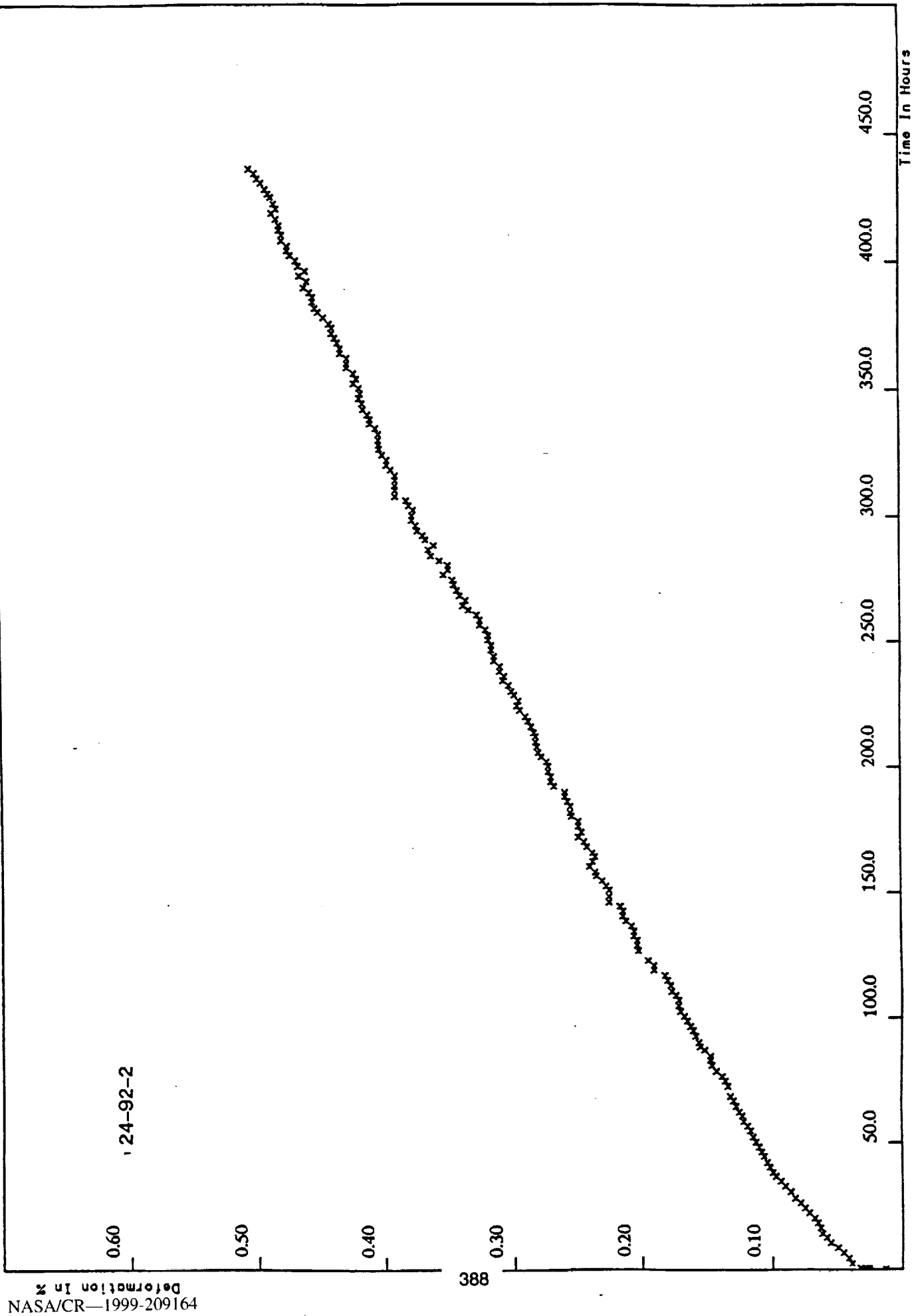
1430 F - 36.0 KSI CREEP DATA FOR PMCR3CT					
Time In Hours	Deformation %	Time In Hours	Deformation %	Time In Hours	Deformation %
0.10	0.014	103.70	0.314	263.60	0.568
0.60	0.044	107.70	0.317	267.70	0.583
0.80	0.052	111.60	0.324	271.70	0.590
1.00	0.060	115.50	0.326	275.70	0.601
1.80	0.087	120.10	0.333	279.60	0.609
3.30	0.120	123.80	0.345	283.80	0.620
6.00	0.139	127.80	0.348	287.90	0.624
7.80	0.140	131.70	0.354	292.10	0.632
9.80	0.143	135.50	0.357	295.80	0.642
11.40	0.146	140.10	0.370	299.80	0.644
15.70	0.154	143.80	0.370	303.70	0.653
19.30	0.163	147.20	0.378	307.60	0.659
24.10	0.177	151.80	0.381	311.70	0.668
27.60	0.184	155.70	0.383	315.30	0.672
31.70	0.198	159.70	0.394	319.90	0.683
35.40	0.194	164.20	0.401	323.80	0.685
39.70	0.205	167.80	0.408	327.50	0.696
43.30	0.207	171.30	0.413	331.90	0.710
48.10	0.224	175.90	0.422	335.90	0.717
51.40	0.234	179.30	0.429	339.20	0.722
53.60	0.236	183.70	0.431	343.70	0.729
55.70	0.239	187.30	0.437	347.20	0.740
57.70	0.236	192.30	0.446	351.90	0.744
59.60	0.237	195.40	0.450	355.70	0.757
61.60	0.239	199.70	0.457	359.80	0.766
63.60	0.242	203.40	0.468	363.60	0.775
65.60	0.253	207.70	0.474	367.80	0.784
67.60	0.255	211.30	0.481	370.50	0.790
69.50	0.261	216.00	0.487	374.60	0.799
71.60	0.263	219.30	0.494	378.00	0.805
73.50	0.268	224.00	0.507	382.90	0.816
75.80	0.271	227.80	0.513	386.20	0.826
77.60	0.269	231.60	0.518	390.70	0.831
79.70	0.273	235.20	0.522	394.70	0.846
81.50	0.279	239.70	0.531	398.50	0.851
83.60	0.281	243.80	0.536	402.70	0.853
87.50	0.281	247.70	0.548	406.60	0.872
91.80	0.289	251.70	0.553	410.40	0.882
95.60	0.294	255.50	0.555	414.80	0.895
99.90	0.304	259.20	0.559	418.70	0.905



SAMPLE	STRESS	TEMP.	SPECIMEN	TOTAL %EL.	RUPTURE
I.D.	(KSI/MPA)	(K)		(%)	(YES\NO)
			ROUND D TESTS		
24-92-1	36/248	1050	THIN	0.5	NO
24-92-2	36/248	1050	THIN	0.5	NO



1430 F - 36.0 KSI CREEP DATA FOR 24-92-1					
Time In Hours	Deformation %	Time In Hours	Deformation %	Time In Hours	Deformation %
0.10	0.000	131.00	0.130	291.30	0.288
0.30	0.009	134.70	0.131	294.90	0.294
0.50	0.013	138.90	0.138	299.20	0.295
0.70	0.015	143.10	0.144	303.10	0.299
2.80	0.017	146.70	0.146	306.90	0.306
4.80	0.018	150.90	0.151	311.20	0.308
7.10	0.023	155.20	0.153	314.90	0.310
9.00	0.024	158.80	0.155	319.30	0.314
11.00	0.029	162.80	0.161	323.10	0.315
12.90	0.031	166.20	0.164	327.30	0.325
14.40	0.033	170.60	0.168	331.00	0.325
17.10	0.034	174.90	0.171	335.30	0.329
18.90	0.037	179.10	0.174	339.00	0.329
22.80	0.045	182.70	0.173	343.20	0.336
26.80	0.050	186.90	0.178	347.40	0.338
30.80	0.050	190.50	0.181	351.20	0.342
35.10	0.057	194.60	0.189	359.00	0.353
38.60	0.062	199.10	0.190	366.70	0.359
42.80	0.061	203.10	0.194	375.90	0.367
46.70	0.062	206.30	0.196	382.50	0.375
50.60	0.065	211.00	0.199	390.50	0.385
55.10	0.069	214.60	0.204	398.60	0.394
59.10	0.072	218.70	0.213	406.50	0.404
62.60	0.074	222.90	0.222	414.60	0.409
67.20	0.084	226.50	0.224	423.10	0.424
70.60	0.090	230.40	0.224	431.20	0.430
74.70	0.093	235.00	0.226	438.80	0.439
78.90	0.098	238.50	0.230	447.10	0.450
83.30	0.100	242.60	0.235	450.80	0.452
87.30	0.103	246.70	0.242	455.10	0.463
90.80	0.103	250.90	0.243	459.10	0.467
95.10	0.103	255.20	0.243	462.90	0.471
98.70	0.108	259.00	0.249	467.20	0.478
103.00	0.112	262.70	0.254	471.00	0.482
107.10	0.118	266.80	0.260	475.00	0.486
110.70	0.116	270.90	0.268	479.40	0.493
115.00	0.121	275.20	0.269	483.00	0.497
117.10	0.127	279.20	0.267	486.90	0.502
122.90	0.129	282.90	0.276	491.10	0.506
126.60	0.129	287.10	0.284	491.70	0.509



1430 F - 36.0 KSI CREEP DATA FOR 24-92-2					
Time In Hours	Deformation %	Time In Hours	Deformation %	Time In Hours	Deformation %
0.10	0.013	76.60	0.139	158.50	0.236
0.30	0.026	78.90	0.143	160.90	0.241
0.50	0.028	81.10	0.146	162.80	0.238
0.70	0.033	83.30	0.147	164.80	0.236
2.50	0.039	84.90	0.147	166.30	0.238
4.70	0.041	87.30	0.152	168.90	0.243
6.80	0.046	88.70	0.155	170.80	0.245
8.90	0.050	90.40	0.156	172.70	0.249
10.90	0.055	92.90	0.158	174.60	0.247
13.00	0.059	95.20	0.160	177.00	0.249
14.50	0.062	96.60	0.163	179.00	0.249
16.90	0.063	98.80	0.165	181.00	0.255
18.90	0.065	100.70	0.167	182.40	0.256
20.70	0.067	102.60	0.170	184.90	0.256
22.90	0.072	104.90	0.171	186.80	0.258
24.60	0.075	107.00	0.171	188.90	0.260
26.70	0.078	109.00	0.173	190.30	0.260
28.50	0.082	110.50	0.177	192.90	0.269
31.00	0.086	112.80	0.178	194.70	0.271
33.20	0.090	114.80	0.180	196.70	0.271
35.10	0.093	116.90	0.182	198.60	0.273
37.00	0.098	119.00	0.191	200.80	0.273
38.50	0.100	120.90	0.191	202.70	0.274
40.60	0.102	122.90	0.195	204.60	0.279
42.50	0.104	126.80	0.203	206.30	0.281
45.00	0.106	129.00	0.204	208.70	0.282
46.60	0.108	131.00	0.204	210.70	0.283
48.60	0.111	132.90	0.206	212.90	0.283
50.60	0.113	134.60	0.206	214.40	0.284
52.70	0.115	136.80	0.208	216.60	0.286
55.10	0.117	138.90	0.212	218.80	0.288
57.00	0.119	140.90	0.215	220.60	0.290
58.90	0.122	142.80	0.215	223.10	0.295
61.00	0.124	144.70	0.217	224.90	0.297
62.50	0.126	146.40	0.225	226.90	0.296
64.90	0.128	148.70	0.225	229.20	0.299
67.00	0.130	151.10	0.225	230.50	0.301
68.60	0.132	152.90	0.228	233.00	0.303
72.70	0.134	155.00	0.231	234.80	0.308
74.90	0.137	157.00	0.235	236.50	0.307

1430 F - 36.0 KSI CREEP DATA FOR 24-92-2					
Time In Hours	Deformation %	Time In Hours	Deformation %	Time In Hours	Deformation %
238.50	0.310	306.90	0.381	374.60	0.440
240.50	0.310	308.50	0.390	376.20	0.442
242.70	0.314	311.00	0.390	378.60	0.446
244.50	0.314	312.70	0.390	380.90	0.451
247.00	0.316	314.80	0.390	382.30	0.453
248.80	0.316	316.60	0.390	384.80	0.455
251.00	0.319	319.00	0.393	386.70	0.455
252.70	0.319	320.90	0.397	388.50	0.457
255.00	0.321	322.90	0.397	390.30	0.462
256.80	0.325	324.90	0.400	392.90	0.459
258.80	0.325	327.20	0.402	395.00	0.465
260.90	0.327	328.70	0.403	396.90	0.461
262.80	0.334	330.60	0.403	398.60	0.466
264.50	0.338	332.90	0.403	400.90	0.468
266.70	0.336	335.10	0.405	402.80	0.472
268.50	0.340	337.00	0.410	404.60	0.475
270.60	0.342	338.60	0.410	406.30	0.475
273.00	0.345	340.50	0.412	408.50	0.479
274.90	0.346	342.70	0.415	410.70	0.479
277.00	0.352	345.00	0.416	412.60	0.481
279.00	0.349	347.00	0.418	414.40	0.481
280.90	0.349	348.90	0.417	416.80	0.483
282.70	0.355	351.00	0.418	419.10	0.487
284.70	0.362	352.80	0.423	420.90	0.483
287.10	0.364	354.70	0.420	422.90	0.485
288.90	0.360	356.80	0.423	425.50	0.488
291.10	0.366	359.10	0.428	426.80	0.490
292.80	0.368	360.70	0.428	428.70	0.492
294.70	0.373	362.80	0.428	431.20	0.495
296.90	0.374	364.60	0.433	432.80	0.498
299.00	0.377	366.50	0.433	435.00	0.501
300.90	0.377	368.90	0.436	436.70	0.505
303.20	0.376	370.70	0.438		
304.80	0.379	372.50	0.440		

SAMPLE	STRESS	TEMP.	SPECIMEN	TOTAL %EL.	RUPTURE
I.D.	(KSI/MPA)	(K)		(%)	(YES\NO)
	ROUND E TESTS				
E1A	36/248	1095	STANDARD	4.7	YES
E1B	36/248	1095	STANDARD	3.2	YES
E2A	10/69	1110	THIN	0.5	NO
E2B	10/69	1110	THIN	0.5	NO

1.80

1.50

1.20

0.90

0.60

0.30

E1A

JML

2700.0

2400.0

2100.0

1800.0

1500.0

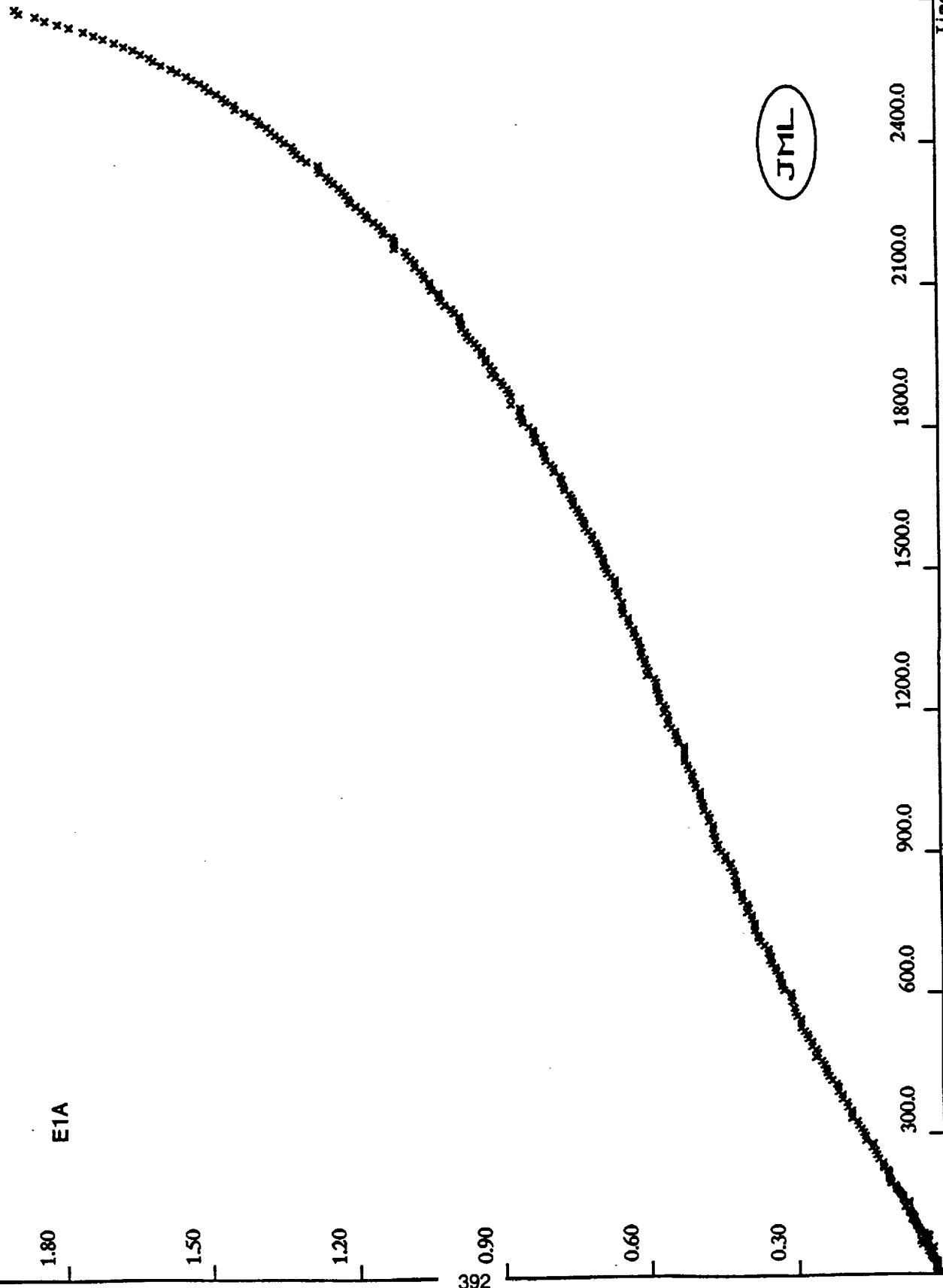
1200.0

900.0

600.0

300.0

Time In Hours



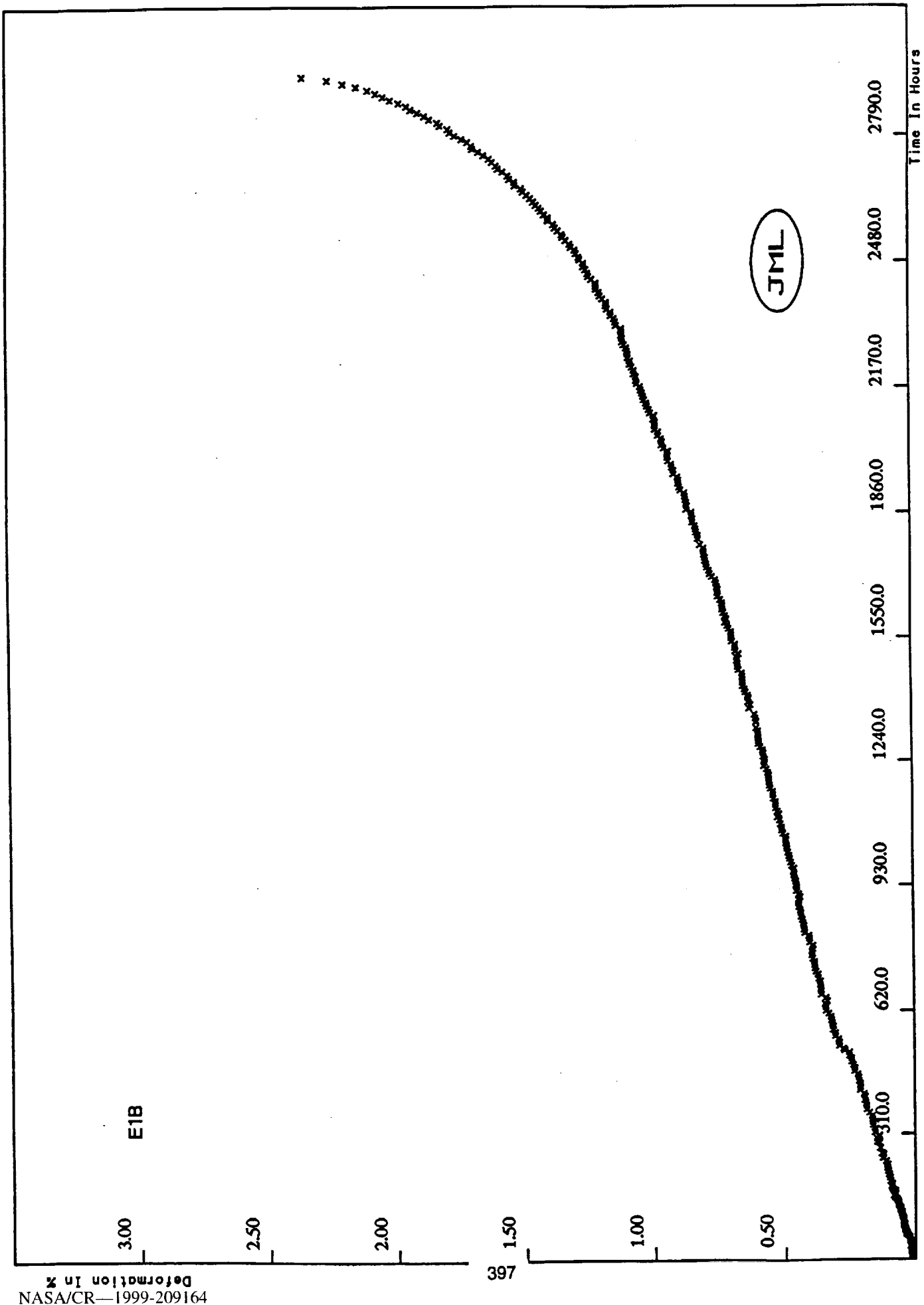


1512 F - 36.0 KSI CREEP DATA FOR E1A					
Time In Hours	Deformation %	Time In Hours	Deformation %	Time In Hours	Deformation %
0.10	0.008	75.40	0.040	174.80	0.094
0.30	0.008	77.90	0.042	179.30	0.097
0.50	0.011	79.40	0.040	183.40	0.101
0.70	0.015	81.60	0.036	187.60	0.101
3.50	0.015	83.80	0.040	191.20	0.103
5.10	0.019	85.70	0.055	195.00	0.111
7.30	0.019	87.80	0.046	199.10	0.111
9.70	0.019	89.80	0.054	203.80	0.113
11.70	0.021	91.80	0.054	207.30	0.115
13.90	0.019	93.90	0.057	211.40	0.115
15.10	0.023	95.70	0.057	215.10	0.115
17.40	0.023	97.50	0.057	219.20	0.115
19.40	0.019	99.30	0.057	223.10	0.119
21.40	0.021	101.60	0.061	227.70	0.124
23.10	0.019	103.40	0.061	231.80	0.126
25.40	0.019	105.80	0.061	239.40	0.126
27.30	0.019	107.80	0.063	247.20	0.134
29.40	0.023	109.80	0.063	255.70	0.138
31.60	0.027	111.60	0.065	263.70	0.141
33.60	0.029	113.80	0.065	271.40	0.147
35.90	0.027	115.70	0.069	279.80	0.145
38.10	0.032	117.80	0.071	287.30	0.161
39.30	0.032	119.60	0.071	295.70	0.161
41.70	0.031	121.40	0.065	303.60	0.164
43.60	0.031	123.30	0.069	311.70	0.168
45.60	0.034	125.30	0.069	319.20	0.174
47.50	0.036	127.90	0.069	327.60	0.176
49.30	0.038	129.70	0.073	335.40	0.187
51.40	0.031	131.90	0.076	343.50	0.187
53.40	0.034	133.70	0.073	351.20	0.187
55.40	0.040	135.70	0.076	359.10	0.195
57.70	0.027	139.60	0.076	367.40	0.197
59.70	0.038	143.60	0.084	376.30	0.206
61.70	0.040	147.20	0.084	384.50	0.206
63.30	0.050	151.40	0.076	392.40	0.214
65.70	0.042	155.70	0.076	400.70	0.214
67.70	0.038	159.80	0.088	408.40	0.218
69.60	0.054	163.80	0.088	416.30	0.227
71.70	0.054	167.60	0.088	424.70	0.233
73.50	0.054	171.30	0.092	432.50	0.237

1512 F - 36.0 KSI CREEP DATA FOR E1A					
Time In Hours	Deformation %	Time In Hours	Deformation %	Time In Hours	Deformation %
440.20	0.239	768.60	0.388	1088.30	0.514
448.80	0.243	776.20	0.398	1096.60	0.520
456.60	0.248	784.60	0.394	1104.20	0.520
464.70	0.260	792.60	0.398	1112.00	0.520
472.70	0.256	800.20	0.405	1120.70	0.520
480.60	0.260	808.70	0.407	1128.50	0.520
488.20	0.268	816.50	0.407	1136.20	0.533
496.80	0.268	824.50	0.417	1143.90	0.535
504.50	0.275	832.70	0.417	1151.80	0.539
512.60	0.277	840.50	0.419	1160.30	0.539
520.30	0.283	843.30	0.420	1168.20	0.547
528.20	0.291	856.20	0.420	1176.20	0.554
536.10	0.291	864.20	0.424	1184.30	0.552
544.40	0.291	872.40	0.430	1192.00	0.554
552.20	0.298	880.50	0.428	1200.10	0.562
560.20	0.302	888.20	0.440	1208.20	0.558
568.40	0.304	896.50	0.440	1216.10	0.562
584.30	0.308	904.70	0.447	1224.00	0.570
592.60	0.310	912.00	0.455	1232.20	0.571
600.80	0.310	920.30	0.453	1240.50	0.573
608.40	0.325	928.70	0.459	1248.70	0.577
616.80	0.329	936.50	0.459	1256.10	0.577
624.40	0.329	944.50	0.464	1264.60	0.577
632.80	0.334	952.80	0.463	1272.50	0.581
640.70	0.333	960.50	0.463	1280.20	0.596
648.70	0.340	968.70	0.472	1288.50	0.593
656.40	0.342	976.70	0.470	1296.30	0.596
664.80	0.348	984.60	0.474	1304.80	0.600
672.10	0.352	992.20	0.482	1312.50	0.600
680.50	0.350	1000.60	0.482	1320.30	0.608
688.30	0.356	1008.10	0.485	1328.10	0.606
696.40	0.356	1016.30	0.489	1336.50	0.608
704.30	0.363	1024.10	0.489	1344.00	0.612
712.30	0.371	1032.10	0.489	1352.20	0.614
720.20	0.375	1040.20	0.497	1360.20	0.619
725.40	0.375	1048.10	0.499	1368.10	0.623
736.60	0.382	1056.00	0.505	1376.20	0.623
744.50	0.382	1064.30	0.503	1384.00	0.631
752.30	0.382	1072.60	0.505	1392.10	0.635
760.60	0.388	1080.10	0.512	1400.20	0.635

1512 F - 36.0 KSI CREEP DATA FOR E1A	
Time In Hours	Deformation %
2384.20	1.305
2392.10	1.311
2400.00	1.315
2408.20	1.330
2416.60	1.338
2424.00	1.347
2431.60	1.357
2440.70	1.365
2448.20	1.380
2455.60	1.384
2464.50	1.399
2472.30	1.411
2480.30	1.430
2488.50	1.433
2496.30	1.449
2503.60	1.456
2512.60	1.468
2519.90	1.483
2527.50	1.491
2536.10	1.502
2543.90	1.518
2552.40	1.529
2560.40	1.548
2567.90	1.562
2576.10	1.583
2584.60	1.598
2592.40	1.606
2599.50	1.625
2608.60	1.640
2616.10	1.659
2623.60	1.678
2632.60	1.701
2640.20	1.720
2648.50	1.741
2656.70	1.770
2664.20	1.793
2671.60	1.820
2680.70	1.839
2688.10	1.873
2695.50	1.881

1512 F - 36.0 KSI CREEP DATA FOR E1A					
Time In Hours	Deformation %	Time In Hours	Deformation %	Time In Hours	Deformation %
1408.50	0.644	1736.20	0.801	2064.10	1.005
1416.60	0.646	1744.50	0.803	2073.00	1.013
1424.00	0.648	1752.50	0.807	2080.60	1.017
1432.60	0.646	1760.30	0.805	2088.50	1.017
1448.20	0.656	1768.60	0.810	2096.20	1.032
1456.60	0.654	1776.40	0.822	2104.50	1.036
1464.30	0.661	1784.20	0.822	2111.90	1.036
1472.60	0.661	1792.60	0.826	2120.20	1.047
1480.50	0.661	1800.20	0.826	2128.50	1.049
1488.30	0.669	1808.30	0.835	2136.10	1.055
1496.00	0.677	1816.60	0.847	2144.00	1.067
1504.50	0.679	1824.10	0.849	2152.60	1.067
1512.00	0.684	1832.30	0.854	2160.10	1.074
1519.60	0.684	1839.90	0.852	2168.30	1.082
1527.60	0.686	1847.90	0.852	2176.60	1.086
1536.60	0.692	1856.20	0.872	2184.40	1.109
1544.20	0.694	1872.10	0.872	2192.20	1.107
1552.40	0.698	1880.40	0.875	2200.20	1.109
1560.40	0.700	1888.30	0.879	2208.10	1.112
1568.00	0.707	1896.10	0.887	2216.20	1.130
1576.50	0.707	1904.50	0.891	2224.20	1.131
1584.60	0.715	1912.70	0.902	2231.90	1.139
1592.00	0.722	1920.30	0.910	2240.20	1.149
1600.60	0.722	1928.20	0.906	2248.60	1.162
1608.10	0.726	1936.70	0.914	2256.30	1.166
1616.30	0.730	1944.50	0.921	2263.60	1.174
1624.70	0.734	1952.20	0.921	2272.60	1.185
1632.10	0.738	1960.70	0.929	2280.50	1.196
1640.70	0.745	1968.20	0.929	2287.90	1.200
1648.70	0.745	1976.30	0.938	2296.50	1.206
1656.20	0.749	1984.60	0.944	2304.30	1.212
1664.10	0.753	1992.20	0.952	2312.20	1.219
1672.70	0.763	1999.30	0.959	2320.60	1.231
1680.10	0.765	2007.90	0.963	2328.40	1.239
1688.30	0.770	2016.00	0.971	2335.90	1.244
1696.00	0.768	2024.10	0.971	2344.50	1.258
1704.20	0.772	2032.10	0.975	2352.00	1.261
1712.30	0.786	2040.10	0.975	2359.70	1.261
1720.40	0.786	2048.10	0.986	2368.20	1.284
1728.00	0.791	2056.20	0.992	2376.00	1.296



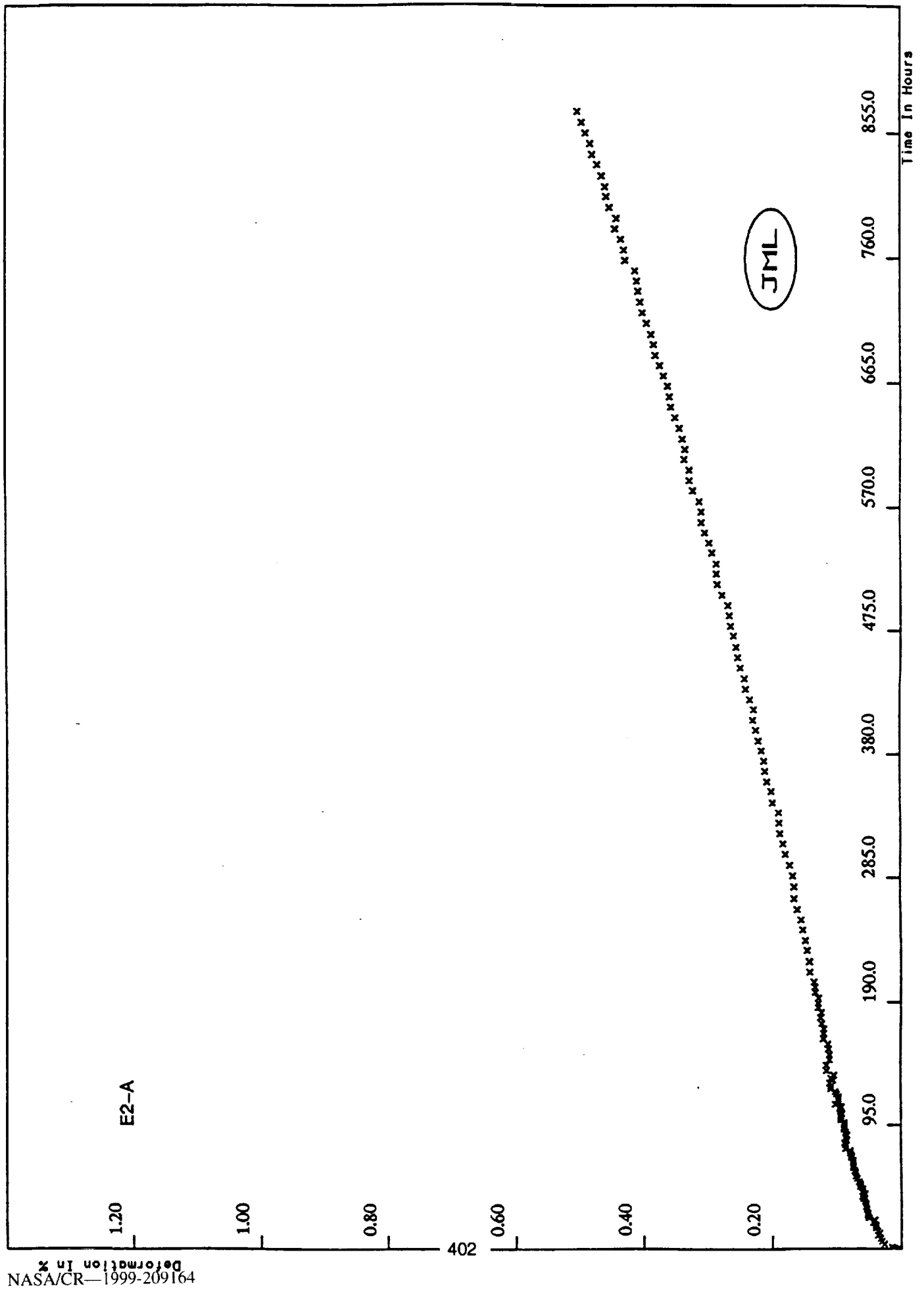
1512 F - 36.0 KSI CREEP DATA FOR E1B					
Time In Hours	Deformation %	Time In Hours	Deformation %	Time In Hours	Deformation %
0.10	0.004	71.00	0.038	235.10	0.107
0.30	0.004	73.00	0.040	242.50	0.111
0.50	0.004	74.80	0.042	250.90	0.122
0.70	0.004	76.70	0.040	258.80	0.122
2.80	0.008	78.60	0.042	261.00	0.126
5.00	0.011	80.69	0.042	274.40	0.134
7.40	0.017	83.20	0.044	287.90	0.138
9.40	0.013	85.00	0.048	290.60	0.145
11.50	0.010	87.10	0.048	298.80	0.145
12.80	0.015	89.00	0.042	306.40	0.138
15.00	0.015	90.90	0.046	314.30	0.153
17.10	0.015	94.70	0.046	322.60	0.151
19.10	0.017	98.90	0.046	331.40	0.160
20.80	0.017	102.50	0.046	339.70	0.160
23.00	0.017	106.70	0.050	347.60	0.162
25.00	0.017	111.00	0.052	356.00	0.164
27.00	0.017	115.10	0.053	363.70	0.174
29.20	0.017	119.10	0.053	371.60	0.183
31.30	0.019	122.80	0.057	379.90	0.183
33.60	0.021	126.50	0.057	387.70	0.187
35.70	0.019	130.00	0.059	395.60	0.191
36.90	0.019	134.50	0.063	404.10	0.189
39.40	0.019	138.60	0.065	411.80	0.193
41.30	0.019	142.80	0.065	420.00	0.208
43.40	0.019	146.50	0.069	428.00	0.206
45.50	0.019	150.30	0.073	435.90	0.206
46.90	0.019	154.40	0.078	443.50	0.212
49.00	0.023	159.00	0.084	452.00	0.214
51.10	0.023	162.60	0.076	459.80	0.218
52.10	0.023	166.60	0.078	467.90	0.229
52.30	0.023	170.30	0.078	475.60	0.229
52.90	0.023	174.40	0.086	483.50	0.233
54.70	0.023	178.30	0.090	491.30	0.241
56.80	0.023	183.00	0.090	499.60	0.241
58.70	0.029	187.10	0.088	507.40	0.248
61.10	0.031	194.60	0.095	515.40	0.248
63.00	0.036	202.50	0.097	520.70	0.267
65.00	0.032	211.00	0.099	521.60	0.267
66.90	0.034	219.00	0.103	522.10	0.267
69.00	0.034	226.60	0.107	524.70	0.271

1512 F - 36.0 KSI CREEP DATA FOR E1B					
Time In Hours	Deformation %	Time In Hours	Deformation %	Time In Hours	Deformation %
532.30	0.286	852.60	0.432	1172.70	0.546
540.70	0.286	860.30	0.432	1180.00	0.550
548.30	0.290	868.30	0.435	1188.50	0.554
556.70	0.302	876.60	0.439	1196.40	0.554
564.60	0.302	884.30	0.439	1204.20	0.554
572.30	0.309	892.60	0.439	1212.50	0.558
580.30	0.309	900.60	0.435	1220.30	0.561
588.70	0.313	908.50	0.439	1228.70	0.571
596.00	0.317	916.10	0.449	1236.50	0.569
604.40	0.319	924.50	0.447	1244.20	0.569
612.20	0.327	932.10	0.451	1252.10	0.573
620.30	0.336	940.20	0.453	1260.40	0.573
628.20	0.336	948.00	0.455	1268.00	0.577
636.20	0.340	956.00	0.458	1276.10	0.584
644.10	0.332	964.10	0.460	1284.10	0.592
652.30	0.336	972.10	0.458	1292.00	0.592
660.50	0.355	980.00	0.466	1300.20	0.592
668.40	0.355	988.20	0.470	1308.60	0.594
676.20	0.357	996.50	0.474	1316.00	0.594
684.50	0.359	1004.60	0.477	1324.10	0.600
692.50	0.359	1012.30	0.481	1337.50	0.600
700.10	0.365	1021.50	0.483	1340.50	0.600
708.50	0.367	1028.20	0.485	1348.00	0.604
716.50	0.374	1036.00	0.489	1356.60	0.607
724.10	0.378	1044.60	0.489	1372.10	0.626
732.60	0.380	1052.50	0.489	1380.60	0.623
740.40	0.380	1060.20	0.498	1388.20	0.630
748.40	0.388	1067.90	0.504	1396.50	0.628
756.60	0.390	1075.80	0.504	1404.50	0.632
764.40	0.390	1084.30	0.508	1412.20	0.640
772.20	0.388	1092.60	0.512	1420.00	0.644
780.20	0.388	1100.10	0.519	1428.50	0.649
788.10	0.399	1108.20	0.514	1436.00	0.649
796.30	0.399	1116.00	0.519	1443.50	0.649
804.40	0.401	1124.10	0.527	1451.50	0.651
812.00	0.416	1132.10	0.527	1460.50	0.653
820.30	0.420	1140.10	0.527	1468.10	0.665
828.50	0.420	1147.90	0.535	1476.40	0.668
835.90	0.424	1156.20	0.537	1484.40	0.668
844.10	0.426	1164.40	0.539	1492.00	0.672

1512 F - 36.0 KSI CREEP DATA FOR E1B					
Time In Hours	Deformation %	Time In Hours	Deformation %	Time In Hours	Deformation %
1500.50	0.672	1828.40	0.829	2148.10	1.024
1508.50	0.665	1836.60	0.837	2155.90	1.028
1516.00	0.676	1844.30	0.837	2164.10	1.031
1524.50	0.678	1852.20	0.840	2172.50	1.035
1532.10	0.678	1860.60	0.840	2180.20	1.047
1540.30	0.689	1868.50	0.859	2187.50	1.050
1548.60	0.691	1876.10	0.858	2196.50	1.050
1556.10	0.691	1884.70	0.859	2203.90	1.058
1564.70	0.693	1892.20	0.863	2211.90	1.058
1572.70	0.701	1900.30	0.865	2220.50	1.068
1580.10	0.707	1908.60	0.867	2228.30	1.073
1588.00	0.714	1916.10	0.882	2236.10	1.073
1596.60	0.710	1923.20	0.886	2244.50	1.081
1604.00	0.714	1931.80	0.890	2252.20	1.081
1612.20	0.722	1939.80	0.890	2259.80	1.085
1620.00	0.726	1948.10	0.894	2268.50	1.089
1628.20	0.726	1956.00	0.909	2276.00	1.096
1636.30	0.728	1964.00	0.909	2283.40	1.104
1644.20	0.733	1972.10	0.915	2292.10	1.104
1652.00	0.741	1980.10	0.917	2299.90	1.108
1660.20	0.743	1988.10	0.928	2308.20	1.108
1668.50	0.741	1996.90	0.932	2316.00	1.108
1676.40	0.745	2004.50	0.932	2324.00	1.127
1684.30	0.749	2012.60	0.928	2332.10	1.131
1692.50	0.752	2020.10	0.945	2340.60	1.134
1700.40	0.764	2028.40	0.953	2348.00	1.146
1708.20	0.772	2035.80	0.951	2355.60	1.146
1716.50	0.775	2044.10	0.955	2364.60	1.161
1724.20	0.783	2052.40	0.966	2372.20	1.165
1732.20	0.785	2060.10	0.966	2379.50	1.165
1740.60	0.791	2068.00	0.978	2388.50	1.178
1748.00	0.791	2076.50	0.978	2396.20	1.188
1756.30	0.795	2084.00	0.978	2404.30	1.194
1763.70	0.795	2092.20	0.985	2412.50	1.203
1771.80	0.795	2100.50	0.982	2420.20	1.205
1780.10	0.808	2108.40	0.997	2427.50	1.205
1796.10	0.817	2116.20	1.003	2436.50	1.222
1804.30	0.817	2124.20	1.008	2443.90	1.234
1812.20	0.823	2132.00	1.012	2451.40	1.238
1820.10	0.825	2140.20	1.020	2460.10	1.245

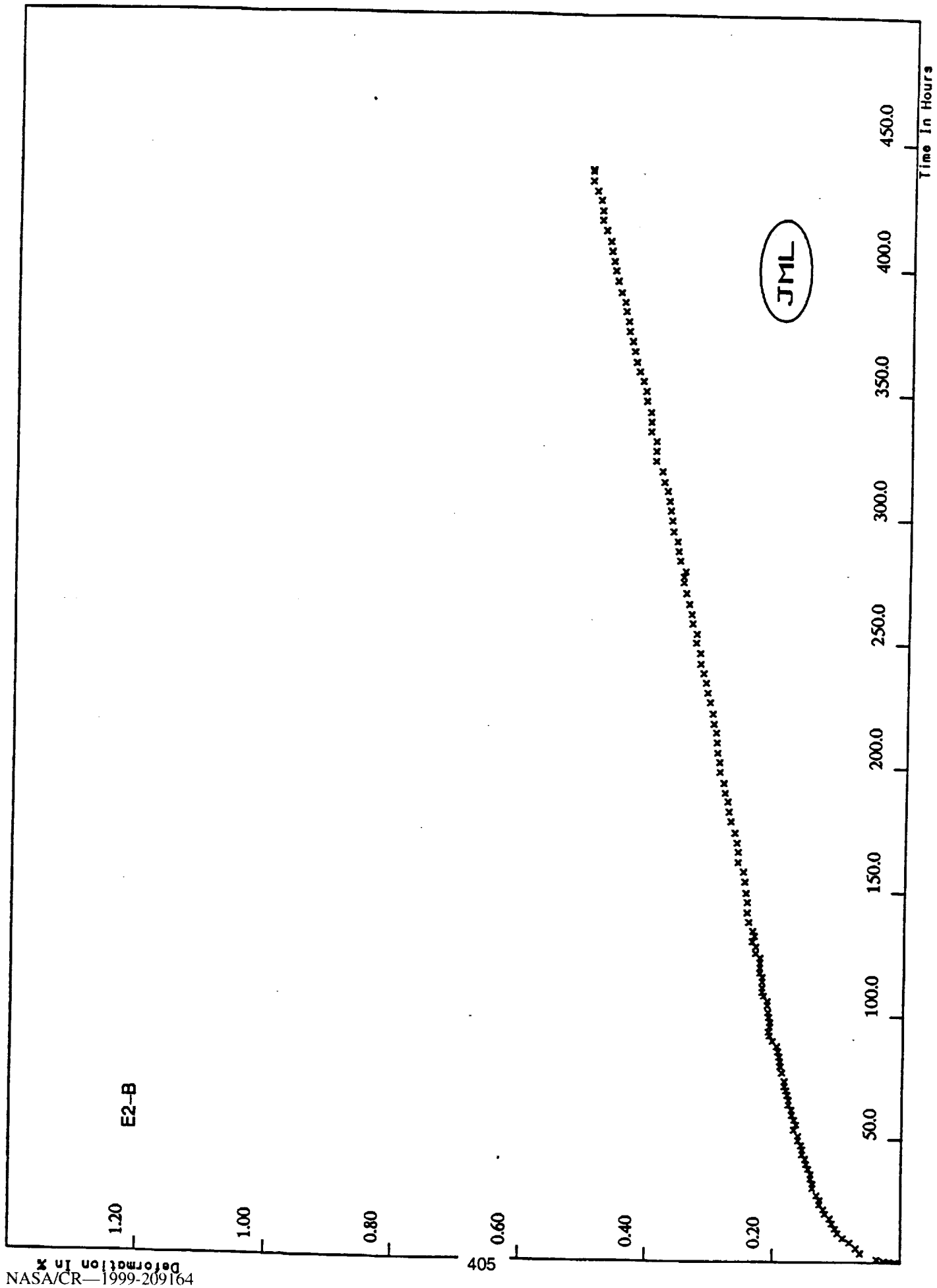


1512 F - 36.0 KSI CREEP DATA FOR E1B			
Time In Hours	Deformation %	Time In Hours	Deformation %
2467.90	1.253	2708.10	1.585
2476.30	1.253	2715.60	1.593
2484.90	1.268	2724.50	1.608
2491.40	1.272	2732.10	1.620
2500.00	1.282	2740.10	1.642
2508.50	1.287	2748.40	1.662
2516.30	1.303	2756.00	1.684
2523.50	1.306	2763.10	1.688
2532.50	1.322	2772.50	1.704
2541.00	1.333	2780.10	1.727
2547.50	1.337	2787.50	1.753
2556.50	1.352	2796.00	1.772
2564.10	1.364	2804.00	1.780
2572.50	1.369	2812.40	1.811
2580.60	1.390	2820.10	1.820
2588.10	1.390	2827.90	1.853
2595.50	1.406	2836.30	1.872
2604.60	1.417	2844.50	1.898
2612.00	1.425	2852.20	1.925
2619.40	1.436	2860.10	1.942
2628.30	1.446	2868.50	1.971
2636.00	1.459	2876.00	2.005
2644.20	1.472	2884.20	2.034
2652.10	1.486	2892.60	2.063
2660.00	1.494	2900.00	2.093
2668.10	1.518	2908.50	2.139
2676.50	1.520	2916.50	2.191
2684.10	1.539	2924.40	2.250
2691.50	1.547	2932.10	2.349
2700.60	1.566		



1539 F - 10.0 KSI CREEP DATA FOR E2-A					
Time In Hours	Deformation %	Time In Hours	Deformation %	Time In Hours	Deformation %
0.10	0.002	73.50	0.079	173.70	0.122
0.30	0.011	75.20	0.079	178.10	0.125
0.50	0.011	77.00	0.086	182.00	0.124
0.70	0.011	79.30	0.086	185.80	0.128
1.40	0.014	81.40	0.087	189.40	0.128
3.70	0.026	83.30	0.085	193.50	0.128
5.80	0.031	85.30	0.086	197.90	0.132
8.00	0.033	87.50	0.084	202.10	0.133
10.00	0.036	89.70	0.086	205.70	0.135
11.90	0.034	91.90	0.088	213.60	0.141
13.70	0.037	93.40	0.088	221.40	0.142
15.90	0.040	95.50	0.088	229.80	0.146
17.80	0.040	97.20	0.088	237.60	0.148
19.90	0.044	99.40	0.093	245.90	0.152
21.80	0.042	101.40	0.093	253.30	0.154
23.50	0.051	104.00	0.092	261.20	0.161
25.40	0.053	106.10	0.094	269.40	0.165
27.40	0.053	107.80	0.095	278.30	0.165
30.20	0.054	109.60	0.093	286.40	0.168
31.90	0.055	111.50	0.101	294.50	0.172
34.10	0.055	113.60	0.097	302.80	0.179
35.80	0.057	115.60	0.097	310.60	0.183
37.90	0.060	117.20	0.097	318.60	0.187
39.90	0.061	119.40	0.099	326.80	0.189
41.80	0.057	121.40	0.101	334.60	0.190
43.70	0.061	123.40	0.108	342.40	0.199
45.90	0.061	125.40	0.108	351.00	0.201
47.50	0.064	127.80	0.110	358.80	0.207
49.50	0.064	130.01	0.105	367.00	0.211
51.30	0.066	131.90	0.108	374.90	0.212
53.80	0.068	134.00	0.104	382.90	0.216
55.90	0.071	137.60	0.115	390.40	0.221
58.10	0.072	141.50	0.115	399.00	0.225
59.80	0.073	145.50	0.110	406.70	0.229
61.90	0.075	149.50	0.110	414.70	0.228
63.60	0.075	153.90	0.111	422.50	0.234
65.70	0.075	157.70	0.112	430.40	0.240
67.80	0.075	161.70	0.119	438.30	0.243
69.80	0.077	165.80	0.119	446.60	0.249
71.40	0.077	169.50	0.119	454.30	0.254

1539 F - 10.0 KSI CREEP DATA FOR E2-A			
Time In Hours	Deformation %	Time In Hours	Deformation %
462.20	0.256	670.80	0.368
470.70	0.260	678.50	0.375
478.60	0.265	686.70	0.382
486.60	0.267	694.80	0.384
494.80	0.269	702.40	0.388
502.60	0.278	710.80	0.395
510.70	0.286	718.70	0.401
519.00	0.287	726.80	0.405
526.60	0.287	734.90	0.408
535.00	0.293	742.70	0.410
542.80	0.298	750.50	0.412
550.70	0.304	758.50	0.428
558.70	0.310	766.30	0.430
566.90	0.310	774.60	0.434
574.40	0.313	782.60	0.443
582.60	0.323	790.30	0.441
590.50	0.329	798.50	0.452
598.50	0.329	806.70	0.457
606.90	0.336	814.10	0.459
614.50	0.335	822.40	0.464
622.30	0.340	830.80	0.471
630.50	0.344	838.60	0.479
638.70	0.351	846.70	0.482
646.70	0.357	854.80	0.490
654.50	0.360	862.60	0.495
662.80	0.362	870.90	0.502



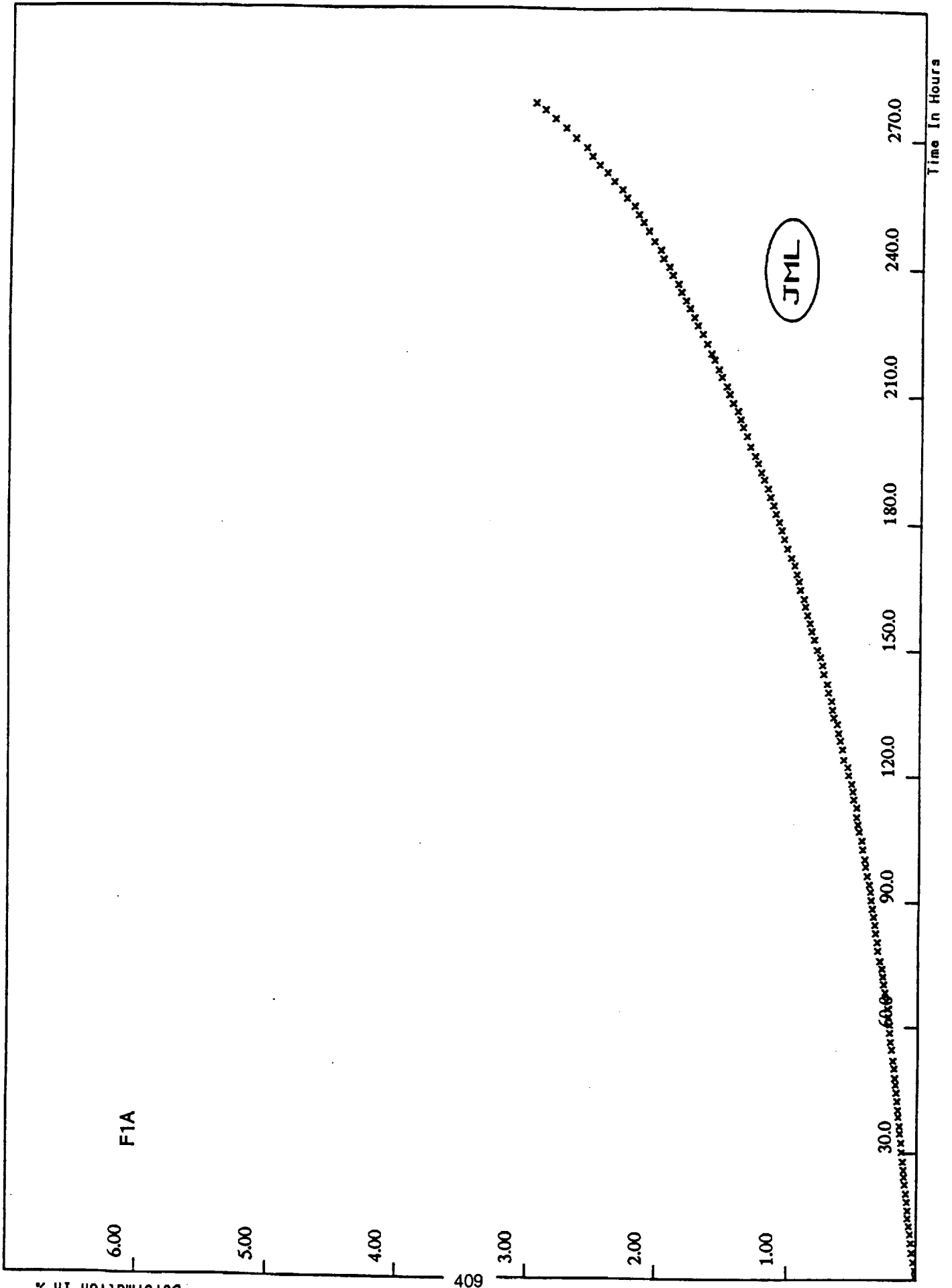
1539 F - 10.0 KSI CREEP DATA FOR E2-B					
Time In Hours	Deformation %	Time In Hours	Deformation %	Time In Hours	Deformation %
0.10	0.009	73.40	0.184	178.00	0.273
0.30	0.018	76.90	0.188	181.90	0.276
0.50	0.018	79.30	0.190	185.80	0.278
0.70	0.026	81.40	0.192	189.40	0.282
1.30	0.037	83.30	0.193	193.40	0.285
3.70	0.063	85.40	0.195	197.80	0.291
5.60	0.070	87.50	0.197	201.90	0.292
8.00	0.080	89.60	0.204	205.70	0.296
9.90	0.091	91.80	0.208	209.80	0.297
11.90	0.099	93.40	0.210	213.80	0.298
13.70	0.103	95.50	0.208	217.40	0.302
15.90	0.107	97.10	0.208	221.40	0.304
17.80	0.111	99.40	0.210	225.90	0.309
19.80	0.118	101.30	0.211	229.70	0.313
21.70	0.120	104.10	0.212	233.70	0.315
23.60	0.127	105.90	0.212	237.50	0.320
25.40	0.127	108.00	0.219	241.30	0.324
27.40	0.131	109.50	0.221	245.70	0.325
30.10	0.138	111.40	0.221	249.90	0.332
31.90	0.138	113.58	0.221	253.30	0.331
34.00	0.141	115.50	0.221	257.50	0.337
35.70	0.141	117.20	0.225	261.20	0.339
37.90	0.146	119.40	0.225	265.20	0.344
39.80	0.149	121.30	0.225	269.50	0.348
41.80	0.151	123.30	0.225	273.80	0.352
43.70	0.155	125.20	0.232	276.10	0.352
45.70	0.155	127.90	0.232	278.30	0.350
47.40	0.158	129.90	0.238	282.60	0.359
49.40	0.162	132.10	0.234	286.50	0.361
51.20	0.162	134.00	0.236	290.50	0.363
53.60	0.169	137.70	0.243	294.50	0.370
55.90	0.165	141.50	0.245	298.80	0.372
57.90	0.169	145.60	0.245	302.80	0.374
59.80	0.172	149.40	0.247	306.70	0.377
61.90	0.173	153.80	0.250	310.60	0.380
63.80	0.177	157.80	0.252	314.40	0.385
65.80	0.177	161.70	0.261	318.58	0.389
67.80	0.180	165.80	0.261	322.80	0.398
69.70	0.182	169.50	0.263	326.80	0.398
71.40	0.184	173.50	0.266	330.80	0.398

1539 F - 10.0 KSI CREEP DATA FOR E2-B	
Time In Hours	Deformation %
334.60	0.407
338.50	0.407
342.40	0.408
346.80	0.415
350.90	0.416
354.80	0.420
358.70	0.427
362.50	0.431
366.90	0.435
370.80	0.438
374.90	0.443
378.80	0.444
382.80	0.449
386.50	0.451
390.40	0.456
394.90	0.462
399.00	0.466
402.60	0.468
406.60	0.473
410.50	0.475
414.90	0.482
418.90	0.488
422.50	0.488
426.60	0.490
430.30	0.497
434.30	0.504
438.20	0.504
438.90	0.504

SAMPLE	STRESS	TEMP.	SPECIMEN	TOTAL %EL.	RUPTURE
I.D.	(KSI/MPA)	(K)		(%)	(YES\NO)
			ROUND F TESTS		
F1A	36/248	1095	STANDARD	4.0	YES
F1B	36/248	1095	STANDARD	3.3	YES

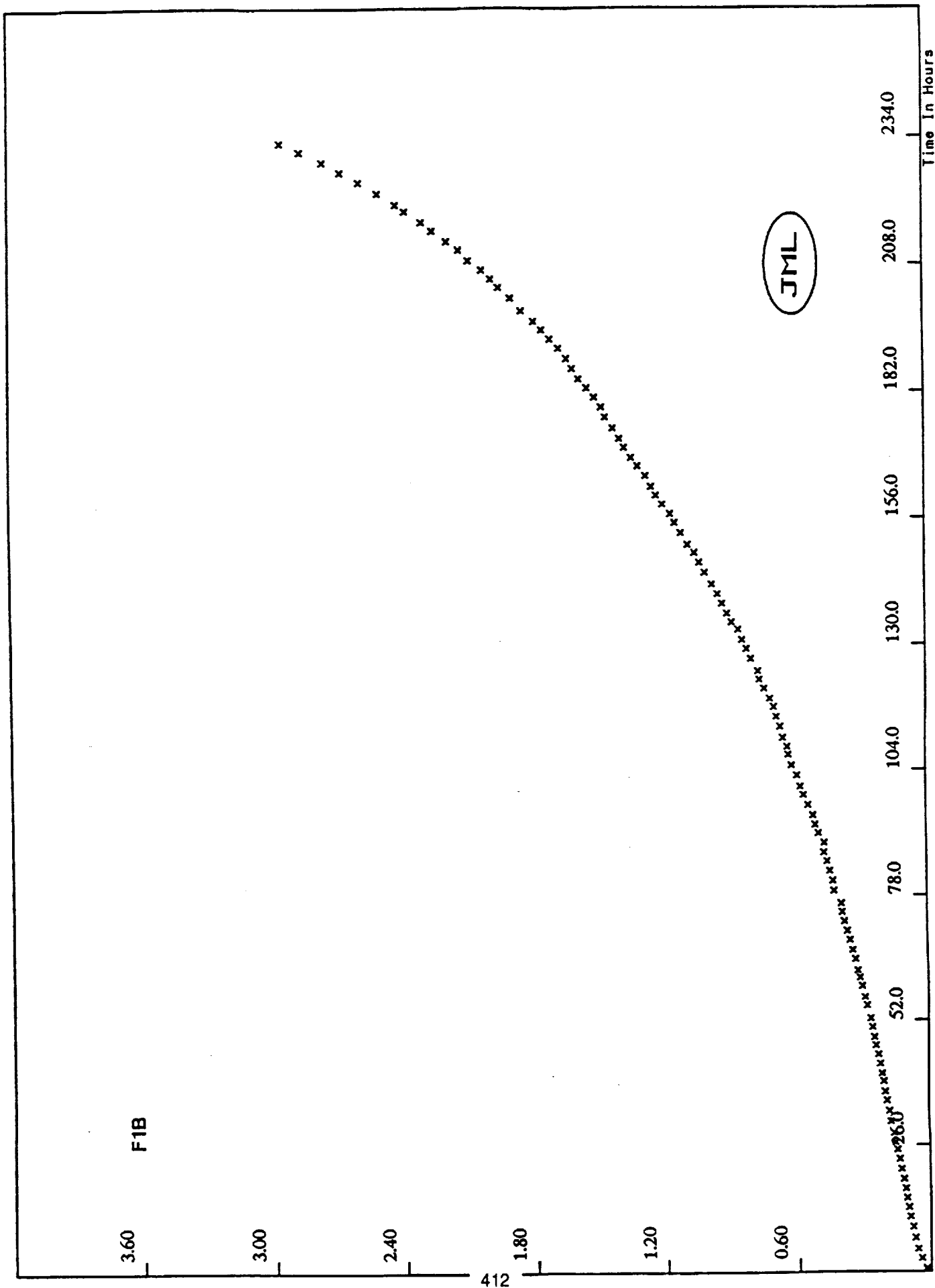
CW = CAST WROUGHT  
 PM = POWDER PROCESSED (-270 MESH)  
 CR = CR HEAT TREATMENT  
 HS = HS HEAT TREATMENT  
 + = U720LI CONSOLIDATED FROM -140 MESH POWDER





1512 F - 36.0 KSI CREEP DATA FOR F1A					
Time In Hours	Deformation %	Time In Hours	Deformation %	Time In Hours	Deformation %
0.10	0.000	74.10	0.281	154.60	0.830
0.30	0.003	75.90	0.296	156.50	0.844
0.50	0.004	78.40	0.313	158.40	0.865
0.70	0.006	80.50	0.317	160.40	0.879
2.20	0.010	82.60	0.330	162.20	0.890
4.10	0.025	84.60	0.336	164.40	0.920
6.30	0.036	86.50	0.348	166.40	0.931
8.60	0.044	88.40	0.357	168.10	0.946
10.70	0.051	90.40	0.368	170.20	0.964
12.60	0.061	92.40	0.375	172.00	0.990
14.50	0.069	94.10	0.383	174.20	1.021
16.40	0.071	96.10	0.401	176.50	1.043
18.40	0.077	98.30	0.412	178.50	1.063
20.40	0.084	100.00	0.419	180.50	1.085
22.60	0.095	102.40	0.438	182.40	1.111
24.40	0.099	104.50	0.445	184.40	1.126
26.00	0.105	106.70	0.464	186.30	1.152
28.00	0.110	108.40	0.473	188.30	1.170
30.30	0.121	110.20	0.482	190.40	1.199
32.50	0.124	112.50	0.482	192.10	1.225
34.70	0.132	114.50	0.508	194.20	1.247
36.50	0.138	116.40	0.515	195.90	1.269
38.70	0.146	118.20	0.522	198.10	1.306
40.30	0.150	120.30	0.548	200.60	1.332
42.40	0.156	122.20	0.552	202.70	1.363
44.40	0.164	124.00	0.585	204.50	1.383
46.30	0.171	126.50	0.592	206.40	1.402
47.80	0.178	128.60	0.609	208.30	1.439
50.10	0.184	130.40	0.624	210.40	1.468
51.90	0.192	132.60	0.633	212.20	1.486
54.60	0.203	134.10	0.659	214.40	1.527
56.40	0.212	135.90	0.670	216.20	1.549
58.60	0.221	138.00	0.677	218.50	1.582
60.50	0.221	140.00	0.699	219.90	1.608
62.50	0.231	142.00	0.710	222.20	1.641
64.40	0.236	144.40	0.736	224.50	1.674
66.40	0.248	146.50	0.747	226.50	1.713
68.40	0.257	148.40	0.765	228.40	1.740
70.30	0.266	150.10	0.787	230.50	1.773
72.20	0.274	152.60	0.809	232.30	1.803

1512 F - 36.0 KSI CREEP DATA FOR F1A	
Time In Hours	Deformation %
234.30	1.840
236.20	1.862
238.30	1.906
240.14	1.935
242.20	1.979
244.20	2.001
246.20	2.049
248.60	2.092
250.70	2.138
252.50	2.173
254.50	2.208
256.40	2.266
258.40	2.303
260.30	2.366
262.30	2.421
264.10	2.483
266.10	2.539
268.10	2.583
270.20	2.671
272.50	2.748
274.60	2.829
276.60	2.908
278.10	2.976

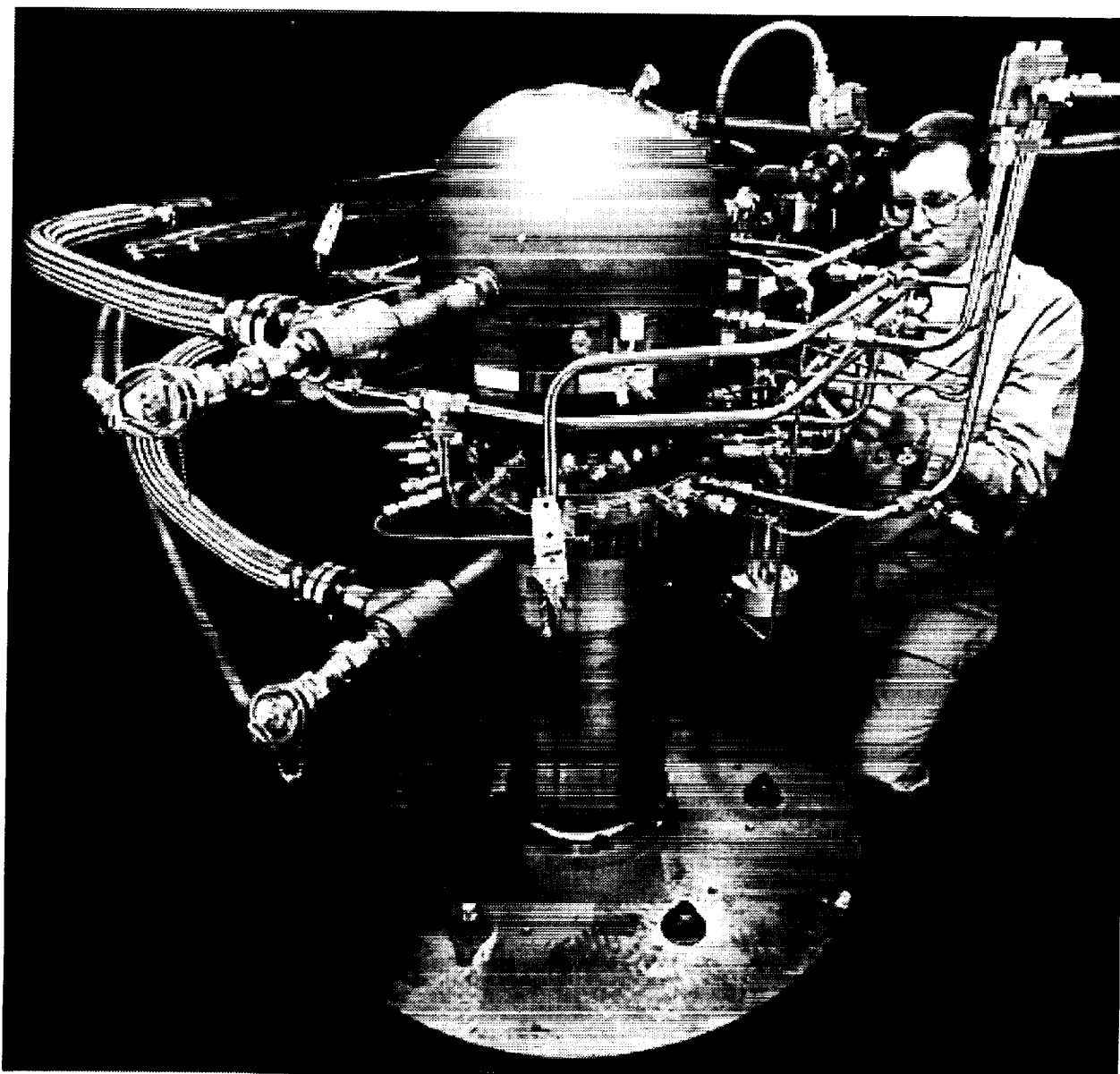


1512 F - 36.0 KSI CREEP DATA FOR F1B					
Time In Hours	Deformation %	Time In Hours	Deformation %	Time In Hours	Deformation %
0.10	0.007	74.60	0.390	155.10	1.141
0.30	0.014	76.40	0.394	157.00	1.159
0.50	0.018	78.90	0.426	158.90	1.196
0.70	0.022	81.00	0.431	160.90	1.227
2.70	0.044	83.10	0.444	162.70	1.247
4.60	0.060	85.10	0.455	164.90	1.273
6.80	0.072	86.90	0.470	166.90	1.310
9.10	0.082	88.90	0.467	168.60	1.339
11.20	0.095	90.90	0.493	170.70	1.372
13.10	0.100	92.60	0.508	172.50	1.394
15.00	0.109	94.60	0.519	174.70	1.424
16.90	0.114	96.70	0.541	177.00	1.461
18.90	0.123	98.80	0.559	179.00	1.477
21.00	0.132	100.50	0.574	181.00	1.510
23.10	0.141	102.90	0.589	183.00	1.545
25.00	0.150	105.00	0.613	184.80	1.582
26.50	0.157	107.20	0.625	186.80	1.611
28.50	0.165	108.90	0.629	188.80	1.637
30.80	0.176	110.70	0.651	190.90	1.674
33.00	0.183	113.00	0.662	192.70	1.714
35.20	0.192	115.00	0.681	194.70	1.751
37.00	0.199	117.00	0.692	196.40	1.788
39.20	0.207	118.70	0.710	198.60	1.843
40.80	0.214	120.80	0.736	201.10	1.891
42.90	0.223	122.70	0.758	203.30	1.946
44.90	0.231	124.50	0.765	205.00	1.981
46.80	0.241	127.00	0.797	206.90	2.024
48.50	0.248	129.10	0.817	208.80	2.086
50.60	0.256	130.90	0.835	210.90	2.130
52.40	0.264	133.10	0.854	212.70	2.185
55.10	0.280	134.60	0.885	214.90	2.252
56.90	0.290	136.40	0.905	216.70	2.299
59.20	0.301	138.50	0.927	219.00	2.377
61.00	0.312	140.50	0.946	220.40	2.417
62.50	0.322	142.50	0.971	222.70	2.502
64.90	0.332	144.90	1.004	225.00	2.588
66.80	0.343	147.00	1.030	227.00	2.675
68.90	0.355	149.00	1.052	229.00	2.756
70.80	0.368	150.60	1.082	231.00	2.859
72.70	0.380	153.10	1.111	232.80	2.947



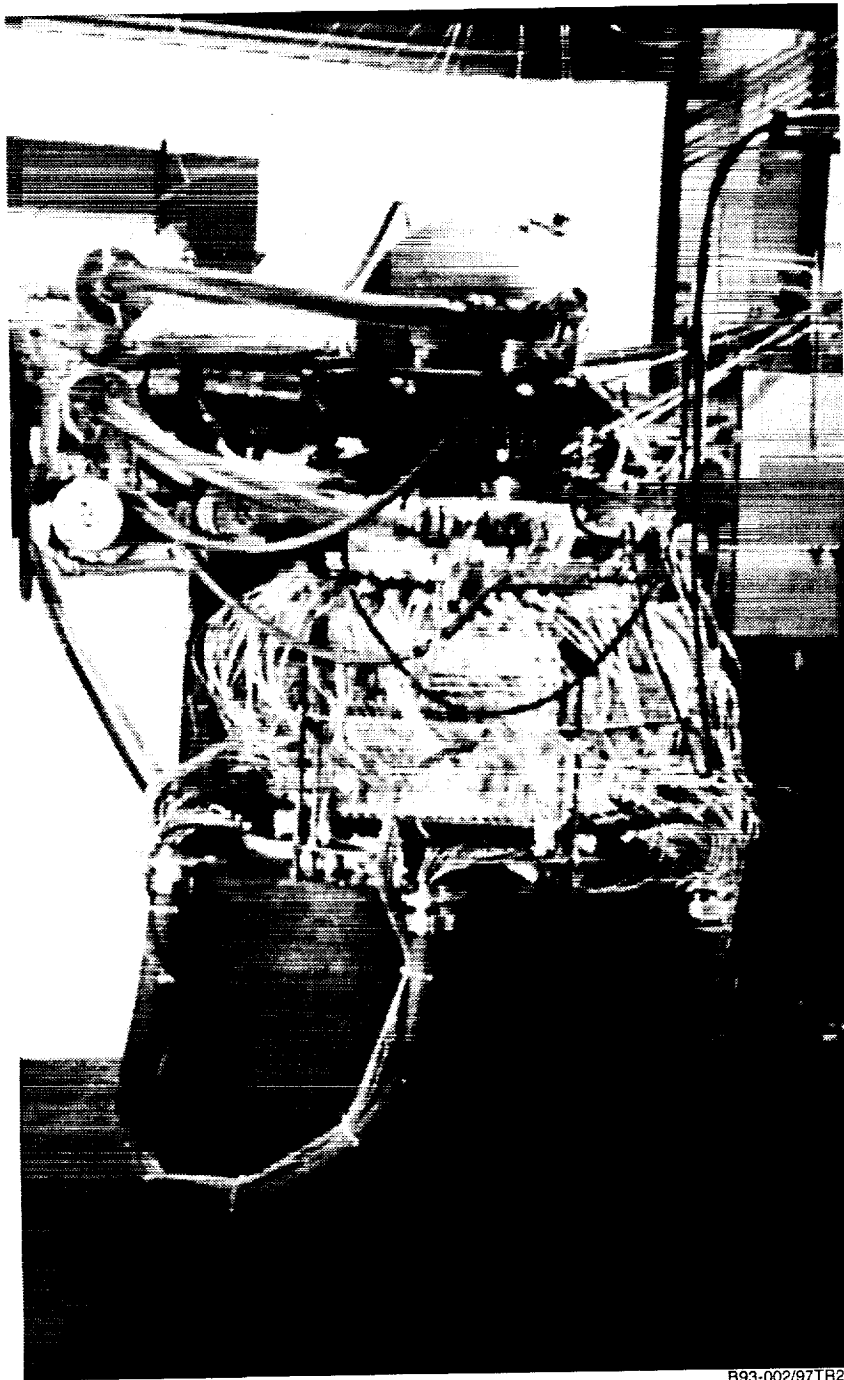
## APPENDIX D. CTPC COMPONENT DEVELOPMENT PHOTOS

This gallery of photographs presents several of the key hardware components of the CTPC and offers impressive proof of the high level of Stirling engine technology development achieved during this program.



B91-0046/97TR21

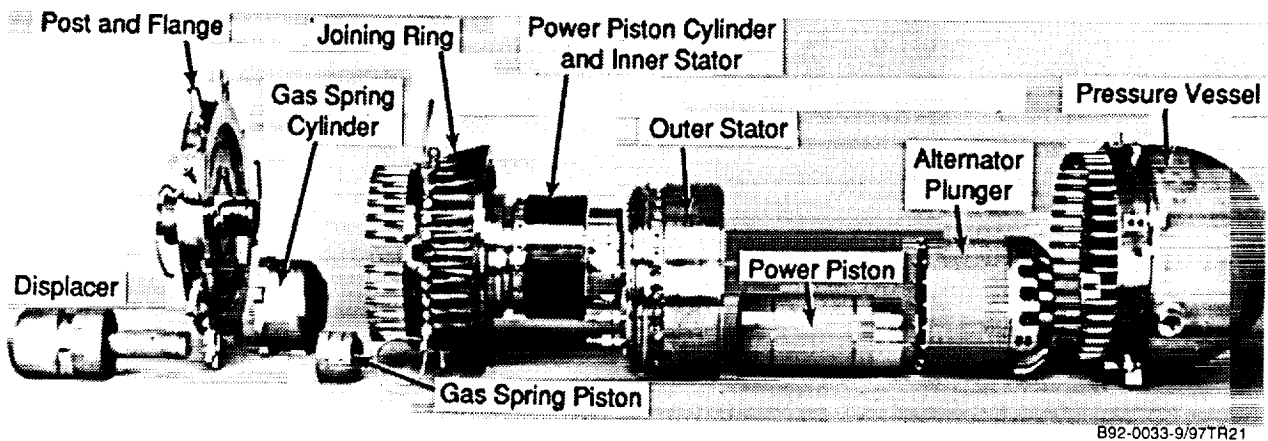
*CTPC Cold End on Test*



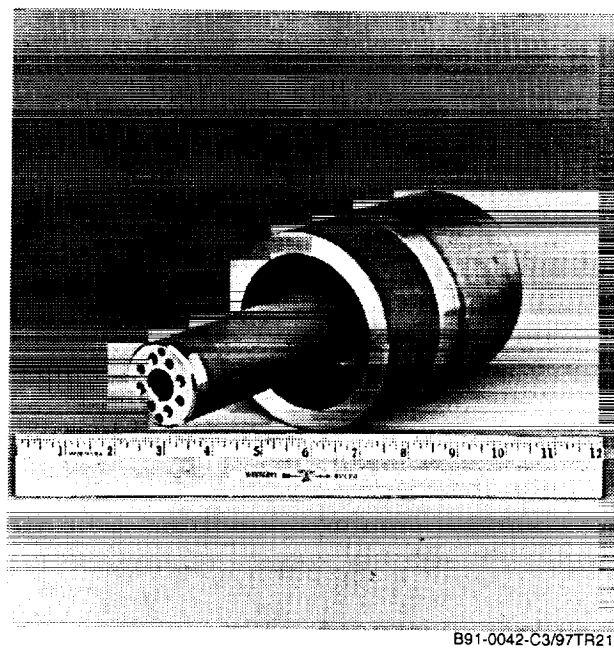
B93-002/97TR21

*CTPC Test Configuration*

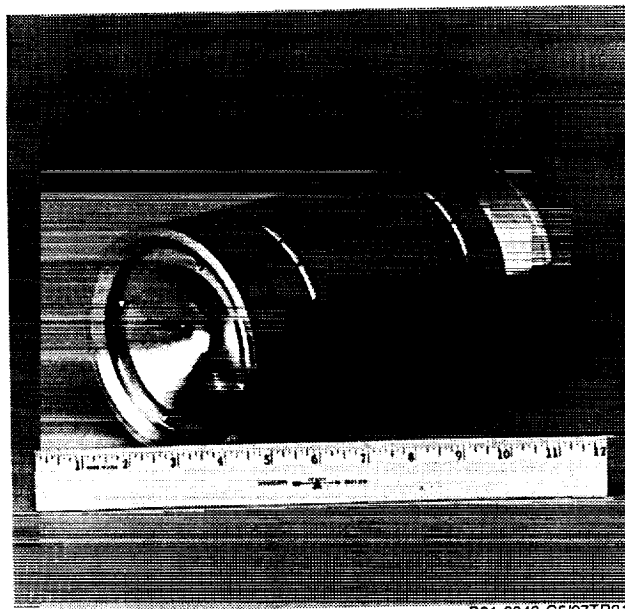




*Hardware Layout of CTPC*

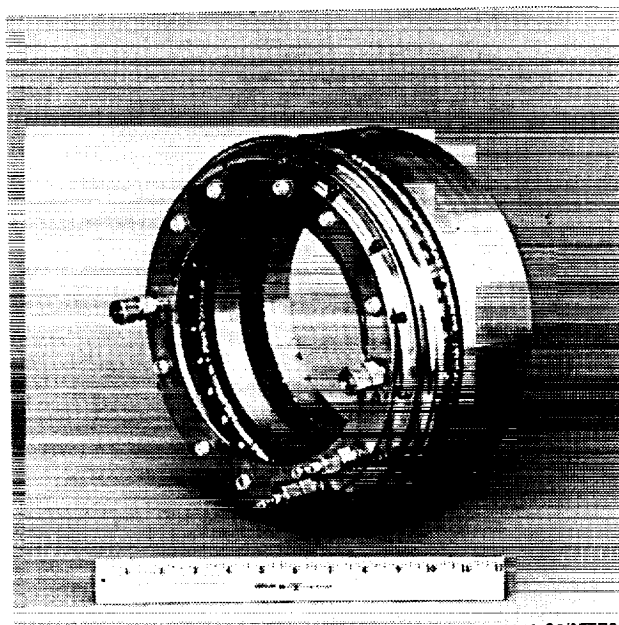


*CTPC Displacer and Rod*



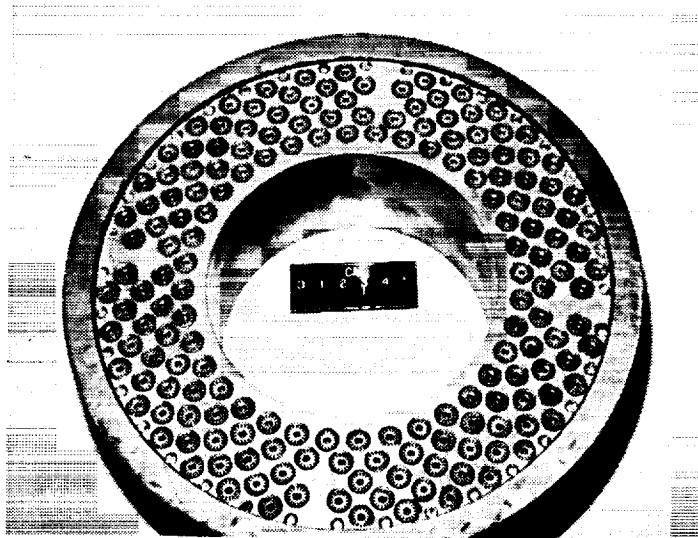
B91-0042-C5/97TR21

***CTPC Power Piston***



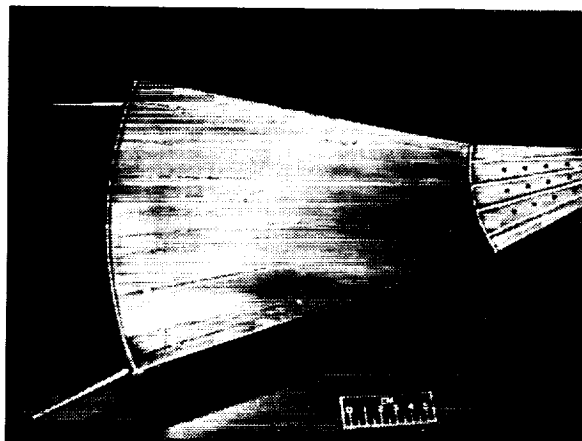
B91-0042-C5/97TR21

***CTPC Alternator Outer Stator***



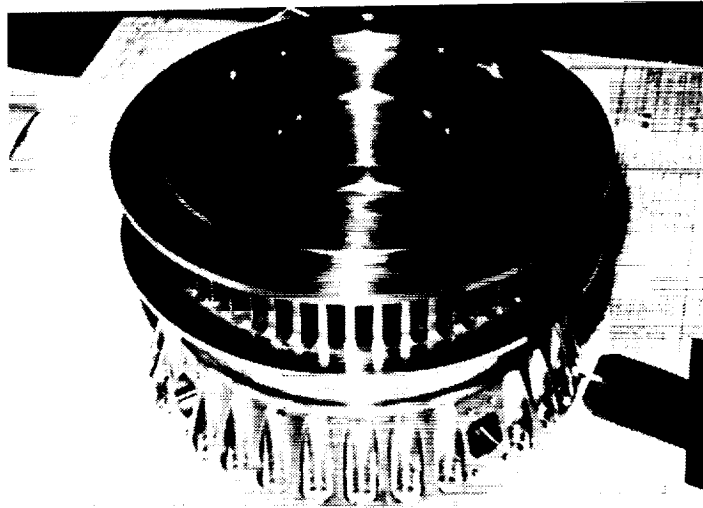
B92-0033-1/97TR21

*CTPC Cooler*



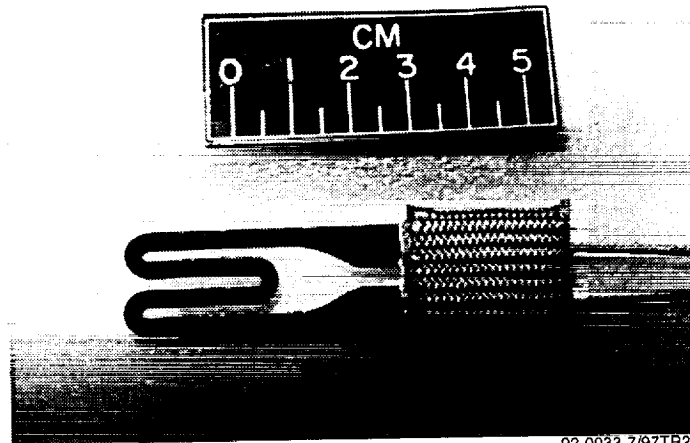
B92-0033-3/97TR21

*CTPC 1/10<sup>th</sup> Heat Pipe Segment*



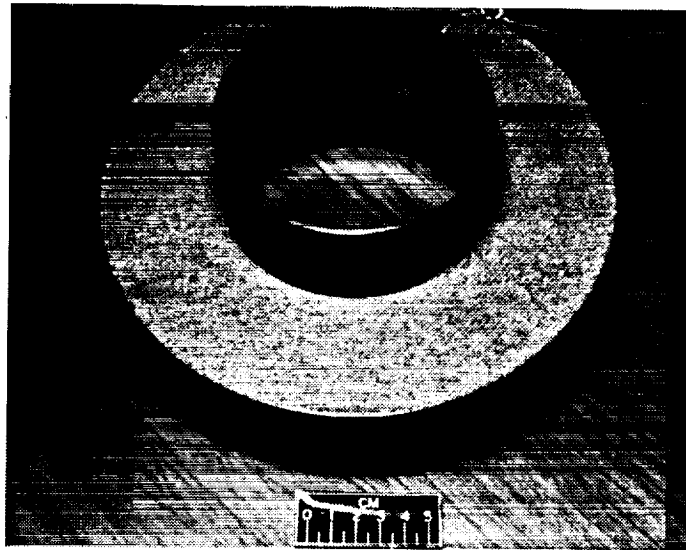
92-0033-5/97TR21

***CTPC Heater Head***



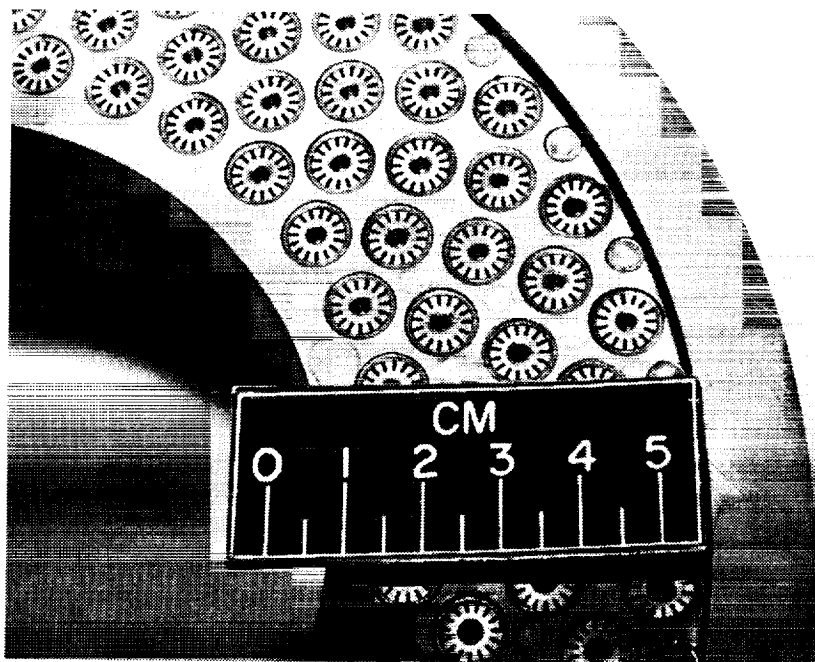
92-0033-7/97TR21

***CTPC Slot Radiant Heater***

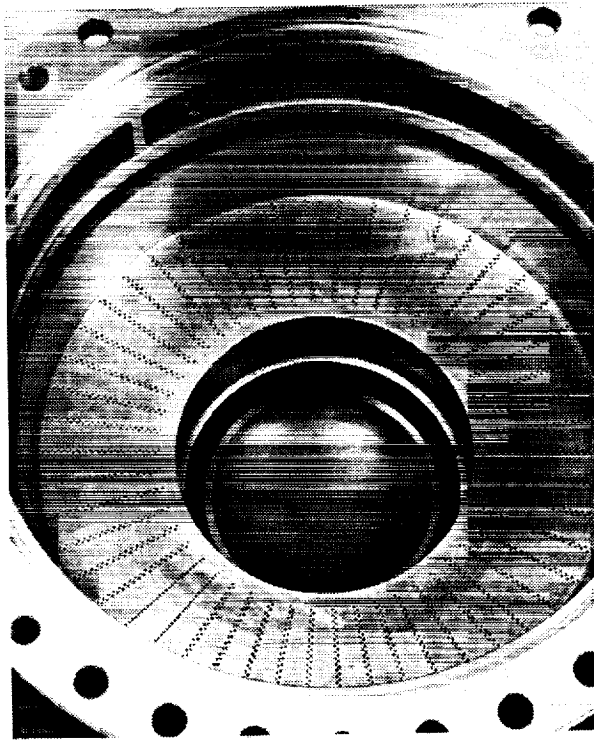


92-0033-6/97TR21

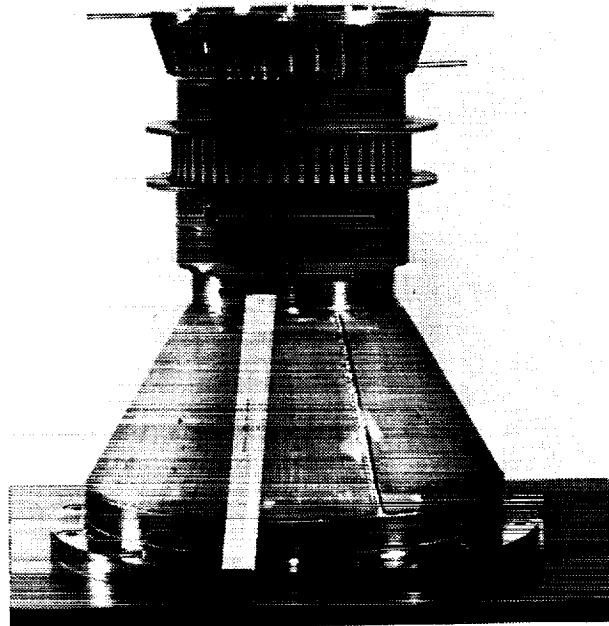
*CTPC Regenerator*



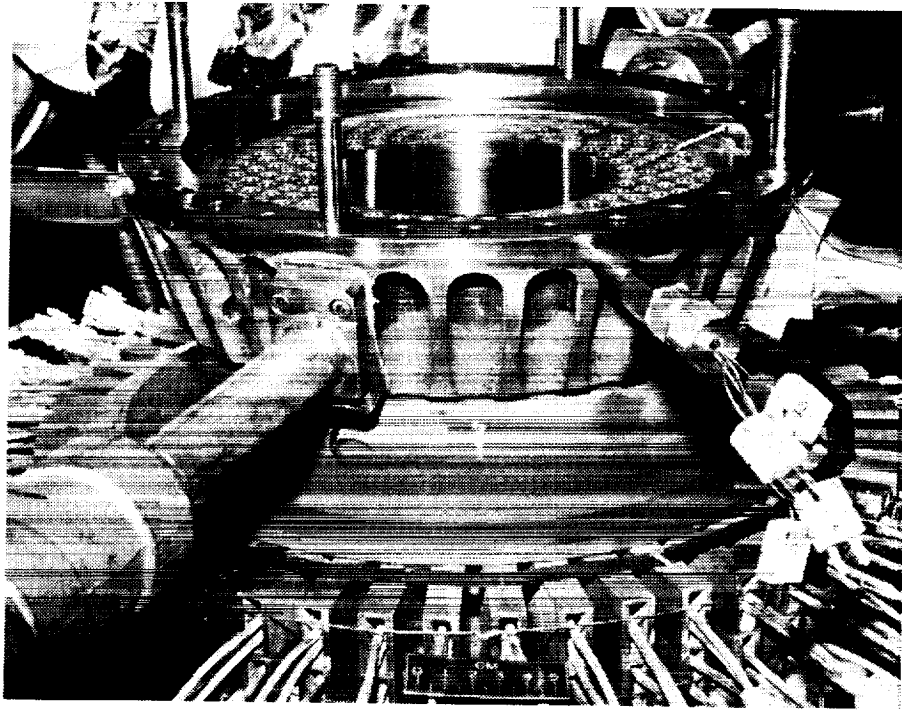
*CTPC Cooler Helium Flow Passages*



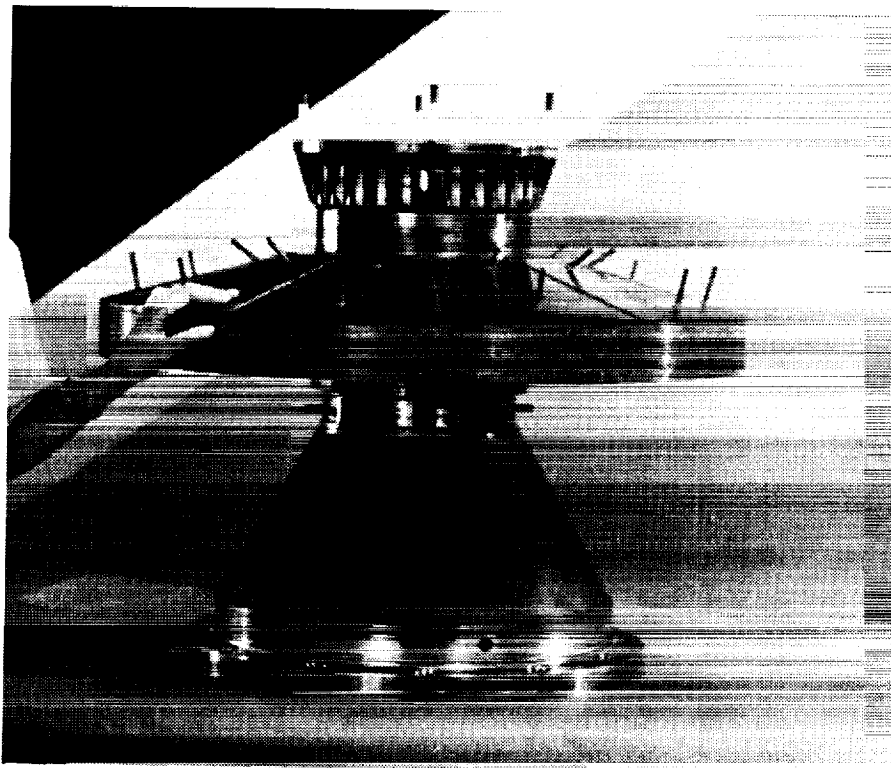
*CTPC Starfish Heater Helium Flow Passages*



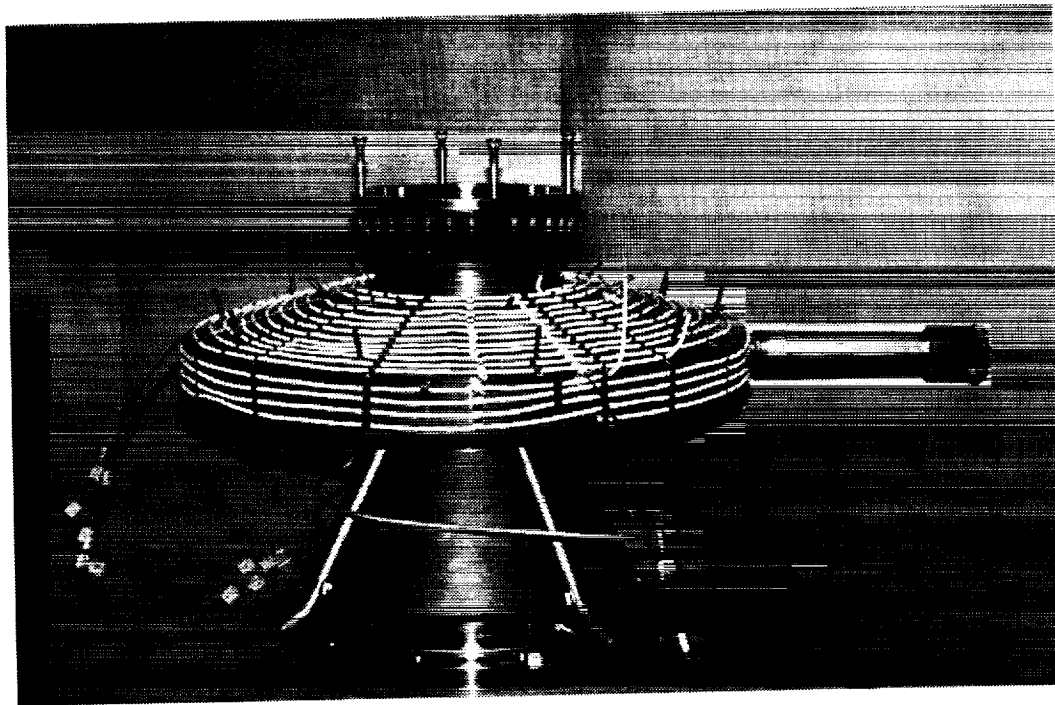
*CTPC Heater Head Assembly with Closure Plates and Mounting Plate*



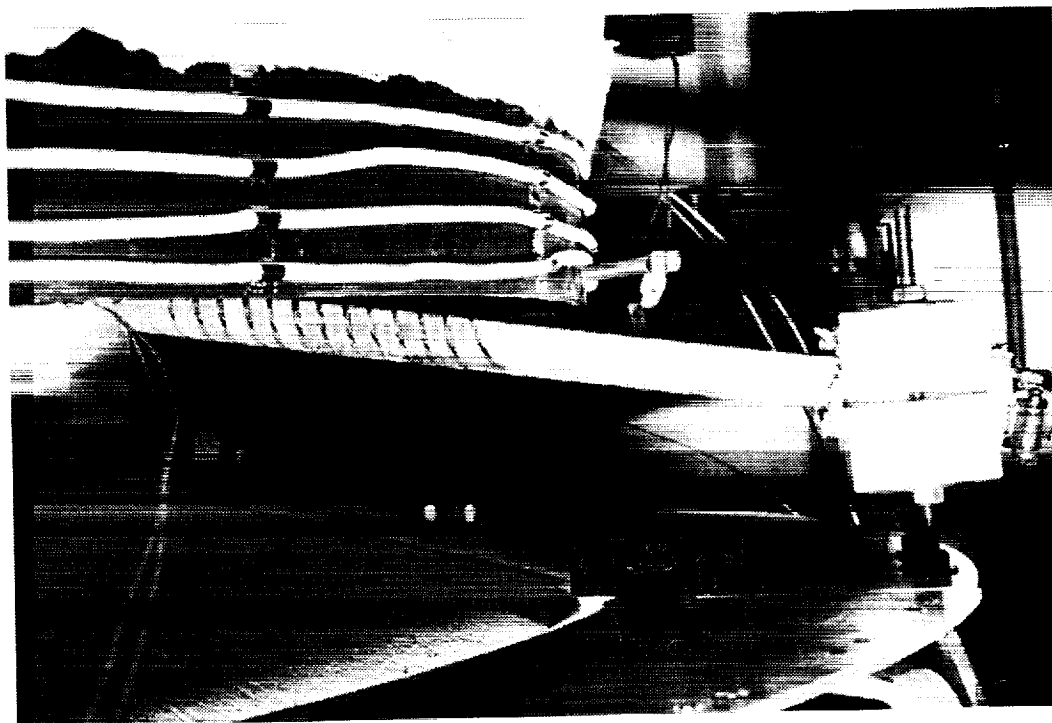
*Test Setup for Radiant Heater Engine Tests, Showing Heater Head, Cooler and Radiant Heaters*



*CTPC Hot-End Assembly with Heat Pipe*

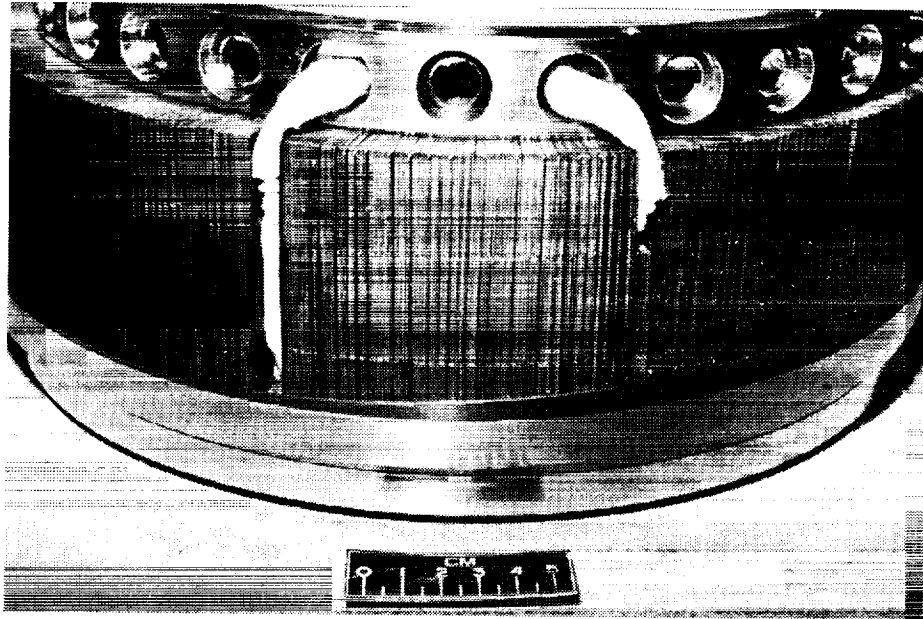


*CTPC Heat Pipe, Showing Trace Heaters for Warm-up*

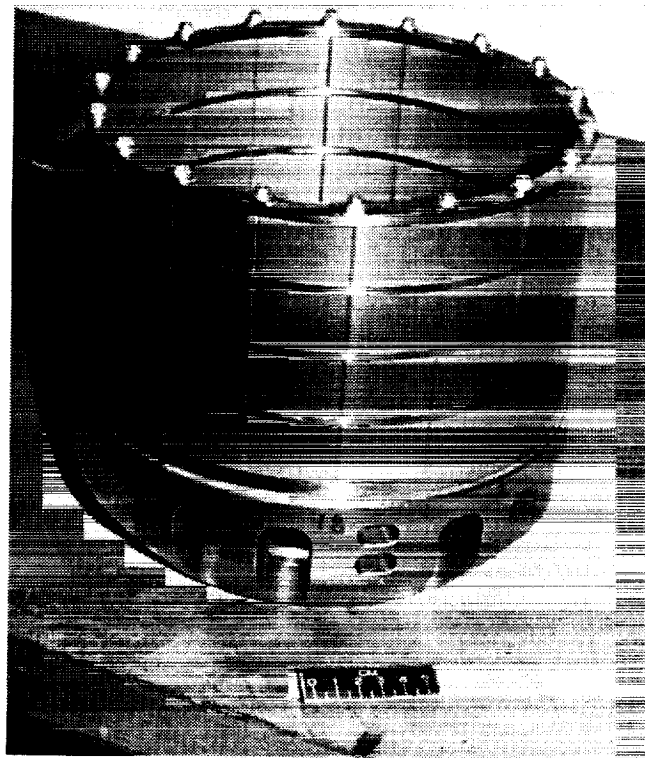


*Silicon Carbide Radiant Heaters (1 of 40) for CTPC Heat Pipe*

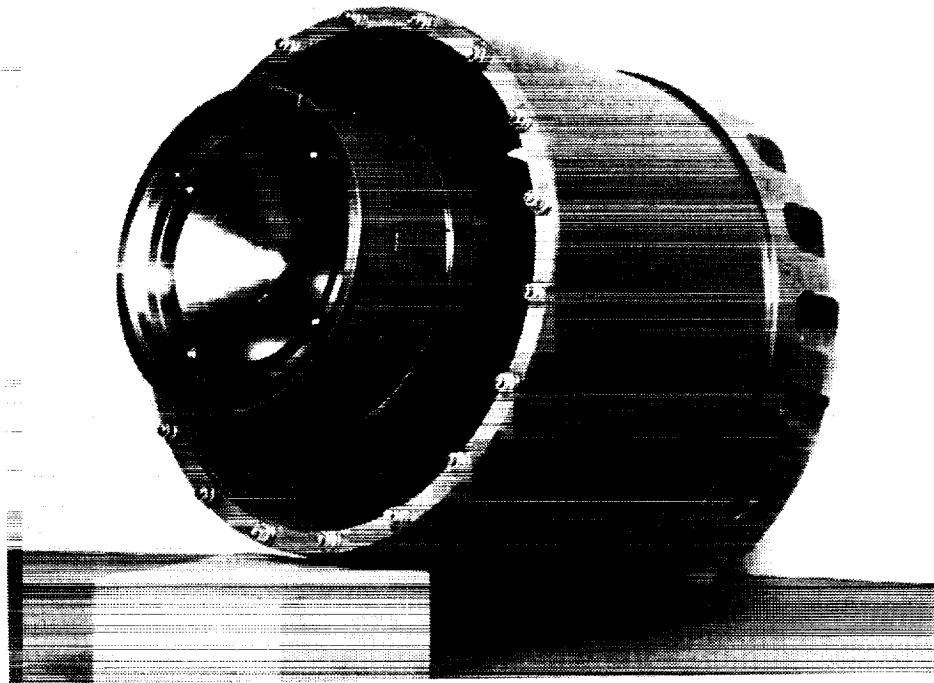




***CTPC Alternator Outer Stator Laminations and Directional Orifices for Alternator Cooling***



***CTPC Alternator Plunger, Showing Samarium Cobalt Magnets***



*CTPC Power Piston and Alternator Plunger Assembly*



REPORT DOCUMENTATION PAGE			Form Approved OMB No. 0704-0188	
Public reporting burden for this collection of information is estimated to average 1 hour per response, including the time for reviewing instructions, searching existing data sources, gathering and maintaining the data needed, and completing and reviewing the collection of information. Send comments regarding this burden estimate or any other aspect of this collection of information, including suggestions for reducing this burden, to Washington Headquarters Services, Directorate for Information Operations and Reports, 1215 Jefferson Davis Highway, Suite 1204, Arlington, VA 22202-4302, and to the Office of Management and Budget, Paperwork Reduction Project (0704-0188), Washington, DC 20503.				
1. AGENCY USE ONLY (Leave blank)		2. REPORT DATE August 1999		3. REPORT TYPE AND DATES COVERED Final Contractor Report
4. TITLE AND SUBTITLE Stirling Space Engine Program Volume 2—Appendixes A, B, C, and D			5. FUNDING NUMBERS  WU-632-1A-1G-00 NAS3-25463	
6. AUTHOR(S)  Manmohan Dhar				
7. PERFORMING ORGANIZATION NAME(S) AND ADDRESS(ES)  Mechanical Technology Incorporated 968 Albany-Shaker Road Latham, New York 12110			8. PERFORMING ORGANIZATION REPORT NUMBER  E-11751-2	
9. SPONSORING/MONITORING AGENCY NAME(S) AND ADDRESS(ES)  National Aeronautics and Space Administration John H. Glenn Research Center at Lewis Field Cleveland, Ohio 44135-3191			10. SPONSORING/MONITORING AGENCY REPORT NUMBER  NASA CR—1999-209164-VOL2 MTI 97TR21	
11. SUPPLEMENTARY NOTES  Technical Agent, D. Alger, Sverdrup Technology, Inc. Project Manager, James E. Dudenhoefer, Power and On-Board Propulsion Technology Division, NASA Glenn Research Center, organization code 5440, (216) 433-6140.				
12a. DISTRIBUTION/AVAILABILITY STATEMENT  Unclassified - Unlimited Subject Categories: 20 and 44  This publication is available from the NASA Center for AeroSpace Information, (301) 621-0390.			12b. DISTRIBUTION CODE	
13. ABSTRACT (Maximum 200 words)  The objective of this program was to develop the technology necessary for operating Stirling power converters in a space environment and to demonstrate this technology in full-scale engine tests. Hardware development focused on the Component Test Power Converter (CTPC), a single cylinder, 12.5-kWe engine. Design parameters for the CTPC were 150 bar operating pressure, 70 Hz frequency, and hot- and cold-end temperatures of 1050 K and 525 K, respectively. The CTPC was also designed for integration with an annular sodium heat pipe at the hot end, which incorporated a unique "Starfish" heater head that eliminated highly stressed brazed or weld joints exposed to liquid metal and used a shaped-tubed electrochemical milling process to achieve precise positional tolerances. Selection of materials that could withstand high operating temperatures with long life were another focus. Significant progress was made in the heater head (Udimet 700 and Inconel 718 and a sodium-filled heat pipe); the alternator (polyimide-coated wire with polyimide adhesive between turns and a polyimide-impregnated fiberglass overwrap and samarium cobalt magnets); and the hydrostatic gas bearings (carbon graphite and aluminum oxide for wear couple surfaces). Tests on the CTPC were performed in three phases: cold end testing (525 K), engine testing with slot radiant heaters, and integrated heat pipe engine system testing. Each test phase was successful, with the integrated engine system demonstrating a power level of 12.5 kWe and an overall efficiency of 22% in its maiden test. A 1500-hour endurance test was then successfully completed. These results indicate the significant achievements made by this program that demonstrate the viability of Stirling engine technology for space applications.				
14. SUBJECT TERMS  Free-Piston Stirling Engines; Stirling Space Power Systems; Nuclear electric power generation			15. NUMBER OF PAGES 417	
			16. PRICE CODE A18	
17. SECURITY CLASSIFICATION OF REPORT  Unclassified	18. SECURITY CLASSIFICATION OF THIS PAGE  Unclassified	19. SECURITY CLASSIFICATION OF ABSTRACT  Unclassified	20. LIMITATION OF ABSTRACT	



